Effet Bystander en Radiobiologie et Hadronthérapie

François Chevalier

Laboratoire
d'accueil
et de recherche
avec les ions accélérés

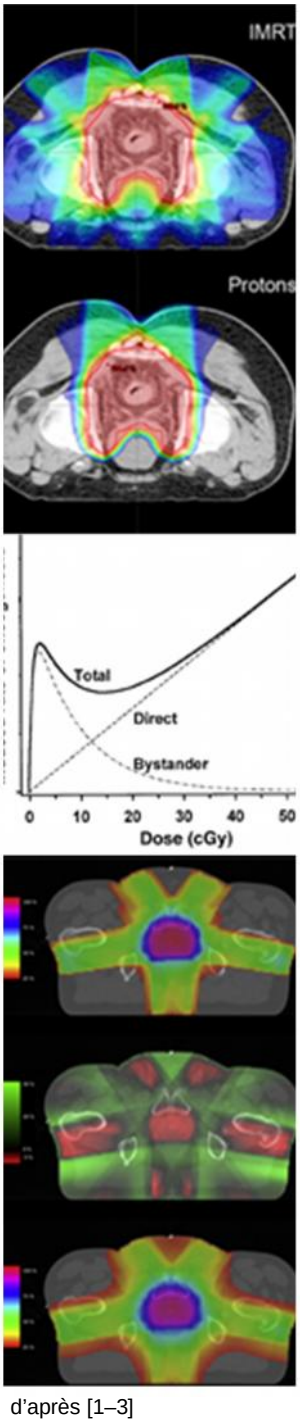

d'après [1–3]

Mémoire

présenté par

Monsieur François CHEVALIER

Le 3 février 2015

en vue de l'obtention du diplôme de l'

HABILITATION A DIRIGER DES RECHERCHES

« Effet Bystander en Radiobiologie et Hadronthérapie »

Jury :

Président :	Professeur F. Confalonieri	(Université Paris Sud Orsay)
Rapporteurs :	Docteur F. Leteurtre, HDR	(CEA)
	Docteur C. Hirtz, HDR	(CHRU Montpellier)
	Docteur J. Armengaud, HDR	(Directeur de Recherche CEA)
Examinateur :	Docteur J.- L. Lefaix, HDR	(CEA)

Table des matières

Coordonnées

François CHEVALIER

Age : 40 ans
Date de naissance : 30 octobre 1974
Lieu de naissance : Clermont-Ferrand (63)
Nationalité : Française

Adresse professionnelle :

Commissariat à l'Energie Atomique
LARIA (Laboratoire d'accueil et de recherche avec des ions accélérés) DSV- iRCM
GANIL
Bd Becquerel
14070 Caen Cedex 5
Tel : 02 31 45 48 60
francois.chevalier@cea.fr
chevalier@ganil.fr

Parcours

1992 : Baccalauréat, série D (Ussel)

1994 : BTS Biotechnologie (Le Puy en Velay)

1995 : L3 : Biochimie (La Rochelle)

1996 : Master 1 Biochimie (La Rochelle)

1996-1997 : Master 2 “Activité biologique des substances naturelles”
MNHN de Paris *mention assez-bien*
Sujet : Clonage et expression d’une carboxylestérase humaine
Lieu : Service d’Oncologie, Rhône-Poulenc Rorer à Vitry-sur-Seine

1998-2001 : Doctorat de biochimie de l’Université de Bordeaux I
Soutenance le 24 octobre 2001 *mention très honorable*
Sujet : Propriétés techno-fonctionnelles et biologiques de la bêta-lactoglobuline modifiée par la réaction de Maillard
Lieu : LEIMA, INRA à Nantes

2001-2005 : Post-Doctorat 1 en analyses protéomiques
Sujet : Analyse protéomique de la variabilité naturelle chez *Arabidopsis*
Lieu : Unité de Protéomique de l’INRA à Montpellier

2006-2007 : Post-Doctorat 2 en analyses protéomiques
Projet : Analyse protéomique de la qualité du lait
Lieu : Dept Food Nutritional Science, University College Cork, Irlande

Depuis 2007 : Chercheur en Radiobiologie et analyses protéomiques
Lieu : plateforme protéomique, iRCM, CEA de Fontenay-aux-Roses (2007-2013)
Lieu : LARIA, iRCM, CEA de Caen (depuis 2013)

Encadrement

Etudiants en Master 2

Novembre 1998 - juin 1999
Master 2 de Biologie Cellulaire Université de Nantes (Stéphanie Prigent)
Sujet : Glycation de la caséine bêta : propriétés physico-chimiques, fonctionnelles et biologiques des dérivés obtenus

Juin - septembre 2002
Master 2 de Biologie Cellulaire, Université de Montpellier II (Mickaël Pata)
Sujet : Analyse morphologique de la réponse racinaire en condition de carence en phosphate de différents écotypes d'*Arabidopsis thaliana*

Avril - juin 2003
Master 2 de Biologie Cellulaire, Université de Caen (Samuel Barteau)
Sujet : Analyse protéomique de la réponse à la carence en phosphate chez différents écotypes d'*Arabidopsis thaliana*

Juin - juillet 2003
Master 2 de Biologie Moléculaire et Cellulaire (Anne-Dominique Devauchelle)
Sujet : Analyse protéomique racinaire de différents écotypes d'*Arabidopsis thaliana* : étude de la réponse en condition de carence en phosphate, étude de la variabilité naturelle inter-écotypes

Etudiants en thèse

2006-2007
Co-encadrant de doctorat University College Cork (Emmanuele Armaforte)
Sujet : Innovative separation techniques for the evaluation of the quality of food products

Co-encadrant de doctorat à 25% (Daniela Voigt)
Sujet : Effect of high-pressure treatment on proteolysis in mature blue-veined cheese

Personnel technique

Gestion de techniciens de laboratoire en biochimie des protéines et protéomique
2000-2001 : Marie-Georgette Nicolas (50%)
2001-2004 : Valérie Rofidal (50%)
2007-2013 : Jordane Dépagne (100%)

Enseignement

2014 : Cours de radiobiologie sur l'effet Bystander radio-induit (2h)
Etudiants en M2 « Imagerie médicale »
Faculté de médecine de Caen

Rayonnement

Critique scientifique de revues internationales

- Proteomics
- Proteomic Insights
- Proteome Science
- PlosOne
- Planta
- Mutation Research
- Journal of Proteomics
- Journal of Proteome Research
- Journal of Food Processing & Technology
- Journal of Food engineering
- Journal of Dairy Science
- Journal of Dairy Research
- Journal of Agricultural and Food Chemistry
- International Dairy Journal
- Analytical biochemistry

Société savante

Membre de la SFEAP (Société Française d'Electrophorèse et d'Analyse Protéomique)
Membre de l'HUPO (Human Proteome Organisation)

Distinctions Scientifiques

1998-2001	Bourse de thèse, Ministère de la recherche (MENRT)
2001-2004	Lauréat de la bourse de post-doc GVE (Growth, vigour, environment - molecular breeding for plant growth and yield, funded under the FP5-LIFE QUALITY of the European Commission)
2006-2007	Lauréat de la bourse de post-doc FIRM (Food Institutional Research Measure, funded by the Irish Government under the National Development Plan)
2007 :	Best Poster Award (category 4 : Nutritional and Health Care) Cork University Hospital Annual Research Day University College Cork, Cork, Ireland 15 June 2007

Liste des publications

36 publications, 682 citations, citations moyennes référencées : 27.3, H Factor : 14 (Web of Science)

Publications dans des revues avec comité de lecture :

1. **Chevalier F**., Chobert J.-M., Genot C., Haertlé T. (2001)
   Scavenging of free radicals, anti-microbial and cytotoxic activities of the Maillard reaction products of ß-lactoglobulin glycated with several sugars.
   Journal of Agricultural and Food Chemistry 49, 5031-5038.

2. **Chevalier F**., Chobert J.-M., Popineau Y., Nicolas M. G., Haertlé T. (2001)
   Improvement of the functional properties of ß-lactoglobulin glycated through the Maillard reaction is related to the sugar nature.
   International Dairy Journal 11, 145-152.

3. **Chevalier F**., Chobert J.-M., Dalgalarrondo M., Haertlé T. (2001)
   Characterization of the Maillard reactions product of ß-lactoglobulin glucosylated in mild conditions.
   Journal of Food Biochemistry 25, 33-55.

4. **Chevalier F**., Chobert J.-M., Mollé D., Haertlé T. (2001)
   Maillard glycation of ß-lactoglobulin with several sugars : comparative study of the properties of the obtained polymers and of the substituted sites.
   Le Lait 81, 655-666.

5. **Chevalier F**., Chobert J.-M., Choiset Y., Dalgalarrondo M., Haertlé T. (2002)
   Maillard glycation of ß-lactoglobulin induces conformation changes.
   Nahrung 46, 58-63.

6. **Chevalier F***., Pata M., Nacry P., Doumas P., Rossignol M. (2003)
   Effects of phosphate availability on the root system architecture : large-scale analysis of the natural variation between *Arabidopsis* accessions.
   Plant Cell & Environment 26, 1839-1850.

7. **Chevalier F***., Martin O., Rofidal V., Devauchelle A.-D., Rossignol M. (2004)
   Proteomic investigation of natural variation between *Arabidopsis* ecotypes.
   Proteomics 4, 1372-1381.

8. **Chevalier F**., Rofidal V., Vanova P., Bergoin A., Rossignol M. (2004)
   Proteomic capacity of recent fluorescent dyes for protein staining.
   Phytochemistry 65, 1499-1506.

9. Hirtz C., **Chevalier F**., Rossignol M., Sommerer N., Deville de Periere D. (2005)
   MS characterization of multiple forms of alpha-amylase in human saliva.
   Proteomics 5, 4597-4607

10. **Chevalier F**., Centeno D., Rofidal V., Sommerer N., Rossignol M. (2005)
    Different Impact of Staining Procedures Using Visible Stains and Fluorescent Dyes for Large-Scale Investigation of Proteomes by MALDI-TOF Mass Spectrometry
    Journal of Proteome Research, 5, 512-520.

11. Hirtz C., **Chevalier F**., Egea J. C., Rossignol M., Deville de Periere D. (2006)
    Complexity of the human whole saliva proteome.
    Journal of Physiology and Biochemistry, 61, 469-480.

12. Hirtz C., **Chevalier F**., Raingeard I., Bringer J., Rossignol M., Deville de Periere D. (2006) Salivary Protein Profiling in Type 1 Diabetes Using Two-Dimensional Electrophoresis and Mass Spectrometry
    Clinical proteomics, 2, 117-128.

13. **Chevalier F***., Hirtz C., Chay S., Cuisinier F., Sommerer N., Rossignol M., Deville de Périère D. (2007)
    Proteomic Studies of Saliva: A Proposal for a Standardized Handling of Clinical Samples.
    Clinical proteomics, 3, 13-21.

14. Lodaite K., **Chevalier F**., Armaforte E. and Kelly A. L. (2009)
Effect of high-pressure homogenization on rheological properties of rennet-induced skim milk and standardized milk gels
Journal of Dairy Research, 76 (3), 294-300.

15. **Chevalier F***., Hirtz C., Sommerer N., Kelly A. L. (2009)
Use of reducing/non-reducing two-dimensional electrophoresis for the study of disulphide-mediated interactions between proteins in raw and heated bovine milk
Journal of Agricultural and Food Chemistry, 57, 5948-5955.

16. Voigt D. D., **Chevalier F**., Qian M., Kelly A. L. (2010)
Effect of high-pressure treatment on microbiology, proteolysis, lipolysis and levels of flavour compounds in mature blue-veined cheese
Innovative Food Science and Emerging Technologies, 11, 68-77.

17. **Chevalier F***. (2010)
Highlights on the capacities of "Gel-based" proteomics
Proteome Science 2010, 8:23 Highly accessed on Biomed Central

18. **Chevalier F***. and Kelly A. L. (2010)
Proteomic quantification of disulfide-linked polymers in raw and heated bovine milk
Journal of Agricultural and Food Chemistry, 58, 7437–7444.

19. Armaforte E., Curran E., Huppertz T., Ryan C. A., Caboni M. F., O'Connor P., Hirtz C., Sommerer N., **Chevalier F**., Kelly A. L. (2010)
Proteins and proteolysis in pre-term and term human milk and possible implications for infant formulae
International Dairy Journal, 20, 715-723.

20. **Chevalier F***. (2010)
Standard dyes for total protein staining in gel-based proteomic analysis
Materials, 3(10), 4784-4792. Special Issue "Advances in Dyes and Pigments"

21. Laulier C., Barascu A., Guirouilh-Barbat J., Pennarun G., Le Chalony C., **Chevalier F**., Palierne G., Bertrand P., Verbavatz J.- M. and Lopez B. S. (2011)
Bcl-2 inhibits nuclear homologous recombination by localizing BRCA1 to the endomembranes
Cancer research, 71(10), 3590-3602.

22. **Chevalier F***. and Rossignol M.
Proteomic analysis of *Arabidopsis thaliana* ecotypes with contrasted root architecture in response to phosphate deficiency (2011)
Journal of Plant Physiology 168(16), 1885-1890.

23. Voigt D. D., **Chevalier F**., Donaghy J. A., Patterson M. F., Qian M., Kelly A. L.
Effect of high-pressure treatment of milk for cheese manufacture on proteolysis, lipolysis, texture and functionality of Cheddar cheese during ripening (2012)
Innovative Food Science and Emerging Technologies 13, 23-30.

24. **Chevalier F***., Depagne J., Hem S., Chevillard S., Bensimon J., Bertrand P., and Lebeau J. (2012)
Accumulation of Cyclophilin A isoforms in conditioned medium of irradiated breast cancer cells
Proteomics, 12(11): 1756–1766.

25. Peric D., Labarre J., **Chevalier F***., and Rousselet G. (2012)
Impairing the micro-RNA pathway induces proteome modifications characterized by size bias and enrichment in anti-oxidant proteins.
Proteomics, 12(13): 2295–2302.

26. Dépagne J., **Chevalier F***. (2012)
Technical updates to basic proteins focalization using IPG strips
Proteome Science 10:54 Highly accessed on Biomed Central

27. Uniacke-Lowe T., **Chevalier F***., Hem S., Fox P. F. and Mulvihill D. M. (2013)
Proteomic comparison of Equine and Bovine Milk Systems on Renneting.
Journal of Agricultural and Food Chemistry, 61, 2839-2850.

28. **Chevalier F***., Hamdi D. H., Saintigny Y. and Lefaix J.- L. (2014)
Proteomic overview and perspectives of the Radiation-Induced Bystander Effects
Mutation Research/ Reviews in Mutation Research *in press*

29. Saintigny Y., Cruet-Hennequart S., Hamdi D. H., **Chevalier F**. and Lefaix J.- L. (2015)
Impact of therapeutic irradiation on healthy articular cartilage
Radiation Research *in press*

Chapitres d'ouvrage :

1. **Chevalier F**., Chobert J.-M., Haertlé T. (2002)
Interfacial properties of glycated ß-lactoglobulin.
In "Recent Advances in Agricultural and Food Chemistry", Research Signpost.

2. **Chevalier F**., Rofidal V., Rossignol M. (2007)
Visible and fluorescent staining of two-dimensional gels.
In " Plant Proteomics : Methods in Molecular Biology ", Humana Press, USA.
Methods Mol Biol. 355, 145-156

3. **Chevalier F***. (2011)
What future for "Gel-based proteomic" approaches? In: Giselle C. Rancourt (Eds), " Proteomics: Methods, Applications and Limitations", pp 31-52 Series: Protein Biochemistry, Synthesis, Structure and Cellular Functions Nova Science Publishers, Inc. Hauppauge NY 11788-3619 USA

4. **Chevalier F***. (2011)
Analytical Methods: Electrophoresis. In: Fuquay JW, Fox PF and McSweeney PLH (eds.), Encyclopedia of Dairy Sciences, Second Edition, vol. 1, pp. 185–192. San Diego: Academic Press.

5. **Chevalier F***., Sommerer N. (2011)
Analytical Methods: Mass Spectrometric Methods. In: Fuquay JW, Fox PF and McSweeney PLH (eds.), Encyclopedia of Dairy Sciences, Second Edition, vol. 1, pp. 198–205. San Diego: Academic Press.

6. **Chevalier F***. (2011)
Milk Proteins : Proteomics. In: Fuquay JW, Fox PF and McSweeney PLH (eds.), Encyclopedia of Dairy Sciences, Second Edition, vol. 3, pp. 843–847. San Diego: Academic Press.

7. **Chevalier F***., Chicheportiche A, Daynac M., Depagne J., Bertrand P. Boussin F., Mouthon M.- A. (2012)
Identification of factors involved in neurogenesis recovery following irradiation of the adult mouse subventricular zone, a preliminary study.
In "Proteomics", InTech Publisher

*** : corresponding author**

Présentations scientifiques / Participation à des Congrès :

Une trentaine de participation à des congrès nationaux ou internationaux sous forme d'affiche ou de présentation orale.

1 - Activités de Recherche : Doctorat - Post-doctorats

Avant-propos

Depuis mon doctorat, et jusqu'à maintenant, mes activités de recherche ont eu pour fil conducteur l'analyse biochimique des relations structures/fonctions des protéines après modification ou en mélanges complexes en réponse à un stress dans des domaines aussi variés que la biologie végétale, l'agroalimentaire ou la cancérologie et la médecine.

Lors de mon doctorat, J'ai étudié une protéine modèle du lait, la bêta-lactoglobuline, après traitement thermique ou modification chimique. Ses propriétés physico-chimiques et biologiques, sa structure et ses capacités fonctionnelles ont été modulées en vue de son utilisation dans l'industrie agroalimentaire. Ayant par la suite totalement changé de thématique, la connaissance sur le sujet a évolué et l'état des lieux actuel n'est pas évoqué dans le texte.

En post-doctorat, j'ai analysé les mécanismes moléculaires gouvernant la réponse à la carence en phosphate chez *Arabidopsis thaliana* en fonction des écotypes de cette plante. L'avènement de l'étude de mélanges complexes de protéines par électrophorèse bidimensionnelle m'a permis de mettre en évidence des profils caractéristiques entre écotypes et conditions de culture. J'ai ensuite appliqué cette technologie lors de mon second post-doctorat pour étudier la qualité du lait et les associations entre protéines laitières après traitement thermique.

Mon activité de recherche actuelle en radiobiologie vise à mettre en évidence des réponses cellulaires caractéristiques à différents types de rayonnements ionisants. Les protéines du métabolisme cellulaire ou les protéines sécrétées en réponse à un stress sont analysées par différents outils de radiobiologie et de biochimie des protéines et protéomique. Plus particulièrement, le projet proposé porte sur l'étude des effets indirects des rayonnements ionisants et leurs conséquences sur les tissus sains en utilisant un modèle 3D de cartilage reconstitué.

Afin de donner une vision d'ensemble des recherches menées lors de mon doctorat, de mes deux contrats postdoctoraux et dans le cadre de mon activité de recherche au CEA, j'ai choisi de présenter d'une part, un résumé des résultats obtenus et, d'autre part, une sélection des principaux articles scientifiques correspondant, publiés dans des journaux internationaux avec comité de lecture et dans lesquels j'apparais comme premier auteur, ou principal auteur de l'étude.

1.1 - Doctorat : Biochimie de la β-lactoglobuline modifiée par glycation

Le travail réalisé au cours de ma thèse consistait à modifier par la réaction de Maillard une protéine alimentaire et à étudier l'influence des composés formés sur les caractéristiques physico-chimiques et structurales de la protéine. L'objectif était d'améliorer les propriétés techno-fonctionnelles et de générer de nouvelles fonctions biologiques aux protéines et peptides modifiés. Depuis sa première description en 1912 par L. C. Maillard, la réaction du même nom fait l'objet de nombreuses recherches dans le domaine des sciences des aliments. Une grande quantité de publications scientifiques a été rédigée sur la réaction complexe entre les composés aminés et les sucres réducteurs. De nombreux composés ont été identifiés afin de mieux appréhender les mécanismes de dégradation et de polymérisation des sucres et des composés aminés ainsi que la formation d'arômes. Bien que cette réaction soit couramment rencontrée lors de processus industriels et dans la cuisson des aliments, son influence sur les propriétés fonctionnelles et la valeur nutritive des protéines alimentaires ainsi modifiées est encore assez mal connue.

1.1.1 - Caractérisation des protéines modifiées

1.1.1.1 - Caractérisation physico-chimique

La glycation de la béta-lactoglobuline (BLG) par différents sucres a permis d'étudier l'influence de la nature du sucre sur l'avancée de la réaction de Maillard lors d'un chauffage de 72 heures à 60°C. Les sucres utilisés ont induit différents taux de glycation en fonction de leur nature chimique.

Le lactose, un diholoside, a conduit au plus faible taux (35%) de modification de la BLG. Les hexoses (galactose, glucose et rhamnose) ont conduit à un taux intermédiaire d'environ 40 %. Le plus fort taux de modification a été obtenu avec les pentoses pour respectivement 60 % et 68 % de glycation en présence d'arabinose et de ribose. Une diminution du point isoélectrique a été observée, proportionnelle au taux de glycation. Plus le taux de glycation était élevé, plus les points isoélectriques étaient acides et homogènes.

1.1.1.2 - Caractérisation structurale

L'analyse de la composition en acides aminés des échantillons de BLG modifiée par le glucose pendant différentes périodes a montré que d'autres acides aminés que la lysine pouvaient être modifiés au cours de la réaction de Maillard. En plus de la lysine, la tyrosine, l'arginine et l'histidine ont semblé être modifiées par le glucose ou par des sous-produits de la réaction.

Des études par spectrométrie de masse ont permis de mettre en évidence sept sites de glycation de la BLG (les lysines 14, 47, 69, 75, 100 et 135 et la leucine 1) en fonction du sucre utilisé. Un, trois, quatre et six sites ont ainsi été observés pour la BLG modifiée respectivement par le rhamnose, le galactose, le lactose ou le glucose.

L'analyse des hydrolysats trypsiques de la BLG modifiée par le glucose a par ailleurs révélé que l'arginine 40 et la lysine 14 ne sont pas des sites préférentiels de glycation ; ces expériences ont aussi montré que la lysine 70 est modifiée au cours du chauffage avant la lysine 69. Ces résultats ont été

interprétés par la localisation différente de ces acides aminés au sein de la structure tridimensionnelle de la BLG.

Les techniques de dichroïsme circulaire, de microcalorimétrie et d'hydrolyse pepsique ont été utilisées afin d'évaluer la conformation de la protéine modifiée par les différents sucres. Ces trois techniques ont révélé que le traitement thermique (72 heures à 60°C) n'induisait pas de modifications conformationnelles fondamentales de la BLG en absence de sucre. En présence de sucres, la modification de la conformation de la protéine était proportionnelle au taux de glycation. D'après les résultats des hydrolyses pepsiques, la glycation par l'arabinose ou le ribose a dénaturé à plus de 65 % la BLG. 57 % et 38 % de dénaturation ont été observés avec la BLG modifiée respectivement en présence de galactose / glucose et en présence de rhamnose / lactose.

1.1.1.3 - Comportement vis-à-vis de l'association – polymérisation

Des polymères ont été mis en évidence dans les échantillons de BLG modifiée par le glucose. L'étude de la nature des liaisons intervenant dans la stabilisation de ces polymères a révélé la présence de pontages covalents induits par les sucres.

Selon le sucre utilisé, différents types de liaisons ont été impliqués dans la stabilisation des polymères. Tous les polymères de BLG modifiée par le ribose ou l'arabinose ont été stabilisés par des pontages covalents.

Dans le cas de la BLG modifiée par le galactose, le glucose ou le rhamnose, des ponts disulfures, des interactions hydrophobes et des pontages covalents ont semblé être impliqués dans la stabilisation de ces polymères. Seule la BLG modifiée par le lactose n'a pas présenté de pontages covalents induits par les sucres ; seuls des ponts disulfures ont été identifiés dans cet échantillon.

1.1.2 - Etude des propriétés techno-fonctionnelles des protéines modifiées

Une amélioration de la stabilité thermique, des propriétés émulsifiantes et moussantes a été observée en utilisant les protéines modifiées dans certaines conditions de pH ou de température. Les échantillons les plus modifiés ont présenté la meilleure solubilité à la suite d'un traitement thermique. La fixation de sucre à la surface de la protéine, par modification de la charge globale, et par augmentation des possibilités d'hydratation, a ainsi amélioré la stabilité thermique de la bêta-lactoglobuline. Le maintien des propriétés émulsifiantes obtenues avec les protéines les plus modifiées lors du changement de pH de 7,0 à 5,0 était sûrement lié en grande partie à la solubilité de ces échantillons aux différents pH.

Un taux de modification moyen (obtenu avec le glucose ou le galactose) a présenté le meilleur compromis pour obtenir des mousses stables avec un faible drainage. Un taux de modification élevé déstabilise la mousse (en partie à cause de la déstructuration de la protéine) et un taux de modification faible augmente le drainage.

1.1.3 - Etude des propriétés biologiques des protéines modifiées

1.1.3.1 - Susceptibilité à l'hydrolyse pepsique et trypsique de la BLG native ou modifiée par la réaction de Maillard

La susceptibilité des différents échantillons de BLG à l'hydrolyse pepsique ou trypsique était directement liée au taux de modification par la réaction de Maillard. Une quantité variable de peptides a donc été obtenue en fonction des échantillons testés. Plus la protéine était modifiée, plus elle était sensible à l'hydrolyse pepsique et moins elle était sensible à l'hydrolyse trypsique.

1.1.3.2 - Tests d'activité antiradicalaire

Des activités antiradicalaires ont été observées dans les échantillons de BLG modifiée par la réaction de Maillard, alors que les protéines non modifiées (BLG native ou chauffée, SAB) ont présenté une faible aptitude à capter les radicaux libres. Cette activité était liée au taux de modification (plus la protéine est modifiée, plus son activité antiradicalaire est forte) et à la nature du sucre utilisé pour modifier la protéine (pour une même quantité de groupe NH2 réactif, la modification de la BLG par le ribose a induit une plus forte activité antiradicalaire que la modification de la BLG par le lactose). L'hydrolyse des échantillons de BLG modifiée par la réaction de Maillard a diminué leur activité antiradicalaire. Cependant, celle-ci était tout de même maintenue à un niveau supérieur à celui des échantillons de BLG non modifiée, révélant la capacité des protéines modifiées à capter les radicaux libres même après leur hydrolyse.

1.1.3.3 - Tests d'activité cytotoxique

La réaction de Maillard est connue pour induire des composés mutagènes et cytotoxiques au cours de la fabrication et de la cuisson des aliments. Les composés avancés de la réaction de Maillard et les amines hétérocycliques sont certainement impliqués dans ces propriétés. De tels composés n'ont pas semblé être formés dans les conditions de réaction utilisées pour modifier la BLG puisque aucune différence de cytotoxicité n'a pu être observée entre la protéine non modifiée et la protéine modifiée. Le traitement thermique relativement doux utilisé (72 heures à 60°C) n'a donc pas semblé générer l'apparition de composés mutagènes et/ou toxiques pour les cellules.

1.1.4 - Sélection de publications du doctorat

Chevalier F., Chobert J.-M., Choiset Y., Dalgalarrondo M., Haertlé T. (2002)
Maillard glycation of ß-lactoglobulin induces conformation changes.
Nahrung 46, 58-63.

Chevalier F., Chobert J.-M., Popineau Y., Nicolas M. G., Haertlé T. (2001)
Improvement of the functional properties of ß-lactoglobulin glycated through the Maillard reaction is related to the sugar nature.
International Dairy Journal 11, 145-152.

Chevalier F., Chobert J.-M., Genot C., Haertlé T. (2001)
Scavenging of free radicals, anti-microbial and cytotoxic activities of the Maillard reaction products of ß-lactoglobulin glycated with several sugars.
Journal of Agricultural and Food Chemistry 49, 5031-5038.

Research Papers

Maillard glycation of β-lactoglobulin induces conformation changes

F. Chevalier, J.-M. Chobert, M. Dalgalarrondo, Y. Choiset and T. Haertlé

Glycation by the Maillard reaction is an ubiquitous reaction of condensation of a reducing sugar with amino groups of proteins, which products could improve the functional and/or biological properties for food and non-food uses. It can induce structural modifications in proteins, modifying their properties. The aim of this work was to investigate the association behavior and the conformational changes of β-lactoglobulin (BLG) after its glycation by the Maillard reaction with several alimentary sugars (arabinose, galactose, glucose, lactose, rhamnose and ribose). Protein samples were heated in the presence or in the absence (heated control) of different sugars during 3 days at 60 °C. Glycation induced oligomerization of BLG monomers. Depending on the reactivity of the sugar, the population of produced oligomers showed smaller or greater heterogeneity in molecular masses. Analysis of modified BLG by circular dichroism and by its susceptibility to pepsinolysis showed that the conditions of heating used did not significantly alter the conformation of BLG. Heating of BLG in presence of sugars induced only minor structural modification, when using the less reactive sugars such as lactose and rhamnose. It was, however, at the origin of major three-dimensional destructuring in the case of the more reactive sugars such as arabinose and ribose. Pepsinolysis of glycated BLG did not affect about 62 and 35% of the protein molecules modified with lactose or rhamnose, and arabinose or ribose, respectively. The increase of susceptibility of glycated BLG to pepsinolysis could be related to the alteration of the conformation of the protein when glycation was performed with highly reactive sugars, as observed by circular dichroism and calorimetry analysis.

1 Introduction

β-Lactoglobulin (BLG) is the major whey protein present in milks of various mammalian species [1, 2], which is absent in human milk. This well-characterized protein with a molecular mass of about 18 300 Da can be classified together with the retinol-binding protein (RBP) and other similar proteins in the superfamily of the proteins able to bind hydrophobic ligands called lipocalins [3, 4]. Crystallographic analysis of the BLG 3-D structure has shown a hydrophobic pocket formed by eight-stranded anti-parallel β-barrel [5, 6]. This protein was studied intensively because of its interesting capacity to bind numerous aromatic compounds [7–9], retinoids [10–12], vitamin D and cholesterol [13], benzopyrene, ellipticine and *cis*-parinaric acid [14, 15], vitamin A [16], and fatty acids [17, 18]. Although BLG is able to bind a lot of compounds *in vitro*, its function in milk is still unknown. The folding of BLG renders it resistant to peptic hydrolysis [19–21], since its peptic cleavage sites (hydrophobic or aromatic amino acid side chains) are buried well inside the β-barrel forming a strong hydrophobic core. This may suggest that particular conformation adopted by BLG could be a solution to trap and transport some molecules through the gastric part of digestive tract.

Thanks to its good nutritional properties and to its availability in large quantity, the use of BLG as a food additive increases [22]. BLG has been modified by several methods [23] as phosphorylation [24], esterification [25, 26], alkylation [27], and amidation [28] in order to improve its functional and physicochemical properties. Functional properties of BLG can also be improved by glycation [29, 30], which occurs naturally in food products during heating and storage [31]. Maillard reaction or nonenzymatic browning is the most frequent reaction in food industry. It occurs between proteins, amino acids and amines on one hand, and sugars as well as sometimes also aldehydes and ketones functions of other compounds on the other hand [32, 33]. This is also the principal pathway of final degradation of organic matter in nature. This reaction, first described by the French biochemist Louis Maillard at the beginning of the 20th century [34] was and is extensively studied because of the high quantity and complexity of the products formed during its different stages [35]. Conformational modification of the native structures of proteins induced by glycation can influence their functional or/and biological properties. Consequently, structural studies of glycated proteins can give many useful informations about their structure-function relationships.

In this study, the effects of glycation on both chemical and conformational changes of BLG modified with several sugars were investigated. Glycation yield was analyzed measuring free primary amino groups of proteins and by isoelectric focusing of the treated proteins. Aggregation was studied by sodium dodecyl sulfate-polyacrylamide gel electrophoresis (SDS-PAGE). Conformational changes were studied measuring peptic susceptibility of glycated BLG and also by microcalorimetry and circular dichroism.

Correspondence: Dr. J.-M. Chobert, Institut National de la Recherche Agronomique, Laboratoire d'Étude des Interactions des Molécules Alimentaires, BP 71627, F-44316 Nantes Cedex 3, France
E-mail: chobert@nantes.inra.fr
Fax: +332-4067-5084

Abbreviations: BLG, β-lactoglobulin; **CD**, circular dichroism; **OPA**, *ortho*-phthaldialdehyde; **RP**, reversed phase

Keywords: Maillard glycation / β-Lactoglobulin / Protein conformation / Circular dichroism / Calorimetry

2 Materials and methods

2.1 Protein purification and reagents

BLG (variant A) was purified according to the procedure of Mailliart and Ribadeau Dumas [36]. The purity of BLG (99%)

  0027-769X/2002/0203-0058$17.50+.50/0

was assessed by reversed phase-high performance liquid chromatography (RP-HPLC). D-Arabinose, D-galactose, D-glucose, D-lactose, D-rhamnose, D-ribose monohydrates and porcine pepsin were obtained from Sigma Chemical Co. (St. Louis, MO, USA). All other reagents were of analytical grade.

2.2 Glycation experiments

BLG (0.217 mM) and the different sugars (0.217 M) were dissolved in 0.1 M phosphate buffer, pH 6.5. After filtration on 0.22 μm acetate cellulose filters (Millipore, Bedford, MA, USA), mixtures of protein and sugar were put in well-capped flasks and heated in a water bath at 60 °C for 72 h. This mild heat treatment limited self-aggregation of BLG. All experiments were performed under strictly anaerobic and sterile conditions, all media were purged and saturated with N_2. After heating, the different fractions were dialyzed against distilled water, freeze-dried, and stored at −20 °C. BLG heated without sugar (heated control) was named "heated BLG", and BLG heated in the presence of sugar was named "glycated BLG".

2.3 Determination of available amino groups

The quantity of available amino groups was determined by the modified *ortho*-phthaldialdehyde (OPA) method [37]. The OPA reagent was prepared daily by mixing 40 mg of OPA (dissolved in 1 mL of methanol), 50 mL of 0.1 M sodium borate buffer, pH 9.3, 100 mg of *N*-dimethyl-2-mercaptoethyl-ammonium chloride (DMMAC), and 1.25 mL of 20% w/w SDS in water. Fifty μL of protein solution (2 g/L in 50 mM sodium phosphate buffer, pH 7.8) was added to 1 mL of OPA reagent. The absorbency was read at 340 nm after a minimal delay of 5 min. A calibration curve was obtained by using 0.25–2.00 mM L-leucine as a standard.

2.4 SDS-PAGE

SDS-PAGE was performed using a Mini Protean II gel electrophoresis apparatus (Bio-Rad, Richmond, CA, USA) as described by Laemmli [38]. Isoelectric focusing was performed in the pH range 3–6 on ready-to-use isoelectric focusing gels (Servalyt Precotes, Serva, Heidelberg, Germany).

2.5 Hydrolysis of BLG by porcine pepsin

BLG (2 mg/mL or 0.11 mM) was dissolved in 10 mM glycine-HCl, pH 2.5. Porcine pepsin, previously solubilized in distilled water (1 mg/mL) was added to the reaction mixture at an enzyme/substrate molar ratio of 1/100. The mixture was incubated at 37 °C and at intervals, the reaction was stopped by the addition of 1 volume of 2 M Tris-HCl, pH 8.8, and the hydrolysates were stored at 4 °C before analysis.

2.6 RP-HPLC

The HPLC equipment consisted of a Waters™ 2690 Separation Module system with an integrated solvent, a sample management platform and a photodiode array detector Model 996. The HPLC system was driven by a Millenium®32 program (Waters, Milford, MA, USA). Peptic peptides of BLG and glycated BLG were separated by RP-HPLC on a Symmetry 300A C_{18} column (3.9 mm × 150 mm; Waters) equilibrated in 80% solvent A (0.11% TFA in H_2O) and 20% solvent B (80% acetonitrile, 19.91% H_2O, 0.09% TFA, v/v/v). Elution was performed with linear gradient from 80% to 0% solvent A for 28 min. The temperature of the column and solvents was maintained at 30 °C. The flow rate was 0.6 ml/min. Eluted peaks were detected by UV-absorbency (214 nm). Peak area corresponding to the non hydrolyzed form of the protein was calculated. All results were reported to the peak area of the non hydrolyzed sample, which represents 100%.

2.7 Circular dichroism (CD) spectroscopy

CD spectra were recorded using a Jobin Yvon CD 6 dichrograph equipped with a thermostated cell holder. The cylindrical cells used had a path length of 0.01 cm in the far-UV region (185–260 nm) and of 1 cm in the near-UV region (250–320 nm). An average of five scans was recorded in the far-UV region and one scan was recorded in the near-UV region. All spectra were obtained at 25 °C using a BLG concentration of 2 mg/mL (or 0.11 mM) in a 10 mM glycine-HCl buffer, pH 2.5. BLG concentration was determined by the bicinchoninic acid (BCA) method (Pierce, Rockford, JL, USA) with bovine serum albumin as a standard. The baseline spectrum of buffer was subtracted from each spectrum and the resultant values were converted into molar ellipticity (Θ). The method of Provencher and Glockner [39] was used to estimate the α-helix and β-sheet content of native and heated BLG.

2.8 Calorimetry

The calorimetric measurements were carried out with the high-sensitivity differential scanning microcalorimeter (MCS System, Microcal) within the temperature range of 5–110 °C at the heating rate of 1 K/min and excess pressure 1.2 atm. Protein samples (2 mg/mL or 0.11 mM) were dissolved in 10 mM glycine-HCl buffer, pH 2.5.

3 Results and discussion

3.1 Determination of the yield of glycation

3.1.1 Changes in glycation degree

The BLG sequence contains 16 potential reactive primary amino groups including 1 α-NH_2 and 15 ε-NH_2 of lysyl residues. The quantity of modified amino groups and glycation degree were deduced from OPA results (Table 1). BLG heated in the absence of sugar showed a glycation degree of 6.2% (1 modified amino group). This corresponds to an artifact in the method used probably due to a small conformation change of BLG, hampering the OPA reaction. On average, 11.0, 8.8, 6.7, 6.6, 6.5, and 5.5 amino groups were modified when proteins were heated in the presence of ribose, arabinose, galactose, glucose, rhamnose and lactose, respectively. As expected,

Table 1. Determination of the glycation degree of BLG

Samples	Modified amino groups	Glycation degree (%)
Native BLG	0	0
Heated BLG	1.0	6.2
BLG-lactose	5.5	34.4
BLG-rhamnose	6.5	40.6
BLG-glucose	6.6	41.2
BLG-galactose	6.7	41.9
BLG-arabinose	8.8	55.0
BLG-ribose	11.1	69.4

the modification degree was in direct relation with the sugar size and reactivity [40, 41]. The shorter the carbon backbone of the sugar, the more open chain form exists and the more reactive is the sugar towards the amino groups of proteins [30, 42].

3.1.2 Changes in the global net charge (pHi)

As glycation substitutes basic amino acid side-chains, it induces a slight loss of basicity, and consequently, a moderate acidification of the BLG molecule. Isoelectric focusing, which allows the separation of proteins according to their global net charge (pHi), could be a good method for evaluation of the yield of glycation (Fig. 1). The native BLG pattern (path 1) showed a major band near pH 5.15 representing the variant A of the protein. Comparable pattern was observed after heating the BLG in absence of sugar (path 2). After heating BLG for 72 h in the presence of galactose, glucose, lactose and rhamnose (paths 4–7, respectively), several bands ranging between pH 5.15 and pH 4 appeared, demonstrating the heterogeneity of the derivatives obtained. Only the protein modified with lactose still presented a band at pH 5.15 showing a residual native form. BLG glycated with galactose, glucose and rhamnose showed about the same isoelectric pattern. This agrees well with their comparable degree of modification measured by the OPA method. BLG modified with arabinose (path 3) and ribose (path 8) presented a relatively homogeneous population (pHi 4.00–4.15), showing a saturation of the reactive sites on the surface of BLG molecule, what agrees with previous results on glucosylation of BLG as a function of time [43].

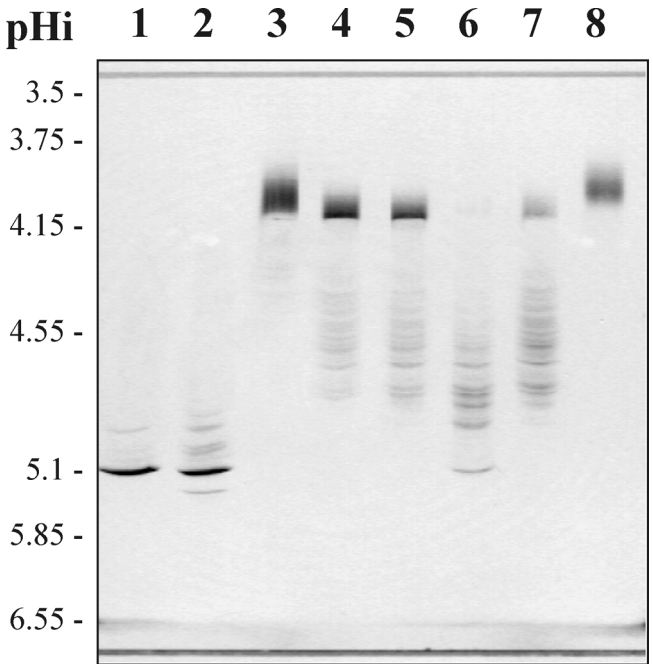

Figure 1. Isoelectric focusing of (1) native BLG, (2) BLG heated without sugar and BLG heated in the presence of (3) arabinose, (4) galactose, (5) glucose, (6) lactose, (7) rhamnose and (8) ribose.

3.2 Aggregation of glycated BLG

Changes in molecular masses of BLG derivatives formed during glycation were estimated by SDS-PAGE (Fig. 2). Native BLG showed one single band of about 18 kDa corresponding to its monomeric form. When heating BLG without addition of sugar, the monomeric form was still observed together with other bands corresponding to the dimeric, trimeric and tetrameric forms. At the same time, protein with higher molecular mass resulting from polymerization was retained in the stacking gel. Such a polymerization of BLG upon heating is well-known and occurs by disulfide exchange due to the presence of the free cysteine 121 [44].

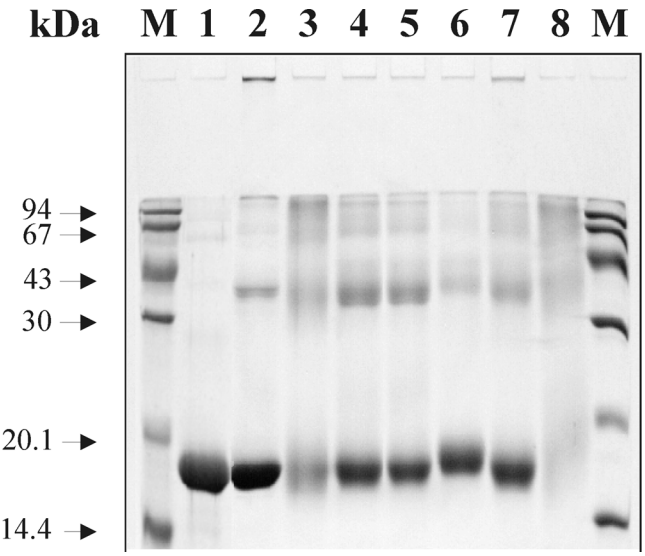

Figure 2. SDS-PAGE of (1) native BLG, (2) BLG heated without sugar and BLG heated in the presence of (3) arabinose, (4) galactose, (5) glucose, (6) lactose, (7) rhamnose and (8) ribose. M: molecular mass markers containing α-lactalbumin (14.4 kDa), trypsin inhibitor (20.1 kDa), carbonic anhydrase (30 kDa), ovalbumin (43 kDa), bovine serum albumin (67 kDa) and phosphorylase *b* (94 kDa).

When BLG was heated in the presence of sugars, several bands corresponding to molecular masses of about 18, 36, 67 kDa and higher were observed. However, these bands became less and less perceptible with the increase of the glycation degree, showing an apparently enhanced heterogeneity of the molecular masses of glycated samples. A smaller amount of glycated BLG was retained in the stacking gel when compared with the protein heated in the absence of sugar. During glycation, numerous polymers were obtained showing different electrophoretic patterns when compared with the heated control [45]. In a previous study it was shown that all the polymers formed during glycation were not stabilized by disulfide bonds only, but also by covalent linkages involving sugar cross-links [42].

3.3 Conformation state of glycated BLG

3.3.1 Characterization by peptic susceptibility

Native BLG resists peptic hydrolysis because of its stable conformation and because most of the peptic cleavage sites are concealed inside the β-barrel [21]. Consequently, changes in susceptibility of BLG to peptic attack can result from changes in its three-dimensional structure. Previous studies demonstrated that upon heating [19], in hydroethanolic media [20] or after its esterification [25], the conformation of BLG was modified allowing its pepsinolysis. In order to observe if structural changes occurred during glycation of BLG, kinetics of peptic hydrolysis were performed with native, heated and glycated samples. Bovine serum albumin (BSA) was used as a control.

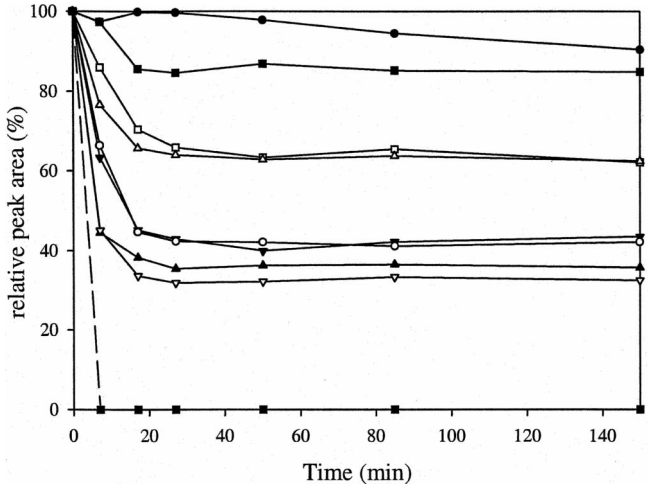

Figure 3. Time course of peptic hydrolysis of (●) native BLG, (■) heated BLG, (■ and dashed line) BSA and BLG heated in the presence of (▲) arabinose, (▼) galactose, (○) glucose, (□) lactose, (△) rhamnose and (▽) ribose.

After 150 min hydrolysis, only 10% of native BLG was hydrolyzed showing a high resistance of the protein to this protease (Fig. 3). When BLG was preheated for 72 h at 60 °C (heated control), about 15% of the protein was hydrolyzed during the first 30 min, then a plateau was reached. Consequently, only 5% of protein were denatured during preheating when compared to the native sample. In case of all glycated samples, pepsin hydrolysis progressed rapidly in the first 30 min. After glycation of BLG with lactose or rhamnose, 62% of protein were still unhydrolyzed after 150 min incubation. About 43% of BLG glycated with galactose or glucose and about 35% of BLG glycated with arabinose or ribose were still unhydrolyzed after 150 min incubation. From the results of peptic lysis as a method to follow the denaturation of glycated proteins, it can be concluded that BLG aliquots modified with lactose and rhamnose were the less denatured (38% of hydrolysis), aliquots modified with glucose and galactose were moderately denatured (57% of hydrolysis) and those modified with arabinose and ribose were the most denatured (65% of hydrolysis). Apparently the intensities of denaturation (corresponding to the percentage of hydrolyzed proteins) are directly related to glycation degree, showing the influence of glycation in destabilization of the native conformation of BLG in an aqueous medium, what agrees well with the results of Morgan *et al.* [46, 47].

3.3.2 Characterization of glycation-induced BLG folding changes by CD

3.3.2.1 Near-UV CD

The near-UV CD signal is due to the chirality of the environment of the side chain of aromatic amino acids such as tryptophan, tyrosine and phenylalanine, as well as of disulfide bonds. A characteristic profile was observed in the case of native BLG (Fig. 4 A). Two minima observed at about 262 and 269 nm in near-UV CD spectrum are due to phenylalanyl residues and the two characteristic deep minima observed at 286 and 293 nm involve tryptophanyl residues of proteins [48, 49]. In the case of BLG, these minima are due to Trp^{19} [50]. After heating BLG at 60 °C for 3 days, a decrease of intensity of two minima at 286 and 293 nm was observed, which agrees well

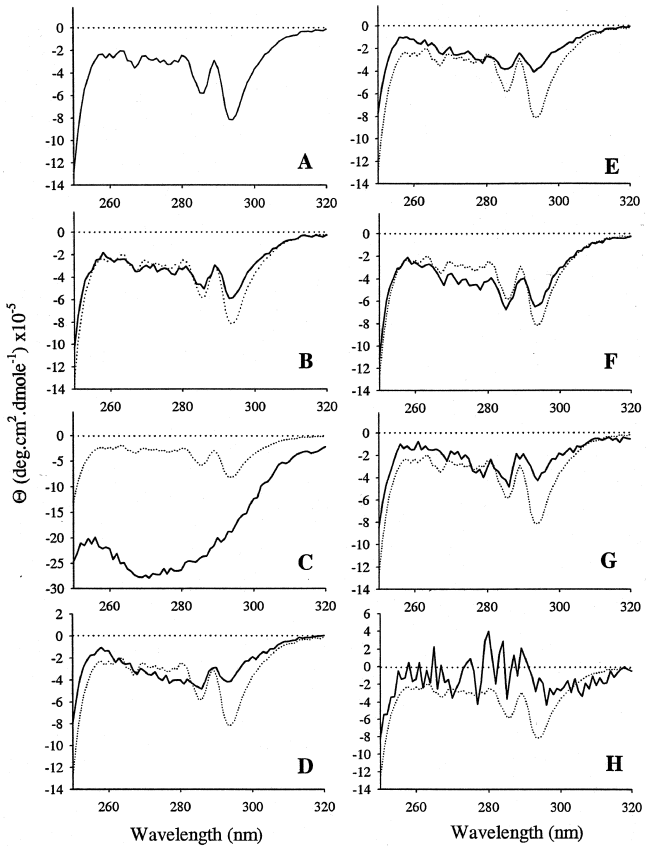

Figure 4. Near-UV CD spectra of native BLG (solid line in A and dashed line in B–H), (B) heated BLG and BLG heated in the presence of (C) arabinose, (D) galactose, (E) glucose, (F) lactose, (G) rhamnose and (H) ribose.

with results of Manderson *et al.* [50]. Such changes in CD spectra result probably from the changes in the environment of Trp^{19}. BLG samples modified with galactose (D), glucose (E), lactose (F) and rhamnose (G) showed similar profiles in the near-UV region when compared with heated BLG. However, the intensity of two minima observed at 286 and 293 nm decreased for each sample with some slight differences in its extent. CD profile of the less glycated sample modified with lactose was relatively similar to what was observed with native protein at 286 nm, but showed a decrease in the intensity of the minimum at 293 nm. These results correlate well with data of peptic hydrolysis showing that these samples conserved their tertiary structure relatively well. However, no significant differences could be observed, by near-UV spectra analysis, between samples modified with lactose and rhamnose and those modified with galactose and glucose. Unfortunately, CD spectra of BLG modified with arabinose (C) and ribose (H) were not interpretable because of a total loss of information in the near-UV region. The profiles obtained could be explained either by a disappearance of the tertiary structure of the glycated proteins and/or by the presence of chromophores resulting from the Maillard reactions, which interfered strongly with CD spectra of aromatic amino acid moieties.

3.3.2.2 Far-UV CD

Far-UV CD signal arises from the peptide bonds absorption and reflects the secondary structure of proteins. According to the method of Provencher and Glockner [39], native BLG

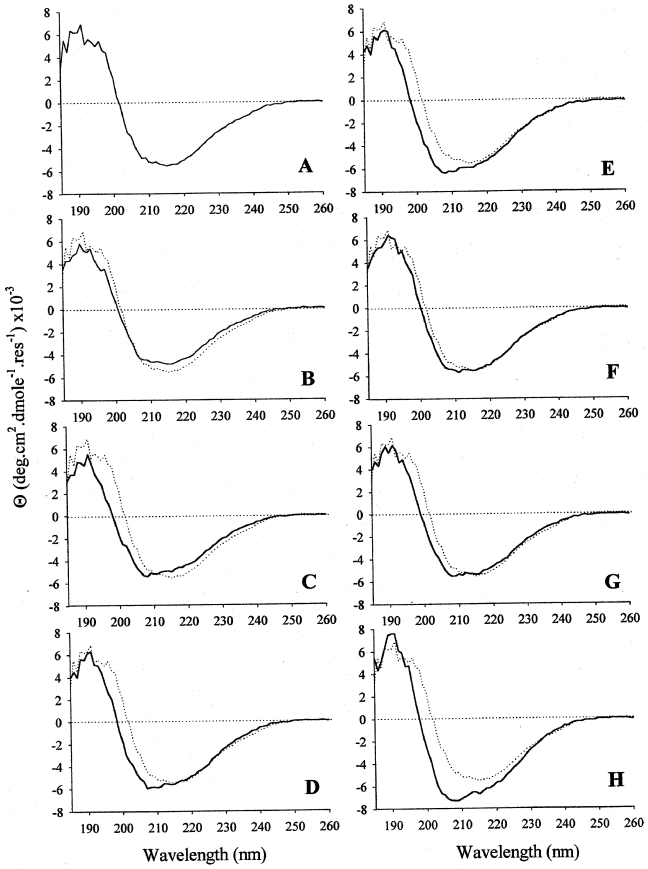

Figure 5. Far-UV CD spectra of native BLG (solid line in A and dashed line in B–H), (B) heated BLG and BLG heated in the presence of (C) arabinose, (D) galactose, (E) glucose, (F) lactose, (G) rhamnose and (H) ribose.

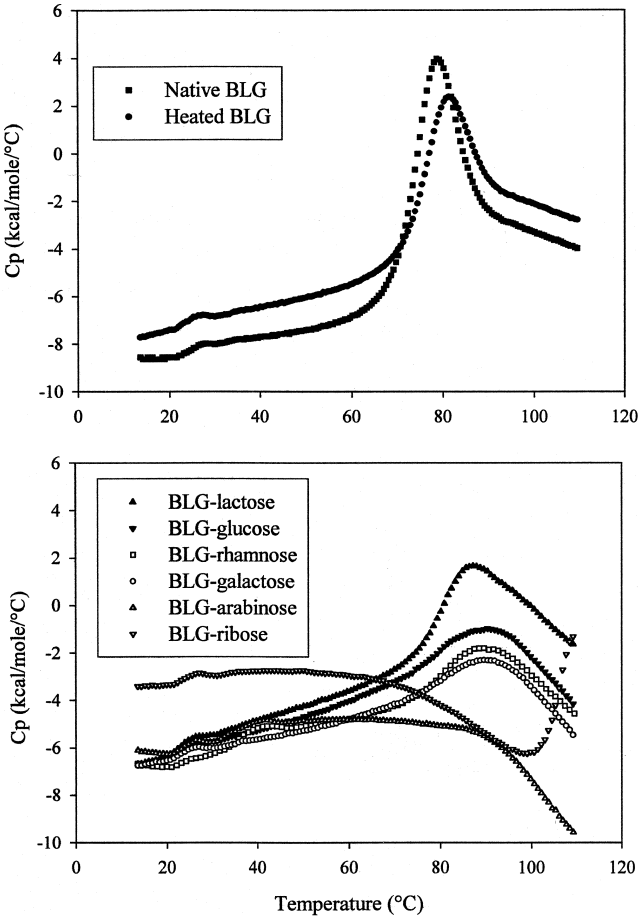

Figure 6. Thermograms of denaturation of native, heated and glycated BLG.

(Fig. 5A) presented ~47% of β-sheet region and ~14% of α-helix region. These results are in agreement with those of Qi *et al.* [51] and X-ray crystal structures [5]. Even though a slight decrease in the intensity of the signal was seen in case of heated BLG when compared with native protein (Fig. 5B), no global secondary structure disorganization could be observed, implying that BLG has retained its secondary and tertiary structures as it was already shown in the case of tertiary structure, in the near-UV region (Fig. 4B). The minimum observed at about 216 nm with native and heated BLG in the case of glycated samples, shifted towards lower wavelengths with a more marked minimum at about 207 nm, especially in the case of BLG glycated with arabinose (Fig. 5C), galactose (Fig. 5D), glucose (Fig. 5E), and ribose (Fig. 5H). In contrast, BLG modified with lactose (Fig. 5F) and rhamnose (Fig. 5G) showed quite similar profile in the far-UV region when compared with native BLG. Spectrum of BLG glycated with ribose was the most modified when compared with native and heated BLG spectra, demonstrating an important modification of its secondary structure. No secondary structure calculation could be done from the spectra of glycated samples because of the presence of chromophores resulting from the Maillard reactions.

3.3.3 Characterization of glycation-induced BLG folding changes by calorimetry

Characteristic transition with T_m at 78.8 and 81.4 °C, respectively, was obtained in the case of native and heated BLG. Consequently, 72 h heating of BLG at 60 °C induced only minor conformational changes, with an increase by 2.6 °C of the temperature of denaturation. Polymerization and association of BLG monomers during heating could be at the origin of this small shift of the temperature of denaturation. When BLG was heated in the presence of sugars, very different data were obtained. Thermograms of BLG glycated with lactose, rhamnose, glucose or galactose showed a maximum value of T_m at 87.5, 89.6, 90.4 and 88.5 °C, respectively. All the obtained thermograms were very broad proving the heterogeneity of the samples and heterogeneity of protein conformations. The shift of about 10 °C of the temperature of denaturation of these glycated proteins indicated a protective effect of glycation on the thermal denaturation of BLG when compared with what was obtained in the case of native BLG. No transition could be observed on thermograms of BLG modified with ribose or arabinose, demonstrating the extensive denaturation of these samples (Fig. 6).

4 Concluding remarks

Heating of BLG for 3 days at 60 °C did not induce major conformational changes, as observed by peptic hydrolysis, since only an additional 5% of the protein was hydrolyzed when compared with native BLG. Only minor modifications could be observed studying far- and near-UV CD spectra of

these proteins. Nevertheless, some changes in aggregation behavior was observed by SDS-PAGE, showing polymerization of BLG after heating. When BLG was heated in the presence of sugars, larger structural modifications were observed depending on the sugar used. Conformational modification of BLG was related with the degree of glycation. The higher the reactivity of the sugar, the more denaturation was observed for the glycated protein. According to peptic hydrolysis data, near- and far-UV CD spectra and microcalorimetry analysis, proteins modified with ribose or arabinose (the most reactive sugars) showed important conformational changes. In contrast, proteins modified with lactose or rhamnose (the less reactive sugars) showed quite similar three-dimensional structures when compared with native BLG. According to previous work [42] and as shown by SDS-PAGE, glycation of BLG induced polymerization of protein monomers. Moreover, as observed by calorimetry analysis, Maillard glycation increased the temperature of denaturation of proteins glycated with galactose, glucose, lactose or rhamnose. These results correlate well with those obtained in a previous study of functional properties of glycated BLG [30], which demonstrated the importance of the sugar used for the improvement of emulsifying and foaming properties of the derivatives. Additionally, this work showed the difficulty to interpret the structural analysis of glycated samples by spectral methods, especially because of the heterogeneity of the Maillard products obtained and because of formation of powerful chromophores during the Maillard reactions.

The authors thank Marie-Georgette Nicolas for BLG purification. The funding by a fellowship from the Ministère de la Recherche et de la Technologie to François Chevalier is acknowledged. The funding of this work by INRA and the Région Pays de Loire in the scope of the VANAM program "Interactions moléculaires et activités biologiques" is also gratefully acknowledged.

5 References

[1] Godovac-Zimmermann, J., Conti, A., Sheil, M., Napolitano, L., *Biol. Chem. Hoppe-Seyler* 1990, *371*, 871–879.
[2] Godovac-Zimmermann, J., Krause, I., Buchberger, J., Weiss, G., Klostermeyer, H., *Biol. Chem. Hoppe-Seyler* 1990, *371*, 255–260.
[3] Monaco, H. L., Zanotti, G., *Biopolymers* 1992, *32*, 457–465.
[4] Sansom, C. E., North, A. C., Sawyer, L., *Biochim. Biophys. Acta* 1994, *1208*, 247–255.
[5] Papiz, M. Z., Sawyer, L., Eliopoulos, E. E., North, A. C. T., Findlay, J. B. C., Sivaprasadrao, R., Jones, T. A., Newcomer, M. E., Kraulis, P. J., *Nature* 1986, *324*, 383–385.
[6] Brownlow, S., Morais Cabral, J. H., Cooper, R., Flower, D. R., Yewdall, S. J., Polikarpov, I., North, A. C., Sawyer, L., *Structure* 1997, *5*, 481–495.
[7] Farrel, Jr., H. M., Behe, M. J., Enyeart, J. A., *J. Dairy Sci.* 1987, *70*, 252–258.
[8] O'Neill, T. H., Kinsella, J. E., *J. Agric. Food Chem.* 1987, *35*, 770–774.
[9] Pelletier, E., Sostmann, K., Guichard, E., *J. Agric. Food Chem.* 1998, *46*, 1506–1509.
[10] Dufour, E., Haertlé, T., *Biochim. Biophys. Acta* 1991, *1079*, 316–320.
[11] Cho, Y., Batt, C. A., Sawyer, L., *J. Biol. Chem.* 1994, *269*, 11102–11107.
[12] Wang, Q., Allen, J. C., Swaisgood, H. E., *J. Dairy Sci.* 1997, *80*, 1047–1053.
[13] Wang, Q., Allen, J. C., Swaisgood, H. E., *J. Dairy Sci.* 1997, *80*, 1054–1059.
[14] Dodin, G., Andrieux, M., al Kabbani, H., *Eur. J. Biochem.* 1990, *193*, 697–700.
[15] Dufour, E., Roger, P., Haertlé, T., *J. Prot. Chem.* 1992, *11*, 645–652.
[16] Hemley, R., Kohler, B. E., Siviski, P., *Biophys. J.* 1979, *28*, 447–455.
[17] Frapin, D., Dufour, E., Haertlé, T., *J. Prot. Chem.* 1993, *12*, 443–449.
[18] Narayan, M., Berliner, L. J., *Prot. Sci.* 1998, *7*, 150–157.
[19] Reddy, M., Kella, N. K. D., Kinsella, J. E., *J. Agric. Food Chem.* 1988, *36*, 737–741.
[20] Dalgalarrondo, M., Dufour, E., Chobert, J.-M., Bertrand-Harb, C., Haertlé, T., *Int. Dairy J.* 1995, *5*, 1–14.
[21] Guo, M. R., Fox, P. F., Flynn, A., Kindstedt, P. S., *J. Dairy Sci.* 1995, *78*, 2336–2344.
[22] Smithers, G. W., Ballard, F. J., Copeland, A. D., de Silva, K. J., *J. Dairy Sci*. 1996, *79*, 1454–1459.
[23] Haertlé, T., Chobert, J.-M., *J. Food Biochem*. 1999, *23*, 367–407.
[24] Sitohy, M., Chobert, J.-M., Haertlé, T., *J. Agric. Food Chem*. 1995, *43*, 59–62.
[25] Chobert, J.-M., Briand, L., Grinberg, Y. V., Haertlé, T., *Biochim. Biophys. Acta* 1995, *1248*, 261–269.
[26] Sitohy, M., Chobert, J.-M., Haertlé, T., *Nahrung/Food* 2001, *45*, 87–93.
[27] Kitabatake, N., Cuq, J. L., Cheftel, J. C., *J. Agric. Food Chem.* 1985, *33*, 125–130.
[28] Mattarella, N. L., Richardson, T., *J. Agric. Food Chem*. 1983, *31*, 972–978.
[29] Aoki, T., Kitahata, K., Fukumoto., T., Sugimoto, Y., Ibrahim, H. R., Kimura, T., Kato, Y., Matsuda, T., *Food Res. Int.* 1997, *30*, 401–406.
[30] Chevalier, F., Chobert, J.-M., Popineau, Y., Nicolas, M.-G., Haertlé, T., *Int. Dairy J.* 2001, *11*, 145–152.
[31] Ledl, F., Schleicher, E., *Angew. Chem. Int.* 1990, *29*, 565–594.
[32] Ames, J. M., *Trends Food Sci. Technol.* 1990, *1*, 150–154.
[33] Chuyen,, N. V., *Adv. Exp. Med. Biol.* 1998, *434*, 213–235.
[34] Maillard, L. C., *C. R. Acad. Sci.* 1912, *154*, 66–68.
[35] Friedman, M., *J. Agric. Food Chem.* 1996, *44*, 631–653.
[36] Mailliart, P., Ribadeau Dumas, B., *J. Food Sci.* 1988, *53*, 743–752.
[37] Frister, H., Meisel, H., Schlimme, E., *Fresenius Z. Anal. Chem.* 1988, *330*, 631–633.
[38] Laemmli, U. K., *Nature* 1970, *227*, 680–685.
[39] Provencher, S. W., Glockner, J., *Biochemistry* 1981, *20*, 33–37.
[40] Prabhakaram, M., Ortwerth, B. J., *Anal. Biochem*. 1994, *216*, 305–312.
[41] Nacka, F., Chobert, J.-M., Burova, T., Léonil, J., Haertlé, T., *J. Prot. Chem.* 1998, *17*, 495–503.
[42] Chevalier, F., Chobert, J.-M., Mollé, D., Haertlé, T., *Lait* 2001, *81*, 651–666.
[43] Chevalier, F., Chobert, J.-M., Dalgalarrondo, M., Haertlé, T., *J. Food Biochem.* 2001, *25*, 33–55.
[44] Dunnil, P., Green, D. W., *J. Mol. Biol.* 1965, *15*, 147–151.
[45] Bouhallab, S., Morgan, F., Henry, G., Mollé, D., Léonil, J., *J. Agric. Food Chem.* 1999, *47*, 1489–1494.
[46] Morgan, F., Mollé, D., Henry, G., Vénien, A., Léonil, J., Peltre, G., Levieux, D., Maubois, J.-L., Bouhallab, S., *Int. J. Food Sci. Technol.* 1999, *34*, 429–435.
[47] Morgan, F., Vénien, A., Bouhallab, S., Mollé, D., Léonil, J., Peltre, G., Levieux, D., *J. Agric. Food Chem.* 1999, *47*, 4543–4548.
[48] Strickland, E. H., *CRC Crit. Rev. Biochem.* 1974, *2*, 113–175.
[49] Kahn, P. C., *Methods Enzymol.* 1979, *61*, 339–378.
[50] Manderson, G. A., Creamer, L. K., Hardman, M. J., *J. Agric. Food Chem.* 1999, *47*, 4557–4567.
[51] Qi, X. L., Holt, C., McNulty, D., Clarke, D. T., Brownlow, S., Jones, G. R., *Biochem. J.* 1997, *324*, 341–346.

Received May 25, 2001
Accepted August 29, 2001

ELSEVIER

International Dairy Journal 11 (2001) 145–152

INTERNATIONAL DAIRY JOURNAL

www.elsevier.com/locate/idairyj

Improvement of functional properties of β-lactoglobulin glycated through the Maillard reaction is related to the nature of the sugar ☆

François Chevalier[a], Jean-Marc Chobert[a,*], Yves Popineau[b], Marie Georgette Nicolas[a], Thomas Haertlé[a]

[a] *Laboratoire d'Étude des Interactions des Molécules Alimentaires, Institut National de la Recherche Agronomique, BP 71627, 44316 Nantes Cedex 3, France*

[b] *Laboratoire de Biochimie et de Technologie des Protéines, Institut National de la Recherche Agronomique, BP 71627, 44316 Nantes Cedex 3, France*

Received 24 October 2000; accepted 2 March 2001

Abstract

The improvement of functional properties of proteins available in large quantity using non-toxic chemical modifications is of a great interest for the food industry. In this study, the Maillard reaction was used to improve the functional properties (solubility, heat stability, emulsifying and foaming properties) of β-lactoglobulin (BLG) glycated with several sugars (arabinose, galactose, glucose, lactose, rhamnose or ribose). Protein samples were heated in the presence or absence (heated control) of different sugars for three days at 60°C. Subsequent glycation induced a modification of the solubility profile shifting minimum solubility towards more acidic pH. Glycated proteins exhibited a better thermal stability when heated at pH 5 as compared to native or heated control. Glycation of BLG with arabinose or ribose (the most reactive sugars) improved its emulsifying properties. Foaming properties were better when BLG was glycated with glucose or galactose (moderately reactive sugars). These results suggest that the nature of the sugar is an essential factor for improving the functional properties of glycated proteins by processes of Maillard reaction.

Keywords: Glycation; Maillard reactions; β-lactoglobulin; Functional properties

1. Introduction

Whey issued from cheese and casein manufacturing contains approximately 20% of all milk proteins. It represents a rich and varied mixture of secreted proteins with wide-ranging chemical, physical and functional properties (Smithers, Ballard, Copeland, & de Silva, 1996). Due to their beneficial functional properties, whey proteins are used as ingredients in many industrial food products (Cheftel & Lorient, 1982). According to Kinsella and Whitehead (1989), functional properties of foods can be explained by the relation of intrinsic property of proteins (amino acid composition and disposition, flexibility, net charge, molecular size, conformation, hydrophobicity, etc.), and extrinsic factors (method of preparation and storage, temperature, pH, modification process, etc.).

Numerous attempts were made to further improve the functional properties of whey proteins through physical, chemical and/or enzymatic treatments (Haertlé & Chobert, 1999). Many studies were carried out with β-lactoglobulin (BLG), the major whey protein. Focusing on the improvement of solubility, heat stability, foaming properties and emulsifying properties, this protein has been conjugated with ester (Mattarella & Richardson, 1983; Sitohy, Chobert, & Haertlé, 2001), gluconic or melibionic acids (Kitabatake, Cuq, & Cheftel, 1985), carbohydrates (Waniska & Kinsella, 1988; Bertrand-Harb, Charrier, Dalgalarrondo, Chobert, & Haertlé, 1990) and phosphoric acid (Sitohy, Chobert, & Haertlé, 1995; Sitohy, Chobert, Popineau, & Haertlé, 1995).

However, most of these methods utilize toxic chemical products and are not permitted for potential industrial applications. Recently, some attempts were made to improve the functional properties of BLG by the conjugation of glucose-6-phosphate (Aoki et al., 1997).

☆ A part of this work was presented at the "Milk Protein Conference", March 30–April 2 2000, Vinstra, Norway.

*Corresponding author. Tel.: +33-240-67-5085; fax: +33-240-67-5084.

E-mail address: chobert@nantes.inra.fr (J.-M. Chobert).

0958-6946/01/$ - see front matter
PII: S0958-6946(01)00040-1

The Maillard reaction, or non-enzymatic browning, occurs frequently during industrial processing and in domestic cooking for the enhancement of colour, aroma and flavour (O'Brien & Morrissey, 1989; Chuyen, 1998; Ames, 1998). This reaction was first described by the French biochemist Louis Maillard at the beginning of the 20th century (Maillard, 1912). It consists of a condensation of the reducing sugar with the ε-amino group of lysyl residues of proteins and results in the so-called Amadori product via the formation of a Schiff's base and the Amadori rearrangement (Ledl & Schleicher, 1990; Friedman, 1996). Through this reaction, the conjugation of the sugar to the protein does not require chemical catalysis, but just heating in order to accelerate the spontaneous reaction. Well-controlled Maillard reaction can thus be a good method for protein processing in food industry.

The aim of this study was to check how the functional properties of BLG glycated with several common sugars evolve. Solubility, heat stability, emulsifying and foaming properties of modified proteins were investigated at different pHs, temperatures and heating times.

2. Material and methods

2.1. Protein purification

β-Lactoglobulin (BLG), variant A was purified from fresh milk as described by Mailliart and Ribadeau Dumas (1988). The purity of BLG (99%) was assessed by RP-HPLC.

2.2. Reagents

D-Arabinose, D-galactose, D-glucose, D-lactose, D-rhamnose and D-ribose monohydrates were obtained from Sigma Chemical Co. (St Louis, MO, USA). All other reagents were of analytical grade.

2.3. Glycation experiments

BLG ($4\,mg\,mL^{-1}$ or $0.217\,mmol\,L^{-1}$) and the different sugars ($0.217\,mol\,L^{-1}$) were dissolved in $0.1\,mol\,L^{-1}$ phosphate buffer, pH 6.5. After filtration on 0.22 μm acetate cellulose filters (Millipore), mixtures of protein and sugars were put in tightly-capped flasks and heated in a water bath at 60°C for 72 h. All experiments were performed under strictly anaerobic and sterile conditions, all media were purged and saturated with N_2. After heating, the different fractions were dialysed for 36 h at 4°C against distilled water to remove unreacted sugars, freeze-dried, and stored at −20°C. BLG heated without sugar (heated control) was named "heated BLG", and BLG heated in the presence of sugar was named "glycated BLG".

2.4. Determination of available amino groups

The quantity of available amino groups was determined by the modified ortho-phthaldialdehyde (OPA) method (Frister, Meisel, & Schlimme, 1988). The OPA reagent was prepared daily by mixing 40 mg of OPA (dissolved in 1 mL of methanol), 50 mL of $0.1\,mol\,L^{-1}$ sodium borate buffer, pH 9.3, 100 mg of *N*-dimethyl-2-mercaptoethylammonium chloride (DMMAC), and 1.25 mL of 20% (w/w) SDS in water. 50 μL of protein solution ($2\,g\,L^{-1}$ in $50\,mmol\,L^{-1}$ sodium phosphate buffer, pH 7.8) was added to 1 mL of OPA reagent. The absorbance was read at 340 nm after a minimal delay of 5 min. A calibration curve was obtained by using $0.25–2\,mmol\,L^{-1}$ L-leucine as a standard.

2.5. Solubility

Native, heated and glycated BLG were diluted in distilled water ($2\,mg\,mL^{-1}$). The pH of the solution was then adjusted from 2 to 10 using concentrated HCl or NaOH. Samples were centrifuged for 15 min (Sigma 201 centrifuge) at 15 000 g. Protein content in the supernatant was determined by the bicinchoninic acid (BCA) method (Pierce) with bovine serum albumin as a standard. Solubility was expressed as a percentage of protein content in supernatant to the total protein content. All experiments were performed at room temperature (25°C).

2.6. Heat stability

Native, heated and glycated BLG were diluted ($2\,mg\,mL^{-1}$), in $0.1\,mol\,L^{-1}$ sodium acetate buffer at pH 4, 4.5 and 5, and in $0.1\,mol\,L^{-1}$ sodium phosphate buffer for pH 7. After solubilization in the appropriate buffer, samples were heated in a water bath at different temperatures (25–90°C) for up to 1 h. After heating, samples were cooled for 15 min at 4°C and centrifuged for 15 min at 15 000 g in order to precipitate aggregates. UV absorbance (280 nm) of the supernatant was measured to estimate protein concentration, and was compared with that of the corresponding untreated sample.

2.7. Emulsifying properties

Native, heated and glycated BLG were diluted ($2\,mg\,mL^{-1}$), in $0.1\,mol\,L^{-1}$ sodium acetate buffer, pH 5, or in $0.1\,mol\,L^{-1}$ sodium phosphate buffer, pH 7. Oil-in-water emulsions were prepared with protein solution and purified sunflower oil with a constant oil volume fraction of 15%. Emulsion premixes were prepared using the rotor stator system Polytron PT3000 (Kinematica, Littau, Switzerland) equipped with a 12 mm head working at 20 000 rpm for 30 s. Homogenisation of

the coarse emulsions was then achieved with a pressure valve homogeniser (Stansted Fluid Power, Stansted, UK). The emulsion (20 mL) was allowed to recirculate in the homogeniser for 90 s at a flow rate of 120 mL min^{-1} and at a pressure of 50 bar. After emulsification, 1 mL of the emulsion was diluted in 9 mL of 0.1% SDS. The oil droplet size distribution was estimated by laser light scattering using a Malvern Mastersizer 3600 (Malvern Instruments, Malvern, UK). The system was equipped with a lens of 45 mm focal length and the manufacturer presentation code 0503 was selected to take into account the oil refractive index. The volume-surface mean diameter of the oil droplets size distribution ($d_{3,2}$ in μm) was recorded. All $d_{3,2}$ results represent a mean value of three determinations.

2.8. Foaming properties

Foaming properties were determined by the method of Hagolle, Relkin, Popineau, and Bertrand (2000). Native, heated and glycated BLG were diluted (1 mg mL^{-1}) in 0.1 mol L^{-1} sodium phosphate buffer, pH 7. Determinations were made in a transparent plastic tube (2 cm × 22.5 cm) equipped with a pair of vertical rod electrodes located at the base of the column and with a metallic porous disk (2 μm average pore size) through which air at the pressure of 1 bar and a flow rate of 15 mL min^{-1} was passed and forced through the test liquid ($T_l = 8$ mL), creating foam. The gas flow was directed by a driven valve, either to the column or to a counter pressure device that prevented the solution from flowing downwards in the absence of bubbling. The conductivity during the test, volume of foam and air incorporated were recorded by a computer and a linear camera (Schmersal OM-1024 with cosmicar 25 mm television lens). All experiments were performed in triplicate.

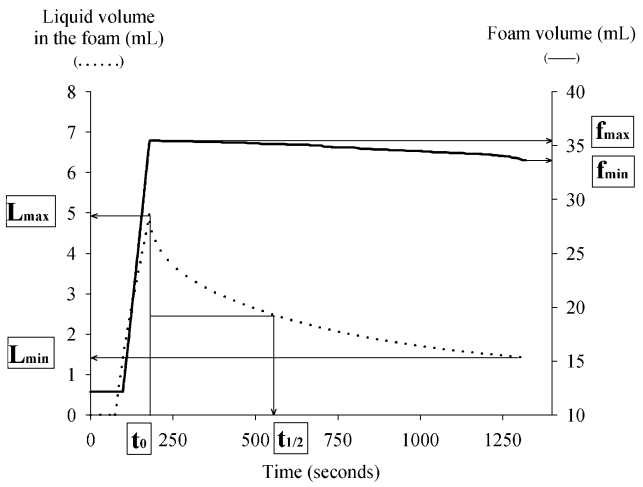

Fig. 1. Experimental foam curves obtained with the bubbling apparatus (heated BLG sample was used): f_{max} is the observed maximum foam volume at the end of bubbling (bubbling stopped when f_{max} equals 35 mL); f_{min} the observed foam volume at the end of the experiment (after 20 min); L_{max} the maximum liquid volume in the foam at the end of bubbling; L_{min} the liquid volume in the foam at the end of the experiment; t_0 the time (s) at the end of bubbling; $t_{1/2} = L_{max}/2$.

Conductivity measurements as a function of time (C_t) and with reference to the conductivity of the buffer test solution (C_{init}) were used to calculate the volume of liquid drained in the foam (L):

$$L = V_{init}[1 - (C_t/C_{init})].$$

The different parameters analysed during the experiment are reported in Fig. 1.

These parameters allowed for the characterization of the foaming properties of the samples:

Foaming capacity was determined by

- the maximum foam volume (F_{max})
  $F_{max} = f_{max} - (T_l - L_{max})$,
- the foam density (FD)
  $FD = (L_{max}/F_{max})$.

Foam stability was determined by

- the half-life of drainage ($T_{1/2}$):
  $T_{1/2} = t_{1/2} - t_0$,
- the minimum foam volume (F_{min}):
  $F_{min} = f_{min} - (T_l - L_{min})$,
- the stability index (S_i):
  $S_i = (F_{min}/F_{max}) \times 100$.

3. Results and discussion

3.1. Determination of the extent of glycation

The quantities of free amino groups were measured using the OPA modified method. The BLG sequence contains 16 potential reactive amino-groups including 1 α-NH_2 and 15 ε-NH_2 on lysyl residues. Modified amino groups (Table 1) were deduced from OPA results. Only 80.1% of the 16 amino groups of native BLG could be detected. Since no amino groups were modified on native BLG, all results are reported relative to 100% of amino groups of native protein. In the heated control protein, one amino group was modified. This could be explained by a structural modification of BLG such as a polymerization, inducing a masking of a single site of modification.

On an average, 11.0, 8.8, 6.7, 6.6, 6.5 and 5.5 amino groups were modified when proteins were heated in the

Table 1
Determination of the quantity of free primary amino groups (OPA method)

Samples	Amino groups detected (%)	Modified amino groups
Native BLG	80.1	0
Heated BLG	75.1	1.0
BLG-ribose	24.5	11.1
BLG-arabinose	36.0	8.8
BLG-galactose	46.6	6.7
BLG-glucose	47.1	6.6
BLG-rhamnose	47.6	6.5
BLG-lactose	52.6	5.5

presence of ribose, arabinose, galactose, glucose, rhamnose and lactose, respectively.

As expected, the modification degree was in direct relation with the sugar size (Prabhakaram & Ortwerth, 1994; Nacka, Chobert, Burova, Léonil, & Haertlé, 1998). The shorter the carbonic chain of the sugar is, the more open chain forms exist and the more reactive is the sugar with the amino groups of proteins.

3.2. Effect of pH on solubility

Solubility in water of native, heated and glycated BLG was measured as a function of pH (Fig. 2). Native BLG was soluble in the whole pH range studied (Fig. 2A). After heating, a 50% decrease of solubility was observed in the pH range 4.0–5.5 with a minimum observed at pH 5, which is near the pI of the protein (Fig. 2A).

After heating BLG in the presence of arabinose or ribose, the resulting glycated derivatives exhibited 35% solubility at pH 4 (Fig. 2B) that is lower than the solubility obtained with heated BLG and BLG glycated with the other sugars. Major conformational modification induced by the glycation could explain such a decrease. However, due to the shift of their isoelectric point, these derivatives showed an increased solubility at pH 5 as compared with heated BLG.

In case of proteins modified with galactose, glucose, lactose or rhamnose, 75% solubility was observed at pH 4.5 (Fig. 2C), showing a protective effect of glycation by these sugars against the decrease of solubility due to heating.

3.3. Effect of temperature of heating on solubility

Native, heated and glycated BLG were heated at different temperatures (from 25°C to 90°C) and at two pH (5 and 7) (Fig. 3).

All the samples were almost 100% soluble after 1 h heating at pH 7 regardless of the temperature of the reaction. When the samples were heated at pH 5, differences between native, heated and glycated BLG

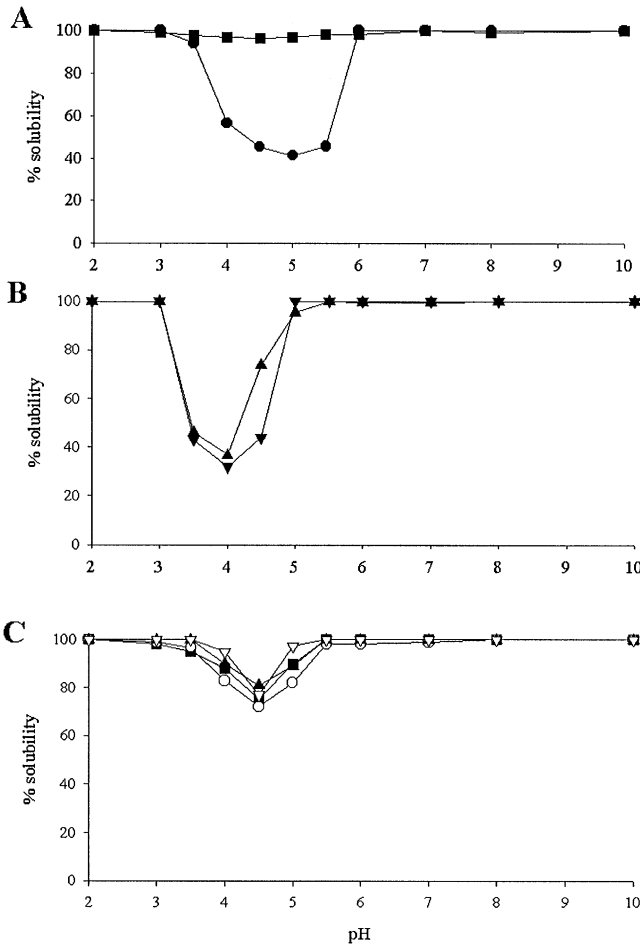

Fig. 2. Solubility of native, heated and glycated BLG as a function of pH. The protein concentration was 2 mg mL^{-1}: (A) native (■) and heated (●) BLG; (B) BLG glycated with arabinose (▲) and ribose (▼); (C) BLG glycated with galactose (■), glucose (○), lactose (▲) and rhamnose (▽).

were observed. Native BLG was about 98% soluble at this pH even after heating up to 60°C. Upon heating from 60°C to 90°C, a constant decrease in solubility from 90% to 5% was observed. The effect of heating on BLG is well known, the protein showing an irreversible denaturation up to 70°C (De Wit & Klarenbeck, 1984; Iametti, de Gregori, Vecchio, & Bonomi, 1996). The heating of BLG near its pI favours protein aggregation as compared with what was observed at pH 7. The same phenomenon was observed in case of heated BLG which exhibited a constant decrease in solubility for temperatures up to 60°C, with an initial decrease in solubility of 60%, as compared with native BLG, corresponding to the pre-heating of the protein. Proteins glycated with galactose, glucose, lactose or rhamnose (Fig. 3C) showed a relatively identical solubility profile as a function of temperature of heating with a constant decrease in solubility from about 80% (50°C) to about 40–50% (90°C) demonstrating a relatively high thermal stability as compared to the native protein and heated

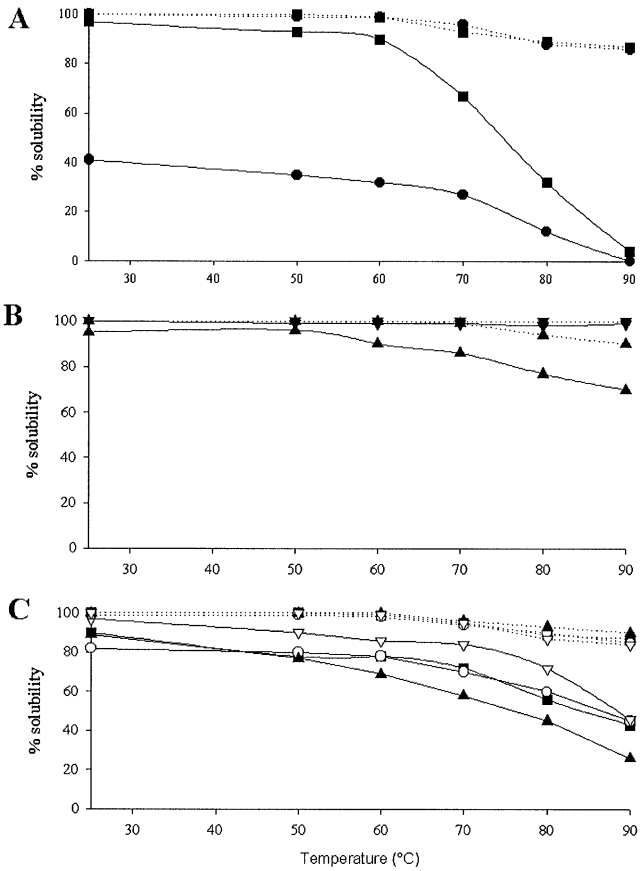

Fig. 3. Heat stability at pH 5 (——) and at pH 7 (------) of native, heated and glycated BLG as a function of temperature. The protein concentration was 2 mg mL^{-1}: (A) native (■) and heated (●) BLG; (B) BLG glycated with arabinose (▲) and ribose (▼); (C) BLG glycated with galactose (■), glucose (○), lactose (▲) and rhamnose (▽).

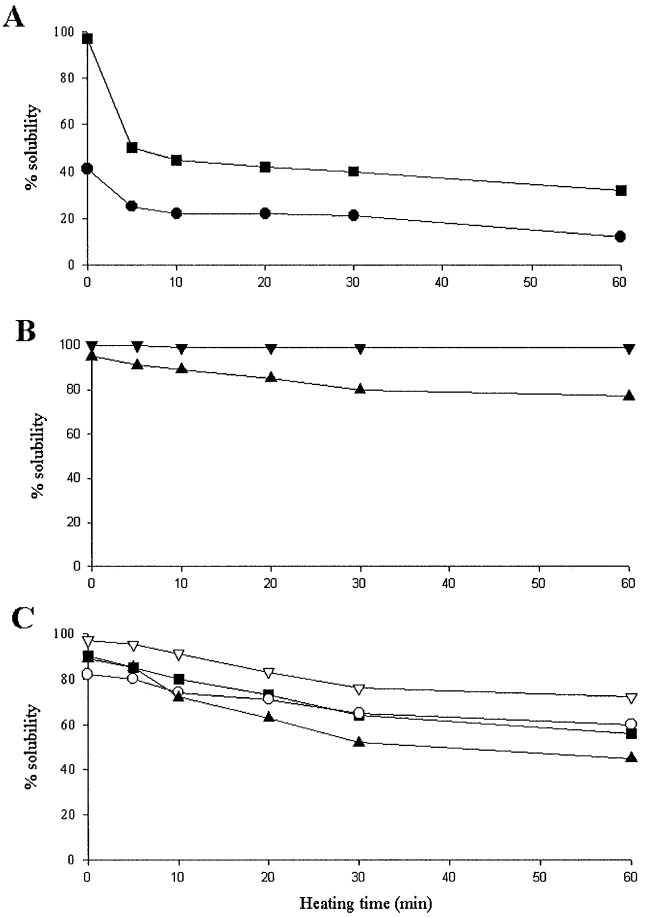

Fig. 4. Heat stability of native, heated and glycated BLG at 80°C and pH 5 as a function of heating time. The protein concentration was 2 mg mL^{-1}: (A) native (■) and heated (●) BLG; (B) BLG glycated with arabinose (▲) and ribose (▼); (C) BLG glycated with galactose (■), glucose (○), lactose (▲) and rhamnose (▽).

control. Nevertheless, proteins glycated with lactose presented a constant decrease of solubility as a function of the temperature of heating, whereas proteins glycated with rhamnose, glucose and galactose showed a decrease of solubility only for a temperature higher to 70°C. The solubility of proteins modified with ribose or arabinose (Fig. 3B) was less affected by a heat treatment as after 1 h heating at 90°C, 70% and 99% solubility, respectively, were measured.

The kinetics of precipitation have been studied at 80°C and pH 5 (Fig. 4). A rapid decrease in solubility from 100% to 45% (native BLG) and from 40% to 25% (heated control) was obtained in the first 10 min of heating. At the opposite, a slow decrease in solubility was observed in case of glycated proteins.

Native BLG and the heated control were highly sensitive to heating at pH values near the pI of BLG and near the pH corresponding to the minimum of solubility of the heated control. In order to understand the role of pH, proteins modified with arabinose or ribose were also heated at different temperatures at pH 4 (Fig. 5A), and proteins modified with galactose, glucose, lactose or rhamnose were heated at different temperatures at pH 4.5 (Fig. 5B). Proteins modified with arabinose or ribose exhibited a constant solubility from about 35% (25°C) to about 30% (90°C) suggesting an excellent stability at this pH. Proteins modified with galactose, glucose, lactose or rhamnose exhibited a constant solubility from 77% (25°C) to about 70% (70°C), and a decrease to about 40% after heating up to 90°C.

At pH 4, the effect of heating on the solubility of the proteins modified with ribose or arabinose (Fig. 5A) was comparable to that obtained at pH 5 and 7 (Fig. 3B) with a constant solubility between 25°C and 90°C. The same conclusion was made between pH 4.5 (Fig. 5B) and pH 5 (Fig. 3C) for the proteins modified with the other sugars.

Sugars in solution (0–300 g L^{-1}) are known to protect proteins from heat denaturation (Jou & Harper, 1996). In order to ensure that heat treatment did not cleave the

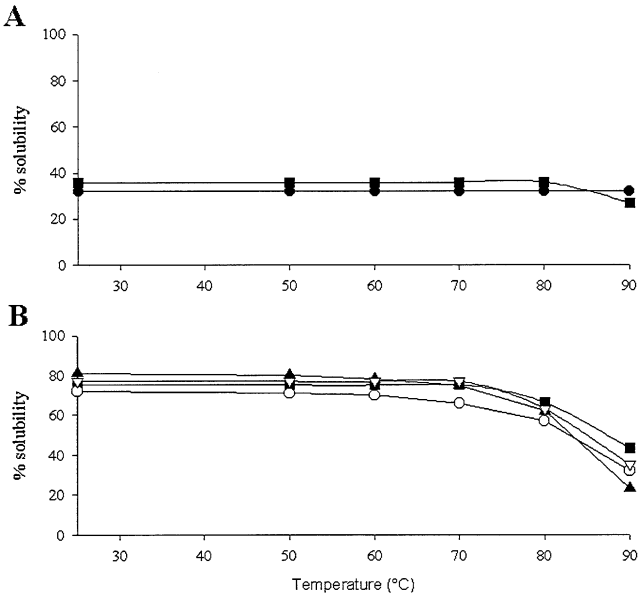

Fig. 5. Heat stability of glycated BLG as a function of temperature. The protein concentration was $2\,mg\,mL^{-1}$: (A) BLG glycated with arabinose (■) and ribose (●), pH 4; (B) BLG glycated with galactose (■), glucose (○), lactose (▲) and rhamnose (▽), pH 4.5.

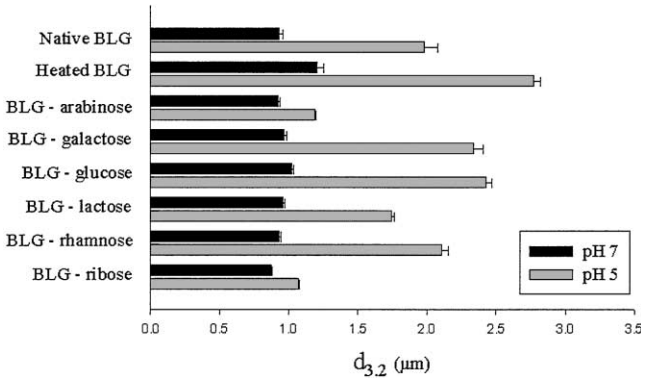

Fig. 6. Emulsifying properties of native, heated and glycated BLG: volume-surface mean diameter of the oil droplet size distribution ($d_{3,2}$) of emulsion realized with $2\,mg\,mL^{-1}$ protein and 15% purified sunflower oil.

sugar–protein bonds, the quantities of primary amino groups of modified BLG were measured before and after heat treatment (OPA method). No differences could be observed (results not shown), indicating the absence of cleavage of sugar–protein bonds in the tested solutions.

3.4. Emulsifying properties

Emulsifying properties of native, heated and glycated BLG ($2\,mg\,mL^{-1}$) measured at pH 5 and 7 in the presence of 15% sunflower oil were evaluated (Fig. 6) by measuring the mean diameter of the oil droplet size distribution ($d_{3,2}$).

At pH 7, where all samples are 100% soluble (Fig. 3), no significant differences were observed between the emulsifying properties of glycated proteins. For all these samples, $d_{3,2}$ was equal to 1 µm. Nevertheless, the smallest particles were obtained with the ribosylated BLG. A difference of about 0.4 µm was measured between glycated samples and the heated control, showing a relative improvement of emulsifying properties after glycation of BLG, which is in agreement with the results of Aoki et al. (1997). Heating induces disulfide exchange of native BLG and leads to polymerizations (Chevalier, Chobert, Dalgalarrondo, & Haertlé, 2001). These structural changes could explain the low $d_{3,2}$ value of heated BLG sample as compared with other samples.

At pH 5, the $d_{3,2}$ value of all the samples increased significantly. Proteins modified with arabinose or ribose had the smallest particle diameters. For these samples, a change of pH from 7 to 5 did not have a major influence on their emulsifying activity. Hydrophobicity changes and conformational modifications could explain the improved ability of these samples to adsorb onto the oil–water interface.

In contrast, in the case of all the other samples studied, the $d_{3,2}$ values were about twice as large as those obtained when experiments were performed at pH 7. In the case of heated BLG, this difference could be explained by a loss of solubility at this pH (Fig. 2A). Solubility is a determining factor for a protein's ability to form an emulsion (Kinsella & Whitehead, 1989). Despite the fact that native BLG is highly soluble in the pH range 2–10, its emulsifying activity index is low at acidic pH and increases with increasing pH (Shimizu, Saito, & Yamauchi, 1985), suggesting that structural changes occur in BLG at acidic pH and influence its emulsifying properties. Such effects close to pH value near the pI of BLG could be at the origin of the decrease of emulsion stability (Klemaszewski, Das, & Kinsella, 1992) observed in the $d_{3,2}$ values.

Recent studies have shown that lactosylation of BLG in a dry system did not significantly alter the three-dimensional structure of the protein. In contrast, in an aqueous system, an important structural change was observed at the protein–protein interface (Morgan, Léonil, Mollé, & Bouhallab, 1999a; Morgan et al., 1999b, c). This suggests that protein modified with galactose, glucose, lactose or rhamnose could present structural changes as compared with the native protein. Polymerization observed with glycated BLG (Bouhallab, Morgan, Henry, Mollé, & Léonil, 1999; Chevalier, Chobert, Dalgalarrondo, & Haertlé, 2001) could be involved in these changes.

Proteins modified with galactose, glucose, lactose or rhamnose were the less glycated samples. Consequently, they may have conserved a globular three-dimensional

Table 2
Foaming properties of native, heated and glycated BLG

Samples	L_{max} (mL)	L_{min} (mL)	F_{max} (mL)	$T_{1/2}$ (s)	F_{min} (mL)	S_i (%)	FD ($\times 10^{-2}$)
BLG	3.01 ± 0.21	0.73 ± 0.07	30.4 ± 0.06	100 ± 4	21.8 ± 2.47	71.7 ± 0.41	10.0 ± 0.05
Heated BLG	4.90 ± 0.13	1.28 ± 0.12	32.3 ± 0.04	346 ± 14	27.6 ± 0.68	85.5 ± 0.17	15.0 ± 0.09
BLG-arabinose	4.25 ± 0.10	0.93 ± 0.09	31.7 ± 0.15	270 ± 15	11.9 ± 1.19	37.5 ± 0.79	13.4 ± 0.17
BLG-galactose	4.56 ± 0.01	1.38 ± 0.05	32.1 ± 0.14	413 ± 29	27.4 ± 0.76	85.5 ± 0.54	14.2 ± 0.07
BLG-glucose	4.40 ± 0.13	1.35 ± 0.13	31.8 ± 0.10	413 ± 40	26.9 ± 0.18	84.7 ± 1.25	13.8 ± 0.13
BLG-lactose	3.99 ± 0.05	0.98 ± 0.06	31.4 ± 0.03	297 ± 6	21.8 ± 3.13	69.4 ± 0.10	12.7 ± 0.12
BLG-rhamnose	4.33 ± 0.07	1.23 ± 0.14	31.8 ± 0.07	387 ± 34	23.6 ± 2.83	74.3 ± 0.40	13.6 ± 0.10
BLG-ribose	4.38 ± 0.16	1.12 ± 0.15	31.8 ± 0.10	313 ± 35	12.0 ± 1.81	37.8 ± 1.81	13.8 ± 0.11

structure close to the conformation of the native protein, accounting for the increase in $d_{3,2}$ at pH 5.

3.5. Foaming properties

Native, heated and glycated BLG were able to produce foam by bubbling, as measured by determining their foam capacity (F_{max}), which was the same for all the samples studied (Table 2). The foam volume at the end of the experiment (F_{min}) measuring the foam stability showed differences between proteins glycated with arabinose or ribose ($F_{min} \sim 12$ mL), native BLG and BLG glycated with lactose or rhamnose ($F_{min} \sim 22$ mL), and heated BLG and BLG glycated with glucose or galactose ($F_{min} \sim 27$ mL). The foams obtained with highly glycated proteins (modified with arabinose or ribose) were not stable, while less glycated proteins (modified with lactose or rhamnose) exhibited the same foam stability as compared with the native protein. However, a modification with glucose or galactose improved the foam stability in the same way as the heated protein samples. The stability index (S_i) followed the same behaviour (as F_{max} was constant for all the samples, S_i was only dependent on F_{min}). Half-life of drainage ($T_{1/2}$) measurement showed that native protein presented the lowest value. Although proteins modified with arabinose or ribose had a small foam volume value at the end of the experiment ($F_{min} \sim 12$ mL), a three-fold longer half-life of drainage value was obtained as compared with the native protein ($T_{1/2\ ribose} \sim 310$ s; $T_{1/2}$ native BLG ~ 100 s), showing an improvement of the liquid retention by the sugar. It was interesting to observe the differences between the experimental curves (foam volume and liquid in the foam as a function of time) of foams obtained with BLG modified with either glucose or ribose glycated at different degrees (Fig. 7). The foam broke easily in the case of ribosylated BLG, whereas good foam stability was observed in the case of glucosylated BLG. On the other hand, small differences were observed in the case of liquid drainage, suggesting that the negative effect on foam stability introduced by a high modification of the protein was offset by liquid retention.

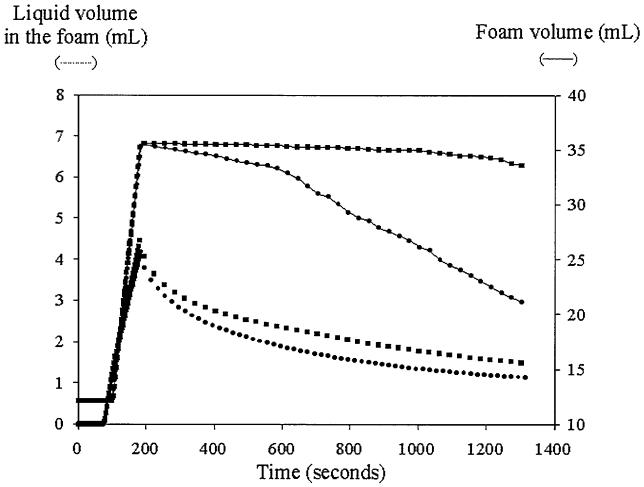

Fig. 7. Foam curves of BLG modified with glucose (■) and ribose (●) representing the liquid volume in the foam (- - -) and the foam volume (——).

Foam density which is highly dependent on the liquid staying in the foam at the end of the experiment (L_{min}) was higher for the foam produced with heated or glycated proteins (FD ~ 14) than for that obtained with native protein (FD ~ 10). In conclusion, a moderate degree of glycation (obtained with glucose or galactose) appears to be the best condition for obtaining foam with better stabilities and low drainages.

Acknowledgements

The funding by a fellowship from the Ministère de la Recherche et de la Technologie to François Chevalier is acknowledged. The funding of this work by INRA and the Région Pays de Loire in the scope of the VANAM program "Interactions moléculaires et activités biologiques" is also gratefully acknowledged. The authors thank Mickaël Le Denmat and Marc Anton for their helpful discussion.

References

Ames, J. M. (1998). Application of the Maillard reaction in the food industry. *Food Chemistry*, *62*, 431–439.

Aoki, T., Kitahata, K., Fukumoto, T., Sugimoto, Y., Ibrahim, H. R., Kimura, T., Kato, Y., & Matsuda, T. (1997). Improvement of functional properties of β-lactoglobulin by conjugation with glucose-6-phosphate through the Maillard reaction. *Food Research International*, *30*, 401–406.

Bertrand-Harb, C., Charrier, B., Dalgalarrondo, M., Chobert, J. M., & Haertlé, T. (1990). Condensation of glycosidic and aromatic structures on amino groups of β-lactoglobulin B via reductive alkylation. Solubility and emulsifying properties of the protein derivatives. *Le Lait*, *71*, 205–215.

Bouhallab, S., Morgan, F., Henry, G., Mollé, D., & Léonil, J. (1999). Formation of stable covalent dimer explains the high solubility at pH 4.6 of lactose-β-lactoglobulin conjugates heated near neutral pH. *Journal of Agricultural and Food Chemistry*, *47*, 1489–1494.

Cheftel, J. C., & Lorient, D. (1982). Aspects technologiques. Les propriétés fonctionnelles des proteines laitières et leur amélioration. *Le Lait*, *62*, 435–483.

Chevalier, F., Chobert, J. M., Dalgalarrondo, M., & Haertlé, T. (2001). Characterization of the Maillard reactions products of β-lactoglobulin glucosylated in mild conditions. *Journal of Food Biochemistry*, *25*, 33–55.

Chuyen, N. V. (1998). Maillard reaction and food processing. Application aspects. *Advances in Experimental Medicine and Biology*, *434*, 213–235.

De Wit, J. N., & Klarenbeek, G. (1984). Effect of various heat treatments on the structure and stability of whey proteins. *Journal of Dairy Science*, *67*, 2701–2710.

Friedman, M. (1996). Food browning and its prevention: An overview. *Journal of Agricultural and Food Chemistry*, *44*, 631–653.

Frister, H., Meisel, H., & Schlimme, E. (1988). OPA method modified by used of N,N-dimethyl-2-mercaptoethylammoniumchloride as thiol component. *Fresenius Zeitschrift für Analytische Chemie*, *330*, 631–633.

Haertlé, T., & Chobert, J. M. (1999). Recent progress in processing of dairy proteins: A review. *Journal of Food Biochemistry*, *23*, 367–407.

Hagolle, N., Relkin, P., Popineau, Y., & Bertrand, D. (2000). Study of the stability of egg white protein-based foams: Effect of heating protein solution. *Journal of the Science of Food and Agriculture*, *80*, 1245–1252.

Iametti, S., de Gregori, B., Vecchio, G., & Bonomi, F. (1996). Modifications occur at different structural levels during the heat denaturation of beta-lactoglobulin. *European Journal of Biochemistry*, *237*, 106–112.

Jou, K. D., & Harper, W. J. (1996). Effect of disaccharides on the thermal properties of whey proteins determined by differential scanning calorimetry (DSC). *Milchwissenschaft*, *51*, 509–512.

Kinsella, J. E., & Whitehead, D. M. (1989). Protein in whey: Chemical, physical and functional properties. *Advances in Food and Nutrition Research*, *33*, 343–438.

Kitabatake, N., Cuq, J. L., & Cheftel, C. (1985). Covalent binding of glycosyl residues to β-lactoglobulin: Effects on solubility and heat stability. *Journal of Agricultural and Food Chemistry*, *33*, 125–130.

Klemaszewski, J. L., Das, K. P., & Kinsella, J. E. (1992). Formation and covalence stability of emulsions stabilized by different milk proteins. *Journal of Food Science*, *57*, 366–371.

Ledl, F., & Schleicher, E. (1990). New aspects of the Maillard reaction in foods and in the human body. *Angewandte Chemie International (Edition in English)*, *29*, 565–594.

Maillard, L. C. (1912). Action des amines sur les sucres: Formation des mélanoïdines par voie méthodique. *Comptes Rendus de l'Académie des Sciences*, *154*, 66–68.

Mailliart, P., & Ribadeau Dumas, B. (1988). Preparation of β-lactoglobulin and β-lactoglobulin-free proteins from whey retentate by NaCl salting out at low pH. *Journal of Food Science*, *53*, 743–752.

Mattarella, N. L., & Richardson, T. (1983). Physicochemical and functional properties of positively charged derivatives of bovine β-lactoglobulin. *Journal of Agricultural and Food Chemistry*, *31*, 972–978.

Morgan, F., Léonil, J., Mollé, D., & Bouhallab, S. (1999a). Modification of bovine β-lactoglobulin by glycation in a powdered state or in an aqueous solution: Effect on association behavior and protein conformation. *Journal of Agricultural and Food Chemistry*, *47*, 83–91.

Morgan, F., Mollé, D., Henry, G., Vénien, A., Léonil, J., Peltre, G., Levieux, D., Maubois, J. L., & Bouhallab, S. (1999b). Glycation of bovine β-lactoglobulin: Effect on the protein structure. *International Journal of Food Science and Technology*, *34*, 429–435.

Morgan, F., Vénien, A., Bouhallab, S., Mollé, D., Léonil, J., Peltre, G., & Levieux, D. (1999c). Modification of bovine β-lactoglobulin by glycation in a powdered state or in aqueous solution: Immunological characterization. *Journal of Agricultural and Food Chemistry*, *47*, 4543–4548.

Nacka, F., Chobert, J. M., Burova, T., Léonil, J., & Haertlé, T. (1998). Induction of new physicochemical and functional properties by the glycosylation of whey proteins. *Journal of Protein Chemistry*, *17*, 495–503.

O'Brien, J., & Morrissey, P. A. (1989). Nutritional and toxicological aspects of the Maillard browning reaction in foods. *Critical Review in Food Science and Nutrition*, *28*, 211–248.

Prabhakaram, M., & Ortwerth, B. J. (1994). Determination of glycation crosslinking by the sugar-dependent incorporation of [^{14}C] lysine into protein. *Analytical Biochemistry*, *216*, 305–312.

Shimizu, M., Saito, M., & Yamauchi, K. (1985). Emulsifying and structural properties of β-lactoglobulin at different pHs. *Agricultural and Biological Chemistry*, *49*, 189–194.

Sitohy, M., Chobert, J. M., & Haertlé, T. (1995). Phosphorylation of β-lactoglobulin under mild conditions. *Journal of Agricultural and Food Chemistry*, *43*, 59–62.

Sitohy, M., Chobert, J. M., Haertlé, T. (2001). Simplified short-time method for the esterification of milk proteins. *Milchwissenschaft, 56*(3), 127–131.

Sitohy, M., Chobert, J. M., Popineau, Y., & Haertlé, T. (1995). Functional properties of β-lactoglobulin phosphorylated in the presence of different aliphatic amines. *Le Lait*, *75*, 503–512.

Smithers, G. W., Ballard, F. J., Copeland, A. D., & de Silva, K. J. (1996). Symposium: Advances in dairy foods proceeding and engineering. New opportunities from the isolation and utilization of whey proteins. *Journal of Dairy Science*, *79*, 1454–1459.

Waniska, R. D., & Kinsella, J. E. (1988). Foaming and emulsifying properties of glycosylated β-lactoglobulin. *Food Hydrocolloïd*, *2*, 439–449.

Scavenging of Free Radicals, Antimicrobial, and Cytotoxic Activities of the Maillard Reaction Products of β-Lactoglobulin Glycated with Several Sugars

François Chevalier, Jean-Marc Chobert,* Claude Genot, and Thomas Haertlé

Laboratoire d'Étude des Interactions des Molécules Alimentaires, INRA, B.P. 71627, 44316 Nantes Cedex 3, France

The Maillard reaction occurs during many industrial and domestic thermal treatments of foods. It is widely used because of its role in creating colors, flavors, textures, and other functional properties in foodstuffs. Proteins glycated without the use of conventional chemical reagents have improved technofunctional properties such as heat stability, emulsifying, and foaming properties. The present study was carried out to determine the extent to which this reaction can convey antioxidant, antimicrobial, or cytotoxic activities to β-lactoglobulin (BLG) and to its tryptic and peptic hydrolysates. BLG was modified with six different sugars in solution at 60 °C. Antiradical properties were estimated using a radical scavenging activity test. Antimicrobial activities against different bacterial strains were studied with a diffusion disk method. Cytotoxic tests were performed using two cell lines and the 3-(4,5-dimethylthiazoyl-2-yl)-2,5-diphenyltetrazolium bromide (MTT) rapid colorimetric assay. Glycation induced a radical scavenging activity to BLG, the intensity of which depended on the sugar used for modification. Proteins modified with ribose and arabinose showed the highest radical scavenging activities depicted by about 80 and 60% of 2,2-diphenyl-1-picrylhydrazyl (DPPH) absorption decrease at 515 nm. No antimicrobial effect of any glycated form of BLG against *Escherichia coli*, *Bacillus subtilis*, *Listeria innocua*, and *Streptococcus mutans* was observed. The MTT test showed no enhancement of cytotoxicity by modified proteins and peptides against COS-7 and HL-60 cells. Thus, glycated proteins could be used in formulated food as functional ingredients with a radical scavenging activity able to delay deterioration due to oxidation. This use could be even more advisable considering the lack of toxicity to eukaryotic and prokaryotic cell cultures demonstrated in this work.

Keywords: *Free radical scavenger; antimicrobial; cytotoxicity; glycation; β-lactoglobulin*

INTRODUCTION

The protein fraction of milk is known to contain many valuable components and biologically active substances, which confer special properties for the support of infant development and growth (*1*). Many milk-borne bioactivities are latent, requiring proteolytic release of bioactive peptides from inactive native proteins (*2*). Milk protein-derived bioactive peptides include a variety of substances that are potential modulators of various regulatory processes and reveal multifunctional bioactivities (*3*). Opioid agonist (*4*), opioid antagonist (*5*), inhibitor of angiotensin converting enzyme (ACE) (*6*, *7*), immunomodulator (*8*), antimicrobial (*9*, *10*), and antithrombotic (*11*) activities have been largely described (*12*).

β-Lactoglobulin (BLG) is known to contain an ACE-inhibitory sequence (*13*), but its biological function in milk is still not well-known (*14*).

Because many attempts are made to control food storage and to preserve food from oxidation and microorganism contamination, it is interesting to subject protein to oxidoreductive modification to see whether new biological properties could be induced. The Maillard reaction is one of the major reactions modifying proteins in food and in nature. The examination of how it can influence biological properties of derived proteins and peptides is of particular interest. This reaction, also called nonenzymatic browning or glycation, was first described by the French biochemist Louis Maillard at the beginning of the 20th century (*15*). It corresponds to a spontaneous reaction between amino groups and reducing compounds. In food, it consists of a condensation of the reducing sugars with essentially the ε-amino group of lysyl residues of proteins (*16*). The Maillard reaction occurs frequently during industrial processing, during prolonged storage, and in domestic cooking (*17*), enhancing color, aroma, and flavor. The consequences of this reaction on the biological properties of the modified products have been largely studied on model systems, which consist of heating a single amino acid with a reducing sugar. The Maillard reaction induced (i) antioxidative activity of glucose−glycine (*18*), xylose−lysine (*19*), and xylose−arginine reacting systems (*20*); (ii) antimicrobial activity of xylose−arginine and glucose−histidine systems (*21*−*23*) and of glucose−glycine system (*24*); (iii) cytotoxic activity of glucose−lysine and fructose−lysine systems (*25*); and (iv) clastogenic activity of ribose−lysine (*26*) and glucose−lysine systems (*27*). Proteins modified by the Maillard reaction can also present some of these properties. For example, lysozyme

* Corresponding author [telephone 33 (0) 2 40 67 50 85; fax 33 (0) 2 40 67 50 84; e-mail chobert@nantes.inra.fr].

10.1021/jf010549x CCC: $20.00
Published on Web 09/26/2001

modified with dextran by glycation developed a significant antimicrobial activity against both Gram-negative and Gram-positive bacteria (*28*); glycation of casein with glucose or lactose resulted in an enhancement of antioxidant activity when compared with native casein (*29*).

Recent work (*30*) has shown that functional properties, such as thermal stability and emulsifying and foaming properties, of BLG modified by the Maillard reaction are improved, depending on the sugar used during modification. Glycated BLG used as a food ingredient for its functional properties may also decrease the oxidative reactions and/or can influence cellular and microorganism growth.

The aim of this study was to determine how glycation of BLG could induce new biological properties when compared with native protein. Whole glycated BLG and its peptic and tryptic hydrolysates were tested for their free radical scavenging, antimicrobial, and cytotoxic properties.

MATERIALS AND METHODS

Protein Purification. β-Lactoglobulin (variant A) was purified according to the procedure of Mailliart and Ribadeau Dumas (*31*). The purity of BLG (99%) was assessed by RP-HPLC.

Reagents. D-Arabinose, D-galactose, D-glucose, D-lactose, D-rhamnose, D-ribose monohydrates, bovine trypsin TPCK-treated, porcine pepsin, 3-(4,5-dimethylthiazoyl-2-yl)-2,5-diphenyltetrazolium bromide (MTT), and bovine serum albumin (BSA) were obtained from Sigma Chemical Co. (St. Louis, MO). *Escherichia coli* HB-101 was from the collection of the Institute of Microbiology, Bulgarian Academy of Science (Sofia, Bulgaria), *Bacillus subtilis* ATCC 6633 was from the American Type Culture Collection (Rockville, MD), *Listeria innocua* F was from the collection of the Ecole Nationale d'Ingénieur des Techniques des Industries Agricoles et Alimentaires (Nantes, France), and *Streptococcus mutans* CIP 103220 T was from the collection of the Institut Pasteur (Paris, France). All other reagents were of analytical grade.

Achievement of Modified Proteins. BLG (0.217 mM) and the different sugars (0.217 M) were dissolved in 0.1 M phosphate buffer, pH 6.5. After filtration on an acetate cellulose membrane filter (0.22 μm diameter, Millipore), mixtures of protein and sugar were put in well-capped flasks and heated in a water bath at 60 °C for 72 h. This mild heat treatment was chosen to limit autoaggregation of BLG. All experiments were performed under strictly anaerobic and sterile conditions; all media were purged and saturated with N_2. After heating, the different fractions were dialyzed against distilled water, freeze-dried, and stored at −20 °C. BLG heated without sugar (heated control) was named "heated BLG", and BLG heated in the presence of sugar was named "glycated BLG" or "BLG-sugar".

The quantities of free amino groups were measured using the OPA modified method (see next section). The BLG sequence contains 16 potential reactive amino groups including 1 α-NH_2 and 15 ϵ-NH_2 on lysyl residues. Modified amino groups were deduced from OPA results. According to previous work (*30*, *32*), on average, 11.0, 8.8, 6.7, 6.6, 6.5, and 5.5 amino groups were modified when proteins were heated in the presence of ribose, arabinose, galactose, glucose, rhamnose, and lactose, respectively.

Determination of Available Amino Groups. The quantity of available amino groups was determined according to the modified *o*-phthaldialdehyde (OPA) method (*33*). The OPA reagent was prepared daily by mixing 40 mg of OPA, dissolved in 1 mL of methanol, 50 mL of 0.1 M sodium borate buffer, pH 9.3, 100 mg of *N*-dimethyl-2-mercaptoethylammonium chloride (DMMAC), and 1.25 mL of 20% (w/w) SDS in water. Fifty microliters of protein solution (2 mg/mL in 50 mM sodium phosphate buffer, pH 7.8) was added to 1 mL of OPA reagent. The absorbance was read at 340 nm after a minimal delay of 5 min. A calibration curve was obtained by using 0.25−2.00 mM L-leucine as a standard.

Hydrolysis of BLG. Native, heated, and glycated BLG (2 mg/mL or 0.11 mM) were dissolved in 0.2 M acetic acid buffer, pH 2.5, for peptic hydrolysis and in 30 mM ammonium carbonate buffer, pH 7.9, for tryptic hydrolysis. Protein samples were dissolved in volatile buffers to allow efficient lyophilization without dialysis after hydrolysis. Porcine pepsin, previously solubilized in distilled water (1 mg/mL), was added to the reaction mixture at an enzyme/substrate (E/S) molar ratio of 1:100. Bovine trypsin, previously solubilized in 0.01 M HCl (1 mg/mL), was added to the reaction mixture at an E/S molar ratio of 1:100. The mixtures were incubated at 37 °C for 120 min. The extent of hydrolysis was controlled by RP-HPLC by measuring the percentage of nonhydrolyzed proteins before freezing at −20 °C, and then hydrolysates were lyophilized.

Reversed Phase High-Performance Liquid Chromatography (RP-HPLC). The HPLC equipment consisted of a Waters 2690 separation module system with an integrated solvent, a sample management platform, and a photodiode array detector model 996. The HPLC system was driven with the Millenium32 program (Waters).

Fifty microliters of hydrolyzed and nonhydrolyzed samples was separated by RP-HPLC on a Symmetry 300A C_{18} column (3.9 × 150 mm, Waters) equilibrated in 80% (v/v) solvent A (trifluoroacetic acid/H_2O, 0.11:99.89, v/v) and 20% solvent B (acetonitrile/H_2O/trifluoroacetic acid, 80:19.91:0.09, v/v/v). Elution was performed with a linear gradient from 80 to 0% solvent A for 30 min. The temperature of the column and solvent was maintained at 30 °C. The flow rate was 0.6 mL/min. Eluted peaks were detected by UV absorbance (214 nm). Peak area corresponding to the nonhydrolyzed form of the protein was integrated. All results were reported to the peak area of the nonhydrolyzed sample that represents 100%.

Antiradical Activity Tests. Free radical scavenging activity was measured by using 2,2-diphenyl-1-picrylhydrazyl (DPPH) as stable free radical. Tests solutions of proteins and peptides were dissolved in bidistilled H_2O at different concentrations, and 0.1 mL of each sample was mixed with 0.9 mL of 6×10^{-5} M DPPH in methanol solution.

Kinetics experiments were performed on a Cary 1 UV−visible spectrophotometer. Measures were realized every 30 s during 30 min with a constant concentration of proteins of 5 mg/mL. The decrease in absorbance at 515 nm was recorded. After ∼10 min, a plateau was reached. Reaction was considered to be complete after 30 min.

End point measurements were realized with different concentrations of proteins and peptides (varying from 5 to 0.1 mg/mL). The mixture of proteins or peptides with DPPH was left standing at 25 °C for 30 min, and then absorbance at 515 nm was measured.

For all experiments, bidistilled water instead of sample solution was used as control. Gallic acid (60 μM) was used as positive free radical scavenger control. All experiments were performed in triplicate.

The free radical scavenging activity (R. S. Act.) of a sample was defined as follows:

$$\text{R. S. Act.} = [1 - (\text{Abs}_{515\text{nm}}\ \text{sample}/\text{Abs}_{515\text{nm}}\ \text{blank})] \times 100$$

Inhibitory concentration 50 (IC_{50}) and inhibitory concentration 10 (IC_{10}) correspond to the concentrations of sample necessary to obtain R. S. Act. values of 50 and 10%, respectively.

Antibacterial Activity Tests. Different bacterial strains were used for these tests. *E. coli* and *B. subtilis* were grown on plate count agar (Biokar), *L. innocua* F was grown on Elliker agar (Biokar), and *S. mutans* was grown on Columbia agar (Biokar).

Antibacterial activity was determined according to the disk diffusion method. Protein and peptide samples were dissolved in bidistilled water (1 mg/mL), filtered on 0.22 μm membranes (Millipore), and stored at 4 °C. Ampicillin (Oxoid) was used as a standard.

Test solutions (10, 25, or 50 μL) were transferred into separate 6 mm diameter paper disks (Whatman No. 1) and left to dry at room temperature under laminar flux. Distilled water was used as a blank.

A preculture of the different strains was realized the day before the manipulation using brain heart infusion (Biokar). Ten microliters of saturated overnight culture was mixed with 10 mL of distilled water and applied at the surface of a Petri dish containing the suitable agar medium. Excess of suspension was eliminated, and dishes were left to dry under laminar flux for 5 min. Paper disks containing proteins or peptides were put at the surface of the inoculated Petri dishes. Finally, Petri dishes were incubated at 37 °C (for *E. coli*, *S. mutans*, and *B. subtilis*) or 30 °C (for *L. innocua*), for 24 or 48 h. Inhibition zones were observed and measured.

Cytotoxic Activity Tests. *Cercopithecus aethiops* (monkey, African green) kidney fibroblast COS-7 cells were grown as a monolayer in Dulbecco's Modified Eagle Media (DMEM; Gibco) supplemented with 10% (v/v) fetal calf serum, penicillin (50 units/mL), and streptomycin (50 μg/mL). Exponentially growing cultures were maintained in an atmosphere of 5% CO_2/95% relative humidity at 37 °C.

Human promyeloblast cells HL-60 were grown in Roswell Park Memorial Institute (RPMI; Biomedia) supplemented with 20% (v/v) fetal calf serum, penicillin (50 units/mL), and streptomycin (50 μg/mL). Exponentially growing cultures were maintained in an atmosphere of 5% CO_2/95% relative humidity at 37 °C.

Assays were based on the cleavage of the tetrazolium salt (MTT) into a blue product (formazan) by a mitochondrial enzyme (succinate dehydrogenase) (*34*). The conversion takes place only in living cells, and the amount of formazan produced is proportional to the number of cells present. The assay is based on the method of Edmondson et al. (*35*) with a modification in the protocol of solubilization of formazan, as follows: a solution of 10% (w/v) SDS in 0.01 M HCl was used instead of a solution of 0.04 M HCl in 2-propanol in order to limit the use of toxic chemicals.

Single-cell suspensions were obtained by mechanical deaggregation of the floating cell line HL-60 and by trypsination of the monolayer cell line COS-7. Cell lines (50 μL) were inoculated in 96-well plates at a concentration of 40000 cells/mL (2000 cells/well). Fifty microliters of protein and peptide samples at different concentrations in culture medium was added to each well (columns 4−11). Blanks were realized with 100 μL of culture medium (column 2), and control was obtained with a mixture of 50 μL of cells (40000 cells/mL) and 50 μL of culture medium (column 3). All samples and the control were made in triplicate. After 72 h of incubation at 37 °C, 25 μL of MTT at 2.5 mg/mL in PBS (phosphate-buffered saline) was added to each well. After 4 h of incubation at 37 °C with MTT, 100 μL of 10% (w/v) SDS in 0.01 M HCl was added to each well. After 24 h of incubation at 37 °C, plates were read at 540 nm.

Percentage of cytotoxicity (PC) was calculated as follows:

$$PC\ (\%) = [1 - (Abs_{540nm}\ \text{test wells})/(Abs_{540nm}\ \text{control wells})] \times 100$$

RESULTS AND DISCUSSION

Hydrolysis by Pepsin and Trypsin: Determination of the Susceptibility to Hydrolysis of Native, Heated, and Glycated BLG. Protein samples were hydrolyzed by trypsin and pepsin during 120 min at 37 °C. The quantity of protein left nonhydrolyzed was determined by RP-HPLC. The peak area corresponding to nonhydrolyzed protein was calculated and related to the peak area of the control without addition of enzyme (Table 1). BSA was used as a positive control of hydrolysis.

Native BLG and heated BLG were rapidly hydrolyzed by trypsin. Because glycation sites are located on lysyl and arginyl residues, which are also tryptic cleavage sites, such a modification inhibited tryptic hydrolysis. As expected, and according to previous work (*16*, *32*), glycated BLG resisted to tryptic hydrolysis as a function of its glycation degree. BLG glycated with ribose, which was the most modified sample (11 sites modified of 16 possible), presented 97% of protein left nonhydrolyzed after trypsinolysis. Half the amount of BLG modified with arabinose was still present after trypsinolysis. BLG modified by other sugars exhibited 13−24% of intact proteins after tryptic action, showing a relatively high susceptibility to this protease.

Table 1. Comparison of Tryptic and Peptic Digestion of Native, Heated, and Glycated BLG and BSA

	residual area of nonhydrolyzed protein (%)	
sample	after peptic hydrolysis	after tryptic hydrolysis
native BLG	95	7
heated BLG	85	3
BLG−arabinose	39	48
BLG−galactose	40	19
BLG−glucose	42	17
BLG−lactose	74	13
BLG−rhamnose	56	24
BLG−ribose	28	97
BSA	0	0

Peptic hydrolysis gave completely different results. Native BLG is known to resist peptic hydrolysis due to its particular three-dimensional conformation (*36*, *37*). Only 5% of native BLG was hydrolyzed by pepsin in the conditions used. After 72 h of heating at 60 °C, 85% of BLG was left nonhydrolyzed, confirming a high stability of BLG structure after heating. Pepsin susceptibility of BLG depended on its glycation degree (*38*). The most hydrolyzed sample was the ribosylated form of BLG, which showed only 28% of protein left nonhydrolyzed.

DPPH Test: Effect of Maillard Glycation on the Free Radical Scavenging Activity of BLG. In these experiments, DPPH in methanol was used as a free radical. This compound is stable and allows evaluation of the antiradical activity of samples. In its radical form, DPPH absorbs at 515 nm, and after its reduction by an antiradical compound, its absorption disappears (*39*). Native, heated, and glycated BLG and their tryptic and peptic hydrolysates were tested for their free radical scavenging activities.

Kinetics experiments were realized first to estimate the time necessary to obtain a relatively stable absorbency of DPPH after being in contact with the protein samples. For all compounds, reaction was very fast in the first 5 min, and then a plateau was rapidly attained. After 30 min, reaction was considered to be achieved and final points were measured.

Radical scavenging activities, IC_{50} and IC_{10}, are reported in Figure 1 and Table 2. IC_{50} and IC_{10} of native BLG, heated BLG, and BSA could not be calculated because the highest concentration used (5 mg/mL) was not sufficient to obtain 10% of radical scavenging activity. This is the reason in Table 2, ">5 mg/mL" is indicated for IC_{50} and IC_{10} values of these samples. Radical scavenging activities of nonhydrolyzed native proteins and their peptic and tryptic hydrolysates were ∼7%, showing a weak antiradical activity of proteins before glycation.

Nonhydrolyzed BLG modified by the Maillard reaction showed a marked antiradical scavenging activity (Figure 1). Ribosylated BLG showed the highest radical

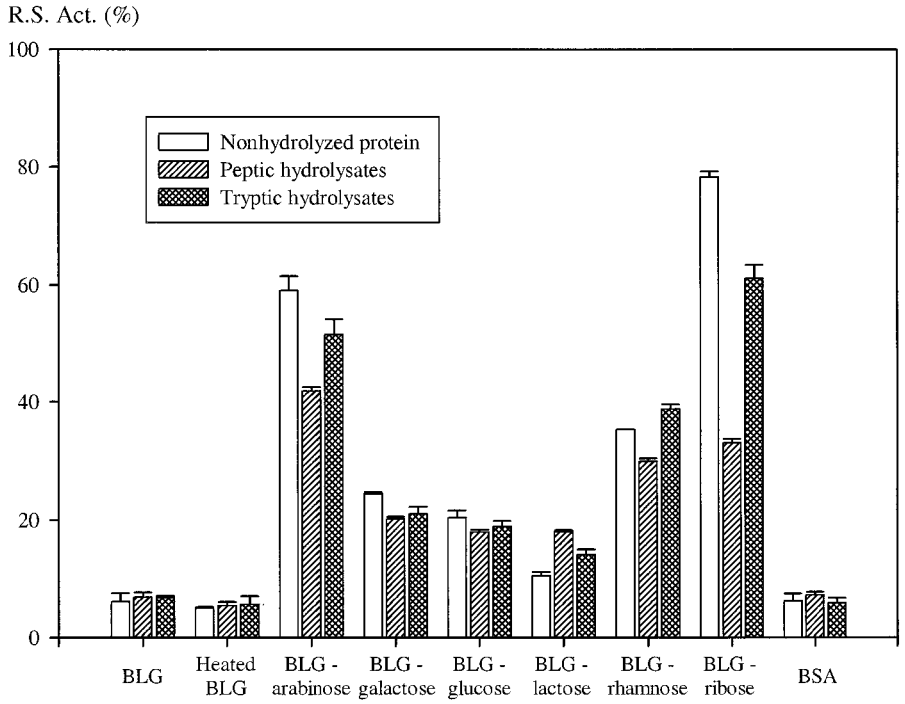

Figure 1. Radical scavenging activity (R. S. Act. %) of nonhydrolyzed and peptic and tryptic hydrolysates of native BLG, heated BLG, BLG glycated with arabinose, galactose, glucose, lactose, rhamnose, or ribose, and BSA. Protein concentration was 5 mg/mL. All results were derived from triplicates.

Table 2. Inhibitory Concentrations of Native, Heated, and Glycated BLG and of BSA against Free Radical of DPPH

	proteins		peptic hydrolysates		tryptic hydrolysates	
sample	IC_{10} (mg/mL)	IC_{50} (mg/mL)	IC_{10} (mg/mL)	IC_{50} (mg/mL)	IC_{10} (mg/mL)	IC_{50} (mg/mL)
native BLG	>5	>5	>5	>5	>5	>5
heated BLG	>5	>5	>5	>5	>5	>5
BLG−arabinose	0.9	4.0	1.4	>5	1.0	4.8
BLG−galactose	2.0	>5	2.5	>5	2.4	>5
BLG−glucose	2.1	>5	2.4	>5	2.6	>5
BLG−lactose	4.7	>5	2.8	>5	3.5	>5
BLG−rhamnose	1.4	>5	1.7	>5	1.3	>5
BLG−ribose	0.6	2.7	1.5	>5	0.8	3.8
BSA	>5	>5	>5	>5	>5	>5

scavenging activity with ~80% of DPPH absorption decrease. BLG modified with arabinose had ~60% of radical scavenging activity. BLG modified with rhamnose, glucose, galactose, and lactose had about 35, 24, 20, and 10% of radical scavenging activity, respectively. These results clearly indicate the role of the Maillard reaction in the free radical scavenging activity of modified proteins, which is in agreement with Nishino et al. (*40*), who showed a radical scavenging activity of milk products prepared by the Maillard reaction.

The free radical scavenging activity of glycated proteins was not directly related to the glycation degree. Although the extent of glycation of BLG modified with rhamnose is about the same as that obtained in the case of glycation with glucose and galactose (see Achievement of Modified Proteins), the rhamnosylated BLG sample exhibited a higher radical scavenging activity than the other two glycated proteins. Formation of melanoidins and heterocycles in the advanced stage of the Maillard reaction (*41*−*43*) could explain the ability of glycated proteins to react with radical compounds (*40*). Nevertheless, BLG modified with rhamnose exhibited a still lower radical scavenging activity than BLG modified with arabinose and ribose, which could be explained by the higher glycation degree obtained with these BLG derivatives.

Free radical scavenging activity of glycated BLG versus the number of moles of reactional primary amino groups, according to the quantity of proteins used during the test and the degree of glycation of each sample, has been measured (Figure 2). This emphasized that activity was also related to the nature of the sugar used for the modification. For example, in the case of BLG glycated with lactose and ribose, the radical scavenging activity corresponding to 150 nmol of reactional primary amino groups was about 10 and 46%, respectively. If radical scavenging activities of samples were related only to glycation degree, for the same amount of reactional primary amino groups, the same activity should be observed, which was not the case in our experiments. According to Figure 2, the nature of the sugar used is another factor influencing the radical scavenging activity of glycated proteins. Such results could be explained, on the one hand, by a more rapid action of ribose during heating, inducing a larger quantity of advanced Maillard products (AMP) as compared with lactose and, on the other hand, by structural and/or chemical differences between sugars, inducing the formation of diversified Maillard reaction products.

According to the results obtained with nonhydrolyzed proteins, modified BLG samples can be ordered from the weakest to the strongest reactant for radical scav-

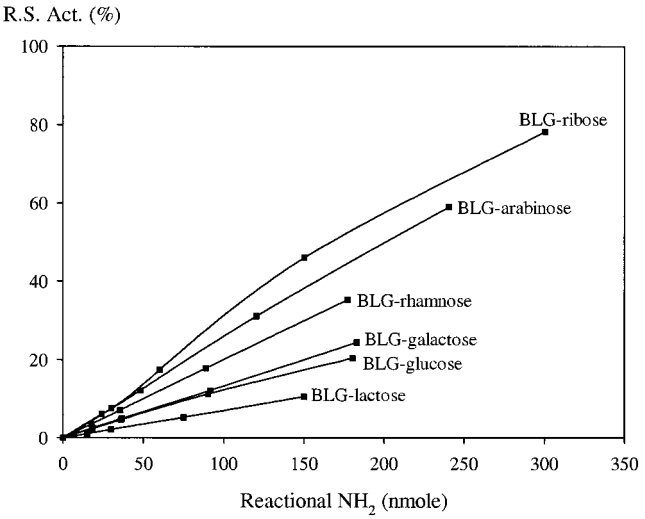

Figure 2. Radical scavenging activity (R. S. Act. %) of BLG glycated with arabinose, galactose, glucose, lactose, rhamnose, or ribose as a function of the number of reactional primary amino groups of BLG.

enging activity of DPPH as follows: BLG−lactose < BLG−glucose ≈ BLG−galactose < BLG−rhamnose < BLG−arabinose < BLG−ribose.

The antiradical properties of peptic and tryptic hydrolysates of modified BLG were also studied to assess the influence of hydrolysis on radical scavenging activity of glycated proteins. All proteins did not reach the same extent of hydrolysis as shown by the residual area of nonhydrolyzed proteins (Table 1). Consequently, three parameters could influence radical scavenging activity: glycation degree, nature of the sugar (as was observed for nonhydrolyzed proteins), and hydrolysis degree.

In the case of tryptic hydrolysis, only 25% of proteins remained nonhydrolyzed except for BLG modified with arabinose and ribose. Only minor differences in radical scavenging activity were observed between whole proteins and their tryptic hydrolysates in the case of BLG modified with galactose, glucose, and rhamnose (Figure 1). In contrast, the IC_{10} of BLG modified with lactose decreased by 1.2 mg/mL after tryptic hydrolysis (Table 2), showing a better radical scavenging activity for this sample. Such a result is difficult to explain because, in contrast, the IC_{10} of tryptic hydrolysates of BLG modified with glucose and galactose increased by 0.5 and 0.4 mg/mL, respectively, as compared with nonhydrolyzed proteins. It could be thought that tryptic hydrolysis of BLG modified with lactose exposed new antiradical moieties previously hidden in the core of the globulin molecule. In comparison, IC_{10} and IC_{50} values of BLG modified with arabinose and ribose increased by about 0.1 and 0.2 mg/mL for IC_{10} and by 0.8 and 1.1 mg/mL for IC_{50}. BLG modified with arabinose was nearly 50% hydrolyzed by trypsin, whereas BLG modified with ribose was almost not hydrolyzed at all (Table 1). In this case, such activity changes could be explained by additional treatments of these samples during hydrolysis and lyophilization processes as compared with nonhydrolyzed samples.

These observations were even more pronounced when glycated BLG was hydrolyzed with pepsin. In this case, IC_{10} of BLG modified by arabinose and ribose increased by 0.5 and 0.9 mg/mL, respectively, corresponding to a decrease of about 20 and 45% in radical scavenging activity (Figure 1). Other glycated samples did not show such a decrease. Radical scavenging activity of BLG modified with rhamnose, galactose, and glucose decreased by about 5, 4, and 2%, respectively, only. Moreover, an 8% increase of this activity was observed with BLG modified with lactose, representing a decrease by 1.9 mg/mL of its IC_{10}.

Nevertheless, even if the radical scavenging activity generally decreased after tryptic or peptic hydrolysis of glycated BLG, it was still higher when compared with that of nonglycated protein.

Antibiotic Activity: Effect of Glycation of BLG on the Inhibition of Bacterial Growth. Four different bacteria strains were used to study the antibiotic activity of BLG modified by the Maillard reaction and of its tryptic and peptic hydrolysates. Gram-positive (*B. subtilis* and *S. mutans*) and Gram-negative bacteria (*E. coli* and *L. innocua*) were used to test a variety of morphologically different bacteria.

All of the experiments performed (results not shown) showed that no antibiotic activity against these microorganisms was present in native, heated, or glycated BLG and its hydrolysates.

Einarsson (*21*, *22*) and Einarsson et al. (*23*) observed an inhibition of bacterial growth by Maillard reaction products prepared with arginine−glucose, arginine−xylose, and histidine−glucose model systems. Antimicrobial activity has also been observed in the case of lysozyme modified with dextran by the Maillard reaction (*28*). Nonmodified lysozyme inhibits the growth of only Gram-positive bacteria. Conjugation of dextran to lysozyme resulted in an extension of its antimicrobial spectrum to Gram-negative bacteria. Recently, four bactericidal domains (residues 15−20, 25−40, 78−833, and 92−100) were isolated after tryptic digestion and characterized in the bovine BLG (*44*). In the present study, native BLG did not show any antimicrobial activity with the techniques used. Only the appearance of new antimicrobial activity could be expected. Such an activity is certainly more difficult to induce by a nonspecific chemical modification because of the large spectrum of resistance mechanisms in bacteria.

Cytotoxic Activity: Effect of Glycation of BLG on the Inhibition of Cellular Growth. COS-7 and HL-60 cells were used to study the effects of nonhydrolyzed BLG and of tryptic and peptic hydrolysates of BLG modified by the Maillard reaction on cellular growth inhibition. BSA, together with its peptic and tryptic hydrolysates, was used as nonactive control.

Native BLG, heated BLG, BSA, and BLG modified with arabinose, galactose, glucose, lactose, rhamnose, and ribose were used in concentrations ranging from 100 to 0.1 μg/mL. Because BLG modified with arabinose, galactose, lactose, or rhamnose gave very similar results when compared with native or BLG modified with glucose and in order to ensure the clarity of presentation, only the results obtained with native BLG (A), heated BLG (B), BLG glycated by glucose (C) or ribose (D), and BSA (E) are presented in Figure 3.

About 60% of the growth of COS-7 cells was inhibited with nonhydrolyzed BLG at the maximum of protein concentration used (100 μg/mL). The same was observed with heated BLG and BLG glycated with glucose. BLG glycated with ribose and BSA exhibited about 40 and 15% inhibition, respectively. A dose−concentration effect was observed: the smaller the concentration of proteins, the lower the inhibition of cellular growth. The

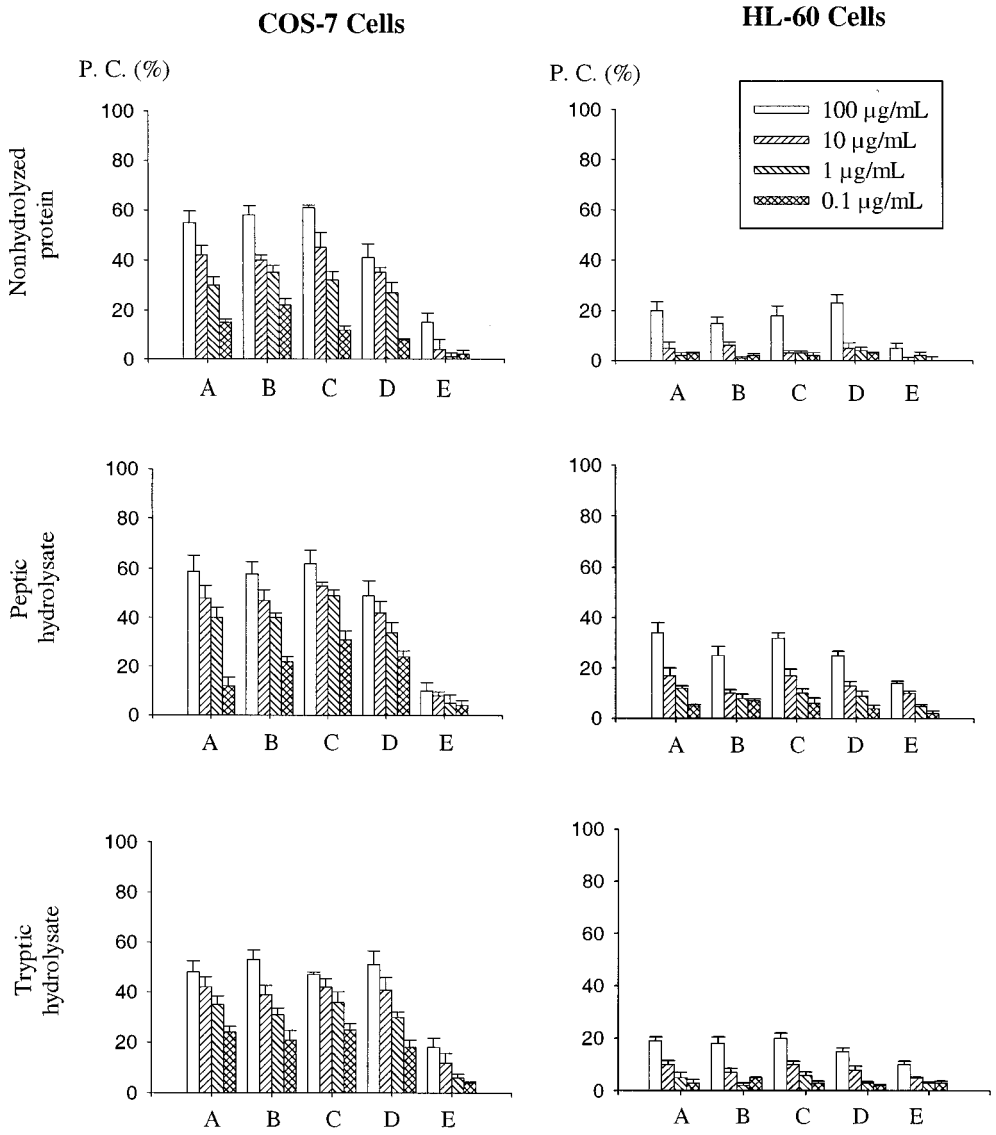

Figure 3. Inhibition of growth of COS-7 and HL-60 cells as a function of protein concentration. Nonhydrolyzed and peptic and tryptic hydrolysates of native BLG (A), heated BLG (B), BLG glycated with glucose (C) or ribose (D), and BSA (E) were studied. All results were derived from triplicates.

growth inhibition of COS-7 cells was about the same in the case of peptic and tryptic hydrolysates. Consequently, differences in their inhibiting activity of COS-7 cell growth between native, heated, and glycated BLG did not seem to exist. However, a significant difference was observed between BLG samples and BSA. BLG samples inhibited ~40% more COS-7 cell growth as compared with BSA. However, this certainly could not be related to glycation but rather to the protein used.

Inhibition of HL-60 cell growth with BLG samples was not so efficient as that observed in the case of COS-7 cells. Only 20% of growth inhibition was observed with nonhydrolyzed and tryptic hydrolysates of BLG samples, and ~30−35% of growth inhibition was observed with peptic hydrolysates of BLG samples. Growth inhibition induced by BSA samples was nearly the same in the case of HL-60 cells when compared with COS-7 cells. In the case of tryptic hydrolysates of BLG samples and BSA, quite similar growth inhibitions were observed, showing the very low activity of tryptic hydrolysates of BLG samples. BLG and its peptic hydrolysates showed higher activity when compared with BSA samples.

COS-7 cell growth inhibition might reasonably be related to the cell adhesion because nonadherent HL-60 cells were less inhibited than COS-7 cells. No specific mechanism can be involved in growth inhibition because of too high concentrations used during the experiment. Only a nonspecific inhibition, due to an excess of proteins or peptides, is likely at the origin of such a low inhibition. However, a question can be raised: why was such an activity present only in the case of BLG samples and not in the case of BSA samples? Physicochemical characteristics of BLG such as its amphiphilic properties or its isoelectric point might be involved in the higher activity of BLG as compared to BSA. Meanwhile, no inhibitory activity was induced by glycation whatever. All activities observed were nearly identical in the cases of native, heated, and glycated BLG.

Maillard reactions are known to produce mutagenic, DNA-damaging, and cytotoxic substances especially during food processing and cooking (*45*). This certainly concerns AMP, the so-called advanced Maillard products. Heterocyclic amines are the most potent mutagens known to be formed during the heat processing of food

(*41*). Such compounds should not be formed (at least in detectable quantity) under the conditions used in the present study because of the mild heat treatment applied (72 h at 60 °C). Consequently, in the case of earlier studied products, some innocuousness can be expected.

ABBREVIATIONS USED

ACE, angiotensin converting enzyme; BLG, β-lactoglobulin; DMEM, Dulbecco's Modified Eagle Media; DPPH, 2,2-diphenyl-1-picrylhydrazyl; MTT, 3-(4,5-dimethylthiazoyl-2-yl) 2,5-diphenyltetrazolium bromide; OPA, orthophthalaldehyde; PBS, phosphate-buffered saline; RPMI, Roswell Park Memorial Institute.

ACKNOWLEDGMENT

We thank X. Dousset (ENITIAA, Nantes, France) and O. Reboul (Dental Surgery Faculty, Nantes, France) for the gift of bacterial strains.

LITERATURE CITED

(1) Meisel, H.; Schlimme, E. Milk proteins: precursors of bioactive peptides. *Trends Food Sci. Technol.* **1990**, *1*, 41−43.

(2) Schanbacher, F. L.; Talhouk, R. S.; Murray, F. A.; Gherman, L. I.; Willett, L. B. Milk-borne bioactive peptides. *Int. Dairy J.* **1998**, *8*, 393−403.

(3) Meisel, H. Overview on milk proteins-derived peptides. *Int. Dairy J.* **1998**, *8*, 363−373.

(4) Meisel, H. Chemical characterization and opioid activity of an exorphin isolated from in vivo digests of casein. *FEBS Lett.* **1986**, *196*, 223−227.

(5) Tani, F.; Iio, K.; Chiba, H.; Yoshikawa, M. Isolation and characterization of opioid antagonist peptides derived from human lactoferrin. *Agric. Biol. Chem.* **1990**, *54*, 1803−1810.

(6) Yamamoto, N. Antihypertensive peptides derived from food proteins. *Biopolymers* **1997**, *43*, 129−134.

(7) Pihlanto-Leppälä, A.; Rokka, T.; Korhonen, H. Angiotensin I converting enzyme inhibitory peptides derived from bovine milk proteins. *Int. Dairy J.* **1998**, *8*, 325−331.

(8) Brantl, V.; Teschemacher, H.; Blasig, J.; Henschen, A.; Lottspeich, F. Opioid activities of β-casomorphins. *Life Sci.* **1981**, *28*, 1903−1909.

(9) Zucht, H.-D.; Raida, M.; Adermann, K.; Mägert, H.-J.; Forssmann, W.-G. Casocidin-I: a casein-α_{S2} derived peptide exhibits antibacterial activity. *FEBS Lett.* **1995**, *372*, 185−188.

(10) Dionysius, D. A.; Milne, J. M. Antibacterial peptides of bovine lactoferrin: purification and characterization. *J. Dairy Sci.* **1997**, *80*, 667−674.

(11) Chabance, B.; Jollès, P.; Izquierdo, C.; Mazoyer, E.; Francoual, C.; Drouet, L.; Fiat, A. M. Characterization of an antithrombotic peptide from κ-casein in newborn plasma after milk ingestion. *Br. J. Nutr.* **1995**, *73*, 583−590.

(12) Meisel, H. Biochemical properties of bioactive peptides derived from milk proteins; potential nutraceuticals for food and pharmaceutical applications. *Livest. Prod. Sci.* **1997**, *50*, 125−138.

(13) Mullally, M. M.; Meisel, H.; Fitzgerald, R. J. Identification of a novel angiotensin-I-converting enzyme inhibitory peptide corresponding to a tryptic fragment of bovine β-lactoglobulin. *FEBS Lett.* **1997**, *402*, 99−101.

(14) Sawyer, L.; Brownlow, S.; Polikarpov, I.; Wu, S.-Y. β-lactoglobulin: structural studies, biological clues. *Int. Dairy J.* **1998**, *8*, 65−72.

(15) Maillard, L. C. Action des amines sur les sucres: formation des mélanoïdines par voie méthodique. *C. R. Acad. Sci.* **1912**, *154*, 66−68.

(16) Chevalier, F.; Chobert, J. M.; Dalgalarrondo, M.; Haertlé, T. Characterization of the Maillard reactions product of β-lactoglobulin glucosylated in mild conditions. *J. Food Biochem.* **2001**, *25*, 33−55.

(17) Ames, J. M. Control of the Maillard reaction in food systems. *Trends Food Sci. Technol.* **1990**, *1*, 150−154.

(18) Anese, M.; Nicoli, M. C.; Lerici, C. R. Influence of pH on the oxygen scavenging properties of heat-treated glucose-glycine systems. *Ital. J. Food Sci.* **1994**, *3*, 339−343.

(19) Yen, G.-C.; Hsieh, P.-P. Antioxidative activity and scavenging effects on native oxygen of xylose-lysine Maillard reaction products. *J. Sci. Food Agric.* **1995**, *67*, 415−420.

(20) Beckel, R. W.; Waller, G. R. Antioxidative arginine-xylose Maillard reaction products: conditions of synthesis. *J. Food Sci.* **1983**, *48*, 996−997.

(21) Einarsson, H. The effect of time, temperature, pH and reactants on the formation of antibacterial compound in the Maillard reaction. *Lebensm.-Wiss. -Technol.* **1987**, *20*, 51−55.

(22) Einarsson, H. The effect of pH and temperature on the antibacterial effect of Maillard reaction products. *Lebensm.-Wiss. -Technol.* **1987**, *20*, 56−58.

(23) Einarsson, H.; Snygg, B. G.; Eriksson, C. Inhibition of bacterial growth by Maillard reaction products. *J. Agric. Food Chem.* **1983**, *31*, 1043−1047.

(24) Stecchini, M. L.; Giavedoni, P.; Sarais, I.; Lerici, C. R. Antimicrobial activity of Maillard reaction products against *Aeromonas hydrophilia*. *Ital. J. Food Sci.* **1993**, *2*, 147−150.

(25) Jing, H.; Kitts, D. D. Comparison of the antioxidative and cytotoxic properties of glucose-lysine and fructose-lysine Maillard reaction. *Food Res. Int.* **2000**, *33*, 509−516.

(26) Vagnarelli, P.; de Sario, A.; Cuzzoni, M. T.; Mazza, P.; de Carli, L. Cytotoxic and clastogenic activity of ribose-lysine browning model system. *J. Agric. Food Chem.* **1991**, *39*, 2237−2239.

(27) Kitts, D. D.; Wu, C. H.; Stich, H. F.; Powrie, W. D. Effect of glucose-lysine Maillard reaction product on bacterial and mammalian cell mutagenesis. *J. Agric. Food Chem.* **1993**, *41*, 2353−2358.

(28) Nakamura, S.; Kato, A.; Kobayashi, K. New antimicrobial characteristics of lysozyme-dextran conjugate. *J. Agric. Food Chem.* **1991**, *39*, 647−650.

(29) McGookin, B. J.; Augustin, M. A. Antioxidant activity of casein and Maillard reaction product from casein-sugar mixtures. *J. Dairy Res.* **1991**, *58*, 313−320.

(30) Chevalier, F.; Chobert, J. M.; Popineau, Y.; Nicolas, M. G.; Haertlé, T. Improvement of the functional properties of β-lactoglobulin glycated through the Maillard reaction is related to the sugar nature. *Int. Dairy J.* **2001**, *11*, 145−152.

(31) Mailliart, P.; Ribadeau Dumas, B. Preparation of β-lactoglobulin and β-lactoglobulin-free proteins from whey retentate by NaCl salting out at low pH. *J. Food Sci.* **1988**, *53*, 743−752.

(32) Chevalier, F.; Chobert, J. M.; Mollé, D.; Haertlé, T. Maillard glycation of β-lactoglobulin with several sugars: Comparative study of the properties of the obtained polymers and of the substituted sites. *Lait* **2001**, *81*, 651−666.

(33) Frister, H.; Meisel, H.; Schlimme, E. OPA method modified by used of *N*,*N*-dimethyl-2-mercaptoethylammoniumchloride as thiol component. *Fresenius' Z. Anal. Chem.* **1988**, *330*, 631−633.

(34) Mosmann, T. Rapid colorimetric assay for cellular growth and survival: application to proliferation and cytotoxic assays. *J. Immunol. Methods* **1983**, *65*, 55−63.

(35) Edmondson, J. M.; Armstrong, L. S.; Martinez, A. O. A rapid and simple MTT-based spectrophotometric assay for determining drug sensitivity in monolayer cultures. *J. Tissue Cult. Methods* **1988**, *11*, 15−17.

(36) Dalgalarrondo, M.; Dufour, E.; Chobert, J. M.; Bertrand-Harb, C.; Haertlé, T. Proteolysis of β-lactoglobulin and β-casein by pepsin in ethanolic media. *Int. Dairy J.* **1995**, *5*, 1−14.
(37) Guo, M. R.; Fox, P. F.; Flynn, A. Susceptibility of β-lactoglobulin and sodium caseinate to proteolysis by pepsin and trypsin. *J. Dairy Sci.* **1995**, *78*, 2336−2344.
(38) Chevalier, F.; Chobert, J. M.; Choiset, Y.; Dalgalarrondo, M.; Haertlé, T. Maillard glycation of β-lactoglobulin induces conformational changes. *Nahrung* **2002**, *46*, in press.
(39) Brand-Williams, W.; Cuvelier, M. E.; Berset, C. Use of free radical method to evaluate antioxidant activity. *Lebensm.-Wiss. -Technol.* **1995**, *28*, 25−30.
(40) Nishino, T.; Shibahara-Sone, H.; Kikuchi-Hayakawa, H.; Ishikawa, F. Transit of radical scavenging activity of milk products prepared by Maillard reaction and *Lactobacillus casei* strain Shirota fermentation through the hamster intestine. *J. Dairy Sci.* **2000**, *83*, 915−922.
(41) Friedman, M. Food browning and its prevention: an overview. *J. Agric. Food Chem.* **1996**, *44*, 631−653.
(42) Ledl, F.; Schleicher, E. New aspects of the Maillard reaction in foods and in the human body. *Angew. Chem., Int. Ed. Engl.* **1990**, *29*, 565−594.
(43) Chuyen, N. V. Maillard reaction and food processing. Application aspects. *Adv. Exp. Med. Biol.* **1998**, *434*, 213−235.
(44) Pellegrini, A.; Dettling, C.; Thomas, U.; Hunziker, P. Isolation and characterization of four bactericidal domains in the bovine β-lactoglobulin. *Biochim Biophys. Acta* **2001**, *1526*, 131−140.
(45) O'Brien, J.; Morrissey, P. A. Nutritional and toxicological aspects of the Maillard browning reaction in foods. *C. R. Food Sci. Nutr.* **1989**, *28*, 211−248.

Received for review April 26, 2001. Revised manuscript received July 26, 2001. Accepted August 2, 2001. Funding by a fellowship from the Ministère de la Recherche et de la Technologie to F.C. is acknowledged. Funding of this work by INRA and the Région Pays de Loire in the scope of the VANAM program Interactions Moléculaires et Activités Biologiques is also gratefully acknowledged.

JF010549X

1.2 - Post-Doctorat 1 : Carence en phosphate chez des écotypes d'*Arabidopsis thaliana*

1.2.1 - Architecture racinaire en réponse à la carence en phosphate

La première étape de ce travail consistait à sélectionner des écotypes de la plante modèle *Arabidopsis thaliana* ayant une réponse caractéristique à la carence en phosphate (phosphore inorganique, ou Pi) au niveau de leur architecture racinaire. La plasticité de développement constitue un composant principal des réponses adaptatives des plantes à la disponibilité des nutriments. Dans ce travail, nous avons étudié la variation naturelle existant chez *Arabidopsis* pour les réponses de croissance à la disponibilité de phosphate. A cette fin, nous avons comparé les effets de la carence en phosphate pour quatre écotypes communs d'*Arabidopsis thaliana*. Un ensemble de dix paramètres de croissance, au niveau de la partie aérienne et du système de racine, a été mesuré. La longueur de la racine primaire et le nombre de parties latérales se sont avérés être conjointement réduits lors de la carence en phosphate chez les quatre accessions.

Ces deux paramètres ont été choisis pour examiner un ensemble de 73 accessions provenant de différents habitats. En condition de carence en phosphate, la moitié des accessions a montré une réduction de la longueur de la racine primaire et du nombre de racines latérales, 25 % n'étaient pas sensibles à la disponibilité de phosphate. Pour 25 % des accessions étudiées, la carence en phosphate n'a affecté qu'un des deux paramètres de croissance sélectionnés, indiquant l'occurrence de différentes stratégies adaptatives.

1.2.2 - Analyse protéomique de la variabilité naturelle

Le premier objectif de ce travail était d'évaluer la capacité des analyses classiques de protéomique comme outil moléculaire de caractérisation de la biodiversité chez *Arabidopsis thaliana*. Pour cela, huit écotypes ont été choisis, provenant d'habitats différents et ayant des réponses contrastées à la carence en phosphate. Les protéines solubles, extraites des racines, ont été séparées par électrophorèse bidimensionnelle. Nous avons utilisé des strips de 18 centimètres (pH 4 - 7) pour la séparation en première dimension et une deuxième dimension couvrant une gamme de poids moléculaires allant de 15 à 150 kDa. Afin d'obtenir une information aussi quantitative que possible, des gels ont été colorés avec le bleu de Coomassie colloïdal. La comparaison des cartes bidimensionnelles a montré que seulement un quart des spots était commun à tous les écotypes. En outre, l'identification des spots principaux de chaque écotype a montré de grandes différences entre les fonctions principales de ces protéines. Une classification hiérarchique des protéomes de chaque écotype a alors été réalisée en fonction de la quantité des spots anonymes. La classification effectuée avec l'ensemble des spots a regroupé les mêmes écotypes que celle effectuée avec seulement les 25 spots majoritaires, ainsi que celle effectuée avec les fonctions de ces spots majoritaires. Cette étude a suggéré que la comparaison de protéomes aurait la capacité de démontrer des différences de statut physiologique entre écotypes. La protéomique classique pourrait ainsi constituer un outil puissant pour révéler la biodiversité entre les écotypes d'une même espèce.

1.2.3 - Analyse protéomique de la réponse à la carence en phosphate

Comme le phosphate présente une faible disponibilité dans le sol, pour l'acquérir, les plantes ont développé de nombreuses capacités d'adaptation tant morphologiques que physiologiques. L'identification et la caractérisation des gènes clés impliqués dans les mécanismes d'adaptation à la carence en Pi pourraient fournir des indices sur les étapes initiales de la signalisation du Pi.
Une approche par électrophorèse sur gel en deux dimensions a été réalisée afin d'analyser la réponse protéomique à la carence en phosphate chez *Arabidopsis*. Deux écotypes ont été sélectionnés grâce à la réponse contrastée de leur système racinaire en condition limitante en phosphate.
Après séparation et analyse des protéomes, sur les 30 spots modulés par une carence en phosphate, 14 sont augmentés et 10 diminués avec l'écotype Be-0, alors que seulement 13 spots ont été observés comme régulés à la baisse pour écotype Ll-0. De plus, des réponses systématiques et opposées à la carence en phosphate ont été observées entre les deux écotypes.
Les 30 protéines exprimées de manière différentielle ont été identifiées par spectrométrie de masse. Ces protéines sont impliquées pour la plupart dans le stress oxydatif ou le métabolisme des glucides et des protéines.
Ces résultats suggèrent que la modulation de deux enzymes, l'alcool déshydrogénase et l'aconitate hydratase, peut contribuer à la stratégie d'adaptation opposée des écotypes Be-0 et Ll-0.
L'analyse approfondie de l'aconitate hydratase a montré une réponse inverse entre les deux écotypes. Cette protéine, aussi potentiellement impliquée dans l'homéostasie du fer, pourrait contribuer, au moins indirectement, à l'architecture particulière des racines de ces écotypes en réponse à la carence en phosphate.

1.2.4 - Sélection de publications du Post-doctorat 1

Chevalier F., Pata M., Nacry P., Doumas P., Rossignol M. (2003)
Effects of phosphate availability on the root system architecture : large-scale analysis of the natural variation between *Arabidopsis* accessions.
Plant Cell & Environment 26, 1839-1850.

Chevalier F., Martin O., Rofidal V., Devauchelle A.-D., Rossignol M. (2004)
Proteomic investigation of natural variation between *Arabidopsis* ecotypes.
Proteomics 4, 1372-1381.

Chevalier F. and Rossignol M.
Proteomic analysis of *Arabidopsis thaliana* ecotypes with contrasted root architecture in response to phosphate deficiency (2011)
Journal of Plant Physiology 168(16), 1885-1890.

Plant, Cell and Environment (2003) **26**, 1839–1850

Effects of phosphate availability on the root system architecture: large-scale analysis of the natural variation between *Arabidopsis* accessions

F. CHEVALIER*, M. PATA, P. NACRY, P. DOUMAS & M. ROSSIGNOL*

Laboratoire de Biochimie & Physiologie Moléculaire des Plantes, UMR 5004, INRA/ENSA-M/CNRS/Université Montpellier 2, 2 place Viala, F-34060 Montpellier Cedex 1, France

ABSTRACT

Developmental plasticity is one main adaptative response of plants to the availability of nutrients. In the present study, the naturally occurring variation existing in *Arabidopsis* for the growth responses to phosphate availability was investigated. Initially details of the effects of phosphate starvation for the four currently used accessions Cvi, Col, Ler and Ws were compared. A set of 10 growth parameters, concerning the aerial part and the root system, was measured in both single-point and time-course experiments. The length of the primary root and the number of laterals were found to be consistently reduced by phosphate starvation in all four accessions. These two robust parameters were selected to further screen a set of 73 accessions originating from a wide range of habitats. One-half of the accessions showed also a reduced primary root and less lateral roots when phosphate-starved, and 25% were not responsive to phosphate availability. For the last quarter of accessions, phosphate starvation was found to affect only one of the two growth parameters, indicating the occurrence of different adaptative strategies. These accessions appear to offer new tools to investigate the molecular basis of the corresponding growth responses to phosphate availability.

Key-words: *Arabidopsis*; accessions; natural variation; phosphate availability; root system architecture.

INTRODUCTION

Re-orientation of growth constitutes one of the main adaptative responses of plants to changes in nutrient availability. For numerous plant species, this leads to an increased growth of roots relative to the aerial part. As a general consequence, large alterations of the root system architecture are observed (Drew 1975), although different kinds of modifications occur depending on the nature of the limiting nutrient and on the plant species. Changes reported in *Arabidopsis* concern, for instance, the growth of the primary root in phosphate-starved plants (Williamson *et al*. 2001), the growth of lateral roots in nitrate-, phosphate- or iron-starved plants (Moog *et al*. 1995; Zhang & Forde 1998; Williamson *et al*. 2001), the density of lateral roots in phosphate- or iron-starved plants (Moog *et al*. 1995; Williamson *et al*. 2001), or the formation of root hairs in phosphate- or iron-starved plants (Bate & Lynch 1996; Schmidt & Schikora 2001), whereas phosphate starvation promotes the formation of proteoid roots in *Lupinus albus* (Johnson, Carroll & Allan 1996), or affects the growth angle of roots in *Phaseolus vulgaris* (Bonser, Lynch & Snapp 1996) while simultaneously altering the growth and density of lateral roots (Borch *et al*. 1999).

Up to now, the search for the genes controlling such growth responses to nutrient availability was based mainly on genetic studies of mutants. In *Arabidopsis*, an important success was the discovery of the MADS box transcription factor *ANR1*, involved in the adaptative increase in lateral root elongation in nitrate-rich regions (Zhang & Forde 1998). Selective involvement of hormones in the growth responses to nitrate, phosphate and iron availability was also demonstrated from the behaviour of mutants affected in their sensitivity to specific hormones (Schmidt & Schikora 2001; Williamson *et al*. 2001; Linkohr *et al*. 2002; Lopez-Bucio *et al*. 2002; Al-Ghazi *et al*. 2003). On another hand, relatively little attention was paid to the variation occurring naturally among accessions as an alternative way to search for genes having large effects in growth responses (Alonso-Blanco & Koornneef 2000). A notable exception in *Arabidopsis* concerns the characterization of phosphate acquisition efficiency, a parameter which includes, among others, growth responses to phosphate availability (Narang, Bruene & Altmann 2000; Narang & Altmann 2001). In these studies quite large variations were observed between accessions. However, due to the limited number of accessions that were characterized, it was not possible to decide whether these variations corresponded to more or less pronounced responses among accessions, or revealed the occurrence of different adaptative strategies.

The present study was aimed at investigating the extent

Correspondence: Dr François Chevalier. Fax: +33 (0)467 525737; e-mail: chevalie@ensam.inra.fr

**Present address: Laboratoire de Protéomique; UR 1199, INRA; 2 place Viala, F-34060 Montpellier Cedex 1, France.*

of the biodiversity of growth responses to phosphate starvation in *Arabidopsis*, with the goal of identifying accessions showing contrasted responses and, eventually, different growth adaptative strategies. For this purpose, the behaviour of four accessions that are widely used in genetic studies was first characterized in details. Two of the growth parameters displaying the more robust responses to phosphate starvation were further selected, and measured among a set of 73 accessions originating from a wide range of habitats.

MATERIALS AND METHODS

Plant material

Arabidopsis thaliana accessions (Table 1) were progenies from NASC (http://nasc.nott.ac.uk) and provided by Dr Gerrit Beemster (Department of Plant Genetics, University of Gent, Belgium), with the exception of accession Ws-4 (obtained from INRA, Versailles, France).

Chemicals

$CaSO_4$, KH_2PO_4 and H_3Bo_3 were from Merck-Eurolab (Darmstadt, Germany); KNO_3, MES, $MnCl_2$ and $CuCl_2$ were from Sigma-Aldrich (St Louis, MO, USA); NaFe-EDTA and NH_4Mo were from Fluka (Buchs, Switzerland); Bactoagar was from Difco (Detroit, MI, USA). All other reagents were of analytical grade.

Plant culture

Seeds of each accession were first sterilized under stirring for 15 min in 20 mL of 50% (v/v) ethanol and 4% (w/v) bayrochlor® (Bayrol, Planegg, Germany) and then washed three times in 100% ethanol and three times in sterile H_2O. The sterile seeds were carefully sown on 12 cm × 12 cm Petri dishes (Greiner Bio-one, Frickenhausen, Germany) containing the culture medium (CM) and 1 mM KH_2PO_4 (termed below as 'normal culture medium'). The CM had the following composition: 0.5 mM $CaSO_4$, 2 mM KNO_3,

Table 1. Overview of the *Arabidopsis thaliana* accessions investigated. NASC numbering is given according to *http://nasc.nott.ac.uk*

Accession	Origin	NASC number	Accession	Origin	NASC number
Aa-0	Aua/Rhön, Germany	N935	In-0	Innsbruck, Austria	N1239
An-1	Antwerpen, Belgium	N945	Is-0	Isenburg, Germany	N1241
Bd-0	Berlin, Germany	N963	Jl-1	Jelinka, Czech Republic	N1249
Be-0	Bensheim, Germany	N965	Jm-0	Jamolice, Czech Republic	N1259
Bl-1	Bologna, Italy	N969	Kä-0	Kärnten, Austria	N1267
Bla-1	Blane, Spain	N971	Kil-0	Killean, England	N1271
Blh-1	Bulhary, Czech Republic	N1031	Kin-0	Kindalville, USA	N1273
Bs-1	Basel, Switzerland	N997	Kondara	Tajikistan	N916
Bur-0	Burren, Eire	N1029	Ler-1	Landsberg, Poland	N1642
C24	Coimbra, Portugal	N906	Ll-0	Llagostera, Spain	N1339
Ca-0	Camberg, Germany	N1061	Ma-0	Marburg, Germany	N1357
Can-0	Canary Islands	N1065	Mv-0	Martha's Vineyard, USA	N1387
Chi-0	Chisdra, Russia	N1073	Nd-0	Niederzenz, Germany	N1391
Co-0	Coimbra, Portugal	N1085	Nok-0	Noordwijk, Netherlands	N1399
Col-0	Landsberg, Poland	N1093	Nw-0	Neuweilnau, Germany	N1409
Col-4	Landsberg, Poland	N933	Ob-0	Oberursel, Germany	N1419
Ct-1	Catania, Italy	N1095	Per-1	Perm, Russia	N1445
Cvi-0	Cape Verdian Islands	N902	Pi-0	Pitztal/Tirol, Austria	N1455
Db-0	Dombachtal, Germany	N1101	Pla-0	Playa de Aro, Spain	N1459
Dijon	Dijon, France	N919	Pog-0	Point Grey, Canada	N1477
Dra-0	Drahonin, Czech Republic	N1117	Rak-2	Raksice, Czech Republic	N1485
Edi-0	Edinburgh, England	N1123	Rld-1	Netherlands	N913
Ei-2	Eifel, Germany	N1125	Rsch-0	Rschew, Russia	N1491
El-0	Ellershausen, Germany	N1135	S-96	Netherlands	N914
En-1	Enkheim, Germany	N1137	Sap-0	Slapy, Czech Republic	N1507
Er-0	Erlangen, Germany	N1143	Sav-0	Slavice, Czech Republic	N1515
Est	Estonia	N911	Stw-0	Stobowa, Russia	N1539
Fi-0	Frickhofen, Germany	N1157	Tsu-1	Tsu, Japan	N1640
Fr-2	Frankfurt, Germany	N1169	Ty-0	Taynuilt, England	N1573
Ga-0	Gabelstein, Germany	N1181	Wc-1	Westercelle, Germany	N1589
Gd-1	Gudow, Germany	N1185	Wei-0	Weiningen, Switzerland	N3110
Gö-0	Göttingen, Germany	N1195	Wil-1	Wilna, Russia	N1595
Gr-1	Graz, Austria	N1199	Ws-0	Wassilewskija, Russia	N1603
Gü-0	Gückingen, Germany	N1213	Ws-1	Wassilewskija, Russia	N2223
Gy-0	La Miniere, France	N1217	Ws-4	Wassilewskija, Russia	N5390
Ha-0	Hannover, Germany	N1219	Wt-4	Wietze, Germany	N1610
Hl-0	Holtensen, Germany	N1229			

0.5 mM $MgCl_2$, 50 μM NaFe-EDTA, 2.5 mM MES, 50 μM H_3Bo_3, 12 μM $MnCl_2$, 1 μM $CuCl_2$, 1 μM $ZnCl_2$, 30 nM NH_4Mo, Bactoagar 8 g L^{-1}, adjusted to pH 5.7 with 1 M KOH and autoclaved at 120 °C for 20 min. After sowing, the plates were cold-treated at 4 °C for 24 h and subsequently placed in a near vertical position in a culture room: 20 °C, 70% relative humidity, 16 h light (250 μmol m^{-2} s^{-1}) using high pressure sodium lamps (Vialox® Nav-T 400 Super; Osram Ltd, Langley, Berkshire, UK) and metallic halogens lamps (Powerstar® HQI-BT 400 D; Osram Ltd). At day 6, the plantlets were either maintained under normal culture conditions, by transfer into Petri dishes containing CM and 1 mM KH_2PO_4, or phosphate-deprived, by transfer into Petri dishes containing CM supplemented with 1 mM KCl. For phosphate-deprived plants, it should be pointed out that, due to the slight phosphate content of Bactoagar, the CM contained approximately 1 μM phosphate. Accordingly, this medium will hereafter be termed 'low-phosphate medium'. The Petri dished were scanned daily using a flat-bed scanner (300 dpi).

Measurement of growth parameters

Images corresponding to different growth times (T) were analysed using Optimas® software version 6.1 (Media Cybernetics, Silver Spring, MD, USA). The projected leaf area (A_L) and the total root length (L_{TR}) were automatically detected on the corresponding region of the picture. The primary root length (L_{PR}), the branched zone length (L_{BZ}) and the lateral root number (N_{LR}) were manually determined.

Data were then exported to a spreadsheet to calculate additional parameters: the total lateral root length (L_{LR}): $L_{LR} = L_{TR} - L_{PR}$; the lateral root density (D_{LR}): $D_{LR} = N_{LR}/L_{PR}$; the mean distance between lateral roots (DI_{LR}): $DI_{LR} = L_{BZ}/N_{LR}$; the primary root growth rate (GR_{PR}): $GR_{PR} = \Delta L_{PR}/\Delta T$; and the average lateral root growth rate (GR_{LR}): $GR_{LR} = \Delta L_{LR}/\Delta T$. All parameters corresponded to the mean value from seven plants.

Statistical analysis

All results were statistically analysed using the Statistica® software (Statsoft, Tulsa, OK, USA). For the analysis of variance, two and three factor analysis of variance (ANOVA) with a LSD *post-hoc* test were used for assessing differences ($P = 0.05$), respectively, at day 14 (A_L, L_{TR}, L_{PR}, L_{LR}, L_{BZ}, N_{LR}, D_{LR} and DI_{LR}) and in temporal analysis (GR_{PR}, GR_{LR} and N_{LR}).

RESULTS

Current accessions display different architectures and variations in their response to phosphate availability

Previous work about the effects of phosphate availability on *Arabidopsis* growth parameters concerned mainly the architecture of the root system (Williamson *et al*. 2001; Linkohr *et al*. 2002; Lopez-Bucio *et al*. 2002; Al-Ghazi *et al*. 2003) and was nearly exclusively performed using the *Columbia* accession. In order to delineate those effects of general importance in *Arabidopsis*, we first selected a small subset of accessions (Col, Cvi, Ler and Ws) that are widely used to generate mutant collections or RILs. Figure 1 compares 2-week-old-plantlets from the four accessions Cvi-0, Col-4, Ler-1 and Ws-1, when cultured under normal medium (1 mM phosphate) or low-phosphate medium (1 μM). Quite large differences in the architecture of the root system can be seen (Fig. 1). In addition, a low phosphate availability seemed to induce contrasting responses between accessions (Fig. 1).

The distribution of growth between roots and leaves (Fig. 2, left), and the effects of phosphate availability on this distribution (Fig. 2, right), were first investigated by

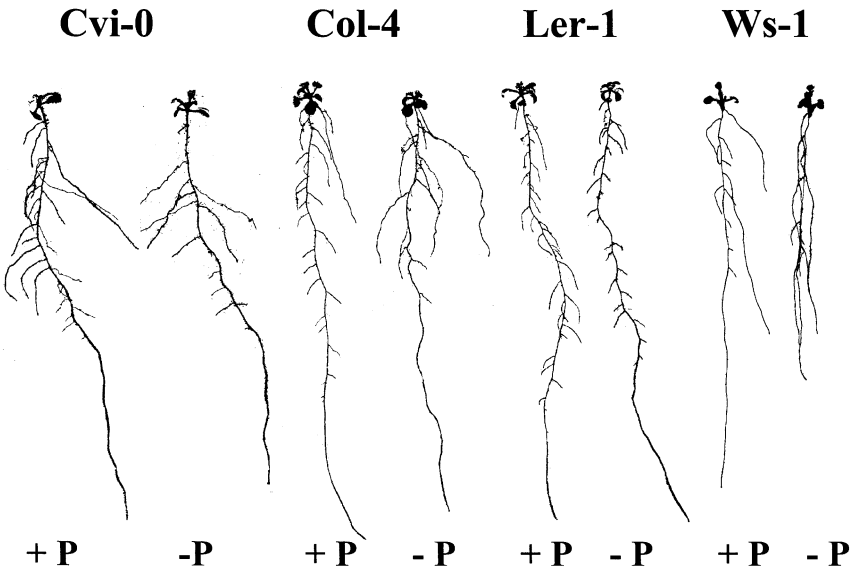

Figure 1. Root system architecture of current *Arabidopsis* accessions. Plants were grown for 2 weeks either on normal culture medium (+ P, 1 mM phosphate) or on low-phosphate medium (– P, 1 μM phosphate).

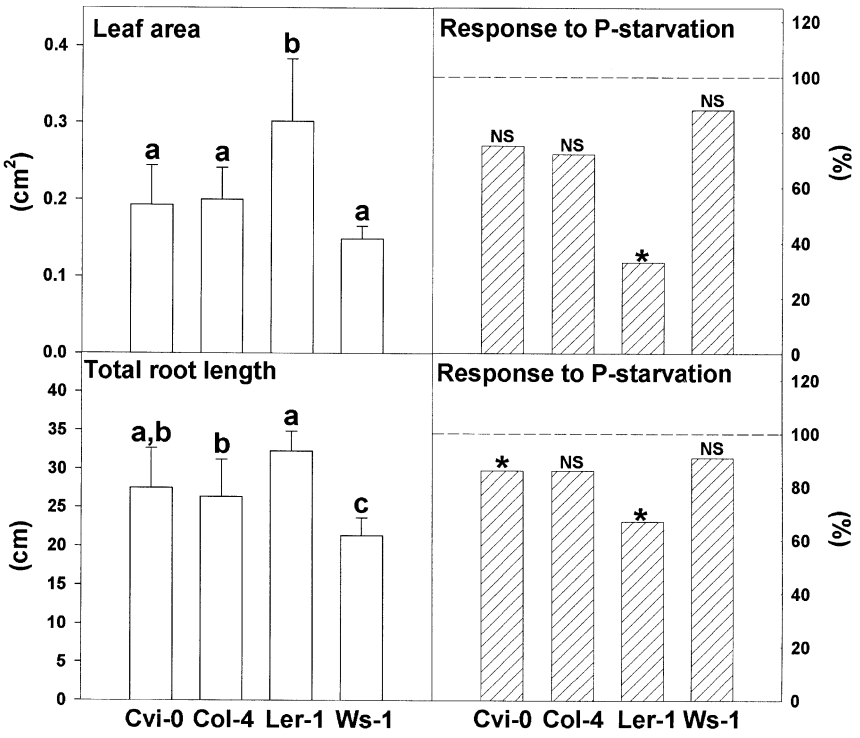

Figure 2. Effects of phosphate availability on plant growth. The relative leaf area and total root length were measured at day 14. Left: parameters values for control plants cultured on normal culture medium; letters and errors bars represent groups that differed significantly and confidence intervals ($P = 0.05$), respectively. Right: changes induced by P-starvation, normalized to the corresponding control; non-significant (NS) and significant (*) responses at $P = 0.05$. All results were the average value from seven seedlings.

global image analysis of the plants. In terms of leaf area (Fig. 2, top), the four accessions were found to fall into two groups: accessions Cvi-0, Col-4 and Ws-1 showed similar leaf area ($A_L \sim 0.18$ cm^2 at day 14), which was significantly smaller than that of Ler-1 ($A_L \sim 0.3$ cm^2) when grown in normal medium. At the same time, only this latter was significantly affected by P availability, and the projected leaf area decreased by 60% in phosphate-starved Ler-1. A slightly more complex pattern was observed under normal conditions concerning the total length of the root system (Fig. 2, bottom). In this case, differences were observed between accessions Col-4, Ler-1 and Ws-1, but Cvi-0 differed significantly only from Ws-1. However, when the plants were grown in low-phosphate medium, a significant decrease in the total root length was only observed with accessions Cvi-0 and Ler-1.

Detailed characterization of growth in 2-week-old current accessions

Taken together, the observations above suggested that more natural variation was to be expected in root development than in leaf growth. In order to get more details concerning variations in root growth, the total root length was decomposed into three parameters: the primary root length, the total lateral root length and the length of the branched zone (Fig. 3). Primary root length was a highly consistent parameter, showing only little variability (Fig. 3, top panel). Accordingly, although extreme values differed by less than 20% ($L_{PR} \sim 9.6$ cm for Cvi-0 and Ws-1 and ~11.2 cm for Ler-1), significant differences were detected between accessions Cvi-0 and Ws-1 and the two others, as well as between Col-4 and Ler-1. For all accessions, phosphate starvation significantly reduced the length of the primary root; the highest effect (44%) concerning the Ws-1 accession. Very similar features (Fig. 3, middle panel) were observed for the length of the branched zone, whatever the culture conditions used (the length of the branched zone accounted to about 50–60% of the primary root length for plants cultured under normal conditions, and was reduced by 20–35% in phosphate-starved plants). By contrast, the total length of lateral roots showed both large differences between accessions (ranging between ~12 cm for Ws-1 and ~21 cm for Ler-1, at day 14) and a relatively complex distribution (Fig. 3, bottom panel). Accessions Cvi-0 and Col-4 displayed similar behaviour, Cvi-0 being in addition not discernable from Ler-1. On the other hand, Ws-1 had shorter lateral roots. However, for most accessions, P-starvation had no significant effect on the lateral root length. The only exception concerned Ler-1 in which L_{LR} for P-starved plantlets was nearly half that of control.

In addition to length parameters, another crucial feature of the root system architecture concerns the distribution of lateral roots along the primary root. This was investigated by measuring the number of lateral roots and further calculating their density and the mean distance between lateral roots. It was found that the number of lateral roots at day 14 displayed up to a two-fold variation between accessions (Fig. 4, top panel). Moreover, both the number of lateral roots and the lateral root density distinguished two accessions from the two others (Fig. 4, top and middle panels), and phosphate starvation promoted a significant decrease in both the number and density of laterals for most accessions. By contrast, the

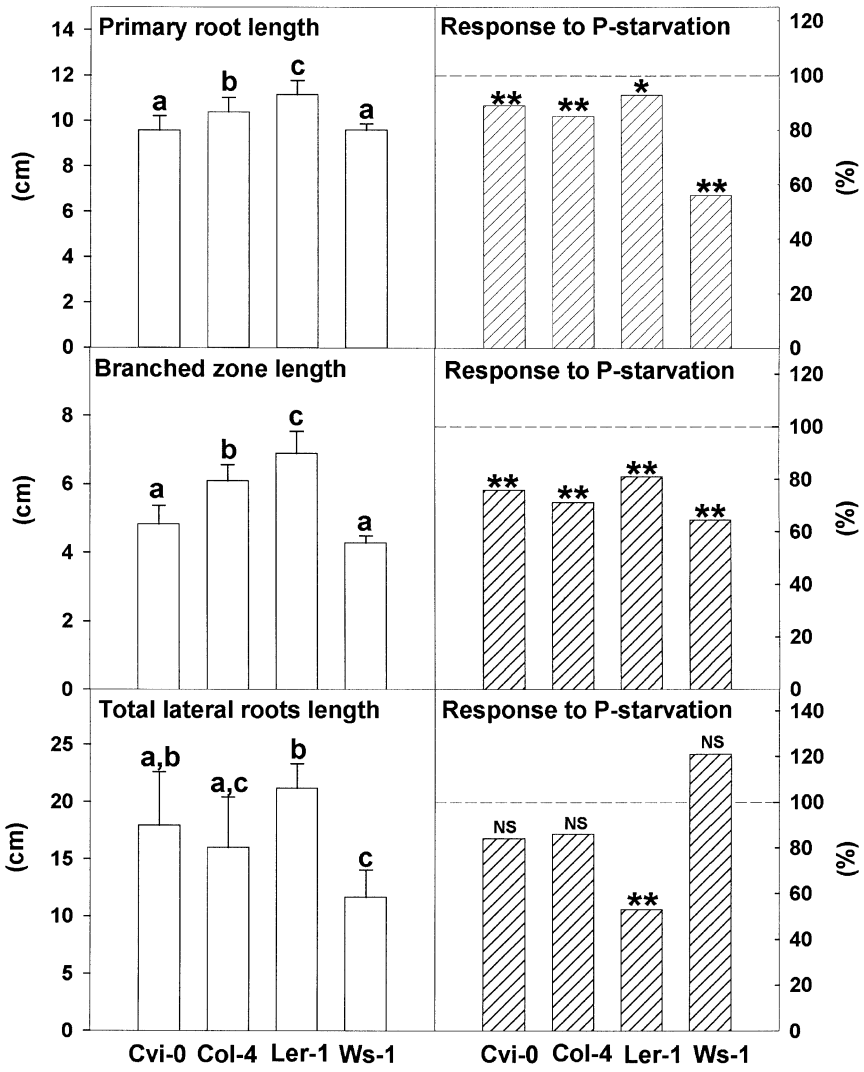

Figure 3. Effects of phosphate availability on root length parameters. The primary roots length, total lateral root length and branched zone length were measured at day 14. Left: parameters values for control plants cultured on normal culture medium; letters and errors bars represent groups that differed significantly and confidence intervals ($P = 0.05$), respectively. Right: changes induced by P-starvation, normalized to the corresponding control; non-significant (NS) and significant (*) responses at $P = 0.05$; highly significant (**) responses ($P = 0.01$). All results were the average value from seven seedlings.

mean distance between lateral roots was very accession-dependent and remained unaffected by phosphate starvation (Fig. 4, bottom panel).

Effect of phosphate availability on time-related growth parameters

The results above suggested that, for 2-week-old plantlets, length parameters for the primary root and the number of lateral roots strongly discriminated the four accessions, especially with respect to the effects of phosphate availability. However, it can not be excluded that variations in the overall plant development rate could occur between accessions and this would affect the simple comparison of plantlets at only one age. Therefore, a complementary analysis was performed on a temporal basis. In a first step, markers for development were researched on plants grown under normal condition by calculating the time required for arbitrarily selected parameters, such as a 4-cm length for the primary root or the emission of five lateral roots (Fig. 5). In both cases, significant differences were observed, Ler-1 showing the fastest development and Ws-1 the slowest one. Therefore, a more detailed analysis was performed from day 7 on, using plants grown up to that time on normal medium. When maintained under normal conditions, all the accessions displayed changes with time in the growth rate of the primary root (Fig. 6, full symbols). With the exception of Col-4, they elongated first with a continuously increased growth rate. In addition, at the end of the period, all accessions slowed their elongation, this event occurring earlier for Ler-1. This biphasic behaviour disappeared in the low-phosphate medium, with the exception of Ler-1 (Fig. 6, open symbols), whereas the three other accessions showed highly significant differences in their time-course of elongation. Completely different features were observed for the elongation of lateral roots (Fig. 7). In this case, elongation rates displayed no decrease with time (Fig. 7, full symbols). In addition, they were less sensitive to phosphate availability and a significant effect of phosphate availability on the time-course of elongation was observed only for Ler-1 (Fig. 7, open symbols).

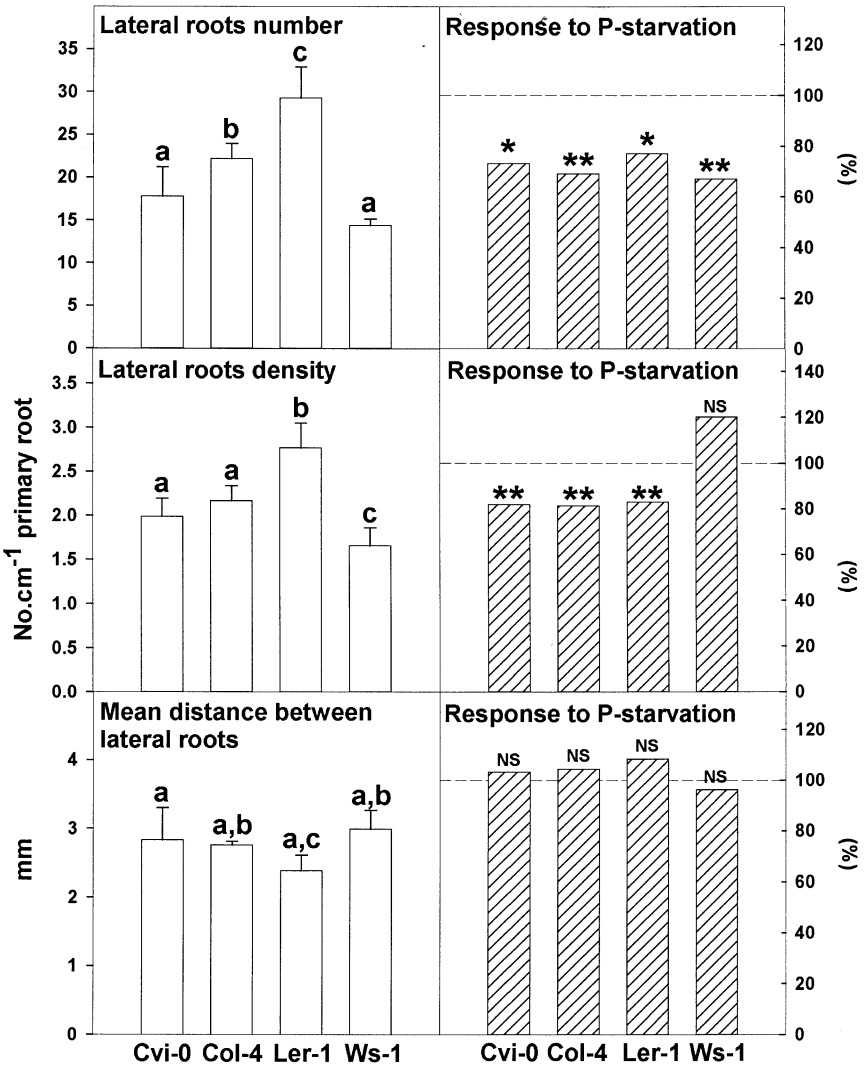

Figure 4. Effects of phosphate availability on lateral root parameters. The lateral root number, lateral roots density and mean distance between lateral roots were measured at day 14. Left: parameters values for control plants cultured on normal culture medium; letters and errors bars represent groups that differed significantly and confidence intervals ($P = 0.05$), respectively. Right: changes induced by P-starvation, normalized to the corresponding control; non-significant (NS) and significant (*) responses at $P = 0.05$; highly significant (**) responses ($P = 0.01$). All results were the average value from seven seedlings.

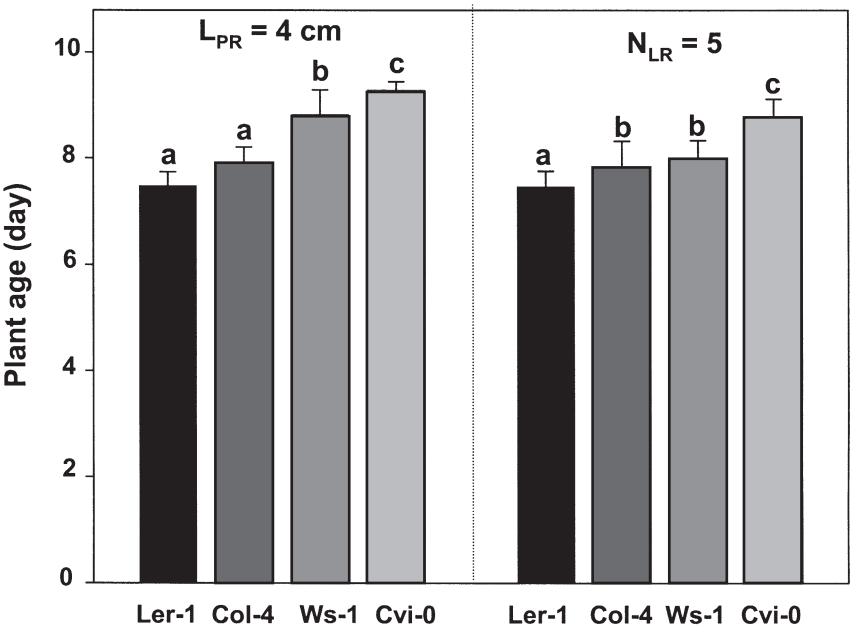

Figure 5. Effects of natural variation between accessions on markers of the rate of development. Developmental markers were estimated by calculating the time required to observe a 4-cm primary root (left) and five lateral roots (right). Letters and errors bars represent groups that differed significantly and confidence intervals ($P = 0.05$), respectively. All results were the average value from seven seedlings.

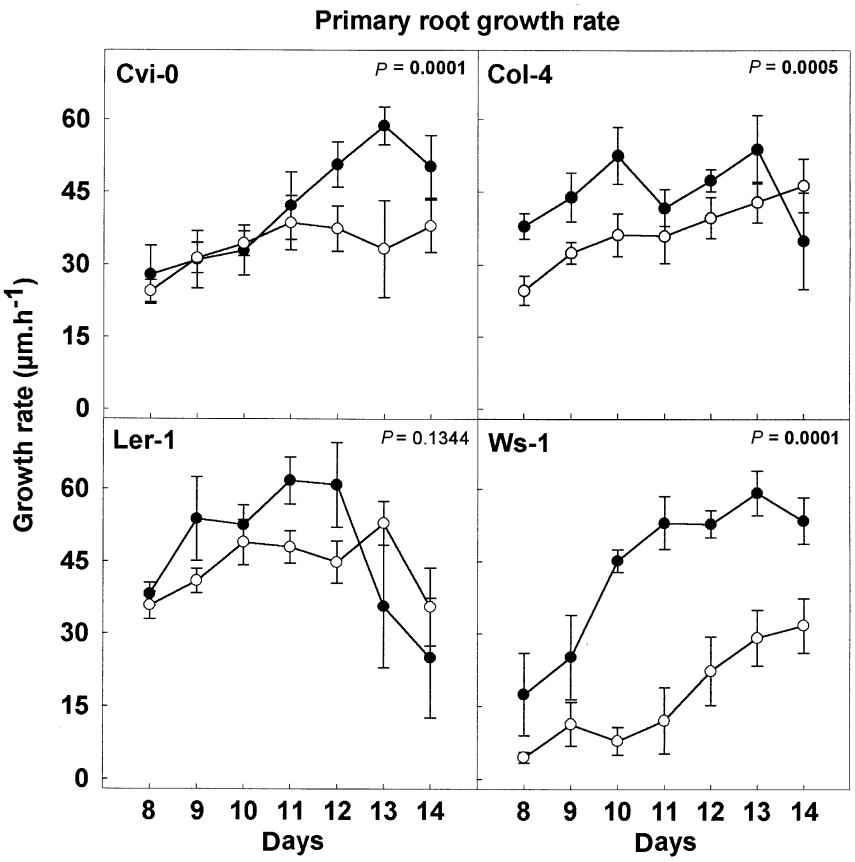

Figure 6. Effects of phosphate availability on the primary root growth rate. Plants were grown either on normal culture medium (full symbols) or on low-phosphate medium (open symbols). All results were the average value (± SD) from seven seedlings ($P = 0.05$). The probability for a difference between the entire time-courses are at the right top of each panel, and shown in bold for significant differences.

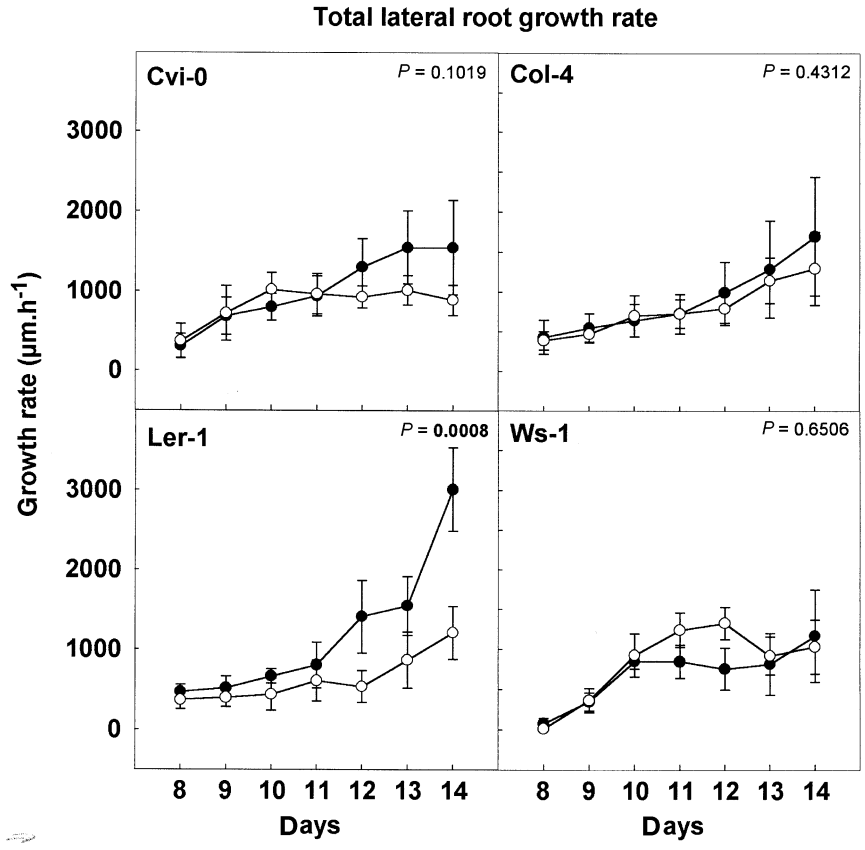

Figure 7. Effects of phosphate availability on the average lateral root growth rate. Plants were grown either on normal culture medium (full symbols) or on low-phosphate medium (open symbols). All results were the average value (± SD) from seven seedlings ($P = 0.05$). The probability for a difference between the entire time-courses are at the right top of each panel, and shown in bold for significant differences.

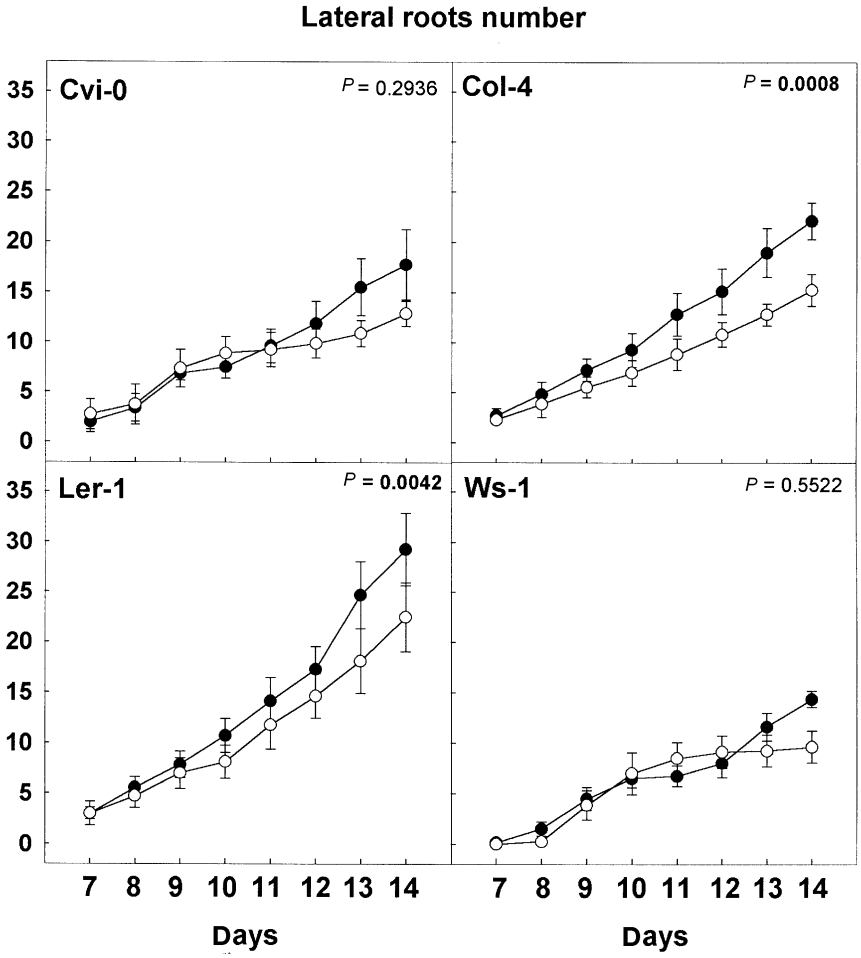

Figure 8. Effects of phosphate availability on lateral root production. Plants were grown either on normal culture medium (full symbols) or on low-phosphate medium (open symbols). All results were the average value (± SD) from seven seedlings ($P = 0.05$). The probability for a difference between the entire time-courses are at the right top of each panel, and shown in bold for significant differences.

A similar characterization was made concerning the evolution of the number of lateral roots with time (Fig. 8). For all four accessions, this number was found to increase nearly linearly with time, suggesting that the production rate of lateral roots was almost constant over the analysed period (Fig. 8, full symbols). In addition, the corresponding time-courses were affected by phosphate availability only for Ler-1 and Col-4 (Fig. 8, open symbols), suggesting a lowering of the production rate of lateral roots in the low-phosphate medium.

Large-scale comparison between accessions

Taken together, the time-based results above confirmed that, generally speaking, more pronounced responses to phosphate availability were observed at the level of primary roots in comparison with the lateral roots. Simultaneously, both the opposite behaviour of Ler-1 for the elongation rates and the contrasted responses in terms of production rates of lateral roots suggested that different adaptative strategies could be found among accessions. In order to obtain further insights concerning this hypothesis, a large-scale comparison was undertaken between available accessions, on the basis of the two parameters showing the most robust response to phosphate availability, the primary root length and the lateral root number. For this purpose, a set of 73 accessions originating from a wide range of habitats was selected (Table 1).

After 2-week culture, 50% of the accessions were found to show both a decrease in the length of primary roots and a reduced number of lateral roots in response to phosphate starvation, similarly to the four previous accessions (Fig. 9, full circles). Within this group, the greatest effect was observed for the accession Er-0 in which P starvation promoted a more than two-fold reduction of each parameter. This group contained in addition the commonly used Col-0 accession. However, one-quarter of the accessions did not appear to be sensitive to phosphate availability (Fig. 9, open circles). On the other hand, the low-phosphate medium only affected some accessions for one of the two parameters (Fig. 9, grey symbols), either the length of primary roots (16% of accessions) or the number of lateral roots (9% of accessions). Extreme behaviours within this group were displayed by accessions Rld-1 and Be-0 which, in response to low phosphate availability, only decreased either the length of the primary root or the number of lateral roots. Moreover, among this latter group, two acces-

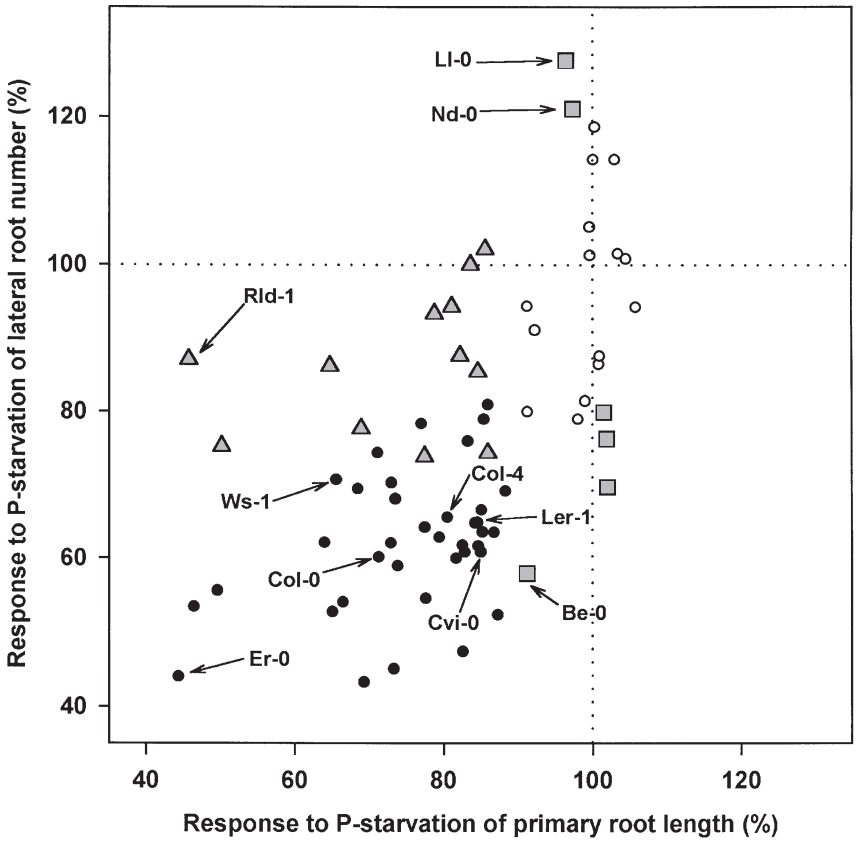

Figure 9. Variations in the phosphate effects between accessions. The effects of phosphate starvation on the length of the primary root and the number of lateral roots were measured for 73 *Arabidopsis* accessions at day 14, and normalized to the corresponding values under control conditions. Full and open circle symbols represent accessions showing significant and non-significant responses, respectively, for both parameters ($P = 0.05$). Grey symbols represent accessions showing a significant response for only one of the two parameters (triangles, primary root length; squares, lateral root number). Accession numbers refer to Table 1.

sions (Ll-0 and Nd-0) displayed statistically significant but opposite responses in terms of lateral root number, namely an over-production of lateral roots in response to P-limitation. The root system architecture of these latter accessions is illustrated in Fig. 10.

DISCUSSION

In recent years, a renewed interest in understanding of the growth responses to phosphate availability has emerged, using the model plant *Arabidopsis*, particularly at the level

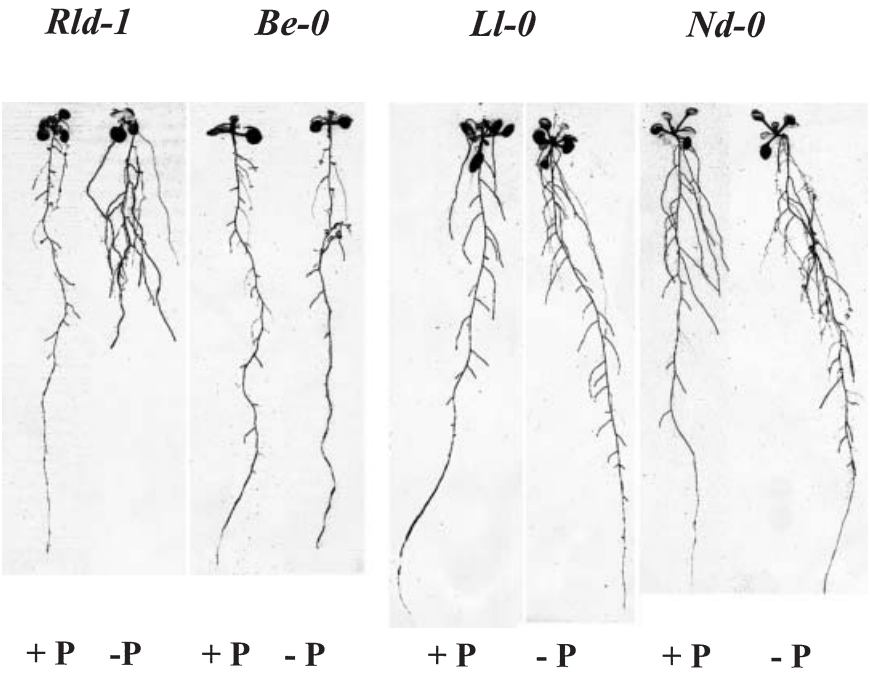

Figure 10. Contrasted strategies for the adaptation of the root system architecture to phosphate availability. Plants were grown as in Fig. 1, either on normal culture medium (+ P, 1 mM phosphate) or on low-phosphate medium (– P, 1 μM phosphate). Accession numbers refer to Table 1 and Fig. 8.

of hormone signalling (Schmidt & Schikora 2001; Williamson *et al*. 2001; Linkohr *et al*. 2002; Lopez-Bucio *et al*. 2002; Al-Ghazi *et al*. 2003). These studies have taken advantage of both the availability of various mutants and of improvements in non-invasive image acquisition and analysis devices, allowing refined quantitative characterization of the effects of phosphate on plant growth, and particularly on the root system architecture. Nevertheless, in some cases, contradictory results were reported. For instance, phosphate starvation was claimed either to reduce or to increase the number of lateral roots. The origin of such discrepancies is not clear. One tentative explanation is that different accessions could display different adaptative strategies in terms of growth responses to phosphate availability. In the present study, in order to assess this working hypothesis, we decided to compare the effects of phosphate starvation on various *Arabidopsis* accessions. As no growth parameter could be chosen a *priori* to screen the accessions, due to the discrepancies between available results, a three-step strategy was selected. First, the growth of a small number of accessions was characterized in detail. These data were then analysed in order to identify those growth parameters displaying the more discriminant responses to phosphate starvation. Finally a large set of accessions was screened using this limited number of robust parameters. For the first step, we selected the four accessions Cvi-0, Col-4, Ler-1 and Ws-1 because they corresponded to accessions previously selected to generate both recombinant inbred lines (Lister & Dean 1993; Alonso-Blanco *et al*. 1998; Alonso-Blanco & Koornneef 2000) and mutant collections (Bechtold, Ellis & Pelletier 1993; Martienssen 1998; Wisman *et al*. 1998; Tissier *et al*. 1999).

Currently used accessions display large and robust variations in root growth

Quite large variations among accessions concerning the plant size and the leaf number of the rosette have previously been reported in *Arabidopsis* (Karlsson, Sills & Nienhuis 1993; Li, Suzuki & Hara 1998), suggesting that variations could also be expected concerning the leaf surface. Here, by monitoring the growth of aerial parts from the projected leaf area, Ler-1 was indeed found to display a superior growth, but the three other accessions were indistinguishable. As previous parameters describing the growth of aerial parts have been shown to be very sensitive to environmental factors (Karlsson *et al*. 1993), this suggests that our *in vitro* culture conditions would trigger weak variations concerning leaves. Therefore, more attention was given to characterize the root growth in greater detail.

By contrast, much more variation was observed concerning the root system. For the primary root, the two accessions Ws-1 and Cvi-0 showed similar length but differed from both Col-4 and Ler-1. More generally, each of the four length parameters (L_{TR}, L_{PR}, L_{LR} and L_{BZ}) classified the accessions into three significantly different groups, the grouping of accessions depending in addition on the parameters. Similarly, all three parameters used to describe the contribution of lateral roots to the root system architecture (N_{LR}, D_{LR} and DI_{LR}) also classified the accessions into three other significantly different groups. Furthermore, when looking at growth rate parameters, three kinds of time-course were observed, both for the primary root and total lateral roots. As the parameters included both raw data and derived traits, it is important to note that these variations emerged from all the independently measured parameters (L_{TR}, L_{PR}, L_{BZ} and N_{LR}), indicating an intrinsic diversity. Previous work has already pointed to such variations when considering different accessions. For instance, Krannitz, Aarssen & Lefebvre (1991) compared 25 accessions and showed that the total root length differed by up to 70%, whereas Lopez-Bucio *et al*. 2002) reported smaller differences among four accessions. Therefore, the 50% variation quoted here among four accessions, is in quite good agreement with published data, allowing for the differences in culture conditions. Similar conclusions can be derived for other parameters (such as the primary root, lateral root lengths or lateral root density) from comparisons with the data of Lopez-Bucio *et al*. 2002). Finally, in time-course studies, Beemster *et al*. (2002) demonstrated the occurrence of very large variations for the elongation rate of the primary root (up to 370% at day 9, among a set of 18 accessions grown under continuous light and in the presence of sucrose). In the present work, in which the plants experienced a photoperiod and the medium lacked sucrose, variations below 120% were observed at day 9, but this ratio increased to 380% later on. Therefore, the fact that, although performed under different environmental conditions, all of these studies still led to similar conclusions suggests that the occurrence of very large variations in both the growth and architecture of the root system constitutes a robust response among *Arabidopsis* accessions, in contrast to that observed for leaf growth. In addition, the accessions selected here to illustrate currently used accessions appeared to be also easily distinguishable with respect to root-related features.

Phosphate availability consistently affects the length of the primary root and the number of lateral roots in all the currently used accessions

The effects of phosphate availability were investigated by comparing plants cultured on a sufficient medium (1 mM phosphate) with plants grown on a low-phosphate medium (approximately 1 μM phosphate). According to phosphate availability, very little variation between accessions was observed for global parameters such as total leaf area or total root length, although, for the four accessions studied, the root length seemed to be more subject to variation than the leaf area. Much more variation emerged when looking at more specific root parameters. For the four accessions, both the length of the primary root, the length of the branched zone and the number of lateral roots were found to be significantly reduced in low-phosphate medium. On the other hand, the time-course of elongation

was affected by phosphate for three of the four accessions in the case of the primary root, but only Ler-1 was sensitive to phosphate level in terms of both total lateral root length and their time-course of elongation. As the total length of lateral roots constitutes an average parameter, it can not be ruled out that significant responses might be observed when measuring the length of individual roots, thus taking into account a possible role of root age. In addition, as the accessions were shown to differ in their overall rate of development, the response to phosphate availability might also simply reflect such differences. However, although both Ler-1 and Col-4 displayed similar and fast growth for the primary root, only Col-4 showed a time-course response that was sensitive to phosphate. A similar disconnection between intrinsic development features and the effect of phosphate availability on time-course responses was observed for the lateral root production rate. Therefore, taken together, all the observations above suggest that the parameters related to the length of the primary root and to the number of lateral roots are among the most discriminant parameters concerning the response to phosphate availability. These conclusions are in full agreement with those from all the previously published studies demonstrating that phosphate starvation reduces the length of the primary root (Williamson *et al*. 2001; Linkohr *et al*. 2002; Lopez-Bucio *et al*. 2002; Al-Ghazi *et al*. 2003). A reduction in the number of lateral roots in low-phosphate medium was also shown in most previous studies (Williamson *et al*. 2001; Linkohr *et al*. 2002; Al-Ghazi *et al*. 2003) with the exception of that by Lopez-Bucio *et al*. (2002).

As, in addition, the measurement of the two parameters L_{PR} and N_{LR} is straightforward and easier to achieve than that of other parameters that also appeared to be sensitive to phosphate availability in all or most accessions, such as the length of the branched zone or the density of lateral roots, L_{PR} and N_{LR} were further selected to screen the behaviour of a large collection of accessions with respect to phosphate availability. In terms of screening strategy, it could be pointed out that the choice to select very discriminant parameters might limit the observation of variations between accessions, and that less stringent parameters could lead to evidence of other variations. In this view, it can not be excluded that other accessions than those identified here could constitute privileged material with which to further investigate the molecular basis of adaptative responses to phosphate starvation. Finally, it should be also emphasized that, for the four accessions cultured under normal medium, a very strong correlation (with coefficients ranging between 0.96 and 0.99) could be calculated between the primary root length and the number of lateral roots. Therefore, the use of two possibly linked parameters could be hypothesized a *priori* to introduce a bias. The subsequent observation that, for one-quarter of the analysed accessions, only one of the two parameters was affected by phosphate starvation suggests that the number of lateral roots is probably not directly linked to the length of the primary root.

Not all accessions display the same adaptative strategy according to phosphate availability

In order to assess the variation between accessions on a larger scale, we selected a set of 73 accessions originating from 18 countries, corresponding mostly to European and American continental stations, in addition to four insular stations. Large amplitudes of variations, by factors of 2.4 and 2.9 for the effects on the primary root length and lateral root number, respectively, were observed for the two measured parameters in response to phosphate availability. In addition, half the accessions displayed the same behaviour as the currently used accessions above, showing that the simultaneous reduction of the growth of the primary root and of the number of lateral roots constitutes a main adaptative response to phosphate starvation in *Arabidopsis*. Interestingly, other accessions showed only one of the two responses. Furthermore, some accessions showed an inverse response. In this way, phosphate starvation appears capable of having either null or negative effects on the primary root, whereas it can have either null, negative or positive effects on the lateral root number. In terms of regulation, these results together suggest that the control of root growth by phosphate availability is not linked to that of branching, although both pathways are likely to share some initial signalling steps. Finally, no clear correlation was found between the geographical origin of accessions and their behaviour.

Up to now, current approaches to elucidate the molecular basis for phenotypic plasticity relied almost exclusively on the search for mutants not displaying the wild-type adaptative response. It can be emphasized that the characterization of clear-cut differential responses between accessions has the capacity to open new routes for the identification of both large-effect genes and favourable allelic variations (Alonso-Blanco & Koornneef 2000). In this respect, several of the accessions studied here could constitute convenient parents to generate populations that would be suitable for the analysis of the developmental plasticity in response to phosphate availability.

ACKNOWLEDGMENTS

The authors are grateful to H. Baudot for valuable assistance. This work was supported by the EU research program *Quality of Life and Management of Living Resources (*contract QLK5-CT-2001–01871).

REFERENCES

Al-Ghazi Y., Muller B., Pinloche S., Tranbarger T.J., Nacry P., Rossignol M., Tardieu F. & Doumas P. (2003) Temporal responses of *Arabidopsis* root architecture to phosphate. starvation: evidences for the involvement of auxin signalling. *Plant, Cell & Environment* **26,** 1053–1066.

Alonso-Blanco C. & Koornneef M. (2000) Naturally occurring variation in *Arabidopsis*: an underexploited resource for plant genetics. *Trends in Plant Sciences* **5,** 22–29.

Alonso-Blanco C., Peeters A.J., Koornneef M., Lister C., Dean C.,

van den Bosch N., Pot J. & Kuiper M.T. (1998) Development of an AFLP based linkage map of L*er*, Col and Cvi *Arabidopsis thaliana* accessions and construction of a L*er*/Cvi recombinant inbred line population. *Plant Journal* **14,** 259–271.

Bates T.R. & Lynch J.P. (1996) Stimulation of root hair elongation in *Arabidopsis thaliana* by low phosphorus availability. *Plant, Cell and Environment* **19,** 529–538.

Bechtold N., Ellis J. & Pelletier G. (1993) *In planta Agrobacterium* mediated gene transfer by infiltration of adult *Arabidopsis thaliana* plants. *Comptes Rendus Academie des Sciences Paris* **316,** 1194–1199.

Beemster G.T., De Vusser K., De Tavernier E., De Bock K. & Inze D. (2002) Variation in growth rate between *Arabidopsis* accessions is correlated with cell division and A-type cyclin-dependent kinase activity. *Plant Physiology* **129,** 854–864.

Bonser A.M., Lynch J.P. & Snapp S. (1996) Effect of phosphorus deficiency on growth angle of basal roots in *Phaseolus vulgaris*. *New Phytologist* **132,** 281–288.

Borch K., Bouma T.J., Lynch J.P. & Brown K.M. (1999) Ethylene: a regulator of root architectural responses to soil phosphorus availability. *Plant, Cell and Environment* **22,** 425–431.

Drew M.C. (1975) Comparison of the effects of a localized supply of phosphate, nitrate, ammonium and potassium on the growth of seminal root system, and shoot, in barley. *New Phytologist* **75,** 479–490.

Johnson J.F., Carroll P.V. & Allan D.L. (1996) Phosphorus deficiency in *Lupinus albus*. *Plant Physiology* **112,** 31–41.

Karlsson B.H., Sills G.R. & Nienhuis J. (1993) Effects of photoperiod and vernalization on the number of leaves at flowering in 32 *Arabidopsis thaliana* (Brassicaceae) accessions. *American Journal of Botany* **80,** 646–648.

Krannitz P.G., Aarssen L.W. & Lefebvre D.D. (1991) Relationship between physiological and morphological attributes related to phosphate uptake in 25 genotypes of *Arabidopsis thaliana*. *Plant and Soil* **133,** 169–175.

Li B., Suzuki J.I. & Hara T. (1998) Latitudinal variation in plant size and relative growth rate in *Arabidopsis thaliana*. *Oecologia* **115,** 293–301.

Linkohr B.I., Williamson L.C., Fitter A.H. & Leyser H.M. (2002) Nitrate and phosphate availability and distribution have different effects on root system architecture of *Arabidopsis*. *Plant Journal* **29,** 751–760.

Lister C. & Dean C. (1993) Recombinant inbred lines for mapping RFLP and phenotypic markers in *Arabidopsis thaliana*. *Plant Journal* **4,** 745–750.

Lopez-Bucio J., Hernandez-Abreu E., Sanchez-Calderon L., Nieto-Jacobo M.F., Simpson J. & Herrera-Estrella L. (2002) Phosphate availability alters architecture and causes changes in hormone sensitivity in the *Arabidopsis* root system. *Plant Physiology* **129,** 244–256.

Martienssen R. (1998) Functional genomics: probing plant gene function and expression with transposons. *Proceedings of the National Academy of Sciences of the USA* **95,** 2021–2026.

Moog P.R., van der Kooij T.A.W., Brüggemann W., Schiefelbein J.W. & Kuiper P.J.C. (1995) Responses to iron deficiency in *Arabidopsis thaliana*: the turbo iron reductase does not depend on the formation of root hairs and transfer cells. *Planta* **195,** 503–513.

Narang R.A. & Altmann T. (2001) Phosphate acquisition heterosis in *Arabidopsis thaliana*: a morphological and physiological analysis. *Plant and Soil* **234,** 91–97.

Narang R.A., Bruene A. & Altmann T. (2000) Analysis of phosphate acquisition efficiency in different *Arabidopsis* accessions. *Plant Physiology* **124,** 1786–1799.

Schmidt W. & Schikora A. (2001) Different pathways are involved in phosphate and iron stress-induced alterations of root epidermal cell development. *Plant Physiology* **125,** 2078–2084.

Tissier A.F., Marillonnet S., Klimyuk V., Patel K., Torres M.A., Murphy G. & Jones J.D. (1999) Multiple independent defective suppressor-mutator transposon insertions in *Arabidopsis*: a tool for functional genomics. *Plant Cell* **11,** 1841–1852.

Williamson L.C., Ribrioux S.P., Fitter A.H. & Leyser H.M. (2001) Phosphate availability regulates root system architecture in *Arabidopsis*. *Plant Physiology* **126,** 875–882.

Wisman E., Hartmann U., Sagasser M., Baumann E., Palme K., Hahlbrock K., Saedler H. & Weisshaar B. (1998) Knock-out mutants from an En-1 mutagenized *Arabidopsis thaliana* population generate phenylpropanoid biosynthesis phenotypes. *Proceedings of the National Academy of Sciences of the USA* **95,** 12432–12437.

Zhang H. & Forde B.G. (1998) An *Arabidopsis* MADS box gene that controls nutrient-induced changes in root architecture. *Science* **279,** 407–409.

Received 25 March 2003; received in revised form 3 July 2003; accepted for publication 3 July 2003

Proteomic investigation of natural variation between *Arabidopsis* ecotypes

François Chevalier, Olivier Martin, Valérie Rofidal, Anne-Dominique Devauchelle, Samuel Barteau, Nicolas Sommerer and Michel Rossignol

Laboratoire de Protéomique, INRA, Montpellier, France

Two-dimensional (2-D) gel electrophoresis and peptide mass fingerprinting were used to investigate the natural variation in the proteome among 8 *Arabidopsis thaliana* ecotypes, of which 3 were previously shown to display atypical responses to environmental stress. Comparison of 2-D maps demonstrated that only one-quarter of spots was shared by all accessions. On the other hand, only 15% of the 25 majors spots accounting for half the total protein amount could be classified as major spots in all ecotypes. Identification of these major spots demonstrated large differences between the major functions detected. Accordingly, the proteomes appeared to reveal important variations in terms of function between ecotypes. Hierarchical clustering of proteomes according to either the amount of all anonymous spots, that of the 25 major spots or the functions of these major spots identified the same classes of ecotypes, and grouped the three atypical ecotypes. It is proposed that proteome comparison has the capacity to evidence differences in the physiological status of ecotypes. Results are discussed with respect to the possibility to infer such differences from limited comparisons of major proteins. It is concluded that classical proteomics could constitute a powerful tool to mine the biodiversity between ecotypes of a single plant species.

Received	6/10/03
Revised	19/1/04
Accepted	21/1/04

Keywords: *Arabidopsis* ecotypes / Hierarchical clustering / Peptide mass fingerprinting / Two-dimensional gel electrophoresis

1 Introduction

Proteomics is becoming an essential field to investigate plant growth and evolution. Very early, the exploration of proteome was successfully used to characterize the relationships between populations [1–4]. In recent years, such approaches allowed the establishment of distances for instance between different species of the Brassicaceae family [5], various wheat cultivars [6], or oriental and American ginseng [7]. On the other hand, to date, little attention was paid to the natural variation occurring among plant ecotypes by opposition to recent works in animal field [8, 9]. However, biodiversity constitutes a high potential resource for searching genes of interest, as it is well established for the model plant *Arabidopsis thaliana* [10–12]. On this model, large differences between ecotypes were observed for a variety of features such as, for instance, light and hormone sensitivity [13], seed size [14], the light-dependent hypocotyls growth [15], or the growth rate [16]. In a previous study on *Arabidopsis* root system architecture, we recently demonstrated that, whereas a majority of ecotypes responds to phosphate starvation by decreasing both growth of the primary root and initiation of lateral roots, other ecotypes use only one of these responses [17].

The present work was undertaken to explore the potential of proteomics to investigate natural variation within *Arabidopsis* ecotypes. For this purpose we selected a small number of ecotypes encompassing the four ones most commonly used in genetic or genomic studies and a variant from one of them as a control for close genetic distance (all of the five displaying the major response to phosphate starvation), as well as three ecotypes showing alternative responses to phosphate

Correspondence: Dr. François Chevalier, UR 1199 – Laboratoire de Protéomique, INRA, 2 place Viala, F-34060 Montpellier Cedex 1, France
E-mail: chevalie@ensam.inra.fr
Fax: +33-4-9961-3014

Abbreviations: MP, major protein; **TGS**, Tris-Glycine – SDS buffer

starvation. Classical 2-DE and MALDI-TOF-MS were used to compare the distances between the proteomes of these ecotypes, with special emphasis to the proteins accounting for the majority of the protein amount in each ecotype.

2 Materials and methods

2.1 Plant material, culture conditions, and chemicals

Arabidopsis thaliana ecotypes Ws-1, Cvi-0, Col-0, Col-4, Ler-1, Be-0, and Ll-0 (Table 1) were progenies from NASC (http://nasc.nott.ac.uk). Plants were grown under hydroponic conditions [18] for 42 days before sample harvest. Urea, phosphoric acid, and acetic acid were from VWR (Fontenay-ss-Bois, France); CHAPS, Triton X-100, iodoacetamide, bromophenol blue and Comassie blue were from Sigma-Aldrich (St. Louis, MO, USA); glycerol, SDS, DTT, TGS, and Tris were from Euromedex (Mundolshein, France). IPG strips and buffer were from Amersham Biosciences (Buckinghamshire, UK), and acrylamide from Bio-Rad (Hercules, CA, USA).

Table 1. Origin of selected *Arabidopsis thaliana* ecotypes (http://nasc.nott.ac.uk)

Ecotype	NASC No.	Origin
Col-0	N1093	Columbia (USA)
Col-4	N933	Columbia (USA)
Be-0	N965	Bensheim (Germany)
Ll-0	N1339	Llagostera (Spain)
Rld-1	N 913	Netherlands (Koornneef group)
Cvi-0	N902	Cape Verdian Islands
Ws-1	N2223	Wassilewskija (Russia)
Ler-1	N1642	Landsberg (Poland)

2.2 Protein extraction

For each ecotype, one root sample corresponding to more than 150 root systems was grinded in liquid nitrogen, and the fine powder was mixed with 90% v/v acetone, 10% v/v TCA solution (100% w/v) and 0.07% v/v 2-mercaptoethanol. After incubation at −20°C for 30 min, insoluble material was pelleted at $42\,000 \times g$ with a TL 100 ultracentrifuge using a TLA 100.3 rotor (Beckman Coulter, Palo Alto, CA, USA). Pellets were washed three times with pure acetone containing 0.07% v/v 2-mercaptoethanol, air-dried, and solubilized in buffer containing 9 M urea, 4% w/v CHAPS, 0.05% v/v Triton X-100, and 65 mM DTT. Protein amount was estimated using the Bradford method. All manipulations were performed at 4°C.

2.3 Two-dimensional electrophoresis

For each ecotype sample, 2-DE was performed in triplicate from the same extract using 18 cm linear pH 4–7 IPG strips. 200 μg protein samples were supplemented with 0.5% v/v IPG buffer pH 4–7 and 0.002% w/v bromophenol blue. Strips were hydrated directly with protein solution. Isoelectric focusing was performed using an IPG-Phor device until 100 000 $kV \cdot h^{-1}$. Before the second dimension, the strips were reduced (50 mM Tris-HCl, pH 8.8, 6 M urea, 30% v/v glycerol, 2% w/v SDS, 130 mM DTT) and alkylated in the same buffer containing 130 mM iodoacetamide instead DTT for 15 min. Strips were then embedded using 0.6% w/v low-melt agarose in running buffer containing traces of bromophenol blue on the top of a 11% acrylamide gel. SDS-PAGE was carried out, using a 2-D electrophoresis DALT system, at 15 mA per gel overnight at 10°C. Gels were stained using colloidal Coomassie blue [19]. Images from stained gels were digitalized at 300 dpi with a GS 710 densitometer (Bio-Rad, Hercules, CA, USA) and analyzed using the Progenesis software (Nonlinear Dynamics, Newcastle upon Tyne, UK). Gel triplicates were matched to create an average gel with spots present at least on two of the three gels. Average gels corresponding to the different *Arabidopsis* ecotypes were compared and spots of interest were selected for subsequent protein identification by MALDI-TOF-MS analysis.

2.4 Protein identification by MALDI-TOF-MS

Spots were picked from preparative gels (500 μg proteins) using a spot picker robot (Perkin Elmer, Wellesley, MA, USA). Acrylamide pieces were collected in 96-well microplates with 50 μL acetic acid (1% v/v). Pieces of gel were then washed using a Multiprobe II robot (Perkin Elmer) in several steps with water, 25 mM ammonium carbonate, and acetonitrile. Proteins were digested with trypsin (12.5 μg/mL in 25 mM ammonium carbonate). Supernatants were mixed with equal volumes of matrix solution (α-cyano-4-hydroxycinnamic acid) and spotted onto targets. Peptide mass fingerprints were acquired using a Biflex III mass spectrometer (Bruker Daltonics, Bremen, Germany). Spectra were calibrated internally and annotated automatically. The MASCOT search engine software (Matrix Science, London, UK) was used to search NCBInr database. The following parameters were used for database search: mass tolerance of 100 ppm, a minimum of four matched peptides and one miscleavage allowed.

2.5 Data analysis

Protein amount in each spot was estimated from its volume after normalization with respect to the total volume of all spots detected in the gel. Euclidean or Manhattan

distances between protein amounts among ecotypes were further used to compute a similarity matrix between ecotypes [20]. For hierarchical clustering, aggregation was made using the Ward criteria [20].

3 Results

3.1 Comparison of 2-D protein maps from *Arabidopsis* ecotypes

The first goal of this work was to evaluate the capacity of classical proteomics as a molecular tool to characterize the natural biodiversity in *Arabidopsis thaliana*. Therefore, eight different ecotypes (Table 1), originating from contrasted habitats and previously shown to display different developmental strategies [17] were selected, and root soluble protein extracts were separated by 2-DE. Based on preliminary work, 18 cm IPG (pH 4–7) and a second dimension covering the 15–150 kDa range were used to get large insights into the proteomes of these ecotypes. In order to obtain an information as quantitative as possible, gels were stained with colloidal Coomassie blue. Triplicate gels were first matched to create an average gel containing those spots observed at least two times among the three gels; thereafter, average gels from the different ecotypes were matched using the ecotype Col-0 as reference (Fig. 1). Over an average of *ca.* 250 spots

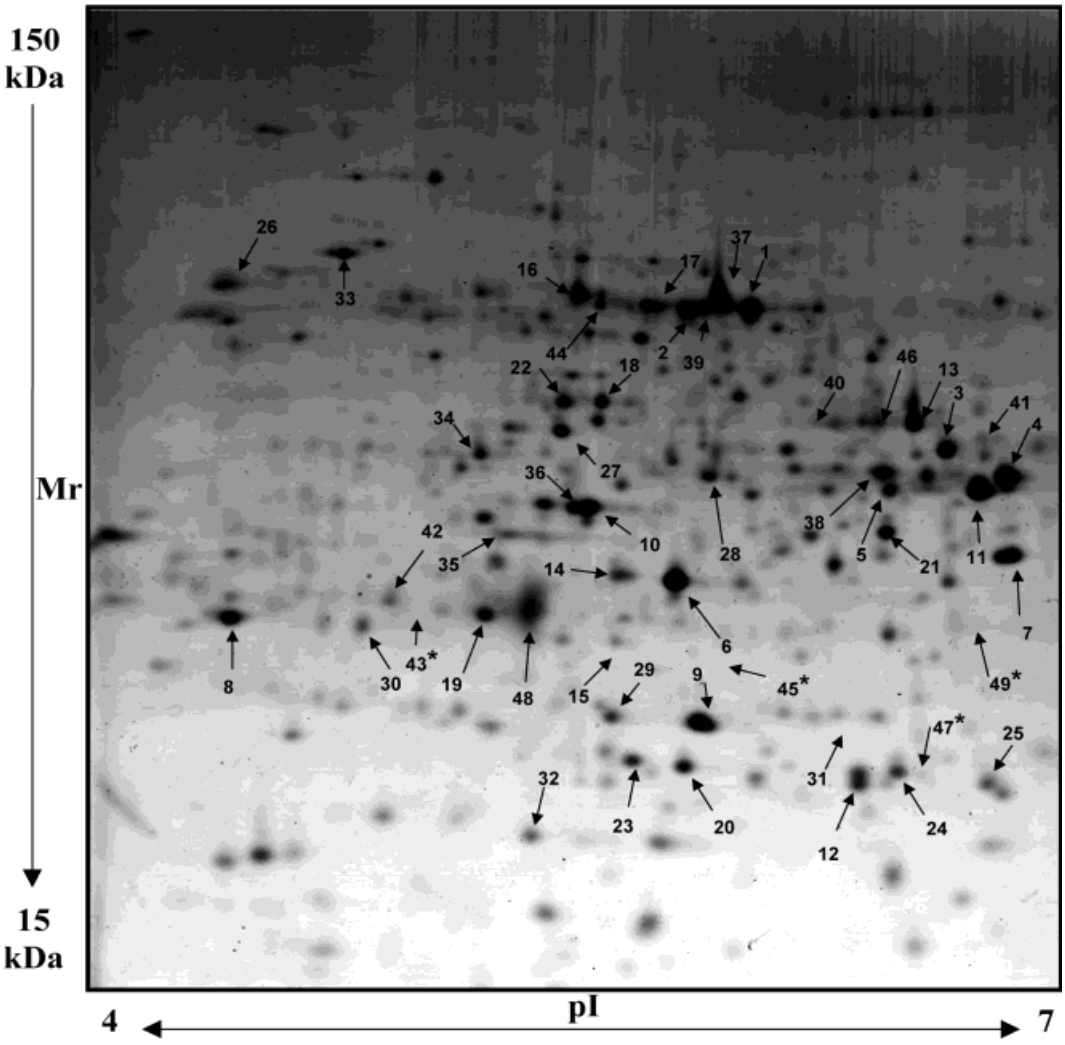

Figure 1. 2-D PAGE reference map of *Arabidopsis thaliana* soluble root proteins from ecotype Col-0. 2-D PAGE conditions: pH 4–7 IPG (first dimension) and 11% SDS-PAGE (second dimension). Proteins spots are visualized by colloidal Coomassie blue staining. Arrows indicate major spots analyzed by MALDI-TOF-MS. Spot numbers with star superscripts refer to spots from other ecotypes and not detected in ecotype Col-0.

for each ecotype, one-quarter was found in all the ecotypes (Fig. 2), and half of them was shared by at least 75% of ecotypes. On the other hand, about 10% of all spots appeared to be specific for one ecotype.

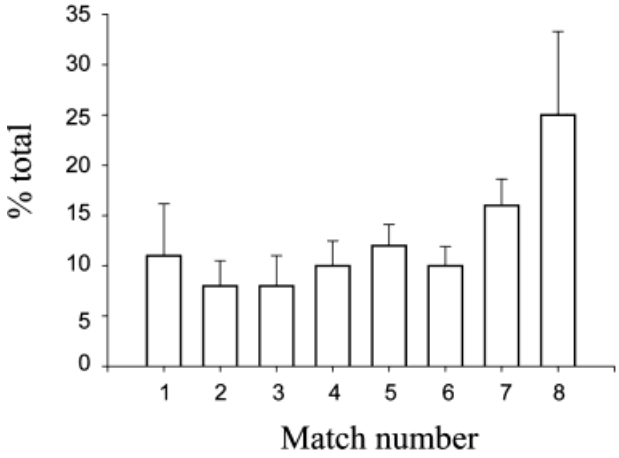

Figure 2. Distribution of spots according to the number of ecotypes where they were detected.

As simple gel comparison seemed to reveal specific features between the proteomes of *Arabidopsis* ecotypes, a classification was made by hierarchical clustering (Fig. 3a). For this purpose, the amount of each spot was estimated by its normalized volume as obtained by image analysis. Euclidian distances were then computed for all spots to build the similarity matrix for ecotypes, and clustering was performed using the Ward's method to link the variables. A first cluster corresponding to the two closest ecotypes was observed for Col-0 and Col-4. Another cluster grouped the ecotypes Be-0 and Ll-0, as well as the ecotype Rld-1, whereas the three last ecotypes defined a third cluster.

3.2 Comparison of *Arabidopsis* ecotypes from their major protein patterns

Above comparison of total 2-D maps indicated both the occurrence of contrasted proteomes between ecotypes and proximity between some of them. Additional analysis showed that the 25 most abundant spots from each *Arabidopsis* ecotype cumulated half the total protein amount detected on the p*I* and MW range investigated (50.2% $\pm$ 6.0% of the total signal computed by image analysis). In a first attempt to get more insights into the molecular basis of this structure, focus was given on these major proteins (MPs). Over the eight ecotypes, the 25 MPs from each defined a total subset of 49 differently matching spots accounting individually for between 0.7% and 6.7% of the total protein amount in their respective 2-D map.

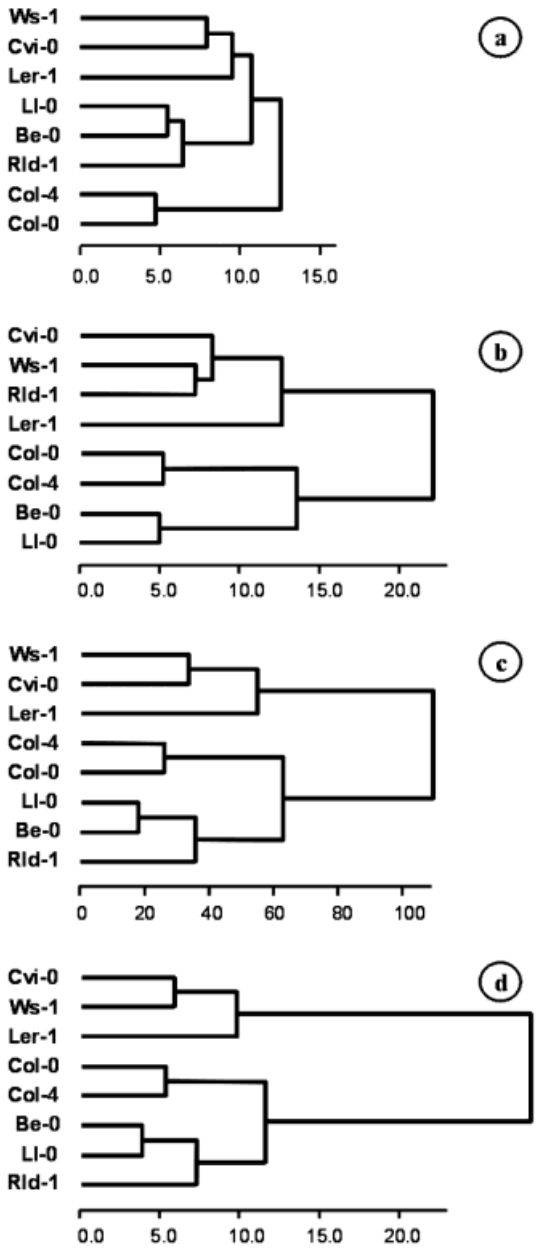

Figure 3. Classification of the proteomes from the eight ecotypes. Hierarchical clustering was performed using (a), (b), (d) the Euclidian distance or (c) the Manhattan distance as metric and the Ward criterion for linkage. (a) Spot abundance (all spots); (b), (c) abundance of MP spots; (d) function of MP spots.

Only 15% of these spots was ranked as MPs in all ecotypes and one-half contributed to the MPs in half or more the ecotypes, indicating the occurrence of large differences in expression level throughout the ecotypes (Fig. 4). Simultaneously, one-quarter of the MPs was not detected in at least another ecotype, whereas the remaining was observed at lower abundance and not classified as MP.

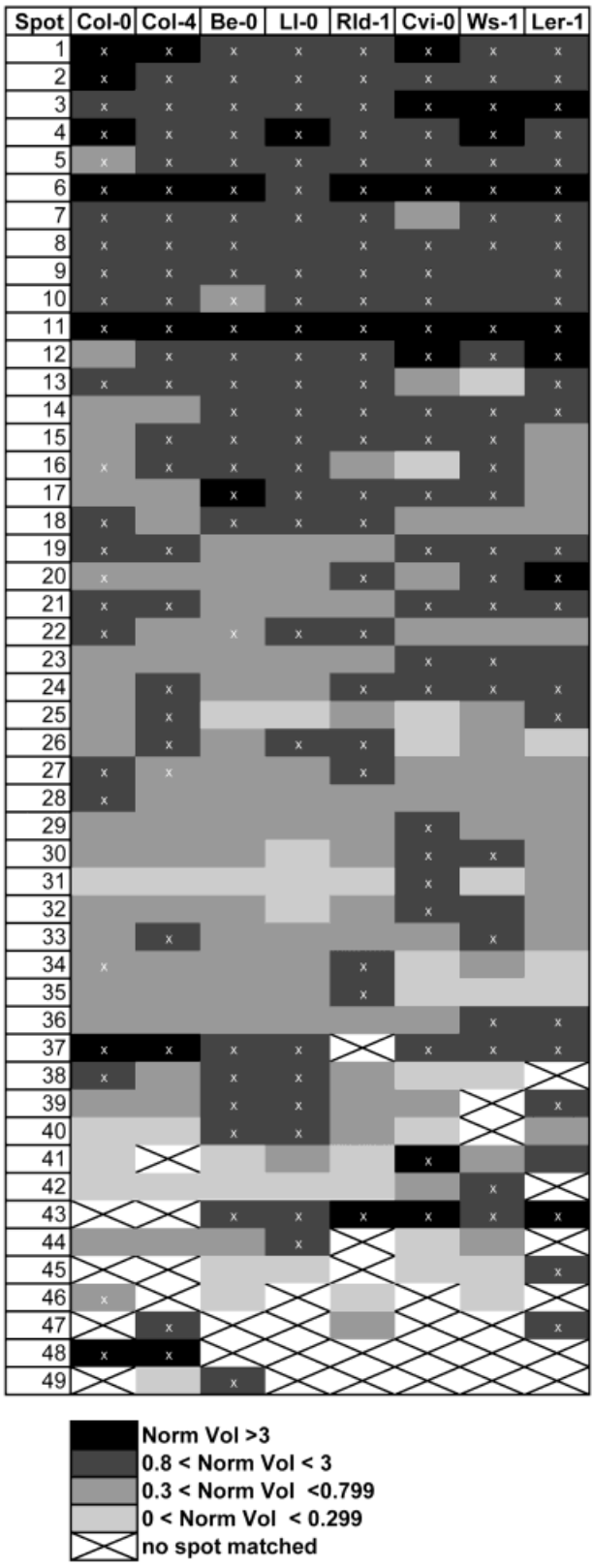

Figure 4. Expression of the 49 spots ranked as MPs in the eight ecotypes. Cross within cells indicate that the spot was ranked as MP in the corresponding ecotype.

As large differences in proteome features appeared to be detectable soon at the MPs' level, the different ecotypes were also classified by taking into account only the MPs. Figure 3b shows that, when using Euclidian distances as metric and the Ward's criterion for clustering, both the previous Col-0/Col-4 cluster and Be-0/Ll-0 cluster were still obtained. By opposition to the classification over the whole proteomes, however, the Rld-1 ecotype was no longer clustered with Be-0/Ll-0, but with the three remaining ecotypes. Nevertheless, the whole proteome-based classification could observed again by using other metric, such as the Manhattan distance (Fig. 3c), suggesting that the position of Rld-1 could be less stable.

3.3 Comparison of *Arabidopsis* ecotypes from the functions of major proteins

The 25 MPs of each ecotype were picked out from gels and processed for MALDI-TOF-MS analysis. In no case, contradictory identifications were obtained for spots that had been matched by image analysis. On the whole, 32 different protein accessions were identified in 44 from the 49 MP spots, and 5 could not be assigned to any protein accession (Table 2). Simultaneously, one half of the identified MPs was found to be present in 2 or 3 different protein spots. In this latter case, the difference between spots concerned mostly the p*I*, suggesting the occurrence of post-translational modifications or the presence of punctual protein variations between ecotypes. However, this encompassed different situations within ecotypes: (i) a same jasmonate-inducible protein was identified, for instance, in spots 6 and 14 (Fig. 5). These two spots showed a shift of 0.14 pH unit in p*I* and were observed simultaneously for the 8 *Arabidopsis* ecotypes, indicating that the protein existed under different states whatever the genotype was. However, only spot 6 corresponded to a MP in all ecotypes, the spot 14 showing a low abundance in the two Col accessions. Similar situations were observed for several other proteins, like the β-chain of the mitochondrial ATPase, a malate dehydrogenase, and a triose phosphate isomerase, indicating that the most frequent form of a protein could be ecotype-dependent. (ii) On the other hand, a same glutathione *S*-transferase could be detected in spots 25 and 47, differing by 0.17 pH unit in p*I* (Fig. 6). However, these two spots constituted MPs only in two ecotypes (Col-4 and Ler-1), and where either present at low abundance (spot 25) or not detected (spot 47) in other ecotypes. A similar situation was also observed for an alcohol dehydrogenase, suggesting that the occurrence of the modification itself could be ecotype-dependent. (iii) An even more contrasted situation was observed for a same blue-copper binding protein that was identified as MP in two spots

Table 2. Identified MPs in *Arabidopsis thaliana* ecotypes

Spot	Protein		Score	Coverage (%)	p*I*		MW (kDa)	
	Accession No.	Name			calc.	meas.	calc.	meas.
1	JQ1187	Phosphopyruvate hydratase	137	36	5.54	5.76	47.7	51.4
2	Q9C5B0	H+-Transporting ATP synthase β-chain	195	35	6.18	5.59	59.6	50.9
3	T02507	Peroxidase	94	18	5.66	6.29	38.7	35.8
4	T47550	Fructose bisphosphate aldolase-like protein	185	50	6.05	6.42	38.5	32.3
5	B86176	Malate dehydrogenase	110	31	6.11	6.13	35.5	31.6
6	AAK43865	Jasmonate inducible protein isolog	181	39	5.46	5.57	32.1	26.9
7	T51311	Malate dehydrogenase	66	15	8.54	6.43	36.0	27.9
8	T52558	Translation elongation factor eEF1Bα	69	26	4.42	4.47	24.2	25.9
9	T50646	Triose-phosphate isomerase	82	22	5.24	5.63	27.1	22.8
10	B84720	Probable fructokinase	183	42	5.31	5.33	35.3	30.3
11	B86176	Malate dehydrogenase	105	34	6.11	6.38	35.5	32.3
12	AAD00509	Germin-like oxalate oxydase	65	26	5.82	6.08	23.2	21.8
13	DEMUAM	Alcohol dehydrogenase	119	29	5.77	6.18	41.1	36.9
14	AAK43865	Jasmonate inducible protein isolog	123	35	5.46	5.52	32.1	26.7
15	T47550	Fructose bisphosphate aldolase	139	36	6.05	6.25	38.5	32.6
17	Q9C5B0	H+-Transporting ATP synthase β-chain	65	15	6.18	5.48	59.6	51.6
18	S68107	Actin 7	193	37	5.31	5.36	41.7	38.8
20	AAF98403	GSH-dependent dehydroascorbate reductase	78	23	5.56	5.59	23.6	22.1
21	T51862	Malate dehydrogenase	91	22	8.48	6.11	42.4	29.2
22	S18600	Glutamate-ammonia ligase	116	24	6.43	5.26	47.4	38.7
23	T52613	Chaperonin 21 precursor	124	36	8.86	5.47	26.8	22.4
24	BAA97523	1,4-Benzoquinone reductase like	78	40	5.96	6.17	21.8	22.3
25	G86159	Glutathione *S*-transferase	58	16	5.8	6.43	23.5	22.1
26	C96605	Calreticulin	85	21	4.46	4.42	48.7	54.3
27	AAG45246	Adenosine kinase	71	23	5.29	5.25	38.3	35.9
28	AAF02115	Reversibly glycosylated polypeptide	99	24	5.61	5.66	41.1	32.7
29	T50646	Triose-phosphate isomerase	157	54	5.24	5.42	27.1	23.1
30	Q9SS67	Putative peroxidase	87	20	5.04	4.73	34.5	25.2
31	APX1	L-Ascorbate peroxidase	60	19	5.72	5.81	27.4	22.3
32	AAD28242	Peroxyredoxin TPX1	82	25	5.21	5.18	17.4	21.3
33	AAD41430	Disulfide isomerase	203	49	4.64	4.76	55.6	62.9
34	H96686	Probable glutamine synthetase	76	23	5.14	5.10	39.3	33.7
35	AAD56335	60S ribosomal protein	64	24	4.52	5.13	24.3	28.5
36	Q9LSM8	Pyruvate dehydrogenase E1	106	19	5.67	5.30	31.2	30.1
37	JQ1187	Phosphopyruvate hydratase	141	33	5.54	5.66	47.7	51.5
38	T47550	Fructose bisphosphate aldolase	198	49	6.05	6.10	38.5	32.9
39	JQ1187	Phosphopyruvate hydratase	85	19	5.54	5.73	47.7	51.2
40	DEMUAM	Alcohol dehydrogenase	122	22	5.77	6.02	41.8	37.8
41	T13020	Peroxidase ATP 19A	96	28	6.53	6.40	35.6	35.2
42	Q9SS67	Putative peroxidase	87	20	5.04	4.89	34.5	26
43	T52408	Blue copper-binding protein II	60	22	5.47	4.84	20.5	26.1
45	S59519	Tryptophan synthase	82	26	6.77	5.66	33.3	24.7
47	G86159	Glutathione *S*-transferase	110	28	5.80	6.26	23.5	22.2
48	T52408	Blue copper-binding protein II	65	15	5.47	5.18	20.5	25.7

Proteins were identified from their peptide mass fingerprint by searching the NCBInr database (scores greater than 58 are significant at $p < 0.05$).

(spot No. 43 and 48) with a shift of 0.31 pH unit in p*I* (Fig. 5). In this case, only one or the other of the two spots could be detected in a given *Arabidopsis* ecotype, suggesting the occurrence of ecotype-specific isoforms.

In terms of function, most MPs corresponded to proteins involved in energy metabolism and oxydoreduction processes (Table 3), and different functions participating to a same pathway, such as glycolysis (3 functions in 8 MP

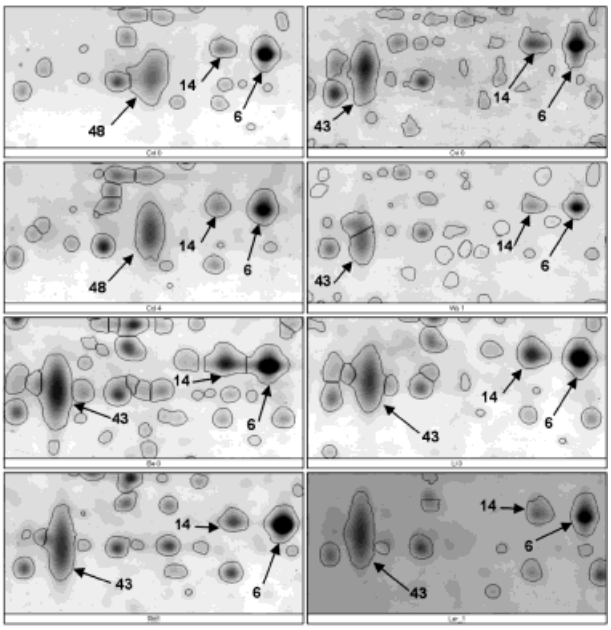

Figure 5. Example of proteins isoforms showing quantitative differences or ecotype-specific expression.

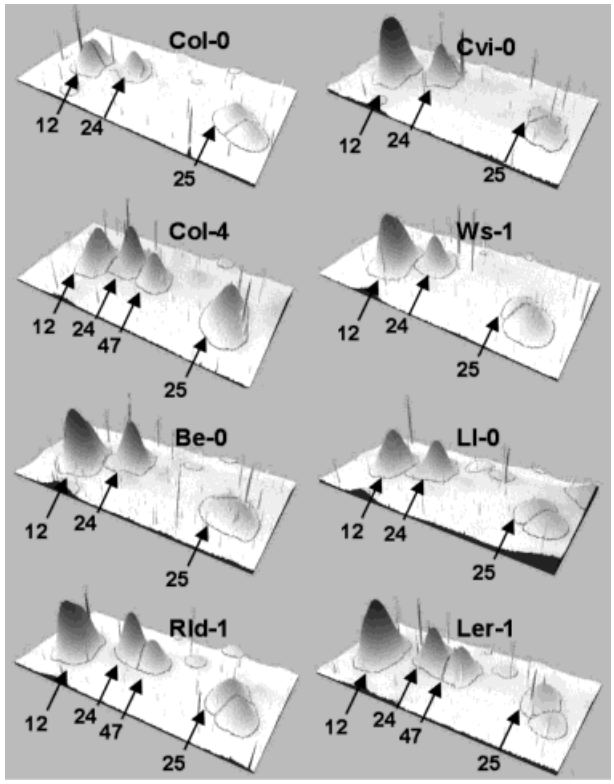

Figure 6. Example of proteins isoforms showing quantitative and ecotype-dependent expression.

spots), were identified as MPs. However, large differences in the functional classification were observed among ecotypes. For the majority of functional classes, these relative differences were in a twofold to fourfold range. For nitrogen assimilation, however, qualitative differences were also observed, no corresponding enzyme being found as MPs for half ecotypes. Accordingly, this suggested that MPs distinguished ecotypes not only in terms of protein isoforms but also on a function basis. Therefore, ecotypes were further classified according to the major functions identified. Figure 3d shows that, when using Euclidian distances to calculate a similarity matrix from the data of Table 3, and the Ward's criterion for linkage, three main

Table 3. Functional distribution of MPs in *Arabidopsis thaliana* ecotypes

Function	Col-0	Col-4	Be-0	Ll-0	Rld-1	Cvi-0	Ws-1	Ler-1
	(% total amount)							
Energy and *C*-metabolism								
glycolysis	16.6	13.3	11.0	11.2	8.0	12.8	9.7	8.8
TCA cycle	8.0	8.7	5.8	6.5	5.7	10.1	12.0	9.0
mitochondrial respiration	3.2	3.7	6.2	3.4	4.6	5.7	5.1	3.9
other	4.4	2.8	3.6	5.1	3.4	1.0		2.6
Electron transfer	3.3	5.0	2.7	1.7	4.1	4.3	2.7	6.3
Oxidative processes	2.5	4.5	2.4	2.8	2.7	10.8	7.5	11.6
Hormone response/stress	4.3	3.5	4.4	3.9	6.1	5.1	4.6	6.8
N-Metabolism	1.5		0.8	1.2	2.1			
Protein expression	1.4	3.6	1.0	2.9	3.7	2.5	4.3	1.5
Other	2.6	2.1	2.3	2.1	4.6	4.0	2.9	7.7
Unidentified proteins	3.4	2.3	3.9	2.4		0.9	2.8	1.4

Lacking values correspond to proteins either not ranked as MPs or not detected.

clusters could be obtained. Furthermore, this tree was almost identical to those obtained when classifying ecotypes on the basis of their whole proteome (Fig. 3a) or according to the anonymous MP subset (Figs. 3b, c).

4 Discussion

To date, little effort was devoted to investigate the differences eventually observed between proteomes of ecotypes from a same plant species. Even in the case of the model plant *Arabidopsis thaliana*, the only available data concern a pair of ecotypes that was included into an inter-species comparison within the Brassicaceae family, with no attempt to identify proteins [3]. Therefore, presently available data do not allow to decipher, for instance, whether eventual differences between ecotypes originate from the expression of different ecotype-specific isoforms of proteins showing the same function or from the differential expression of proteins with different functions.

4.1 Different *Arabidopsis* ecotypes display contrasted proteomes

In the present work, two main series of evidences were obtained arguing for the existence of large differences between the proteomes of the eight *Arabidopsis* ecotypes analyzed.

(i) In terms of protein patterns, gel comparison demonstrated first that at least one-third of the spots was not detected in half the accessions. On the other hand, ranking the spots in terms of MPs showed that only one-quarter of these constituted MPs in all the ecotypes, several MPs for one ecotype displaying lower abundance or being not detected in others. Further identification of MPs gave examples for different types of variations, to which quantitative differences were also superimposed: simultaneous expression of the different spots in all the ecotypes, expression of one or two forms of the protein in all ecotypes, whereas another form was ecotype-dependent, or exclusive expression of one form of the protein in an ecotype-specific manner. Therefore, collectively, these results demonstrate the occurrence of a qualitative and quantitative plasticity of the protein profiles between ecotypes which concerns both low-abundance and high-abundance proteins. The nature of these differences was not investigated here and could be hypothesized to rely as well on post-translational modifications as on allelic variations for those proteins identifying the same accession. Overall, very little information is presently available concerning the variations in proteome among *Arabidopsis* ecotypes, more extensive information being available for some other plant species. Using metrics based on the presence or absence of spots, the two *Arabidopsis* ecotypes Landsberg and Columbia were shown to be first merged together when compared to other species from the Brassicaceae family [5]. For maritime pine [4], plants from seven origins were compared, and less than 20% of spots was observed simultaneously in all patterns. However, in none of these works, a specific analysis according to the protein abundance was made. Accordingly, our results both constitute a novel example of the proteome plasticity among plant ecotypes and give the first evidences that the major proteins could contribute strongly to the variations observed. Colloidal Coomassie blue staining of 2-DE gels is known to favor the visualization of abundant proteins. Therefore, as the proteins ranked here as MPs constituted half of the amount of this subset, the accumulation of MPs is likely to have a major cost for the cell. Accordingly, it can be speculated whether, beside the selection of isoforms or allelic forms conferring a superiority with respect to some functions, the variations demonstrated in the proteomes of ecotypes reveal also physiological re-equilibrations.

(ii) In terms of functions associated to MPs, large variations were also observed, mostly as quantitative differences, showing that not the same abundant proteins are accumulated in all ecotypes. Actually, whenever more than one-quarter of MPs was not detected in some ecotypes, for most of them the same accession was identified in other spots indicating the occurrence of isoforms or protein modifications. On the other hand, in several cases, given functions were highly expressed in some ecotypes, but minor in others. A striking example concerns the alcohol dehydrogenase function, that constitutes a major function in two MP spots for LI-0 ecotype (where it cumulates 3.7% of the total protein amount), but a minor function in Ws-1 ecotype (0.1% of the total). Such amplitude suggests the occurrence of strong functional variations between ecotypes. Moreover, the fact that several of the major functions participate to the same pathway support the hypothesis that the plasticity of the proteome reveals different physiological equilibriums between ecotypes. For instance, in terms of MPs, Cvi-0 ecotype appears to dedicate 13% of its protein amount to glycolysis and 27-fold less to nitrogen assimilation, whereas this ratio is 7 times lower for Rld-1 ecotype. In terms of experimental strategy, it should be emphasized that, although a small proportion of proteins was characterized here, the conclusions derived can be assumed to be robust as it is unlikely that such ratio could be strongly modified by the identification of minor proteins. However, it should be also noticed that the five spots that could not be identified from their peptide mass fingerprint contribute substantially to the variation between ecotypes (3.9% of the total protein amount in

Be-0 ecotype, not detected in Rld-1 ecotype). Beside the important question of the function of these MPs, this leaves open the possibility that they participate to some of the pathways identified, thus altering their contribution in the present analysis.

A large part of identified proteins corresponds to enzymes involved in energy metabolism. This is not unexpected owing to their functional importance, although little reference data is presently available. Very recently, a first large-scale quantification of genes expressed in *Arabidopsis* root was made using the SAGE approach [21]. None of the 25 most frequent tags ($>$ 12 700 different tags) corresponds to any of the 25 MPs identified here in one or the other of the 8 ecotypes, although the product of some of these genes, like a glyceraldehyde-3-phosphate dehydrogenase, falls clearly in the p*I* and MW ranges investigated. Differences in physiological state of roots between these experiments are likely. Nevertheless, this suggests that the major functions expressed could be not deducible from a transcript analysis. As these functions appear to discriminate ecotypes and possibly to reveal different physiological status, this would confer to the proteome analysis an unique advantage in characterizing the plant biodiversity.

Taken together, the differences quoted in terms of protein pattern and of protein function appear to encompass both a genetic and a physiological information. The former, which corresponds to approaches already well established in plants [2], was not analyzed here, although some of the observed examples (position shifts, presence/absence of spots) suggest the possible occurrence of allelic variations. The latter was not addressed up to now in ecotypes. On this basis, proteomic analysis of naturally occurring variations can be speculated to constitute a new powerful way to get insights into functional traits.

4.2 Proteomes as signatures for ecotype classification

Hierarchical clustering was used to get insights into the structure of the differences in the proteome that were quoted among ecotypes. This resulted in a classification into three groups: the two ecotypes known to be very close according to their origin, the three ecotypes introduced for their alternative root growth responses, and the three last currently used ecotypes. The same structure holds as well for the whole and anonymous protein pattern, or when restricting the focus on the 25 anonymous MPs accounting for half the protein amount in each ecotype, as for the main functions deduced from the identification of MPs. It should be emphasized that these classifications rely on both quantitative (protein abundance), qualitative (protein presence or absence), and functional features (protein function class). Therefore, it can be speculated whether they reveal characteristic proteomic signatures. This was not investigated into more details, and no similar analysis was published to date for plant ecotypes. In the case of *Arabidopsis* mutants, however, the classification of anonymous protein patterns was previously shown to group the *cri* mutant with the corresponding wild-type ecotype when grown in the presence of cytokinins, and this mutant was demonstrated thereafter to overproduce cytokinins [22]. Although such examples are rare, they suggest that different but close genotypes can be classified from their proteome in a way reflecting the physiological status of plants. Therefore, owing to the important differences quoted here among proteomes in terms of major functions, both these data and ours support the working hypothesis that the proteomic signature includes a physiological information.

One striking result is that the three ecotypes that were introduced in the study for their alternative response to environmental stress were grouped in a same cluster. According to the discussion above, this would suggest that Be-0, Ll-0, and Rld-1 ecotypes would share major physiological features. To date, however, the only data available about these ecotypes concern their atypical response to phosphate starvation. On the other hand, a close link between phosphate and energy metabolisms is well known [23], and the present proteome analysis was performed with plants grown under normal conditions. Therefore, one tentative hypothesis is that the three ecotypes would display specific and constitutive features in their energy metabolism that would be detectable at the proteome level. Under this hypothesis, their original response to phosphate starvation would result from these specific features.

A noticeable point in this work is that only a small part of the total proteomic information was used. According to the experimental conditions, the analysis concerned a defined window in terms of p*I* and MW and was restricted to soluble proteins. The classification obtained can address therefore only the functions associated to the corresponding subset of abundant and soluble proteins, illustrated here by enzymes involved in energy metabolism. Accordingly, a different classification would be not unexpected when looking at other classes of proteins, such as, for instance, transporters which include numerous basic and hydrophobic proteins. On the other hand, both anonymous and function-based classifications of MPs led to the same classification that was obtained when exploiting all the protein pattern. This suggests that MPs

would be responsible for a main part of variations between ecotypes, and that an analysis focusing on a limited number of proteins bearing major functions may have the capacity to reveal specific features of the proteomes. No attempt was made here to assess these points, for instance by changing the number of MPs selected and the proportion of the total protein amount taken into account to classify the proteomes. Further work remains therefore required to rationalize a general strategy suitable for large-scale classification of ecotypes from a limited but detailed characterization of proteomes.

In conclusion, we report here a first use of proteomics to investigate variations between *Arabidopsis* ecotypes. The result obtained demonstrate that the differences in the proteomes originate both from the expression of different ecotype-specific isoforms of proteins showing the same function and from the differential expression of proteins with different functions. Furthermore, the approach appears to have the capacity to discriminate ecotypes and to generate a classification according to their physiological status, directly from the features of their major proteins. Owing to the throughput of the present proteomic technology and to the hundreds of ecotypes available for *Arabidopsis*, it can be speculated that such proteomic approach will constitute a robust tool for mining the natural biodiversity in plants.

This work was supported by the EU research program Quality of Life and Management of Living Resources (contract QLK5-CT-2001-01871) and by the Proteome Platform of the Montpellier-LR Génopole.

5 References

[1] De Vienne, D., Burstin, J., Gerber, S., Leonardi, A. *et al.*, *Heredity* 1996, *76*, 166–177.

[2] Thiellement, H., Bahrman, N., Damerval, C., Plomion, C. *et al.*, *Electrophoresis* 1999, *20*, 2013–2326.

[3] Burstin, J., de Vienne, D., Dubreuil, P., Damerval, C., *Theor. Appl. Genet.* 1994, *89*, 943–950.

[4] Bahrman, N., Zivy, M., Damerval, C., Baradat, P., *Theor. Appl. Genet.* 1994, *88*, 407–411.

[5] Marquès, K., Sarazin, B., Chané-Favre, L., Zivy, M., Thiellement, H., *Proteomics* 2001, *11*, 1457–1462.

[6] Jacobsen, S., Nesic, L., Petersen, M., Sondergaard, I., *Electrophoresis* 2001, *22*, 1242–1245.

[7] Lum, J. H., Fung, K. L., Cheung, P. Y., Wong, M., S. *et al.*, *Proteomics* 2002, *2*, 1123–1130.

[8] Fullaondo, A., Vicario, A., Aguirre, A., Barrena, I., Salazar, A., *Heredity* 2001, *87*, 266–272.

[9] Mosquera, E., López, J. L., Alvarez, G., *Heredity* 2003, *90*, 432–442.

[10] Pigliucci, M., *Trends Plant. Sci.* 1998, *3*, 485–489.

[11] Alonso-Blanco, C., Koornneef, M., *Trends Plant. Sci.* 2000, *5*, 22–29.

[12] Mitchell-Olds, T., *Trends Ecol. Evol.* 2001, *16*, 693–700.

[13] Maloof, J. N., Borevitz, J. O., Dabi, T., Lutes, J. *et al.*, *Nat. Genet.* 2001, *29*, 441–446.

[14] Alonso-Blanco, C., Blankestijn-de Vries, H., Hanhart, C. J., Koornneef, M., *Proc. Natl. Acad. Sci. USA* 1999, *96*, 4710–4717.

[15] Pepper, A. E., Corbett, R. W., Kang, N., *Plant Cell. Environ.* 2002, *25*, 591–600.

[16] Beemster, G. T., De Vusser, K., De Tavernier, E., De Bock, K., Inze, D., *Plant Physiol.* 2002, *129*, 854–864.

[17] Chevalier, F., Pata, M., Nacry, P., Doumas, P., Rossignol, M., *Plant Cell. Environ.* 2003, *26*, 1839–1850.

[18] Lejay, L., Tillard, P., Lepetit, M., Olive, F. D. *et al.*, *Plant J.* 1999, *18*, 509–519.

[19] Schele, C., Lamer, S., Pan, Z., Li, X. P. *et al.*, *Electrophoresis* 1998, *19*, 918–927.

[20] Hartigan, J. A., *Clustering Algorithms*, Wiley, New York 1975.

[21] Eckman, D. R., Lorenz, W. W., Przybyla, A. E., Wolfe, N. L., Dean, J. F. D., *Plant Physiol.* 2003, *133*, 1397–1406.

[22] Santoni, V., Delarue, M., Caboche, M., Bellini, C., *Planta* 1997, *202*, 62–69.

[23] Plaxton, W. C., in: Lynch, J. P., Deikman, J. (Eds.), *Phosphorus in Plant Biology*, ASPP, Rockville, USA 1998, 229–241.

Journal of Plant Physiology 168 (2011) 1885–1890

Contents lists available at ScienceDirect

Journal of Plant Physiology

journal homepage: www.elsevier.de/jplph

Proteomic analysis of *Arabidopsis thaliana* ecotypes with contrasted root architecture in response to phosphate deficiency

François Chevalier[a,b,*], Michel Rossignol[a]

[a] *INRA UR 1199, Protéomique Fonctionnelle, Place Viala, 34060 Montpellier, Cedex 2, France*
[b] *CEA DSV/iRCM, Plateforme de Protéomique, Route du Panorama, 92265 Fontenay-aux-Roses, Cedex, France*

ARTICLE INFO

Article history:
Received 8 March 2011
Received in revised form 16 May 2011
Accepted 21 May 2011

Keywords:
Aconitase
Ecotypes
Phosphate deficiency
Proteomics

ABSTRACT

Owing to a weak availability in soil, plants have developed numerous morphological, physiological and biochemical adaptations to acquire phosphate (Pi). Identification and characterisation of key genes involved in the initial steps of Pi-signalling might provide clues about the regulation of the complex Pi deficiency adaptation mechanism. A two-dimensional gel electrophoresis approach was performed to investigate proteome responses to Pi starvation in *Arabidopsis*. Two ecotypes were selected according to contrasting responses of their root system architecture to low availability of Pi. Thirty protein spots were shown to be affected by Pi deficiency. Fourteen proteins appeared to be up-regulated and ten down-regulated with ecotype Be-0, wheras only thirteen proteins were observed as down-regulated for ecotype Ll-0. Furthermore, systematic and opposite responses to Pi deficiency were observed between the two ecotypes. The sequences of these 30 differentially expressed protein spots were identified using mass spectrometry, and most of the proteins were involved in oxidative stress, carbohydrate and proteins metabolism. The results suggested that the modulation of alcohol dehydrogenase, malic enzyme and aconitate hydratase may contribute to the contrasted adaptation strategy to Pi deficiency of Be-0 and Ll-0 ecotypes. A focus on aconitate hydratase highlighted a complex reverse response of the pattern of corresponding spots between the two ecotypes. This protein, also potentially involved in iron homeostasis, was speculated to contribute, at least indirectly, to the root architecture response of these ecotypes.

Introduction

Like nitrogen and potassium, phosphate is one of the three essential macronutrients of plants. Phosphate is not only a constituent of such key cell molecules as ATP, nucleic acids and phospholipids, but also acts as a regulator in many metabolisms, including energy transfer, protein activation, and carbon metabolic processes. Because of its low mobility in the soil, inorganic orthophosphate (Pi), the assimilated form of phosphorus, is one of the most limiting nutrients for plant growth and crop productivity, and low-Pi availability is a major constraint for plant productivity in alkaline and acid soils (Raghothama and Karthikeyan, 2005). As developmental plasticity is one main adaptative response of plants to the availability of nutrients, limitation in Pi induces both molecular and developmental adjustment (Fang et al., 2009; Raghothama, 1999).

In *Arabidopsis*, Pi starvation was described to result in an increase of the size of the root apparatus that could favour Pi uptake (Al-Ghazi et al., 2003). Such responses of the root architecture may involve various modifications, of which several are also triggered by other stresses. For instance, they may concern the growth of the primary root in Pi-starved plants (Chevalier et al., 2003), the growth of lateral roots in nitrate-, Pi- or iron-starved plants, the density of lateral roots in Pi- or iron-starved plants (Moog et al., 1995; Williamson et al., 2001) or the formation of root hairs in Pi- or iron-starved plants (Bates and Lynch, 1996; Schmidt and Schikora, 2001). In other plant species, Pi starvation may promote the formation of proteoid roots as in *Lupinus albus* (Johnson et al., 1996) or affect the growth angle of roots in *Phaseolus vulgaris* (Bonser et al., 1996) whilst altering simultaneously the growth and density of lateral roots (Borch et al., 1999).

Several gene and transcription factors were related to Pi starvation and plant adaptation (Camacho-Cristóbal et al., 2008; Liu et al., 2009; Richardson, 2009; Ticconi et al., 2009; Wang et al., 2010; Yang et al., 2010; Yuan and Liu, 2008). In a previous work, we analysed the capacity of *Arabidopsis* ecotypes to develop a specific root

Abbreviations: TAIR, The *Arabidopsis* Information Resource; Pi, inorganic phosphate; 2-DE, two-dimensional electrophoresis.

* Corresponding author at: Proteomic Platform, iRCM, CEA, Fontenay aux Roses, France. Tel.: +33 (0)1 46 548 326; fax: +33 (0)1 46 549 138.
E-mail address: francois.chevalier@cea.fr (F. Chevalier).

0176-1617/$ – see front matter © 2011 Elsevier GmbH. All rights reserved.
doi:10.1016/j.jplph.2011.05.024

architecture under low-Pi growth conditions (Chevalier et al., 2003). A wide range of ecotypes was studied and an increase or a decrease in the primary root length and/or the lateral roots number were observed, indicating the occurrence of different and contrasting adaptative strategies. Among all ecotypes analysed, 66% presented a decrease in primary root length and 25% presented no modification of the primary root length nor of the lateral root number. From the remaining 9%, ecotypes Ll-0 and Be-0 displayed opposite responses, with an increase or a decrease of the lateral root number, respectively, and no change in the primary root length. In addition, under conditions of Pi-deficiency, the decrease in primary root length was proposed to be linked to root Fe toxicity, and the atypical response of accession Ll-0 was associated with an increased resistance to root Fe toxicity (Ward et al., 2008).

A previous proteomic study using two-dimensional electrophoresis (2-DE) and MALDI-TOF mass spectrometry allowed the analysis of the natural variability at the protein level, with a special focus on proteins accounting for the majority of the protein amount in each ecotype (Chevalier et al., 2004a; Chevalier, 2010). The proteomes appeared to reveal important variations in terms of function between the 5 studied ecotypes under normal growth conditions, without any stress. It was proposed that proteomic comparison has the capacity to evidence differences in the physiological status of ecotypes.

In this work, in order to further analyse key proteins involved in plant adaptation to Pi-deficiency, we compared ecotypes Ll-0 and Be-0, previously shown to be very close in terms of global proteome but distant in terms of their root system under low-Pi growth conditions. A gel-based proteomic strategy was used for total soluble proteins from hydroponic roots of the two ecotypes grown on control or Pi-deficient medium. Several spots appeared to display opposite responses between the two ecotypes, and a specific emphasis was proposed for aconitase hydratase, which seemed to be characteristic of contrasted ecotype responses to Pi starvation.

Materials and methods

Plant material and culture conditions

Arabidopsis ecotypes Be-0 and Ll-0 were progenies from NASC (http://nasc.nott.ac.uk). Plants were grown under hydroponic conditions as previously described (Lejay et al., 1999) at the vegetative stage with complete medium for 6 weeks and then again with complete medium (control) or with Pi deficiency medium (treated) during the last 8 days before sample harvest.

Protein extraction

A TCA/acetone extraction protocol was used to extract and solubilise proteins from plant root as previously described (Chevalier et al., 2004b). Briefly, for each ecotype and growth condition, root sample corresponding to more than 150 root systems was ground in liquid nitrogen, and the fine powder was mixed with precipitation solution (90% acetone, 10% TCA and 0.07% 2-mercaptoethanol). After incubation at −20 °C, insoluble material was pelleted at 42,000 × *g* with a TL 100 ultracentrifuge using a TLA 100.3 rotor (Beckman Coulter, CA, USA). Pellets were washed with acetone containing 0.07% 2-mercatoethanol (v/v), air-dried and solubilised in buffer containing 9 M urea, 4% CHAPS (w/v), 0.05% Triton X100 (v/v) and 65 mM DTT. Protein level was estimated using the Bradford method. All manipulations were performed on ice.

Two-dimensional electrophoresis

For each ecotype sample, 2-DE was performed as previously described (Chevalier et al., 2004a). Triplicate gels with 18 cm linear pH 4–7 IPG strips for the first dimension and 12% acrylamide gel for the second dimension were used. Protein samples (200 μg) were loaded on each gel and gels were stained using colloidal Coomassie blue (Chevalier et al., 2004b, 2007).

Image analysis

Images from stained gels were digitalized at 300 dpi with a GS 710 densitometer (Biorad, Hercules, CA, USA) and analysed using the Samespots software v4.0 (Non-linear Dynamics, UK). Gel triplicates were grouped to create an analysis with the 12 gels corresponding to 2 ecotypes and 2 growth conditions. Spots of each ecotypes were compared between control and Pi deficiency growth conditions. A multivariate statistical analysis was performed using the statistic mode of the Samespots software v4.0 (Non-linear Dynamics, UK). Spots with significant differences between control and Pi deficiency growth conditions (Anova *t*-test, $p < 0.05$) were first selected for each ecotypes separately. Then, only spots with a *q* value <0.05 and a power >0.8 were finally selected for subsequent protein identification by MALDI-TOF MS analysis.

Protein identification by MALDI-TOF MS

Spots were picked from preparative gels (500 μg proteins) using a spot picker robot (Perkin Elmer, Wellesley, MA, USA) as previously described (Chevalier et al., 2006). Briefly, acrylamide pieces were collected in microplates with acetic acid 1% (v/v). Pieces of gel were washed using a Multiprobe II robot (Perkin Elmer, Wellesley, MA, USA) with water, 25 mM ammonium carbonate and acetonitrile. Proteins were digested with trypsin (12.5 μg/ml in 25 mM ammonium carbonate), mixed with α-cyano-4-hydroxy-cinnamic acid and spotted onto MALDI targets. Peptide mass fingerprints were acquired using a Biflex III mass spectrometer (Bruker Daltonics, Bremen, Germany). Spectra were calibrated internally and annotated automatically. The MASCOT search engine software (Matrix Science, London, UK) was used to search NCBInr database. The following parameters were used for database search: mass tolerance of 100 ppm, a minimum of four matched peptides and one missed cleavage allowed.

Results and discussion

Proteomic variations in responses to Pi-deficiency

Root system architecture was analysed on a set of *Arabidopsis* ecotypes (Chevalier et al., 2003). These ecotypes have adapted to strongly contrasting growth conditions and thus display highly variable growth characteristics (Table 1). Dramatic differences in growth and architecture were observed within the first few weeks after germination and several parameters were compared, such as primary root length, lateral root number, lateral root length, leaf area or primary root growth rate. It appeared that the length of the primary root and the number of laterals were two robust parameters to discriminate accessions. Be-0 and Ll-0 ecotypes were selected as they displayed differential and atypical root architecture, with no modification of the primary root length, combined with a decrease or an increase of the lateral root number, respectively (Chevalier et al., 2003).

Quantitative changes in root proteins were analysed by comparing the proteomic map of ecotypes under two growth conditions (normal hydroponic medium, or Pi deficiency medium). A total of 465 proteins were detected on colloidal Coomassie blue stained 2D-PAGE gels using Non-linear Samespots software. To analyse the Pi-responsive proteins, significant differences in spot volume between control and “treated” samples were assessed and protein

Table 1
Ecological and morphological characteristics of *Arabidopsis* ecotypes Be-0 and Ll-0 according to (Chevalier et al., 2003) and TAIR.

Ecotype	Be-0	Ll-0
Location	Bensheim/Bergstr. (Germany)	Llagostera (Spain)
NASC Id	N965	N1338
Ecological characteristics (TAIR)		
Altitute (Min/Max)	100/200	1/100
Latitute (Min/Max)	49/50	42/42
Longitute (Min/Max)	8/9	3/3
Monthly preciptation spring (Min/Max)	30/40	30/40
Monthly preciptation autumn (Min/Max)	30/40	30/40
Morphological characteristics (Chevalier et al., 2003)		
Primary root length (control *vs* Pi deficiency)	No modification	No modification
Lateral root number (control *vs* Pi deficiency)	Decrease	Increase

spots displaying significant up- or down-regulation were regarded as candidates and submitted to MS analysis.

On the whole, thirty spots, representing 6.4% of all spots on the experiment (Fig. 1), showed significant variations ($p < 0.05$). They corresponded to respectively 24 and 13 spots differentially accumulated between growth conditions in respectively ecotypes Be-0 and Ll-0. Nearly one quarter of them were common to both ecotypes (Table 2) and displayed a systematically an opposite response to phosphate availability. Other spots were affected in only one of the two ecotypes.

The functional distribution of identified proteins was inferred from "The *Arabidopsis* Information Resource, TAIR" (http://www.arabidopsis.org) and the "Protein knowledgebase" of UniprotKB (http://www.uniprot.org). Accordingly, proteins could be classified into 4 main groups: oxidative stress-related proteins, carbohydrate and energy metabolism, proteins, nucleic acids and lipid metabolisms, other metabolic groups.

Modulation of oxidative stress-related proteins

Pi deficiency was previously shown to induce an oxidative stress in bean plants and a major role of oxidase was highlighted in stabilizing the reduction level of ubiquinone, and thus preventing active oxygen species formation (Juszczuk et al., 2001).

In this study, oxidative stress-related proteins were identified in 15 spots, corresponding to 7 different protein accessions. Alcohol dehydrogenase (spot 529) was modulated under Pi deficiency. This protein, known to be involved in alcohol oxido-reduction *via* NADH, contains several zinc–metal binding sites with catalytic activity. Spot 529 was under-expressed in the Ll-0 ecotype, and over-expressed in ecotype Be-0. Disulfide-isomerase (spot 274) catalyzes the rearrangement of –S–S– bonds in proteins and participates in cell redox homeostasis. L-Ascorbate peroxidase 1 (spot 429) plays a key role in hydrogen peroxide removal and constitutes a central component of the reactive oxygen gene network (Davletova et al., 2005). Malic enzyme (spot 68) acts as an oxidoreductase especially in malate metabolic process. Methylmalonate-semialdehyde dehydrogenase (spot 119) is a mitochondrial oxido-reductase. Monodehydroascorbate reductase (spots 167 and 207) catalyzes the conversion of monodehydroascorbate to ascorbate, oxidizing NADH in the process. Most of these proteins were previously described as involved under cadmium, hypoxia, heat and/or salt stress. A modulation of such proteins under Pi deficiency may play a role in antioxidant defense and redox signalling during oxidative stress.

Aconitate hydratase was identified in 8 spots (spots 13, 16, 17, 19–21, 517, and 518) modulated during Pi deficiency. It was the most relevant protein, identified in our proteomic analysis. Aconitase hydratase 2 is a mitochondrial enzyme, with a citrate hydro-lyase catalytic activity, involved in several biological processes, such as glyoxylate cycle and tricarboxylic acid cycle. The protein was described as implicated in response to abscisic acid stimulus and cadmium, oxidative, salt and acid stresses (TAIR). Recently, aconitase was described as playing a key role in regulating resistance to oxidative stress and cell death in *Arabidopsis* (Moeder et al., 2007). The authors speculated that plant aconitase mediates resistance to oxidative stress and regulates cell death by modulating the expression of genes whose products control intracellular ROS levels.

Regulation of carbohydrate and energy metabolism

Proteins involved in carbohydrate and energy metabolism were identified in 5 different spots. ATP synthase subunit beta (spots 519 and 520) is a mitochondrial membrane ATP synthase (F1F0 ATP synthase or Complex V) which produces ATP from ADP in the presence of a proton gradient across the membrane, which is generated by electron transport complexes of the respiratory chain. Citrate synthase 4 (spot 183) is involved in cellular carbohydrate metabolic process in the biosynthesis of citrate from oxaloacetate and acetyl CoA. Enolase (spot 521) is one of the major glycolysis enzyme, catalysing the synthesis of phosphoenolpyruvate from 2-phospho-D-glycerate. Isopentenyl-diphosphate Delta-isomerase II (spot 54) catalyzes the 1,3-allylic rearrangement of the homoallylic substrate isopentenyl to its highly electrophilic allylic isomer, dimethylallyl diphosphate. Modulation of carbohydrate and energy metabolism enzymes is a well known biochemical process following Pi starvation (Raghothama, 1999). In such nutriment stress, enzymes that do not require Pi as substrate are activated. These enzymes are considered to be adaptive enzymes of the glycolytic pathway during Pi starvation, and they are involved in "bypass reactions" that circumvent Pi in glycolysis, thus permitting carbon metabolism to proceed during starvation (Duff et al., 1989).

Alteration of proteins, nucleic acids and lipid metabolisms

Several proteins involved in different processes appeared also to be modulated under low Pi growth condition. Calreticulin-1 (spot 549) was under-expressed in Ll-0 ecotype. Calreticulin-1 is a calcium-binding chaperone promoting folding, oligomeric assembly and quality control in the ER *via* the calreticulin/calnexin cycle. This protein was affected by cadmium, oxidative or salt stresses, indicating that protein folding could have a general function during stress responses in *Arabidopsis*. Protease regulatory subunit 26S (spots 173) was over-expressed under Pi deficiency in Be-0 ecotype. This protease is involved in the degradation of ubiquitinated proteins (ATP-dependent). S-adenosylmethionine synthase 1 (spot 195) and tryptophan synthase alpha chain (spot 397), involved in amino acid metabolism, were over-expressed under Pi deficiency in Be-0 ecotype, whereas hydroxymethylglutaryl-CoA synthase (spot 123) implicated in lipid synthesis, was under-expressed under Pi deficiency in Be-0 ecotype. This suggested a general modification

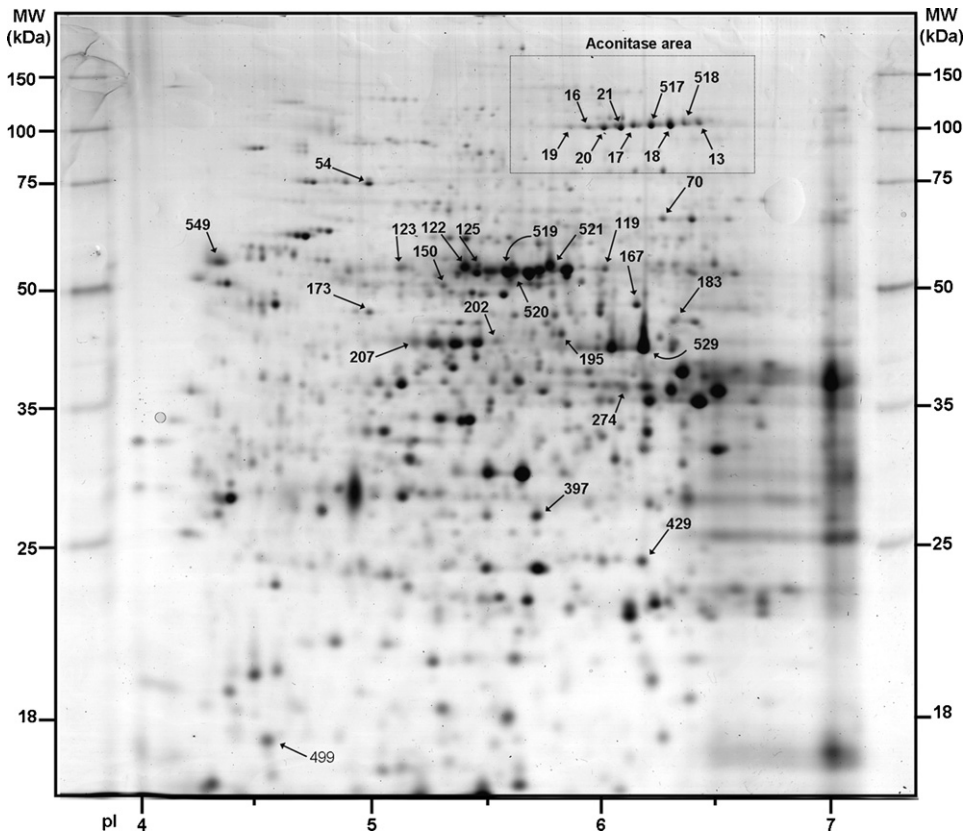

Fig. 1. Two-dimensional electrophoresis of root proteins of Be-0 ecotype, separated under reducing conditions using a 18-cm pH 4–7 pI range strip for the first dimension and a 12% acrylamide gel for the second dimension. Spots differentially accumulated in response to Pi deficiency, as indicated by arrows, were submitted to mass spectrometry identification by MALDI-TOF peptide mass fingerprinting (Table 1).

of the cell machinery with a rapid biochemical adjustment system to overcome low Pi availability.

Be-0 and Ll-0 ecotypes displayed opposite protein variations

Several modulated proteins under low Pi conditions were common to Be-0 and Ll-0 ecotypes. It is striking that opposite variations (i.e. over-accumulation in Be-0 and under-accumulation in Ll-0) were systematically observed (bold proteins in Table 2). These included alcohol dehydrogenase, malic enzyme and aconitate hydratase. Moreover, 7 spots were over-expressed and 10 spots under-expressed in ecotype Be-0, whereas they were unaffected by Pi availability in Ll-0 ecotype; similarly, 6 spots were under-accumulated in ecotype Ll-0, but were stable in Be-0 ecotype. Collectively, these responses suggest that the two ecotypes would have divergent adaptive strategies to low Pi.

In Fig. 2, a special focus is given to aconitate hydratase (aconitase) spots, as this protein was identified in 8 different spots. Most of isoforms were similarly modified, with an under-expression in ecotypes Ll-0 (7/8 spots) and with an over-expression in ecotype Be-0 (6/8 spots).

Possible relationship between proteomic responses and root architecture

Pi deficiency and iron availability were correlated with primary root elongation (Ward et al., 2008). In a P-deficient medium, inhibition of primary root elongation was demonstrated as a result of iron (Fe) toxicity. A reverted phenotype was observed when the Fe concentration in P-deficient medium is reduced, with an elongation of the primary root without an increase in Pi availability or a corresponding change in the expression of Pi deficiency-regulated genes (Ward et al., 2008). Here, it was shown that aconitase displayed different responses to Pi deficiency between ecotypes Be-0 and Ll-0 (Table 2). In Be-0 ecotype, levels of spots for aconitase were increased under P-deficient growth condition (Fig. 2), whereas the opposite observation was obtained with ecotype Ll-0. These two ecotypes were selected for this study on a basis of specific and atypical root architecture responses under low-Pi growth conditions. Indeed, a reduction of the primary root length was observed with 2/3 of all analysed *Arabidopsis* ecotypes (Chevalier et al., 2003), but no reduction of the primary root length was observed ecotypes Be-0 and Ll-0. Thus, Ll-0 accession was proposed to be more resistant to root Fe toxicity, with an increased tissue concentration of Fe (Ward et al., 2008).

Aconitase, an iron–sulfur protein that contains a [4Fe–4S]-cluster, catalyzes the interconversion of isocitrate and citrate *via* a cis-aconitate intermediate, and the cytoplasmic isoform of the enzyme is known to be sensitive to iron availability (Shlizerman et al., 2007). In addition, a change in iron cellular concentration was previously observed under similar conditions for the Ll-0 ecotype (Ward et al., 2008). Whether the decrease in the accumulation of the mitochondrial isoform observed here is related to the iron concentration and potentially to the root architecture response, needs further dedicated gene-based experiments.

In conclusion, our results showed that phosphate deficiency induced a modulation of several root proteins involved in oxidative stress, energy and biomolecule metabolism. Under low-Pi conditions, ecotypes Be-0 and Ll-0, selected following to their contrasted root architecture, displayed a systematic and opposite proteomic response for alcohol dehydrogenase, malic enzyme and aconitate hydratase. The striking response of this latter protein, potentially involved in iron homeostasis, opens speculation

Table 2
Identified root proteins from *Arabidopsis* ecotypes Be-0 and Ll-0 showing significant changes in abundance between control and Pi deficiency growth conditions. *+, spots over-accumulated in low Pi condition; −, spots under-accumulated in low Pi conditions. **Bold, proteins with opposite response to low Pi between Be-0 and Ll-0 ecotypes.

Metabolic group	Spot	Protein name**	No accession	Mol mass (kDa)		pI		Be-0*		Ll-0*	
				Theor.	Obs.	Theor.	Obs.	Diff.	Anova (*p*)	Diff.	Anova (*p*)
Oxidative stress related proteins	529	**Alcohol dehydrogenase**	P06525	41.18	42.10	5.83	6.19	+1.238	0.042	−1.284	0.015
	274	Disulfide-isomerase A6	O22263	37.17	36.23	5.65	6.03			−1.123	0.041
	429	L-Ascorbate peroxidase 1	Q05431	27.43	24.39	5.72	6.18	+2.467	0.001		
	70	**Malic enzyme**	Q9LYG3	64.41	66.00	6.01	6.27	+1.718	0.003	−1.460	0.034
	119	Methylmalonate-semialdehyde dehydrogenase	Q0WM29	63.02	54.69	8.46	6.00	−1.530	0.019		
	167	Monodehydroascorbate reductase	P92947	47.64	47.60	5.79	6.16	+1.835	0.000		
	207	Monodehydroascorbate reductase isoform 4	Q93WJ8	47.48	43.14	5.25	5.19			−2.124	0.041
	13	Aconitate hydratase 2	Q9SIB9	99.74	108.57	5.86	6.43	+1.674	0.043		
	16	**Aconitate hydratase 2**	Q9SIB9	99.74	106.21	5.86	5.92	+1.935	0.001	−1.911	0.016
	17	**Aconitate hydratase 2**	Q9SIB9	99.74	105.68	5.86	6.15	+1.529	0.009	−1.540	0.006
	19	**Aconitate hydratase 2**	Q9SIB9	99.74	105.06	5.86	5.87	+2.470	0.003	−1.615	0.040
	20	**Aconitate hydratase 2**	Q9SIB9	99.74	103.95	5.86	6.01	+1.710	0.007	−1.877	0.003
	21	**Aconitate hydratase 2**	Q9SIB9	99.74	103.97	5.86	6.09	+1.642	0.002	−1.815	0.001
	517	Aconitate hydratase 2	Q9SIB9	99.74	105.41	5.86	6.22			−1.523	0.022
	518	Aconitate hydratase 2	Q9SIB9	99.74	108.28	5.86	6.39			−1.868	0.025
Carbohydrate and energy metabolism	519	ATP synthase subunit beta	P19023	54.06	53.34	5.19	5.60	−1.840	0.011		
	520	ATP synthase subunit beta-1	P83483	54.22	53.33	5.37	5.61	−1.879	0.000		
	183	Citrate synthase 4	P20115	50.84	45.60	5.99	6.31	+1.663	0.016		
	521	Enolase	P25696	47.72	54.78	5.54	5.78	−1.479	0.003		
	54	Isopentenyl-diphosphate Delta-isomerase II	Q42553	32.61	74.12	6.10	5.35	−1.808	0.001		
Protein, nucleic acid and lipid metabolism	549	Calreticulin-1	O04151	46.16	57.49	4.42	4.40			−1.844	0.000
	173	26S protease regulatory subunit 6A homolog A	Q9SEI2	47.48	46.87	4.91	5.00	+1.728	0.005		
	195	S-adenosylmethionine synthase 1	P49612	39.94	44.00	6.45	5.83	+2.368	0.001		
	397	Tryptophan synthase alpha chain	Q42529	33.20	27.20	6.76	5.72	+1.676	0.002		
	123	Hydroxymethylglutaryl-CoA synthase	P54873	51.09	54.64	5.98	5.13	−1.591	0.003		
Others	122	F28N24.3 protein	Q9LP57	51.43	54.61	9.03	5.41	−1.903	0.000		
	125	F28N24.3 protein	Q9LP57	51.43	54.27	9.03	5.46	−1.612	0.000		
	150	Tubulin alpha-3/alpha-5 chain	P20363	49.65	50.49	4.95	5.32	−1.517	0.021		
	202	Actin-8	Q96293	41.86	43.52	5.37	5.56	−1.486	0.008		
	499	Uncharacterized protein	O80858	16.94	16.90	4.92	4.56			−1.359	0.001

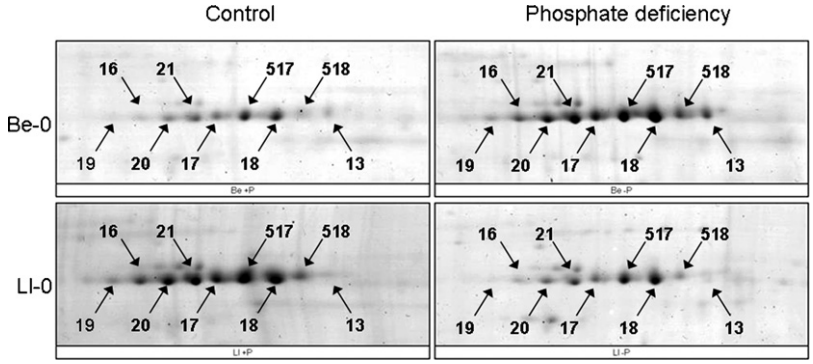

Fig. 2. Comparison of "aconitase area" from Fig. 1 for Be-0 and Ll-0 ecotypes, in response to Pi deficiency. Spots identified as aconitase were indicated by arrows (Table 2).

about its contribution to the root architecture response of these ecotypes.

Acknowledgements

F.C. was supported by fellowships from the EU research program Quality of Life and Management of Living Resources (contract QLK5-CT-2001–01871).

The authors thank the members of their laboratories for valuable discussions, Hugues Baudot for seed amplification and plant growth, Samuel Barteau and Anne-Dominique Devauchelle for technical support in proteomic, Delphine Centeno and Valérie Rofidal for technical support in mass spectrometry, Nicolas Sommerer for expertise in mass spectrometry, Olivier Martin for expertise in bio-statistics and Prof. Alan L. Kelly from University College Cork for valuable comments.

References

Al-Ghazi Y, Muller B, Pinloche S, Tranbarger TJ, Nacry P, Rossignol M, et al. Temporal responses of *Arabidopsis* root architecture to phosphate starvation: evidence for the involvement of auxin signalling. Plant Cell and Environment 2003;26:1053–66.

Bates TR, Lynch JP. Stimulation of root hair elongation in *Arabidopsis thaliana* by low phosphorus availability. Plant Cell and Environment 1996;19:529–38.

Bonser AM, Lynch J, Snapp S. Effect of phosphorus deficiency on growth angle of basal roots in *Phaseolus vulgaris*. New Phytologist 1996;132:281–8.

Borch K, Bouma TJ, Lynch JP, Brown KM. Ethylene: a regulator of root architectural responses to soil phosphorus availability. Plant Cell and Environment 1999;22:425–31.

Camacho-Cristóbal JJ, Rexach J, Conéjéro G, Al-Ghazi Y, Nacry P, Doumas P. PRD, an *Arabidopsis* AINTEGUMENTA-like gene, is involved in root architectural changes in response to phosphate starvation. Planta 2008;228:511–22.

Chevalier F, Pata M, Nacry P, Doumas P, Rossignol M. Effects of phosphate availability on the root system architecture: large-scale analysis of the natural variation between *Arabidopsis* accessions. Plant Cell and Environment 2003;26:1839–50.

Chevalier F, Martin O, Rofidal V, Devauchelle AD, Barteau S, Sommerer N, et al. Proteomic investigation of natural variation between *Arabidopsis* ecotypes. Proteomics 2004a;4:1372–81.

Chevalier F, Rofidal V, Vanova P, Bergoin A, Rossignol M. Proteomic capacity of recent fluorescent dyes for protein staining. Phytochemistry 2004b;65: 1499–506.

Chevalier F, Centeno D, Rofidal V, Tauzin M, Martin O, Sommerer N, et al. Different impact of staining procedures using visible stains and fluorescent dyes for large-scale investigation of proteomes by MALDI-TOF mass spectrometry. Journal of Proteome Research 2006;5:512–20.

Chevalier F, Rofidal V, Rossignol M. Visible and fluorescent staining of two-dimensional gels. Methods in Molecular Biology 2007:145–56.

Chevalier F. Highlights on the capacities of gel-based proteomics. Proteome Science 2010;8:23.

Davletova S, Rizhsky L, Liang H, Shengqiang Z, Oliver DJ, Coutu J, et al. Cytosolic ascorbate peroxidase 1 is a central component of the reactive oxygen gene network of *Arabidopsis*. Plant Cell 2005;17:268–81.

Duff SM, Moorhead GB, Lefebvre DD, Plaxton WC. Phosphate starvation inducible bypasses of adenylate and phosphate dependent glycolytic enzymes in *Brassica nigra* suspension cells. Plant Physiology 1989;90:1275–8.

Fang ZY, Shao C, Meng YJ, Wu P, Chen M. Phosphate signaling in *Arabidopsis* and *Oryza sativa*. Plant Science 2009;176:170–80.

Johnson JF, Vance CP, Allan DL. Phosphorus deficiency in *Lupinus albus*—altered lateral root development and enhanced expression of phosphoenolpyruvate carboxylase. Plant Physiology 1996;112:31–41.

Juszczuk I, Malusa E, Rychter A. Oxidative stress during phosphate deficiency in roots of bean plants (*Phaseolus vulgaris* L.). Journal of Plant Physiology 2001;158:1299–305.

Lejay L, Tillard P, Lepetit M, Olive FD, Filleur S, Daniel-Vedele F, et al. Molecular and functional regulation of two NO_3-uptake systems by N- and C-status of *Arabidopsis* plants. Plant Journal 1999;18:509–19.

Liu H, Yang HX, Wu CM, Feng JJ, Liu X, Qin HJ, et al. Overexpressing HRS1 confers hypersensitivity to low phosphate-elicited inhibition of primary root growth in *Arabidopsis thaliana*. Journal of Integrative Plant Biology 2009;51:382–92.

Moeder W, Del Pozo O, Navarre DA, Martin GB, Klessig DF. Aconitase plays a role in regulating resistance to oxidative stress and cell death in *Arabidopsis* and *Nicotiana benthamiana*. Plant Molecular Biology 2007;63:273–87.

Moog PR, Vanderkooij TAW, Bruggemann W, Schiefelbein JW, Kuiper PJC. Responses to iron-deficiency in *Arabidopsis thaliana*—the turbo iron reductase does not depend on the formation of root hairs and transfer cells. Planta 1995:505–13.

Raghothama KG. Phosphate F acquisition. Annual Review of Plant Physiology and Plant Molecular Biology 1999;50:665–93.

Raghothama KG, Karthikeyan AS. Phosphate acquisition. Plant and Soil 2005;274:37–49.

Richardson AE. Regulating the phosphorus nutrition of plants: molecular biology meeting agronomic needs. Plant and Soil 2009;322:17–24.

Schmidt W, Schikora A. Different pathways are involved in phosphate and iron stress-induced alterations of root epidermal cell development. Plant Physiology 2001;125:2078–84.

Shlizerman L, Marsh K, Blumwald E, Sadka A. Iron-shortage-induced increase in citric acid content and reduction of cytosolic aconitase activity in Citrus fruit vesicles and calli. Plant Physiology 2007;131:72–9.

Ticconi CA, Lucero RD, Sakhonwasee S, Adamson AW, Creff A, Nussaume L, et al. ER-resident proteins PDR2 and LPR1 mediate the developmental response of root meristems to phosphate availability. Proceedings of the National Academy of Sciences of the United States of America 2009;106:14174–9.

Wang XM, Du GK, Meng YJ, Li YY, Wu P, Yi KK. The function of LPR1 is controlled by an element in the promoter and is independent of SUMO E3 ligase SIZ1 in response to low Pi stress in *Arabidopsis thaliana*. Plant and Cell Physiology 2010;51:380–94.

Ward JT, Lahner B, Yakubova E, Salt DE, Raghothama KG. The effect of iron on the primary root elongation of *Arabidopsis* during phosphate deficiency. Plant Physiology 2008;147:1181–91.

Williamson LC, Ribrioux S, Fitter AH, Leyser HMO. Phosphate availability regulates root system architecture in *Arabidopsis*. Plant Physiology 2001;126:875–82.

Yang M, Ding GD, Shi L, Feng J, Xu FS, Meng JL. Quantitative trait loci for root morphology in response to low phosphorus stress in *Brassica napus*. Theoretical and Applied Genetics 2010;121:181–93.

Yuan H, Liu D. Signaling components involved in plant responses to phosphate starvation. Journal of Integrative Plant Biology 2008;50:849–59.

1.3 - Post-Doctorat 2 : Analyse de la qualité de laits après différents traitements

Ce contrat post-doctoral à l'University College of Cork était financé dans le cadre d'une mission gouvernementale Irlandaise du « Department of Agriculture and Food » pour le projet FIRM (Food Institutional Research Measure). Le laboratoire d'Alan Kelly avait pour mission l'analyse de la qualité du lait et des produits laitiers par des outils protéomiques.

1.3.1 - Analyse de la qualité du lait après traitement thermique

Ce projet était articulé autour de cinq objectifs visant à caractériser le lait et les produits laitiers ayant subi différents traitements physiques (chaleur, haute pression), chimiques et enzymatiques.
La première étape consistait à caractériser le protéome typique du lait de vache cru ou chauffé. A cet effet, une étude cinétique de lait chauffé à 90°C pendant 30 minutes a été réalisée. Afin de comprendre les interactions qui se produisent entre les protéines du lait suite à un traitement thermique, des échantillons de lait chauffés ont été incubés avec des agents réducteurs avant et/ou après isoélectrofocalisation des protéines, ce qui constitue la première étape de l'électrophorèse bidimensionnelle. Les protéines clés qui sont censées interagir pendant le traitement thermique sont la bêta-lactoglobuline et la caséine kappa. Ces deux protéines présentent des résidus cysteil libres qui peuvent interagir suite à un traitement thermique et ainsi former des hétérodimères. Dans cette analyse, les cartes du protéome de lait non chauffé et chauffé à 90°C ont été comparées en fonction des trois conditions de séparation afin d'observer la présence d'interactions entre protéines, principalement par des liaisons dissulfures. Un petit nombre de protéines en grande abondance sont caractéristiques du protéome du lait cru. Certains complexes protéiques réticulés ont été observés dans des conditions natives/non chauffées par électrophorèse bidimensionnelle. Lorsque le lait écrémé a été chauffé à 90ºC pendant 10 minutes, la quantité de protéines natives de lactosérum a diminué en parallèle avec une augmentation de complexes, y compris hétéropolymères très complexes, par exemple, des polymères caséines/protéines de lactosérum contenant de multiples espèces. La stratégie d'analyse utilisée dans cette étude révèle que de nombreuses interactions font intervenir des ponts disulfures.
Les polymères ainsi formés ont ensuite été quantifiés : en condition native, 18% de alpha S2-caséine, 25% de β-lactoglobuline, et 46% de kappa-caséine sont impliqués dans des complexes. Après traitement thermique à 90 °C pendant 30 minutes, une grande quantité de sérum albumine, de β-lactoglobuline et la kappa-caséine sont sous forme de polymères. En effet, homo-polymères et hétéro-polymères de kappa caséine et d'alpha-S2-caséine ont été identifiés par spectrométrie de masse. La quantité des spots correspondant aux monomères de kappa-caséine diminue progressivement avec le temps de chauffage à 90 °C, avec une plus grande proportion pour les points isoélectriques acides.

1.3.2 - Analyse du lait de jument après coagulation enzymatique

Un deuxième projet a été mené en collaboration avec Therese Uniacke-Lowe et le Prof. P. F. Fox sur la caractérisation du lait de jument pendant sa coagulation par électrophorèse bidimensionnelle en comparaison avec les résultats obtenus avec du lait de vache.

La coagulation du lait de vache induite par la présure est un mécanisme complexe dans lequel la chymosine hydrolyse spécifiquement la κ-caséine, une protéine responsable de la stabilité de la micelle de caséine. Dans le lait équin, ce mécanisme n'était pas encore clair et la cible protéique de la chymosine restait inconnue.
Pour connaitre les protéines impliquées, l'étude de la capacité de coagulation du lait équin par la chymosine a été réalisée par analyse protéomique comparative en utilisant le lait bovin comme contrôle. L'analyse par RP-HPLC de laits bovin et équin a montré la libération de plusieurs peptides suite à une incubation avec la chymosine. Les principaux peptides obtenus à partir de lait équin ont été identifiés par spectrométrie de masse comme des fragments de β-caséine. L'analyse effectuée par l'électrophorèse bidimensionnelle a confirmé que la β-caséine équine était la principale cible de la chymosine après 24 h à 30°C et pH 6,5. De plus, l'analyse de ces gels d'électrophorèse a permis une bonne séparation des différentes protéines du lait équin avec, pour la première fois, l'observation de la gamme d'isoformes de κ-caséine équine. En comparaison avec le lait de vache, les isoformes de κ-caséine de lait équin ne semblent pas impliquées dans la coagulation du lait induite par la chymosine. De plus, l'intensité des spots de β-caséine équine a diminué après l'addition de la chymosine, mais à un rythme plus lent que la κ-caséine bovine.

1.3.3 - Analyse du lait maternel et implication des enzymes endogènes

La compréhension des différences entre le système de protéines du lait maternel et celui du lait de vache est crucial pour permettre le développement de préparations pour nourrissons.
Dans cette étude, les protéines de lait de vache et une préparation pour nourrisson d'origine bovine ont été comparées par électrophorèses 1D et 2D avec les protéines du lait maternel produit pour les nourrissons nés prématurément ou à terme.
La distribution des protéines de la préparation pour nourrissons diffère significativement de celle des autres types de lait. L'analyse du protéome du lait humain pour prématurés a montré une réduction des niveaux de caséines béta et d'alpha S et une augmentation de peptides issus de ces protéines. De plus, le lait pour prématurés contient une concentration plus élevée en azote total et de la plasmine, en accord avec les données protéomiques. Ces résultats suggèrent un mécanisme physiologique qui permet d'ajuster l'expression d'enzymes ou de certaines protéines pour améliorer la digestibilité des protéines pour des prématurés. Cette observation pourra faciliter la conception des préparations pour nourrissons, plus proche du lait maternel, en particulier pour les enfants prématurés.

1.3.4 - Sélection de publications du Post-doctorat 2

Chevalier F., Hirtz C., Sommerer N., Kelly A. L. (2009)
Use of reducing/non-reducing two-dimensional electrophoresis for the study of disulphide-mediated interactions between proteins in raw and heated bovine milk
Journal of Agricultural and Food Chemistry, 57, 5948-5955.

Chevalier F. and Kelly A. L. (2010)
Proteomic quantification of disulfide-linked polymers in raw and heated bovine milk
Journal of Agricultural and Food Chemistry, 58, 7437–7444.

Armaforte E., Curran E., Huppertz T., Ryan C. A., Caboni M. F., O'Connor P., Hirtz C., Sommerer N., Chevalier F., Kelly A. L.
Proteins and proteolysis in pre-term and term human milk and possible implications for infant formulae (2010) International Dairy Journal, 20, 715-723.

Uniacke-Lowe T., Chevalier F., Hem S., Fox P. F. and Mulvihill D. M. (2013)
Proteomic comparison of Equine and Bovine Milk Systems on Renneting.
Journal of Agricultural and Food Chemistry, 61, 2839-2850.

DOI:10.1021/jf900518n

JOURNAL OF AGRICULTURAL AND FOOD CHEMISTRY
ARTICLE

Use of Reducing/Nonreducing Two-Dimensional Electrophoresis for the Study of Disulfide-Mediated Interactions between Proteins in Raw and Heated Bovine Milk

François Chevalier,*,† Christophe Hirtz,§ Nicolas Sommerer,§ and Alan L. Kelly†

†Department of Food and Nutritional Sciences, University College Cork, Cork, Ireland, and §Proteomic Platform, INRA, Montpellier, France

The composition and interactions of proteins in bovine milk, and modifications resulting from milk storage and processing, are complex and incompletely understood. Analysis of the milk proteome can elucidate milk protein expression, structure, interaction, and modifications. Raw milk was analyzed by two-dimensional electrophoresis (isolelectric focusing followed by sodium dodecyl sulfate−polyacrylamide gel electrophoresis) under reducing and nonreducing, or combined, conditions, followed by mass spectrometry of separated protein spots; a small number of high-abundance proteins, that is, caseins (α_{S1}-, α_{S2}-, β-, κ-, and γ-), β-lactoglobulin, α-lactalbumin, and serum albumin, represented the vast majority of protein spots on the two-dimensional electrophoretograms of raw milk samples, but some cross-linked protein complexes (mainly homopolymers of κ-casein and α_{S2}-casein but also some heteropolymeric complexes) were resolved under native/unheated conditions. When skim milk was heated to 90 °C for up to 10 min, the level of native whey proteins decreased in parallel with an increase in disulfide-linked complexes, including very complex heteropolymers, for example, casein/whey protein polymers containing multiple species. The analysis strategy used in this study reveals numerous disulfide-mediated interactions and can be proposed to analyze reduction/oxidation of milk and dairy product proteins following processing treatments applied for processing and storage.

KEYWORDS: Milk proteins; proteome; interactome; disulfide bridges; heat treatment; mass spectrometry

INTRODUCTION

Heat treatment is applied in the processing of milk for both hygienic and technological reasons and is today an essential operation in commercial dairy processes to provide acceptable safety and shelf life of dairy products. As a consequence of heat treatment, milk proteins may undergo structural changes, such as unfolding and aggregation. Heat treatment of milk at >70 °C results in a number of physicochemical changes in the milk constituents, in particular, denaturation of whey proteins and the formation of hydrophobic interactions or disulfide-bonded aggregates with casein micelles, particularly through interactions with κ-casein. Such protein−protein interactions can significantly affect the stability of milk and contribute to heat-induced coagulation of the milk. Numerous studies have been performed on model systems to elucidate the mechanism of interactions between milk proteins after heat treatment (*1*−*5*).

Zittle et al. (*6*) provided the first conclusive evidence of complex formation between β-lactoglobulin (β-LG) and κ-casein (κ-CN). Sawyer et al. (*7*) demonstrated the involvement of thiol groups and suggested that the free thiol group of β-LG is involved in the interaction and that intermolecular disulfide bonds are formed between κ-CN and β-LG. Subsequent investigations have tended to focus on determining the types of bonding involved in complex formation and the stoichiometry of the complexes formed (*5*, *8*−*16*). Sawyer (*7*) and McKenzie et al. (*17*) showed that the self-aggregation of β-LG was limited when κ-CN was present and suggested that κ-CN forms complexes with intermediate species of aggregated β-LG. In contrast, Euber and Brunner (*14*) reported that the aggregation of β-LG is not a prerequisite for interaction with κ-CN. Cho et al. (*5*) examined the interaction of β-LG with κ-CN using a "natural" κ-CN isolated without reduction or chromatography. Only denatured β-LG interacted with κ-CN (*18*), and many of the possible pathways involved in the aggregation of β-LG with κ-CN were elucidated. It has been proposed that, on heating β-LG and κ-CN, the free thiol group of β-LG is exposed, which initiates a series of reactions with other denatured molecules of β-LG or with κ-CN. The products formed depend on the ratio of κ-CN to β-LG and included 1:1 β-LG−κ-CN complexes and a range of large heterogeneous aggregates that were held together by disulfide bonds and/or hydrophobic interactions (*7*, *19*−*21*).

*Author to whom correspondence should be addressed [telephone +33 (0)146 548 326; fax +33 (0)146 549 138; e-mail francois.chevalier@cea.fr].

 Published on Web 06/15/2009

Milk is considerably more complex than purified protein model systems. Although β-LG is the major whey protein in bovine milk, several other whey proteins with free thiol groups and/or disulfide bonds are present, such as serum albumin and α-lactalbumin (*22*). Of the caseins, both κ-CN and α_{S2}-CN have disulfide bonds, and therefore both could participate in thiol−disulfide interchange reactions (*23*). As a consequence, many more thiol−disulfide interaction pathways exist, and the separation and the analysis of the reaction products increase in complexity. Despite this, it appears that reactions between β-LG and κ-CN similar to those observed in the model systems occur in heated milk, although, as expected, other denatured whey proteins are also involved in complex formation (*11*, *15*, *16*, *24*−*29*).

Tools for the study of proteins and protein−protein interactions in complex systems have developed significantly in recent years with the introduction of proteomic tools, such as two-dimensional electrophoresis combined with mass spectrometry for the identification of specific separated proteins (*30*−*32*). A number of recent studies have applied two-dimensional electrophoretic separation approaches to the study of protein−protein interactions in heated milk systems, most often using sodium dodecyl sulfate−polyacrylamide gels under nonreducing and reducing conditions as the two dimensions for the separation of proteins, particularly disulfide-bonded complexes (*18*, *33*−*35*). Fewer studies have used the classic proteomic strategy of separation on the basis of isoelectric point (isoelectric focusing) followed by SDS-PAGE under reducing conditions (*36*), although this may yield information significantly different from that obtained through the previous approach mentioned.

The objective of this study was to investigate the interactions between proteins in raw skim milk and milk heated under laboratory conditions to identify the principal pathways and complexes involved, using proteomic approaches to protein separation and identification.

MATERIALS AND METHODS

Milk Samples and Reagents. Fresh bulk cow's milk was obtained from a dairy farm in Cork. The milk was warmed to 50 °C and skimmed using a pilot-scale cream separator (final fat content of < 0.1%, w/w). Sodium azide (0.02%, w/v) and a protease inhibitor cocktail, one tablet for 10 mL of milk (Complete Mini EDTA-free, Roche Diagnostics, Mannheim, Germany), were added to the fresh skim milk before analysis. Phosphoric and acetic acids were obtained from VWR (Ballycoolin, Dublin, Ireland); glycerol, urea, SDS, DTT, CHAPS, Triton X-100, iodoacetamide, bromophenol blue, and Coomassie blue were obtained from Sigma-Aldrich (St. Louis, MO); acrylamide was obtained from Bio-Rad (Hercules, CA).

Heat Treatment and Protein Preparation. Aliquots (2 mL) of skim milk were placed in glass tubes (1.5 cm diameter) with a parafilm cap and heated in a water bath at 90 °C for 30 min and then cooled rapidly in iced water and stored at −20 °C until analyzed. Following thawing, heat-treated milk samples were diluted (1/10) according to the method of Chevalier et al. (*37*) in 9 M urea, 4% CHAPS, w/v, and 0.05% Triton X-100, v/v, with (reduced samples) or without (unreduced samples) 65 mM DTT. The protein content of the solubilized samples was estimated using the Bradford method (*38*).

Analytical Two-Dimensional Electrophoresis. Precast 7-cm strips, pH range 4−7, or 17-cm strips, pH range 4−7 or 3−10 (Bio-Rad), as appropriate, were rehydrated in the presence of 100 μg (7-cm strips) or 300 μg (17-cm strips) of milk protein. Isoelectric focusing was carried out using a Protean IEF Cell (Bio-Rad) isoelectric focusing system until 50 kV h^{-1}. The strips were then incubated in the first equilibration solution [50 mM Tris-HCl, pH 8.8, 6 M urea, 30% (v/v) glycerol, 2% (w/v) SDS] with 130 mM DTT (reduced samples) or without DTT (unreduced samples) and then in the second equilibration solution [50 mM Tris-HCl, pH 8.8, 6 M urea, 30% (v/v) glycerol, 2% (w/v) SDS] with 130 mM iodoacetamide (reduced samples) or without iodoacetamide (unreduced samples). Strips were then embedded using 0.6% (w/v) low-melt agarose on the top of the acrylamide gel. SDS-PAGE was carried out on a 10−18% acrylamide gradient SDS−polyacrylamide gel (produced using a model 485 Gradient Former, Bio-Rad), using a Criterion Dodeca Cell electrophoresis unit (Bio-Rad). Gels were stained with colloidal Coomassie blue (*39*) and scanned to images, which were digitized with a GS 800 densitometer (Bio-Rad) and analyzed using PDQuest software v.7.3.1 (Bio-Rad).

Preparative Two-Dimensional Electrophoresis. Precast 17-cm strips pH 4−7 or pH 3−10 L (Bio-Rad) were rehydrated with 300 μg of protein samples, and isoelectric focusing was carried as described above. The strips were incubated in the first equilibrated solution with DTT (reduced samples) or without DTT (unreduced samples) and then in the SDS solution with iodoactamide. SDS-PAGE was carried out on linear 12.5% SDS−polyacrylamide gels, using the Criterion Dodeca Cell electrophoresis unit (Bio-Rad). Gels were stained with colloidal Coomassie blue (*39*), and images were digitized with a GS 800 densitometer (Bio-Rad) and analyzed using PDQuest software v.7.3.1 (Bio-Rad).

Image Analysis. An averaged gel experiment was performed with analytical two-dimensional electrophoresis gels using the gels of control unheated milk as reference with the PD Quest software (Bio-Rad). At least three experimental repetitions of each sample were used in this analysis. For each sample, the same gel areas were selected and compared. The spot volume was determined as percentage of total volume of all spots on respective gels.

MALDI-TOF and TOF/TOF Analysis. Spots were analyzed according to the method of Chevalier et al. (*40*). Briefly, spots were excised from preparative two-dimensional electrophoresis gels by hand and processed using a Packard Multiprobe II liquid-handling robot (Perkin-Elmer, Courtaboeuf, France). After successive washings with water, 25 mM ammonium bicarbonate, acetonitrile/25 mM ammonium bicarbonate (1:1, v/v), and acetonitrile, gel fragments were dried at 37 °C. Protein digestion was carried out at 37 °C for 5 h following addition of 0.125 μg of trypsin (sequencing grade, modified, Promega, Charbonières, France), and resulting fragments were extracted twice with 50 μL of acetonitrile/water (1:1, v/v) containing 0.1% trifluoroacetic acid for 15 min. Pooled supernatants were concentrated with a Speedvac to a final volume of ca. 20 μL. Peptides were simultaneously desalted and concentrated with C18 Zip-Tip microcolumns to a final volume of 3 μL, an aliquot of each sample was mixed (1/1) with the α-cyano-4-hydroxycinnamic acid matrix at half saturation in acetonitrile/water (1:1, v/v), and the mixture was immediately spotted on the MALDI target by the Multiprobe II robot. Mass spectra were recorded in the reflector mode on a UltraFlex II MALDI-TOF/TOF mass spectrometer (Bruker Daltonics, Bremen, Germany). Automatic annotation of monoisotopic masses was performed using Bruker's SNAPTM procedure. The MASCOT search engine software (Matrix Science, London, U.K.) was used to search the NCBInr database. The following parameters were used: mass tolerance of 30 ppm, a minimum of five peptides matching to the protein, carbamidomethylation of cysteine as fixed modification, oxidation of methionine as variable modifications, and one missed cleavage allowed. MALDI-TOF/TOF experiments were performed under LID conditions with the LIFT cell voltage parameters set at 19.0 kV for a final acceleration of 29.5 kV (reflector voltage) and a pressure in the LIFT cell around 4×10^{-7} mbar. MASCOT parameters were adjusted as follows: parent ion mass tolerance of 20 ppm, fragment ion mass tolerance of 100 ppm.

Nano-LC MS Analysis. Stained protein spots were manually excised, washed, digested with trypsin as above, and extracted using formic acid instead of trifluoroactetic acid. Protein digests were analyzed using an ion trap mass spectrometer (Esquire HCT plus; Bruker Daltonics) coupled to a nanochromatography system (HPLC 1200, Agilent) interfaced with an HPLC-Chip system (Chip Cube, Agilent). MS/MS data were searched against National Center for Biotechnology Information (NCBI) and MSDB databases using Mascot software with the following parameters: parent and fragment ion mass tolerance of 0.6 Da for doubly and triply charged peptides.

RESULTS AND DISCUSSION

Reducing Two-Dimensional Electrophoresis Analysis of Raw Skim Milk Proteins: Reference Proteomic Map. A two-dimensional electrophoretogram of raw milk (**Figure 1**) highlighted the

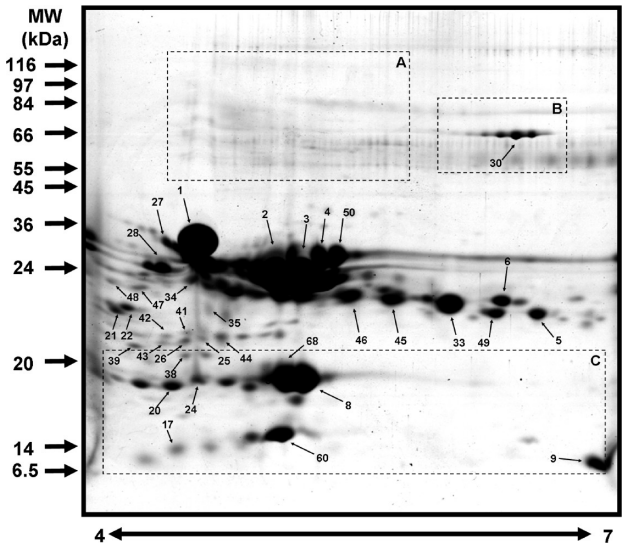

Figure 1. Two-dimensional gel electrophoretogram of proteins in raw milk (100 μg) separated under reducing conditions using a 7-cm pH 4−7 p*I* range strip for the first dimension and a 10−18% gradient acrylamide gel for the second dimension. The most abundant spots as indicated by arrows were submitted to mass spectrometry identification by MALDI-TOF peptide mass fingerprinting (**Table 1**). Three areas of interest indicated were compared according to heating time and reducing/nonreducing conditions of 2D separation (areas A, B, and C correspond to **Figures 4**, **5**, and **6**, respectively).

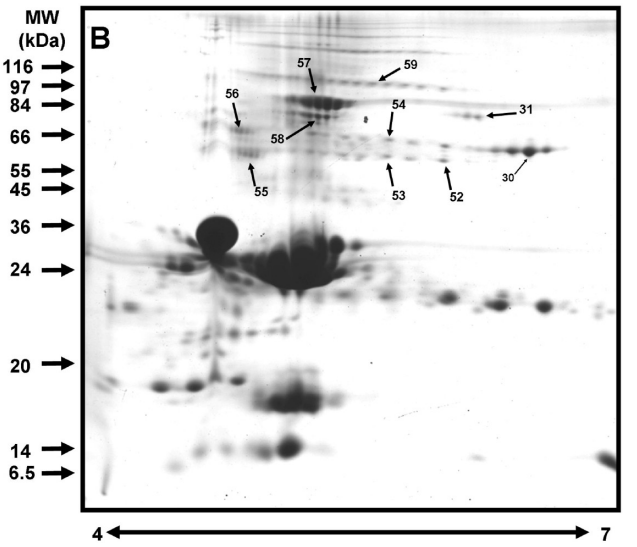

Figure 2. Two-dimensional gel electrophoretogram of proteins in raw milk (100 μg) separated under nonreducing conditions using a 7-cm pH 4−7 p*I* range strip for the first dimension and a 10−18% gradient acrylamide gel for the second dimension. The specific/interesting spots as indicated by arrows were submitted to mass spectrometry identification by MALDI-TOF peptide mass fingerprinting (**Table 1**).

complex heterogeneity of the milk protein system; this proteomic map of milk protein was prepared with 100 μg of reduced milk proteins using a wide p*I* range (4−7) for the first dimension and a gradient acrylamide gel (10−18%) for the second dimension (**Figure 1**). Between the two dimensions, the proteins were equilibrated with SDS in the presence of DTT followed by iodoacetamide, for reduction and alkylation of the proteins, respectively.

Despite the presence of dozens of proteins in milk identified using a global proteomic analysis, it is clear that the major proteins present were caseins (α_{S1}-, α_{S2}-, β-, κ-, and γ-), β-LG, α-lactalbumin (α-LA), and serum albumin, as would be expected (*41*) and which were found in positions roughly corresponding to those previously reported in similar two-dimensional analyses (*31*, *32*, *43*). Additional spots were clearly derived from these by alterations such as proteolysis, post-translational modification (e.g., spots 5, 6, 45, and 46 represent differently glycosylated forms of κ-CN), and interaction and association of the major milk proteins. For example, spot 9 is apparently a low molecular weight breakdown product of β-CN that has a very high isoelectric point, whereas spots 17, 20−22, 24−26, and 42−44 were all apparently proteolysis products of the caseins, probably originating from the activity of the principal indigenous milk protease, plasmin, or other indigenous (or exogenous, e.g., bacterial) protease activities in milk. Interestingly, there were far more proteolysis products originating from α_{S1}-CN than from β-CN and none from κ-CN, despite β-CN being the preferred substrate for plasmin.

Nonreducing Two-Dimensional Electrophoresis Analysis of Raw Skim Milk: Study of the Native Milk Interactome. When raw milk was subjected to two-dimensional analysis using nonreducing SDS-PAGE in the second dimension, a more complex pattern was obtained (**Figure 2**). By comparison to the reference proteomic map (**Figure 1**), the same separation parameters were applied to raw skim milk, but without the use of reducing agent, to prevent the reduction/cleavage of disulfide links between milk proteins: milk protein was prepared with 100 μg of unreduced milk proteins using a p*I* range (4−7) for the first dimension and a gradient acrylamide gel (10−18%) for the second dimension (**Figure 1**). Between the two dimensions, the proteins were equilibrated with SDS in the presence of iodoacetamide (without the DTT step) to fix the naturally reduced cysteines and to retain the naturally formed disulfide bonds. This strategy, which has been applied very recently and successfully to study the oxidative stress in chronic obstructive pulmonary disease (*42*), allowed observation of the naturally occurring disulfide interactions between the same proteins (homopolymers), and between different proteins (heteropolymers), in relation to the oxidized/reduced status of cysteine residues.

Comparison of the reducing and nonreducing milk proteomic maps highlighted significantly contrasting results (**Figure 2**). Most of the milk protein spots observed at molecular mass below 36 kDa were common to both conditions (bottom of the gel). In contrast, many high molecular weight spots appeared in the nonreducing proteomic map, showing new populations of disulfide-linked polymers (top of the gel). It can be noted that the spots observed in the reducing proteomic map between 14 and 36 kDa seemed to be less intense on the nonreducing proteomic map. As the same amount of protein was loaded for both conditions, the decrease in intensity of the low molecular weight resulted almost certainly from the presence of the disulfide-linked high molecular weight spots.

The use of a gel gradient (10−18%) for the second dimension of the two-dimensional electrophoresis was very powerful for the separation of these high molecular weight populations. At least 20 or 30 new spot populations were observed on the top of the gel of the nonreducing proteomic map. These spots were very heterogeneous in terms of isoelectic point (4.6−6.4) as well as molecular mass (45−150 kDa). The nine most intense spots of these disulfide-linked polymers were analyzed using mass spectrometry (**Table 1**, spots 31 and 52−59).

These complexes included some spots that may correspond to homopolymers of κ-CN (spots 52 and 53) and α_{S2}-CN (likely dimers at spots 57 and 58); these proteins, being the only CNs to contain cysteine residues, are known to form homomultimers (*43*).

Several heteropolymers consisting of various milk proteins at least in part disulfide-linked were also found, including complexes of α_{S2}/κ-CN (spot 54), α_{S1}-/α_{S2}/κ-CN (spots 55 and 56), α_{S1}-/α_{S2}/κ-CN/ β-Lg (spot 59), and α_{S2}/β-CN/serum albumin (spot 31), of different molecular weights and p*I* values, depending presumably on the glycosylated and phosphorylated forms of the CN involved. It can be noted that new proteins species were also identified in some of these complexes, including phenylethanolamine *N*-methyltransferase and α-actin 2 (spot 55), showing the complexity of the heteropolymeric complexes observed using such nonreducing two-dimensional electrophoresis. The observation of these stable complexes under "native-like" separation

Table 1. Principal Species Identified in Heated and Unheated Bovine Milk Samples by IEF/SDS-PAGE followed by (a) MALDI MS-PMF, (b) MALDI TOF/TOF, or (c) Nano-LC-MS/MS[a]

					MALDI-TOF (a)		MALDI-TOF/TOF (b)			nano-LC-MS/MS (c)	
spot	MW[b] theor/obsd	p*I* theor/ obsd[c]	identified protein	accession no.[d]	Mascot score	% coverage	peptide mass	Mascot score	sequence	score	matching peptides
1	22.97/27.3	4.91/4.61	α_{S1}-casein	P02662	84.4	31.8					
2	23.58/23.52	5.13/4.98	β-casein	P02666	39	15.6					
3	23.58/21.95	5.13/5.29	β-casein	P02666	52.4	19.2					
4	24.35/28.31	8.34/5.21	α_{S2}-casein	P02663	77.9	26.1				250	9
5	18.97/20.82	5.93/6.59	κ-casein	O02782	33	31.1					
6	18.97/21.26	5.93/6.34	κ-casein	O02782	31.9	27				139	2
8	18.28/18.27	4.83/5.16	β-lactoglobulin	P02754	55.7	44.4				461	10
9	23.58/14.2	5.13/6.95	β-casein	P02666	55.6	21.9				55	3
17	22.97/13.87	4.91/4.36	α_{S1}-casein	P02662	32	21.5					
20	23.58/17.92	5.13/4.46	β-casein	P02666			2061.81	44.9	FQSEEQQQ-TEDELQDK		
21	22.97/20.88	4.91/4.03	α_{S1}-casein	P02662	41.9	36.9					
22	22.97/20.75	4.91/4.12	α_{S1}-casein	P02662	42	26.2					
24	23.58/18.39	5.13/4.60	β-casein	P02666			2061.81	44.9	FQSEEQQQ-TEDELQDK		
25	22.97/19.93	4.91/4.61	α_{S1}-casein	P02662	69.8	24.3					
26	22.97/19.80	4.91/4.54	α_{S1}-casein	P02662	56.6	24.3					
27	22.97/31.09	4.91/4.34	α_{S1}-casein	P02662	61.2	31.8					
28	22.97/24.40	4.91/4.40	α_{S1}-casein	P02662	87.1	33.2					
30	66.43/65.11	5.6/6.39	serum albumin	P02769	85.3	16				923	19
31	24.35/70.32	8.34/6.18	α_{S2}-casein	P02663	49.1	18					
31	66.43/70.32	5.6/6.18	serum albumin	P02769	39.9	12.5					
31	23.58/70.32	5.13/6.18	β-casein	P02666	20.6	28.1					
33	18.97/21.15	5.93/6.01	κ-casein	O02782	28.7	30.5	1752.955	41.95	HPHPHLSFM-AIPPKK	198	3
34	22.97/21.80	4.91/4.56	α_{S1}-casein	P02662	51.5	24.3					
35	22.97/20.94	4.91/4.64	α_{S1}-casein	P02662	67.4	31.8					
38	23.58/19.22	5.13/4.54	β-casein	P02666			1029.54	36.35	HKEMPFPK		
39	22.97/19.33	4.91/4.18	α_{S1}-casein	P02662	41.5	16.8					
41	22.97/20.06	4.91/4.55	α_{S1}-casein	P02662	45.4	22.4					
42	22.97/19.92	4.91/4.44	α_{S1}-casein	P02662	51.5	24.3					
43	22.97/19.66	4.91/4.42	α_{S1}-casein	P02662	37.9	22.4					
44	22.97/19.95	4.91/4.71	α_{S1}-casein	P02662	54.5	22.4					
45	18.97/21.20	5.93/5.63	κ-casein	O02782	27.5	30.5					
46	18.97/21.28	5.93/5.38	κ-casein	O02782	27.9	42.4				102	3
47	24.35/21.53	8.34/4.26	α_{S2}-casein	P02663	35.4	15.7					
48	24.35/21.72	8.34/4.07	α_{S2}-casein	P02663	37.4	15.7					
49	18.97/20.74	5.93/6.19	κ-casein	O02782						40	1
50	24.35/28.94	8.34/5.32	α_{S2}-casein	P02663						264	7
52	18.97/55.27	5.93/5.98	κ-casein	O02782						171	3
53	18.97/56.66	5.93/5.63	κ-casein	O02782						120	1
54	18.97/61.37	5.93/5.65	κ-casein	O02782						120	2
54	24.35/61.37	8.34/5.65	α_{S2}-casein	P02663						83	4
55	41.77/56.38	5.24/4.81	α-actin 2	P62739						362	7
55	24.35/56.38	8.34/4.81	α_{S2}-casein	P02663						95	3
55	18.97/56.38	5.93/4.81	κ-casein	O02782						61	1
55	22.97/56.38	4.91/4.81	α_{S1}- casein	P02662						43	1
55	30.92/56.38	5.91/4.81	phenylethanol amine *N*-methyl-transferase	P10938						41	1
56	22.97/65.11	4.91/4.71	α_{S1}-casein	P02662						193	3
56	24.35/65.11	8.34/4.71	α_{S2}-casein	P02663						146	5
56	18.97/65.11	5.93/4.71	κ-casein	O02782						109	2
57	24.35/76.90	8.34/5.22	α_{S2}-casein	P02663	68.5	24.8					
57	24.35/76.90	8.34/5.22	α_{S2}-casein	P02663						251	7
58	24.35/70.85	8.34/5.21	α_{S2}-casein	P02663						112	2

Table 1. Continued

spot	MW[b] theor/obsd	p*I* theor/obsd[c]	identified protein	accession no.[d]	MALDI-TOF (a) Mascot score	MALDI-TOF (a) % coverage	MALDI-TOF/TOF (b) peptide mass	MALDI-TOF/TOF (b) Mascot score	MALDI-TOF/TOF (b) sequence	nano-LC-MS/MS (c) score	nano-LC-MS/MS (c) matching peptides
59	18.28/89.38	4.83/5.55	β-lactoglobulin	P02754						202	4
59	22.97/89.38	4.91/5.55	α_{S1}- casein	P02662						181	3
59	18.97/89.38	5.93/5.55	κ-casein	O02782						175	3
59	24.35/89.38	8.34/5.55	α_{S2}-casein	P02663						140	4
60	14.19/14.73	4.8/5.04	α-lactalbumin	P00711						252	5
61	18.28/18.50	4.83/6.73	β-lactoglobulin	P02754						420	8
62	18.28/18.50	4.83/6.95	β-lactoglobulin	P02754						486	10
63	18.97/21.15	5.93/6.73	κ-casein	O02782						138	2
64	18.97/21.15	5.93/6.95	κ-casein	O02782						117	1
65	66.43/65.32	5.6/6.73	serum albumin	P02769						977	21
66	66.43/65.32	5.6/6.95	serum albumin	P02769						979	22
67	18.28/18.50	4.83/6.32	β-lactoglobulin	P02754						285	7
68	18.28/18.27	4.99/5.16	β-lactoglobulin	P02754						415	9

[a] Spot numbers correspond to **Figures 1**, **2**, **4**, **5**, **6**, and **7**. [b] Observed molecular mass from the gel (kDa)/theoretical molecular mass (kDa, calculated from the primary amino acid sequence using sequence analysis tools). [c] Observed isoelectric point from the gel/theoretical isoelectric point (calculated from the primary amino acid sequence using sequence analysis tools). [d] Accession number in the Swiss-Prot database.

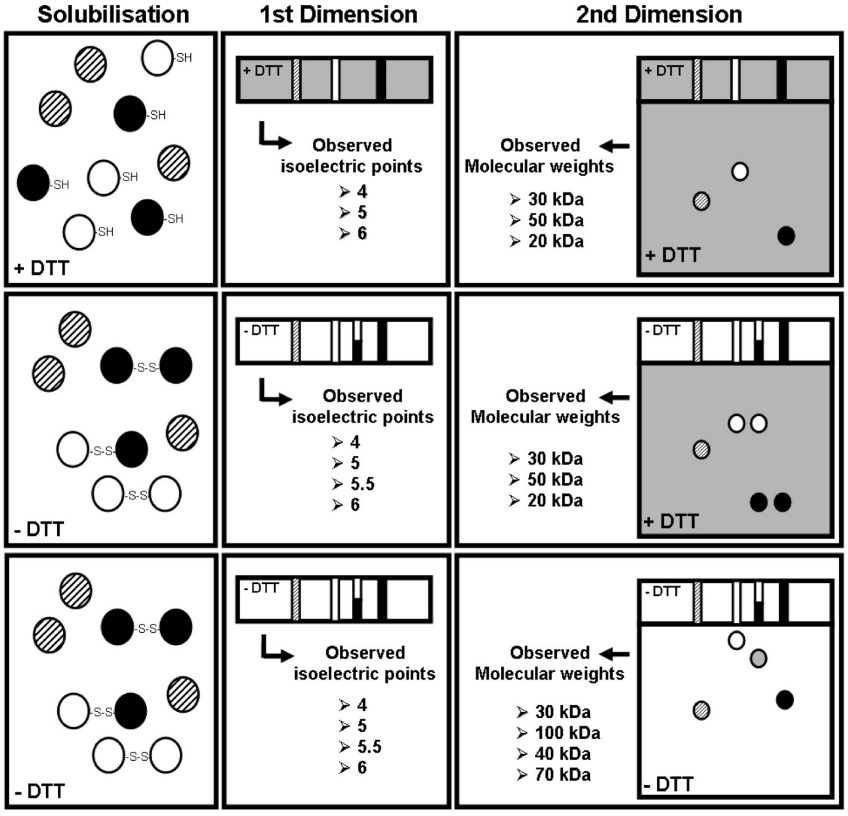

Figure 3. Schematic representation of the 2DE R/R, NR/R, and NR/NR strategies of analysis and the resulting expected results concerning the spots characteristic modification in term of isoelectric point and molecular weight. Milk samples were first diluted with solubilization buffer containing DTT (top panel, reduced samples) or without DTT (middle and bottom panel, unreduced samples) and then separated through 2D electrophoresis. Three samples conditions were set up to analyze and compare disulfide bridge exchanges (according to Miller et al. 2004): (a) samples completely reduced before and during 2-dimensional electrophoresis (top panel); (b) samples unreduced before 2-dimensional electrophoresis and reduced only after isoelectric focusing (middle panel); (c) samples unreduced before and during 2-dimensional electrophoresis (bottom panel).

conditions (i.e., without ionic detergents or reducing agents) may reveal natural interactions between milk proteins with a potential biological function, still unknown. The interaction of whey proteins (i.e., especially β-LG) and caseins (α_{S1}-/α_{S2}/κ-/β-CN) at the micellar surface can explain, at least in part, the initiation of a three-dimensional gel matrix during ultrahigh-temperature treatment involving whey proteins and caseins (*44*).

Nonreducing versus Reducing Two-Dimensional Electrophoresis of Heated Milk: Analysis of Heat-Induced Interactions. The changes in milk during heating at 90 °C for up to 30 min were analyzed by two-dimensional electrophoresis under three different sets of conditions of treatment (the principle is schematically described in **Figure 3**): 2DE R/R corresponds to samples analyzed under reducing conditions in both dimensions (i.e., all disulfide bonds were reduced during the full analysis, and complexes were resolved into their constituent proteins); 2DE NR/R corresponds to samples reduced only after isoelectric focusing (i.e., disulfide-bonded complexes resolved during IEF, but the bonds were

reduced during SDS-PAGE); and 2DE NR/NR corresponds to fully unreduced samples (i.e., disulfide-bonded complexes remained cross-linked throughout both dimensions of analysis). This strategy of analysis was first described by Miller et al. (*45*) for the specific study of disulfide-bond-mediated interactions between urinary proteins. This strategy, thanks to the powerful precision of IEF, represents a more accurate alternative to the strategy of consecutive steps of SDS-PAGE under nonreducing and reducing conditions (*33*). Analysis under R/R conditions corresponds to the conventional technique used to separate a complex mixture of reduced proteins through two-dimensional electrophoresis and was used to prepare the raw skim milk proteomic reference map (**Figure 1**), whereas analysis under NR/NR conditions was used to study the disulfide-bonded interactome in raw milk (**Figure 2**).

Samples of raw skimmed milk after heating for 0, 5, 10, and 30 min at 90 °C were submitted to these three different conditions of 2DE in triplicate experiments; the resulting gels were analyzed and spots of interest were identified using tryptic digestion followed by mass spectrometry, that is, MALDI-TOF mass spectra. Three areas of particular interest were selected and are highlighted in **Figure 1** (A, B, and C).

Area A corresponds to high molecular weight proteins or complexes (**Figure 4**), which were almost all observed only when 2-DE was carried out under completely nonreducing conditions (2DE NR/NR); consequently, these complexes were clearly disulfide-linked. After identification of the spots by MALDI-TOF MS, β-LG, κ-CN, β-CN, and α_{S1}-CN were identified as being involved in some of these spots. The former proteins are well-known to undergo heat-induced complex formation through thiol−disulfide interchange reactions (*19*, *46*), but the participation of the other two caseins determined is less widely reported, showing the capacity of this analysis strategy to identify constituent proteins in complex polymers. Under complete (R/R) or partial (NR/R) reducing conditions, only spot 56 can be matched with the NR/NR conditions for both heated times. This spot corresponds to a mixture of α_{S1}-/α_{S2}-/κ-CN. This heteropolymer was naturally observed under "native" nonreducing 2DE of raw milk and seemed to be partially resistant to reduction after heat treatment at 90 °C. It can be hypothesized that such high temperature can denature proteins and complexes and consequently hide disulfide bonds inside the three-dimensional structures, protecting them in part from reduction by DTT. Such high temperatures can also increase the glycation reactions between proteins and lactose and can induce covalently linked complexes, resistant to reducing agents (*47*). These oxidized complexes included disulfide bridges and a possible formation of a protein cross-link from initial Amadori adducts of lactose and ε-lysyl residues involving an imidazole function (*48*, *49*). Proteins without cysteine residues (β-CN and α_{S1}-CN) were possibly linked to these complexes by sugar-type bonds catalyzed by a nonenzymatic glycation process.

Spots in area B, which corresponds to several isoforms (spot 30) of bovine serum albumin (BSA), were also compared by heat treatment time and conditions of separation (**Figure 5**). These spots were observed in the control (unheated milk) sample under reducing and nonreducing conditions. However, when the milk was heated at 90 °C, the spots disappeared when IEF was carried out under nonreducing conditions. Thus, it appeared that BSA readily formed heat-induced complexes of high molecular weight which could not be resolved unless DTT was present in the initial stage of electrophoresis. BSA contains one free sulfhydryl of its 35 cysteines and is consequently highly susceptible to denaturation and aggregation on heating (*3*).

Area C (**Figure 6**) contained spots corresponding to the major whey proteins, β-LG (spots 8 and 68) and α-LA (spot 60). The two major genetic variants of β-LG (A and B) were identified by mass spectrometry as β-LG, but without any additional information concerning the nature of the analyzed variant. β-LG variants A and B differ only by two amino acids in position 80 (D/G) and 134 (D/A), respectively, according to the Swiss-Prot database

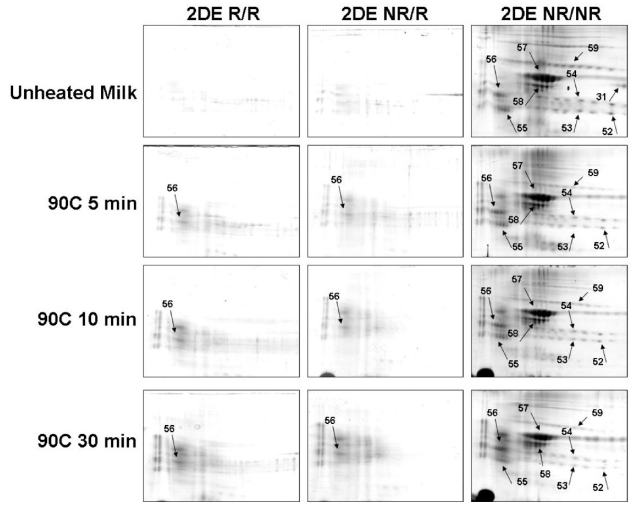

Figure 4. Comparison of changes in spots in area A of **Figure 1** as a function of heating time and different conditions of 2D electrophoresis.

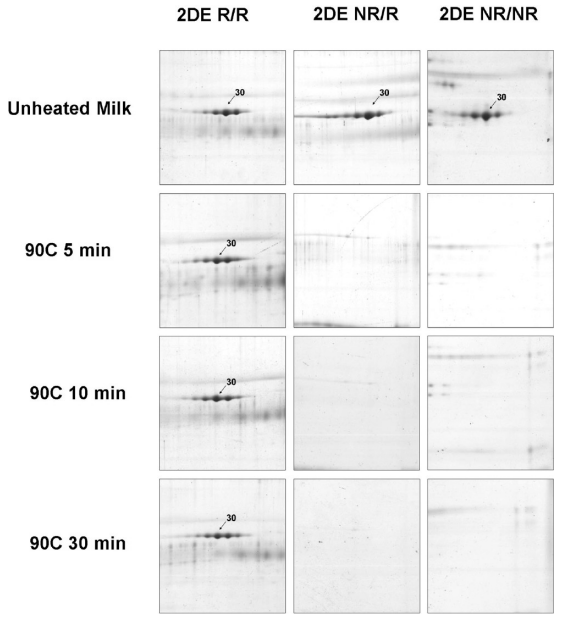

Figure 5. Comparison of changes in spots in area B of **Figure 1** as a function of heating time and reducing/nonreducing conditions of 2D electrophoresis.

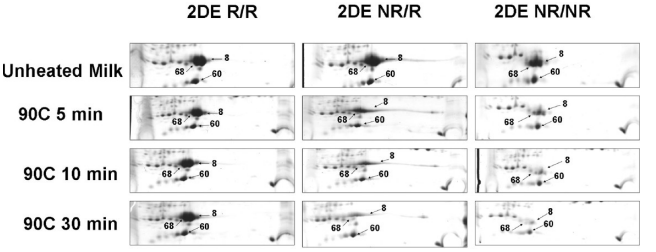

Figure 6. Comparison of changes in spots in area C of **Figure 1** as a function of heating time and reducing/nonreducing conditions of 2D electrophoresis.

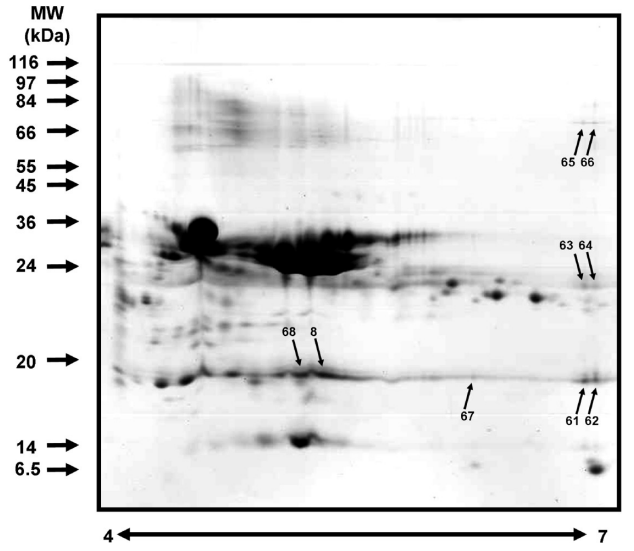

Figure 7. Two-dimensional gel electrophoretogram of milk protein (100 μg) separated under nonreducing conditions of solubilization and isoelectric focusing and then reducing condition of SDS-PAGE second dimension, using a 7-cm pH 4−7 p*I* range for the first dimension and a 10−18% gradient acrylamide gel for the second dimension. The specific/interesting spots are shown with arrows and were submitted to mass spectrometry identification by MALDI-TOF peptide mass fingerprint (**Table 1**).

(http://expasy.org/sprot), using the β-LG B accession number (P02754) as reference. From the primary sequence of the protein, the theoretical isoelectric point is 4.83 for β-LG variant B and 4.76 for variant A. Consequently, we can reasonably propose to identify spot 68 as variant A and spot 8 as variant B. These two variants of β-LG (A and B) were apparent in control samples and in heated milk samples analyzed under completely reducing conditions (top three panels and left four panels of **Figure 6**). Under completely nonreducing conditions, however, the intensity of the two protein spots decreased progressively and, after 30 min at 90 °C, the spots had almost completely disappeared. Over the same time, spot 60, corresponding to α-LA, showed the same pattern as β-LG's spots, with no intensity changes under 2DE R/R conditions, but with a progressive decrease of spot intensity under NR/R and NR/NR conditions as a function of heating time, showing that a part of α-LA was also involved in disulfide-linked polymers, even if no α-LA was identified in such oxidized complexes.

Part of the disulfide-cross-linked complex of β-LG could be reduced when DTT was added during the second dimension (NR/R), but with a range of isoelectric points from 5 to 7, revealed by a nonfocused smear on the right of the β-LG spots 8 and 68. The disulfide-bonded complexes of β-LG showed a large heterogeneity of isoelectric points, presumably due to the high molecular weights of polymers, which were difficult to focus normally during the first nonreducing dimension of the 2DE.

To further understand the protein species involved in these complexes, a preparative gel was prepared under NR/R reducing conditions using a milk sample heated for 30 min at 90 °C (**Figure 7**). On the basis of molecular weight, β-LG was identified in spots 61, 62, 67, and 68; κ-CN in spots 63 and 64; and serum albumin in spots 65 and 66. In contrast, the isoelectric point of the identified protein is far from the theoretical isoelectric point. The reducing conditions for the second dimension allowed determination of the correct molecular weight of all of these proteins. Nevertheless, the nonreducing condition of the first dimension did not result in dissociation of the complexes formed with disulfides bridges. This condition clearly showed a heterotrimer complex between one or more molecules of β-LG, κ-CN, and BSA formed by disulfide bonding, which focused near pH 7, the isoelectric point of spots 61−66. It can also be hypothesized that spot 67, which corresponds to β-LG, was involved in a complex of the same origin but involving other proteins. Although these complexes were clearly observed using nonreducing versus reducing 2DE conditions, the disulfide bridges involved in the homo/heteropolymer formation is still unknown. The next step of the present study will be the identification and localization of the disulfide bridges, as previously performed on goat's milk (*50*).

Conclusions. The strategy of separation selected for this study showed new findings on the "native-like" disulfide interactions between milk proteins, with or without any heat treatments. The proteomic tools resolved clearly a complex mixture of proteins in raw milk, including some natural disulfide-linked complexes; heating milk fundamentally altered the milk proteome and resulted in a range of cross-linked protein adducts, many of which were identified by mass spectrometry. In this study, it was shown that different two-dimensional electrophoresis separations followed by mass spectrometry have the capacity to identify the protein partners involved inside oxidized complexes, which can potentially be used as potential markers of milk oxidation (*51*). The reduced or oxidized state of proteins in a very complex environment of reducing sugar and lipids such as milk can be an indicator of the quality and storage capacity of dairy products.

ACKNOWLEDGMENT

We thank Professor Patrick Fox of University College Cork for helpful comments on the manuscript.

LITERATURE CITED

(1) Sawyer, W. H. Complex between β-lactoglobulin and κ-casein. A review. *J. Dairy Sci.* **1969**, *52*, 1347–1355.
(2) Gezimati, J.; Creamer, L. K.; Singh, H. Heat-induced interactions and gelation of mixtures of β-lactoglobulin and alpha-lactalbumin. *J. Agric. Food Chem.* **1997**, *45*, 1130–1136.
(3) Havea, P.; Singh, H.; Creamer, L. K. Characterization of heat-induced aggregates of β-lactoglobulin, α-lactalbumin and bovine serum albumin in a whey protein concentrate environment. *J. Dairy Res.* **2001**, *68*, 483–497.
(4) Bertrand-Harb, C.; Baday, A.; Dalgalarrondo, M.; Chobert, J.- M.; Haertle, T. Thermal modifications of structure and co-denaturation of α-lactalbumin and β-lactoglobulin induce changes of solubility and susceptibility to proteases. *Nahrung* **2002**, *46*, 283–289.
(5) Cho, Y.; Singh, H.; Creamer, L. K. Heat-induced interactions of β-lactoglobulin A and κ-casein B in a model system. *J. Dairy Res.* **2003**, *70*, 61–71.
(6) Zittle, C. A.; Thompson, M. P.; Custer, J. H.; Cerbulis, J. κ-Casein−β-lactoglobulin interaction in solution when heated. *J. Dairy Sci.* **1962**, *45*, 807–810.
(7) Sawyer, W. H.; Coulter, S. T.; Jenness, R. Role of sulfhydryl groups in the interaction of κ-casein and β-lactoglobulin. *J. Dairy Sci.* **1963**, *46*, 564–565.
(8) McKenzie, H. A. α-Lactoglobulins. In *Milk Proteins: Chemistry and Molecular Biology*; McKenzie, H. A., Ed.; Academic Press: New York, 1971; pp 257−330.
(9) Hill, A. R. The β-lactoglobulin−κ-casein complex. *Can. Inst. Food Sci. Technol. J.* **1989**, *22*, 120–123.
(10) Jang, H. D.; Swaisgood, H. E. Disulfide bond formation between thermally denatured β-lactoglobulin and κ-casein in casein micelles. *J. Dairy Sci.* **1990**, *73*, 900–904.
(11) Corredig, M.; Dalgleish, D. G. Effect of temperature and pH on the interactions of whey proteins with casein micelles in skim milk. *Food Res. Int.* **1996**, *29*, 49–55.
(12) Corredig, M.; Dalgleish, D. G. The binding of α-lactalbumin and β-lactoglobulin to casein micelles in milk treated by different heating systems. *Milchwissenschaft* **1996**, *51*, 123–127.

(13) Corredig, M.; Dalgleish, D. G. The mechanisms of the heatinduced interaction of whey proteins with casein micelles in milk. *Int. Dairy J.* **1999**, *9*, 233–236.
(14) Euber, J. R.; Brunner, J. R. Interaction of κ-casein with immobilized β-lactoglobulin. *J. Dairy Sci.* **1982**, *65*, 2384–2387.
(15) Anema, S. G.; Li, Y. Effect of pH on the association of denatured whey proteins with casein micelles in heated reconstituted skim milk. *J. Agric. Food Chem.* **2003**, *51*, 1640–1646.
(16) Anema, S. G.; Li, Y. Association of denatured whey proteins with casein micelles in heated reconstituted skim milk and its effect on casein micelle size. *J. Dairy Res.* **2003**, *70*, 73–83.
(17) McKenzie, G. H.; Norton, R. S.; Sawyer, W. H. Heat-induced interaction of β-lactoglobulin and κ-casein. *J. Dairy Res.* **1971**, *38*, 343–351.
(18) Creamer, L. K.; Bienvenue, A.; Nilsson, H.; Paulsson, M.; van Wanroij, M.; Lowe, E. K.; Anema, S. G.; Boland, M. J.; Jiménez-Flores, R. Heat-induced redistribution of disulfide bonds in milk proteins. 1. Bovine α-lactoglobulin. *J. Agric. Food Chem.* **2004**, *52*, 7660–7668.
(19) Lowe, E. K.; Anema, S. G.; Bienvenue, A.; Boland, M. J.; Creamer, L. K.; Jimenez-Flores, R. Heat-induced redistribution of disulfide bonds in milk proteins. 2. Disulfide bonding patterns between bovine β-lactoglobulin and κ-casein. *J. Agric. Food Chem.* **2004**, *52*, 7669–7680.
(20) Jang, H. D.; Swaisgood, E. Disulphide bond formation between thermally denatured β-lactoglobulin and κ-casein in casein micelles. *J. Dairy Sci.* **1990**, *73*, 900–904.
(21) Livney, Y. D.; Dalgleish, D. G. Specificity of disulphide bond formation during thermal aggregation in solutions of β-lactoglobulin B and κ-casein A. *J. Agric. Food Chem.* **2004**, *52*, 5527–5532.
(22) Swaisgood, H. E. Chemistry of the caseins. In *Advanced Dairy Chemistry. s1. Proteins*; Fox, P. F., Ed.; Elsevier Applied Science: London, U.K., 1992; pp 63−110.
(23) Rasmussen, L. K.; Johnsen, L. B.; Tsiora, A.; Sørensen, E. S.; Thomsen, J. K.; Nielsen, N. C.; Jakobsen, H. J.; Petersen, T. E. Disulphide-linked caseins and casein micelles. *Int. Dairy J.* **1999**, *9*, 215–218.
(24) Guyomarc'h, F.; Law, A. J. R.; Dalgleish, D. G. Formation of soluble and micelle-bound protein aggregates in heated milk. *J. Agric. Food Chem.* **2003**, *51*, 4652–4660.
(25) Smits, P.; van Brouwershaven, J. H. Heat-induced association of β-lactoglobulin and casein micelles. *J. Dairy Res.* **1980**, *47*, 313–325.
(26) Singh, H.; Creamer, L. K. Denaturation, aggregation and heat stability of milk protein during the manufacture of skim milk powder. *J. Dairy Res.* **1991**, *58*, 269–283.
(27) Vasbinder, A. J.; de Kruif, C. G. Casein−whey protein interactions in heated milk: the influence of pH. *Int. Dairy J.* **2003**, *13*, 669–677.
(28) Nabhan, M. A.; Girardet, J. M.; Campagna, S.; Gaillard, J. L.; Le Roux, Y. Isolation and characterization of copolymers of β-lactoglobulin, α-lactalbumin, κ-casein, and α_{S1}-casein generated by pressurization and thermal treatment of raw milk. *J. Dairy Sci.* **2004**, *87*, 3614–3622.
(29) Oldfield, D. J.; Singh, H.; Taylor, M. W. Kinetics of heat-induced whey protein denaturation and aggregation in skim milks with adjusted whey protein concentration. *J. Dairy Res.* **2005**, *72*, 369–378.
(30) Galvani, M.; Hamdan, M.; Righetti, P. G. Two-dimensional gel electrophoresis/matrix-assisted laser desorption/ionization mass spectrometry of a milk powder. *Rapid Commun. Mass Spectrom.* **2000**, *14*, 1889–1897.
(31) Holland, J. W.; Deeth, H. C.; Alewood, P. F. Proteomic analysis of κ-casein micro-heterogeneity. *Proteomics* **2004**, *4*, 743–752.
(32) Holland, J. W.; Deeth, H. C.; Alewood, P. F. Resolution and characterisation of multiple isoforms of bovine κ-casein by 2-DE following a reversible cysteine-tagging enrichment strategy. *Proteomics* **2006**, *6*, 3087–3095.
(33) Patel, H. A.; Singh, H.; Anema, S. G.; Creamer, L. K. Effects of heat and high hydrostatic pressure treatments on disulphide bonding interchanges among the proteins in skim milk. *J. Agric. Food Chem.* **2006**, *54*, 3409–3420.
(34) Creamer, L. K.; Bienvenue, A.; Nilsson, H.; Paulsson, M.; van Wanroij, M.; Lowe, E. K.; Anema, S. G.; Boland, M. J.; Jiménez-Flores, R. Heat-induced redistribution of disulphide bonds in milk proteins. 1. Bovine β-lactoglobulin. *J. Agric. Food Chem.* **2004**, *52*, 7660–7668.
(35) Livney, Y. D.; Dalgleish, D. G. Specificity of disulfide bond formation during thermal aggregation in solutions of β-lactoglobulin B and κ-casein A. *J. Agric. Food Chem.* **2004**, *52*, 5527–5532.
(36) Yamada, M.; Murakami, K.; Wallingford, J. C.; Yuki, Y. Identification of low-abundance proteins of bovine colostral and mature milk using two-dimensional electrophoresis followed by microsequencing and mass spectrometry. *Electrophoresis* **2002**, *23*, 1153–1160.
(37) Chevalier, F.; Martin, O.; Rofidal, V.; Devauchelle, A. -D.; Rossignol, M. Proteomic investigation of natural variation between *Arabidopsis* ecotypes. *Proteomics* **2004**, *4*, 1372–1381.
(38) Bradford, M. M. A rapid and sensitive method for the quantitation of microgram quantities of protein utilizing the principle of protein−dye binding. *Anal. Biochem.* **1976**, *72*, 248–254.
(39) Chevalier, F.; Rofidal, V.; Vanova, P.; Bergoin, A.; Rossignol, M. Proteomic capacity of recent fluorescent dyes for protein staining. *Phytochemistry* **2004**, *65*, 1499–1506.
(40) Chevalier, F.; Centeno, D.; Rofidal, V.; Tauzin, M.; Sommerer, N.; Rossignol, M. Differential capacity of visible stains and fluorescent dyes for large-scale investigation of proteomes by MALDI-TOF MS. *J. Proteome Res.* **2006**, *5*, 512–520.
(41) Fox, P. F.; McSweeney, P. L. H. *Dairy Chemistry and Biochemistry*; Blackie Academic and Professional Publishers: London, U.K., 1998.
(42) Lehtonen, S. T.; Ohlmeier, S.; Kaarteenaho-Wiik, R.; Harju, T.; Pääkkö, P.; Soini, Y.; Kinnula, V. L. Does the oxidative stress in chronic obstructive pulmonary disease cause thioredoxin/peroxiredoxin oxidation? *Antioxid. Redox. Signal.* **2008**, *10*, 813–819.
(43) Holland, J. W.; Deeth, H. C.; Alewood, P. F. Analysis of disulphide linkages in bovine κ-casein oligomers using two-dimensional electrophoresis. *Electrophoresis* **2008**, *29*, 2402–2410.
(44) Datta, N.; Deeth, H. C. Age gelation of UHT milk: a review. *Food Bioprod. Proc.* **2001**, *79*, 197–210.
(45) Miller, I.; Teinfalt, M.; Leschnik, M.; Wait, R.; Gemeiner, M. Non-reducing two-dimensional gel electrophoresis for the detection of Bence Jones proteins in serum and urine. *Proteomics* **2004**, *4*, 257–260.
(46) Considine, T.; Patel, H. A.; Anema, S. G.; Singh, H.; Creamer, L. K. Interactions of milk proteins during heat and high hydrostatic pressure treatments—a review. *Innovative Food Sci. Emerg. Technol.* **2007**, *8*, 1–23.
(47) Chevalier, F.; Chobert, J.-M.; Mollé, D.; Haertlé, T. Maillard glycation of β-lactoglobulin with several sugars: comparative study of the properties of the obtained polymers and of the substituted sites. *Lait* **2001**, *81*, 655–666.
(48) Chevalier, F.; Chobert, J.-M.; Dalgalarrondo, M.; Haertlé, T. Characterization of the Maillard reactions product of β-lactoglobulin glucosylated in mild conditions. *J. Food Biochem.* **2001**, *25*, 33–55.
(49) Pongor, S.; Ulrich, P. C.; Bencsath, F. A.; Cerami, A. Aging of proteins: isolation and identification of a fluorescent chromophore from the reaction of polypeptides with glucose. *Proc. Natl. Acad. Sci. U.S.A.* **1984**, *81*, 2684–2688.
(50) Henry, G.; Mollé, D.; Morgan, F.; Fauquant, J.; Bouhallab, S. Heat-induced covalent complex between casein micelles and β-lactoglobulin from goat's milk: identification of an involved disulfide bond. *J. Agric. Food Chem.* **2002**, *50*, 185–191.
(51) Wait, R.; Begum, S.; Brambilla, D.; Carabelli, A. M.; Conserva, F.; Rocco Guerini, A.; Eberini, I.; Ballerio, R.; Gemeiner, M.; Miller, I.; Gianazza, E. Redox options in two-dimensional electrophoresis. *Amino Acids* **2005**, *28*, 239–272.

Received February 13, 2009. Revised manuscript received April 29, 2009. Accepted May 13, 2009. Funding for this research was provided under the National Development Plan 2007-2013, through the Food Institutional Research Measure, administered by the Department of Agriculture, Fisheries and Food, Ireland. This work was also supported by the Proteomic Platform of Montpellier-LR Genopole.

JOURNAL OF AGRICULTURAL AND FOOD CHEMISTRY
ARTICLE

J. Agric. Food Chem. 2010, 58, 7437–7444 7437
DOI:10.1021/jf1010879

Proteomic Quantification of Disulfide-Linked Polymers in Raw and Heated Bovine Milk

François Chevalier*,†,‡ and Alan L. Kelly†

†School of Food and Nutritional Sciences, University College Cork, Cork, Ireland, and
‡Proteomic Platform, CEA, Fontenay aux Roses, France

Disulfide bond formation between milk protein molecules was quantified in raw and heated bovine milk using reducing and nonreducing two-dimensional electrophoresis. Analysis of protein profiles in raw milk indicated that 18% of α_{S2}-casein, 25% of β-lactoglobulin, and 46% of κ-casein molecules were involved in disulfide-linked complexes (calculated through differences in spot volumes on two-dimensional electrophoretograms under reducing and nonreducing conditions), whereas levels of α_{S1}- and β-caseins were similar under both conditions. Following heat treatment at 90 °C for 30 min, spot volumes of serum albumin, β-lactoglobulin, and κ-casein decreased by 85%, 75%, and 75%, respectively, with the formation of several spots on nonreducing gels corresponding to polymers. Homopolymers and heteropolymers of κ-casein and α_{S2}-casein were identified by mass spectrometry in raw milk samples; polymers involving only α_{S2}-casein or only κ-casein accounted for 43% and 12% of the total polymers present, respectively. In addition, 45% of polymers in raw milk involved α_{S2}-casein in association with other proteins as heteropolymers, indicating the key role of this protein in intermolecular disulfide bridging between proteins in raw milk. The intensity of monomeric κ-casein spots decreased progressively with heating time at 90 °C, with greatest changes in spots with acidic isoelectric points. Interactions and association of milk proteins via disulfide bridges are discussed in relation to the proteins involved and their potential protective function against formation of fibril aggregates.

KEYWORDS: Milk proteome; polymer quantification; interactome; heat treatment; disulfide bridges; mass spectrometry

INTRODUCTION

One of the major objectives of dairy biochemistry is understanding of functional and biological properties of biomolecules. For this purpose, the techniques most widely used to visualize and analyze proteins are SDS−PAGE and two-dimensional electrophoresis (2DE) under denaturing conditions. Milk proteins have been analyzed extensively using proteomic tools (*1*−*13*). Based on two independent biochemical characteristics of proteins, 2DE combines isoelectric focusing (IEF), which separates proteins according to their isoelectric point (related to amino acid characteristics, i.e., acid/basic/neutral), and SDS−PAGE, which separates them further according to their molecular mass. At present, 2DE allows simultaneous detection and quantification of up to thousands of protein spots in the same gel (*14*, *15*). Combined with subsequent mass spectrometry analysis, 2DE offers the possibility of identifying proteins and comparing isoform abundance and posttranslational modifications (*16*−*19*).

Despite numerous proteomic studies analyzing milk proteins, many questions concerning milk protein expression, modification, and interactions remain unanswered. Milk is a very complex fluid secretion, composed of a colloidal emulsion of fat globules and casein micelles in a water-based fluid containing soluble proteins, lactose, and many trace elements such as vitamins and minerals (*20*). In this biological system, caseins are organized and stabilized in micelles (*21*−*23*). The biological function of the caseins is largely nutritional; casein micelles serve as calcium-transport vesicles, providing young mammals with a concentrated, yet soluble, form of calcium as well as essential amino acids (*24*). Another biological function of caseins was described recently (*25*), where these proteins can act as chaperones to protect proteins against aberrant aggregations, including formation of amyloid fibrils, when exposed to stress conditions such as elevated temperature or reducing environment (*26*−*29*).

During processing, bovine milk is submitted to several physical treatments, especially homogenization and pasteurization. These processes are well-known to induce modifications in protein organizations (*30*−*32*). Heat treatment of milk results in a number of physicochemical changes in the milk constituents, in particular, denaturation of whey proteins, leading to hydrophobic interactions or disulfide-bonded aggregation with κ-casein at the surface of casein micelles (*31*−*35*). Two disulfide bridges and a free sulfhydryl group present in the native structure of the whey protein β-lactoglobulin seem to play a critical role in its heat-induced interactions with κ-casein (*36*−*42*). Patel et al. (*43*) recently developed a system based on a two-dimensional PAGE method to explore the differences in the irreversible disulfide bond changes among the milk proteins after heat pressure treatments. They

*To whom correspondence should be addressed. Tel: +33 (0)146 548 326. Fax: +33 (0)146 549 138. E-mail: francois.chevalier@cea.fr.

Published on Web 05/26/2010

observed disulfide-bonded aggregates that included a high proportion of all the whey proteins and κ-casein and a proportion of the α_{S2}-casein. Following these important novel findings, a similar method to analyze milk protein complexes, based on the strategy of Miller et al. (*44*), using a combination of nonreducing and reducing steps with a high resolutive conventional proteomic approach (*45*), was developed. Nonreducing IEF was first performed to separate disulfide-linked polymers, and then reducing or nonreducing SDS−PAGE was used as a second dimension to separate protein complexes. Protein spots were analyzed by mass spectrometry to identify the proteins involved in each complex.

Based on the same analysis strategy, in the present study, the complexes formed under native-like conditions or after heat treatment were characterized, quantified, and compared with the corresponding nonaggregated protein spots to understand a possible biological function of such interactions. Following the approach of Holland et al. (*46*), a special focus was placed on κ-casein spots to understand and quantify the milk proteins which preferentially interact in the native environment or after heat treatment.

MATERIALS AND METHODS

Milk Treatment and Protein Solubilization. Fresh raw milk was obtained, skimmed, and preserved as described in ref *45*; subsamples of skim milk were also heated in a water bath at 90 °C for time periods up to 30 min. Samples were then prepared for electrophoresis with or without reducing agent, and protein content was measured as described in ref *45*.

One-Dimensional Gel Electrophoresis. Separation of milk samples was carried out according to the method of Laemmli (*47*) on 12.5% acrylamide gels using the Protean II system (Bio-Rad, Hercules, CA). The gels were stained with Coomassie Blue (R250) and scanned to digital images with a GS-800 densitometer (Bio-Rad).

Two-Dimensional Gel Electrophoresis. Each milk sample was analyzed using two-dimensional gel electrophoresis as described previously (*45*). Briefly, precast 7 cm strips, pH range 4−7 (Bio-Rad, Hercules, CA), were rehydrated in the presence of 100 μg of reduced or unreduced milk protein. Isoelectric focusing was carried out using a Protean IEF cell (Bio-Rad, Hercules, CA) until 50 kV h^{-1} and submitted to the second dimension. SDS−PAGE was carried out on a 10−18% acrylamide gradient (Gradient former 485; Bio-Rad) using a Criterion Dodeca Cell electrophoresis unit (Bio-Rad). Gels were stained with colloidal Coomassie Blue (*48*) and scanned to images with a GS 800 densitometer (Bio-Rad). Two-dimensional gels were analyzed with the Progenesis Samespots software V3.3 (Nonlinear). The same gel area was selected and compared, and the spot volume was quantified as a mean of each replicate. For each picture used, the same spots were reproduced, and when no spot was detected, a background value was automatically created by the software and used in the analysis. All spots and isoforms were detected, and spot volumes were compared between samples, and apparent isoelectric points and molecular weights were calculated from spot localization in the 2DE maps.

Mass Spectrometry Analysis. Stained protein spots were excised manually, washed, digested with trypsin as previously described (*45*), and extracted using formic acid. Protein digests were analyzed using an ion-trap mass spectrometer (Esquire HCT plus; Bruker Daltonics) coupled to a nanochromatography system (HPLC 1200; Agilent) interfaced with an HPLC-Chip system (Chip Cube; Agilent). MS/MS data were searched against NCBI (National Center for Biotechnology Information) and MSDB databases using Mascot software with a parent and fragment ion mass tolerance of 0.6 Da for doubly and triply charged peptides.

RESULTS

Electrophoretic Analysis (One-Dimensional) of Raw and Heated Skim Milk. Separation of milk proteins using SDS−PAGE is a conventional technique to visualize the different protein species in a given sample; electrophoretic separation of proteins in the milk sample is shown in **Figure 1**. Under reducing conditions (**Figure 1**, left part), BSA, κ-casein, β-lactoglobulin, and α-lactalbumin were well separated. However, α_{S1}-, α_{S2}-, and β-caseins were badly separated owing to their very similar molecular weights. No modification of the protein pattern under reducing condition was observed between the raw milk sample (**Figure 1**, lane 1) and samples heated for 5, 10, or 30 min at 90 °C (**Figure 1**, lanes 2, 3, and 4, respectively).

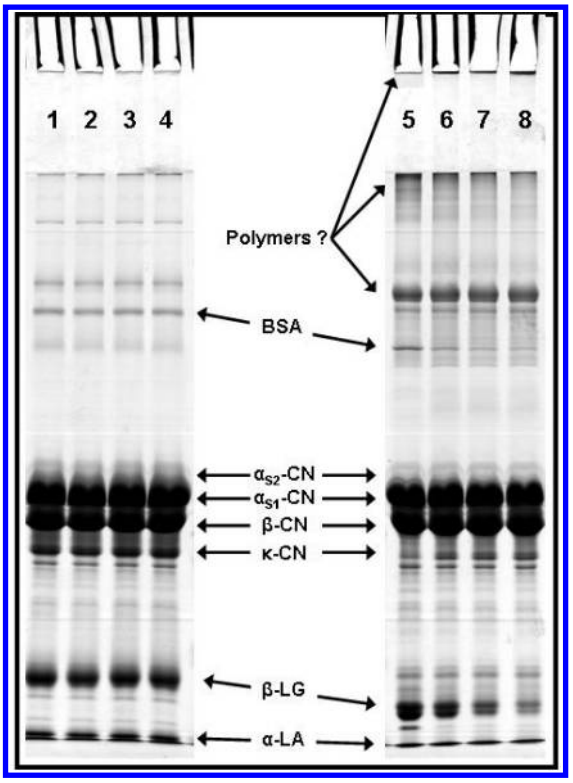

Figure 1. SDS−PAGE electropherogram of raw milk (lanes 1 and 5) or milk heated for 5 min (lanes 2 and 6), 10 min (lanes 3 and 7), or 30 min (lanes 4 and 8) at 90 °C under reducing (left part) and nonreducing (right part) conditions.

Under nonreducing conditions (SDS−PAGE without β-mercaptoethanol) some differences can be observed. Compared to reduced monomeric κ-casein, the amount of unreduced protein was considerably decreased in raw milk (**Figure 1**, lane 5) and remained at the same level during heat treatment, whereas amounts of unreduced BSA and β-lactoglobulin bands disappeared progressively during heat treatment (**Figure 1**, lanes 6−8), with concomitant appearance of polymers in the upper part of the gel. These polymers were expected to be formed by the interaction of κ-casein, β-lactoglobulin, and other milk proteins containing available sulfhydryl groups. The reactivity of milk proteins in forming polymers has been largely described using model systems. However, many questions concerning the composition and the amount of polymers cannot be answered owing to the low separation power of SDS−PAGE. Thus, a new strategy based on proteomic analysis, using high-resolution IEF followed by SDS−PAGE, was developed (*45*).

Comparison of Nonreducing and Reducing 2DE of Proteins in Raw Milk. Two-dimensional electrophoresis of proteins in unheated milk was performed under reducing and nonreducing conditions (**Figure 2**). The proteomic map obtained under reducing conditions was characteristic of a milk sample. Several spots for each casein and whey protein were observed and identified using mass spectrometry (**Table 1**). The use of IEF as the first dimension resolved multiple protein isoforms in comparison with the 1D analysis (right part of the 2D gel), without IEF. Most of the κ-casein spots were easily observed and corresponded to

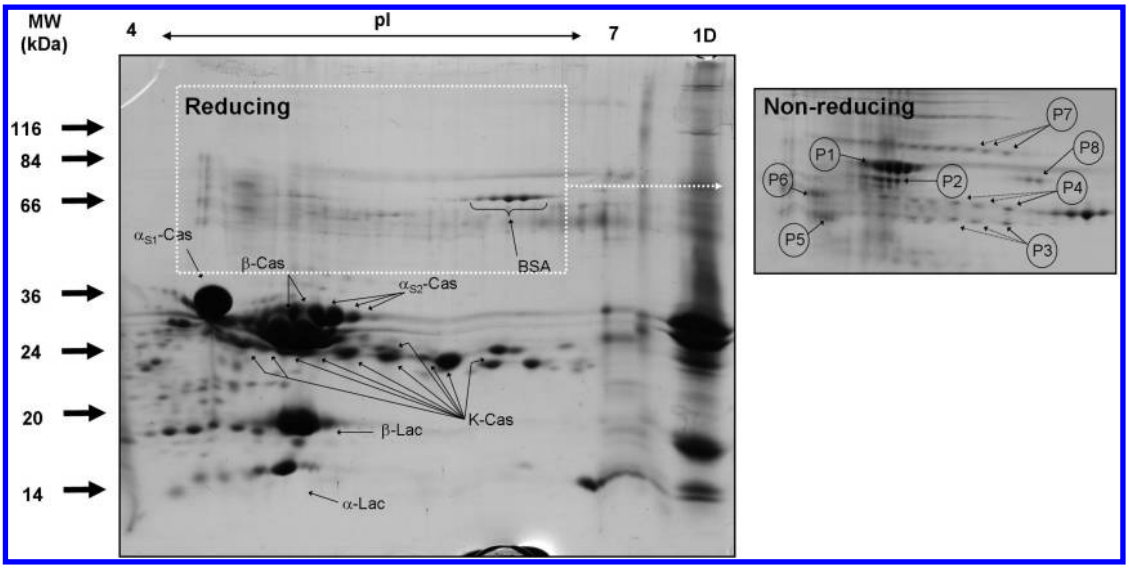

Figure 2. Two-dimensional electropherogram of proteins in raw milk under reducing (left-hand side) or nonreducing (right-hand side, part shown only corresponding to area indicated on left-hand figure) conditions. The major milk proteins are indicated with arrows under reducing conditions; polymers from **Tables 1** and **2** are labeled with arrows only under nonreducing conditions.

Table 1. Characteristics of Protein and Polymer Spots Separated by Two-Dimensional Electrophoresis in Raw Milk under Reducing (*) or Nonreducing (**) Conditions from Image Analysis of Gels Presented in **Figure 2**[a]

	theor/app MW (kDa)	theor/app p*I*	no. of spot isoforms
α_{S1}-casein	22.97/33.6	4.91/4.66	1*
α_{S2}-casein	24.35/33.0	8.34/5.15−5.33	3*
β-casein	23.58/30.3	5.13/4.96−5.05	2*
κ-casein	18.97/24.4−26.1	5.93/4.64−6.24	10*
β-lactoglobulin	18.28/18.7	4.83/4.9−5.01	2*
α-lactalbumin	14.19/14.8	4.80/4.99	1*
serum albumin	66.43/65.4	5.6/5.88−6.25	6*
P1	Ø/79.1	Ø/4.95−5.29	7**
P2	Ø/75.9	Ø/5.02−5.23	6**
P3	Ø/64.1	Ø/4.94−5.76	9**
P4	Ø/69.2	Ø/4.94−5.76	9**
P5	Ø/64.6	Ø/4.69−4.82	5**
P6	Ø/71.9	Ø/4.62−4.78	5**
P7	Ø/86.2	Ø/4.74−5.85	18**
P8	Ø/75.9	Ø/5.81−5.92	3**

[a] Ø indicates that theoretical molecular weight (MW) or isoelectric point (p*I*) was not calculated for polymers P1 to P8.

isoforms arising from posttranslational modifications such as phosphorylation and glycosylation (*16*−*19*, *45*).

Under nonreducing conditions (**Figure 2**, right-hand side), several new spots appeared (P1 to P8), ranging from p*I* 4.62 to 6.25 and 64.1 to 86.2 kDa (**Table 1**). These polymers, naturally present in unheated milk, were only observed under nonreducing conditions (*45*, *46*) and were likely formed by disulfide cross-links between milk proteins. All of these species were analyzed by an ion-trap mass spectrometer coupled to a nanochromatography system, and the proteins identified as being involved in these complexes are reported in **Table 2**. All of the observed polymers were composed of α_{S2}-casein and/or κ-casein (P1 to P4), with α_{S1}-casein (P5, P6, and P7), β-casein (P8), β-lactoglobulin (P7), and serum albumin (P8). These polymers were observed with several spot isoforms (**Table 1**), from 3 spots (P8) to 18 spots (P7). The spot patterns were likely due to the biochemical characteristic of the proteins involved. For example, in the case of the homopolymer "P3", composed exclusively of κ-casein (*46*), 9 spots were

Table 2. Presence of Caseins and Whey Proteins in Polymers Observed in Raw Milk under Nonreducing 2DE according to Ref *45* and This Study

	α_{S1}-casein	α_{S2}-casein	β-casein	κ-casein	β-lactoglobulin	serum albumin
P1		x				
P2		x				
P3				x		
P4		x		x		
P5	x	x		x		
P6	x	x		x		
P7	x	x		x	x	
P8		x	x			x

observed and corresponded to the different posttranslational modifications of the protein. These results were in agreement with the data of Patel et al. (*43*), using a similar strategy for separation (PAGE instead of IEF for the first dimension), in which disulfide-bonded polymers of whey proteins, κ-casein, and α_{S2}-casein were identified after severe heat treatment (70−140 °C) of milk samples.

Quantification of Milk Proteins in Raw and Heated Milk. The total amount of each major milk protein separated under nonreducing 2DE was estimated for raw milk and milk heated for 5, 10, or 30 min at 90 °C (**Figure 3**). The quantification of these milk proteins was performed using the 2DE proteomic map of raw milk separated under reducing conditions as reference sample; each value corresponded to a percentage of the same protein on the reducing 2DE.

In raw milk (T0), 75% of β-lactoglobulin, 82% of α_{S2}-casein, and 54% of κ-casein spot volumes were present on nonreducing gels compared to gels run under reducing conditions. This decrease of spot amount implies that a significant proportion of these proteins are present in polymers in a native environment without any heat treatment. In contrast, serum albumin, α_{S1}-casein, and β-casein spots in heated milk were not significantly different under reducing and nonreducing conditions. After heating milk at 90 °C, serum albumin was the protein most affected, as around 85% of the protein disappeared on nonreducing 2DE gels after 5 min at 90 °C. Levels of β-lactoglobulin and κ-casein decreased gradually when milk samples were heated for 5, 10, and 30 min, until about 25% of protein remained. Under

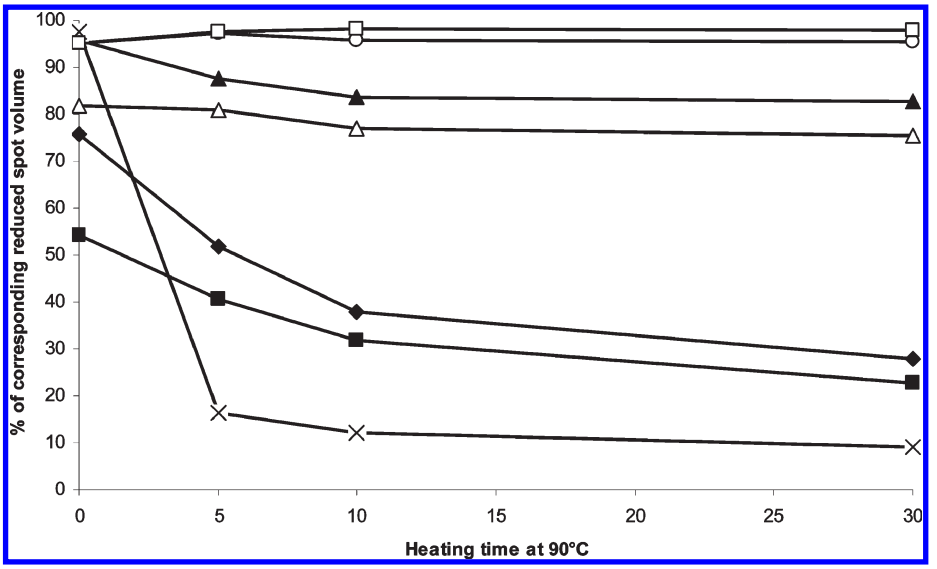

Figure 3. Levels of β-lactoglobulin (◆), κ-casein (■), α-lactalbumin (▲), serum albumin (×), α_{S1}-casein (○), α_{S2}-casein (△), and β-casein (□) separated under nonreducing 2DE normalized as a percentage of the corresponding spots separated under reducing 2DE as a function of heating time of milk at 90 °C.

nonreducing conditions, levels of α_{S1}-, α_{S2}-, and β-caseins were similar in unheated and heated samples. In contrast, the level of α-lactalbumin decreased from 95% (in raw milk) to 82% (heated for 30 min at 90 °C) under nonreducing conditions.

Quantification of Nonreduced Polymers in Raw and Heated Milk. As with the major milk proteins, all polymers observed under nonreducing conditions were quantified, and the proportion of each polymer under nonreducing 2DE was estimated (**Figure 4**, top part). In raw milk, the two most abundant polymers, P1 and P2, were composed of α_{S2}-casein only. Relative to the total of all polymer spot volumes, polymers involving only α_{S2}-casein represented 43% of all polymers, demonstrating the significance of intermolecular disulfide bonding for this protein. Polymers P2 to P7, which showed a larger p*I* range, were composed of homopolymers of κ-casein (12%), as observed by Holland et al. (*46*) and/or a combination of α_{S1}-casein, α_{S2}-casein, and β-lactoglobulin. Serum albumin and β-casein were only identified in polymer P8, which represented only 2% of the amount of all polymers. It can be noticed that α_{S2}-casein and κ-casein were involved in 45% and 31% of polymers, respectively, as heteropolymers. This emphasizes the key role of the cysteine residues of these two proteins in forming naturally occurring interchain disulfide bridges between proteins in raw milk (*22*, *49*, *50*).

In heated milk, changes in the level of each polymer using the level of all polymers observed in raw milk as reference was also analyzed (**Figure 3** bottom part). Polymers P1, P3, P6, and P7 remained constant and polymers P2, P4, P5, and P8 were significantly decreased as a function of heating time. Polymer P8 was the most affected by heat treatment, with a reduction of 80% of the polymer level being observed after 5 min at 90 °C.

As polymers P1 and P2 were composed of homopolymers of α_{S2}-casein and level of P1 remained constant, but that of P2 decreased, as a function of heating time, it is proposed that polymer P2 may be a stable transition complex, which can be converted to P1 during heat treatment.

Quantification of Individual κ-Casein Spots in Raw and Heated Milk. In raw milk, 10 κ-casein spots were observed under reducing conditions (**Figures 2** and **5A**), using an IEF range p*I* 4−7. This spot pattern was consistent with the study of Holland et al. (*16*), who analyzed the posttranslational modifications of κ-casein in bovine milk, using 2DE (p*I* 4−7 and 14% acrylamide SDS−PAGE).

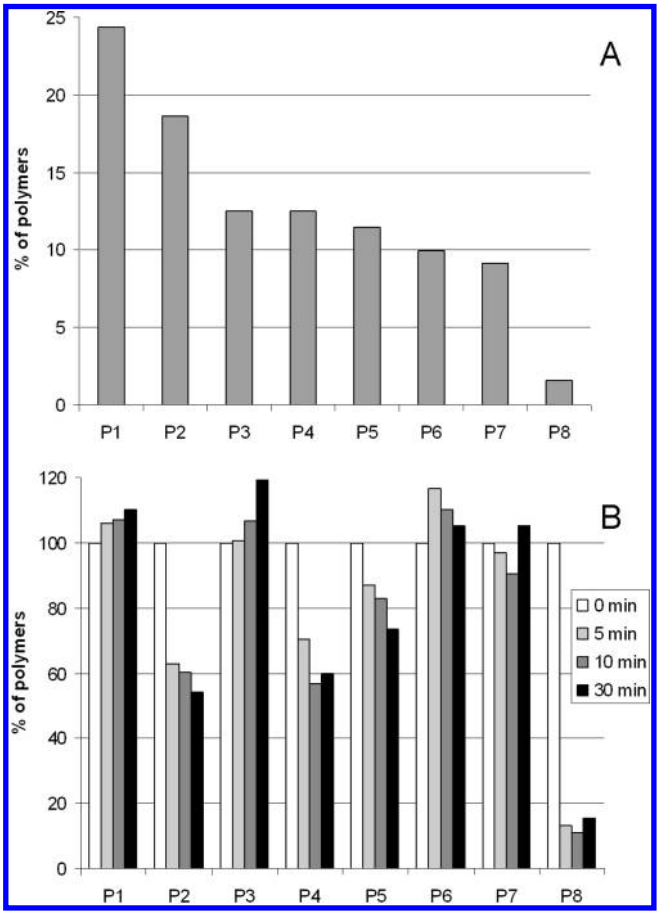

Figure 4. Proportion (%) of each polymer among all polymers observed in raw milk under nonreducing 2DE (**A**) and as a function of heating time of milk at 90 °C (0, 5, 10, and 30 min) using the corresponding spots of raw milk as reference (**B**).

Under nonreducing 2DE conditions, most of the spot volumes of κ-casein decreased (**Figure 5B**) as compared with reducing conditions, but not in the same proportions.

The 10 spots observed under reducing conditions were used as a reference to analyze spot volume under nonreducing conditions

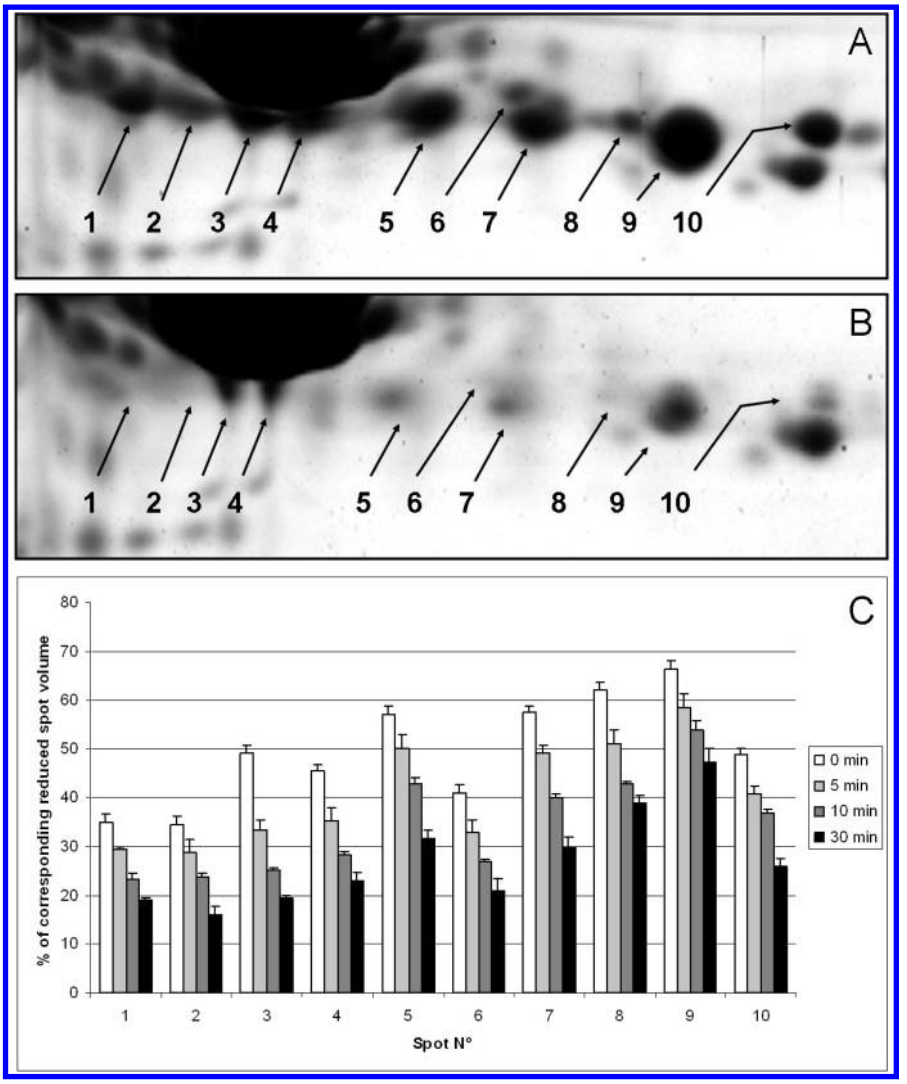

Figure 5. Quantification of individual κ-casein spots. The 10 observed κ-casein spots were labeled on the 2DE map of raw milk proteins separated under reducing conditions (**A**) or under nonreducing conditions (**B**). Each spot, separated under nonreducing conditions, was quantified and displayed as a percentage of the corresponding spots separated under reducing 2DE as a function of heating time of milk at 90 °C (**C**).

in raw milk (T0) or following heat treatment of milk at 90 °C (**Figure 5C**). In raw milk, the two spots with the greatest decrease under nonreducing condition were the most acidic κ-casein spots, and the least affected spots were the most basic κ-casein spots (except spot 10). During heat treatment at 90 °C, all spot volumes decreased, but the same proportions between acidic and basic κ-casein spots remained.

This quantitative analysis of κ-casein spots showed that sensitivity of the isoforms to heat treatment was potentially related to posttranslational modifications of the proteins, which is related to protein localization and orientation inside the casein micelle (*21*−*23*, *51*).

DISCUSSION

The analysis of complexes formed during heat treatment of bovine milk is very difficult due to the inherent complexity of the milk system. In particular, the caseins are organized as casein micelles in which proteins are held together by a combination of hydrophobic associations and covalent cross-links (*20*, *23*, *52*). To study all protein interactions in their natural form, or after heat treatment, an original strategy was developed which involved nonreducing and reducing combination steps during the two-dimensional gel electrophoresis protocol (*45*). Under nonreducing conditions, milk protein solubilization and all of the steps of the 2DE separation were performed without DTT. Prior to the second dimension, strips were incubated in equilibration buffer containing urea and SDS, followed by an equilibration step containing iodoacetamide. In the case of the reduced samples, solubilization of milk proteins was achieved with DTT as well as the first equilibration step. To obtain a good separation of polymers on the top of the 2D gel, homemade gradient polyacrylamide gels (10−18%) were used during the second dimension. After image analysis, and identification of proteins and polymers by mass spectrometry, a detailed and quantitative description of native interactions between milk proteins can be performed, and possible roles of each major milk protein can be described.

Presence of κ-Casein Polymers under Native Conditions. Bovine κ-casein consists of multiple isoforms due to several genetic variants and differential phosphorylation and glycosylation. This casein also contains two cysteine residues, allowing the formation of an intramolecular disulfide bond (*50*) or the assembly of disulfide-linked polymers (*53*−*55*). Isoforms of κ-casein can be separated by 2DE in the p*I* range 4−7 as 10 major spots (*16*, *45*). Spots corresponding to genetic variant, or forms differing in phosphorylation and/or glycosylation, have been identified and the posttranslational modifications located, using a mass spectrometry approach (*17*, *19*). In the present study, using a global 2DE approach to separate all major milk proteins on the same gel,

10 spots of monomeric κ-casein were observed under reducing conditions (**Figures 2** and **5**) ranging from p*I* 4.6 to p*I* 6.2. Under nonreducing conditions, the intensity of most spots was decreased, showing the presence of polymers. Image analysis focused on monomeric κ-casein revealed that the most acidic spots were highly involved in polymer formation (**Figure 5C**). These spots corresponded to the proteins with a complex pattern of posttranslational modifications. The most acidic spots observed on a 2DE gel of milk are reported to have three glycosylations and one phosphorylation site (*16*). According to the spot volume quantification, it seemed that such posttranslational modifications increased oligomerization of κ-casein. Phosphorylation and glycosylation modified the charge of κ-casein, as observed on a 2DE gel by a shift in isoelectric points.

As previously described for the tau protein with self-assembly modification into paired helical filaments (*56*), phosphorylation could also generate structural modifications of κ-casein inside the casein micelle, inducing a potential higher reactivity of cysteine residues to form interchain disulfide polymers. Oligopolymers of κ-casein were observed on 2DE gels of bovine milk under nonreducing conditions (*46*). Trains of spots corresponding to monomers to hexamers were observed as a result of the participation of different glycoforms and phosphoforms in oligomer formation. In this study, the polymers were observed at the same molecular weight range as in ref *46*, but sometimes with a more complex protein composition (**Figure 2** and **Table 2**).

This strategy of analysis not only focused on identification of κ-casein polymers but also allowed the complete study of all species involved in polymer formation. In agreement with ref *46*, κ-casein was observed in polymers P3, P4, and P7, but α_{S2}-casein was also identified in polymer P4, and a mixture of α_{S2}-casein, α_{S1}-casein, and β-lactoglobulin was identified in polymer P7. No polymer of α_{S2}-casein and κ-casein has been described previously. Disulfide-linked homopolymers of α_{S2}-casein and homopolymers of κ-casein have been observed under various environments and treatments (*50*, *57*). As no disulfide linkage between proteins was analyzed and identified by mass spectrometry, it is not possible to distinguish between heteropolymers and a mixture of homopolymers inside the same spot. Nevertheless, only single and well-separated spots were excised and analyzed by mass spectrometry (**Figure 2**). As all analyzed and quantified polymers displayed a characteristic pattern (**Table 1**), it is unlikely that two different homopolymers can be identified inside the same spot, even if this cannot be totally excluded. In addition, α_{S2}-casein has been shown to display an increased accessibility and ability to form complexes involving κ-casein and whey proteins after high-pressure treatment (*43*, *58*). Thus, there is substantial evidence for the capacity of κ-casein and α_{S2}-casein to form disulfide-linked heteropolymers.

Involvement of α_{S2}-Casein in Native Milk Polymers. Of the four caseins, only α_{S2}-casein and κ-casein contain cysteines. Of these, α_{S2}-casein naturally occurs as monomers and dimers in bovine milk (*59*). In the present study, the two major polymers observed under nonreducing 2DE corresponded to homopolymers of α_{S2}-casein, representing 43% of all polymers observed in raw milk. Since α_{S2}-casein contains two cysteine residues (amino acids 36 and 40), a dimer could be linked by one or two disulfide bridges. If two monomers are linked by one intermolecular disulfide bridge, free cysteine residues remain and can react with other proteins to form several kind of polymers. In this study, several proteins in raw milk containing cysteine residues, i.e., κ-casein, β-lactoglobulin, and serum albumin (**Table 2**), were identified inside complexes involving α_{S2}-casein. Using a similar approach, Bouguyon et al. (*52*) observed several homopolymers and heteropolymers involving rat or mouse α_S-casein, β-casein, and κ-casein linked by disulfide bridges. As observed in **Figure 3**, only a low percentage of monomeric α_{S2}-casein was involved in polymers, but this amount was enough to promote disulfide-linked polymers under native conditions. Interactions between casein in micelles are governed mainly by a balance of attractive hydrophobic interactions and electrostatic repulsion (*21*), but disulfide bridges between caseins are now considered to help in contributing to stabilization of the casein micelle (*22*, *23*).

Interaction of Whey Proteins with the Casein Micelle during Heat Treatment. κ-Casein is located mainly at the micelle surface, where it plays a role in regulating micelle size and in maintaining them in suspension in milk (*21*). The peripheral location of κ-casein in the micelle stabilizes the protein and acts as a bridge to link proteins of the whey fraction and caseins hidden inside the micelle. In this study, β-lactoglobulin was identified in polymer P7 in raw milk samples, mixed with κ-casein, α_{S1}-casein, and α_{S2}-casein. Serum albumin was also identified in polymer P8, mixed with α_{S2}-casein and β-casein (**Table 2**). As α_{S2}-casein and κ-casein are the only caseins which contain cysteines, α_{S1}-casein and β-casein were not linked to the other proteins by disulfides bridges but possibly by other bonds such as glycation cross-links (*60*) or strong ionic/hydrophobic interactions, not broken by SDS during electrophoresis. Levels of monomeric β-lactoglobulin and serum albumin decreased rapidly with heating time (**Figures 1** and **3**), probably through the formation of polymers involving caseins and whey proteins (*32*−*34*, *61*−*63*). Polymer formation involving β-lactoglobulin and κ-casein has been studied extensively for 40 years under a huge variety of environments and treatments (*38*, *64*−*68*). However, according to the present study, only a few detectable polymers contained whey proteins (P7 and P8), and these represented only 11% of the polymers observed on the 2D gels of raw milk samples under nonreducing conditions (**Figure 4**). Using a nonreducing/reducing discontinuous strategy (nonreduced isoelectric focusing and then reduced SDS−PAGE), we previously showed the presence of large polymers composed of serum albumin, κ-casein, and β-lactoglobulin in milk heated at 90 °C (*45*). Using such a strategy, proteins were visualized on the 2D gel as polymers were reduced to monomers. In the present study, polymers were only observed under nonreducing conditions, and larger polymers/aggregates, which were not able to enter the second dimension gel, cannot be visualized and quantified. A gradient gel (10−18% acrylamide) was used as second dimension to reduce this problem, but this limitation still remains for polymers greater than 200 kDa.

Interactions of Caseins To Prevent Formation of Fibrils: A Possible Biological Mechanism. Under nonreducing conditions, α_{S2}-casein and κ-casein were associated in milk as homodimers and/or heterodimers or multimers (this study and refs *22*, *46*, *49*, *50*, *53*, *54*, and *57*). Under physiological conditions, caseins have little secondary or tertiary structure with extensive regions of disordered structure (*20*−*22*, *51*). These proteins are organized and stabilized with calcium inside micelles, but under stress conditions such as heat treatment or a reducing environment, associations between caseins can be disrupted, and proteins can adopt amyloid fibril structures associated with degenerative diseases (*26*−*28*, *69*−*72*). Native κ-casein is organized as a series of disulfide-bonded polymers (*46*), ranging from dimers to octamers and above. When cysteine residues are chemically modified to prevent disulfide bond formation (by reduction and carboxymethylation), κ-casein increases in molecular weight and shows a tendency toward self-association, in particular the formation of fibrillar structures (*70*).

Of the caseins, α_{S2}-casein is the least abundant and perhaps the most difficult to isolate in a pure form. Consequently, it has been the least studied. After reduction of disulfide bridges, α_{S2}-casein is particularly susceptible to fibril formation under physiological

conditions (*27*). Consequently, self-associations and interactions between caseins inside the casein micelle can prevent such aberrant fibrillar structures.

In conclusion, α_{S2}-casein and κ-casein in raw milk were shown to participate in a complex pattern of homopolymers and heteropolymers in association with the other caseins and whey proteins under native-like nonreducing conditions, and α_{S2}-casein was the milk protein most implicated in polymer establishment and heterogeneity. Only a small proportion of α_{S2}-casein was present in polymers, but this corresponded to a large proportion of all polymers identified. This protein appeared as a platform which was able to connect several milk proteins using disulfide bonds and probably other kinds of links with cysteine-free proteins. The technical strategy using two-dimensional electrophoresis under reducing and nonreducing conditions was very useful in revealing the partners involved in polymers, but it also showed the limit of gel-based electrophoresis, which was not effective in analysis of large complexes. Posttranslational modification of κ-casein increased its sensitivity to oligomerization, but further study is required to further define the role of the protein in polymer formation. All major milk proteins appeared to interact, suggesting a very intricate system inside casein micelles and between caseins and whey proteins. Prevention against aberrant fibril structures of caseins is proposed to explain at least in part milk protein interactions and polymer stability.

ACKNOWLEDGMENT

The authors thank Professor Patrick Fox of University College Cork for helpful comments on the manuscript.

LITERATURE CITED

(1) O'Donnell, R.; Holland, J. W.; Deeth, H. C.; Alewood, P. Milk proteomics. *Int. Dairy J*. **2004**, *14* (12), 1013–1023.
(2) Gagnaire, V.; Jardin, J.; Jan, G.; Lortal, S. Invited review: Proteomics of milk and bacteria used in fermented dairy products: From qualitative to quantitative advances. *J. Dairy Sci*. **2009**, *92* (3), 811–825.
(3) Kuckova, S.; Crhova, M.; Vankova, L.; Hnizda, A.; Hynek, R.; Kodicek, M. Towards proteomic analysis of milk proteins in historical building materials. *Int. J. Mass Spectrom*. **2009**, *284* (1−3), 42–46.
(4) Manso, M. A.; Leonil, J.; Jan, G.; Gagnaire, V. Application of proteomics to the characterisation of milk and dairy products. *Int. Dairy J*. **2005**, *15* (6−9), 845–855.
(5) Cavaletto, M.; Giuffrida, M. G.; Conti, A., Milk fat globule membrane components—A proteomic approach. In *Bioactive Components of Milk*; Springer-Verlag: Berlin, 2008; Vol. 606, pp 129−141.
(6) Bertino, E.; Coscia, A.; Testa, T.; Boni, L.; Maiorca, D.; Dileo, L.; Giuffrida, G.; Fortunato, D.; Conti, A.; Fabris, C. Proteomics analysis of human milk fat globule membrane proteins. *Pediatr. Res*. **2005**, *58* (2), 374.
(7) Boehmer, J. L.; Bannerman, D. D.; Shefcheck, K.; Ward, J. L. Proteomic analysis of differentially expressed proteins in bovine milk during experimentally induced *Escherichia coli* mastitis. *J. Dairy Sci*. **2008**, *91* (11), 4206–4218.
(8) Mange, A.; Bellet, V.; Tuaillon, E.; de Perre, P. V.; Solassol, J. Comprehensive proteomic analysis of the human milk proteome: Contribution of protein fractionation. *J. Chromatogr., Sect. B: Anal. Technol. Biomed. Life Sci*. **2008**, *876* (2), 252–256.
(9) Pampel, L. W.; Duboc, P.; Vidal, K.; Gysler, C.; Bhou-Habib, G.; van den Broek, P. Proteomics in the food industry: Development of a high-throughput system for the expression of bioactive milk proteins. *Abstr. Pap. Am. Chem. Soc*. **2002**, *224*, 233-BIOT.
(10) Reinhardt, T. A.; Lippolis, J. D. Bovine milk fat globule membrane proteome. *J. Dairy Res*. **2006**, *73* (4), 406–416.
(11) Ruhlen, R. L.; Sauter, E. R. Proteomics of nipple aspirate fluid, breast cyst fluid, milk, and colostrum. *Proteomics Clin. Appl*. **2007**, *1* (8), 845–852.
(12) Vanderghem, C.; Blecker, C.; Danthine, S.; Deroanne, C.; Haubruge, E.; Guillonneau, F.; De Pauw, E.; Francis, F. Proteome analysis of the bovine milk fat globule: Enhancement of membrane purification. *Int. Dairy J*. **2008**, *18* (9), 885–893.
(13) Yamada, M.; Murakami, K.; Wallingford, J. C.; Yuki, Y. Identification of low-abundance proteins of bovine colostral and mature milk using two-dimensional electrophoresis followed by microsequencing and mass spectrometry. *Electrophoresis* **2002**, *23* (7−8), 1153–1160.
(14) Galvani, M.; Hamdan, M.; Righetti, P. G. Two-dimensional gel electrophoresis/matrix-assisted laser desorption/ionisation mass spectrometry of a milk powder. *Rapid Commun. Mass Spectrom*. **2000**, *14* (20), 1889–1897.
(15) Gorg, A.; Weiss, W.; Dunn, M. J. Current two-dimensional electrophoresis technology for proteomics. *Proteomics* **2004**, *4* (12), 3665–3685.
(16) Holland, J. W.; Deeth, H. C.; Alewood, P. F. Proteomic analysis of K-casein micro-heterogeneity. *Proteomics* **2004**, *4* (3), 743–752.
(17) Holland, J. W.; Deeth, H. C.; Alewood, P. F. Analysis of O-glycosylation site occupancy in bovine kappa-casein glycoforms separated by two-dimensional gel electrophoresis. *Proteomics* **2005**, *5* (4), 990–1002.
(18) Holland, J. W.; Deeth, H. C.; Alewood, P. F. Resolution and characterisation of multiple isoforms of bovine kappa-casein by 2-DE following a reversible cysteine-tagging enrichment strategy. *Proteomics* **2006**, *6* (10), 3087–3095.
(19) Poth, A. G.; Deeth, H. C.; Alewood, P. F.; Holland, J. W. Analysis of the human casein phosphoproteome by 2-D electrophoresis and MALDI-TOF/TOF MS reveals new phosphoforms. *J. Proteome Res*. **2008**, *7* (11), 5017–5027.
(20) Holt, C. Structure and stability of bovine casein micelles. *Adv. Protein Chem*. **1992**, *43*, 63–151.
(21) Horne, D. S. Casein interactions: Casting light on the black boxes, the structure in dairy products. *Int. Dairy J*. **1998**, *8* (3), 171–177.
(22) Rasmussen, L. K.; Johnsen, L. B.; Tsiora, A.; Sorensen, E. S.; Thomsen, J. K.; Nielsen, N. C.; Jakobsen, H. J.; Petersen, T. E. Disulphide-linked caseins and casein micelles. *Int. Dairy J*. **1999**, *9* (3−6), 215–218.
(23) Creamer, L. K.; Plowman, J. E.; Liddell, M. J.; Smith, M. H.; Hill, J. P. Micelle stability: kappa-casein structure and function. *J. Dairy Sci*. **1998**, *81* (11), 3004–3012.
(24) Fox, P. F.; McSweeney, P. L. H., Milk proteins. In *Dairy Chemistry and Biochemistry*, Professional, B. A. a., ed.; Springer-Verlag: London, 1998; pp 150−169.
(25) Morgan, P. E.; Treweek, T. M.; Lindner, R. A.; Price, W. E.; Carver, J. A. Casein proteins as molecular chaperones. *J. Agric. Food Chem*. **2005**, *53* (7), 2670–2683.
(26) Thorn, D. C.; Meehan, S.; Sunde, M.; Rekas, A.; Gras, S. L.; MacPhee, C. E.; Dobson, C. M.; Wilson, M. R.; Carver, J. A. Amyloid fibril formation by bovine milk kappa-casein and its inhibition by the molecular chaperones alpha(s-) and beta-casein. *Biochemistry* **2005**, *44* (51), 17027–17036.
(27) Thorn, D. C.; Ecroyd, H.; Sunde, M.; Poon, S.; Carver, J. A. Amyloid fibril formation by bovine milk alpha(s2)-casein occurs under physiological conditions yet is prevented by its natural counterpart, alpha-(s1)-casein. *Biochemistry* **2008**, *47* (12), 3926–3936.
(28) Thorn, D. C.; Ecroyd, H.; Carver, J. A. The two-faced nature of milk casein proteins: Amyloid fibril formation and chaperone-like activity. *Aust. J. Dairy Technol*. **2009**, *64* (1), 34–40.
(29) O'Kennedy, B. T.; Mounsey, J. S. Control of heat-induced aggregation of whey proteins using casein. *J. Agric. Food Chem*. **2006**, *54* (15), 5637–5642.
(30) Oldfield, D. J.; Singh, H.; Taylor, M. W. Kinetics of heat-induced whey protein denaturation and aggregation in skim milks with adjusted whey protein concentration. *J. Dairy Res*. **2005**, *72* (3), 369–378.
(31) Guyomarc'h, F.; Law, A. J. R.; Dalgleish, D. G. Formation of soluble and micelle-bound protein aggregates in heated milk. *J. Agric. Food Chem*. **2003**, *51* (16), 4652–4660.
(32) Corredig, M.; Dalgleish, D. G. The mechanisms of the heat-induced interaction of whey proteins with casein micelles in milk. *Int. Dairy J*. **1999**, *9* (3−6), 233–236.

(33) Anema, S. G.; Li, Y. M. Association of denatured whey proteins with casein micelles in heated reconstituted skim milk and its effect on casein micelle size. *J. Dairy Res*. **2003**, *70* (1), 73–83.
(34) Vasbinder, A. J.; de Kruif, C. G. Casein-whey protein interactions in heated milk: The influence of pH. *Int. Dairy J*. **2003**, *13* (8), 669–677.
(35) Corredig, M.; Dalgleish, D. G. Effect of temperature and pH on the interactions of whey proteins with casein micelles in skim milk. *Food Res. Int*. **1996**, *29* (1), 49–55.
(36) Swaisgood, H. E.; Brunner, J. R.; Lillevik, H. A. Physical parameters of k-casein from cows milk. *Biochemistry* **1964**, *3* (11), 1616.
(37) Heth, A. A.; Swaisgood, H. E. Examination of casein micelle structure by a method for reversible covalent immobilization. *J. Dairy Sci*. **1982**, *65* (11), 2047–2054.
(38) McKenzie, G. H.; Norton, R. S.; Sawyer, W. H. Heat-induced interaction of beta-lactoglobulin and kappa-casein. *J. Dairy Res*. **1971**, *38* (3), 343.
(39) Haque, Z.; Kinsella, J. E. Interaction between heated kappa-casein and beta-lactoglobulin—Predominance of hydrophobic interactions in the initial-stages of complex-formation. *J. Dairy Res*. **1988**, *55* (1), 67–80.
(40) Hae, D. J.; Swaisgood, H. E. Disulfide bond formation between thermally denatured beta-lactoglobulin and kappa-casein in casein micelles. *J. Dairy Sci*. **1990**, *73* (4), 900–904.
(41) Cho, Y. H.; Singh, H.; Creamer, L. K. Heat-induced interactions of beta-lactoglobulin A and kappa-casein B in a model system. *J. Dairy Res*. **2003**, *70* (1), 61–71.
(42) Livney, Y. D.; Dalgleish, D. G. Specificity of disulfide bond formation during thermal aggregation in solutions of beta-lactoglobulin B and kappa-casein A. *J. Agric. Food Chem*. **2004**, *52* (17), 5527–5532.
(43) Patel, H. A.; Singh, H.; Anema, S. G.; Creamer, L. K. Effects of heat and high hydrostatic pressure treatments on disulfide bonding interchanges among the proteins in skim milk. *J. Agric. Food Chem*. **2006**, *54* (9), 3409–3420.
(44) Miller, I.; Teinfalt, M.; Leschnik, M.; Wait, R.; Gemeiner, M. Nonreducing two-dimensional gel electrophoresis for the detection of Bence Jones proteins in serum and urine. *Proteomics* **2004**, *4* (1), 257–260.
(45) Chevalier, F.; Hirtz, C.; Sommerer, N.; Kelly, A. L. Use of reducing/nonreducing two-dimensional electrophoresis for the study of disulfide-mediated interactions between proteins in raw and heated bovine milk. *J. Agric. Food Chem*. **2009**, *57* (13), 5948–5955.
(46) Holland, J. W.; Deeth, H. C.; Alewood, P. F. Analysis of disulphide linkages in bovine kappa-casein oligomers using two-dimensional electrophoresis. *Electrophoresis* **2008**, *29* (11), 2402–2410.
(47) Laemmli, U. K. Cleavage of structural proteins during assembly of head of bacteriophage-T4. *Nature* **1970**, *227* (5259), 680.
(48) Chevalier, F.; Rofidal, V.; Vanova, P.; Bergoin, A.; Rossignol, M. Proteomic capacity of recent fluorescent dyes for protein staining. *Phytochemistry* **2004**, *65* (11), 1499–1506.
(49) Talbot, B.; Waugh, D. F. Micelle-forming characteristics of monomeric and covalent polymeric kappa-caseins. *Biochemistry* **1970**, *9* (14), 2807.
(50) Rasmussen, L. K.; Hojrup, P.; Petersen, T. E. Disulfide arrangement in bovine caseins—Localization of intrachain disulfide bridges in monomers of kappa-casein and alpha(s2)-casein from bovine-milk. *J. Dairy Res*. **1994**, *61* (4), 485–493.
(51) Dalgleish, D. G. Casein micelles as colloids: Surface structures and stabilities. *J. Dairy Sci*. **1998**, *81* (11), 3013–3018.
(52) Bouguyon, E.; Beauvallet, C.; Huet, J. C.; Chanat, E. Disulphide bonds in casein micelle from milk. *Biochem. Biophys. Res. Commun*. **2006**, *343* (2), 450–458.
(53) Groves, M. L.; Dower, H. J.; Farrell, H. M. Reexamination of the polymeric distributions of kappa-casein isolated from bovine-milk. *J. Protein Chem*. **1992**, *11* (1), 21–28.
(54) Rasmussen, L. K.; Hojrup, P.; Petersen, T. E. The multimeric structure and disulfide-bonding pattern of bovine kappa-casein. *Eur. J. Biochem*. **1992**, *207* (1), 215–222.
(55) Groves, M. L.; Wickham, E. D.; Farrell, H. M. Environmental effects on disulfide bonding patterns of bovine kappa-casein. *J. Protein Chem*. **1998**, *17* (2), 73–84.
(56) Mandelkow, E. M.; Schweers, O.; Drewes, G.; Biernat, J.; Gustke, N.; Trinczek, B.; Mandelkow, E. Structure, microtubule interactions, and phosphorylation of tau protein. In *Neurobiology of Alzheimer's Disease*; Wurtman, R. J., Corkin, S., Growdon, J. H., Nitsch, R. M., Eds.; **1996**; Vol. *777*, pp 96−106.
(57) Rasmussen, L. K.; Petersen, T. E. Purification of disulfide-linked alpha-s2-casein and kappa-casein from bovine-milk. *J. Dairy Res*. **1991**, *58* (2), 187–193.
(58) Considine, T.; Patel, H. A.; Anema, S. G.; Singh, H.; Creamer, L. K. Interactions of milk proteins during heat and high hydrostatic pressure treatments—A review. *Innovative Food Sci. Emerging Technol*. **2007**, *8* (1), 1–23.
(59) Annan, W. D.; Manson, W. A fractionation of alphas-casein complex of bovine milk. *J. Dairy Res*. **1969**, *36* (2), 259–268.
(60) Chevalier, F.; Chobert, J. M.; Molle, D.; Haertle, T. Maillard glycation of beta-lactoglobulin with several sugars: Comparative study of the properties of the obtained polymers and of the substituted sites. *Lait* **2001**, *81* (5), 651–666.
(61) Lucey, J. A.; Tamehana, M.; Singh, H.; Munro, P. A. Effect of interactions between denatured whey proteins and casein micelles on the formation and rheological properties of acid skim milk gels. *J. Dairy Res*. **1998**, *65* (4), 555–567.
(62) Donato, L.; Guyomarc'h, F.; Amiot, S.; Dalgleish, D. G. Formation of whey protein/kappa-casein complexes in heated milk: Preferential reaction of whey protein with kappa-casein in the casein micelles. *Int. Dairy J*. **2007**, *17* (10), 1161–1167.
(63) Donato, L.; Guyomarc'H, F. Formation and properties of the whey protein/kappa-casein complexes in heated skim milk—A review. *Dairy Sci. Technol*. **2009**, *89* (1), 3–29.
(64) Zittle, C. A.; Custer, J. H.; Cerbulis, J.; Thompson, M. P. Kappa-casein−beta-lactoglobulin interaction in solution when heated. *J. Dairy Sci*. **1962**, *45* (7), 807.
(65) Creamer, L. K.; Bienvenue, A.; Nilsson, H.; Paulsson, M.; van Wanroij, M.; Lowe, E. K.; Anema, S. G.; Boland, M. J.; Jimenez-Flores, R. Heat-induced redistribution of disulfide bonds in milk proteins. 1. Bovine beta-lactoglobulin. *J. Agric. Food Chem*. **2004**, *52* (25), 7660–7668.
(66) Lowe, E. K.; Anema, S. G.; Bienvenue, A.; Boland, M. J.; Creamer, L. K.; Jimenez-Flores, R. Heat-induced redistribution of disulfide bonds in milk proteins. 2. Disulfide bonding patterns between bovine beta-lactoglobulin and kappa-casein. *J. Agric. Food Chem*. **2004**, *52* (25), 7669–7680.
(67) Sawyer, W. H.; Jenness, R.; Coulter, S. T. Role of sulfhydryl groups in interaction of k-casein and beta-lactoglobulin. *J. Dairy Sci*. **1963**, *46* (6), 564.
(68) Sawyer, W. H. Complex between beta-lactoglobulin and kappa-casein. A review. *J. Dairy Sci*. **1969**, *52* (9), 1347.
(69) Uversky, V. N.; Fink, A. L. Conformational constraints for amyloid fibrillation: the importance of being unfolded. *Biochim. Biophys. Acta* **2004**, *1698* (2), 131–153.
(70) Farrell, H. M.; Cooke, P. H.; Wickham, E. D.; Piotrowski, E. G.; Hoagland, P. D. Environmental influences on bovine kappa-casein: Reduction and conversion to fibrillar (amyloid) structures. *J. Protein Chem*. **2003**, *22* (3), 259–273.
(71) Lencki, R. W. Evidence for fibril-like structure in bovine casein micelles. *J. Dairy Sci*. **2007**, *90* (1), 75–89.
(72) Sokolovski, M.; Sheynis, T.; Kolusheva, S.; Jelinek, R. Membrane interactions and lipid binding of casein oligomers and early aggregates. *Biochim. Biophys. Acta* **2008**, *1778* (10), 2341–2349.

Received for review March 23, 2010. Revised manuscript received May 6, 2010. Accepted May 07, 2010. Funding for this research was provided under the National Development Plan 2007−2013, through the Food Institutional Research Measure, administered by the Department of Agriculture, Fisheries and Food, Ireland. The work was also partly supported by the Proteomic Platform of Montpellier-LR Genopole.

International Dairy Journal 20 (2010) 715–723

Contents lists available at ScienceDirect

International Dairy Journal

journal homepage: www.elsevier.com/locate/idairyj

Proteins and proteolysis in pre-term and term human milk and possible implications for infant formulae

Emanuele Armaforte [a,c], Erika Curran [a], Thom Huppertz [a,d], C. Anthony Ryan [b], Maria F. Caboni [c], Paula M. O'Connor [e], R. Paul Ross [e], Christophe Hirtz [f], Nicolas Sommerer [f], François Chevalier [a,g], Alan L. Kelly [a,*]

[a] Department of Food and Nutritional Sciences, University College, Cork, Ireland
[b] Cork University Maternity Hospital, Department of Paediatrics and Child Health, University College, Cork, Ireland
[c] Department of Food Science, University of Bologna, Cesena, Italy
[d] NIZO food research, Ede, The Netherlands
[e] Moorepark Food Research Centre, Fermoy, Ireland
[f] Proteomic Platform, UR1199, INRA, Montpellier, France
[g] Proteomic Platform, CEA-FAR/DSV-IRCM, Fontenay aux Roses, France

ARTICLE INFO

Article history:
Received 15 November 2009
Received in revised form
4 March 2010
Accepted 8 March 2010

ABSTRACT

Understanding the differences between the protein system of human milk and bovine milk is critical in the development of infant formulae. In this study, the proteins of bovine milk and a bovine-based whey-dominant infant formula were compared with those of human milk for infants born prematurely (pre-term) or at full term (term). The protein distribution of infant formula differed significantly from that of either type of human milk. A proteomic comparison between pre-term and term human milk showed a reduction of levels of β-casein and α_s-casein and appearance of additional products, corresponding to low molecular weight hydrolysis products of the caseins, in pre-term milk. Pre-term milk samples also had higher total nitrogen concentration and plasmin activity, consistent with the proteomic data. These results suggest the operation of a physiological mechanism that may adjust enzyme and/or protein expression to modify protein digestibility, and may facilitate design of infant formulae, closer to maternal milk, particularly for premature infants.

1. Introduction

Human milk has long been recognized as the optimal form of nutrition for the newborn period (Work Group on Breastfeeding, 1997). Human milk contains a wide array of proteins that contribute to its unique qualities and that provide biological activities, ranging from antimicrobial effects to immunostimulatory functions. In addition, they provide adequate amounts of essential amino acids to growing infants (Jensen, 1995).

Although casein is the principal class of protein in milk from most species, this is not the case for human milk. Caseins in human milk comprise 10–50% of total protein, and whey proteins account for the remainder (Kunz & Lönnerdal, 1989). The contents of casein and whey proteins change profoundly in early lactation. In fact, during the first days of lactation and in milk from mothers delivering prematurely, the concentration of whey proteins is very high, whereas casein is virtually undetectable (Kunz & Lönnerdal, 1990, 1992). Subsequently, casein synthesis commences in the mammary gland and casein concentration increases, whereas the concentration of total whey proteins decreases, partially because of an increased volume of milk being produced. As a result, casein constitutes a progressively larger proportion of human milk protein with increasing duration of lactation after birth (Conti, Giuffrida, & Cavaletto, 2007; Kunz & Lönnerdal, 1989) and there is no "fixed" ratio of whey to casein in human milk (Lönnerdal, 2003). Human milk does not contain β-lactoglobulin or α_{s2}-casein.

Human milk has a high non-protein nitrogen (NPN) content (20–25% of total nitrogen) and is generally considered to provide adequate protein and nitrogen for the term infant. The concentration of NPN is higher in human milk than that in bovine milk; however, the proportion of NPN in infant formulae is variable, ranging from 5 to 16% in bovine-based formulae (Rudloff & Kunz, 1997). For human milk, it has been shown that, in early lactation, the absolute amount of NPN, such as creatinine, creatine, urea, free amino acids and small peptides, is significantly greater in pre-term milk than term milk (Atkinson, Anderson, & Bryan, 1980). It is

* Corresponding author. Tel.: +353 21 4902810/4903405; fax: +353 21 4270001.
E-mail address: a.kelly@ucc.ie (A.L. Kelly).

0958-6946/$ – see front matter © 2010 Elsevier Ltd. All rights reserved.
doi:10.1016/j.idairyj.2010.03.008

generally believed that the free amino acids and peptides in NPN should be more readily available to the neonate than intact proteins (Atkinson, Schnurr, Donovan, & Lonnerdal, 1989).

Human milk contains active enzymes, hormones and essential nutrients as well as live cells that remain viable in the infant stomach up to 4 h after ingestion. Storrs and Hull (1956) suggested that proteolytic enzymes may provide the breast-fed infant with significant digestive assistance immediately after birth and a subsequent study by Heyndrickx (1963) showed that there are higher levels of proteolytic enzymes in human milk than in bovine milk.

The main proteolytic enzyme in human milk is plasmin. Plasmin activity in milk is controlled by the availability of its precursor plasminogen (PA) and by the levels of plasminogen activators and inhibitors; plasmin is produced by either of two families of serine proteinases encoded by different genes, i.e., urokinase-type plasminogen activators (u-PA) and tissue-type plasminogen activators (t-PA) (Heegaard et al., 1997). The presence of the plasminogen activation system in human milk was first described by Astrup and Sterndorff (1953). Subsequent investigations have demonstrated proteolytic activity attributed to plasmin activity and the presence of plasminogen activators in colostrum and mature milk (Korycka-Dahl, Ribadeau Dumas, Chene, & Martal, 1983). As in bovine milk, plasmin is involved in the hydrolysis of proteins of human milk (Ferranti et al., 2004). Human milk obtained 6–7 days post-partum contained 4.8 ± 4.2 and $12.4 \pm 9.9\ \mathrm{U\,mL^{-1}}$ of plasmin and plasminogen-derived activity, respectively (Korycka-Dahl et al., 1983). The final plasmin activity of milk and, subsequently, hydrolysis of milk casein depends not only on the amount of plasminogen and PA but also on the level of inhibitors.

Whereas the multiple benefits of breast-feeding for human child health are well known and breast-feeding is strongly supported as the ideal form of infant feeding, infant formulae are intended to serve as a substitute for breast milk for infants who cannot be breast-fed, or should not receive breast milk, or for whom breast milk is not available (as stated by the World Health Organization: Thirty-Ninth World Health Assembly; Guidelines concerning the main health and socioeconomic circumstances in which infants have to be fed on breast-milk substitutes). The adequacy of infant formula composition should be determined by a comparing effects on physiological (e.g., growth patterns), biochemical (e.g., plasma markers) and functional (e.g., immune responses) parameters in infants fed formulae with those found in populations of healthy, exclusively breast-fed infants, taking into account the high variable composition of breast milk. The composition of infant formulae should serve to meet the particular nutritional requirements and to promote normal growth and development of the infants for whom they are intended (Koletzko et al., 2005).

This paper describes a detailed biochemical comparison of human milk samples with the aim of investigating differences in total protein content and plasmin activity between samples coming from mothers who gave birth to premature or mature babies. Characterization of the typical human milk proteome and a proteomic comparison of pre-term and term milk was carried out using two-dimensional electrophoresis followed by mass spectrometry. Moreover, a commercial infant formula and bovine milk were analyzed by two-dimensional electrophoresis to understand factors relevant to the composition of infant formulae.

2. Material and methods

2.1. Collection of milk samples

Human milk samples were collected at the Erinville Hospital, Cork, Ireland, over a 24 month period, For human milk, seven term milk samples were collected within 4 weeks after the colostral period from lactating mothers with full-term infants born after 38 weeks of gestation, and seven pre-term milk samples were collected from mothers with infants born between 30 and 37 completed weeks of pregnancy. Both term and pre-term human milk sample were collected with an electrical pump (Medela, McHenry, IL, USA). Ethical approval for the study was granted by the Cork University Hospitals Research Ethics Committee, and consent was subsequently obtained on this basis from all participants in the study. Human milk samples were centrifuged at $10{,}000 \times g$ for 15 min to remove fat, cell and debris and then frozen at $-80\,^{\circ}\mathrm{C}$ and thawed at refrigeration temperature overnight before analysis. Low-heat skim milk powder (NILAC) was obtained from NIZO food research (Ede, The Netherlands). The low-heat skim milk powder contained ~34% protein, ~60% lactose and <1% fat. A powdered sample of a bovine-based whey-dominant first-age commercial infant formula was bought. The powder contained ~11% protein, with the caseins and whey proteins at a ratio of ~40:60. In addition, the powder contained ~26% fat and ~58% carbohydrate.

2.2. One- and two-dimensional electrophoresis

Analytical SDS-PAGE electrophoresis of human milk samples was carried out according to the method of Laemmli (1970) on a 12.5% acrylamide gel using the Protean II system (Bio-Rad, Hercules, CA) under reducing conditions. The gels were stained with Coomassie blue (R250) and digitalized at 300 dpi with a GS-800 densitometer (Bio-Rad, Hercules, CA, USA).

Analytical 2D gel electrophoresis was carried out with 100 μg of protein (7.5 μL of pre-term or term human milk samples) using 7-cm strips and a linear pH gradient from 3 to 10 (Bio-Rad), and preparative 2D gel analysis was carried with 350 μg of protein (25 μL of human milk or 30 μL or 10 μL of reconstituted infant formula or bovine milk respectively) using 17-cm strips and linear pH gradient 3–10 (Bio-Rad). Milk samples were mixed with solubilization buffer (9 M urea, 4% CHAPS, 0.05% Triton X100 and 65 mM dithiothreitol (DTT)). Subsequently, 7 or 17-cm strips (with a linear pH gradient from 3 to 10) were rehydrated in the above solution. Isoelectric focusing was carried out according to the method of Chevalier, Hirtz, Sommerer, and Kelly (2009). The strips were then embedded using 0.6% (w/v), low-melt agarose on the top of a 12.5% acrylamide gel and SDS-PAGE was carried out using a Criterion® Dodeca Cell electrophoresis unit (Bio-Rad) for 7-cm strips and with a Protean® II xi Cell electrophoresis unit (Bio-Rad) for 17-cm strips. Gels were stained using colloidal Coomassie blue (Chevalier, Rofidal, Vanova, Bergoin, & Rossignol, 2004) and stained gels were digitized at 300 dpi using a GS-800 densitometer (Bio-Rad).

2.3. Image analysis of SDS-PAGE electrophoretograms of human milk samples

Images of analytical SDS-PAGE gels were analyzed with Quantity One software (Bio-Rad, Hercules, CA, USA) and gel images from two-dimensional analysis were analyzed with PD Quest software (Bio-Rad, Hercules, CA, USA). All human milk samples were analyzed in triplicate and the replicates were used to provide an averaged gel. All the averaged gels were compared to evaluate differences between samples belonging to the same group, and between the two groups (pre-term and term). The same gel regions were selected and compared, and spot volume was determined as a percentage of total volume of all spots on respective gels. The complete pattern (including all spots) was used for qualitative and quantitative analysis. Qualitative analysis identified specific spots present only in one group, while quantitative analysis determined spots with over- or under-expression (>2-fold difference).

2.4. Protein identification by MALDI-TOF mass spectrometry

Spots of interest were excised from preparative 2D gels of pre-term and term milk samples, washed sequentially with Milli Q (Millipore, Massachusetts, USA) water, 25 mM ammonium carbonate, 25 mM ammonium carbonate–acetonitrile (1:1) and acetonitrile. The spots were dried using with a Speed-Vac (GMI Inc., Minnesota, USA) and the proteins were subsequently digested with trypsin (12.5 $\mu g\,\mu L^{-1}$ in 25 mM ammonium carbonate). Resulting fragments were extracted twice with 50 μL of acetonitrile/water (1:1, v/v) containing 0.1% trifluoroacetic acid for 15 min. Pooled supernatants were concentrated using a Speed-Vac to a final volume of ~20 μL and peptides were immediately spotted onto the MALDI target. Mass spectra were recorded in the reflector mode on an Axima CFR plus MALDI-TOF mass spectrometer (Shimadzu Biotech, Manchester, UK). The MASCOT search engine software (Matrix Science, London, UK) was used to search the NCBInr database (version 20060620, containing 3,682,060 sequences ftp://ftp.ncbi.nih.gov/blast/db/FASTA/nr.gz). The following parameters were used: mass tolerance of 100 ppm, a minimum of four peptides matching to the protein, carbamidomethylation of cysteine as a fixed modification, oxidation of methionine and pyroglutamylation of glutamine as variable modifications, and one missed cleavage allowed.

2.5. Protein identification by nano liquid chromatography–mass spectrometry

Stained protein spots were excised manually, washed, digested with trypsin and extracted using formic acid. Protein digests were analyzed using an ion trap mass spectrometer (Esquire HCT plus; Bruker, Billerica, MA, USA) coupled to a nano-chromatography system (HPLC 1200, Agilent, Santa Clara, CA, USA) interfaced with an HPLC-Chip system (Chip Cube, Agilent). MS/MS data were searched against National Center for Biotechnology Information (NCBI) and Mass Spectrometry protein sequence Data Base (MSDB) databases using Mascot software.

2.6. Determination of nitrogen content and plasmin activity

The total nitrogen content of human milk samples was determined using the Kjeldahl method. Plasmin activity in milk was measured using the method of Richardson and Pearce (1981).

2.7. Statistical analysis of data

Total protein and plasmin activity data were analyzed using SPSS r.11.0.0 statistical software (SPSS Inc., Chicago, IL, USA). Differences at a 5% significance level among means were determined by one-way analysis of variance (ANOVA) using Tukey's test. Two-dimensional analysis data were also analyzed by principal components and classification analysis (Statistica 6.0, Statsoft Inc., Tulsa, OK, USA) to analyse correlations between the analyses and differences between the samples.

3. Results

3.1. Determination of total nitrogen content and plasmin activity of human milk samples

The mean nitrogen content of the seven pre-term milk samples was 1.65-fold higher ($p < 0.001$) than that of the seven term milk samples (Fig. 1, top panel). The mean total nitrogen contents of pre-term and term milk samples were 0.28% and 0.17%, respectively. In addition, the levels of nitrogen in the pre-term milk samples were more variable (range of 0.22–0.35%) than those in the term milk samples (0.12–0.17%). The plasmin activities in pre-term and term milk samples were also significantly different ($p < 0.001$) (Fig. 1,

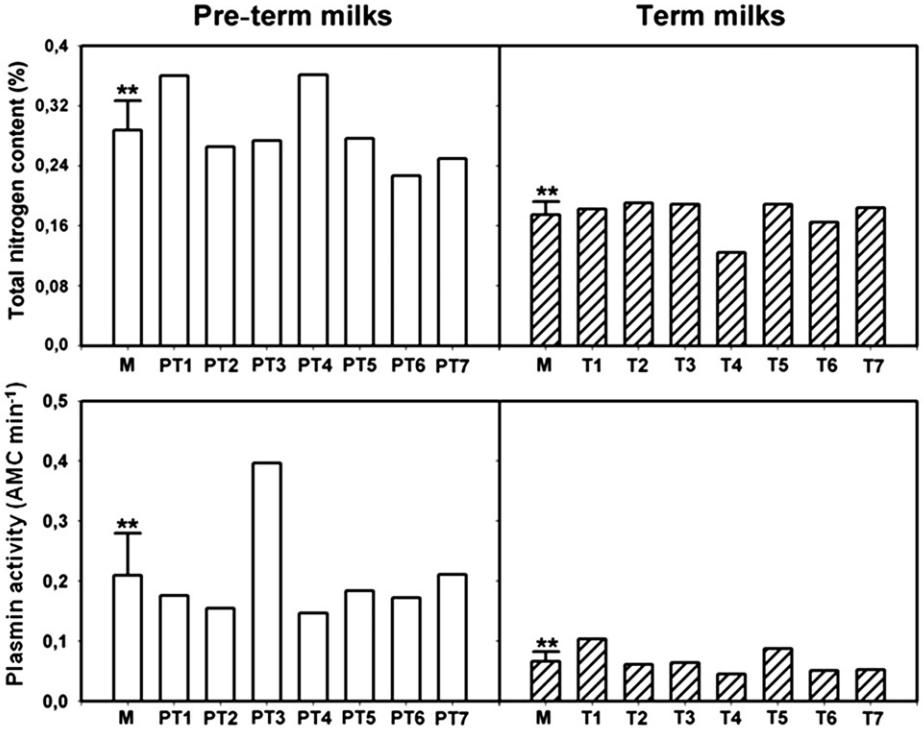

Fig. 1. Total nitrogen content and plasmin activity of the pre-term and term human milk samples; M: average value, PT: pre-term, T: term; **statistically significant differences between the two groups ($p < 0.001$).

bottom panel); the plasmin activity of the seven term milk samples was very consistent and lower (0.045–0.104 amino methyl coumarin (AMC) units per mL milk) than the plasmin activity of the pre-term milk samples (0.147–0.397 AMC units per mL milk).

3.2. SDS-PAGE analysis of human milk samples

SDS-PAGE electrophoresis was performed on 14 human milk samples (7 pre-term and 7 term; Fig. 2). The principal bands in all samples corresponded to lactoferrin, β-casein, α-casein and α-lactalbumin. However, there was significant variation in the intensities of the bands corresponding to these proteins between samples, more so in the case of the caseins than the whey proteins. In addition, several samples showed bands of lower molecular weight than the caseins (i.e., including polypeptides produced by proteolysis). The difference between pre-term and term samples was less than the inter-sample variability.

Subsequently, to determine a characteristic pattern of the milk samples, a correlation matrix derived from the number and the intensity of the mono-dimensional electrophoretic bands was performed with the Quantity One software. According to this correlation matrix, three most representative samples of each group (PT2, PT4, PT7 for pre-term and T1, T2, T7 for term) were chosen and analyzed by two-dimensional electrophoresis.

3.3. Identification of the most abundant protein spots from pre-term human milk

To identify most of the abundant proteins, a two-dimensional electrophoresis reference gel of human pre-term milk was run (Fig. 3). The pre-term sample with the highest number of spots was chosen so as to best exemplify the complexity of the human milk protein profile and to identify the most abundant proteins and proteolysis products. Mass spectrometry identifications of the 50 spots analyzed are shown in Table 1. Two thirds of the proteins identified corresponded to α_{s1}- and β-caseins: 24 spots were identified as α_{s1}-casein isoforms with apparent molecular masses from 18.74 to 32.05 kDa and apparent isoelectric points from 4.03 to 5.56; 18 spots were identified as β-casein isoforms (13.1–35.04 kDa, pI = 4.76–8.44). Together with these two main groups of caseins, other well-known milk proteins were identified, including α-lactalbumin (4 spots), lactoferrin (3 spots), lacto-transferrin (1 spot), κ-casein (1 spot), and several immunoglobulins.

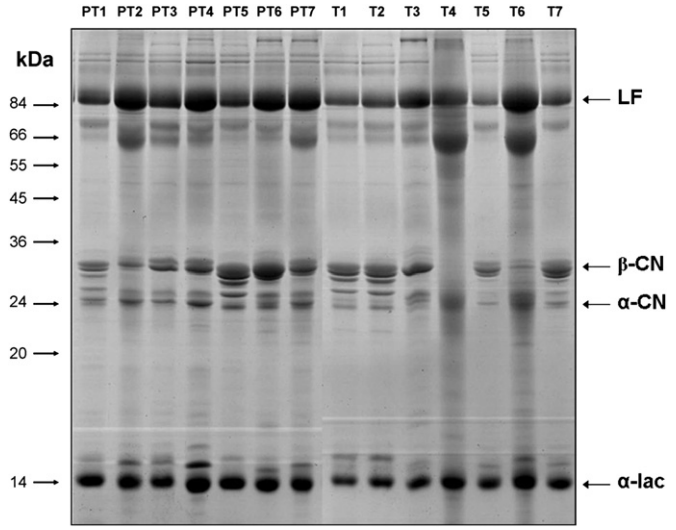

Fig. 2. SDS-PAGE electrophoretograms of 7 human milk samples from mothers giving birth at pre-term (PT) or term (T). LF: lactoferrin; β-CN: β-casein; α-CN: α-casein; α-lac: α-lactalbumin.

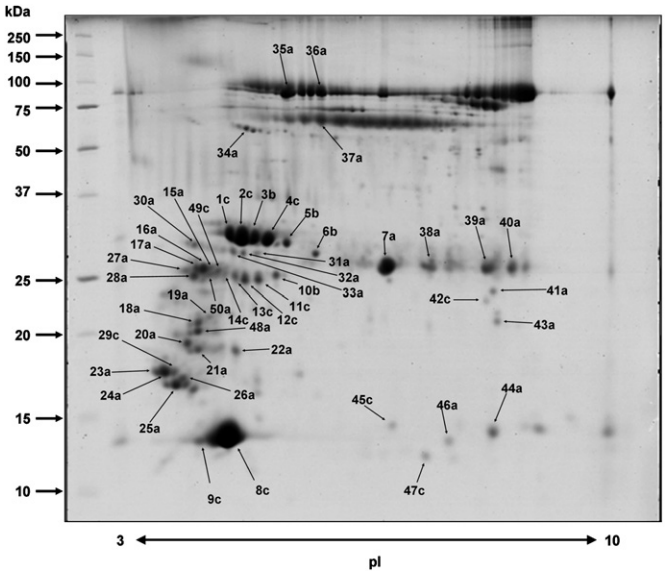

Fig. 3. Reference proteomic map of a human pre-term milk sample: 2D preparative gel of a representative milk sample (~300 μg of proteins) under reducing conditions using a 17 cm pH 3–10 pI range for the first dimension, and a 12% gradient acrylamide gel for the second dimension. The most abundant spots were shown with arrows and were submitted to mass spectrometry identification by MALDI-TOF peptide mass fingerprint and/or nano-LC/MS–MS (results in Table 1). a: Over-expressed in pre-term milk; b: over-expressed in term milk; c: no differences between pre-term and term milk.

Most of these isoforms corresponded to breakdown products or post-translational modifications of the native protein. In the case of human β-casein, different levels of phosphorylation are well known and have been reported previously Greenberg & Groves, 1984; (Greenberg, Groves, & Dower, 1983; Poth, Deeth, Alewood, & Holland, 2008) The same consideration can be applied to α_{s1}-casein, for which, in addition to different phosphorylation levels, there were also many hydrolysis products, presumably originating from the action of proteolytic enzymes, producing a number of peptides with different molecular weight and isoelectric points.

3.4. Comparison of the 2D-electrophoretic patterns of term and pre-term human milk samples

Changes in the human milk proteome for the pre-term and term samples were studied using 2-DE on proteins solubilized directly from the chosen human milk samples. A high resolution 2-DE gel pattern, in a pI range between 3 and 10, was visualised by coomassie blue staining. The three replicates selected by SDS-PAGE electrophoresis were used for image analysis. A mean of 101 and 147 protein spots were reproducibly detected in each term and pre-term gel, respectively (Table 2) and were selected for further analysis. Quantitative analysis, using PD Quest software, revealed that 55 proteins showed more than 2-fold differences in expression value. Among these, a total of 48 proteins were up-regulated and 7 were down-regulated in pre-term milk samples. In addition, 69 unique spots appeared in the 2D map of pre-term samples; in comparison, only 10 unique spots were detected in term samples. Among all spots, the 36 most abundant and varying spots between the pre-term and term milk samples are shown in Fig. 3. Spots labelled with "a" correspond to the spots over-expressed in pre-term milk; spots labelled with "b" correspond to the spots under-expressed in pre-term milk and spots with no intensity modification between pre-term and term milk samples are labelled "c".

Table 1
Identification of the 50 most abundant spots from the two-dimensional gel of human milk (see Fig. 3), by peptide mass fingerprinting (PMF) using MALDI-TOF.[a]

Spot no.	Protein name	Ref. Swiss Prot	Mol. mass (kDa)		pI		PMF/MALDI-TOF			Nano LC–MS/MS		
			Theor.	Obs.	Theor.	Obs.	Score	% Cov.	Peptides	Score	Match peptides	Hit rank
1	β-Casein	P05814	23.86	35.04	5.33	4.97	71	31	3			
2	β-Casein	P05814	23.86	34.78	5.33	5.1	71	31	3			
3	β-Casein	P05814	23.86	33.82	5.33	5.23	92	38	4			
4	β-Casein	P05814	23.86	34.34	5.33	5.41	71	31	3			
5	β-Casein	P05814	23.86	32.49	5.33	5.6	71	31	3			
6	β-Casein	P05814	23.86	31.01	5.33	5.81	71	31	3			
7	β-Casein	P05814	23.86	27.58	5.33	6.4	92	38	4			
8	α-Lactalbumin	P00709	14.08	14.85	4.70	4.97	82	33	5			
9	α-Lactalbumin	P00709	14.08	13.57	4.70	5.09				283	8	1
10	α-Casein	P47710	20.09	27.36	5.17	5.56	68	22	3			
11	α-Casein	P47710	20.09	25.77	5.17	5.32	68	22	3			
12	α-Casein	P47710	20.09	25.59	5.17	5.17	70	30	4			
13	α-Casein	P47710	20.09	25.77	5.17	5.04	70	30	4			
14	α-Casein	P47713	20.09	23.88	5.17	5.24	72	35	5			
15	α-Casein	P47710	20.09	26.66	5.17	4.73	70	30	4			
16	α-Casein	P47710	20.09	26.58	5.17	4.65	70	30	4			
17	α-Casein	P47713	20.09	25.06	5.17	4.75	75	30	4			
18	α_{s1}-Casein	P47712	20.09	21.96	5.17	4.77				87	2	4
	β-Casein	P05814	23.86	21.96	5.33	4.77				40	3	6
19	α_{s1}-Casein	P47711	20.09	22.17	5.17	4.99				102	2	1
	β-Casein	P05814	23.86	22.17	5.33	4.99				43	2	2
20	α_{s1}-Casein	P47712	20.09	21.6	5.17	4.56				159	3	1
21	α_{s1}-Casein	P47713	20.09	21.09	5.17	4.77				98	2	1
22	α_{s1}-Casein	P47710	20.09	21.28	5.17	5.41	72	35	5			
23	Protease serine	Q6ISJ4	26.7	20	5.72	3.75				61	2	1
24	α_{s1}-Casein	P47711	20.09	20.27	5.17	4.03				51	2	1
25	α_{s1}-Casein	P47711	20.09	18.88	5.17	4.29				106	2	1
26	α_{s1}-Casein	P47713	20.09	18.74	5.17	4.5				72	1	1
27	Ig J chain	P01591	15.59	23.89	4.62	4.53	127	11	59			
28	Ig J chain	P01591	15.59	23.64	4.62	4.7	110	9	59			
29	α_{s1}-Casein	P47713	20.09	20.07	5.17	4.23				118	2	1
30	α_{s1}-Casein	P47713	20.09	32.05	5.17	4.71				127	4	2
31	α_{s1}-Casein	P47713	20.09	28.44	5.17	5.5				213	5	5
	β-Casein	P05814	23.86	28.44	5.33	5.5				56	2	13
	Anti-pneumo coccal antibody	Q502W4	25.94	28.44	8.69	5.5				92	3	7
32	α_{s1}-Casein	P47713	20.09	28.44	5.17	5.5				301	8	1
	β-Casein	P05814	23.86	28.44	5.33	5.5				44	2	3
33	α_{s1}-Casein	P47713	20.09	28.61	5.17	5.39				216	5	1
	β-Casein	P05814	23.86	28.61	5.33	5.39				74	2	3
	α-Lactalbumin	P00709	14.08	28.61	4.70	5.39				121	5	2
34	α 1 Antitrypsin	P01009	44.32	69.44	5.37	5.53				799	23	1
	κ-Casein	P07498	18.16	69.44	8.68	5.53				51	2	4
35	Lactoferrin	Q2TUW9	77.99	81.24	8.51	5.11	78	12	5			
36	Lactoferrin	Q2TUW9	77.99	83.29	8.51	5.5	94	15	9			
37	Lacto-transferrin	P02788	76.17	71.4	8.47	6.4				263	7	7
	Immunoglobulin	Q9NPP6	44.79	71.4	5.74	6.4				171	4	9
38	Ig k VLG region	/	28.6	23.68	6.15	7.31				418	11	1
39	IgG k chain	/	23.3	24	7.75	8.07	140	9	52			
40	IgG k chain	/	23.3	24.95	7.75	8.34	103	6	29			
41	β-Casein	P05814	23.86	22.84	5.33	8.28	69	28	3			
42	β-Casein	P05816	23.86	22.7	5.33	8.09	69	28	3			
43	β-Casein	P05815	23.86	22.08	5.33	8.44	69	28	3			
44	β-Casein	P05817	23.86	13.6	5.33	8.31	69	28	3			
45	Fatty acid binding protein	P05413	14	14.73	6.81	6.34				332	9	1
46	β-Casein	P05814	23.86	13.12	5.33	7.59				72	2	2
	α-Lactalbumin	P00709	14.08	13.12	4.70	7.59				55	2	3
47	β 2 Microglobulin	P61769	11.73	12.18	6.07	7.2				160	6	1
48	Lactoferrin	Q2TUW9	77.99	21.65	8.51	4.76				118	2	1
	α_{s1}-Casein	P47713	20.09	21.65	5.17	4.76				82	1	2
	β-Casein	P05814	23.86	21.65	5.33	4.76				37	4	3
49	α_{s1}-Casein	P47710	20.09	26.51	5.17	4.88	75	30	4			
50	α_{s1}-Casein	P47710	20.09	25.73	5.17	4.73	72	35	5			

[a] Protein reference (Ref.) corresponds to the Swiss-Prot/NCBI accession number; % cov. refers to sequence coverage. Theoretical molecular mass and isoelectric point (pI) of proteins are as according to the amino acid primary sequence and without consideration of any post-translational and/or degradation modifications. Observed molecular mass and isoelectric point (pI) are as observed with the position of the corresponding spots on the two-dimensional electrophoresis gel.

Table 2
Number and distribution of spots in two-dimensional electrophoretograms of pre-term and term human milk samples.

	Human milk samples[a]	Common spots	Specific spots	Over-expressed spots	No differences
	$X \pm SD$				
PT2	162 ± 2	84	69	48	29
PT4	143 ± 4				
PT7	136 ± 1				
Mean	147 ± 14				
T1	92 ± 2		10	7	29
T2	112 ± 2				
T7	97 ± 1				
Mean	101 ± 10				

[a] Abbreviations are: *X*, average number of spots among three replicates of the same sample; SD, standard deviation of the number of spots among three replicates of the same sample.

Interestingly, all the under-expressed spots in pre-term milk corresponded to β-casein (spots 3, 5 and 6) and to α_{s1}-casein (spot 10), with an observed molecular mass close to the native proteins. In contrast, most of the varying spots with a low molecular mass appeared to correspond to spots over-expressed in pre-term milk; 6 spots (18, 41, 42, 43, 44 and 48) were identified as originating from β-casein, and 9 spots (18, 20, 21, 22, 24, 25, 26, 46 and 48) were identified as originating from α_{s1}-casein. Thus, these low molecular mass spots correspond to fragments of β-casein and α_{s1}-casein resulting from enzymatic hydrolysis.

3.5. Proteomic comparison of human milk, infant formula and bovine milk

The protein pattern of a commercially available powdered infant formula, evaluated by two-dimensional electrophoresis, is shown in Fig. 4 (F) and compared with a human milk sample (H) and a bovine milk sample (B). The human milk profile was clearly different compared with that of infant formula; moreover, a comparison of Fig. 3 with Fig. 4 (sample F) shows that the proteolysis products, normally present in full-term human milk and, especially, in pre-term human milk are absent in the infant formula sample.

A recently reported two-dimensional reference gel of bovine milk proteins (Chevalier et al., 2009) allowed the identification of the most abundant protein spots in bovine milk and infant formula. As expected, the most abundant proteins of bovine milk were α_{s1}-casein, while 4 different isoforms of α_{s2}-casein, 2 isoforms of β-casein and 5 isoforms of κ-casein were identified in the central area of the gel. Together with these main groups of caseins, other well-known milk proteins were identified, including α-lactalbumin, bovine serum albumin and the two genetic variants of β-lactoglobulin.

Compared with bovine milk there was, as expected, a higher proportion of whey protein in the whey-dominant infant formula. Whey-dominant formulae are commonly formulated at a casein-to-whey protein ratio of ~40:60, compared with the ratio of ~80:20 that is commonly found in bovine milk. In addition, the ratio of α-lactalbumin to β-lactoglobulin was higher in the infant formula than in bovine milk. The selective enrichment of β-lactoglobulin, which further tailors the whey protein composition of the formula towards that of human milk, is a further step in the humanization of infant formula. The amount of high molecular mass proteins, e.g., lactoferrin, was comparable for human milk and infant formula, while these were noticeably lower in bovine milk.

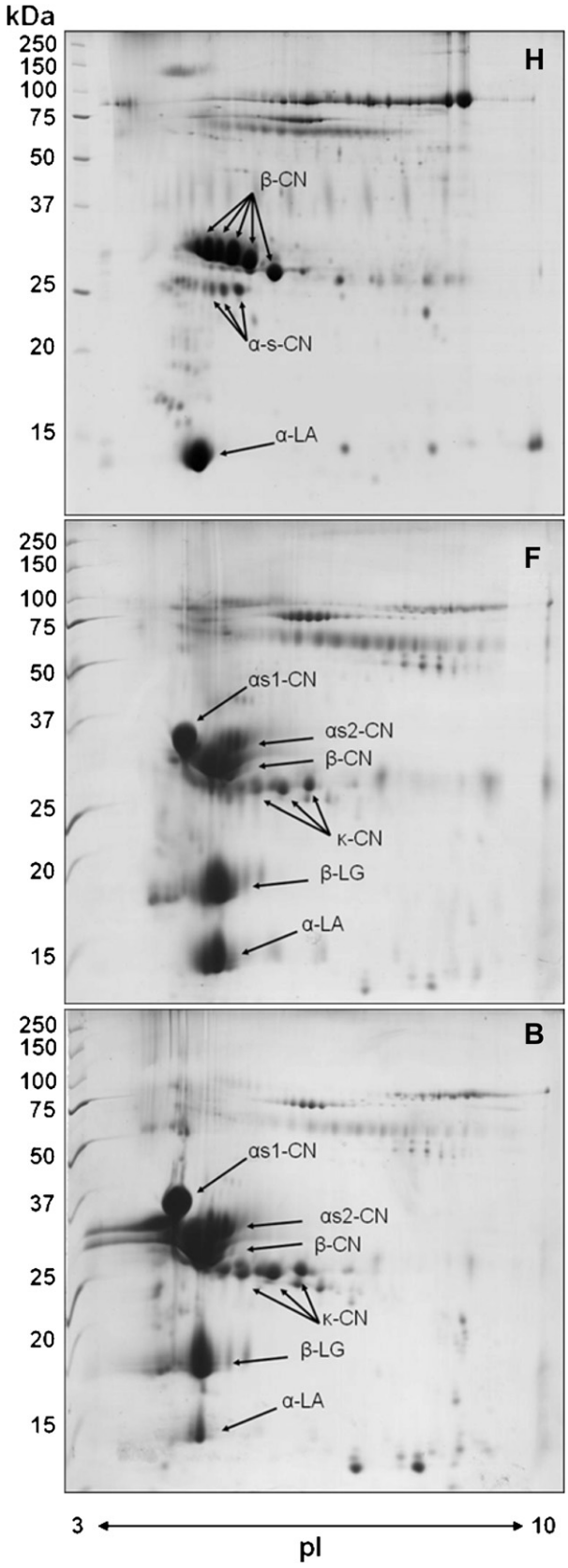

Fig. 4. Two-dimensional preparative gel of 300 μg of (H) human term milk proteins, (F) powdered infant formula proteins and (B) bovine milk proteins, separated under reducing conditions using a 17 cm pH 3–10 pI range for the first dimension, and a 12% gradient acrylamide gel for the second dimension.

4. Discussion

Comparative proteomics, as well as biochemical and enzymatic measurements, were initially used to investigate the modulation of proteins in milk from mothers who gave birth to pre-term and full-term babies. The differences in total nitrogen content were consistent with those reported by Atkinson et al. (1980), i.e., that the total protein concentration of breast milk from women delivering prematurely was considerably higher than that of milk from women delivering at term. It was hypothesized that a higher protein concentration can benefit the premature infant with its rapid catch-up growth and high protein requirement.

Atkinson et al. (1980) also reported that the peptides found in human milk may be indigenous constituents of breast milk or may be formed in expressed milk through the proteolytic action of native enzymes in the milk. Building on these findings, this paper reports, for the first time, increased plasmin activity in milk from mothers delivering prematurely (Fig. 1). Milk proteases present in breast milk, including plasmin, are capable of hydrolysing β-casein in milk (Ferranti et al., 2004; Greenberg & Groves, 1984; Okamoto, Horie, Nagamatsu, & Yamamoto, 1981) and could contribute to the complement-inhibitory activity of human milk (Ogundele, 1999). This study contributes new information about the protein composition of human milk, underlining the key role of plasmin: its higher level in milk for premature infants results in more extensive hydrolysis of protein, leading to the production of small peptides which could facilitate the digestion process.

One-dimensional electrophoretic data showed a more complex pattern for pre-term milk samples than for term milk, consistent with the plasmin activity results. Higher plasmin activity and higher nitrogen content thus result in higher rates of hydrolysis of protein, which results in the formation of lower-molecular mass polypeptides and peptides. The level of the main protein band of α-lactalbumin showed no particular differences between the two groups. The stable concentration of α-lactalbumin is due to its role in the synthesis of lactose, which, in turn, is linked with the osmotic pressure of blood in the mammary gland. This may explain the similar concentration of α-lactalbumin in pre-term and term human milk samples (Fig. 2). In contrast, the casein spots were more intense in the term samples; this could again be a result of the higher proteolytic activity of pre-term samples.

Identification of the spots of interest further elucidated the protein fraction of human milk. The first consideration is related to the breakdown products, present mainly in the pre-term milk samples (Fig. 5), which are mostly polypeptide fragments derived from α_{s1}- and β-caseins (Table 2). This observation is complementary to a previous study that reported that β-casein was the main source of small peptides by proteolytic action in human milk (Ferranti et al., 2004). In that study, trichloroacetic acid (TCA) was used to precipitate casein and separate peptides from milk and then liquid chromatography–mass spectrometry and tandem mass spectrometry were used for the separation and identification of the peptides. In the present study, milk was analyzed directly without additional extraction or enrichment steps and the proteins were separated using two-dimensional electrophoresis. These differences in the experimental methods have a great influence on the determination of proteolysis products from proteins. Firstly, the use of TCA for the purification of peptides and reverse-phase HPLC for the separation gave rise to peptide populations with a molecular mass that was too low to be resolved on a SDS-PAGE gel. On the other hand, two-dimensional electrophoresis allowed direct analysis of the native proteins preferentially hydrolysed by plasmin and the resulting polypeptides. Then, in pre-term human milk, plasmin can hydrolyse both α_{s1}-casein and β-casein (Ferranti et al., 2004), and yields polypeptides from both α_{s1}-casein and β-caseins and small peptides from β-casein (Ferranti et al., 2004). Moreover, Ferranti et al. (2004) reported that, in term milk, the amount of comparatively shorter peptides was higher compared with those of greater size, which indicates a higher quantitative and qualitative level of hydrolysis by plasmin; also, α_{s1}-casein-derived peptides, which are few in pre-term milk, were more abundant in term milk. In bovine milk, proteolytic enzymes, and especially plasmin, preferentially hydrolyse β-casein (Fox & Kelly, 2005), but in human milk this proteolytic activity is apparently carried out on both α_{s1}-casein and β-casein.

The quantitative data from the image analysis highlighted that pre-term milk samples were also richer in immunoglobulins and antibodies, making stronger the hypothesis of milk "naturally

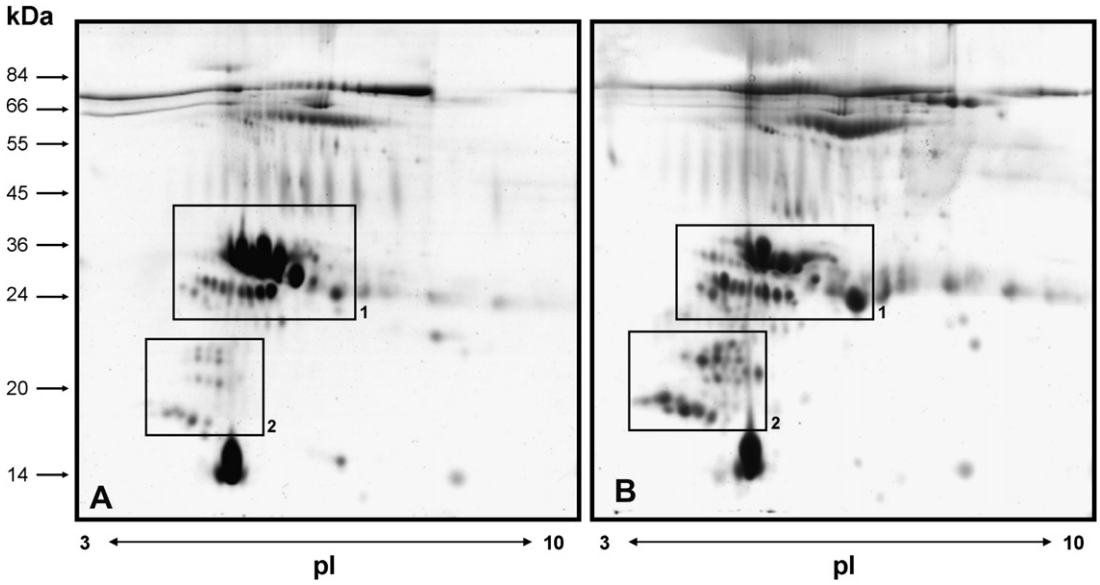

Fig. 5. Comparison between pre-term and term milk samples: 2D analytical gels of a representative term milk sample (A) and a representative pre-term milk sample (B) (~100 μg of proteins) under reducing conditions using a 7 cm pH 3–10 pI range for the first dimension, and a 12% gradient acrylamide gel for the second dimension.

enriched" in proteins and peptides but also in bio-active compounds which are able to protect pre-term infants during early life.

The two-dimensional electrophoretic protein profile of bovine milk was found to be remarkably different from that of human milk. As expected, the most abundant proteins in the bovine milk proteome were α_{s1}-casein, α_{s2}-casein, β-casein (which are grouped in the same area of the gel) and the two genetic variants of β-lactoglobulin, while α-lactalbumin and high molecular mass proteins are present in low concentration (Fig. 4, sample B). In human milk, the most abundant protein was α-lactalbumin, followed by the groups of the isoforms of β-caseins and α-caseins, which are resolved separately from each other; moreover, the high molecular mass proteins (mainly lactoferrin) represented an important fraction of the total protein content (Fig. 4, sample H). Several isoforms of κ-casein are known to be present in bovine milk, while only 1 spot was identified as κ-casein in human milk (Fig. 3, Table 2). In human milk, and especially in pre-term milk, the action of plasmin gives rise to a significant number of hydrolysis products of α- and β-caseins. In the case of bovine milk, inflammation of mammary gland gives rise to higher plasmin activity; high plasmin activity and high concentration of hydrolysis products are undesirable in bovine milk since they are indicators of low quality (Kelly, O'Flaherty, & Fox, 2005). Instead, in human milk, the higher activity of plasmin in pre-term milk may have an important nutritional role for low-birth weight infants.

As expected, the qualitative protein profile of infant formula milk was very similar to that of bovine milk powder, since formula milk is most often formulated with dairy ingredients, i.e., skim milk powder and demineralised whey powder or whey protein concentrated. Infant formula based on soy or protein hydrolysates are available for infant which are allergic to cow milk constituents (Hill, Murch, Rafferty, Wallis, & Green, 2007). From a quantitative point of view, it was observed that a higher level of whey protein was present in powdered formula than in bovine milk. The increased proportion of whey-dominant formula is applied to obtain a casein:whey protein ratio closer to that of human milk. The higher proportion of α-lactalbumin in the formula than in the skim milk powder is a further step towards humanization of the infant formula and can be achieved by the inclusion of an α-lactalbumin-enriched whey protein preparation. In addition, a higher level of high molecular mass proteins was observed, most likely to resemble the average human milk protein composition.

Infant formulae are designed to have a quantitative protein profile as close to that of human milk as possible; however, this protein profile does not always take into account the partial predigestion of the protein and, in particular, these formulae do not contain hydrolysis products of the native human caseins. Formulations based solely on protein hydrolysates are readily available for hypoallergenic purpose but the inclusion of partially hydrolysed casein in formula for neonates is not widely practiced at present. The findings of this study could thus be employed in the further improvement of infant formulae, particularly those for neonates born prematurely. The inclusion of partially hydrolysed milk proteins may be useful for preparation of formulae which mimic the natural human milk as closely as possible. Further study of the composition of these low molecular mass peptides and their possible physiological and nutritional roles will also be required to optimally meet the complex nutritional requirements of newborns.

5. Conclusions

The higher total nitrogen content of milk from women delivering prematurely confirms previous reports by other authors, and a higher content of immunoglobulins and antibodies in that milk was shown. For the first time, elevated plasmin activity and its consequent hydrolysis of caseins in pre-term milk has been elucidated. Moreover, the proteomic patterns of pre-term and term milk samples were investigated in detail and the fifty most abundant proteins identified. The data suggest a physiological response that adjusts enzyme and/or protein expression to improve milk digestibility for breast-fed prematurely newborn babies, a finding that may have relevance for further design of infant formulae for different groups of neonates.

References

Astrup, T., & Sterndorff, I. (1953). A fibrinolytic system in human milk. *Proceedings of the Society for Experimental Biology and Medicine, 84*, 605–609.

Atkinson, S. A., Anderson, G. H., & Bryan, M. H. (1980). Human milk: comparison of the nitrogen composition in milk from mothers of premature and full-term infants. *American Journal of Clinical Nutrition, 33*, 811–816.

Atkinson, S. A., Schnurr, C. M., Donovan, S. M., & Lonnerdal, B. (1989). The non-protein nitrogen components in human milk: biochemistry and potential functional role. In S. A. Atkinson, & B. Lonnerdal (Eds.), *Protein and non-protein nitrogen in human milk* (pp. 117–133). Boca Raton, FL, USA: CRC Press.

Chevalier, F., Hirtz, C., Sommerer, N., & Kelly, A. L. (2009). Use of reducing/non reducing two-dimensional electrophoresis for the study of disulfide-mediated interactions between proteins in raw and heated bovine milk. *Journal of Agricultural and Food Chemistry, 57*, 5948–5955.

Chevalier, F., Rofidal, V., Vanova, P., Bergoin, A., & Rossignol, M. (2004). Proteomic capacity of recent fluorescent dyes for protein staining. *Phytochemistry, 65*, 1499–1506.

Conti, A., Giuffrida, M. G., & Cavaletto, M. (2007). Proteomics of human milk. In G. L. Hortin (Ed.), *Proteomics of human body fluids: Principles, methods and applications* (pp. 437–451). Totowa, NJ, USA: Humana Press.

Ferranti, P., Traisci, M. V., Picariello, G., Nasi, A., Boschi, V., Siervo, M., et al. (2004). Casein proteolysis in human milk: tracing the pattern of casein breakdown and the formation of potential bioactive peptides. *Journal of Dairy Research, 71*, 74–87.

Fox, P. F., & Kelly, A. L. (2005). Indigenous enzymes in milk: overview and historical aspects – part 1. *International Dairy Journal, 16*, 500–516.

Greenberg, R., & Groves, M. L. (1984). Plasmin cleaves human beta-casein. *Biochemical and Biophysical Research Communications, 125*, 463–468.

Greenberg, R., Groves, M. L., & Dower, H. J. (1983). Human β-casein amino acid sequence and identification of phosphorylation sites. *Journal of Biological Chemistry, 259*, 5132–5138.

Heegaard, C. W., Larsen, L. B., Rasmussen, L. K., Højberg, K. E., Petersen, T. E., & Andreasen, P. A. (1997). Plasminogen activation system in human milk. *Journal of Pediatric Gastroenterology and Nutrition, 25*, 159–166.

Heyndrickx, G. V. (1963). Further investigations on the enzymes in human milk. *Pediatrics, 31*, 1019.

Hill, D. J., Murch, S. H., Rafferty, K., Wallis, P., & Green, C. J. (2007). The efficacy of amino acids-based formulas in relieving the symptoms of cow's milk allergy: a systematic review. *Clinical and Experimental Allergy, 37*, 808–822.

Jensen, R. G. (1995). *Handbook of milk composition*. San Diego, USA: Academic Press.

Kelly, A. L., O'Flaherty, F., & Fox, P. F. (2005). Indigenous enzymes in milk: a brief overview of the present state of knowledge. *International Dairy Journal, 16*, 563–572.

Koletzko, B., Baker, S., Cleghorn, G., Neto, U. F., Gopalan, S., Hernell, O., et al. (2005). Global standard for the composition of infant formula: recommendations of an ESPGHAN coordinated international expert group. *Journal of Pediatric Gastroenterology and Nutrition, 41*, 584–599.

Korycka-Dahl, M., Ribadeau Dumas, B., Chene, N., & Martal, J. (1983). Plasmin activity in milk. *Journal of Dairy Science, 66*, 704–711.

Kunz, C., & Lönnerdal, B. (1989). Human milk protein: separation of whey proteins and their analysis by polyacrylamide gradient gel electrophoresis, fast protein liquid chromatography (FPLC), gel filtration and anion-exchange chromatography. *American Journal of Clinical Nutrition, 49*, 464–470.

Kunz, C., & Lönnerdal, B. (1990). Human-milk proteins: analysis of casein and casein subunits by anion-exchange chromatography, gel electrophoresis, and specific staining methods. *American Journal of Clinical Nutrition, 51*, 37–46.

Kunz, C., & Lönnerdal, B. (1992). Re-evaluation of the whey protein/casein ratio of human milk. *Acta Paediatrica, 81*, 107–112.

Laemmli, U. K. (1970). Cleavage of structural proteins during the assembly of the head of bacteriophage T4. *Nature, 277*, 680–685.

Lönnerdal, B. (2003). Nutritional and physiologic significance of human milk proteins. *American Journal of Clinical Nutrition, 77*, 1537S–1543S.

Ogundele, M. O. (1999). Inhibitors of complement activity in human breast-milk: a proposed hypothesis of their physiological significance. *Mediators of Inflammation, 8*, 69–75.

Okamoto, U., Horie, N., Nagamatsu, Y., & Yamamoto, J. I. (1981). Plasminogen-activator in human early milk: its partial purification and characterization. *Thrombosis and Haemostasis, 45*, 121–126.

Poth, A. G., Deeth, H. C., Alewood, P. F., & Holland, J. W. (2008). Analysis of the human casein phosphoproteome by 2-D electrophoresis and MALDI-TOF/TOF MS reveals new phosphoforms. *Journal of Proteomic Research, 7*, 5017–5027.

Richardson, B. C., & Pearce, K. N. (1981). The determination of plasmin in dairy products. *New Zealand Journal of Dairy Science and Technology, 18*, 247–252.

Rudloff, S., & Kunz, C. (1997). Protein and nonprotein nitrogen components in human milk, bovine milk, and infant formula: quantitative and qualitative aspects in infant nutrition. *Journal of Pediatric Gastroenterology and Nutrition, 24*, 328–344.

Storrs, A. B., & Hull, M. E. (1956). Proteolytic enzymes in human and cow milk. *Journal of Dairy Science, 39*, 1097–1100.

Work Group on Breastfeeding. (1997). American Academy of Pediatrics: breastfeeding and the use of human milk. *Pediatrics, 100*, 1035–1039.

JOURNAL OF AGRICULTURAL AND FOOD CHEMISTRY

Article

pubs.acs.org/JAFC

Proteomic Comparison of Equine and Bovine Milks on Renneting

Therese Uniacke-Lowe,[†] François Chevalier,*[,†,§] Sonia Hem,[#] Patrick F. Fox,[†] and Daniel M. Mulvihill[†]

[†]School of Food and Nutritional Sciences, University College, Cork, Ireland

[§]Proteomic Platform, iRCM, CEA, Fontenay aux Roses, France

[#]Proteomic Platform, INRA, Montpellier, France

ABSTRACT: Rennet-induced coagulation of bovine milk is a complex mechanism in which chymosin specifically hydrolyzes κ-casein, the protein responsible for the stability of the casein micelle. In equine milk, this mechanism is still unclear, and the protein targets of chymosin are unknown. To reveal the proteins involved, the rennetability of equine milk by calf chymosin was examined using gel-free and gel-based proteomic analysis and compared to bovine milk. RP-HPLC analysis of bovine and equine milks showed the release of several peptides following chymosin incubation. The hydrolyses of equine and bovine casein by chymosin were different, and the major peptides produced from equine milk were identified by mass spectrometry as fragments of β-casein. Using two-dimensional electrophoresis, equine β-casein was confirmed as the main target of calf chymosin over 24 h at 30 °C and pH 6.5. The gel-based analysis of equine milk discriminated between the different individual proteins and provided information on the range of isoforms of each protein as a result of post-translational modifications, as well as positively identified for the first time several isoforms of κ-casein. In comparison to bovine milk, κ-casein isoforms in equine milk were not involved in chymosin-induced coagulation. The intensity of equine β-casein spots decreased following chymosin addition, but at a slower rate than bovine κ-casein.

KEYWORDS: *equine milk, rennet coagulation, κ-casein, proteomic, bovine milk*

INTRODUCTION

The milk from all species studied to date contains a heterogeneous mixture of proteins within which a few primary proteins dominate. In bovine milk these proteins are α_{s1}-, α_{s2}-, β-, and κ-caseins, β-lactoglobulin, and α-lactalbumin with relative proportions of ∼30:10:30:12:10:4, respectively.[1] Proportions of these proteins vary greatly among species but, apart from whey acidic protein (WAP), which has been identified in several species[2] but not in ruminant or human milk,[3] no major protein, other than one of these families, has yet been found in the milk of any species. The protein content of mature equine milk is lower than that of bovine milk, but the principal classes of proteins, that is, caseins and whey proteins, are similar in both milks.[4−7]

The milk proteome is extremely complex due to post-translational modifications of proteins and the presence of many genetic variants.[8−10] All milk proteins exhibit genetic polymorphism, usually due to the substitution of one or two amino acids, which do not have significant effects on protein functionality. Microheterogeneity of milk proteins also results from post-translational phosphorylation, glycosylation, or proteolysis.

Whereas the principal proteins of equine milk have been fairly well characterized, the presence of κ-casein in equine milk has been an issue of debate for several years, with several authors[11−14] reporting its absence. However, other studies[15−19] reported its presence, albeit at a low concentration, and Lenasi et al.[20] presented the entire cDNA sequence for equine κ-casein.

In bovine milk, κ-casein is located predominately on the surface of casein micelles and plays an important role in the formation, stabilization, and aggregation of the micelles and alters the manufacturing properties and digestibility of milk. The presence of a glycan moiety in the C-terminal region of κ-casein enhances its ability to stabilize the micelle, by electrostatic repulsion, and may increase the resistance by the protein to proteolytic enzymes and high temperatures.[21,22] It has been reported[13] that equine κ-casein is more highly glycosylated than bovine κ-casein, which could significantly contribute to equine micelle stability. Ochirkhuyag et al.[13] and Doreau and Martin-Rosset[23] concluded that the steric stabilization of equine casein micelles by κ-casein may be aided by unphosphorylated β-casein on the surface of the micelle, thus compensating for the low κ-casein content.

Chymosin (EC 3.4.23.4) is a neonatal gastric aspartal proteinase that hydrolyxes the κ-casein of bovine milk into a soluble glycopeptide [caseinomacropeptide (CMP): amino acid residues 106−169] and an insoluble part (para-κ-casein: amino acid residues 1−105), which is crucial for the production of cheese and for the nutrition of newborns.[24,25] The non-enzymatic secondary stage of the coagulation of milk by chymosin involves the aggregation and gelation of para-κ-casein under the influence of Ca^{2+}.[26] Apart from cleavage of the Phe_{105}−Met_{106} bond of κ-casein, chymosin causes limited hydrolysis of κ-casein.[25] Calf chymosin hydrolyzes the Phe_{97}−Ile_{98} bond of equine κ-casein[19] and slowly hydrolyzes the Phe_{105}−Ile_{106} bond of human κ-casein.[27] Although the CMPs released from equine and human κ-casein are less hydrophilic than bovine CMP, in all species CMP is believed to inhibit

Received: November 5, 2012
Revised: February 7, 2013
Accepted: February 15, 2013
Published: February 15, 2013

gastric acid secretion following milk intake[28−30] and to have antibacterial activity.[31,32] The sequence 97−116 of κ-casein is highly conserved across species, suggesting that the limited proteolysis of κ-casein and subsequent coagulation of milk are of major biological significance.[28] The other proteins in bovine milk, α_{s1}-, α_{s2}-, and β-caseins and α-lactalbumin, are hydrolyzed by chymosin but at a much slower rate than κ-casein.[33,34]

Over the past decade, milk from nonbovine mammals (goat, donkey, horse, and camel) have been studied, generally as a means of identifying the best substitute for human milk in infant nutrition.[35−37] Milk proteins have been analyzed extensively using proteomic techniques.[38] Two-dimensional electrophoresis (2-DE) allows simultaneous detection and quantification of several thousand protein spots in the same gel[38−40] when combined with mass spectrometry analysis, and it has been used for the separation and characterization of the proteins in bovine milk or colostrum[41,42] or for identification of specific proteins and isoforms thereof.[43−45] To date, analysis of the effects of various processing treatments on bovine milk proteins using proteomics has been confined to exploring the changes in disulfide bonds in milk proteins after heating or pressure treatment.[45−48] Caseins in human milk have been resolved using 2-DE,[49] and a proteomic comparison between preterm and term human milk has been reported.[50] Recently, Hinz et al.[14] compared the milk of several species, including equine milk, using proteomics. The proteins of equine colostrum and milk have been analyzed by electrophoretic and immunological methods,[39] whereas Egito et al.[13] characterized the casein fraction of equine milk using 1- DE and 2-DE of samples purified by anion exchange chromatography and reverse phase high-performance liquid chromatography (RP-HPLC). Various mass spectrometric approaches have been used to characterize the proteins of asinine[51−56] and equine[17,57,58] milks.

The aim of this study was to examine the rennetability of equine milk by calf chymosin using RP-HPLC and 2-DE followed by mass spectrometry with comparative analysis of a renneted bovine milk sample. The presence and implication of equine κ-casein in equine milk coagulation were also investigated.

MATERIALS AND METHODS

Milk Supply. Equine milk was obtained from Orchid's Paardenmelkerij (Zeeland, The Netherlands) from a bulk supply collected from five milkings over 24 h, from a herd of multiparous New Forest and New Forest/Arabian mares (n > 100) in midlactation, physically separated by day from their foals. The milk was defatted by centrifugation at 1000g using a Sorvall RC 5B centrifuge (Thermo Fisher Scientific Inc., Waltham, MA, USA) at 20 °C for 20 min, followed by filtration through glass wool to remove fat particles. Raw whole bovine milk was obtained from a local dairy farm and was defatted by centrifugation at 2000g for 20 min at 20 °C, followed by filtration through glass wool. Sodium azide (0.5 g L^{-1}) was added to the skimmed milks to prevent microbial growth. All chemicals used were of reagent grade and obtained from Sigma-Aldrich Chemical Co. (St. Louis, MO, USA).

Renneting Equine and Bovine Milks. Skimmed equine and bovine milks were adjusted to pH 6.5 and tempered at 30 °C for 20 min in thin-walled glass tubes in a thermostatically controlled water bath. A 1:10 (v/v) aqueous dilution of fermentation-produced chymosin (10 μL mL^{-1}; Maxiren 180; 180 international milk-clotting units (IMCU) mL^{-1}; DSM Food Specialties, Delft, The Netherlands) was added. Aliquots (1 mL) of renneted bovine milk were removed after 4, 10, 15, 20, 40, 60, 90, and 240 min and from renneted equine milk after 20, 30, 60, 90, 120, and 240 min and at 24 h. Renneted milk samples were diluted (1:1) immediately with 4% trichloroacetic acid (TCA) in Eppendorf tubes, vortexed for 1 min, and then held at 20 °C for 30 min. The samples were centrifuged at 5000g for 10 min in a microcentrifuge (Sigma 1-15, Sigma Laborzentrifuge, Osterode am Harz, Germany). Supernatants were removed carefully and diluted 1:1 with buffer (0.1 M bis-Tris, pH 7.0, 8 M urea, 45 mM citrate) to a final pH of 3.0.[59] Samples were filtered through 0.45 μm filters (Millex-HV, PVDF, 13 mm; Millipore Corp., Billerica, MA, USA) prior to injection onto the RP-HPLC column.

RP-HPLC Analysis of Renneted Equine and Bovine Milk. RP-HPLC was preformed according to the method of Vasbinder et al.[59] for RP-HPLC analysis of CMP. Analysis was carried out using a Waters 626 nonmetallic HPLC system (Waters Corp., Milford, MA, USA) consisting of a Waters 486 UV−vis detector, a Waters 717$^+$ autosampler, a Waters 626 pump with a 600S controller, and an online Degasys DG-2410 degassing unit (Sanwa Tsusho Co., Tokyo, Japan). A Varian Pursuit XRs C18 RP-HPLC column [250 × 4.6 mm, 5 μm particles size, 300 Å pore size (Varian Inc., Lake Forest, CA, USA)] was used. A wash step of 15 min at 70% solvent B followed by a 15 min equilibration with 85% solvent A was included between analyses of samples.

Identification of κ-Casein in Equine Milk. To determine if equine milk contained κ-casein, skimmed equine milk was analyzed by RP-HPLC according to the method of Miranda et al.[48] Prior to analysis, the milk was mixed 1:2 (v/v) with 0.1 M bis-Tris buffer, pH 8.0, containing 8 M urea, 1.3% trisodium citrate, and 0.3% DTT. Chromatographic equipment was as described above, and a Microsorb C4 RP-HPLC column (250 × 4.6 mm, 300 Å pore size, 5 μm particle size) from Varian maintained at 40 °C was used. A 20 min wash step with 60% solvent B was included after protein separation followed by 10 min at 100% solvent A before injection of subsequent samples. A fraction was collected manually in the κ-casein region identified by Miranda et al.,[48] precipitated using TCA/acetone and dephosphorylated as follows: 10 mL of sample was cooled on ice, 750 μL of 100% TCA was added, and the mixture was held on ice for 2 h. The sample was centrifuged at 10000g for 10 min at 4 °C. The supernatant was removed, and 2 mL of acetone (precooled on ice) was added to the pellet. The sample was vortexed for 2 min, followed by centrifugation at 10000g (10 min at 4 °C). The supernatant was removed, and the pellet was washed again with 2 mL of ice-cold acetone; this step was repeated once. Finally, the pellet was dissolved in 45 μL of distilled water, and 2 μL of 20% SDS was added. Prior to electrophoresis, two samples (15 μL each) were prepared as follows: For sample 1, 15 μL was added to 15 μL of a 2× electrophoresis loading buffer. Sample 2 was dephosphorylated using the lambda protein phosphatase (lambda PP) and buffer system from New England Biolabs (Hitchin, Herts., UK); 2 μL of $MnCl_2$, 2 μL of PPase buffer, and 2 μL of phosphatase were added to 15 μL of sample, and the mixture was incubated overnight at 30 °C; 20 μL of single-strength electrophoresis buffer was added to 20 μL of the dephosphorylated sample solution. Samples were denatured in denaturing NuPAGE sample buffer[60] and separated with a Bis-Tris−MOBS buffer system (Invitrogen, Paisley, UK). The selected bands were then

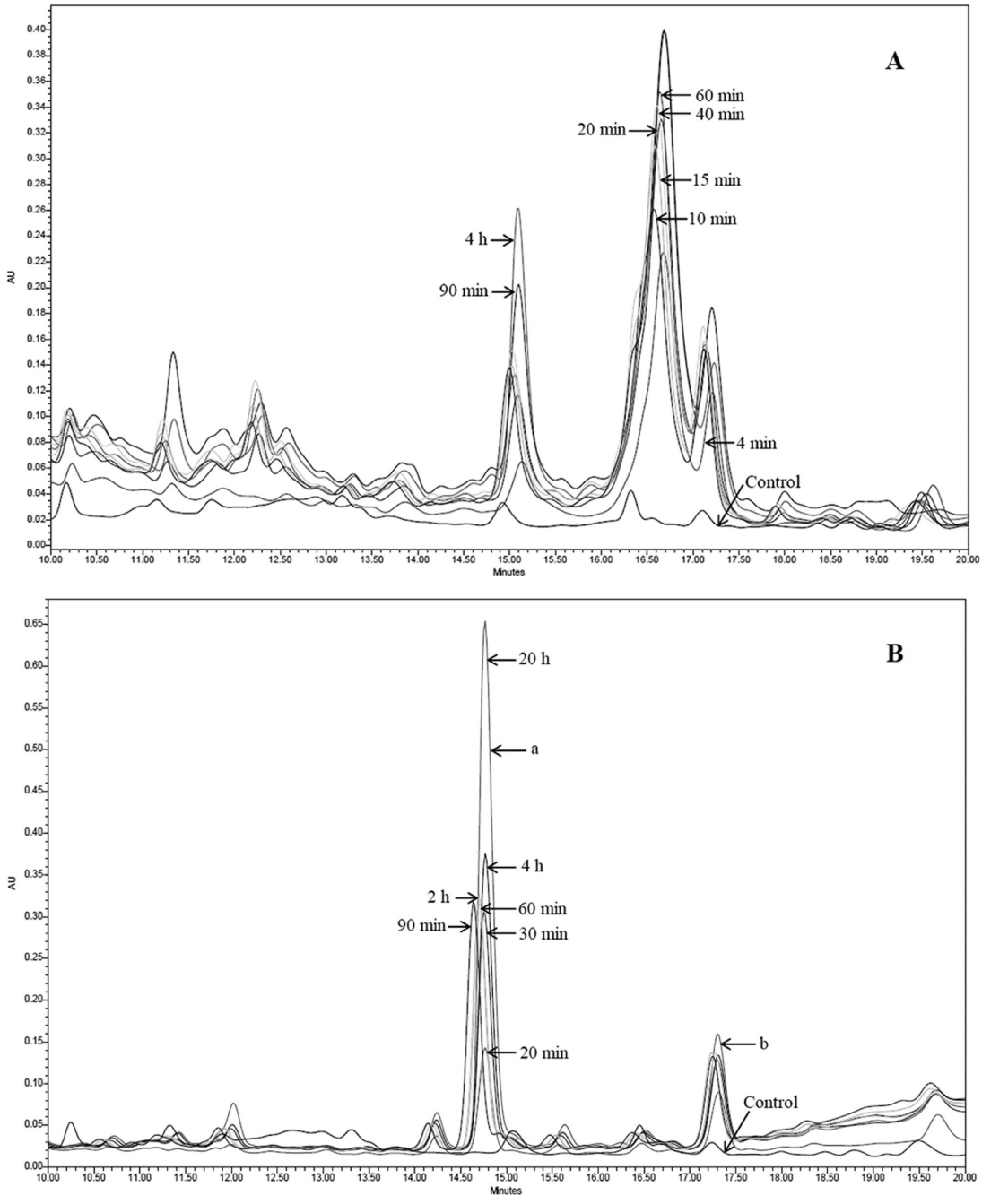

Figure 1. C18 RP-HPLC chromatograms of bovine (A) and equine (B) milks renneted with 10 μL mL^{-1} of 1:10 (v/v) Maxiren 180 at pH 6.5 and 30 °C. Fractions a and b were collected for MALDI-TOF MS/MS analysis.

in-gel digested with trypsin and subjected to nano-LC-MS/MS analysis as described below.

Two-Dimensional Electrophoresis Analysis of Renneted Equine and Bovine Milk. Samples of renneted equine milk were taken at 1, 2, 4, 8, and 24 h. Aliquots of renneted bovine milk were removed at 2 min intervals up to 16 min and at 20, 24, and 60 min. Renneted milk samples were diluted (1:10) immediately with solubilization buffer [9 M urea, 40 g L^{-1} 3-[(3-cholamidopropyl)dimethylammonio]-1-propanesulfonate (CHAPS), 5 g L^{-1} Triton X100, and 65 mM dithiothreitol (DTT)] according to the method of Chevalier et al.[49] The protein content of 100 μL of each sample was determined by the Bio-Rad Protein Assay (No. 500-0002, Bio-Rad Laboratories, Hercules, CA, USA), which is based on the method of Bradford[61] and uses bovine serum albumin (BSA) as standard. Analysis was carried out in at least duplicate at each time point for both equine and bovine milks. Analytical 2-DE was carried out on renneted equine and bovine milks with 100 μg of protein using 7 cm immobilized pH gradient (IPG) strips (ReadyStrip, Bio-Rad, Hercules, CA, USA) with a linear pH gradient from 3 to 10 (Bio-Rad), and preparative 2-DE was carried out on equine and bovine milks with 300 μg of protein using 17 cm IPG strips and a linear pH gradient from 3 to 10 (Bio-Rad). The 7 or 17 cm IPG strips were rehydrated in the protein solubilization buffer solution. Isoelectric focusing was carried out according to the method of Armaforte et al.[38] using a Protean IEF Cell isoelectric focusing system (Bio-Rad). The IPG strips were then embedded using 6 g L^{-1} low melting point

dx.doi.org/10.1021/jf3045846 | J. Agric. Food Chem. 2013, 61, 2839−2850

Table 1. Mass Spectrometry Results for Fractions a and b from C18 RP-HPLC Analysis of Equine Milk Renneted with Maxiren 180 at pH 6.5 and 30 °C; Analysis Carried out Using MALDI-TOF MS/MS

equine protein	obsd MW (Da)	theor MW (Da)	score	sequence[a]	amino acids[b]
			Fraction a		
β-casein	2336.289	2336.274	141	L-GPTGELDPATQPIVAVHNPVI-V	203−225
β-casein	1593.759	1593.867	48	V-APFPQPVVPYPQ-R	175−188
			Fraction b		
β-lg I	1677.872	1677.941	61	L-RPTPEDNLEIIL-R	45−58

[a]Cleavage sites indicated by hyphens. [b]Peptides identified by mass spectrometry include the signal peptide (amino acids 1−15 for β-casein and 1−18 for β-lg).

agarose on top of a 12.5% acrylamide gel, and sodium dodecyl sulfate−gel electrophoresis (SDS-PAGE) was carried out using a Criterion Dodeca Cell electrophoresis unit (Bio-Rad) for the 7 cm strips or a Protean II xi Cell electrophoresis unit (Bio-Rad) for the 17 cm strips. Gels were stained using colloidal Coomassie blue as described by Chevalier et al.[62] and stained gels digitized at 300 dpi using a GS-800 densitometer (Bio-Rad).

Image Analysis of 2-DE Gels. 2-DE gels were analyzed using Progenesis SameSpots V. 4.0 image analysis software (Nonlinear Dynamics, Newcastle-upon-Tyne, UK). The same gel area was selected from duplicate gels of each time point after rennet addition. Gel areas were compared, and the protein spot volumes were quantified as a mean of each replicate; spot quantities of all gels were normalized to remove non-expression-related variations in spot intensity as previously described.[63] To normalize the raw protein spot volume, each spot was expressed relative to the total volume of all spots on that image. Statistical analysis separated proteins that significantly increased or decreased ($p < 0.05$) after the treatments.[64]

In-Gel Digestion. Protein spots were selected for further analysis from preparative 2-DE and excised using a ∼2 mm diameter punch; gel pieces were transferred to 1.5 mL Eppendorf tubes. The gel spots were washed sequentially with Milli-Q water (Millipore Corp., Billerica, MA, USA), 25 mM ammonium bicarbonate, acetonitrile/25 mM ammonium bicarbonate (1:1, v/v), and acetonitrile. Gel fragments were dried using a Speed-Vac (GMI Inc., Ramsey, MN, USA), and the proteins were digested by the addition of sequencing grade trypsin (Promega, Charbonnieres, France) at 12.5 μg μL^{-1} in 25 mM ammonium carbonate, which was added on ice. After 15 min of gel rehydration, the proteins were digested at 37 °C for 2 h. Digested protein fragments were identified either by MALDI-TOF or by nano-LC MS/MS.

Protein Identification by MALDI-TOF Mass Spectrometry. Digested protein fragments were extracted by the addition of 20 μL of 0.1% TFA and sonicated for 15 min. The supernatants were transferred to 500 μL polypropylene microcentrifuge tubes. Peptide extraction was carried out by the addition of 20 μL of a 3:2 (v/v) acetonitrile/TFA solution and sonicated for 15 min. Supernatants were concentrated using a Speed-Vac to a final volume of 10−20 μL. Peptides were simultaneously desalted and concentrated using C18 Zip-Tip microcolumns, and supernatants were spotted directly on an AnchorChip MALDI target with α-cyano-4-hydroxycinnamic acid matrix solution and allowed to cocrystallize. Crystallized samples were washed with 0.1% TFA in water and recrystallized from 6:3:1 (v/v/v) ethanol/acetone/0.1% TFA in water. Peptide mass fingerprinting (PMF) was done using an UltraFlex MALDI-TOF/TOF mass spectrophotometer (Bruker, Bremen, Germany). The following parameters were used for the database search: taxonomy restricted to mammalia, one missed cleavage allowed, carbamidomethylation of cysteines as fixed modification, a mass tolerance of 30 ppm for the parent ion, and a mass tolerance of 0.6 Da for fragment ions. A minimum of five peptides matching the protein was used to validate the PMF identification, and peptide was validated if the p value was <0.05.

Protein Identification by Nano-LC Mass Spectrometry. When low-intensity protein spots could not be identified by MALDI-TOF mass spectrometry, nano-LC MS was used. Protein digests were extracted using formic acid and peptides were analyzed using an ion trap mass spectrometer (Esquire HCT plus; Bruker, Billerica, MA, USA) coupled to a nanochromatography system (HPLC 1200, Agilent, Santa Clara, CA, USA) interfaced with an HPLC-Chip system (Chip Cube, Agilent). Samples were first loaded onto the 4 mm enrichment cartridge at a flow rate of 4 μL min^{-1} using 0.1% formic acid. After preconcentration, peptides were separated on the column (75 μm diameter, 43 mm length) at a flow rate of 0.3 μL min^{-1} using a 15 min linear gradient from 3 to 80% acetonitrile in 0.1% formic acid and eluted into the mass spectrometer. The tandem mass spectrometer was an Esquire HCT+ (Bruker Daltonik GmBH, Bremen, Germany) operating in positive ion mode. The automated data-dependent acquisition parameters were chosen such that only doubly and triply charged precursor ions were selected for CID, excluding singly charged ions. MS/MS raw data were analyzed using Data Analysis software (Bruker Daltonik GmbH) to generate the peak lists. MASCOT search engine software (Matrix Science, London, UK) was used to search the Swissprot database (release 20100121). The following parameters were used for the database search: mass tolerance of 0.6 Da for parent and fragment ions, one missed cleavage allowed, carbamidomethylation of cysteines as fixed modification, peptide charge fixed at 2+ and 3+, and taxonomy restricted to mammalia. A protein was validated once it showed at least one peptide with $p < 0.05$.

RESULTS AND DISCUSSION

RP-HPLC of Renneted Equine and Bovine Milk. Chromatograms of 2% TCA extracts of equine and bovine milks renneted using Maxiren 180 and analyzed using C18 RP-HPLC are shown in Figure 1. Compared to a control bovine milk, renneted bovine milk contained peptides eluting at ∼15 and ∼16−17.5 min, which increased significantly in height about 4 min after rennet addition (Figure 1A) and continued to increase up to 240 min. Renneted equine milk (Figure 1B) had a different RP-HPLC profile from that of bovine milk, and no peptides appeared until ∼20 min after rennet addition. The time after rennet addition was therefore adjusted for equine milk, and samples for RP-HPLC were taken for up to 20 h.

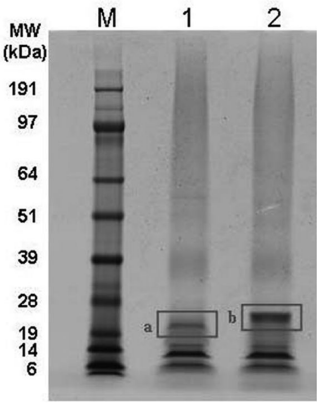

Figure 2. Electrophoretogram of fraction collected from C4 RP-HPLC analysis of equine milk. Lanes: M, molecular weight marker; 1, untreated sample; 2, sample treated with phosphatase. Bands a and b were excised for identification by nano-LC-MS/MS.

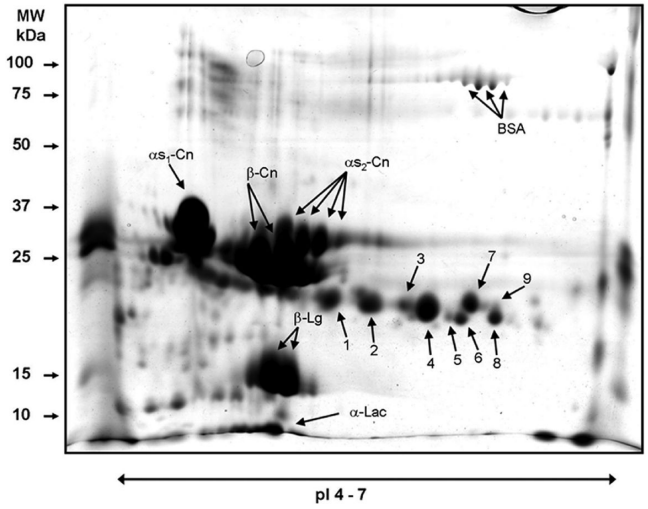

Figure 4. 2-DE preparative gel of a control bovine milk sample (~300 μg of proteins) under reducing conditions using pH 4–7 p*I* range for the first dimension and a 12% acrylamide gel for the second dimension. The numbered spots were submitted to mass spectrometry identification by MALDI-TOF peptide mass fingerprint and/or nano-LC MS/MS (results in Table 2). Proteins identified in figure from Chevalier and Kelly.[45]

Egito et al.[19] reported that calf chymosin readily cleaves equine β-casein at Leu_{190}–Tyr_{191}, and the fragments produced were resistant to hydrolysis even after 24 h of incubation with chymosin. Egito et al.[19] fractionated whole equine casein using affinity chromatography on agarose wheat germ agglutinin (WGA) and demonstrated the relatively slow hydrolysis of equine κ-casein (WGA-bound fraction) by calf chymosin at the bond Phe_{97}–Ile_{98}. Fractions labeled a and b (Figure 1B) in this study were collected and analyzed by MALDI-TOF MS/MS, and the faster eluting peak, a, was identified as originating from equine β-casein (Table 1), which was hydrolyzed quickly by calf chymosin in agreement with Egito et al.[19] Peptides from equine κ-casein were not identified in either fraction by MS.

Identification of κ-Casein in Equine Milk. The fraction containing κ-casein, isolated using C4 RP-HPLC and identified according to Miranda et al.,[48] was collected and treated with phosphatase. The electrophoretograms of the enzymatically treated samples are shown in Figure 2. The phosphatase-treated sample had one band of ~24000 Da, which was selected for MS analysis along with a band of ~19000 Da from the control sample. Using MALDI-TOF and MALDI TOF/TOF analysis, no result was obtained by PMF, and multiple TOF-TOF analyses identified equine lysozyme; however, using nano-LC MS/MS a peptide (YIPIYYVLNSSPR) from equine κ-casein was identified in band b (Figure 3). Band a (Figure 2) was from a control equine milk, which was not dephosphorylated, and κ-

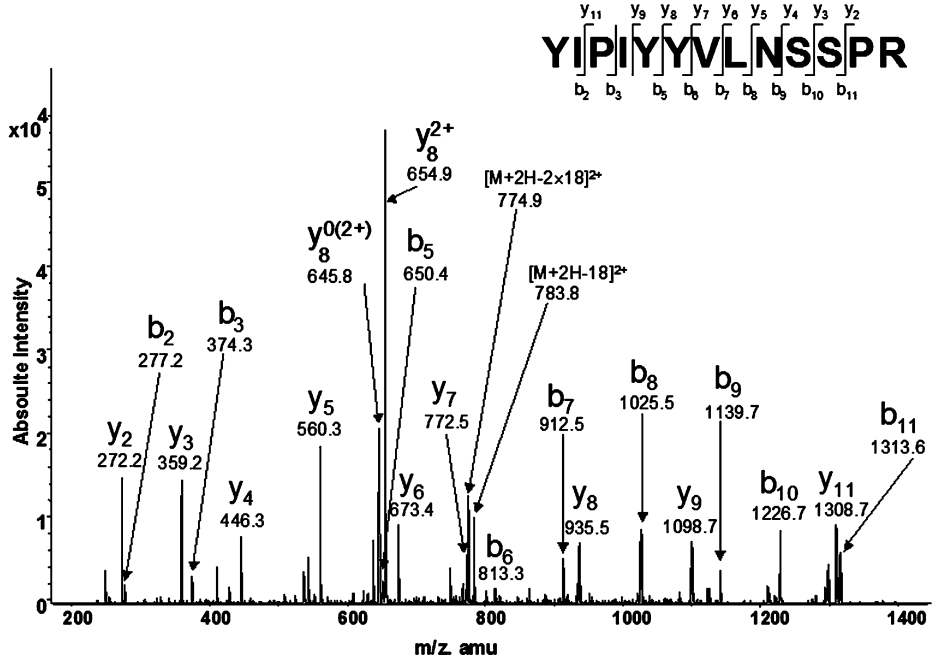

Figure 3. Nano-LC MS/MS spectra of fragmentation process of the YIPIYYVLNSSPR peptide (with m/z 792.9) from equine κ-casein; b^0, b-ion with loss of water (−18 Da); $[M + 2H - 18]^{2+}$, precursor ion with neutral loss of one molecule of water; $[M + 2H - 2 \times 18]^{2+}$, precursor ion with neutral loss of two molecules of water.

dx.doi.org/10.1021/jf3045846 | J. Agric. Food Chem. 2013, 61, 2839–2850

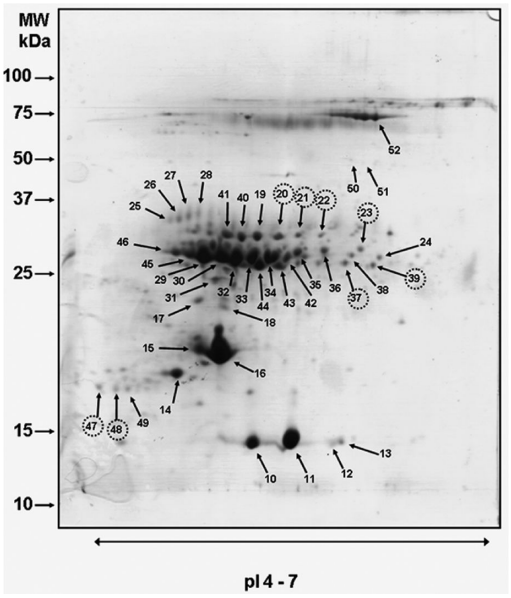

Figure 5. 2-DE preparative gel of equine milk (~300 μg of proteins) under reducing conditions using a 17 cm pH 4−7 p*I* range in the first dimension and a 12% acrylamide gel for the second dimension. The most abundant spots are indicated with arrows, and they were submitted to mass spectrometry identification by MALDI-TOF peptide mass fingerprinting and/or nano-LC/MS-MS (results in Table 3). Gel spots with dashed circles were those identified in subsequent analysis as having decreased following renneting with Maxiren 180 at pH 6.5.

casein was not identified therein. The κ-casein peptide, YIPIYYVLNSSPR, identified in band b, contained several potential phosphorylation sites; the lower ion efficiency of phosphorylated peptides in complex samples makes it difficult for MS identification. Using NetPhos 2.0, 11 phosphorylation sites in equine κ-casein (2 serine, 6 threonine, 3 tyrosine) were predicted, which scored >0.5 in the NetPhos scoring system. In the sequence YIPIYYVLNSSPR, identified from equine κ-casein, the serine residue highlighted in bold scored 0.947 on the NetPhos scale, which indicated a high probability of phosphorylation.

Two-Dimensional Electrophoresis Analysis of Equine and Bovine Milks. Preparative 2-DE gels of skimmed bovine and equine milk samples, performed under reducing conditions, are shown in Figures 4 and 5, respectively. Protein spots in the bovine sample were identified according to the method of Chevalier and Kelly;[45] the spots in the κ-caseins region were identified by MALDI-TOF with PMF, and the results are shown in Table 2. In this region, five κ-caseins, that is protein spots 1, 2, 3, 4, and 6, were identified by MALDI-TOF/TOF with PMF (Table 2). It has been reported that up to 10 isoforms of κ-casein with p*I* values from 4.47 to 5.81 can be identified by 2-DE gels of bovine milk.[43] If α_s- and β-caseins are removed, up to 16 gel spots can be identified as κ-casein isoforms arising from post-translational modifications such as phosphorylation and glycosylation.[44] In this study, within the region of the κ-casein isoforms, several β-casein isoforms were identified (Table 2), which have been reported to migrate to similar regions on a 2-DE gel as the more acidic κ-casein isoforms.[44] Holland et al.[44] and Chevalier and Kelly[45] identified the principal κ-casein spots in bovine milk, but in the present study the effect of added chymosin over time was considered for only the major isoforms.

The most abundant protein spots in equine milk isolated by preparative 2-DE were identified using peptide mass fingerprinting (PMF) with MALDI-TOF or nano-LC-MS/MS. Equine κ-casein was identified in spots 25, 26, and 27, and some κ-casein comigrated with β-casein in spots 40 and 41 (Figure 5 and Table 3). By comparison with bovine κ-casein, the isoelectric points of equine κ-caseins were significantly

Table 2. Identification of the Protein Spots in the κ-Casein Region of Bovine Milk by 2-DE with Peptide Mass Fingerprinting (PMF) Using MALDI-TOF or TOF/TOF[a]

spot	bovine protein	accession no.[b]	obsd p*I*	obsd MW (kDa)	theor p*I*	theor MW (kDa)	score	no. of matching peptides	sequence[c]	amino acids[d]
1	κ-casein	P02668	5.23	20	5.93	18.9	100	2	K-YIPIQYVLSR-Y	45−56
									R-SPAQILQWQVLSNTVPAK-S	89−108
2	κ-casein	P02668	5.45	20	5.93	18.9	76	1	R-SPAQILQWQVLSNTVPAK-S	89−108
3	κ-casein	P02668	5.66	20	5.93	18.9	46	1	K-YIPIQYVLSR-Y	45−56
4	κ-casein	P02668	5.78	19	5.93	18.9	108	1	R-SPAQILQWQVLSNTVPAK-S	89−108
5	κ-casein	P02668	5.94	19	5.93	18.9	55	1	K-YIPIQYVLSR-Y	45−56
6	β-casein fragment	P02666	5.98	18	5.13	23.6	151	4	K-VLPVPQK-A	184−192
									K-AVPYPQR-D	191−199
									K-FQSEEQQQTEDELQDK-I	48−64
									R-DMPIQAFLLYQEPVLGPVR-G	198−218
7	κ-casein	P02668	6.03	20	5.93	18.9	159	2	K-YIPIQYVLSR-Y	45−56
									R-SPAQILQWQVLSNTVPAK-S	89−108
8	β-casein fragment	P02666	6.17	18	5.13	23.6	111	4	R-GPFPIIV	217−224
									K-VLPVPQK-A	184−192
									K-AVPYPQR-D	191−199
									R-DMPIQAFLLYQEPVLGPVR-G	198−218
9	β-casein fragment	P02666	6.17	19	5.13	23.6	50	2	K-VLPVPQK-A	184−192
									K-AVPYPQR-D	191−199

[a]Theoretical molecular mass and isoelectric point (p*I*) of proteins are based on the amino acid primary sequence without taking into account any post-translational and/or degradation modifications. Observed molecular mass and isoelectric points (p*I*) are those observed from the position of the corresponding spot on the two-dimensional electrophores. [b]Accession number corresponds to the Swiss-Prot accession number. [c]Cleavage sites indicated by hyphens. [d]Peptides identified by mass spectrometry include the signal peptide (amino acids 1−15 for β-casein and 1−18 for β-lg.

Table 3. Identification of the Most Abundant Spots from Two-Dimensional Gel of Equine Milk by Nano-LC-MS/MS[a]

spot	equine protein	accession no.[b]	obsd p*I*	obsd MW (kDa)	theor p*I*	theor MW (kDa)	score	no. of matching peptides
10	α-lactalbumin	P08334	5.25	14	4.95	14.2	424	8
11	α-lactalbumin	P08334	5.55	14	4.95	14.2	561	6
12	α-lactalbumin	P08334	5.89	14	4.95	14.2	401	9
	heart-type fatty acid-binding protein	Q9XSI5	5.89	14	5.92	13.9	315	6
13	α-lactalbumin	P08334	5.94	14	4.95	14.2	327	7
	heart-type fatty acid-binding protein	Q9XSI5	5.94	14	5.92	13.9	115	3
14	β-lactoglobulin II	LGHO2	4.78	18	4.71	18.3	245	5
15	β-lactoglobulin I	P08334	4.91	19	4.85	18.5	415	9
16	β-lactoglobulin I	P08334	5.02	20	4.85	18.5	522	11
17	β-lactoglobulin I	P08334	4.87	25	4.85	18.5	330	7
	β-casein	Q9GKK3	4.87	25	5.78	25.5	180	5
	α_{s1}-casein	Q95KZ7	4.87	25	5.57	24.7	114	3
18	β-lactoglobulin I	P08334	4.97	24	4.85	18.5	266	6
	α-lactalbumin	P08334	4.97	24	4.95	14.2	165	3
19	β-casein	Q9GKK3	5.3	28	5.78	25.5	264	7
20	β-casein	Q9GKK3	5.53	28	5.78	25.5	235	6
21	β-casein	Q9GKK3	5.73	28	5.78	25.5	223	6
22	β-casein	Q9GKK3	5.97	28	5.78	25.5	237	6
23	β-casein	Q9GKK3	6.31	29	5.78	25.5	252	7
24	α_{s1}-casein	Q95KZ7	6.53	26	5.57	24.7	329	7
25	κ-casein	P82187	4.72	33	8.03	18.8	138	3
26	κ-casein	P82187	4.75	33	8.03	18.8	181	4
27	κ-casein	P82187	4.79	33	8.03	18.8	61	1
28	β-casein	Q9GKK3	4.85	32	5.78	25.5	82	2
29	β-casein	Q9GKK3	4.9	26	5.78	25.5	212	6
	α_{s1}-casein	Q95KZ7	4.9	26	5.57	24.7	167	2
30	β-casein	Q9GKK3	5.02	27	5.78	25.5	252	6
	α_{s1}-casein	Q95KZ7	5.02	27	5.57	24.7	95	2
31	α_{s1}-casein	Q95KZ7	4.97	24	5.57	24.7	239	5
	β-casein	Q9GKK3	4.97	24	5.78	25.5	177	4
32	β-casein	Q9GKK3	5.1	26	5.78	25.5	168	5
	α_{s1}-casein	Q95KZ7	5.1	26	5.57	24.7	107	2
33	β-casein	Q9GKK3	5.31	26	5.78	25.5	259	7
	α_{s1}-casein	Q95KZ7	5.31	26	5.57	24.7	104	2
34	β-casein	Q9GKK3	5.44	26	5.78	25.5	232	5
	α_{s1}-casein	Q95KZ7	5.44	26	5.57	24.7	59	2
35	β-casein	Q9GKK3	5.75	26	5.78	25.5	194	4
	α_{s1}-casein	Q95KZ7	5.75	26	5.57	24.7	77	3
36	β-casein	Q9GKK3	5.98	26	5.78	25.5	267	7
37	β-casein	Q9GKK3	6.18	25	5.78	25.5	354	9
	α_{s1}-casein	Q95KZ7	6.18	25	5.57	24.7	207	5
38	α_{s1}-casein	Q95KZ7	6.23	26	5.57	24.7	245	5
	β-casein	Q9GKK3	6.23	26	5.78	25.5	225	6
39	α_{s1}-casein	Q95KZ7	6.48	25	5.57	24.7	454	8
	β-casein	Q9GKK3	6.48	25	5.78	25.5	208	6
40	β-casein	Q9GKK3	5.13	27	5.78	25.5	248	6
	κ-casein	P82187	5.13	27	8.03	18.8	180	3
41	β-casein	Q9GKK3	5.01	28	5.78	25.5	254	6
	κ-casein	P82187	5.01	28	8.03	18.8	115	2
42	β-casein	Q9GKK3	5.58	26	5.78	25.5	131	3
	α_{s1}-casein	Q95KZ7	5.58	26	5.57	24.7	118	2
43	α_{s1}-casein	Q95KZ7	5.53	26	5.57	24.7	96	1
	β-casein	Q9GKK3	5.53	26	5.78	25.5	61	1
44	α_{s1}-casein	Q95KZ7	5.38	25	5.57	24.7	282	3
45	β-casein	Q9GKK3	4.85	26	5.78	25.5	220	5
	α_{s1}-casein	Q95KZ7	4.85	26	5.57	24.7	145	3
46	β-casein	Q9GKK3	4.74	27	5.78	25.5	239	5
	α_{s1}-casein	Q95KZ7	4.74	27	5.57	24.7	93	2
47	β-casein	Q9GKK3	4.25	17	5.78	25.5	87	3
48	β-casein	Q9GKK3	4.36	17	5.78	25.5	64	1
49	β-casein	Q9GKK3	4.46	17	5.78	25.5	75	2

dx.doi.org/10.1021/jf3045846 | J. Agric. Food Chem. 2013, 61, 2839−2850

Table 3. continued

spot	equine protein	accession no.[b]	obsd p*I*	obsd MW (kDa)	theor p*I*	theor MW (kDa)	score	no. of matching peptides
50	lactoferrin	O97668	5.93	51	8.32	75.4	793	15
51	lactoferrin	O97668	6.15	50	8.32	75.4	863	16
52	lactoferrin	O97668	6.17	75	8.32	75.4	49	2

[a]Theoretical molecular mass and isoelectric point (p*I*) of proteins are based on the amino acid primary sequence without taking into account any post-translational and/or degradation modifications. Observed molecular mass and isoelectric points (p*I*) are those observed from the position of the corresponding spot on the two-dimensional electrophoresis gel. [b]Accession number corresponds to the Swiss-Prot accession number.

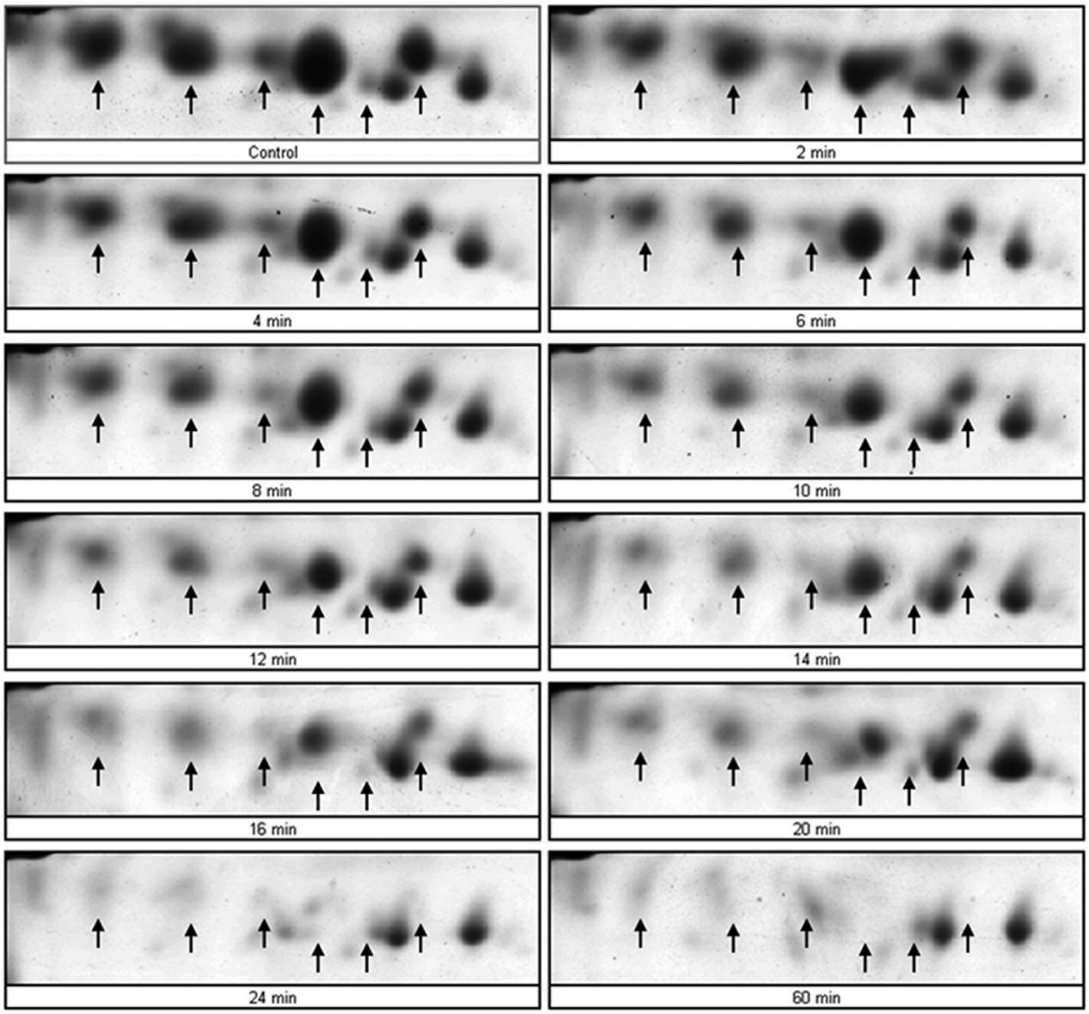

Figure 6. Image analysis of κ-casein modulated protein spots from 2-DE gels of bovine milk renneted over 60 min. Arrows indicate the κ-caseins that change in intensity (amount) over time.

lower than those of their bovine counterparts. Areas of the 2-DE gel of equine milk can be identified where isoforms of proteins are grouped; protein spots 20, 21, 22, 23, 28, and 29 form a cluster of β-casein isoforms, whereas protein spots 30, 31, 33, 34, and 35 represent isoforms of equine α_{s1}-casein (Figure 5 and Table 3). On the basis of spot intensities, approximately ∼35% of protein spots were β-casein isoforms, and a further 35% were α_{s1}-casein isoforms. Together with these two main milk proteins, other well-known milk proteins were identified including α-lactalbumin (4 spots), β-lactoglobulin (5 spots), and lactoferrin (3 spots). This is the first study in which a complete identification of the most abundant proteins in equine milk was achieved. Previously, 2-DE has been used to display the microheterogeneity of equine α_{s1}-[65] and β-caseins.[57,66] The 2-DE gel of equine milk highlighted the complexity of the milk proteome, and although very different from that of bovine milk in general appearance, it contained a multitude of protein spots. The proteome of bovine milk, and the milk of most species, is dominated by 6 gene products that constitute ∼95% of milk protein, but >150 protein spots can be detected using 2-DE of whole bovine milk. Many of the protein spots represent isoforms of the major gene products that have been produced by extensive post-translational modifications, including phosphorylation, glycosylation, and proteolysis.[43] D'Auria et al.[67] conducted a proteomic evaluation of milk from various species, including equine milk, as a means of identifying and evaluating the suitability of such milks for infant nutrition and highlighted the complex pattern of proteins of 2-DE electrophoretograms from human, equine, asinine, caprine, ovine, and bovine milks and reported that phylogenetically

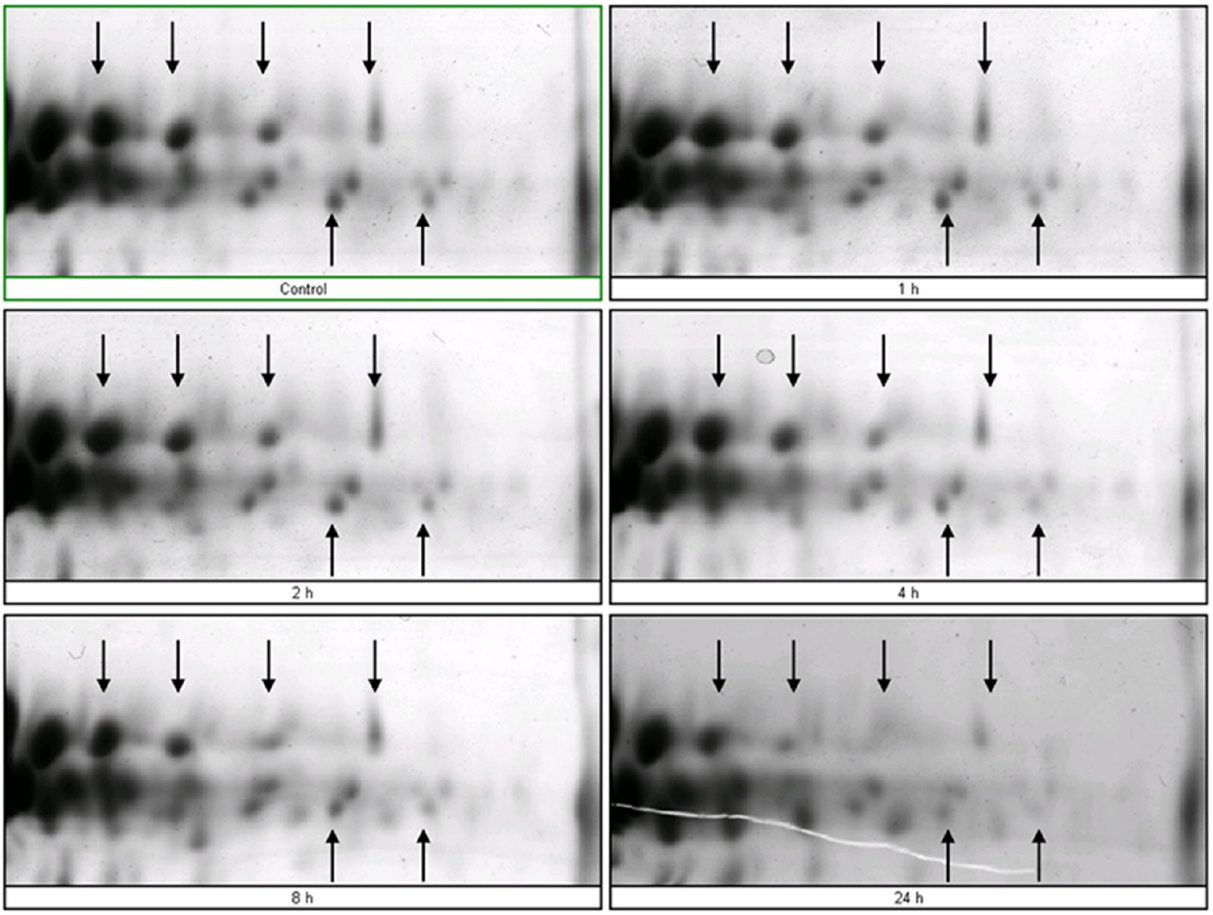

Figure 7. Image analysis of β-casein modulated protein spots from 2-DE gels of equine milk renneted over time. Arrows indicate the β-caseins that change in intensity (amount) over 24 h.

related species such as sheep/goats and horses/donkeys had quite similar protein expressions. Human milk protein expression was reported to be quite similar to both those of the horse and donkey.[67]

Effect of Renneting on Protein Spot Intensity in Equine and Bovine Milk. Two-dimensional analytical gels of renneted bovine and equine milk samples were scanned using SameSpots V4.0 software, and protein spots that changed in intensity over time were identified. The areas of the gels where protein spots susceptible to chymosin hydrolysis were identified and selected for further analysis. In the case of renneted bovine milk, six κ-casein spots decreased over time after chymosin addition (Figure 6). The result showed the decrease in intensity of bovine κ-caseins with time after chymosin addition (Figure 6). Bovine β-caseins were not significantly affected by chymosin during the time course of this experiment.

The proteins in equine milk that were hydrolyzed by chymosin over 24 h were identified as β-caseins only, that is, protein spots 20, 21, 22, 23, 47, and 48 as well as 37 and 39, which were identified as mixtures of β- and α_{s1}-caseins (Figure 3 and Table 3). Image analysis was performed on the 2-DE gel area where the most significant changes in protein spot intensities were detected (Figure 7), which showed the decrease in equine β-casein over 24 h after chymosin addition with the most significant decrease having taken place ~4 h after chymosin addition. According to the picture analysis, no change was observed over time with spots identified as κ-casein. This result was in agreement with the C18-RPLC analysis carried out on renneted equine milk (see RP-HPLC of Renneted Equine and Bovine Milk), where the peptide that increased in intensity following chymosin hydrolysis was identified as a peptide from β-casein. Egito et al.[19] reported the slow hydrolysis of equine κ-casein by chymosin with peptides generated ~10−20 min after chymosin addition when analyzed by C18 RP-HPLC.

Because equine milk contains a low level of κ-casein,[16,18,19,68,69] it has been suggested that the steric stabilization of equine casein micelles by κ-casein may be aided by unphosphorylated β-casein;[8] it is evident from this study that β-casein plays a significant role in equine casein micelle structure, and because it is hydrolyzed preferentially by chymosin, rather than κ-casein, it is likely that a significant proportion has an exposed location. It is not known whether phosphorylated or unphosphorylated forms of equine β-casein may stabilize the casein micelle. Phosphorylated forms would be hydrophilic and, in theory, could contribute to micellar stability, but they may be susceptible to precipitation by calcium. The significance of casein micelle phosphate groups is discussed by Yoshikawa et al.[70]

Unlike bovine κ-casein, the amino acid sequence of equine κ-casein does not have a distinctly hydrophilic C-terminal domain, particularly due to the absence of a strong hydrophilic region at residues 110−120, which, in the case of bovine casein micelles, protrudes from the micellar surface providing steric stabilization. However, equine κ-casein is reported to be heavily glycosylated,[13] which could compensate for the lack of

dx.doi.org/10.1021/jf3045846 | J. Agric. Food Chem. 2013, 61, 2839−2850

hydrophilic amino acid residues. The high level of glycosylation of equine κ-casein means the molecular mass of equine κ-casein prior to post-translational modification is ∼18.8 kDa,[14] whereas after post-translational modification it is ∼25.3 kDa,[28] suggesting that carbohydrate moieties represent ∼35% of total mass of equine κ-casein. For bovine κ-casein, glycosylation increases the mass of κ-casein by <5%.[71] The degree of glycosylation of κ-casein can have considerable effects on the colloidal stability of casein micelles.[72,73]

Conclusion. Isoforms of equine κ-casein were unequivocally observed and identified in several spots of a 2-DE map by MS. Also, a peptide from equine κ-casein was separated by C18 RP-HPLC and identified by MS analysis. This study demonstrated the ability of 2-DE coupled with mass spectrometry and image analysis to follow the effects of renneting on milk proteins over time. 2-DE and MS allowed the simultaneous evaluation of the relative abundance and modification of the endogenous proteins in equine and bovine milk following hydrolysis by calf chymosin. Equine milk was susceptible to hydrolysis by calf chymosin over 24 h at 30 °C and pH 6.5, but the peptides produced were from equine β-casein, which was also confirmed by MS analysis of C18 RP-HPLC peptides. Whereas equine β-casein was hydrolyzed by chymosin, hydrolysis occurred at a much slower rate compared to that of bovine κ-casein. In this study, equine κ-casein was not susceptible to hydrolysis by calf chymosin. The hydrolysis pattern of equine caseins by calf chymosin is not necessarily unique, and other studies have shown that the milk of a particular species is preferentially coagulated by chymosin from that species.[74−79] The isolation of equine chymosin and its ability to coagulate equine milk as well as its hydrolysis of equine caseins warrants investigation.

AUTHOR INFORMATION

Corresponding Author

*Postal address: Proteomic Platform, iRCM, CEA, Fontenay aux Roses, France. Phone: +33 (0)146 548 326. Fax: +33 (0) 146 549 138. E-mail: francois.chevalier@cea.fr.

Notes

The authors declare no competing financial interest.

REFERENCES

(1) Fox, P. F.; McSweeney, P. L. H. *Advanced Dairy Chemistry*; Springer: Berlin, Germany, 2003.

(2) Hajjoubi, S.; Rival-Gervier, S.; Hayes, H.; Floriot, S.; Eggen, A.; Piumi, F.; Chardon, P.; Houdebine, L.-M.; Thépot, D. Ruminants genome no longer contains whey acidic protein gene but only a pseudogene. *Gene* **2006**, *370*, 104−112.

(3) Rival-Gervier, S.; Thépot, D.; Jolivet, G.; Houdebine, L.-M. Pig whey acidic protein gene is surrounded by two ubiquitously expressed genes. *Biochim. Biophys. Acta* **2003**, *1627*, 7−14.

(4) Uniacke-Lowe, T.; Fox, P. F. Milk | equid milk. In *Encyclopedia of Dairy Sciences*, 2nd ed.; Fuquay, J. W., Ed.; Academic Press: San Diego, CA, 2011; pp 518−529.

(5) Uniacke-Lowe, T.; Huppertz, T.; Fox, P. F. Equine milk proteins: chemistry, structure and nutritional significance. *Int. Dairy J.* **2010**, *20*, 609−629.

(6) Uniacke-Lowe, T.; Fox, P. F. Equid milk: chemistry, biochemistry and processing. In *Food Biochemistry and Food Processing*, 2nd ed.; Simpson, B., Ed.; Wiley-Blackwell: Ames, IA, 2012; pp 491−530.

(7) Salimei, E.; Fantuz, F. Equid milk for human consumption. *Int. Dairy J.* **2012**, *24*, 130−142.

(8) Eigel, W. N.; Butler, J. E.; Ernstrom, C. A.; Farrell, H. M., Jr.; Harwalkar, V. R.; Jenness, R.; Whitney, R. M. Nomenclature of proteins of cow's milk: fifth revision. *J. Dairy Sci.* **1984**, *67*, 1599−1631.

(9) Farrell, H. M., Jr.; Jimenez-Flores, R.; Bleck, G. T.; Brown, E. M.; Butler, J. E.; Creamer, L. K.; Hicks, C. L.; Hollar, C. M.; Ng-Kwai-Hang, K. F.; Swaisgood, H. E. Nomenclature of the proteins of cows' milk, sixth revision. *J. Dairy Sci.* **2004**, *87*, 1641−1674.

(10) Cunsolo, V.; Muccilli, V.; Saletti, R.; Foti, S. Review: applications of mass spectrometry techniques in the investigation of milk proteome. *Eur. J. Mass Spectrom. (Chichester, UK)* **2011**, *17*, 305−320.

(11) Visser, S.; Jenness, R.; Mullin, R. J. Isolation and characterization of β- and γ-caseins from horse milk. *Biochem. J.* **1982**, *203*, 131−139.

(12) Ono, T.; Kohno, H.; Odagiri, S.; Takagi, T. Subunit components of casein micelles from bovine, ovine, caprine and equine milks. *J. Dairy Res.* **1989**, *56*, 61−68.

(13) Ochirkhuyag, B.; Chobert, J.-M.; Dalgalarrondo, M.; Haertlé, T. Characterization of mare caseins. Identification of α-S1- and α-S2-caseins. *Lait* **2000**, *80*, 223−235.

(14) Hinz, K.; O'Connor, P. M.; Huppertz, T.; Ross, R. P.; Kelly, A. L. Comparison of the principal proteins in bovine, caprine, buffalo, equine and camel milk. *J. Dairy Res.* **2012**, *79*, 185−191.

(15) Kotts, C.; Jenness, R. Isolation of κ-casein-like proteins from milks of various species. *J. Dairy Sci.* **1976**, *59*, 816−822.

(16) Malacarne, M.; Summer, A.; Formaggioni, P.; Mariani, P. Observations on percentage distribution of the main mare milk caseins separated by reversed-phase HPLC. *Ann. Fac. Med. Vet., Univ. Parma* **2000**, *20*, 143−152.

(17) Iametti, B. S.; Tedeschi, G.; Oungre, E.; Bonomi, F. Primary structure of κ-casein isolated from mares' milk. *J. Dairy Res.* **2001**, *68*, 53−61.

(18) Egito, A. S.; Miclo, L.; López, C.; Adam, A.; Girardet, J. M.; Gaillard, J. L. Separation and characterization of mares' milk α(s1)-, β-, κ-caseins, γ-casein-like, and proteose peptone component 5-like peptides. *J. Dairy Sci.* **2002**, *85*, 697−706.

(19) Egito, A. S.; Girardet, J.-M.; Miclo, L.; Molle, D.; Humbert, G.; Gaillard, J.-L. Susceptibility of equine κ- and β-caseins to hydrolysis by chymosin. *Int. Dairy J.* **2001**, *11*, 885−893.

(20) Lenasi, T.; Rogelj, I.; Dovc, P. Characterization of equine cDNA sequences for αS1-, β- and κ-casein. *J. Dairy Res.* **2003**, *70*, 29−36.

(21) Minkiewicz, P.; Dziuba, J.; Muzinska, B. The contribution of *N*-acetylneuraminic acid in the stabilization of micellar casein. *Pol. J. Food Nutr. Sci.* **1993**, *2*, 39−48.

(22) Dziuba, J.; Minkiewicz, P. Influence of glycosylation on micelle-stabilizing ability and biological properties of C-terminal fragments of cow's κ-casein. *Int. Dairy J.* **1996**, *6*, 1017−1044.

(23) Doreau, M.; Martin-Rosset, W. Dairy animals | horse. In *Encyclopedia of Dairy Sciences*; Roginski, H., Ed.; Elsevier: Oxford, UK, 2002; pp 630−637.

(24) Mercier, J. C.; Brignon, G.; Ribadeau-Dumas, B. [Primary structure of bovine κB casein. Complete sequence]. *Eur. J. Biochem.* **1973**, *35*, 222−235.

(25) Crabbe, M. J. C. Rennets: general and molecular aspects. In *Cheese: Chemistry, Physics and Microbiology*; Patrick, F., Fox, P. L. H. M., Eds.; Academic Press: San Diego, CA, 2004; Vol. *1*, pp 19−45.

(26) Neal A. Bringe, J. E. K. Use of platelet aggregometer to monitor the chymosin-initiated coagulation of casein micelles. *J. Dairy Res.* **1986**, *53*, 359−370.

(27) Plowman, J. E.; Creamer, L. K.; Liddell, M. J.; Cross, J. J. Structural features of a peptide corresponding to human κ-casein residues 84−101 by ^{1}H-nuclear magnetic resonance spectroscopy. *J. Dairy Res.* **1999**, *66*, 53−63.

(28) Mercier, J. C.; Chobert, J. M.; Addeo, F. Comparative study of the amino acid sequences of the caseinomacropeptides from seven species. *FEBS Lett.* **1976**, *72*, 208−214.

(29) Yvon, M.; Beucher, S.; Guilloteau, P.; Le Huerou-Luron, I.; Corring, T. Effects of caseinomacropeptide (CMP) on digestion regulation. *Reprod. Nutr. Dev.* **1994**, *34*, 527−537.

(30) Guilloteau, P.; Romé, V.; Delaby, L.; Mendy, F.; Roger, L.; Chayvialle, J. A. Is caseinomacropeptide from milk proteins, an inhibitor of gastric secretion? *Regul. Pept.* **2010**, *159*, 129−136.

(31) Malkoski, M.; Dashper, S. G.; O'Brien-Simpson, N. M.; Talbo, G. H.; Macris, M.; Cross, K. J.; Reynolds, E. C. Kappacin, a novel antibacterial peptide from bovine milk. *Antimicrob. Agents Chemother.* **2001**, *45*, 2309−2315.
(32) Thomä-Worringer, C.; Sørensen, J.; López-Fandiño, R. Health effects and technological features of caseinomacropeptide. *Int. Dairy J.* **2006**, *16*, 1324−1333.
(33) Carles, C.; Ribadeau Dumas, B. Kinetics of the action of chymosin (rennin) on a peptide bond of bovine α_{s1}-casein. Comparison of the behaviour of this substrate with that of β- and κ o-caseins. *FEBS Lett.* **1985**, *185*, 282−286.
(34) Miranda, G.; Haze, G.; Scanff, P.; Pelissier, J. P. Hydrolysis of α-lactalbumin by chymosin and pepsin. Effect of conformation and pH. *Lait* **1989**, *69*, 451−459.
(35) Businco, L.; Giampietro, P. G.; Lucenti, P.; Lucaroni, F.; Pini, C.; Di Felice, G.; Iacovacci, P.; Curadi, C.; Orlandi, M. Allergenicity of mare's milk in children with cow's milk allergy. *J. Allergy Clin. Immunol.* **2000**, *105*, 1031−1034.
(36) Muraro, M. A.; Giampietro, P. G.; Galli, E. Soy formulas and nonbovine milk. *Ann. Allergy Asthma Immunol.* **2002**, *89*, 97−101.
(37) Restani, P.; Beretta, B.; Fiocchi, A.; Ballabio, C.; Galli, C. L. Cross-reactivity between mammalian proteins. *Ann. Allergy Asthma Immunol.* **2002**, *89*, 11−15.
(38) Chevalier, F. Highlights on the capacities of "gel-based" proteomics. *Proteome Sci* **2010**, *8*, 23.
(39) Galvani, M.; Hamdan, M.; Righetti, P. G. Two-dimensional gel electrophoresis/matrix-assisted laser desorption/ionisation mass spectrometry of a milk powder. *Rapid Commun. Mass Spectrom.* **2000**, *14*, 1889−1897.
(40) Görg, A.; Weiss, W.; Dunn, M. J. Current two-dimensional electrophoresis technology for proteomics. *Proteomics* **2004**, *4*, 3665−3685.
(41) Galvani, M.; Hamdan, M.; Righetti, P. G. Two-dimensional gel electrophoresis/matrix-assisted laser desorption/ionisation mass spectrometry of commercial bovine milk. *Rapid Commun. Mass Spectrom.* **2001**, *15*, 258−264.
(42) Lindmark-Månsson, H.; Timgren, A.; Aldén, G.; Paulsson, M. Two-dimensional gel electrophoresis of proteins and peptides in bovine milk. *Int. Dairy J.* **2005**, *15*, 111−121.
(43) Holland, J. W.; Deeth, H. C.; Alewood, P. F. Proteomic analysis of κ-casein micro-heterogeneity. *Proteomics* **2004**, *4*, 743−752.
(44) Holland, J. W.; Deeth, H. C.; Alewood, P. F. Resolution and characterisation of multiple isoforms of bovine κ-casein by 2-DE following a reversible cysteine-tagging enrichment strategy. *Proteomics* **2006**, *6*, 3087−3095.
(45) Chevalier, F.; Kelly, A. L. Proteomic quantification of disulfide-linked polymers in raw and heated bovine milk. *J. Agric. Food Chem.* **2010**, *58*, 7437−7444.
(46) Patel, H. A.; Singh, H.; Anema, S. G.; Creamer, L. K. Effects of heat and high hydrostatic pressure treatments on disulfide bonding interchanges among the proteins in skim milk. *J. Agric. Food Chem.* **2006**, *54*, 3409−3420.
(47) Chevalier, F.; Hirtz, C.; Sommerer, N.; Kelly, A. L. Use of reducing/nonreducing two-dimensional electrophoresis for the study of disulfide-mediated interactions between proteins in raw and heated bovine milk. *J. Agric. Food Chem.* **2009**, *57*, 5948−5955.
(48) Lodaite, K.; Chevalier, F.; Armaforte, E.; Kelly, A. L. Effect of high-pressure homogenisation on rheological properties of rennet-induced skim milk and standardised milk gels. *J. Dairy Res.* **2009**, *76*, 294−300.
(49) Poth, A. G.; Deeth, H. C.; Alewood, P. F.; Holland, J. W. Analysis of the human casein phosphoproteome by 2-D electrophoresis and MALDI-TOF/TOF MS reveals new phosphoforms. *J. Proteome Res.* **2008**, *7*, 5017−5027.
(50) Armaforte, E.; Curran, E.; Huppertz, T.; Ryan, C. A.; Caboni, M. F.; O'Connor, P. M.; Ross, R. P.; Hirtz, C.; Sommerer, N.; Chevalier, F.; Kelly, A. L. Proteins and proteolysis in pre-term and term human milk and possible implications for infant formulae. *Int. Dairy J.* **2010**, *20*, 715−723.
(51) Cunsolo, V.; Saletti, R.; Muccilli, V.; Foti, S. Characterization of the protein profile of donkey's milk whey fraction. *J. Mass Spectrom.* **2007**, *42*, 1162−1174.
(52) Cunsolo, V.; Cairone, E.; Fontanini, D.; Criscione, A.; Muccilli, V.; Saletti, R.; Foti, S. Sequence determination of alphas1-casein isoforms from donkey by mass spectrometric methods. *J. Mass Spectrom.* **2009**, *44*, 1742−1753.
(53) Marletta, D.; Criscione, A.; Cunsolo, V.; Zuccaro, A.; Muccilli, V.; Bordonaro, S.; Guastella, A. M.; D'Urso, G. Protein fraction heterogeneity in donkey's milk analysed by proteomic methods. *Ital. J. Anim. Sci.* **2010**, *6*, 650−652.
(54) Chianese, L.; Calabrese, M. G.; Ferranti, P.; Mauriello, R.; Garro, G.; De Simone, C.; Quarto, M.; Addeo, F.; Cosenza, G.; Ramunno, L. Proteomic characterization of donkey milk "caseome". *J. Chromatogr., A* **2010**, *1217*, 4834−4840.
(55) Criscione, A.; Cunsolo, V.; Bordonaro, S.; Guastella, A. M.; Saletti, R.; Zuccaro, A.; D'Urso, G.; Marletta, D. Donkeys' milk protein fraction investigated by electrophoretic methods and mass spectrometric analysis. *Int. Dairy J.* **2009**, *19*, 190−197.
(56) Vincenzetti, S.; Amici, A.; Pucciarelli, S.; Vita, A.; Micozzi, D.; Carpi, F. M.; Polzonetti, V.; Natalini, P.; Polidori, P. A proteomic study on donkey milk. *Biochem. Anal. Biochem.* **2012**, *1*, 1−8.
(57) Girardet, J.-M.; Miclo, L.; Florent, S.; Mollé, D.; Gaillard, J.-L. Determination of the phosphorylation level and deamidation susceptibility of equine β-casein. *Proteomics* **2006**, *6*, 3707−3717.
(58) Miclo, L.; Girardet, J.-M.; Egito, A. S.; Mollé, D.; Martin, P.; Gaillard, J.-L. The primary structure of a low-Mr multiphosphorylated variant of β-casein in equine milk. *Proteomics* **2007**, *7*, 1327−1335.
(59) Vasbinder, A. J.; Rollema, H. S.; De Kruif, C. G. Impaired rennetability of heated milk; study of enzymatic hydrolysis and gelation kinetics. *J. Dairy Sci.* **2003**, *86*, 1548−1555.
(60) Chevalier, F.; Depagne, J.; Hem, S.; Chevillard, S.; Bensimon, J.; Bertrand, P.; Lebeau, J. Accumulation of cyclophilin A isoforms in conditioned medium of irradiated breast cancer cells. *Proteomics* **2012**, *12*, 1756−1766.
(61) Bradford, M. M. A rapid and sensitive method for the quantitation of microgram quantities of protein utilizing the principle of protein-dye binding. *Anal. Biochem.* **1976**, *72*, 248−254.
(62) Chevalier, F.; Centeno, D.; Rofidal, V.; Tauzin, M.; Martin, O.; Sommerer, N.; Rossignol, M. Different impact of staining procedures using visible stains and fluorescent dyes for large-scale investigation of proteomes by MALDI-TOF mass spectrometry. *J. Proteome Res.* **2006**, *5*, 512−520.
(63) Peric, D.; Labarre, J.; Chevalier, F.; Rousselet, G. Impairing the microRNA biogenesis pathway induces proteome modifications characterized by size bias and enrichment in antioxidant proteins. *Proteomics* **2012**, *12*, 2295−2302.
(64) Chevalier, F.; Rossignol, M. Proteomic analysis of Arabidopsis thaliana ecotypes with contrasted root architecture in response to phosphate deficiency. *J. Plant Physiol.* **2011**, *168*, 1885−1890.
(65) Matéos, A.; Miclo, L.; Mollé, D.; Dary, A.; Girardet, J.-M.; Gaillard, J.-L. Equine α_{S1}-casein: characterization of alternative splicing isoforms and determination of phosphorylation levels. *J. Dairy Sci.* **2009**, *92*, 3604−3615.
(66) Matéos, A.; Girardet, J.-M.; Mollé, D.; Dary, A.; Miclo, L.; Gaillard, J.-L. Two-dimensional cartography of equine β-casein variants achieved by isolation of phosphorylation isoforms and control of the deamidation phenomenon. *J. Dairy Sci.* **2009**, *92*, 2389−2399.
(67) D'Auria, E.; Agostoni, C.; Giovannini, M.; Riva, E.; Zetterström, R.; Fortin, R.; Greppi, G. F.; Bonizzi, L.; Roncada, P. Proteomic evaluation of milk from different mammalian species as a substitute for breast milk. *Acta Paediatr.* **2005**, *94*, 1708−1713.
(68) Malacarne, M.; Martuzzi, F.; Summer, A.; Mariani, P. Protein and fat composition of mare's milk: some nutritional remarks with reference to human and cow's milk. *Int. Dairy J.* **2002**, *12*, 869−877.
(69) Miranda, G.; Mahé, M.-F.; Leroux, C.; Martin, P. Proteomic tools to characterize the protein fraction of Equidae milk. *Proteomics* **2004**, *4*, 2496−2509.

(70) Yoshikawa, M.; Sasaki, R.; Chiba, H. Effects of chemical phosphorylation of bovine casein components on the properties related to casein micelle formation. *Agric. Biol. Chem.* **1981**, *45*, 909−914.
(71) Vreeman, H. J.; Both, P.; Brinkhuis, J. A.; Van der Spek, C. Purification and some physicochemical properties of bovine κ-casein. *Biochim. Biophys. Acta* **1977**, *491*, 93−103.
(72) Dziuba, J.; Minkiewicz, P. Influence of glycosylation on micelle-stabilizing ability and biological properties of C-terminal fragments of cow's κ-casein. *Int. Dairy J.* **1996**, *6*, 1017−1044.
(73) Cases, E.; Vidal, V.; Cuq, J. L. Effect of κ-casein deglycosylation on the acid coagulability of milk. *J. Food Sci.* **2003**, *68*, 2406−2410.
(74) Mulvihill, D. M. *Proteolysis of Caseins by Chymosins and Pepsins*; National University of Ireland, 1978.
(75) Foltmann, B. Gastric proteinases: structure, function, evolution and mechanism of action. In *Essays in Biochemistry*; Compbell, P. N., Marshall, R. D., Eds.; Academic Press: New York, 1981; Vol. *17*, pp 52−84.
(76) Foltmann, B.; Jensen, A. L.; Lønblad, P.; Smidt, E.; Axelsen, N. H. A developmental analysis of the production of chymosin and pepsin in pigs. *Comp. Biochem. Physiol. Part B: Comp. Biochem.* **1981**, *68*, 9−13.
(77) Wangoh, J.; Farah, Z.; Puhan, Z. Extraction of camel rennet and its comparison with calf rennet extract. *Milchwissenschaft* **1993**, *48*, 322−325.
(78) Kappeler, S. R.; Van den Brink, H. J. M.; Rahbek-Nielsen, H.; Farah, Z.; Puhan, Z.; Hansen, E. B.; Johansen, E. Characterization of recombinant camel chymosin reveals superior properties for the coagulation of bovine and camel milk. *Biochem. Biophys. Res. Commun.* **2006**, *342*, 647−654.
(79) Bela Szecsi, P.; Harboe, M. Chapter 5 − Chymosin. In *Handbook of Proteolytic Enzymes*; Academic Press: San Diego, CA, 2013; pp 37−42.

2 - Activités de Recherche au CEA

2.1 - Responsable de la plateforme de protéomique de l'iRCM

A mon départ de Fontenay-aux-Roses en juillet 2013, et après 6 années de fonctionnement, la plateforme de protéomique a été remplacée par une plateforme d'ingénierie des protéines, axée sur le clonage et l'expression de protéines recombinantes, gérée maintenant par Didier Busso (IR INSERM).

De 2007 à 2013, en tant que responsable titulaire de la plateforme de protéomique du CEA de Fontenay-aux-Roses, j'ai participé à de nombreux projets de recherche parfois comme expert technique ou comme principal intervenant. Pendant cette période, la plateforme de protéomique de l'iRCM a partagé une expertise en biochimie des protéines et en analyse protéomique pour répondre à des questions fondamentales en radiobiologie. L'équipe de la plate-forme protéomique a développé une expertise spécifique pour interpréter et valider les données protéomiques à l'aide de logiciels bio-analytiques spécialisés, tels que le logiciel ProGenesis Samespot.
Depuis la création de la plateforme, 16 projets de laboratoires de l'iRCM ont été réalisés avec différents modèles biologiques (lignées cellulaires de mammifères, de levures, des tissus, des cellules souches) et en utilisant un large choix d'expériences telles que l'extraction des protéines et la quantification, l'immuno-purification, l'électrophorèse bidimensionnelle et western blot.

Les chapitres qui suivent reviennent sur certains développements technologiques en électrophorèse bidimensionnelle (A1), ainsi que sur des projets réalisés en collaboration avec deux laboratoires de l'iRCM (A2 et A3) qui ont donné lieu à des publications scientifiques.

2.1.1 - Développement technologique en analyse protéomique

Les méthodes protéomiques permettent l'analyse et la comparaison de toutes les protéines présentes dans un échantillon biologique choisi. Notre technologie largement basée sur l'électrophorèse bidimensionnelle permet une quantification précise de l'expression des protéines et modifications post-traductionnelles, avec le soutien de plateformes externes de spectrométrie de masse pour l'identification des protéines.

Une attention toute particulière a été portée sur la mise au point de conditions expérimentales convenables pour la séparation des protéines aux caractéristiques biochimiques extrêmes, et plus particulièrement aux protéines basiques, réputées difficiles à focaliser par électrophorèse bidimensionnelle.

Dans cette étude, trois protocoles différents ont été comparés en utilisant des extraits de protéines issues de cellules MCF7 (lignée cellulaire issue d'un cancer du sein). Le protocole classique de réhydration « in gel » des protéines a été comparé aux protocoles de chargement des protéines par « cup loading » ou par « paper-bridge loading » sur des strips de focalisation dans une gamme de pI de 6-11.
Comme cela était attendu, le protocole de réhydration « in gel » des protéines a présenté de larges trainées horizontales alors que le protocole « paper-bridge loading » a permis une bonne focalisation des protéines, mais avec une certaine perte de matériel.
Plusieurs conditions expérimentales ont été comparées afin d'optimiser la focalisation par « cup loading » et la meilleure séparation a été observée avec des mèches cathodiques complétées avec la solution de réhydratation et du DTT.
Le protocole « paper-bridge loading » a finalement été analysé en utilisant des échantillons non-limitant en protéines, telles que les protéines de lait de vache. Dans ce cas, une bonne focalisation a été obtenue, permettant la visualisation de spots uniques jusque-là non séparés.

2.1.2 - Analyse protéomique de la voie des micro-ARNs dans la cancérogénèse

Cette étude a été réalisée en associant trois équipes scientifiquement et techniquement complémentaires : Germain Rousselet (Laboratoire de Génétique de la Radiosensibilité, CEA iRCM), Jean Labarre (Laboratoire de Biologie Intégrative, CEA iBiTecs) et la plateforme de protéomique (CEA iRCM).

Cette étude visait à mieux comprendre comment la perturbation de micro-ARNs individuels joue un rôle dans la cancérogenèse.
Dans certaines cellules cancéreuses, l'inhibition globale de la voie de biogenèse des micro-ARNs (CoGAM : colony growth arrest induced by microprocessor inhibition) conduit à un arrêt de croissance qui peut être restaurée par la réexpression de certains micro-ARNs individuels tels que miR-20a.
En utilisant une stratégie expérimentale d'analyse globale du protéome cellulaire par gels 2D, nous avons observé que l'inhibition de la voie de biogenèse des micro-ARNs induit de multiples changements du profil protéique. En effet, la modification du protéome est caractérisée par une modification de la taille des protéines exprimées, avec l'induction de protéines de faible poids moléculaire et une réduction de l'expression de protéines de haut poids moléculaire.
Cette polarisation de la taille a été observée dans les cellules avec CoGAM, dans des cellules CoGAM résistantes et dans les cellules sensibles à CoGAM secourues par miR-20a. Dans ce cas, l'analyse des protéines identifiées par spectrométrie de masse a révélé un enrichissement significatif en protéines impliquées dans la résistance au stress oxydatif. En outre, un traitement par H_2O_2 chez *Saccharomyces cerevisiae* ou dans des cellules de mammifères conduit aussi à une modification du protéome de même ordre. Nos résultats ont montré le rôle de la taille des protéines comme une lecture pertinente de modifications du protéome, en particulier dans des conditions de stress telles que l'inhibition de la voie de la biogenèse des micro-ARNs ou le stress oxydatif.

2.1.3 - Analyse protéomique d'un effet bystander radio-induit

Les protéines sécrétées jouent un rôle clé dans la signalisation et la communication intercellulaire radio-induite. Les facteurs sécrétés peuvent alors induire une réponse cellulaire proche d'un effet direct radio-induit, on parle alors d'effet bystander.

En utilisant un modèle *in vitro* de cellules mammaires, l'objectif de notre travail était d'identifier les facteurs diffusibles, sécrétés après irradiation gamma et potentiellement impliqués dans la signalisation intercellulaire.

L'analyse protéomique différentielle des milieux conditionnés a été effectuée en utilisant l'électrophorèse bidimensionnelle. Cette analyse a entraîné la détection de nombreux spots modulés de manière significative suivant l'irradiation des cellules. Les protéines correspondantes ont été identifiées par des approches de type MALDI-TOF MS et LC-MS / MS.
Après analyse des résultats, il est intéressant de noter que cinq isoformes de cyclophiline A ont été sécrétées spécifiquement dans le milieu conditionné de cellules irradiées. Cette observation a été confirmée par Western blotting. Ces isoformes diffèrent principalement de par leur point isoélectrique grâce à des modifications post-traductionnelles, comprenant la suppression partielle de la méthionine N-terminale, associée à une combinaison d'acétylation et de méthylation.
Le rôle de la protéine est discuté en relation avec son implication potentielle dans les mécanismes de communications intercellulaires et d'effet bystander.

2.1.4 - Sélection de publications

Dépagne J., Chevalier F.
Technical updates to basic proteins focalization using IPG strips (2012) Proteome Science 10:54 (6 September 2012)

Peric D., Labarre J., Chevalier F., and Rousselet G.
Impairing the micro-RNA pathway induces proteome modifications characterized by size bias and enrichment in anti-oxidant proteins. (2012) Proteomics, 12(13): 2295–2302.

Chevalier F., Depagne J., Hem S., Chevillard S., Bensimon J., Bertrand P., and Lebeau J.
Accumulation of Cyclophilin A isoforms in conditioned medium of irradiated breast cancer cells (2012) Proteomics, 12(11): 1756–1766.

PROTEOME SCIENCE

METHODOLOGY Open Access

Technical updates to basic proteins focalization using IPG strips

Jordane Dépagne and François Chevalier*

Abstract

Background: Gel-based proteomic is a popular and versatile method of global protein separation and quantification. However, separation of basic protein still represents technical challenges with recurrent problems of resolution and reproducibility.

Results: Three different protocols of protein loading were compared using MCF7 cells proteins. In-gel rehydration, cup-loading and paper-bridge loading were first compared using 6–11 IPG strips, as attempted, in-gel rehydration gave large horizontal steaking; paper-bridge loading displayed an interesting spot resolution, but with a predominant loss of material; cup-loading was selected as the most relevant method, but still needing improvement. Twelve cup-loading protocols were compared with various strip rehydration, and cathodic wick solutions. Destreak appeared as better than DTT for strip rehydration; the use of isopropanol gave no improvement. The best 2DE separation was observed with cathodic wicks filled with rehydration solution complemented with DTT. Paper-bridge loading was finally analyzed using non-limited samples, such as bovine milk. In this case, new spots of basic milk proteins were observed, with or without paper wicks.

Conclusion: According to this technical study of basic protein focalization with IPG strips, the cup-loading protocol clearly displayed the best resolution and reproducibility: strips were first rehydrated with standard solution, then proteins were cup-loaded with destreak reagent, and focalisation was performed with cathodic wicks filled with rehydration solution and DTT. Paper-bridge loading could be as well used, but preferentially with non-limited samples.

Keywords: Two-dimensional electrophoresis, Proteomic methods, Isoelectric focusing, IPG, Cup-loading, Paper bridge loading, Basic proteins

Background

Two-dimensional electrophoresis is until now one of the most widely used technique for performing functional proteomics [1]. Indeed, it has the capacity to separate, visualize and quantify several thousands of proteins in a single gel from a complex biological sample, allowing the large-scale analysis of protein expression differences. Gel-to-gel variability has been largely improved thanks to the use of IPG strips and robust gel staining protocols [2,3].

But even now, IEF in the alkaline region is considered as a challenge to separate basic proteins by 2-DE and most of gel-based proteomic studies were performed in the acidic range. Basic proteins are difficult to separate in the first dimension for several reasons. At pH above 8, polymerized acrylamide gel is unstable, and can degrade. So it is very important to use only fresh strips stored at a correct temperature. A degradation of acrylamide can be visualized when the plastic part of the dry strip glues to the acrylamide gel part, with a tendency to twist.

At basic pH, it is mandatory to keep the redox status for cysteines using reducing agent such as DTT [4]. But a problem concerns the migration of DTT towards the anode during IEF at basic pH. This results in depletion of DTT at the cathode and leads to reformation of intra- and inter-molecular disulphide bridges due to the oxidation of sulphydryl groups. DTT is a weak acid and hence it is transported out of the basic part of the IPG strip during focusing, resulting in horizontal streaking [5]. This can cause proteins within the sample to become less soluble, leading to horizontal streaking within the

* Correspondence: francois.chevalier@cea.fr
Proteomic Laboratory, iRCM / DSV / CEA, Fontenay aux Roses, France

gels and thus poor resolution of the basic proteins. Different sample application methods were alternatively proposed to overcome these problems, such as anodic cup-loading, in-gel rehydration, or paper-bridge loading. The addition at the cathodic electrode of a paper wick soaked with DTT was as well proposed to replenish IPG strip with new DTT during focalisation. The use of destreak reagent was proposed to replace DTT to limit unspecific oxidation of protein thiol groups, a combination of isopropanol and glycerol in rehydratation buffer was reported to improve the focusing of proteins in the alkaline IPG strips [6,7]. The paper-bridge loading protocol allowed an improvement of resolution for preparative loading of cardiac mitochondrial samples in the 6–11 pI range [8].

Finally, electroendosmotic flow was reported to occur at high pH values, leading to a basic gap characterized by a zone of streaking and poorly focused proteins close to the cathode. The presence of hydroxide ions in the IPG-strip causes electro-osmotic pumping from the cathode towards the anode with the result that water present in the cathodic paper wick is pumped into the IPG-strip. The authors reported that the gap can therefore be avoided by the use of solutions containing urea in the cathodic electrode wick and DTT should be avoided in the wick as the transport of these components into the IPG-strip will intensify the electro-osmotic transport from the paper wick [9].

In the present article, we first evaluated the separation capacities of three conventional protein loading methods using basic IPG strips. Different conditions and samples were then compared to optimize the cup-loading and the paper-bridge loading protocols.

Results and discussion

Evaluation of methods for protein loading

To analyse the capacity of IPG strips to separate protein, we first compare three protocols of protein loading, with 50 μg proteins (Figure 1). Almost the same buffer conditions were used to investigate the efficiency of each protocols, the same protein sample and the same protein amount were used, *ie*, 50 μg of MCF7 total extract in TUC solution (7 M urea / 2 M thiourea / 4% CHAPS).

In case of protein loading during strip rehydration (Figure 1A), proteins were mixed with RB (7 M urea, 2 M thiourea, 4% CHAPS, 0.05% triton X100, 5% glycerol) complemented with 1.2% destreak reagent and 0.5% IPG buffer 6–11. Large horizontal smears were observed with most of abundant proteins spots, showing a weak focalisation capacity. This observation was in agreement with previous studies, indeed, protein loading during strip rehydration wasn't recommended in case of basic IPG strip [5].

In case of protein loading with the cup loading protocol (Figure 1B), strips were rehydrated with RB complemented with 1.2% destreak reagent and 0.5% IPG buffer 6–11. Protein sample was applied after strip rehydration using a plastic cup. Electrode wicks were soaked with 50 μL of water. Lots of spots appeared as well focalized but some horizontal smears were still observed with the most abundant proteins spots.

In case of protein loading with the paper-bridge loading protocol (Figure 1C), strips were rehydrated with the same buffer conditions as the cup loading protocol. Protein sample was applied after strip rehydration onto the anodic electrode wicks, the cathodic electrode wicks was soaked with 50 μL of water. Very

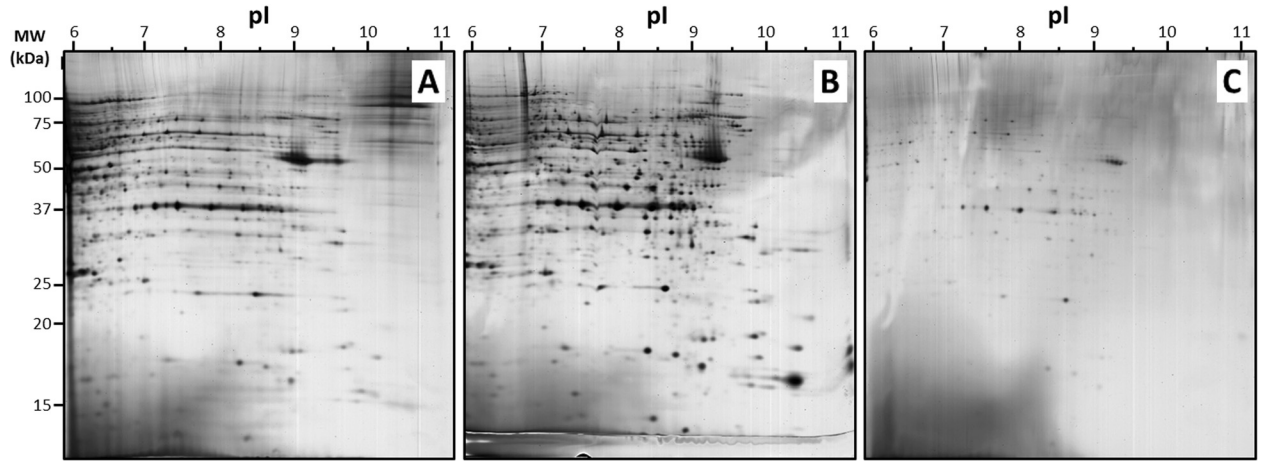

Figure 1 2DE separation of MCF7 basic protein: iso-electric focalisation was performed with 50 μg proteins using 6–11 pH IPG strip and 12% acrylamide was used for the second dimension. Proteins were loaded by in-gel rehydration (**A**), anodic cup loading (**B**), and paper-bridge loading (**C**).

few "well-focalized" spots can be distinguished with this last condition. It appeared clearly that almost 90% of proteins were lost.

We decided to focus our interest on the cup loading protocol as it is the most widely used protocol for basic proteins, and as it appeared to be the most efficient loading protocol in our conditions.

Tests of various buffer conditions with the cup loading protocol

For cup-loading, IPG dry strips are first rehydrated with rehydration buffer containing at least urea, nonionic and / or zwitterionic detergents, a reducing agent and small amounts of carrier ampholytes [5]. Since several decades, protocol developments were proposed to improve basic protein solubilisation and focalisation. DTT was replaced by destreak agent [9], glycerol and isopropanol were included in rehydration buffer [6], but sometimes with contrasted observations, leading to interpretations problems and confusions. Indeed, protein focalisation using IPG strips involved a range of specific and useful chemicals, which interaction could produce unpredictable troubles.

An experimental plan was generated to examine DTT, destreak reagent and isopropanol interactions within strip rehydration and the replacement of water by urea with or without DTT onto cathodic wicks (Figure 2). Twelve experimental conditions (methods) were performed and the 2DE maps were compared. An accurate and regular image analysis using the Samespots software appeared quite difficult since many spot groups presented modified focalisation pattern.

Three evident observations could be depicted even without a complete computer assisted analysis: *(i)* firstly, although most of spots were unmodified and reproducible between samples in the left part of pictures (pI 6 to 8.5), major differences were observed in the right / bottom part of 2DE gel pictures; *(ii)* secondly, the use of isopropanol during strip rehydration gave no modification or improvement of spots pattern; *(iii)* finally, spot

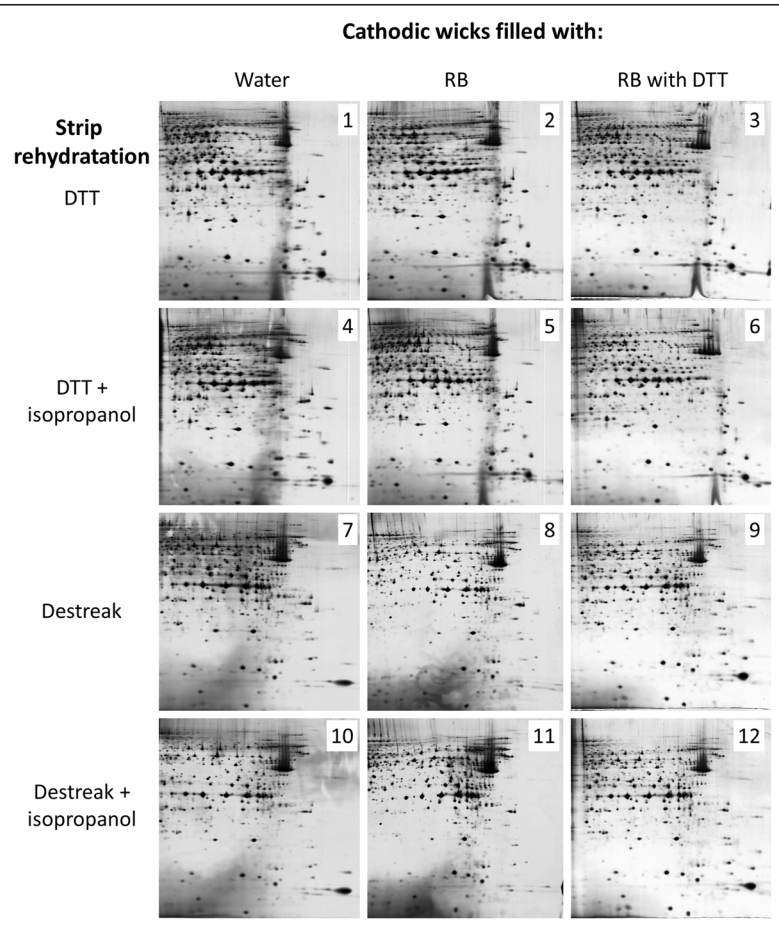

Figure 2 Comparison of MCF7 basic protein 2DE separation using twelve different anodic cup-loading protocols. Iso-electric focalisation was performed with 50 µg proteins using 6–11 pH IPG strip and 12% acrylamide was used for the second dimension. The number reported on each picture corresponded to the cup-loading condition used, as presented in detail in Table 1.

focalisation was improved when cathodic wicks were filled with RB plus DTT instead of RB without DTT, especially in case of strip rehydration with destreak reagent.

As shown in Figure 3, areas A and B (in the right/bottom part of the 2D gel) corresponded to the 2DE regions of particular interest to evaluate the efficiency of protein spot separation. These specific gel areas were further analysed in detail, using the most different spot patterns. Indeed, from the twelve initial conditions, four were selected and further analysed in detail according to these specific areas (Figure 4 and Table 1): cathodic wicks filled with water or with basic solution complemented with DTT; and strip rehydration using DTT or destreak.

In case of strip rehydration with DTT, the use of cathodic wicks filled with RB plus DTT (method 3) instead of water (method 1) allowed a clearer background but without improvement of spot focalisation (Figure 4). In case of cathodic wicks filled with water, the use of desteak reagent (method 7) instead of DTT (method 1) during strip rehydration allowed a better focalisation, but with a decrease in some spot intensity. It appeared that a lot of spots were common between methods 1 and 9, with a higher number of spots in case of method 1, but with a better spot repeatability and an enhanced overall image quality in case of method 9 (Table 1). The use of destreak reagent for strip rehydration, combined with cathodic wicks filled with RB plus DTT (method 9) appeared as the best compromise to give an acceptable reproducibility and the best focalisation efficiency and overall image quality using the cup-loading protocol.

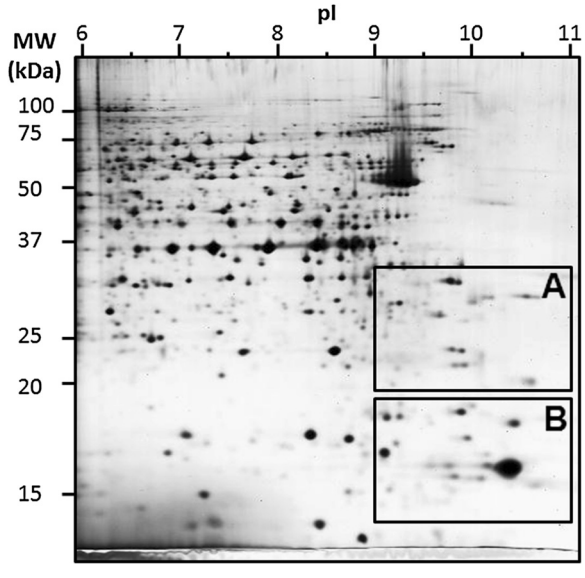

Figure 3 2DE map of MCF7 basic protein separation using anodic cup-loading protocol n°9, as presented in Figure 2 and Table 1. Specific areas **A** and **B** were further analysed.

Paper-bridge loading protocol investigation

Although the paper-bridge loading protocol resulted in a massive loss of protein, this protocol could be useful in case of study of non-limiting protein samples. Actually, it offers a good separation of proteins with few horizontal smears [8]. We decided to work with bovine milk proteins, a largely available source of proteins, and with major nutritional interests [10,11]. These proteins were studied many times using two-dimensional electrophoresis and proteomic tools to reveal a large complexity in term of post-translational modifications and protein relationship [12-14]. Most of bovine milk proteins were focused in the 4–7 pH range, such as caseins (alpha S1, alpha S2, beta and kappa), beta-lactoglobulin and alpha-lactalbumin [15-17]. A paper-bridge strategy to load milk protein in the basic range could be a way to deplete the sample of the most abundant proteins, showing specifically and with a higher resolution basic proteic component.

A conventional protein separation was first performed with protein loading during strip rehydration using a 3–10 pH range (Figure 5A). As attempt, and according to previous results, the major milk proteins were observed in the left part of the gel, with only few proteins in the right part.

The paper-bridge loading protocol was test in a first time with paper wicks placed at both electrodes, and with an anodic application of the milk sample (Figure 6A). Protein sample was loaded from wick into the strip during 16 hours at 200 V according to [8]; anodic wick was then removed and replaced with a paper wick soaked with water. Proteins were then focused until 60 KVh-1. Paper wick with remaining protein was kept and re-used to run a 4–7 pH range strip with the same protocol. In a 6–11 pH range, only few proteins were observed (Figure 5C), with a dark background at the bottom of the 2D gel. Nevertheless, this strategy allowed the separation of the abundant milk proteins in the 4–7 pH range (Figure 5B).

To improve protein focalisation following paper-bridge loading, we tried to remove paper wick bonds between strip and electrode during protein focalisation [8]. With this strategy (Figure 5D), the intensity of some spots around 30 kDa decreased slightly, but a lot of new spots appeared after pH9, and a clear background was observed at the bottom of the gel. These new spots were in fact present as well in the 3–10 pH range performed in a first time with protein loading during strip rehydration (Figure 5A), but with such large pH range, spots were less separated and were certainly superposed.

Conclusion

As attempted, basic protein focalization with IPG strips was a challenge, giving contrasted and surprising results

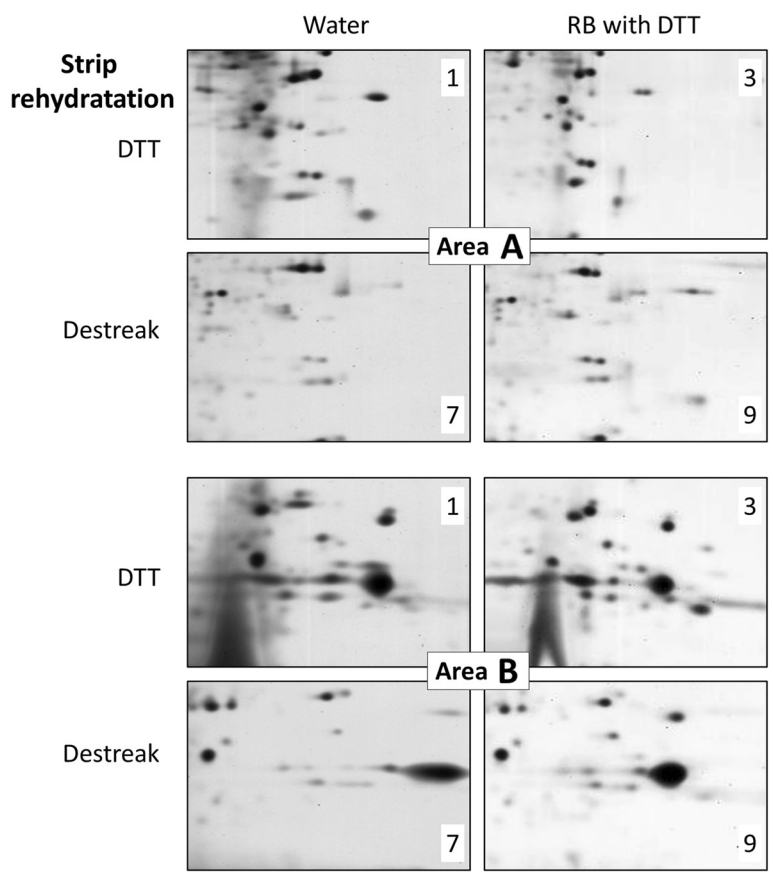

Figure 4 Picture comparison of areas A and B from Figure 3 as a function of different anodic cup-loading protocols. The number of spots within each area was estimated by picture analysis and reported in Table 1.

as a function of the protocol strategy used. After the exclusion of the in-gel loading protocol which is definitively inappropriate for basic pH range, the cup-loading protocol clearly displayed the best resolution and reproducibility when the proteins were rehydrated with destreak reagent, and the focalisation was performed with cathodic wicks filled with rehydration solution coupled with DTT. Paper-bridge loading could be as well used, but preferentially with non-limited samples owing to the loss of protein during active rehydration of IPG strips.

Methods

Chemicals

TRIS base, urea, thiourea, CHAPS, iodoacetamide, TEMED, low-melt agarose, Triton X-100, spermine, phosphatase inhibitor cocktail and bromophenol blue were obtained from Sigma-Aldrich (St. Louis, MO, USA); protease inhibitor cocktail (Complete Mini EDTA-free) was from Roche Diagnostics (Mannheim, Germany); IPG buffers, IPG strips (pH 6–9 and 6–11) and destreak reagent were purchased from GE (GE Healthcare); acrylamide was obtained from Bio-Rad (Hercules, CA); SDS, glycerol, DTT and TGS 10X were from Eudomedex (Mundolshein, France); all other reagents were of analytical grade.

Protein extraction and solubilisation

Proteins were extracted from MCF7 cells as previously described [18] in sample buffer containing 7 M urea, 2 M thiourea, 4% CHAPS, 0.05% Triton X100, 65 mM DTT, 40 mM spermine, protease and phosphatase inhibitor cocktails. This suspension was centrifuged at 68000 rpm for 60 min, supernatants were collected and the protein content was estimated using the Bradford method [19].

Proteins were then precipitated using the 2D clean-up kit (GE Healthcare) and the pellet was solubilized with TUC solution (7 M urea, 2 M thiourea, 4% CHAPS) and quantified with the 2D quant kit (GE Healthcare).

Table 1 Methods tested for basic proteins focalization with the corresponding number of spots in area A and B (Figure 3) and an estimation of each focalization efficiency and overall image quality

Method	Strip rehydration	Cathodic wicks	Spots area A	Spots area B	Focalisation efficiency	Overall image quality
1	160 mM DTT	50 µl water	82 +/− 9,9	79 +/− 14,1	+/−	−
2	160 mM DTT	50 µl RB	73 +/− 7,1	76,5 +/− 3,5	-	-
3	160 mM DTT	50 µl RB 160 mM DTT	67 +/− 4,2	78 +/− 4,2	+/−	+/−
4	160 mM DTT 10% isopropanol	50 µl water	82 +/−8,5	76,5 +/− 4,9	+/−	−
5	160 mM DTT 10% isopropanol	50 µl RB	60 +/− 11,3	70,5 +/− 9,2	-	-
6	160 mM DTT 10% isopropanol	50 µl RB 160 mM DTT	67,5 +/− 9,2	80,5 +/− 0,7	+/−	+/−
7	1,2% destreak reagent	50 µl water	58 +/− 1,4	61,5 +/− 4,9	+/−	+/−
8	1,2% destreak reagent	50 µl RB	40 +/− 24	67 +/− 17	+	-
9	1,2% destreak reagent	50 µl RB 160 mM DTT	71,5 +/− 0,7	72,5 +/− 3,5	++	++
10	1,2% destreak reagent 10% isopropanol	50 µl water	35 +/− 1,4	65,5 +/− 4,9	+/−	+/−
11	1,2% destreak reagent 10% isopropanol	50 µl RB	36,5 +/− 3,5	59 +/− 5,7	+	-
12	1,2% destreak reagent 10% isopropanol	50 µl RB 160 mM DTT	72 +/− 1,4	74 +/− 7,1	++	++

Strip rehydration with protein samples: "sample in-gel rehydration"

Protein sample (50 µg) was mixed with rehydration buffer (RB): 7 M urea, 2 M thiourea, 4% CHAPS, 0.05% triton X100, 5% glycerol complemented with 1.2% destreak reagent, 0.5% ampholytes (IPG buffer 6–11 GE) and adjusted to the correct volume to rehydrate 18 cm strip (here, 320 µl). Strips were then placed acrylamide face down (Figure 6A) in the focusing tray equipped with platinum electrode embedded into the running tray (Protean IEF, Bio-Rad) and passively rehydrated at 20°C without electricity for 16 hours, and then actively rehydrated at 50 V during 9 hours. During protein focalisation, small electrode wicks were placed between acrylamide and electrode. These paper wicks (Ref 1654071, Electrode wicks, Bio-Rad) were in advance soaked with water in order to absorb salts and other contaminant species during active rehydration. The IPG strips were then focused according to the following program: 500 V for 1 h, a linear ramp to 1000 V for 1 h, a linear ramp to 10000 V for 33 KV^{-1} h, and finally 10000 V for 24 KV^{-1} h.

Cup loading of protein samples

Strips were first rehydrated without proteins using 320 µl of RB with 0.5% IPG buffer 6–11), with 160 mM DTT, or 1.2% destreak reagent and/or 10% iso-propanol at 20° for 16 hours. Following this passive rehydration, strips were removed from the rehydration tray, drained from excess of mineral oil and positioned with the acrylamide face on top, gel side up (Figure 6B) in a "cup loading tray" (Protean IEF, Bio-Rad). Plastic cup were placed at the surface of the acrylamide part, 10 mm away from the anodic end and filled with proteins sample. A paper wick (30 x 4 mm, cut from Blot paper TE70, ref TE76, GE), soaked with 50 µL of water was placed at the anodic extremity and a paper wick soaked with 50 µL of solution (water, rehydration buffer with or without 160 mM DTT) to create a bridge between the acrylamide of strip and the movable electrode (Bio-Rad). The IPG strips were then focused according to the following program: active rehydration at 50 V for 9 hours, then, 500 V for 1 h, a linear ramp to 1000 V for 1 h, a linear ramp to 10000 V for 33 KV^{-1} h, and finally 10000 V for 24 KV^{-1} h.

Paper-bridge loading of protein samples

Another possibility consisted to use the "cup loading protocol" described earlier, but instead of using a cup to load proteins, proteins were loaded using the anodic paper wick as described by Kane et al. [8], with some adaptations. In this case, strips were first rehydrated using 320 µl of RB with 1.2% destreak reagent and 0.5% IPG buffer 6–11 at 20° for 16 hours. Following this

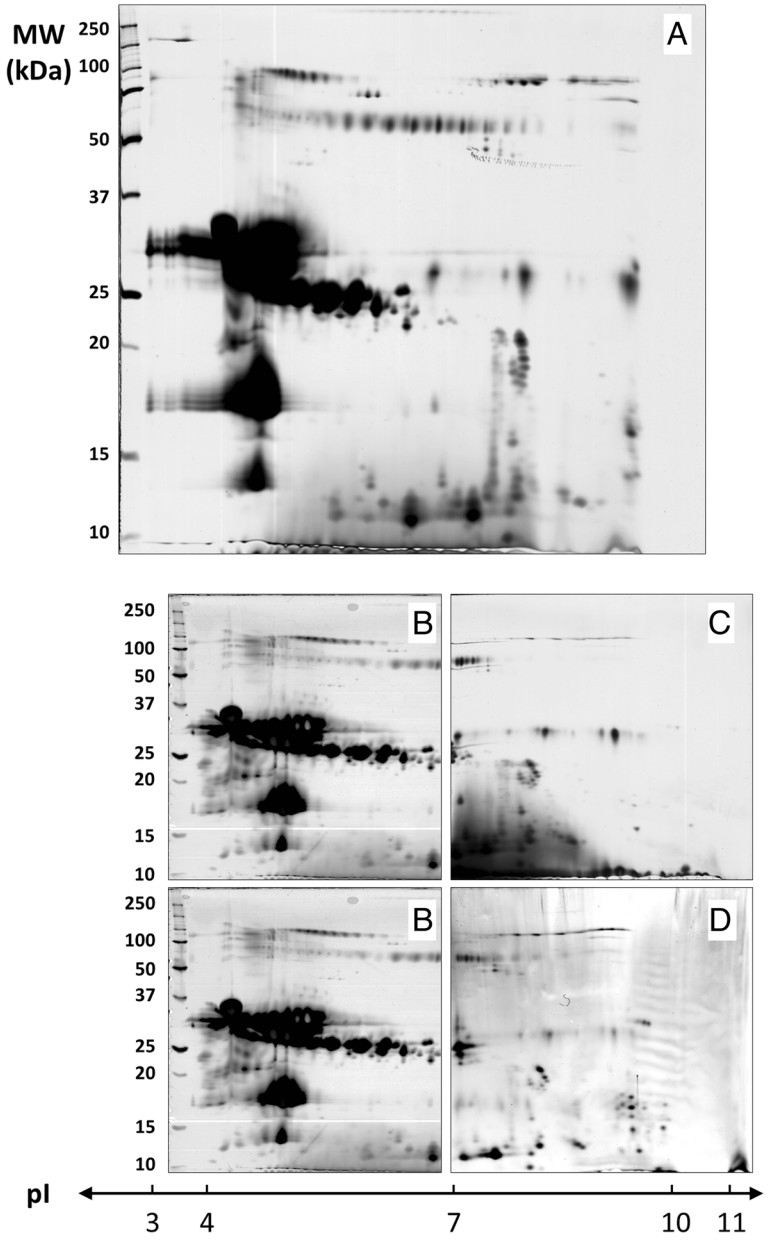

Figure 5 2DE map comparison and alignment of bovine milk proteins using in-gel rehydration or paper-bridge loading. 600 µg of non-fat dry milk proteins were in-gel loaded using 3–10 IPG strips (**A**) or paper-bridge loaded using 6–11 IPG strips with (**C**) or without electrode wicks (**D**) during focalization. In a second time, paper-bridge previously used with 6–11 IPG strip was applied with 4–7 IPG strips (**B**) to focalize remaining proteins.

passive rehydration, strips were removed from the rehydration tray, drained from excess of mineral oil and positioned with the acrylamide face on top, gel side up (Figure 6B) in a "cup loading tray" (Protean IEF, Bio-Rad). A paper wick (30 x 4 mm, cut from Blot paper TE70, ref TE76, GE), was placed at each extremity to create a bridge between the acrylamide of strip and the movable electrode (Bio-Rad). Protein sample (adjusted to 50 µl with rehydration buffer) was applied onto the anodic paper wick and 50 µL of rehydration buffer with 160 mM DTT was applied onto the cathodic paper wick. The IPG strips were then focused according to the following program: 200 V for 16 hours, 500 V for 1 h, a linear ramp to 1000 V for 1 h, a linear ramp to 10000 V for 33 KV^{-1} h, and finally 10000 V for 24 KV^{-1} h.

IPG strips equilibration and second dimension

The strips were incubated two times 10 min in the first equilibration solution (50 mM Tris–HCl pH 8.8, 6 M urea, 30% (v/v) glycerol, 2% (w/v) SDS) with 130 mM DTT and

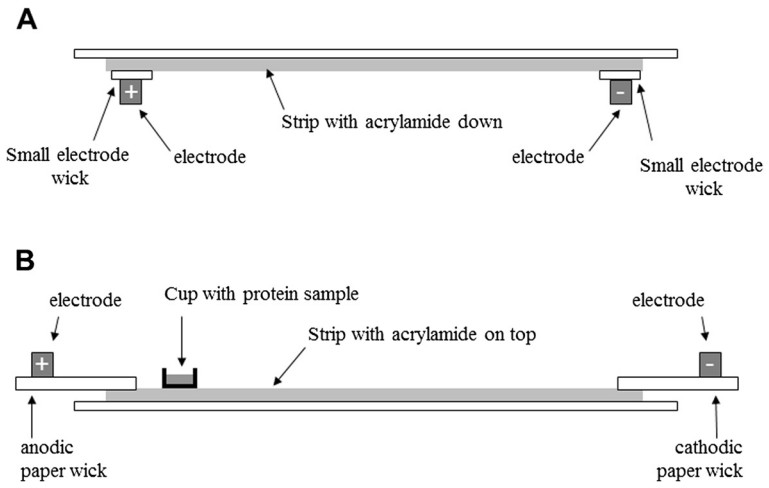

Figure 6 Schematic of IPG strip, electrodes and paper wicks positions as function of protein loading protocols. A: sample in-gel rehydration of IPG strip, with acrylamide face down. **B**: cup-loading of protein sample, with acrylamide face up, a plastic sample cup was placed at the anodic end, paper wicks connected strip with electrodes.

then two times 10 min in the second equilibration solution (50 mM Tris–HCl pH 8.8, 6 M urea, 30% (v/v) glycerol, 2% (w/v) SDS) with 130 mM iodoacetamide.

As described in Figure 7, strips were then embedded using 1% (w/v) low-melt agarose on the top of the acrylamide gel and trapped using plastic blockers. These curved plastic pieces allowed a perfect alignment of the strip with the acrylamide gel, and prevented any displacement before agarose reticulation. A molecular weight marker was prepared with 5 µl of unstained precision plus protein standards (Bio-Rad) on a paper wicks (Ref 1654071, Electrode wicks, Bio-Rad), sealed with a drop of 1% (w/v) low-melt agarose and inserted in the left part of the assembly (Figure 7). SDS-PAGE was carried out on a 12% acrylamide gel (size 20 x 20 cm and 1 mm thickness), using the Dodeca Cell electrophoresis unit (Bio-Rad) at 85 constant voltage, overnight, at 10°C.

Gel staining and picture acquisition

Gels were stained with silver nitrate as previously described [20,21], with some modifications. Briefly, gels were first fixed at least 1 hour with 30% ethanol and 5% acetic acid; washed 3 times 10 min with water; sensibilized 1 min with 0.02% sodium thiosulfate; washed 2 min with water; stained 30 min with 0.2% silver nitrate and 0.011% formaldehyde; washed 10 s with water; developed

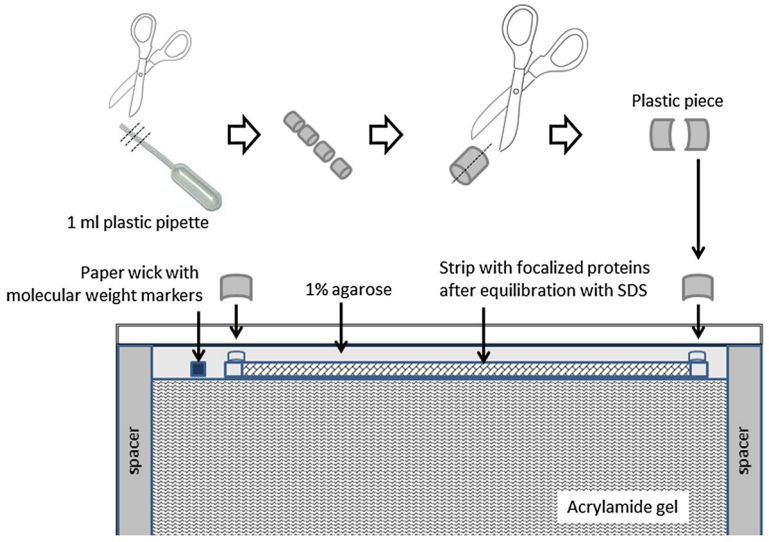

Figure 7 Schematic of IPG strip placement before the second dimension. A special precaution is presented to seal strips with 1% agarose and curved plastic pieces.

5 min with 85 mM sodium carbonate, 0.00125% sodium thiosulfate and 0.011% formaldehyde; stopped with 0.33 M TRIS and 1.7% acetic acid; stored with 5% acetic acid with 2% DMSO.

Gels were scanned to images right after staining to limit polychromatic colour of spots. Images were acquired with a GS 800 densitometer (Bio-Rad). After several hours in storage solution, gels were dried between sheets of cellophane, using the GelAir drying system (Bio-Rad).

Image analysis

Images from stained gels were analysed using the Samespots software v4.5 (Non-linear Dynamics, UK). Gel were grouped to create an global analysis with all conditions. Spots of each samples were compared between conditions, and spots were numbered with the same detection parameters.

Abbreviations

RB: Rehydration buffer; TUC: Thiourea Urea CHAPS.

Competing interests

The authors declare that they have no competing interests.

Authors' contributions

JD and FC performed the experiments. FC designed the experiments and wrote the manuscript. Both authors read and approved the final manuscript.

Acknowledgements

This work was supported by the Institute of Cellular and Molecular Radiobiology (iRCM, DSV, CEA, Fontenay aux Roses).

Received: 12 July 2012 Accepted: 21 August 2012
Published: 6 September 2012

References

1. Van den Bergh G, Arckens L: **High Resolution Protein Display by Two-Dimensional Electrophoresis.** *Curr Anal Chem* 2009, **5:**106–115.
2. Chevalier F: **Highlights on the capacities of "Gel-based" proteomics.** *Proteome Science* 2010, **8:**23.
3. Rabilloud T, Lelong C: **Two-dimensional gel electrophoresis in proteomics: A tutorial.** *J Proteomics* 2011, **74:**1829–1841.
4. Luche S, Diemer H, Tastet C, Chevallet M, Van Dorsselaer A, Leize-Wagner E, Rabilloud T: **About thiol derivatization and resolution of basic proteins in two-dimensional electrophoresis.** *Proteomics* 2004, **4:**551–561.
5. Görg A, Drews O, Lück C, Weiland F, Weiss W: **2-DE with IPGs.** *Electrophoresis* 2009, **30:**S122–S132.
6. Hoving S, Gerrits B, Voshol H, Müller D, Roberts RC, van Oostrum J: **Preparative two-dimensional gel electrophoresis at alkaline pH using narrow range immobilized pH gradients.** *Proteomics* 2002, **2:**127–134.
7. Olsson I, Larsson K, Palmgren R, Bjellqvist B: **Organic disulfides as a means to generate streak-free two-dimensional maps with narrow range basic immobilized pH gradient strips as first dimension.** *Proteomics* 2002, **2:**1630–1632.
8. Kask L, Larsson K, Bjellqvist B: **Elimination of basic gaps at high pH values in 2-DE.** *Proteomics* 2009, **9:**5558–5561.
9. Kane LA, Yung CK, Agnetti G, Neverova I, Van Eyk JE: **Optimization of paper bridge loading for 2-DE analysis in the basic pH region: application to the mitochondrial subproteome.** *Proteomics* 2006, **6**:5683–5687.
10. Chevalier F: **Analytical Methods | Electrophoresis**. In *Encyclopedia of Dairy Sciences*. San Diego: Academic; 2011:185–192.
11. Fox PF, McSweeney PL: **Milk proteins.** In *Dairy Chemistry and Biochemistry*. London: BA; 1998:150–169.
12. Poth AG, Deeth HC, Alewood PF, Holland JW: **Analysis of the Human Casein Phosphoproteome by 2-D Electrophoresis and MALDI-TOF/TOF MS Reveals New Phosphoforms.** *J Proteome Res* 2008, **7:**5017–5027.
13. Holland JW, Deeth HC, Alewood PF: **Analysis of disulphide linkages in bovine kappa-casein oligomers using two-dimensional electrophoresis.** *Electrophoresis* 2008, **29:**2402–2410.
14. Chevalier F, Chobert JM, Dalgalarrondo M, Haertle T: **Characterization of the Maillard reaction products of beta-lactoglobulin glucosylated in mild conditions.** *J Food Biochem* 2001, **25:**33–55.
15. Chevalier F, Hirtz C, Sommerer N, Kelly AL: **Use of Reducing/Nonreducing Two-Dimensional Electrophoresis for the Study of Disulfide-Mediated Interactions between Proteins in Raw and Heated Bovine Milk.** *J Agric Food Chem* 2009, **57:**5948–5955.
16. Chevalier F, Kelly AL: **Proteomic Quantification of Disulfide-Linked Polymers in Raw and Heated Bovine Milk.** *J Agric Food Chem* 2010, **58:**7437–7444.
17. Chevalier F: **Milk Proteins | Proteomics**. In *Encyclopedia of Dairy Sciences*. San Diego: Academic; 2011:843–847.
18. Chevalier F, Depagne J, Hem S, Chevillard S, Bensimon J, Bertrand P, Lebeau J: **Accumulation of Cyclophilin A isoforms in conditioned medium of irradiated breast cancer cells.** *Proteomics* 2012, **12:**1756–1766.
19. Bradford MM: **A rapid and sensitive method for the quantitation of microgram quantities of protein utilizing the principle of protein-dye binding.** *Anal Biochem* 1976, **72:**248–254.
20. Chevalier F, Rofidal V, Vanova P, Bergoin A, Rossignol M: **Proteomic capacity of recent fluorescent dyes for protein staining.** *Phytochemistry* 2004, **65:**1499–1506.
21. Chevalier F, Centeno D, Rofidal V, Tauzin M, Martin O, Sommerer N, Rossignol M: **Different impact of staining procedures using visible stains and fluorescent dyes for large-scale investigation of proteomes by MALDI-TOF mass spectrometry.** *J Proteome Res* 2006, **5:**512–520.

doi:10.1186/1477-5956-10-54
Cite this article as: Dépagne and Chevalier: **Technical updates to basic proteins focalization using IPG strips.** *Proteome Science* 2012 **10**:54.

RESEARCH ARTICLE

Impairing the microRNA biogenesis pathway induces proteome modifications characterized by size bias and enrichment in antioxidant proteins

Delphine Peric[1], *Jean Labarre*[2], *François Chevalier*[3*,**] *and Germain Rousselet*[1*]

[1] CEA, DSV, iRCM, Laboratoire de Génétique de la Radiosensibilité, Fontenay aux Roses, France
[2] CEA, DSV, iBiTecS, Laboratoire de Biologie Intégrative, Gif sur Yvette, France
[3] CEA, DSV, iRCM, Plateforme de Protéomique, Fontenay aux Roses, France

Received: September 2, 2011
Revised: May 2, 2012
Accepted: May 10, 2012

Perturbation of individual microRNAs, or of the microRNA pathway, plays a role in carcinogenesis. In certain cancer cells, inhibition of the microRNA biogenesis pathway leads to a growth arrest state (CoGAM for Colony Growth Arrest induced by Microprocessor inhibition), which can be rescued by re-expression of individual microRNAs such as miR-20a. We now report that inhibition of the microRNA biogenesis pathway induced proteome changes characterized by a size bias in differentially expressed proteins, with induction of small proteins and inhibition of large ones. This size bias was observed in cells undergoing CoGAM, as well as in CoGAM-resistant cells, and in CoGAM-sensitive cells rescued by miR-20a. In this case, GO analysis of induced proteins identified by mass spectrometry revealed a significant enrichment in proteins involved in resistance to oxidative stress. In addition, H_2O_2 treatment of *Saccharomyces cerevisiae* or mammalian cells led to similarly size-biased proteome modifications. Our results point to size bias as a relevant readout of proteome modifications, in particular in conditions of stress such as inhibition of the microRNA biogenesis pathway or oxidative stress. They also suggest research avenues to study the role of the microRNA pathway in proteostasis.

Keywords:
Cell biology / Drosha / Microprocessor / Proteostasis / Stress

1 Introduction

MicroRNAs are a family of ~22 nucleotide RNAs controlling genome expression by inhibiting translation and/or inducing degradation of specific target mRNAs (reviewed in [1]). These small RNAs are encoded in the genome, either in dedicated polymerase II transcription units, or in the introns of protein coding genes. Their biogenesis requires two distinct steps [2]. In the nucleus, the Microprocessor, a complex composed of the RNase III Drosha and its RNA binding partner DGCR8, excises a stem-loop RNA (pre-miRNA) from the primary transcript (pri-miRNA). After export to the cytoplasm, the loop is removed by the RNase III Dicer, and the mature miRNA is loaded onto a functional RNA-induced silencing complex (RISC). Target mRNAs are then recognized by hybridization of the microRNA component of the RISC, leading to decrease of the encoded protein, generally accompanied by mRNA degradation [3].

It is now established that microRNAs participate in multiple biological functions, in particular in relation to cell differentiation and proliferation [4]. In addition, deregulation of microRNAs has been observed in tumor tissues and cells [5], and oncogenic [6] or tumor suppressive [7, 8] properties have been assigned to specific microRNAs. Therefore, functional studies in the context of transformed cells are of primary importance to identify cancer-related microRNAs, as well as the

Correspondence: Dr. Germain Rousselet, Laboratoire Réparation et Transcription dans les cellules Souches, iRCM, CEA, 18 route du panorama, 92260 Fontenay aux Roses, France
E-mail: germain.rousselet@cea.fr
Fax: +33-1-4654-8734

Abbreviation: CoGAM, Colony Growth Arrest induced by Microprocessor inhibition

*Both these authors contributed equally to this work
**Additional corresponding author: Dr. Francois Chevalier, E-mail: francois.chevalier@cea.fr

pathways they control. However, the microRNA pathway is endowed with redundancy, at both structural and functional levels. As a consequence, inhibition of single microRNAs is often phenotypically silent [9], which hampers classical reverse genetics approaches.

As an alternative, we have developed a molecular genetics approach combining a specific inhibition of the microRNA pathway at large, by inhibiting the Microprocessor, and a complementation of the observed phenotypes by re-expression of individual Microprocessor-independent pre-miRNAs [10]. We have used this approach to identify cancer cell lines whose proliferation depends on the Microprocessor, describing a new phenotype of colony growth arrest that we have called CoGAM (Colony Growth Arrest induced by Microprocessor inhibition). This phenotype was observed only in certain cell lines, where it is characterized by a long-term growth arrest with an increase of the fraction of cells in G0/G1 in the absence of senescence. In CoGAM-resistant cells, Microprocessor inhibition led to an increase of the transformed phenotype, as already established in other tumor models [11]. CoGAM could be complemented by re-expression of individual microRNAs, such as miR-20a, showing that it involved microRNA-controlled biological pathways.

In this report, we present the proteomic consequences of the inhibition of the microRNA biogenesis pathway in CoGAM-resistant and sensitive cells, highlighting a size bias in differentially expressed proteins.

2 Materials and methods

2.1 Cell cultures and treatments

MCF-7 (breast carcinoma) and HCT116 (colon carcinoma) cells were grown and transfected as previously described [10]. Cells were selected for at least 14 days before analysis.

2.2 Total protein extraction

Cells were scraped in PBS, washed three times in PBS, and dissolved in proteomic sample buffer (9 M urea, 4% CHAPS, 0.05% Triton-X100, 65 mM DTT and protease inhibitors (cOmplete, Roche, Meylan, France)). After centrifugation at 68 000 rpm for 60 min, supernatants were collected, aliquoted, and stored at −20°C until use. Protein content was estimated using the Bradford method [12].

2.3 2DE

Analytic 2DE was performed as previously described [13] with three technical replicates. Briefly, precast 18 cm strips, pH range 3–10 NL (GE Healthcare, Velizy, France), were rehydrated in the presence of 250 μg of protein. Isoelectric focusing was carried out using a Protean IEF Cell (Bio-Rad, Hercules, CA, USA) isoelectric focusing system until 80 kV h^{-1}. The strips were then incubated in ES1 (50 mM Tris-HCl pH 8.8, 6 M urea, 30% (v/v) glycerol, 2% (w/v) SDS) with 130 mM DTT and then in ES1 supplemented with 130 mM iodoacetamide. Strips were then embedded using 1% low-melt agarose on top of acrylamide gels. SDS-PAGE was carried out on a 12% acrylamide gel, using the Dodeca Cell electrophoresis unit (Bio-Rad). Gels were batch-stained with silver nitrate [14] with a Dodeca stainer unit (Bio-Rad) and scanned to images that were digitized with a GS 800 densitometer (Bio-Rad). Preparative 2DE gels were performed as previously described [15] with 500 μg of proteins using the Coomassie colloidal blue staining protocol [16].

2.4 Image analysis

Images from stained gels were digitalized at 300 dpi with a GS 710 densitometer (Bio-Rad) and analyzed using the Samespots software v4.1 (Non-linear Dynamics, UK). Gel replicates were grouped to create a global analysis with all conditions. Quantitative comparisons of spot intensities were analyzed using Samespots (v4.1, Nonlinear Dynamics, Durham, NC, USA). Background subtraction and spot intensity normalization were automatically performed by Samespots. A multivariate statistic analysis was performed using the statistic mode of the Samespots software v4.1. Spots were considered differentially expressed at $p < 0.05$ (ANOVA *t*-test). Statistical analysis of the distribution of the molecular weights of induced and repressed proteins was performed with a one-tailed Wilcoxon rank sum test.

2.5 MALDI-TOF MS analysis

Spots were excised from preparative 2DE gels, and processed using a Packard Multiprobe II robot (Perkin-Elmer, Courtaboeuf, France). After washing successively with water, 25 mM ammonium bicarbonate, ACN/25 mM ammonium bicarbonate (1:1, v/v), and ACN, gel fragments were dried at 37°C. Protein digestion was carried out at 37°C for 5 h following addition of 0.125 μg trypsin (sequencing grade, modified, Promega, Charbonières, France), and resulting fragments were extracted twice with 50 μL ACN/water (1:1, v/v) containing 0.1% TFA for 15 min. Pooled supernatants were concentrated with a speedvac to a final volume of 20 μL. Peptides were simultaneously desalted and concentrated with C18 Zip-Tip microcolumns to a final volume of 3 μL, an aliquot of each sample was mixed (1/1) with the CHCA matrix at half saturation in ACN/water (1:1, v/v), and the mixture was immediately spotted on the MALDI target by the Multiprobe II robot. Mass spectra were recorded in the reflector mode on a UltraFlex II MALDI-TOF/TOF mass spectrometer (Bruker Daltonics, Bremen, Germany). Automatic annotation of monoisotopic masses was performed using Bruker's SNAPTM procedure. The MASCOT search

engine software (Matrix Science, London, UK) was used to search the NCBInr database. The following parameters were used: mass tolerance of 30–100 ppm, a minimum of five peptides matching to the protein, carbamidomethylation of cysteine as fixed modification, oxidation of methionine as variable modifications, and one missed cleavage allowed.

2.6 Nano LC-MS analysis

When spots could not be identified by PMF, LC-MS/MS analysis was conducted. Stained protein spots were excised manually, washed, digested with trypsin, and extracted using formic acid. Protein digests were analyzed using an ion trap mass spectrometer (Esquire HCT plus; Bruker, Billerica, MA, USA) coupled to a nano-chromatography system (HPLC 1200, Agilent, Santa Clara, CA, USA) interfaced with an HPLC-Chip system (Chip Cube, Agilent). MS/MS data were searched against NCBI and MSDB databases using Mascot software.

3 Results

3.1 Proteome changes during CoGAM reveal a shift in protein size

In order to identify protein expression changes upon CoGAM induction, we transfected the CoGAM-sensitive MCF-7 breast cancer cells with a vector coding or not for a Drosha-targeting shRNA, selected transfected cells in the presence of puromycin for 14–21 days, and extracted total proteins as described in Section 2. Whole cell extracts were separated by 2DE and protein spots were revealed by silver staining. Experiments were performed at least in triplicate. The 3–10 p*I* range allowed the detection of 1332 spots observed at least in one sample. A representative 2DE gel is presented for each sample (Fig. 1A and B). We identified 171 spots (12.8%) as being significantly modified by Drosha inhibition, including 85 decreased (outlined in blue in Fig. 1A) and 86 increased (outlined in red in Fig. 1B).

We noticed that proteins whose expression is reduced appeared larger in size than proteins with increased expression (Fig. 1). Analysis of the fold change as a function of protein size confirmed this observation (Fig. 1C and D). Following Drosha inhibition, induced proteins had a mean size of 27.5 ± 6.0 kDa (mean ± SD), whereas the mean size of repressed proteins was 87.4 ± 25.7 kDa. This difference was significant ($p < 10^{-15}$; one-tailed Wilcoxon rank sum test). In addition, it was specific for the protein size, as induced and repressed proteins were significantly different neither for their p*I*s (6.2 ± 1.3 versus 6.3 ± 1.2, $p > 0.67$; Fig. 1E and F), nor for their level of expression, as approximated by the intensity of staining of spots ($p > 0.95$; Fig. 1G and H). We suspected that this size bias could be due to nonspecific proteolysis during CoGAM, to which large proteins could be more sensitive. Such a nonspecific degradation of proteins should indiscriminately decrease the bulk of large proteins. However, this was not the case. Among the proteins with a size over 60 kDa, only 85 of 535 (15.9%) were decreased. Although these observations do not exclude the possibility that at least part of the decrease of large proteins could be due to CoGAM-induced proteases, they reveal some kind of specificity in this potential mechanism (see also section 3.3). Altogether, they demonstrate a correlation between Drosha inhibition in CoGAM-sensitive cells and a strongly size-biased modification of the proteome.

3.2 Drosha inhibition induces size-biased proteome changes in the absence of CoGAM

We then sought to establish whether Drosha inhibition induced size-biased proteome changes in the absence of CoGAM. To do this, we took advantage of the fact that overexpression of miR-20a was able to rescue the growth of Drosha^{kd} MCF-7 cells [10]. We therefore analyzed the proteomic consequences of Drosha knockdown in MCF-7 cells overexpressing the CoGAM-complementing miR-20a (Dro^{kd}-miR-20a versus miR-20a; Fig. 2). We detected 31 spots that were modified (Fig. 2A), a majority of them being increased (23 versus 8 decreased). Among these spots, 11 (35.5%) had also been found to be modified by Drosha inhibition in the absence of miR-20a. Size analysis (Fig. 2B) revealed that Drosha inhibition in the absence of CoGAM also led to size-biased modifications of the proteome. Induced spots had a mean size of 30.6 ± 7.9 kDa, whereas decreased ones had a mean size of 91.2 ± 24.5 kDa ($p < 10^{-4}$). In addition, we compared the proteomes of Drosha^{kd} and control HCT116 cells, because these cells do not undergo CoGAM upon Microprocessor inhibition [10]. Size analysis of differentially expressed spots again revealed a size bias (Supporting Information Fig. 1 and Fig. 2C and D), with a mean size of 44.9 ± 12.3 kDa for the 12 induced proteins versus 65.0 ± 25.7 kDa for the 12 repressed ones ($p < 10^{-2}$). Altogether, these data demonstrate that Drosha inhibition induces size-biased modifications of the proteome that are independent from the establishment of CoGAM.

3.3 A link between microRNAs, protein size shift, and stress response

To our knowledge, the only reported protein size shift reported in the literature has been suggested in the yeast *Saccharomyces cerevisiae* in response to several types of environmental stresses [17]. In this study, H_2O_2 treatment appeared to be the stress condition causing the most important bias. However, these data were based on transcriptome experiments, from which protein sizes were computed. We therefore re-examined our previous proteome analysis of the yeast

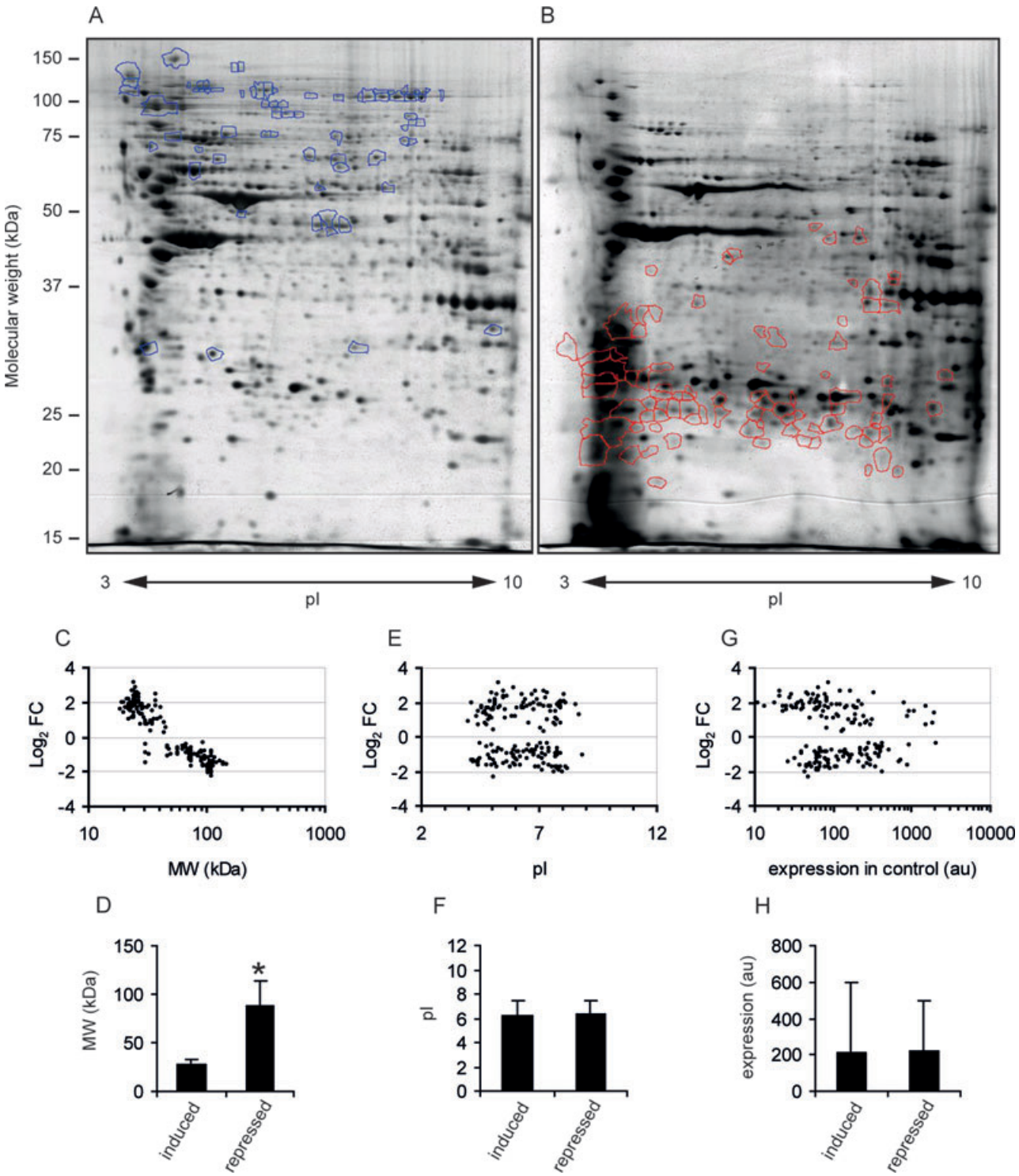

Figure 1. Proteome changes during CoGAM. Whole cell extracts from MCF-7 cells transfected with (A) an empty vector or (B) a vector coding for a Drosha-targeting shRNA were analyzed by 2DE. One representative gel out of three is shown. Differentially expressed spots were delineated either in blue (repressed in Drosha^{kd} cells) or in red (induced in Drosha^{kd} cells). The Log_2 of the fold change (Log_2 FC) of differentially expressed spots between Drosha^{kd} and control MCF-7 cells was individually analyzed as a function of (C) molecular weight, (E) isoelectric point, and (G) level of expression in control cells. We note that level of expression was approximated by staining intensity, although silver staining also depends upon protein sequence [32]. Results were also edited as mean ± SD of induced or repressed spots for (D) molecular weight, (F) isoelectric point, and (H) level of expression in control cells. $*p < 10^{-15}$.

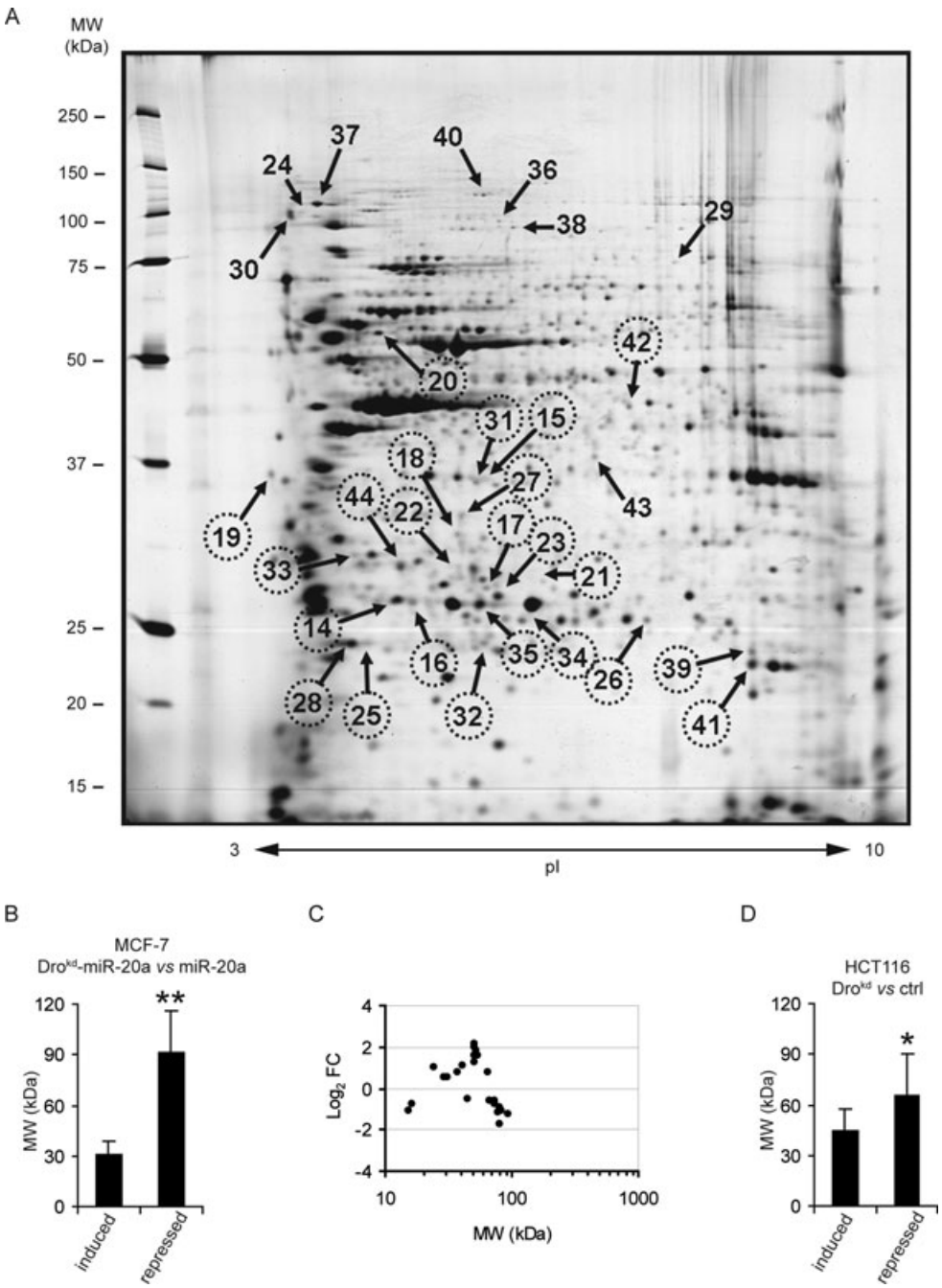

Figure 2. Drosha inhibition induces a size-biased proteome modification in the absence of CoGAM. (A) Whole cell extracts were prepared from MCF-7 cells overexpressing both a Drosha-targeting shRNA and miR-20a (Microprocessor inhibition without CoGAM), and analyzed by 2DE. Numbered spots were significantly increased (circled) or decreased (non circled) when compared to cells expressing miR-20a without Drosha inhibition, and were identified by mass spectrometry (Supporting Information Table S1). (B) A CoGAM-independent size bias in proteome modifications induced by Drosha knockdown was assayed by comparing the mean ± SD of the molecular weights of repressed and induced spots identified in (A). (C) Whole cell extracts were prepared from HCT116 cells transfected with a plasmid expressing or not a Drosha targeting shRNA, and compared by 2DE. The Log_2 of the fold changes of differentially expressed spots (Log_2 FC) was plotted as a function of the molecular weight of the spots. (D) Mean ± SD of the molecular weights of induced or repressed spots identified in (C). $^{*}p < 10^{-2}$; $^{**}p < 10^{-4}$.

response to H_2O_2 [18], probing for a potential size shift. Indeed, upon H_2O_2 treatment, proteins with fold changes higher than 2 had an average MW of 45.0 ± 24.4 kDa (n = 54), compared to an average of 54.6 ± 26.0 kDa (n = 29) for proteins with fold changes under 0.5 (Fig. 3A and B; $p < 5 \times 10^{-2}$).

We therefore wondered whether the size-biased response that we observed upon Drosha inhibition could be interpreted as a stress response. To answer this question, we identified by mass spectrometry the spots that were induced by Drosha knockdown in the presence of miR-20a (Dro^{kd}-miR-20a versus miR-20a; Supporting Information Table S1). All the identified proteins (28 of 31) had theoretical MWs that were consistent with the observed size of the original spots. This result showed that increased proteins were not proteolytic fragments from large degraded proteins, demonstrating that, in this setting, the size-biased proteome modification was not due to proteolysis. Strikingly, out of 18 proteins, three were known to be involved in the cellular response to an oxidative stress by scavenging reactive oxygen species (two

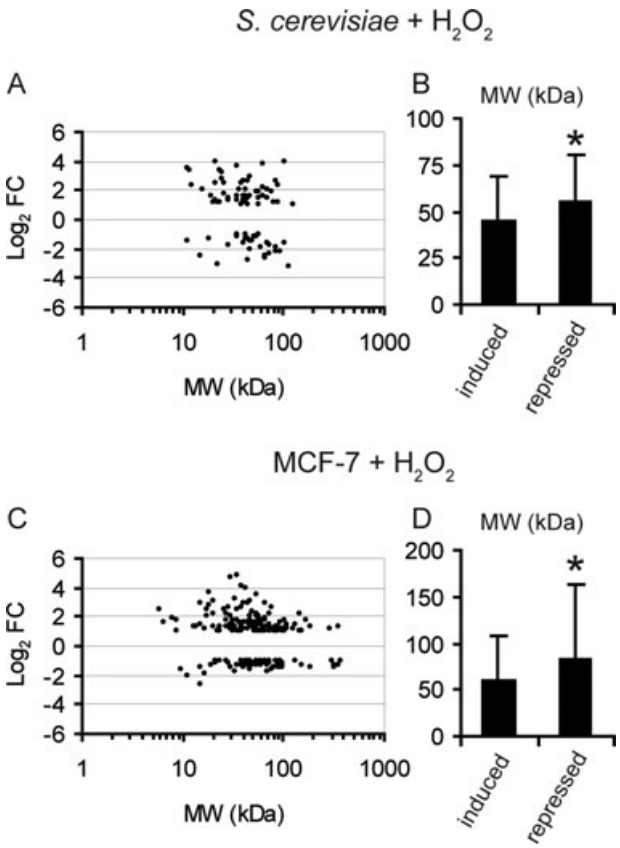

Figure 3. H_2O_2 induces size-biased proteome modifications in *S. cerevisiae* and MCF-7 cells. (A) Proteomic data from *S. cerevisiae* cells treated with 400 μM H_2O_2 were retrieved from [18] and plotted as the Log_2 of the fold change (Log_2 FC) as a function of the observed molecular weight for spots with Log_2 FC >1 or Log_2 FC <-1. (B) The same data as in (A) were analyzed by comparing the mean $\pm$ SD of the molecular weights of repressed and induced protein. (C) The theoretical molecular weight of proteins whose mRNAs were found to be differentially expressed more than twofold after a 100 μM H_2O_2 treatment of MCF-7 cells [23] was retrieved from Uniprot. The Log_2 of the fold change (Log_2 FC) was plotted as a function of this molecular weight. (D) The data shown in (C) were analyzed by comparing the mean $\pm$ SD of the molecular weights of repressed and induced protein. $*p < 5 \times 10^{-2}$.

thioredoxin-dependent peroxidases PRDX1 and PRDX3 [19], and the biliverdin reductase BLVRB [20]), one by reducing $NADP^+$ to NADPH (the NADP-dependent isocitrate dehydrogenase IDH1 [21]), and one as a molecular chaperone (the heat shock protein HSP27 [22]). Western blotting analysis confirmed induction of HSP27 and PRDX1 proteins (Supporting Information Fig. 2). In addition, PRDX3, IDH1, and HSP27 were among the 11 spots that were also found in the comparison between Dro^{kd} and control cells. The statistical significance of this enrichment was tested by performing a GO analysis using DAVID (http://david.abcc.ncifcrf.gov/). Indeed, among the 35 Biological Processes GO terms found to be significantly enriched ($p < 5 \times 10^{-2}$), seven concerned the cellular response to stress (with enrichment folds going from 3.72 for "response to stress" to 92.26 for "hydrogen peroxide catabolic process"), among which six related specifically to oxidative stress (Supporting Information Table S2). The second highly represented biological process was apoptosis inhibition (seven GO terms with enrichment folds going from 4.81 for "regulation of cell death" to 11.42 for "anti-apoptosis"). Therefore, the proteome response to Drosha inhibition has characteristics of a cellular response to oxidative stress.

Reciprocally, we wondered whether the response of a mammalian cell to oxidative stress also involved a size bias in differentially expressed proteins. We therefore analyzed the results of microarray experiments that we performed after H_2O_2 treatment of MCF-7 cells [23]. For genes identified as being induced or repressed more than twofold, we retrieved predicted protein sizes from Uniprot (http://www.uniprot.org/), using the reference isoform when a gene coded for more than one protein. The mean protein size of induced genes was 59.7 ± 49.2 kDa ($n = 143$), and 81.9 ± 80.2 kDa for repressed genes ($n = 67$) (Fig. 3C and D). This size bias was statistically significant ($p < 2 \times 10^{-2}$). We conclude that the mammalian cell response to an oxidative stress also involves a size bias in regulated proteins.

4 Discussion

In this manuscript, we report that impairment of the microRNA biogenesis pathway, obtained by knocking down the Microprocessor RNase Drosha, resulted in a proteome modification characterized by a size bias in differentially expressed proteins. Repressed proteins were found to have a significantly higher mean molecular weight than induced proteins. This seldom described phenotype was reproducible in MCF-7 cells undergoing CoGAM, in MCF-7 cells rescued for CoGAM, and in the CoGAM-resistant HCT116 cells. In addition, such a size bias was also observed in *S. cerevisiae* or MCF-7 cells submitted to an oxidative stress. Reciprocally, proteins induced by the inhibition of Drosha included enzymes involved in reactive oxygen species detoxification and chaperones, leading to a significant enrichment of proteins annotated as participating in the cell response to an oxidative stress.

During the last decade, the sequencing of genomes from several species, including *Homo sapiens*, paved the way for global in silico analyses of protein length. Significant size differences were reported to correlate with different types of protein classification. Morbid genes, i.e. genes whose mutations adversely affect health, code for proteins that are on average longer than other proteins [24]. Conversely, housekeeping genes have been reported to code for short proteins [25]. More generally, mean protein sizes are different in functional classes of proteins characterized in the Clusters of Orthologous Groups (COG) database [26], or when *S. cerevisiae* proteins are grouped according to their biochemical activity [27]. On the other hand, the size of proteins impacts the

cost of their biosynthesis, which constitutes the major energy consuming process of a cell [28]. Balch and collaborators [29] have proposed that the maintenance of a functional proteome (proteostasis) is a bona fide cellular system integrating signals from environmental and intrinsic clues through specialized signaling pathways. This proteostasis network might control protein size, at least as an indirect consequence of energy saving or functional reorientation of the proteome. Indeed, Vilaprinyo et al. [17] have shown that the proteostasis network response to certain stresses in *S. cerevisiae* was characterized by a size-biased modification of protein expression, similar to the one we report herein, and that they attributed to a minimization of biosynthetic costs. Our data confirm that, in different experimental settings, the size of regulated proteins is a readout of modifications of the proteostasis network.

The mechanism leading from Drosha inhibition to size-biased modifications of the proteome has to be explored. Our data already demonstrate that the context of CoGAM dramatically modified the extent of the response, suggesting that this mechanism can be impacted by the cellular environment. This observation is hard to reconcile with the straightforward hypothesis that microRNAs could preferentially target mRNAs coding for small proteins. Alternatively, impairing the microRNA biogenesis pathway could affect the proteostasis network, either because major regulatory proteins of this network are microRNA targets, or because metabolic changes induced by Microprocessor inhibition are sensed by proteostasis regulating pathways.

In this regard, the link between Drosha inhibition, size-biased proteome modifications, and oxidative stress, is puzzling. On the one hand, in *S. cerevisiae*, oxidative stress induces a response marked by a size bias in differentially expressed proteins (this article and [17]). Whether this corresponds to a minimization of biosynthetic costs [17], or to the fact that antioxidant proteins are smaller than average [27], is not clear. Our results extend this observation to the MCF-7 mammalian cell line, suggesting that such a size-biased proteome modification is a general feature of the response to an oxidative stress. On the other hand, proteins induced by Drosha inhibition, at least in miR-20a-complemented MCF-7 cells, are enriched for known effectors of an antioxidative response. Therefore, it would be tempting to hypothesize that Drosha inhibition induces an oxidative stress, which in turn induces a size-biased proteome modification. Conversely, it is intriguing that Dicer, the pre-miRNA maturing RNase III, is transcriptionally inhibited by H_2O_2 in several mammalian cells [23]. Furthermore, DGCR8, the RNA binding partner of Drosha, is a double-cysteine-ligated heme-dependent protein [30, 31], that might thus be sensitive to oxidation. Therefore, we cannot exclude that in mammalian cells, an oxidative stress could induce a global inhibition of the microRNA pathway. These two possibilities, and their possible integration in a double positive feedback loop (see Fig. 4), are under investigation.

In conclusion, our data suggest that size biases in proteome changes should be more systematically analyzed, because they could bring information on the biology of the studied cells in general, and on their proteostasis network and regulatory pathways in particular.

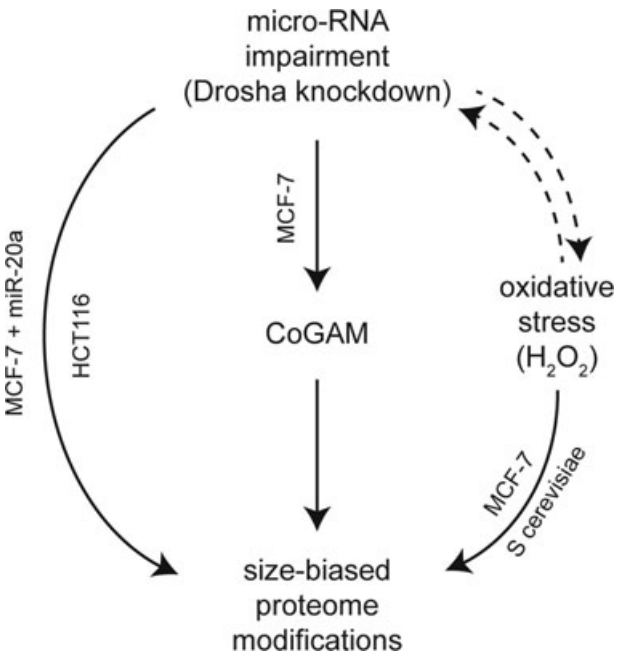

Figure 4. MicroRNAs, oxidative stress response, and protein size shift: a working model. Schematic view of the working model. Solid arrows represent conclusions from 2DE comparisons performed as reported in the text, whereas dotted arrows are hypothetical.

We thank J. Depagne for expert technical assistance, J.-C. Aude for help with the Wilcoxon rank sum test, and acknowledge the support of the Proteomic Platform of Montpellier-LR Genopole. This work was supported by the Electricité de France grant n° V3-104 to GR.

The authors have declared no conflict of interest.

5 References

[1] Bartel, D. P., MicroRNAs: target recognition and regulatory functions. *Cell* 2009, *136*, 215–233.

[2] Kim, V. N., Han, J., Siomi, M. C., Biogenesis of small RNAs in animals. *Nat. Rev. Mol. Cell Biol.* 2009, *10*, 126–139.

[3] Guo, H., Ingolia, N. T., Weissman, J. S., Bartel, D. P., Mammalian microRNAs predominantly act to decrease target mRNA levels. *Nature* 2010, *466*, 835–840.

[4] Ivey, K. N., Srivastava, D., MicroRNAs as regulators of differentiation and cell fate decisions. *Cell Stem Cell* 2010, *7*, 36–41.

[5] Lu, J., Getz, G., Miska, E. A., Alvarez-Saavedra, E. et al., MicroRNA expression profiles classify human cancers. *Nature* 2005, *435*, 834–838.

[6] He, L., Thomson, J. M., Hemann, M. T., Hernando-Monge, E. et al., A microRNA polycistron as a potential human oncogene. *Nature* 2005, *435*, 828–833.

[7] Mayr, C., Hemann, M. T., Bartel, D. P., Disrupting the pairing between let-7 and Hmga2 enhances oncogenic transformation. *Science* 2007, *315*, 1576–1579.

[8] Welch, C., Chen, Y., Stallings, R. L., MicroRNA-34a functions as a potential tumor suppressor by inducing apoptosis in neuroblastoma cells. *Oncogene* 2007, *26*, 5017–5022.

[9] Wang, Y., Baskerville, S., Shenoy, A., Babiarz, J. E. et al., Embryonic stem cell-specific microRNAs regulate the G1-S transition and promote rapid proliferation. *Nat. Genet.* 2008, *40*, 1478–1483.

[10] Peric, D., Chvalova, K., Rousselet, G., Identification of microprocessor-dependent cancer cells allows screening for growth-sustaining micro-RNAs. *Oncogene* 2011, 31, 2039–2048.

[11] Kumar, M. S., Lu, J., Mercer, K. L., Golub, T. R. et al., Impaired microRNA processing enhances cellular transformation and tumorigenesis. *Nat. Genet.* 2007, *39*, 673–677.

[12] Bradford, M. M., A rapid and sensitive method for the quantitation of microgram quantities of protein utilizing the principle of protein-dye binding. *Anal. Biochem.* 1976, *72*, 248–254.

[13] Chevalier, F., Highlights on the capacities of "Gel-based" proteomics. *Proteome. Sci.* 2010, *8*, doi: 10.1186/1477-5956-8-23.

[14] Chevalier, F., Centeno, D., Rofidal, V., Tauzin, M. et al., Different impact of staining procedures using visible stains and fluorescent dyes for large-scale investigation of proteomes by MALDI-TOF mass spectrometry. *J. Proteome. Res.* 2006, *5*, 512–520.

[15] Chevalier, F., Hirtz, C., Sommerer, N., Kelly, A. L., Use of reducing/nonreducing two-dimensional electrophoresis for the study of disulfide-mediated interactions between proteins in raw and heated bovine milk. *J. Agric. Food Chem.* 2009, *57*, 5948–5955.

[16] Chevalier, F., Rofidal, V., Rossignol, M., Visible and fluorescent staining of two-dimensional gels. *Methods Mol. Biol.* 2007, *355*, 145–156.

[17] Vilaprinyo, E., Alves, R., Sorribas, A., Minimization of biosynthetic costs in adaptive gene expression responses of yeast to environmental changes. *PLoS Comput. Biol.* 2010, *6*, e1000674.

[18] Godon, C., Lagniel, G., Lee, J., Buhler, J. M. et al., The H2O2 stimulon in *Saccharomyces cerevisiae*. *J. Biol. Chem.* 1998, *273*, 22480–22489.

[19] Hall, A., Karplus, P. A., Poole, L. B., Typical 2-Cys peroxiredoxins – structures, mechanisms and functions. *FEBS J.* 2009, *276*, 2469–2477.

[20] Baranano, D. E., Rao, M., Ferris, C. D., Snyder, S. H., Biliverdin reductase: a major physiologic cytoprotectant. *Proc. Natl. Acad. Sci. USA* 2002, *99*, 16093–16098.

[21] Reitman, Z. J., Yan, H., Isocitrate dehydrogenase 1 and 2 mutations in cancer: alterations at a crossroads of cellular metabolism. *J. Natl. Cancer Inst.* 2010, *102*, 932–941.

[22] Arrigo, A. P., Virot, S., Chaufour, S., Firdaus, W. et al., Hsp27 consolidates intracellular redox homeostasis by upholding glutathione in its reduced form and by decreasing iron intracellular levels. *Antioxid. Redox Signal.* 2005, *7*, 414–422.

[23] Desaint, S., Luriau, S., Aude, J. C., Rousselet, G. et al., Mammalian antioxidant defenses are not inducible by H_2O_2. *J. Biol. Chem.* 2004, *279*, 31157–31163.

[24] Kondrashov, F. A., Ogurtsov, A. Y., Kondrashov, A. S., Bioinformatical assay of human gene morbidity. *Nucleic Acids Res.* 2004, *32*, 1731–1737.

[25] Eisenberg, E., Levanon, E. Y., Human housekeeping genes are compact. *Trends Genet.* 2003, *19*, 362–365.

[26] Brocchieri, L., Karlin, S., Protein length in eukaryotic and prokaryotic proteomes. *Nucleic Acids Res.* 2005, *33*, 3390–3400.

[27] Warringer, J., Blomberg, A., Evolutionary constraints on yeast protein size. *BMC Evol. Biol.* 2006, *6*, doi:10.1186/1471-2148-6-61.

[28] Russell, J. B., Cook, G. M., Energetics of bacterial growth: balance of anabolic and catabolic reactions. *Microbiol. Rev.* 1995, *59*, 48–62.

[29] Roth, D. M., Balch, W. E., Modeling general proteostasis: proteome balance in health and disease. *Curr. Opin. Cell Biol.* 2011, *23*, 126–134.

[30] Faller, M., Matsunaga, M., Yin, S., Loo, J. A. et al., Heme is involved in microRNA processing. *Nat. Struct. Mol. Biol.* 2007, *14*, 23–29.

[31] Barr, I., Smith, A. T., Senturia, R., Chen, Y. et al., DiGeorge critical region 8 (DGCR8) is a double-cysteine-ligated heme protein. *J. Biol. Chem.* 2011, *286*, 16716–16725.

[32] Richert, S., Luche, S., Chevallet, M., Van Dorsselaer, A. et al., About the mechanism of interference of silver staining with peptide mass spectrometry. *Proteomics* 2004, *4*, 909–916.

DOI 10.1002/pmic.201100319 *Proteomics* 2012, *12*, 1756–1766

RESEARCH ARTICLE

Accumulation of cyclophilin A isoforms in conditioned medium of irradiated breast cancer cells

François Chevalier[1], Jordane Depagne[1], Sonia Hem[2], Sylvie Chevillard[3], Julie Bensimon[3], Pascale Bertrand[1,4] and Jérôme Lebeau[3]

[1] CEA, DSV, iRCM Plateforme de Protéomique, Fontenay-aux-Roses, France
[2] INRA, UR 1199, Laboratoire de Protéomique Fonctionnelle, Montpellier, France
[3] CEA, DSV, iRCM, SREIT Laboratoire de Cancérologie Expérimentale, Fontenay-aux-Roses, France
[4] CEA, DSV, IRCM, SIGRR, Laboratoire des Mécanismes de la Recombinaison, Fontenay-aux-Roses, France

Received: June 17, 2011
Revised: December 16, 2011
Accepted: February 21, 2012

Secreted proteins play a key role in cell signaling and communication. We recently showed that ionizing radiations induced a delayed cell death of breast cancer cells, mediated by the death receptor pathways through the expression of soluble forms of "death ligands." Using the same cell model, the objective of our work was the identification of diffusible factors, secreted following cell irradiation, potentially involved in cell death signaling. Differential proteomic analysis of conditioned media using 2DE resulted in detection of numerous spots that were significantly modulated following cell irradiation. The corresponding proteins were identified using MALDI-TOF MS and LC-MS/MS approaches. Interestingly, five isoforms of cyclophilin A were observed as increased in conditioned medium of irradiated cells. These isoforms differed in isoelectric points and in accumulation levels. An increase of cyclophilin A secretion was confirmed by Western blotting of conditioned media of irradiated or radiosentive mammary cells. These isoforms displayed an interesting pattern of protein maturation and post-translational modifications, including an alternating removal of N-terminal methionine, associated with a combination of acetylations and methylations. The role of the protein is discussed in relation with its potential involvement in the mechanisms of intercells relationships and radiosensitivity.

Keywords:
Breast cancer / Cell biology / Cyclophilin A / Irradiation / Radiosensitivity / Secretome

1 Introduction

The secretome refers to the global study of proteins that are secreted by a cell, a tissue, or an organism [1]. Although the secretome is a potential source suitable for the discovery of new therapeutic targets or biomarker candidates, the access to secreted proteins using proteomic analysis represents a challenge for three reasons: (i) the very low concentration in the culture media of most secreted proteins makes their analysis difficult; (ii) their covering and contamination by cytoplasmic or other normally nonsecreted proteins released following cell lysis and death; (iii) the use of FCS in culture media, mandatory to most cell lines, interferes with proteomics techniques [2]. Several technical possibilities were offered to address these three problems: (i) the high separation power of gel-based proteomics methods [3,4], coupled with enrichment techniques based on trichloroacetic acid (TCA) precipitation allowed the concentration and the study of secreted proteins [2,5]; (ii) additional control samples (cytoplasmic and total cell extracts) can limit false positive spots during gel picture analysis; (iii) secreted proteins were collected from cells grown without FCS in culture media in order to reduce serum protein contamination [6,7].

Correspondence: Dr. François Chevalier, CEA, DSV, iRCM, Plateforme de Protéomique, 92260 Fontenay-aux-Roses, France
E-mail: francois.chevalier@cea.fr
Fax: +33-146-549-138

Abbreviations: Cc, cytoplasmic extract proteins of control cells; **Ci**, cytoplasmic extract proteins of irradiated cells; **CyPA**, cyclophilin A; **IR**, ionizing radiation; **Sc**, conditioned media of control cells; **SFM**, serum free medium; **Si**, conditioned media of irradiated cells; **Tc**, total extract proteins of control cells; **TCA**, trichloroacetic acid; **Ti**, total extract proteins of irradiated cells

While genetic analyses may provide a list of potentially secreted proteins, proteome analysis is essential to identify proteins actually secreted by cells and tissues under certain conditions. Indeed, secreted proteins from cancer cells were able to control many biological and physiological processes [8].

Cellular exposure to ionizing radiation (IR) can result in the secretion of soluble factors by irradiated cells [9]. In this case, a bystander effects can occur in cells that were never themselves irradiated but were either in close proximity to irradiated cells. In vivo, a bystander effect was observed after injecting mice with either neutron irradiated cells [10] or radioactively labeled cells [11], mixing these with nonirradiated cells and observing subsequent effects in the nonirradiated cells.

Following gamma-irradiation, breast tumor displayed a prolonged G2 blockage, accompanied by a mitotic disorder and considered as a frequent mode of cell death [12]. The mechanisms underlying radiation-induced bystander effects are as yet unclear and the identity of the bystander factors is partially defined. Several interleukine and cytokine were described to participate in such bio-cellular mechanisms [13,14], but it is likely that multiple pathways are involved in the bystander phenomenon, and different cell types respond differently to bystander signaling. We have shown previously that irradiation of mammary tumor cells led to late cell death by apoptosis. After a 10-Gy irradiation, the proliferative capacity was almost fully inhibited; only few cell clones were able to emerge, showing the selection of radioresistant cells. This growth inhibition was mediated by the Fas, TRAIL, and TNF-alpha death receptor pathways through the expression of mains ligands/receptors implicated in these three pathways. Moreover, we showed that the three ligands were also produced as soluble forms whose secretion can induce the death of sensitive cells through a "bystander" type effect [15].

The aim of the present work is focused on the research and characterization of new diffusible factors during radioinduced cell death of mammary cancer cells. These diffusible factors could be implicated in cell death and potentially associated with bystander effects. So, using a proteomic strategy specifically developed for secreted proteins, the goal of this study was the investigation of cell secretome for the identification of proteomic changes associated with IRs.

According to a gel-based secretomic analysis, several isoforms of cyclophilin A (CyPA) were observed as specifically over-expressed in conditioned medium from irradiated cells. Spot isoforms were analyzed by MS, and the level of secreted CyPA was estimated in different mammary cell lines. Our study provides evidence that protein secretion was increased following irradiation and protein function could be connected to radiosensibility.

2 Materials and methods

2.1 Cell cultures

T-47D, MCF7, BT-20, ZR-75–1, MDA-MB-157, and MDA-MB-231 cell lines were obtained from the American Type Culture Collection (Rockville, MD, USA). Cells were maintained in DMEM, 4.5 g/L glucose, 0.11 g/L sodium pyruvate, glutamate (GlutaMAX 1^{TM}) and pyridoxine, supplemented with 5% (T-47D, MCF7, and MDA-MB-231), or 10% (BT-20 and MDA-MB-157) FCS, penicillin, streptomycin, and amphotericin B (antibiotic–antimycotic mix) (all from Life Technologies, Cergy-Pontoise, France) in 5% CO_2 and 95% humidity. Cell proliferation and survival analyses were performed in two or more independent experiments, by scoring at least 300 cells each time. Discrimination between viable and dead cells was performed by trypan blue exclusion.

2.2 Irradiation and conditioned medium collection

Cells were plated 48 h prior to irradiation. On day 0 (concentration of 4×10^6 cells per 75 cm^2 flask), cells were 10 Gy-irradiated in a serum-free DMEM, using a 137Cs irradiation unit at dose rate of 2 Gy/min, and then incubated with fresh medium. Six days after irradiation, the medium was removed and the cell layer was washed once with PBS and thrice with serum-free medium (SFM), SFM was added to the cells for an incubation period of 18 h after which cell layer as well as SFM were collected (Fig. 1). In parallel, nonirradiated cells (concentration of 4×10^5 cells per 75 cm^2 flask at day 0, in order to obtain a concentration of 4×10^6 cells per flask at day 6) were similarly treated. Two independent biological replicates were used for subsequent proteomic analyses.

2.3 Conditioned medium, cytosolic, and total protein extraction

Proteins were extracted from conditioned medium by precipitation. Briefly, SFM with secreted proteins was centrifuged at 10 000 × *g* for 10 min at 4°C to remove dead cells and large debris. Proteins were precipitated according to the method of Hirtz et al. applied for secreted salivary proteins [5], with the modification of Chevallet et al. applied for cell secretome [2].

Briefly, secreted proteins in SFM were incubated with 7.5% TCA and 0.1% NLS (N-Lauroyl Sarcosine) at −20°C overnight. The protein suspension was then centrifuged at 42 000 × *g* for 10 min at 4°C and the pellet was washed two times with ice cold acetone/2-ME (0.07% v/v), centrifuged again as previously, and the final pellet was dried in the air. Proteins were resuspended in proteomic sample buffer containing 9 M urea, 4% CHAPS, 0.05% Triton X-100, 65 mM DTT, and a protease inhibitor cocktail (Roche Diagnostics, Meylan, France). Samples were stored at −20°C.

Total proteins were extracted from intact cell as following. Cells were collected following trypsinization and cell pellets were washed three times in PBS. Half of cells were dissolved in proteomic sample buffer to obtain the total protein extract. This suspension was centrifuged at 68 000 rpm for 60 min, supernatants were collected, aliquoted, and stored

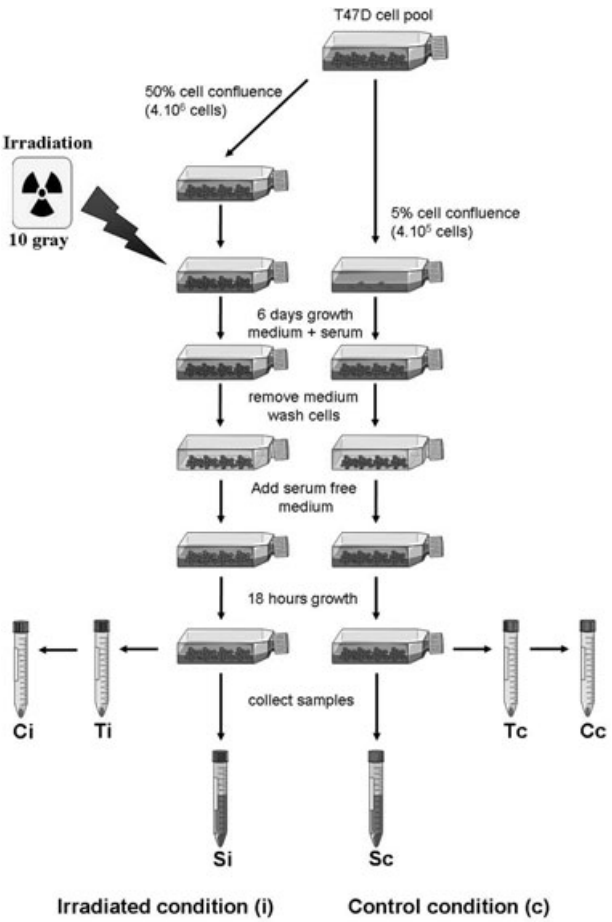

Figure 1. Protocol strategy to produce conditioned media of control (Sc) or irradiated cell (Si); total cell extracts of control (Tc) or irradiated cell (Ti); cytoplasmic cell extracts of control (Cc) or irradiated cell (Ci).

at −20°C until usage. The other half of intact cell was used to extract cytosolic proteins. Cells were resuspended in fresh SFM, cytosolic fraction was obtained after cell membrane disruption with ten strokes in a dounce potter (verified by microscopy) and centrifuge at 10 000 × *g* for 5 min at 4°C to remove cell nuclei and membrane debris. Cytosolic proteins were then precipitated as described previously for the secreted proteins.

The protein content of the solubilized samples was estimated using the Bradford method.

2.4 2DE

2DE was performed as previously described [16] with three technical replicates and two independent biological experiments using precast 18 cm strips, pH range 3–10 NL (GE Healthcare, Buckinghamshire, UK), for the first dimension, and 12% acrylamide SDS-polyacrylamide gel for the second dimension. Gels were batch-stained with silver nitrate [17] with a Dodeca stainer unit (Bio-Rad) and scanned to images that were digitized with a GS 800 densitometer (Bio-Rad).

2.5 Image analysis

Images from stained gels were digitalized at 300 dpi with a GS 710 densitometer (Biorad, Hercules, CA, USA) and analyzed using the Samespots software v4.0 (Non-linear Dynamics, Newcastle upon Tyne, UK). Gel replicates were grouped to create a global analysis with all conditions. Spots of each samples were compared between control and irradiated conditions. A multivariate statistic analysis was performed using the statistic mode of the Samespots software (Non-linear Dynamics). Spots with significant differences between control and irradiated cells (ANOVA *t*-test $p < 0.05$) were first extracted. Then, only spots with a q value < 0.05 and a power > 0.8 were finally selected. Spots of interest were selected for subsequent protein identification by MS analysis.

2.6 In-gel digestion

Spots were excised from gels manually. All subsequent steps were done automatically using a Multiprobe II robot (Perkin-Elmer). Spots were first washed with 300 μL of water and then 300 μL of 25 mM NH_4HCO_3. Destaining was performed twice in the presence of 300 μL of 50% ACN in 25 mM NH_4HCO_3. Gel pieces were then dehydrated twice by 300 μL of 100% CH_3CN, and finally dried at 37°C for 1 h. Eight microliters of a trypsin solution (Sequencing Grade Modified Trypsin, Promega, Madison, WI, USA), at a concentration of 0.0125 μg/μL in 25 mM NH_4HCO_3, was added to every spot. Digestion was performed overnight at 37°C and was stopped by addition of 0.1% TFA. Resulting fragments were extracted twice with 50 μL ACN/water (1:1, v/v) containing 0.1% TFA for 15 min. Pooled supernatants were concentrated with a speedvac to a final volume of ca 20 μL.

2.7 MALDI-TOF MS analysis

For the direct identification of protein, peptides were simultaneously desalted and concentrated with C18 Zip-Tip microcolumns to a final volume of 3 μL. An aliquot of each sample was mixed (1/1) with the CHCA matrix at half saturation in ACN/water (1:1, v/v) and the mixture was immediately spotted on the MALDI target. For the analysis of phosphorylations, protein digests were diluted in loading buffer (80% ACN, 5% TFA) [18], and loaded on TiO_2 home-made microcolumns as described previously [19, 20]. After two washing steps with 10 μL loading buffer and 60 μL buffer 2 (80% ACN,

1% TFA), phosphopeptides were eluted using 2 μL NH_4OH, pH 12 directly onto the MALDI target, then mixed with 1 μL of DHB matrix (20 g/L) in acetonitrile, water, and phosphoric acid (50/44/6). In order to identify the proteins, the flow through of the TiO_2 microcolumns was dried, resuspended in 2 μL of DHB matrix, and spotted onto the MALDI target.

All mass spectra were recorded in the reflector mode on an UltraFlex II MALDI-TOF/TOF mass spectrometer (Bruker Daltonics, Bremen, Germany). Automatic annotation of monoisotopic masses was performed using Bruker's SNAP™ procedure. Protein identification was achieved using the Mascot search engine (v. 2.2.04; Matrix Science, London, UK) to query locally the UniProt-SwissProt database (release July 2011). For PMF identification, the following parameters were used: *Homo sapiens* for the taxonomy, 100 ppm mass accuracy in MS, trypsin as enzyme, one missed cleavage allowed, carbamidomethylation of Cystein as fixed modification and acetylation of N-term protein, deamidation of N or Q, and oxidation of Methionines as variable modification. For the analysis of protein modifications (PMF and MS/MS), mass accuracy was set to 0.5 Da in MS/MS and the following variable modifications were allowed: acetylation of lysines, Pyro-Glutamylation of N-term E or Q, and methylation of D or E. In PMF, protein was validated once they showed identity with *p*-value <0.05. After MS/MS, peptides were validated once they showed identity or extensive homology (p <0.05) or manually checked for validation and assignment of modified sites.

2.8 Nano LC-MS/MS analysis

When low-abundant spots could not be identified by PMF, LC-MS/MS analysis was conducted. The sample preparation was done as above and protein digests were analyzed using a High Capacity ion trap mass spectrometer (Esquire HCT; Bruker Daltonik), interfaced with a nano-HPLC Chip-Cube system (Agilent Technologies, Santa Clara, USA). The chips contained both the precolumn and the column (Zorbax 300SB-C18; Agilent Technologies). Samples were first loaded onto the 4 mm enrichment cartridge at a flow rate of 4 μL/min using 0.1% formic acid. After preconcentration, peptides were separated on the column (75 μm diameter, 43 mm length) at a flow rate of 0.3 μL/min using a 15 min linear gradient from 3% to 80% acetonitrile in 0.1% formic acid, and eluted into the mass spectrometer. A capillary voltage of 1.8–2.1 kV in the positive ion mode was used together with a dry gas flow rate of 4.5 L/min at 250°C. A first full-scan mass spectrum was measured in the 310 m/z to 1800 m/z range, followed by a second scan at higher resolution to measure precisely the mass of the three major ions in the previous scan. Finally, a third scan was performed to acquire the collision-induced MS/MS spectra of the selected ions. MS/MS raw data were analyzed using Data Analysis software (Bruker Daltonik) to generate the peak lists. The UniProt-SwissProt database (release July 2011) database was queried locally using the Mascot search engine (v. 2.2.04; Matrix Science) and the following parameters: *H. sapiens* for the taxonomy, mass accuracy of 0.6 Da in MS and MS/MS, trypsin as enzyme, one missed cleavage allowed, carbamidomethylation of Cystein as fixed modification and acetylation of N-term protein, deamidation of N or Q, and oxidation of Methionine as variable modifications. Proteins were validated once they showed at least one peptide with identity or extensive homology (p <0.05).

2.9 1D and 2D Western blotting analysis

For 1D Western blotting analysis, prestained standards (See Blue 2, Invitrogen) and protein samples were separated by NuPAGE Novex Bis-Tris gels with MOPS (3-(N-morpholino) propane sulfonic acid) SDS running buffer on 4–12% separating gels (Invitrogen). For 2D Western blotting analysis, proteins were separated as previously described in the Section 2.4, with some technical adjustments. Briefly, 20 μg of protein was first separated with 7 cm pI 3–10 NL precast strips (GE Healthcare) and then separated on a 12% acrylamide SDS-polyacrylamide gel, using the Protean 3 electrophoresis unit (Bio-Rad). Following 1D or 2D gel separation, proteins were transferred onto PVDF membrane (GE Healthcare) and blocked with 5% skim milk powder in TBS-T (150 mM NaCl, 10 mM Tris-HCl pH 8, 0.05% Tween-20) for 45 min at 20°C. Blots were incubated with anti-CyPA antibody (1:1000, ref 07–313, Millipore) in TBS-T with 1% skim milk powder overnight at 4°C and were washed 3× for 10 min with TBS-T. The blots were then incubated with secondary antibodies: HRP-conjugated goat antirabbit antibody (1:10 000, GE Healthcare) in TBS-T with 1% skim milk powder for 45 min at 20°C and were washed with TBS-T. Blots were treated with ECL EZ chemiluminescence reagent (ATGC) for 1 min before exposure to Hyperfilms (GE Healthcare) from 1 to 2 min. Films were developed and scanned as JPEGs using a GS 800 Bio-Rad scanner.

2.10 RNA extraction and quantitative real-time RT-PCR

RNA extraction was performed as previously described [15] by Taqman assays (Applied Biosystems, France). The primers: Hs99999904_m1 (CyPA), Hs99999905_m1 (GAPDH), and Hs99999903_m1 (ACTG1/beta-actin) were from Applied Biosciences. Gene expression was estimated as previously described [15].

3 Results and discussion

3.1 Proteomic comparison between conditioned media and control samples

To analyse T47D conditioned medium of irradiated cells, the choice of protein extraction and control samples was fundamental. To explore this proteome, we employed the TCA–NLS protein precipitation protocol by Chevallet et al. [2] for the enrichment of secreted proteins in conditioned medium from control or irradiated T47D cells. This protocol appears to reproducibly provide high recovery rates while maintaining compatibility with 2DE analysis.

To investigate the characteristic secretome of cells following irradiation, conditioned media were analyzed by 2DE in 3–10 nonlinear pH gradient strips. Special care was given to limit contamination by cellular proteins and serum albumin. Indeed, conditioned media were collected during the last 18 h of growth period, when cell were grown with SFM (Fig. 1). Media with secreted proteins were collected and submitted to a centrifugation step before protein precipitation to reduce contamination by floating cells or cell debris. In addition, to demonstrate specificity of findings, respective total and cytosolic cell extracts were analyzed in parallel as proposed previously [21] to limit false positive secreted proteins.

Two-dimensional gel analysis was performed with adequate control samples to highlight specifically secreted proteins following cell irradiation. In a first time, gel pictures of conditioned medium from irradiated cells (Si) were compared with gel pictures of conditioned medium from control cells (Sc) and spots significantly modulated were correspondingly tagged. The same analyses were performed independently with gels of total extract proteins from irradiated cells (Ti) compared with gels of total extract proteins from control cells (Tc); or gels of cytoplasmic extract proteins from irradiated cells (Ci) compared with gels of cytoplasmic extract proteins from control cells (Cc). A set of spots tagged as modulated by cell irradiation on secreted samples was extracted. On this basis, spots specifically modulated in secreted samples were highlighted, and spots common between secreted and total or cytosolic fractions were speculated to come from total cell or cytosolic protein contamination of secretome.

Approximately 1000 distinct protein spots were detected on each of the silver-stained gels, for a total of 1447 spots. The overall spot pattern derived from total protein extract and cytosolic extract of T47D-control cells was very similar. A careful examination of replicate gels for both group samples revealed some significant differences between total extract samples (Tc vs. Ti) and between cytosolic samples (Cc vs. Ci) with 233 spots and 122 spots modulated, respectively. But such differentially expressed spots were used as false positive when differences were shared with the comparison between conditioned medium samples (Sc vs. Si). All differentially expressed spots were grouped as a function of analyzed samples and were visualized using a Venn diagram (Fig. 2).

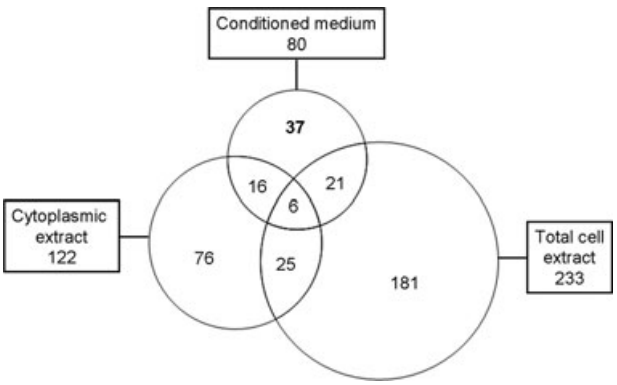

Figure 2. Venn diagram of spots differentially expressed in response to irradiation of T47D cells in conditioned media (Sc vs. Si), cytoplasmic extracts (Cc vs. Ci), and total cell extracts (Tc vs. Ti). Spots in bold were selected as specific.

According to the global analysis of 1447 spots, 80 spots (5.5%) were differentially expressed ($p < 0.05$) between secreted samples of controls and irradiated cells. Among these modulated spots, 37 spots (4.7%) were finally selected as specifically differentially expressed in conditioned medium (Fig. 2). Indeed, more than half of spots were eliminated from the analysis as possible contamination, because they were as well differentially expressed with total extract analysis (Tc vs. Ti) and cytosolic extract analysis (Cc vs. Ci).

Preparative gels, stained with Coomassie blue, were finally performed and 24 spots were effectively visible, picked off, and analyzed using MS (Table 1). From these, 19 spots were over-expressed in Si samples and five over-expressed in Sc samples.

According to MS identification, modulated spots were related to 17 distinct protein accessions. The gel location of these spots was depicted (Fig. 3).

Spots 51 and 101 were increased in Sc samples and corresponded to bovine destrin and BSA. As T47D cells derived from a human ductal breast epithelial tumor, these bovine proteins were considered without any doubt as a contamination from FCS used for in vitro cell growth. Additionally, serum albumin is well known to be a highly cell-sticky and abundant serum protein, and very difficult to eliminate completely. According to our protocol to generate conditioned media, cells were washed three times with PBS before a short growth period without serum to remove as much as possible of such serum protein. Nevertheless, some proteins of bovine origin remained, these contaminant spots were highlighted by MS. When asking databases for protein identification, "mammalia" or "all entries" were selected as taxonomy parameter to include contaminant proteins from others species as well as human proteins from the cell line.

Spots 23, 72, 106, and 113, corresponding to pyruvate kinase isozymes M1/M2, cofilin-1, calreticulin, and ribonucleoprotein K were observed as over-expressed in Sc samples. These proteins were not described as secreted, but belonged

Table 1. Proteins modulated in T47D cells following irradiation

Spot	Protein name[a)]	Si/Sc[b)]	Fold	ANOVA (p)	q value	Power	Identification score[c)]	Accession	Matched peptides	% coverage	Theoric pI	Observed pI	Theoric MW	Observed MW
2	Coatomer protein complex	Si	4.3	3.07×10^{-06}	1.62×10^{-04}	1.00	66	P61923	1	5	4.8	4.4	20.3	19.3
5	Cellular retinoic acid-binding protein 2	Si	3.6	6.00×10^{-06}	2.08×10^{-04}	1.00	133	P29373	4	28	5.4	6.5	15.7	14.4
6	Gamma-glutamyl-cyclotransferase	Si	3.4	5.08×10^{-08}	3.18×10^{-05}	1.00	324	O75223	6	33	8.5	4.5	12.9	21
8	TRAPPC3	Si	3	3.64×10^{-06}	1.62×10^{-04}	1.00	41	O43617	1	4	4.85	4.5	20.2	18.3
11	Myosin regulatory light chain 12B	Si	2.9	3.62×10^{-06}	1.62×10^{-04}	1.00	157	O14950	3	18	4.69	4.4	19.6	18.1
18	26S proteasome non-ATPase regulatory subunit 10	Si	2.6	1.65×10^{-06}	1.03×10^{-04}	1.00	55	O75832	1	3	5.7	7.1	24.4	24.4
19	Cyclophilin A	Si	2.5	5.95×10^{-04}	2.32×10^{-03}	0.99	108*	P62937	13	66	7.7	6.7	18	15.8
21	Gamma-glutamyl-cyclotransferase	Si	2.5	3.02×10^{-04}	1.45×10^{-03}	1.00	271	O75223	5	28	5.1	4.5	21.0	21
23	Pyruvate kinase isozymes M1/M2	Sc	2.4	3.34×10^{-04}	1.59×10^{-03}	1.00	178	P14618	4	8	7.95	6.4	57.8	64.4
28	Proteasome subunit beta type-2	Si	2.3	4.84×10^{-04}	2.09×10^{-03}	1.00	54	P49721	1	4	6.2	6.1	22.3	23.4
32	60S acidic ribosomal protein P0	Si	2.1	1.26×10^{-03}	3.83×10^{-03}	0.98	303	Q8NHW5	7	23	5.7	6.2	34.3	36
38	Glutathione S-transferase Mu 2	Si	2	1.88×10^{-05}	3.39×10^{-04}	1.00	115	Q03013	2	11	6	7	25.7	25.2
51	Destrin (bovine)	Sc	1.8	4.08×10^{-03}	8.83×10^{-03}	0.91	133	P60981	5	21	8.1	7.6	18.5	17.3
72	Cofilin-1	Sc	1.6	1.90×10^{-03}	4.92×10^{-03}	0.96	84*	P23528	8	51	8.2	7.2	18.5	17.5
84	Triosephosphate isomerase	Si	1.5	8.34×10^{-07}	7.26×10^{-05}	1.00	147*	P60174	15	72	6.5	7	26.6	26.3
87	Cellular retinoic acid-binding protein 2	Si	1.5	5.20×10^{-03}	1.03×10^{-02}	0.89	133	P29373	4	28	5.4	5.4	15.6	14.9
89	Cyclophilin A	Si	1.5	2.86×10^{-02}	3.64×10^{-02}	0.84	136*	P62937	17	78	7.7	7.4	18	16.5
92	Cyclophilin A	Si	1.5	7.44×10^{-06}	2.15×10^{-04}	1.00	137*	P62937	17	78	7.7	6.7	18	16.5
97	Cyclophilin A	Si	1.4	2.87×10^{-03}	6.22×10^{-03}	0.94	127*	P62937	14	71	7.7	6.1	18	16.6
101	Serum albumin (bovine)	Sc	1.4	9.16×10^{-04}	3.17×10^{-03}	0.99	161	P02768	4	5	5.7	6	66.5	74
106	Calreticulin variant	Sc	1.3	1.77×10^{-03}	4.78×10^{-03}	0.97	89*	Q53G71	17	52	4.3	4.1	46.9	76.3
113	Heterogeneous nuclear ribonucleoprotein K	Sc	1.6	8.96×10^{-05}	6.98×10^{-04}	1.00	469	P61978	9	21	5.2	4.9	51	68.6
132	Protein DJ-1	Si	1.4	7.68×10^{-05}	6.31×10^{-04}	1.00	248	Q99497	7	31	6.3	5.8	19.9	23.9
159	Cyclophilin A	Si	1.4	4.22×10^{-03}	9.13×10^{-03}	0.91	159*	P62938	20	86	7.7	7.2	18	16.5

ANOVA, q value, and power were obtained from image analysis with the Samespots software using the statistical package. The observed MW and pI of the differentially expressed protein spots and the theoretical values of identified proteins are also listed

a) For each spot, only the protein with the highest score is shown.

b) Si: Spots increased in the conditioned media of irradiated cells, Sc: spots increased in the conditioned media of control (nonirradiated) cells.

c) Scores with asterisks (*) referred to PMF MALDI-TOF identification of proteins; scores without asterisks referred to low-abundant spots, identified with nano-LC-MS/MS.

to structural or cellular metabolism protein families on subcellular compartments and could be release through secretion of exosomes [22, 23].

The 18 other spots appeared as specifically over-expressed in Si samples. According to the ExPASy Proteomics Server (http://expasy.org/sprot/), most of the identified proteins were situated in the cytoplasm and/or extra-cellular compartments. Of course, many proteins were counted in more than one cellular compartment. For example, cellular retinoic acid-binding protein 2 is described as involved in the transports of retinoic acid from the cytoplasm to the nucleus. Upon ligand binding, a conformation change exposes a nuclear localization motif and the protein is transported into the nucleus.

Several proteins described as cytoplasmic were involved in intracellular bio-molecule transport (coatomer protein complex; cellular retinoic acid-binding protein 2), in glutathione biosynthetic process (gamma-glutamylcyclotransferase), in intracellular signal transduction (glutathione S-transferase Mu 2; PAK 2, triosephosphate isomerase), in intracellular chaperone or oxidative stress defence (DJ1), and in extracellular signal transduction (CyPA).

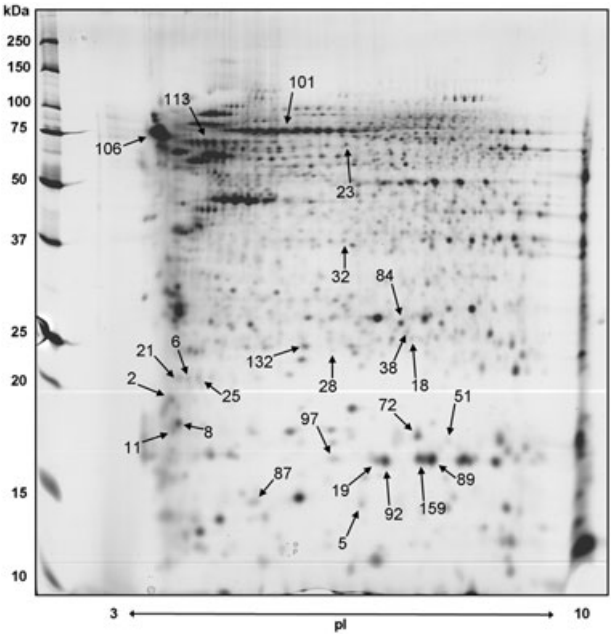

Figure 3. 2DE of proteins from conditioned media of irradiated T47D cells. Fifty micrograms proteins were separated using 18-cm pH 3–10 pI range strips for the first dimension, and 12% acrylamide gels for the second dimension. Spots differentially expressed in response to irradiated treatment as indicated by arrows and identified by mass spectrometry (Table 1).

3.2 Comparison of spots identified as CyPA in conditioned media

We decided to focus our interest and perform further protein validation on CyPA. This later was previously described as secreted by colorectal cancer cells using a gel-based secretomic strategy [24] and by breast tumor using a capillary ultrafiltration probe implanted into the central part of tumor [25].

According to picture analysis of secreted, total, and cytosolic extracts, five spots isoforms of CyPA were identified as specifically over-expressed in the secretome of irradiated cells (Fig. 4). These spots were not modulated following cell irradiation in total protein extract (Tc vs. Ti) and in cytosolic extracts (Cc vs. Ci), but were systematically increased in conditioned media of irradiated cells (Fig. 4A and B).

CyPA is an abundant intracellular protein, considered to be the main target of the immunosuppressive drug cyclosporine A [26]; but it is as well secreted from smooth muscle cells, head, and neck cancer cell line [27] and macrophages in response to oxidative stress and lipopolysaccharide, suggesting a cytokine role for CyPA in inflammation and stress response [28]. Moreover, the protein was previously described for being involved in proliferation rate of stem and progenitor cells in mouse subventricular zone after IR [29]. Consequently, further experiments were performed with this protein and CyPA levels were estimated by Western blotting using conditioned media.

The differential expression of CyPA was further confirmed by 1D and 2D Western blot analysis (Figs. 4C and 5A). According to the 1D Western blotting signal intensity, (Fig. 5A), a band near 14 kDa, corresponding to CyPA appeared upregulated 1.8 times in Si. Using total cell extract as reference, a faint contamination of conditioned media with cytosolic proteins was observed using actin antibody against secreted proteins (Fig. 5A). It was interesting to observe that cytosolic contamination was almost stable between control and irradiated samples, showing the secretion specificity of CyPA and the relevance of protein modulation in conditioned media following irradiation.

A 2DE–Western blotting analysis was performed too with secretory samples to estimate the differential over-expression of CyPA spot isoforms (Fig. 4C). In agreement with 1D Western blotting, the spots over-expressed in Si samples (spots 19, 89, 92, 97, and 159) and identified by MS as CyPA following the secretomic analysis were all observed over-expressed in Si according to the 2D Western blotting analysis. Additionally, new spots recognized by the CyPA antibody appeared at the same molecular weight (spots 139 and 140), but their amount was not modulated by irradiation according to picture analysis of secreted samples. As these spots appeared to be at the same molecular weights of others CyPA spots, they were likely more alkaline CyPA spots isoforms. It is interesting to observe that in one hand, the level of most acidic isoforms of CyPA was the most increased by irradiation treatment, and in the other hand, the level of the most alkaline isoforms of CyPA was not influenced by treatment (Fig. 4C).

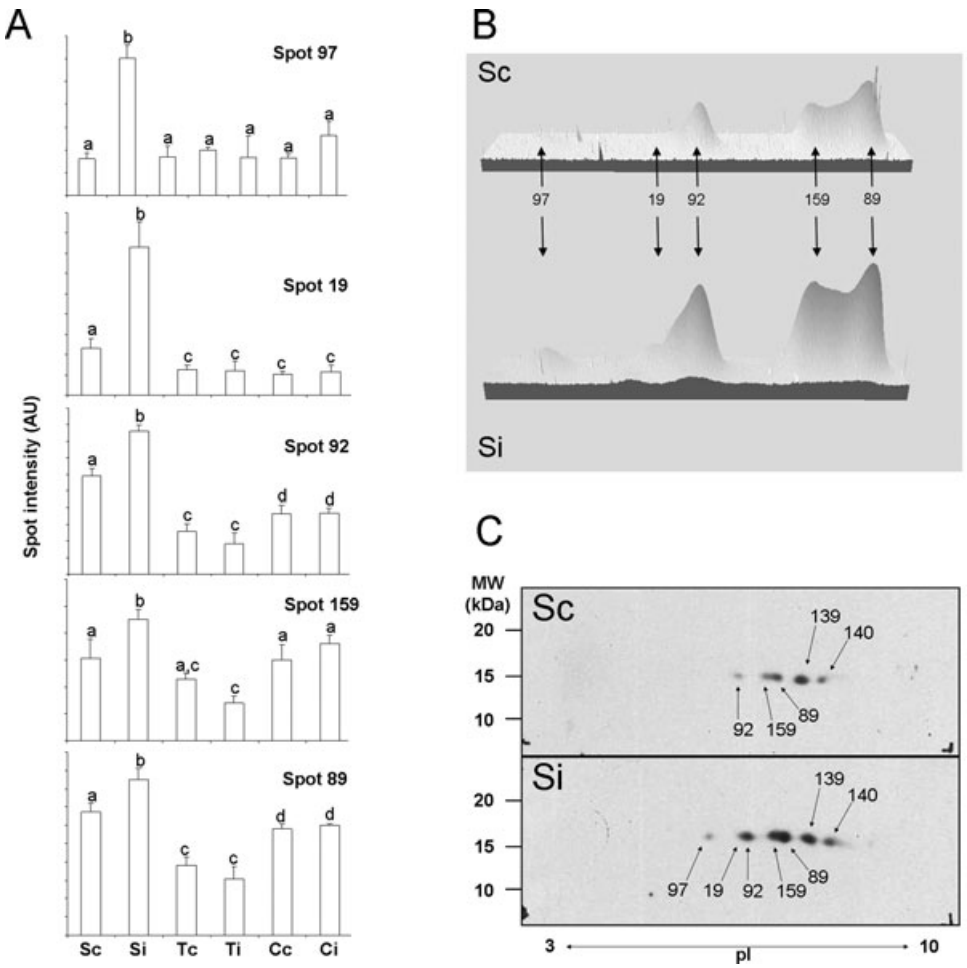

Figure 4. Quantitative comparison of spots 19, 89, 92, 97, and 159, identified as cyclophilin A; (A) amounts in conditioned medium of control cells (Sc), conditioned medium of irradiated cells (Si), total protein extract of control cells (Tc), total protein extract of irradiated cells (Ti), cytoplasmic protein extract of control cells (Cc), and cytoplasmic protein extract of irradiated cells (Ci). Letters represent significantly different groups ($p < 0.05$) on basis of spot intensity; (B) three-dimensional view of spots in Sc (top) and Si (bottom); (C) 2D Western blotting analysis of CyPA, using 7-cm pH 3–10 p*I* range strips for the first dimension, and 12% acrylamide gels for the second dimension.

3.3 CyPA displayed a complex pattern of PTMs

CyPA was described with a lot of potential post-translational modifications. Seven potential N6-acetyllysine were proposed on amino acids 28, 44, 49, 76, 82, 125, and 131 [30]. By similarity, one phosphoserine (position 21) and one phosphothreonine (position 157) were suggested too [31].

Phosphorylations were researched on spots 139 and 159, identified as CyPA and corresponding to respectively unaffected and increased isoforms following irradiation (Fig. 4C) using a titanium dioxide enrichment strategy. No phosphorylated peptide was observed in the binding fraction, but the analysis of the flow through fraction revealed a complex pattern of maturation and post-translational modifications. Indeed, an alternating removal of N-terminal methionine was observed (Supporting Information Table S1). This N-terminal amino acid was detected as partially acetylated (acetyl N-term–Met or acetyl N-term–Val). Moreover, several lysine acetylation (four locations) and methylations of acidic groups (eight locations) were observed for the first time. Most of these forms were validated with MALDI-TOF/TOF MS/MS peptide fragmentation (Supporting Information data).

The initiator amino acid is not systematically processed by methionine aminopeptidase but it depends of the penultimate amino acid [32]. For example, the initiator methionine was cleaved when the penultimate amino acid was serine or alanine, but in contrast, when valine was in such position, the initiator methionine was not systematically removed [33]. In our case, the penultimate amino acid is a valine and we demonstrated the presence of both species (with or without the initiator methionine), in association with acetyl N-terminal modification.

Acetylations and methylations, in association with an alternative removal of initiator methionine, can induce p*I* shifts matching with the 2D spot pattern of CypA (Fig. 3). As at least seven spots were revealed by 2D Western blotting analysis (Fig. 4C), it is likely that a complex combination of such modifications occurred.

Initiator methionine processing and amino acid acetylation/methylation were major modifications of proteins implicated in protein activation and targeting [30]. It can be reasonably hypothesized that CyPA structure/activity was modified by such protein maturation/ post-translational modifications as a consequence of

irradiation treatment, leading to an increased secretion of the protein.

3.4 What is the function of CyPA secretion following cell irradiation?

CyPA is an abundant cytosolic protein, participating in the processes of intracellular protein transport, and acting as an ubiquitinious protein with cis-trans-isomerase activity [34]. Moreover, CyPA participates in the signal transduction from T-cell receptor [35], in regulation of inflammatory responses [36], and is a ligand for cyclosporin A, thus determining its immunosuppressing properties [37, 38]. A recent proteomic study revealed that CyPA could be a potential prognostic factor and therapeutic target in endometrial carcinoma [39]. In our system, the cytosolic form of CyPA was not modulated following irradiation. Indeed, according to 1D Western blotting analysis, CyPA amount was not significantly affected following irradiation, using actin as reference (Fig. 5A). Moreover, an RT-PCR analysis of CyPA mRNA did not show significant variation between control and irradiated proteins (results not shown).

In addition to this well-studied cytosolic form, a secretory form of CyPA also exists. Indeed, activated macrophages were able to secrete this protein into the environment [40]. The secretory form of CyPA has been detected in human milk too [41]. Extracellular CyPA acts as a chemotactic agent regulating the migration of monocytes, neutrophils, eosinophils, and T-cells [42]. This protein possesses immunomodulating activity by stimulation of maturation and antigenic presentation in dendritic cells [43]. Following CyPA secretion in response to inflammatory stimuli, CD147 was described as its surface receptor and as an essential component in the CyPA-initiated signaling cascade that culminates in ERK activation [44] and ERK-induced apoptosis [45].

In our model, we have previously showed that 10-Gy irradiation induced an increased secretion of CyPA (Fig. 5A) and an almost fully inhibition of proliferative capacity with only few cell clones ($\sim 1/10^{-4}$) appearing in culture 3–4 wks after irradiation [15]. To investigate a potential link between CyPA secretion and radiosensitivity phenotype, we have studied the amount of cellular and secreted CyPA from six mammary tumor cell lines displaying various level of radiosensitivity (% of dead cells, 7 days after 10-Gy irradiation). These cell lines were not irradiated, only the basal level of CyPA was estimated and quantification was performed by 1D Western blotting (Fig. 5B). For cellular CyPA expression, no significant variation was observed. In contrast, a strong heterogeneity of expression was observed for secreted CyPA analysis. Spontaneous level of secreted CyPA appeared to be related with intrinsic radiosensitivity of studied cell lines. The highest level of secreted CyPA was observed in MDA-MB-157 cells, i.e. the most radiosensitive cell line. Moreover, the lowest level of expression was observed for the most radioresistant cells (MCF7 and MDA-MB-231) and cells displaying an intermediate radiosensitivity, showed an intermediate amount of secreted CyPA, with the exception of BT20 cells. These results suggest that level of secreted CyPA was related to intrinsic radiosensitivity of mammary cell lines. It is interesting to notice that in accordance with results observed by RT-PCR and 1D Western blotting analysis, the amount of total protein is constant in all the cell lines studied. This could indicate that the level of secreted CyPA was essentially regulated by post-translational mechanisms.

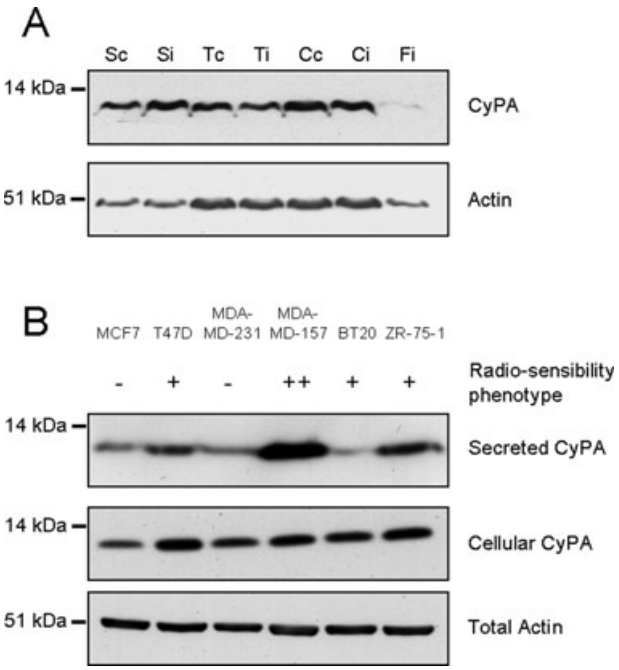

Figure 5. 1D Western blotting analysis of cyclophilin A with actin as loading control; (A) CyPA analysis in conditioned media (S), total cell extract (T), cytosolic extract (C), and floating cells (F), with (i) or without (c) irradiation treatment; (B) secreted and cellular CyPA analysis in several cell lines. (1) MCF7, (2) T47D, (3) MBA-MB-231, (4) MBA-MB-157, (5) BT20, (6) ZR-75-1. The radiosensitivity phenotype is defined according to the percentage of death cells following irradiation treatment: – < 50%; 50% < + < 60%; ++ > 60%.

4 Concluding remarks

In the present study, we used the T47D human breast cancer cells as a model to analyze proteins that are released by the cells following IR treatment. Using high-resolution 2DE, protein differences were observed in conditioned media of irradiated cells using conditioned media of nontreated cells and others intracellular extracts as controls. Several spots of CyPA were observed as up-regulated in conditioned media of irradiated cells. Initiator methionine processing and amino acid acetylation/methylation were identified by MS and can be related to the complex spot pattern of CyPA. Additionally, cells sensible to irradiation displayed an increased level of secreted

CyPA. Taken together, these results showed that this protein could be defined as a cytokine, post-translationally regulated and potentially implicated in the radioinduced apoptotic response in mammary tumor cells. More generally, our results showed the capacity of our approach to select and identify proteins released in conditioned medium, the gel-based proteomic was as usual of a great interest to reveal differences between spots isoforms and discrete modifications of proteomes [3, 46].

This work was supported by the Institute of Cellular and Molecular Radiobiology (DSV, CEA) and the Proteomic Platform of Montpellier-LR Genopole.

The authors have declared no conflict of interest.

5 References

[1] Tjalsma, H., Bolhuis, A., Jongbloed, J. D., Bron, S. et al., Signal peptide-dependent protein transport in *Bacillus subtilis*: a genome-based survey of the secretome. *Microbiol. Mol. Biol. Rev.* 2000, *64*, 515–547.

[2] Chevallet, M., Diemer, H., Van Dorssealer, A., Villiers, C. et al., Toward a better analysis of secreted proteins: the example of the myeloid cells secretome. *Proteomics* 2007, *7*, 1757–1770.

[3] Chevalier, F., Highlights on the capacities of "gel-based" proteomics. *Proteome Sci.* 2010, *8*, 1–10.

[4] Rabilloud, T., Chevallet, M., Luche, S., Lelong, C., Two-dimensional gel electrophoresis in proteomics: past, present and future. *J. Proteomics* 2010, *73*, 2064–2077.

[5] Hirtz, C., Chevalier, F., Centeno, D., Rofidal, V. et al., MS characterization of multiple forms of alpha-amylase in human saliva. *Proteomics* 2005, *5*, 4597–4607.

[6] Dowling, P., Clynes, M., Conditioned media from cell lines: a complementary model to clinical specimens for the discovery of disease-specific biomarkers. *Proteomics* 2011, *11*, 794–804.

[7] Skalnikova, H., Motlik, J., Gadher, S. J., Kovarova, H., Mapping of the secretome of primary isolates of mammalian cells, stem cells and derived cell lines. *Proteomics* 2011, *11*, 691–708.

[8] Gromov, P., Gromova, I., Bunkenborg, J., Cabezon, T. et al., Up-regulated proteins in the fluid bathing the tumour cell microenvironment as potential serological markers for early detection of cancer of the breast. *Mol. Oncol.* 2010, *4*, 65–89.

[9] Sowa Resat, M. B., Morgan, W. F., Radiation-induced genomic instability: a role for secreted soluble factors in communicating the radiation response to non-irradiated cells. *J. Cell. Biochem.* 2004, *92*, 1013–1019.

[10] Watson, G. E., Lorimore, S. A., Macdonald, D. A., Wright, E. G., Chromosomal instability in unirradiated cells induced in vivo by a bystander effect of ionizing radiation. *Cancer Res.* 2000, *60*, 5608–5611.

[11] Xue, L. Y., Butler, N. J., Makrigiorgos, G. M., Adelstein, S. J. et al., Bystander effect produced by radiolabeled tumor cells in vivo. *Proc. Natl. Acad. Sci. USA* 2002, *99*, 13765–13770.

[12] Roninson, I. B., Broude, E. V., Chang, B.-D., If not apoptosis, then what? Treatment-induced senescence and mitotic catastrophe in tumor cells. *Drug Resistance Updates* 2001, *4*, 303–313.

[13] Hei, T. K., Zhou, H., Chai, Y., Ponnaiya, B. et al., Radiation induced non-targeted response: mechanism and potential clinical implications. *Curr. Mol. Pharmacol.* 2011, *4,* 96–105.

[14] Shao, C., Folkard, M., Prise, K. M., Role of TGF-beta1 and nitric oxide in the bystander response of irradiated glioma cells. *Oncogene* 2008, *27*, 434–440.

[15] Luce, A., Courtin, A., Levalois, C., Altmeyer-Morel, S. et al., Death receptor pathways mediate targeted and non-targeted effects of ionizing radiations in breast cancer cells. *Carcinogenesis* 2009, *30*, 432–439.

[16] Chevalier, F., Martin, O., Rofidal, V., Devauchelle, A. D. et al., Proteomic investigation of natural variation between Arabidopsis ecotypes. *Proteomics* 2004, *4*, 1372–1381.

[17] Chevalier, F., Centeno, D., Rofidal, V., Tauzin, M. et al., Different impact of staining procedures using visible stains and fluorescent dyes for large-scale investigation of proteomes by MALDI-TOF mass spectrometry. *J. Proteome Res.* 2006, *5*, 512–520.

[18] Imanishi, S. Y., Kochin, V., Ferraris, S. E., de Thonel, A. et al., Reference-facilitated phosphoproteomics: fast and reliable phosphopeptide validation by microLC-ESI-Q-TOF MS/MS. *Mol. Cell Proteomics* 2007, *6*, 1380–1391.

[19] Hem, S., Rofidal, V., Sommerer, N., Rossignol, M., Novel subsets of the Arabidopsis plasmalemma phosphoproteome identify phosphorylation sites in secondary active transporters. *Biochem. Biophys. Res. Commun.* 2007, *363*, 375–380.

[20] Larsen, M. R., Thingholm, T. E., Jensen, O. N., Roepstorff, P. et al., Highly selective enrichment of phosphorylated peptides from peptide mixtures using titanium dioxide microcolumns. *Mol. Cell Proteomics* 2005, *4*, 873–886.

[21] Zwickl, H., Traxler, E., Staettner, S., Parzefall, W. et al., A novel technique to specifically analyze the secretome of cells and tissues. *Electrophoresis* 2005, *26*, 2779–2785.

[22] Volmer, M. W., Stühler, K., Zapatka, M., Schöneck, A. et al., Differential proteome analysis of conditioned media to detect Smad4 regulated secreted biomarkers in colon cancer. *Proteomics* 2005, *5*, 2587–2601.

[23] Raimondo, F., Morosi, L., Chinello, C., Magni, F. et al., Advances in membranous vesicle and exosome proteomics improving biological understanding and biomarker discovery. *Proteomics* 2011, *11*, 709–720.

[24] Diehl, H. C., Stühler, K., Klein-Scory, S., Volmer, M. W. et al., A catalogue of proteins released by colorectal cancer cells in vitro as an alternative source for biomarker discovery. *Proteomics – Clin. Appl.* 2007, *1*, 47–61.

[25] Chen, S.-T., Pan, T.-L., Juan, H.-F., Chen, T.-Y. et al., Breast tumor microenvironment: proteomics highlights the treatments targeting secretome. *J. Proteome Res.* 2008, *7*, 1379–1387.

[26] Obchoei, S., Wongkhan, S., Wongkham, C., Li, M. et al., Cyclophilin A: potential functions and therapeutic target

for human cancer. *Med. Sci. Monit* 2009, *15*, RA221–RA232.

[27] Ralhan, R., Masui, O., DeSouza, L. V., Matta, A. et al., Identification of proteins secreted by head and neck cancer cell lines using LC-MS/MS: strategy for discovery of candidate serological biomarkers. *Proteomics* 2011, *11*, 2363–2376.

[28] Jin, Z.-G., Lungu, A. O., Xie, L., Wang, M. et al., Cyclophilin A is a proinflammatory cytokine that activates endothelial cells. *Arterioscler. Thromb. Vasc. Biol* 2004, *24*, 1186–1191.

[29] Osato, K., Sato, Y., Ochiishi, T., Osato, A. et al., Apoptosis-inducing factor deficiency decreases the proliferation rate and protects the subventricular zone against ionizing radiation. *Cell Death Dis.* 2010, *1*, e84.

[30] Choudhary, C., Kumar, C., Gnad, F., Nielsen, M. L. et al., Lysine acetylation targets protein complexes and co-regulates major cellular functions. *Science* 2009, *325*, 834–840.

[31] Gevaert, K., Staes, A., Van Damme, J., De Groot, S. et al., Global phosphoproteome analysis on human HepG2 hepatocytes using reversed-phase diagonal LC. *Proteomics* 2005, *5*, 3589–3599.

[32] Link, A. J., Robison, K., Church, G. M., Comparing the predicted and observed properties of proteins encoded in the genome of *Escherichia coli* K-12. *Electrophoresis* 1997, *18*, 1259–1313.

[33] Frottin, F., Martinez, A., Peynot, P., Mitra, S. et al., The proteomics of N-terminal methionine cleavage. *Mol. Cell. Proteomics* 2006, *5*, 2336–2349.

[34] Fischer, G., Bang, H., Mech, C., Determination of enzymatic catalysis for the cis-trans-isomerization of peptide binding in proline-containing peptides. *Biomed. Biochim. Acta.* 1984, *43*, 1101–1111.

[35] Colgan, J., Asmal, M., Neagu, M., Yu, B. et al., Cyclophilin A regulates TCR signal strength in CD4+ T cells via a proline-directed conformational switch in Itk. *Immunity* 2004, *21*, 189–201.

[36] Arora, K., Gwinn, W. M., Bower, M. A., Watson, A. et al., Extracellular cyclophilins contribute to the regulation of inflammatory responses. *J. Immunol.* 2005, *175*, 517–522.

[37] Fruman, D. A., Burakoff, S. J., Bierer, B. E., Immunophilins in protein folding and immunosuppression. *FASEB J.* 1994, *8*, 391–400.

[38] Colgan, J., Asmal, M., Yu, B., Luban, J., Cyclophilin A-deficient mice are resistant to immunosuppression by cyclosporine. *J. Immunol.* 2005, *174*, 6030–6038.

[39] Li, Z., Zhao, X., Bai, S., Wang, Z. et al., Proteomics identification of cyclophilin A as a potential prognostic factor and therapeutic target in endometrial carcinoma. *Mol. Cell. Proteomics* 2008, *7*, 1810–1823.

[40] Sherry, B., Yarlett, N., Strupp, A., Cerami, A., Identification of cyclophilin as a proinflammatory secretory product of lipopolysaccharide-activated macrophages. *Proc. Natl. Acad. Sci. USA* 1992, *89*, 3511–3515.

[41] Spik, G., Haendler, B., Delmas, O., Mariller, C. et al., A novel secreted cyclophilin-like protein (SCYLP). *J. Biol. Chem.* 1991, *266*, 10735–10738.

[42] Xu, Q., Leiva, M. C., Fischkoff, S. A., Handschumacher, R. E. et al., Leukocyte chemotactic activity of cyclophilin. *J. Biol. Chem.* 1992, *267*, 11968–11971.

[43] Bharadwaj, U., Zhang, R., Yang, H., Li, M. et al., Effects of cyclophilin A on myeloblastic cell line KG-1 derived dendritic like cells (DLC) through p38 MAP kinase activation. *J. Surg. Res.* 2005, *127*, 29–38.

[44] Yurchenko, V., Zybarth, G., O'Connor, M., Dai, W. W. et al., Active site residues of cyclophilin A are crucial for its signaling activity via CD147. *J. Biol. Chem.* 2002, *277*, 22959–22965.

[45] Zhuang, S., Schnellmann, R. G., A death-promoting role for extracellular signal-regulated kinase. *J. Pharmacol. Exp. Ther.* 2006, *319*, 991–997.

[46] Rabilloud, T., Vaezzadeh, A. R., Potier, N., Lelong, C. et al., Power and limitations of electrophoretic separations in proteomics strategies. *Mass. Spectrom. Rev.* 2009, *28*, 816–843.

2.2 - Chercheur en radiobiologie au LARIA

En juillet 2013, j'ai rejoint le LARIA, le Laboratoire d'Accueil et de Recherche avec les Ions Accélérés, situé à Caen, sur le site de l'INB du GANIL (Grand Accélérateur National d'Ions Lourds).
Le LARIA, dirigé par Jean-Louis Lefaix, étudie depuis plusieurs années les effets des radiations ionisantes de types photons ou hadrons sur les tissus sains, et plus particulièrement sur le cartilage.
En effet, le laboratoire a choisi de développer un modèle en 3D de cartilage sain, associé et comparé au chondrosarcome, tumeur en première ligne pour l'hadronthérapie ions carbone.

Le cartilage est un tissu naturellement hypoxique car non vascularisé. Le chondrosarcome, qui représente 20% des tumeurs primitives de l'os, est une tumeur chimio- et radiorésistante du cartilage, et l'origine de cette résistance, hors hypoxie, est encore aujourd'hui mal connue.
L'alternative à la chirurgie extensive toujours invalidante pour le patient est la radiothérapie par protons ou ions carbone afin d'allier efficacités balistique et thérapeutique à une tolérance raisonnable du traitement pour le patient.

Le LARIA étudie les réponses des chondrocytes humains sains et tumoraux aux radiations ionisantes, en prenant en compte leur microenvironnement, c'est-à-dire dans un modèle de culture en trois dimensions en biomatériaux (3D) dans des conditions de physioxie au plus proche de la réalité biologique (~3 à 5% d'oxygène).
Afin de reproduire les conditions de physioxie cellulaire, les cellules sont, d'une part, irradiées en culture 2D en condition de physioxie naturelle *in vivo* (~3% O2) comme références internes, puis en culture 3D en éponge de collagène de type I dans ces mêmes conditions de physioxie. Ce modèle de culture en 3D permet de restituer *in vitro* le micro-environnement naturel des cellules et de conserver leurs capacités de différenciation (chondrocyte vers l'ostéocyte et cellules souches mésenchymateuses (CSMs) vers les chondrocyte ou les ostéocytes).

Deux principaux axes de recherche sont développés au LARIA :

- l'analyse des effets directs des rayonnements ionisants (rayons X et ions lourds) sur le modèle 3D de cartilage sain ou tumoral
- l'étude des effets indirects de type bystander des rayonnements ionisants (rayons X et ions lourds) sur le modèle 3D de cartilage sain ou tumoral

Dans ce contexte, et en accord avec le responsable du laboratoire, j'ai choisi de travailler sur ce deuxième axe de recherche, sur l'étude d'un effet bystander radio-induit en utilisant des irradiations par rayons X et ions lourds sur le modèle 3D de cartilage.

Le projet de recherche correspondant à cet axe thématique est développé dans le prochain chapitre.

3 - Projet de Recherche

Avant-propos

Ce projet de recherche fait partie intégrante d'une des thématiques principales du LARIA sur l'analyse des effets indirects des ions accélérés.

Ce projet est structuré en relation avec la mise en place du projet ARCHADE dans lequel notre équipe sera impliquée dans la recherche en radiobiologie. Ce projet tient compte des thématiques scientifiques qui seront liées directement à ce centre de traitement, mais aussi du calendrier de sa mise en place et de la fonctionnalité des deux systèmes de traitement et de recherche qui y seront installés. Dans un premier temps, le S2C2, un appareil de traitement par proton-thérapie, sera mis en place et fonctionnel dès 2017, puis le C400, un prototype de machine dédiée à la recherche en physique, clinique, radiobiologie et produisant des faisceaux de protons et d'ions carbone à partir de 2020.

De plus, dans le cadre de la rédaction de ce projet, une partie de la réflexion sur la place de l'analyse protéomique dans ce contexte de recherche a été valorisée sous forme d'un article de revue, publié dans « Mutation Research : Reviews in Mutation Research ». Pour plus de clarté et pour éviter les redondances, cet article est inséré en texte intégral dans ce projet, après la page 152.

3.1 - Contexte

3.1.1 - Radiobiologie des hadrons dans ARCHADE

Pour préparer la mise en place dans les mois prochains d'ARCHADE (Advanced Resource Centre for Hadrontherapy in Europe), centre européen de protonthérapie et de recherche en hadronthérapie par ions carbone [4,5], basé à Caen sur le site du GANIL (Fig. 1), le LARIA a développé depuis de nombreuses années des thématiques de recherche en lien direct avec la radiobiologie des hadrons. Nous proposons, en particulier, d'étudier l'existence d'un effet « bystander » radio-induit ou RIBE (Radiation-Induced Bystander Effect) lors de radiothérapie conventionnelle (photons) ou d'hadronthérapie (radiothérapie par protons et ions carbone) dont le développement est récent et qui constitue l'une des solutions du futur pour le traitement de certains cancers inopérables, radio-résistants ou chimio-résistants.

Figure 1 : Vue perspective prévue du bâtiment ARCHADE (en haut) et localisation d'ARCHADE sur le site du GANIL (en bas).

3.1.2 - De l'intérêt des ions accélérés en radiothérapie

Le physicien américain Robert Wilson proposa dès 1946 de remplacer les rayons x par des faisceaux d'ions rapides. Il pensait améliorer la balistique de la méthode (le ciblage de la zone visée) et atteindre ainsi certaines tumeurs résistant aux rayons X.
Aujourd'hui, plus de 60 ans après cette première expérience, on sait détruire des tumeurs à l'aide d'ions accélérés. Cette technique – l'hadronthérapie – est déjà utilisée en clinique dans plusieurs centres de cancérologie soit avec des ions carbone, au Japon et en Allemagne, soit avec des protons dans un plus grand nombre de pays dont les États-Unis et la France.
En plus d'une meilleure balistique (précision), les ions accélérés permettent un dépôt de dose plus localisé dans la profondeur que les rayons X. En effet, la propriété pour des particules, comme les protons ou les ions carbone, de perdre le maximum d'énergie avant de s'arrêter a été mise en évidence par le physicien anglais William Bragg (Prix Nobel de Physique en 1915 pour sa contribution à l'analyse de la structure cristalline au moyen des rayons X).

L'énergie déposée par ionisation dans un tissu en fin de parcours est près de 5 fois plus importante qu'au début. La courbe passe par un pic (Fig. 2) appelé « Pic de Bragg ».

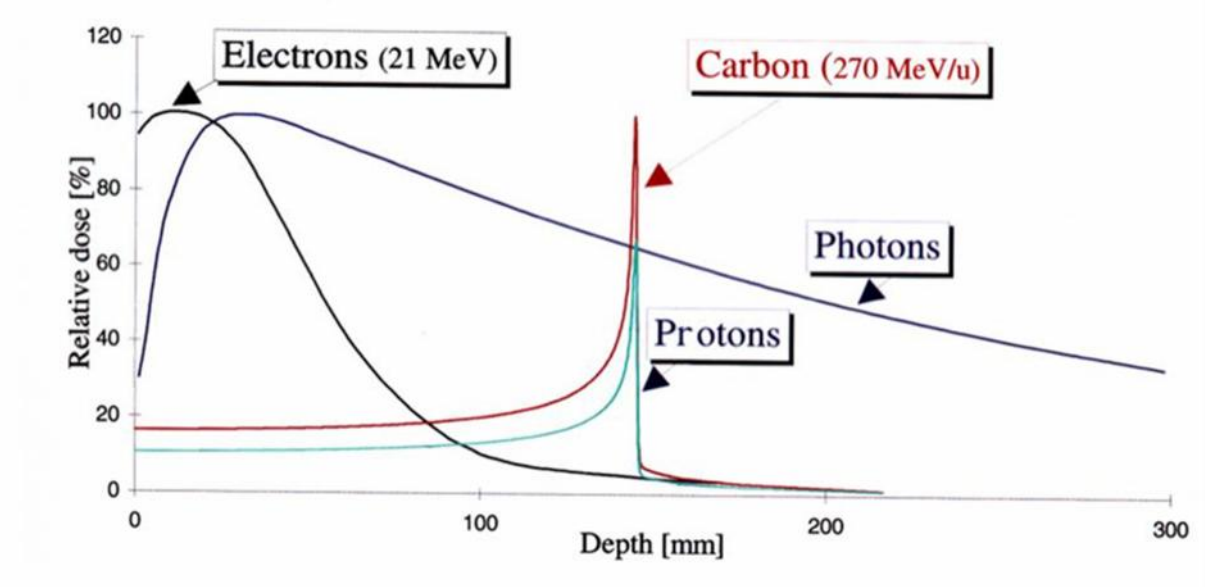

Figure 2 : Pénétration de divers rayonnements ; absorption rapide des électrons, plus lente des photons gamma et pic de Bragg des protons et des ions carbone [6].

En modulant (variant) l'énergie initiale des ions, on diminue la hauteur du pic de Bragg mais on augmente l'épaisseur de la tranche où l'irradiation est plus forte. Cela permet de traiter une tumeur dans son épaisseur, ce qui est appelé le SOBP (Fig. 3), en épargnant au maximum les tissus sains environnants, par exemple la peau, les tissus superficiels et les tissus profonds. Lors d'un protocole d'hadronthérapie avec un faisceau d'ions carbone d'environ 290 MeV/nu, le Transfert d'Energie Linéique (TEL, la quantité d'énergie transférée par une particule ionisante à la matière par unité de distance) à l'entrée dans le corps est ~15 keV/µm et, en routine clinique, le TEL à la tumeur est ~80 keV/µm.

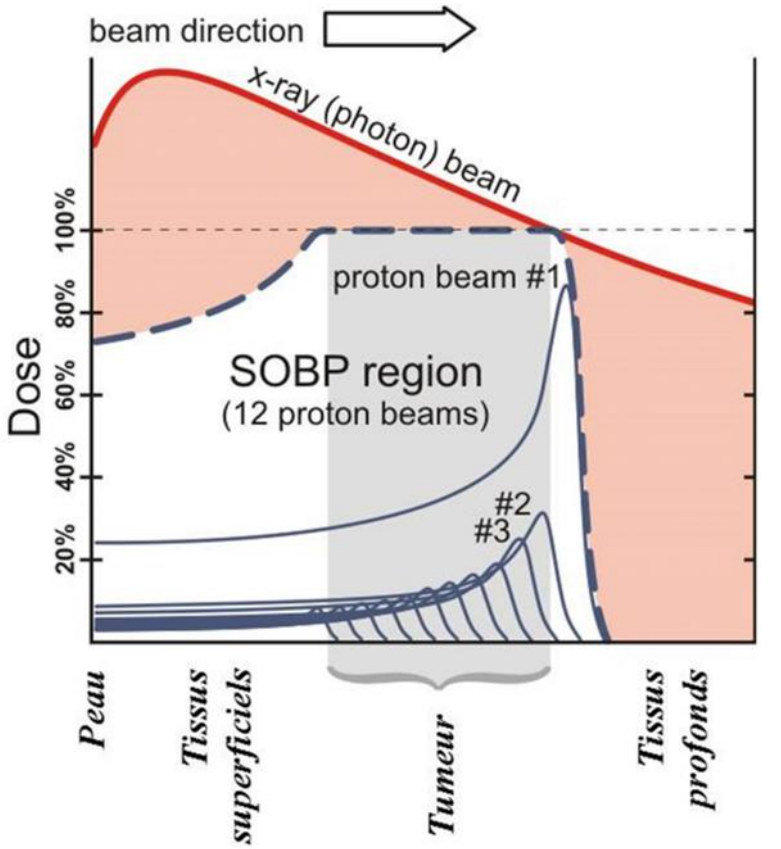

Figure 3 : Dans un plan de traitement typique pour l'hadronthérapie, le pic de Bragg étalé (SOBP : spread out Bragg peak), ligne pointillée bleue, est la distribution de rayonnement thérapeutique.
Le SOBP est la somme de plusieurs pics de Bragg individuels (lignes bleues minces) à des profondeurs échelonnées. La dose en profondeur d'un faisceau de rayons X (ligne rouge) est fournie à titre de comparaison. La zone rose représente la dose additionnelle délivrée lors de radiothérapie conventionnelle (rayons X) qui peut endommager les tissus normaux et provoquer des cancers secondaires, en particulier de la peau.

3.1.3 - Radiothérapie conventionnelle et hadronthérapie

Chaque année en France, 360 000 nouveaux cas de cancers sont diagnostiqués. Seulement la moitié d'entre eux environ pourra guérir avec les armes thérapeutiques dont nous disposons actuellement que sont la chirurgie, la chimiothérapie et la radiothérapie.
Dans ce contexte, l'apparition d'une nouvelle forme de radiothérapie, appelée « hadronthérapie », représente une avancée. Les premiers essais cliniques ont montré des résultats prometteurs, en particulier sur des cancers qui restent aujourd'hui incurables ou inopérables.

Le Centre Européen de Recherche en Hadronthérapie ARCHADE est créé dans cette perspective [5]. Il sera le premier au monde consacré prioritairement à la recherche dans ce domaine (Fig. 4).

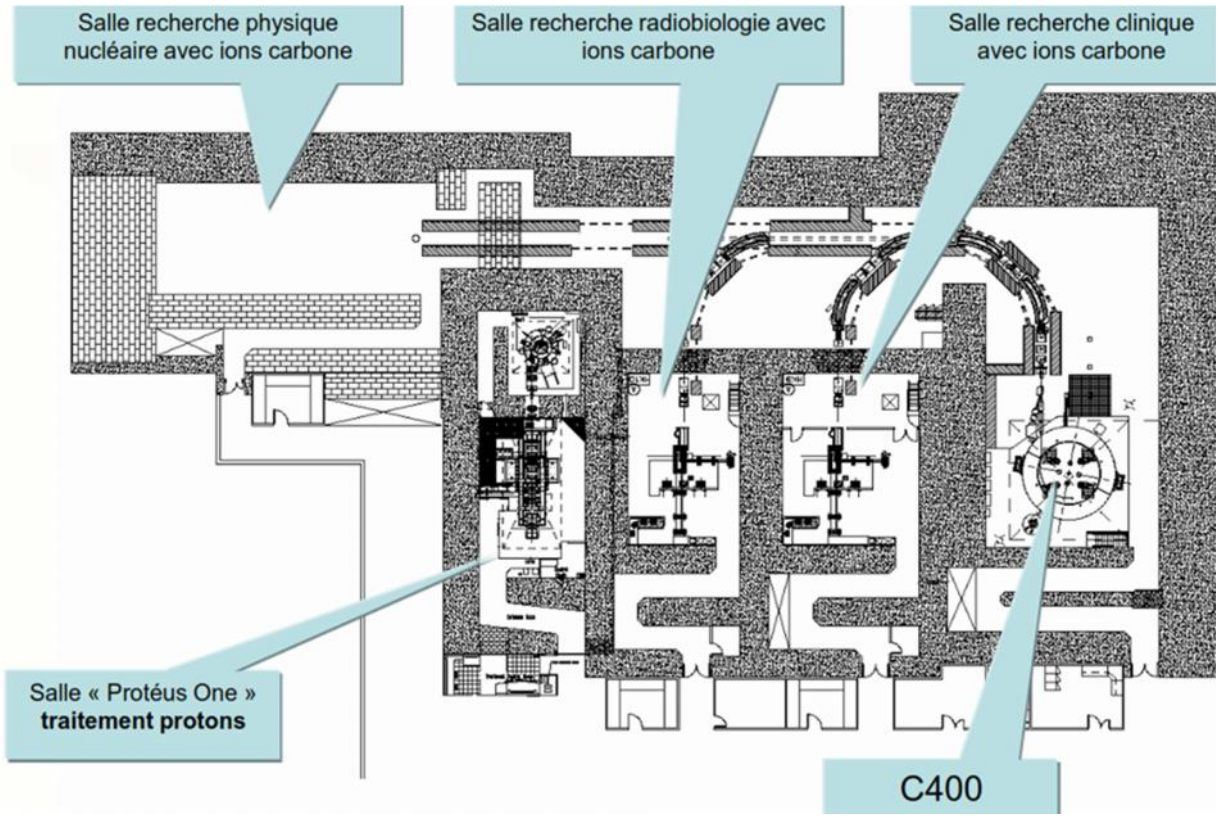

Figure 4 : Plan des salles d'irradiation dans le bâtiment ARCHADE.
Le centre ARCHADE sera en premier doté d'un irradiateur médical de protonthérapie, le « Protéus One » de la société IBA. Dans un second temps, un prototype d'accélérateur de particules (protons et ions carbone), le cyclotron Cyclone®400 (C400) sera mis en place et sera utilisé pour la recherche sur les ions carbone et les soins en protons.

3.1.4 - Un TPS pour l'hadronthérapie

Lors de la mise en place d'un protocole de radiothérapie, il est indispensable de disposer d'un système efficace de planification de traitement, ou TPS (« Treatment Planning System »), qui permettra de préparer ce protocole sur le plan dosimétrique. Ce logiciel détermine l'ensemble des paramètres de l'irradiation en tenant compte des caractéristiques des faisceaux (nature, fluence, débit, énergie, géométrie…), de l'anatomie du patient, de la localisation locorégionale de la tumeur et de son imagerie, de son volume et de sa radiosensibilité. Le TPS permet ainsi de réaliser pour chaque patient un plan de traitement sur mesure qui doit être validé sur le plan médical et physique avant la première fraction de RT afin d'épargner, au mieux, les organes à risque. Il existe actuellement des logiciels qui permettent le calcul de la distribution de la dose physique (Fig. 5) pour la radiothérapie conventionnelle (photons, électrons) et non conventionnelle (protons).

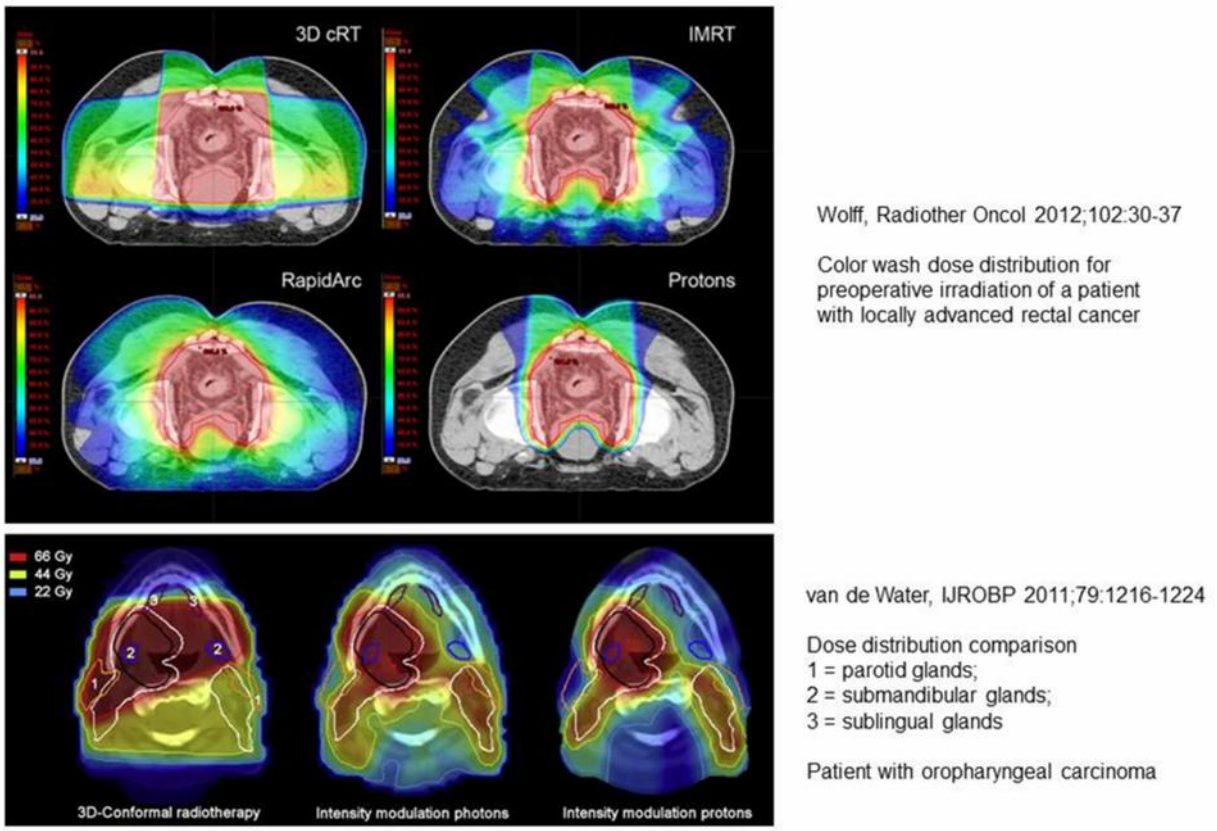

Figure 5 : Simulation de distribution de doses lors de la planification d'un traitement de radiothérapie en fonction de la technologie utilisée [1,7]

Malgré de récentes simulations multiparamétriques satisfaisantes, il n'existe pas actuellement de TPS qui intègre de façon documentée les multiples effets biologiques des ions carbone et des différentes particules produites par ces faisceaux traversant le corps humain. Les EBRs (Efficacité Biologique Relative) généralement utilisées sont obtenues par le rapport des doses d'irradiation induisant une clonogénicité de 10% pour des cultures cellulaires en monocouches irradiées *in vitro* en rayons X *versus* ions carbone en posant un certain nombre d'hypothèses parfois infondées. Les paramètres alpha et bêta, extraits d'un ajustement linéaire quadratique de ces courbes de survie obtenues dans des conditions expérimentales souvent trop hétérogènes, sont trop réducteurs des effets biologiques radio-induits, ciblés et ne prennent pas en compte les effets non ciblés comme par exemple l'effet « bystander » radio-induit. Par ailleurs, le nombre restreint d'outils actuellement disponibles en radiobiologie moléculaire moderne, notamment concernant la visualisation des lésions de l'ADN, représente également un facteur très réducteur.

3.1.5 - Notification d'un « RIBE » à des faibles doses

Dans une démonstration de modélisation développée à partir de résultats de radiobiologie cellulaire *in vitro*, David Brenner et John Little proposaient en 2001 [2,8] l'existence d'un rôle majeur du « RIBE » c'est-à-dire d'un effet de voisinage d'une cellule irradiée vers les cellules adjacentes ou proches dans leur microenvironnement immédiat, dans le risque de prénéoplasie applicable à la loi dite « linéaire avec ou sans seuil » pour des doses uniques inférieures à 50 cGy (Fig. 6). Depuis lors, de nombreux travaux de radiobiologie cellulaire ont tendu à montrer, dans une gamme de doses uniques de 0 à 200 cGy, qu'il y avait un réel « RIBE » avec des rayonnements de haut et bas TEL dans la modulation du métabolisme antiradicalaire ou l'instabilité génétique, mesurables *in vitro* dans différentes conditions expérimentales.

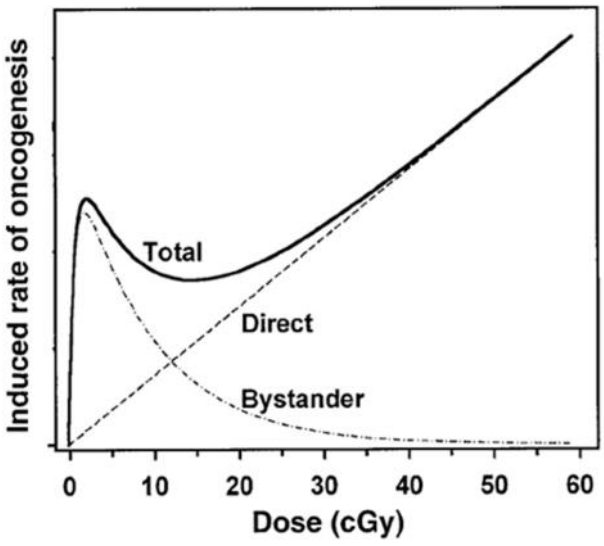

Figure 6 : Simulation proposée pour répondre aux effets biologiques observés à des faibles doses, entre 0 et 30 cGy [2]

3.1.6 - Implication du « RIBE » en radiothérapie

Aujourd'hui, en radiothérapie conventionnelle de nouvelle génération, l'avènement récent de la modulation d'intensité, l'utilisation de la tomothérapie et de ses variantes en arcthérapie, du cyberknife et des faisceaux fins balayés en hadronthérapie posent brutalement des questions essentielles de radiobiologie fondamentale en ce qui concerne le volume de tissus sains exposés à des niveaux élevés de rayonnements et leurs conséquences, ces tissus sains étant adjacents à la tumeur à traiter ou sur le parcours des faisceaux (Fig. 5).

Parmi ces questions, quelle est l'influence d'un « RIBE », un effet indirect des RI, agissant par le biais d'un ou plusieurs « signaux de stress » non encore identifiés au niveau moléculaire, émis par une ou plusieurs cellules irradiées vers les cellules non irradiées adjacentes, voisines ou à distance.

Selon les simulations présentées à la figure 3 et pour une dose d'irradiation d'un protocole standard de 45 à 60 Gy délivrée à la tumeur par fractions quotidiennes de 2 Gy, une rapide estimation permet d'évaluer la dose d'irradiation reçue par le volume de tissus sains aussi bien en radiothérapie conformationnelle 3D, qu'en modulation d'intensité ou en ArcThérapie, à 1/3 de la dose à la tumeur, ce qui correspond à ~15 – 20 Gy cumulés, mais par doses quotidiennes répétitives de ~65 cGy.

Un TPS théorique, proposé dans une étude récente de l'équipe de Kévin Prise [3], permet de mettre en évidence l'importance d'un RIBE lors d'une radiothérapie.
Les auteurs ont paramétré le signal de stress émis par les cellules de la zone irradiée à traiter vers les tissus adjacents (Fig. 7)

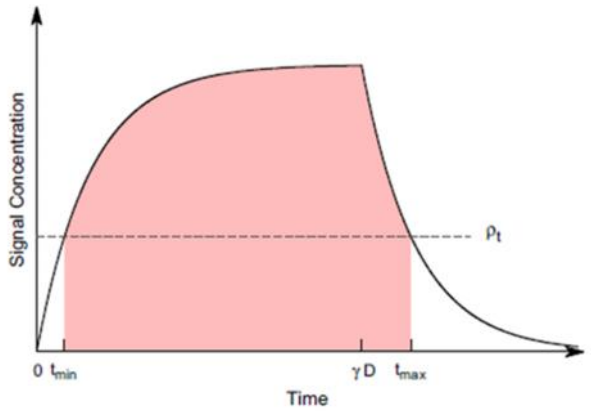

Figure 7 : Modélisation de la cinétique de signalisation de facteurs de stress [3]

Grâce à cette modélisation et à son inclusion dans un TPS, les auteurs mettent en avant l'augmentation des doses sur les tissus adjacents (Fig. 8). Le TPS ajusté montre une augmentation de la dose prescrite jusqu'à 30 % sur les trajets des faisceaux quelle que soit la technologie concernée.

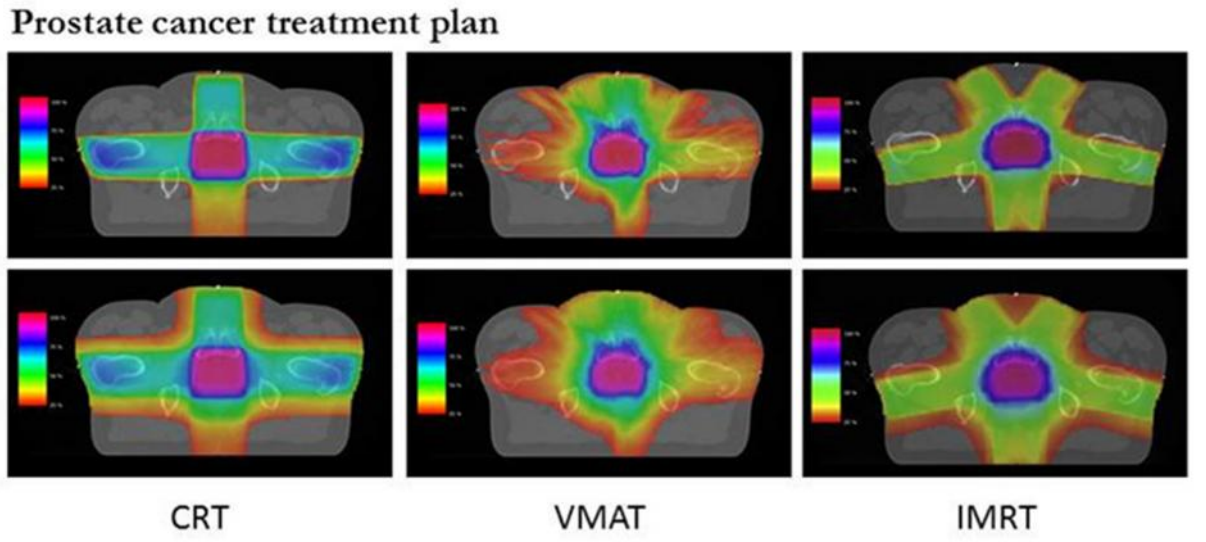

Figure 8 : Illustration de l'impact de l'effet bystander sur les distributions de dose pour un exemple d'IMRT (à gauche), de CRT (au centre) et de VMAT (à droite) lors d'un TPS de cancer de la prostate, avec une plage de signal de 15 mm.
Panel du haut : distribution de dose physique générée par le système de planification de traitement.
Panel du bas : distribution de dose après intégration d'un signal de stress radio-induit sur les tissus adjacents jusqu'à 15 mm de distance [3].

Cette problématique en doses uniques de quelques dizaines de cGy est directement liée aux questions de radioprotection rencontrées chez certaines catégories de personnel potentiellement exposés, comme dans la filière nucléaire ou encore le domaine aéronautique et spatial. Cependant, qu'en est-il pour des doses de 60 cGy répétées plusieurs dizaines de fois comme évoqué précédemment, quant au principe de précaution et à la protection des patients pris en charge dans un protocole de RT, notamment en oncopédiatrie ? Les conséquences à long terme de ces faibles doses sur les tissus sains restent imprévisibles et doivent faire l'objet de recherches approfondies, en particulier vis-à-vis d'un signal de stress comme le « RIBE ».

3.2 - L'effet bystander : mécanismes cellulaires décrits

L'effet bystander repose sur une signalisation intercellulaire : les cellules endommagées par l'irradiation transmettent des signaux (de manière spécifique ou non-spécifique), directement par des connexions ou indirectement par le milieu environnant, aux cellules voisines initialement non traversées par le rayonnement (Fig. 9). Le relargage de facteurs dits clastogènes (c'est-à-dire cassant les chromosomes) observé au niveau cellulaire ainsi que les effets abscopaux observés au niveau de certains tissus d'individus irradiés font partie de ce phénomène.

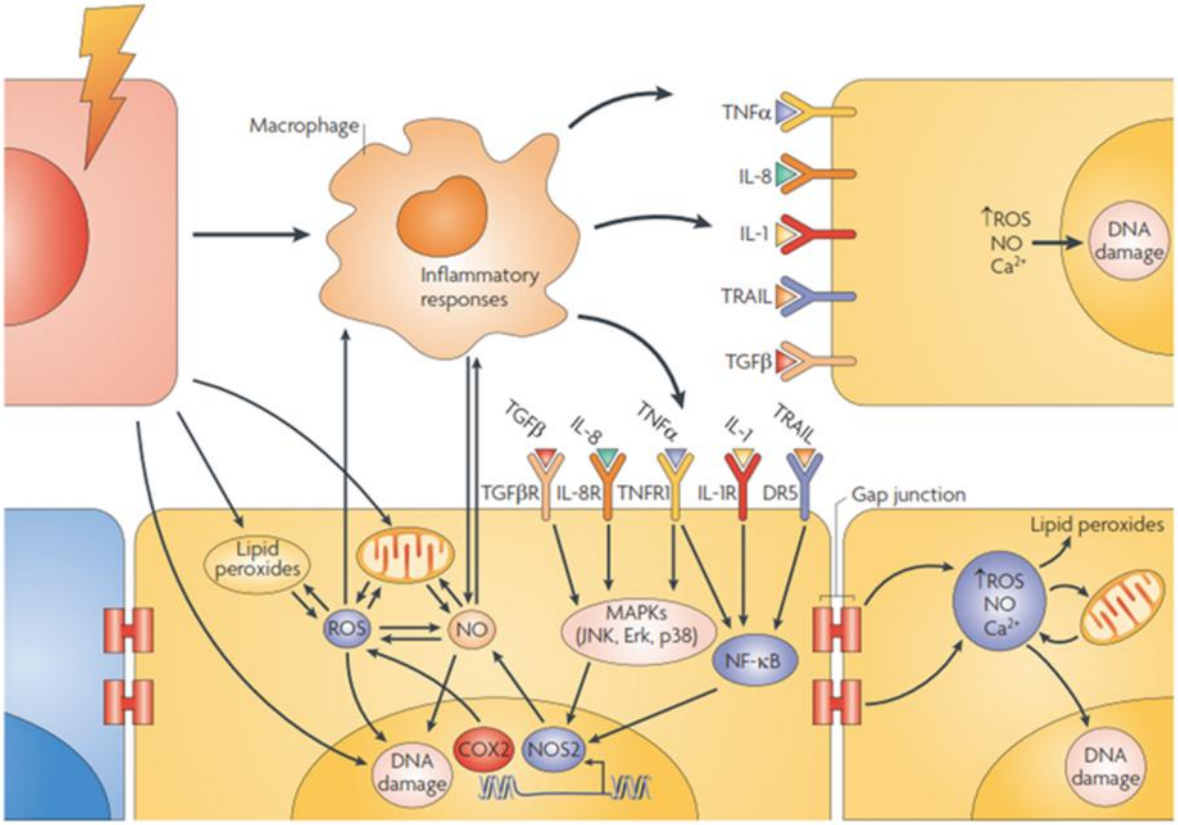

Figure 9 : Mécanismes cellulaires proposés de l'effet bystander radio-induit via une réponse inflammatoire transmise de proche en proche [9].

Nous savons aujourd'hui que cet effet est directement dépendant de la nature des cellules mises en jeu. Il existe des cellules « émettrices » du signal de stress et des cellules « receveuses » de ce signal, le fibroblaste humain sain étant considéré en radiobiologie comme « receveur universel » de ce signal.

Bien sûr, l'observation d'un effet bystander, et son intensité, vont dépendre des protocoles expérimentaux mis en jeu (irradiation par macro- ou microfaisceaux, irradiation directe, irradiation

partiellement collimatée, ou transfert de milieu conditionné de cellules irradiées sur cellules non irradiées), de la nature du rayonnement (bas ou haut TEL) et de son énergie, de la dose engagée voire du débit de dose, du critère d'évaluation de l'effet biologique recherché (lésions à l'ADN, apoptose, sénescence, instabilité génétique, mort cellulaire, marqueurs spécifiques…), du temps d'exposition des cellules receveuses au signal de stress (co-culture ou milieu conditionné) ainsi que de la concentration de ce signal (niveaux de dilutions variables d'un milieu conditionné). Un état des lieux des différents paramètres expérimentaux influençant la mise en évidence d'un effet bystander est présenté dans [10].

Depuis la synthèse de l'UNSCEAR en 2006 [11] sur les effets non ciblés des rayonnements ionisants et sur l'existence du « RIBE » dans la gamme de doses thérapeutiques et du rôle de celui-ci *in vitro*, il apparaît que le modèle expérimental a presque toujours été de la culture cellulaire en monocouche en deux dimensions (2D), ce qui est maintenant considéré comme réducteur et assez éloigné de la réalité biologique.

Basés sur des conditions d'irradiation mimant au mieux *in vitro* les conditions d'un protocole de radiothérapie externe, conditions dérivées du modèle de Suchowerska [12], les récents travaux du groupe de Kevin Prise [3,9,13–19] publiés ces deux dernières années ont fait fortement progresser la connaissance du « RIBE » en pratiquant des irradiations partiellement collimatées de cultures de diverses lignées cellulaires, en rayons X de différentes énergies ([16,17,20–23], irradiation en cuve à eau thermostatée avec écrans équivalents tissus d'épaisseur variable en amont des cultures cellulaires, associée à une dosimétrie physique de qualité médicale) avec le développement d'une modélisation mathématique adaptée [18,24]. Ils ont ainsi pu mettre en évidence notamment la contribution du « RIBE » sur la mortalité cellulaire radio-induite directe en normoxie (~20% d'oxygène de l'air), en faisant intervenir différents antagonistes des espèces radicalaires des voies oxygénées et nitrogénées. Cependant, les résultats de ces travaux souffrent d'incertitudes majeures dans l'aspect biologique des expériences réalisées sur cellules en phase exponentielle de croissance (densité d'ensemencement, temps de doublement cellulaire et phases du cycle, pourcentage d'attachement, fréquence de changement de milieu nutritif), paramètres dont on connaît bien aujourd'hui l'importance dans toutes les expériences de clonogénicité.
Schématiquement, il est donc encore globalement admis après irradiation en bas TEL que le « RIBE » *in vitro* n'est pas mesurable avec des outils moléculaires de la radiobiologie cellulaire moderne autres que la survie cellulaire voire la recherche de micronoyaux. Par ailleurs, des résultats contradictoires ont été obtenus *in vitro* en culture en monocouche après irradiation par des protons médicaux voire même de très haute énergie, alors que cet effet a été mis en évidence avec des rayonnements de haut TEL (particules alpha et ions lourds) dans une gamme de 0 à 200 cGy.
Le groupe d'Edouard Azzam, qui travaille depuis longtemps dans ce domaine [25–36], a récemment montré *in vitro* des modifications définitives du métabolisme anti-radicalaire dans des cellules non irradiées, induites par cinq heures de contact avec des cellules irradiées, mesurables dans différentes conditions expérimentales après vingt cycles cellulaires [30]. Ces résultats étaient confortés par des

expériences similaires à très faibles doses associées à des calculs de micro-dosimétrie et des simulations mathématiques particulièrement élégantes de fragmentations d'ions à hauts TEL [34].

3.3 - Un modèle biologique *in vitro* en 3D

Dans la mise en évidence *in vitro* d'un « RIBE », il apparaît que le modèle expérimental de référence a toujours été la culture cellulaire en monocouche 2D, même si un modèle de culture 3D « équivalent peau » avec des kératinocytes et des fibroblastes humains normaux cultivés dans une matrice de macromolécules est utilisé depuis 2005 sous irradiation par micro-faisceau [37]. Ce modèle expérimental, devenu par ailleurs le « gold standard » en toxicologie chimique cutanée, s'affranchit néanmoins du compartiment microvasculaire dont le rôle est pourtant essentiel quant à l'effet des rayonnements ionisants *in vivo* (revue dans [38]). Ces études *in vitro* 2D et 3D ont toujours été développées dans des conditions de normoxie (~20% de l'oxygène de l'air), bien que cette situation physicochimique artificielle place les cellules dans une condition artéfactuelle de grande radiosensibilité au regard de la physioxie naturelle des tissus humains qui est de ~5% ±2% d'O_2 (revue dans [39]). En conséquence, à aucun moment ces résultats ne sont directement extrapolables à l'homme.

Dans l'objectif de reproduire les conditions de microenvironnement naturel, les différents types cellulaires seront irradiés en culture 2D en condition de physioxie (phase exponentielle et ~3% O_2), modalité de culture qui servira de contrôle interne.
Un modèle de culture en trois dimensions (3D) en biomatériaux (brevet WO2012038668) est développé au laboratoire depuis plusieurs années afin de reproduire les conditions de physiologie cellulaire du cartilage articulaire et pouvant être irradié avec des ions lourds sur la ligne D1 du GANIL. Ce modèle de culture en 3D, proche des nombreux modèles déjà utilisés en radiobiologie avec des irradiations X, protons et ions accélérés, sera ensuite utilisé avec les outils adaptés [37,40–44]. Ce modèle propre aux chondrocytes (cartilage reconstruit *in vitro* en éponge de collagène de type I ; [45]) est utilisé en routine au laboratoire car il permet de restituer *in vitro* le microenvironnement naturel des cellules et leurs différenciations respectives (phase exponentielle de croissance et ~3% O_2 ; [46,47]). Par ailleurs, cette étude en culture 3D est l'alternative ou le préalable aujourd'hui incontournable à toute modélisation *in vivo* chez le rongeur.
La mise en évidence d'un effet bystander dans des conditions mimant au mieux la réalité biologique d'un tissu humain est essentielle dans la perspective d'un protocole d'hadronthérapie par ions carbone ou protons ciblant un sarcome (chordome, ostéo- et chondrosarcomes), tumeur en première ligne pour l'hadronthérapie [48] et le projet ARCHADE [4,5]. La littérature ne rapporte à ce jour qu'un seul article relatif à un signal de type bystander émis par des chondrocytes de chondrosarcome dans des conditions expérimentales en 2D paradoxales (cultures sans CO_2) et normoxie [49], sans le contrôle interne, à savoir les chondrocytes normaux.

3.4 - Plan scientifique du projet de recherche

3.4.1 - Questionnement / étapes clés

Dans le cadre de ce projet de recherche, différentes questions seront posées séquentiellement afin d'organiser une logique scientifique et de structurer la démarche de recherche.

- ***Mise en évidence d'un effet bystander en culture 2D***

La première question consiste à rechercher et à mettre en évidence un effet bystander dans nos conditions d'analyse *in vitro*.
En effet, un tel mécanisme n'a jamais été démontré dans nos conditions opératoires et il reste à déterminer quelle est la combinaison de paramètres permettant sa réalisation. Pour cela, et pour se placer dans les conditions les plus favorables, un système de culture en 2D *in vitro,* développé depuis peu et permettant la co-culture, sera utilisé et les conditions d'irradiation seront comparées afin d'observer un effet biologique sur les cellules non-irradiées.

- ***Analyse d'un effet bystander sur le modèle 3D***

Après la mise en évidence d'un effet biologique sur des cellules en 2D, les mêmes conditions seront appliquées sur le modèle de culture en 3D de cartilage. L'effet bystander sera à nouveau analysé par différents types de protocoles expérimentaux et une analyse protéomique sera mise en place pour connaitre les mécanismes mis en jeu.
La plus grande partie des expériences sera réalisée avec ce modèle de culture en 3D, les effets indirects seront comparés aux effets directs et les sécrétomes seront comparés aux protéomes cellulaires.

- ***Rôle de la matrice extracellulaire dans la réponse biologique***

Le cartilage est un tissu contenant assez peu de cellules (chondrocytes) et, proportionnellement, une grande quantité de matrice extracellulaire. Cette matrice, composée principalement de collagène et de protéoglycans, subit aussi les effets des rayonnements ionisants et les produits de dégradations peuvent avoir une activité biologique de type bystander vers les tissus voisins non-irradiés. Cet aspect de recherche sera aussi analysé en collaboration avec des physiciens, spécialistes des effets des rayonnements ionisants sur la matière.

3.4.2 - Plan d'expériences

Dans la suite de ce projet de recherche, nous allons décrire les différentes conditions opératoires que nous souhaitons développer pour étudier l'effet bystander sur nos différents modèles cellulaires *in vitro* :

- modèles 2D vs modèles 3D
- types cellulaires (chondrocytes immortalisés vs chondrosarcomes vs chondrocytes primaires)
- type d'irradiation (Rayons X vs ions lourds)
- TEL (protons vs ions carbone vs rayons X)
- doses (0 à 2 Gy physiques)
- protocole de transfert de milieu
- protocole de co-culture

La mise en évidence d'un effet bystander sera réalisée à l'aide de techniques classiques de radiobiologie ainsi que de techniques innovantes de protéomique sur différents compartiments comme défini ci-dessous :

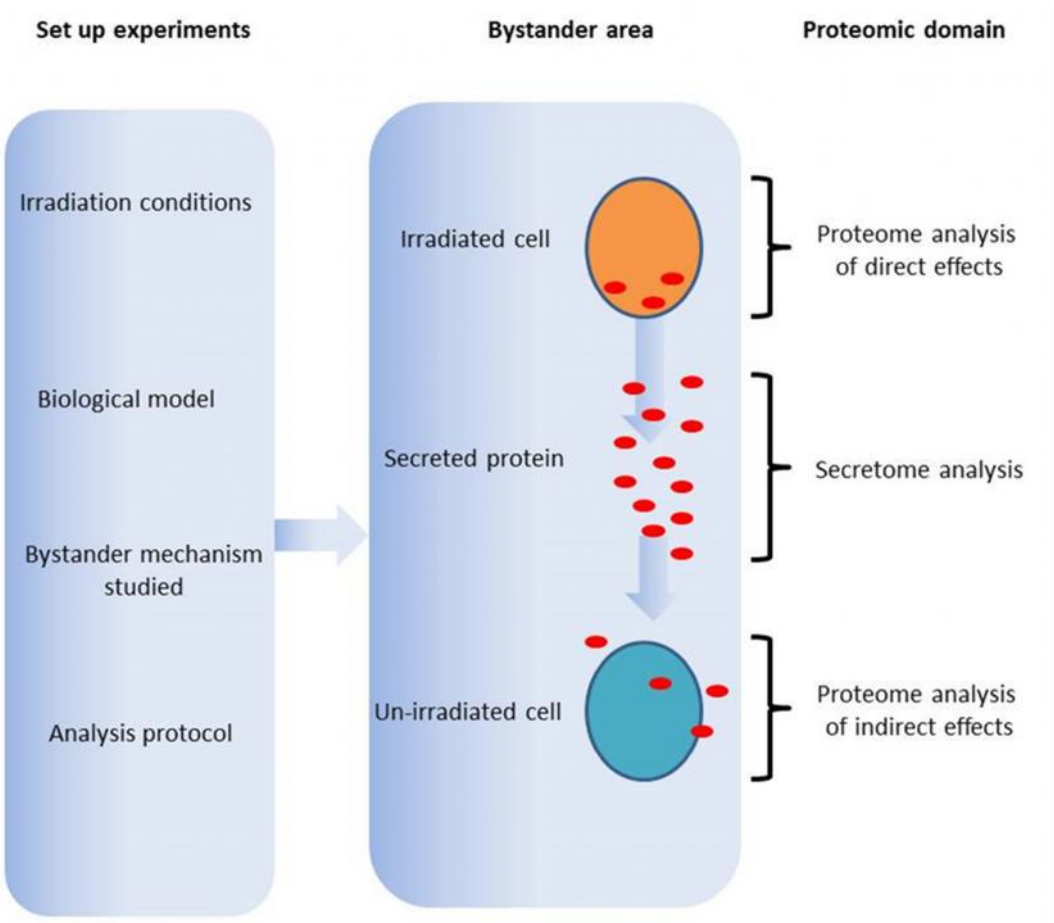

Figure 10 : Plan expérimental de l'étude de l'effet bystander par des stratégies d'analyse protéomique compartimentées (d'après [10]).

3.4.3 - Irradiation par différents types de rayonnements ionisants

Les irradiations conventionnelles seront réalisées grâce au générateur de rayons X de recherche obtenu dans le cadre de l'Equipex « RecHadron 2011 ».
La sensibilité des cellules sera explorée dans la gamme des faibles doses en dessous de 50 cGy (entre 1 et 50 cGy) et jusqu'à 2 Gy pour se placer dans des conditions d'irradiation proches d'une fraction de radiothérapie.
Les irradiations à hauts TEL seront effectuées au GANIL (ions 13C ~35keV/µm et ions 22Ne ~105 keV/µm) sur les cultures 3D de chondrocytes non irradiées et exposées aux milieux conditionnés de cultures 3D irradiées.
Ces deux TEL sont le résultat d'un compromis entre, d'une part, le TEL à l'entrée du faisceau d'ions carbone (~290 MeV/nu) dans le corps (~15 keV/µm) d'un patient lors d'un protocole d'hadronthérapie et le TEL à la tumeur (~80 keV/µm) et, d'autre part, les caractéristiques et régularités de programmations des faisceaux d'ions accélérés accessibles au GANIL.
Des irradiations par protons et ions carbone de qualité médicale seront par la suite réalisées avec les irradiateurs du centre ARCHADE avec respectivement le S2C2 et le C400 lorsqu'ils seront mis en place.

3.5 - Méthodes d'analyse et aspects "protéomiques" de l'effet de voisinage

Dans le cadre de la rédaction de cette HDR, j'ai été amené à réfléchir sur la place de l'analyse protéomique comme outil de recherche et de mise en évidence de cet effet bystander.
Dans cet objectif, une revue de la littérature dans le domaine a été rédigée et cet article a été publié en 2014 [10] dans le journal « Mutation Research : Reviews in Mutation Research ». Cet article est reproduit en version intégrale à la fin de ce chapitre.

3.6 - Critères biologiques

L'existence d'effets biologiques de type bystander sera explorée en phase avec les dernières publications du domaine, notamment par des analyses portant sur le stress oxydatif (Western blot) et les mécanismes de transmission du signal au niveau cellulaire.
La plupart de ces techniques décrites ci-après sont couramment appliquées pour étudier et évaluer les conséquences des effets directs des rayonnements ionisants. Dans notre cas, ces techniques seront d'abord utilisées pour étudier les effets bystander (en comparaison des effets directs), mais nécessiteront certainement une sensibilité adaptée pour mettre en évidence le phénomène.
Les techniques de protéomique seront largement employées, notamment par gel d'électrophorèse en 2D [50] ou par spectrométrie de masse quantitative. L'analyse protéomique est un outil puissant,

permettant de mettre en évidence sans *a priori* les mécanismes mis en jeu suite à une irradiation, ou lors d'un effet bystander. Ces technologies, en complément de techniques plus classiques de radiobiologie, pourront permettre de définir les voies métaboliques impliquées dans la réponse à un stress, ainsi que les acteurs protéiques mobilisés ou réprimés.
Dans la perspective où aucun effet ne serait mis en évidence dans des cultures de chondrocytes utilisées comme « receveuses », des cultures de fibroblastes de derme humain pourront être substituées comme cellules « receveuses » de milieu conditionné, le fibroblaste étant considéré comme « receveur universel » du « RIBE ».

3.6.1 - Radiotoxicité cellulaire et clonogénicité

L'analyse de la radiotoxicité cellulaire peut être réalisée avec des tests portant sur le métabolisme cellulaire. La nécrose cellulaire sera évaluée par la mesure de la libération de l'adénylate kinase dans les milieux de culture par l'utilisation du kit Toxilight. La viabilité cellulaire sera également déterminée par exclusion au bleu trypan et la clonogénicité, déterminée de manière conventionnelle, sera couplée à une analyse de la distribution de taille des colonies permettant de mettre en évidence d'éventuelles pertes de capacité proliférative des cellules irradiées (effets directs) et des cellules bystander (effets indirects).
Cette étude de radiotoxicité/clonogénicité permettra de définir deux à trois situations caractéristiques de dose/débit de dose/effet biologique utilisées ci-dessous comme conditions expérimentales.

3.6.2 - Formation et réparation des lésions de l'ADN

La majorité des cassures double brins (CDBs) induites par rayons X est réparée par la voie NHEJ qui est le mode de prédilection de la réparation en phase G0/G1, alors que la voie HR est favorisée pour les cellules en phase S/G2. Lorsque des cellules sont irradiées en phases S ou G2, de longs segments d'ADN simple brin sont formés et recouverts de RPA qui pourrait représenter un unique «scaffold» pour le recrutement de facteurs comme Rad51 et BRCA1 également impliqués dans les processus de réparation. La radiosensibilité dépend de l'intégrité des systèmes de détection et de réparation des lésions de l'ADN impliquant notamment ATR, ATM et DNA-PK. La réponse ATR dépendante est généralement associée aux lésions de l'ADN induites par des stress réplicatifs. En raison du stress oxydatif connu après irradiation par rayons X, l'implication de ATR en réponse à la formation d'adduits de type 8-oxo-G ne peut être exclue et doit être investiguée. ATM est généralement impliquée dans l'induction des systèmes de réparation, l'arrêt du cycle cellulaire et la régulation de l'apoptose radio-induite, alors que DNA-PK joue un rôle important dans le processus de réparation des CDBs par NHEJ.

La production de CDBs sera mesurée directement dans les cellules par l'analyse de la phosphorylation de l'histone H2AX (foyers gamma-H2AX) par western blot. Les éventuelles modifications quantitatives ou qualitatives radio-induites des foyers gamma-H2AX seront mesurées dans les conditions de doses et de débits de doses définies.

3.6.3 - Apoptose radio-induite et sénescence

Parallèlement à la mesure des CDBs de l'ADN, l'impact direct et indirect de l'irradiation sur la survie à court terme (quelques jours) des modèles cellulaires retenus sera analysé dans les conditions de doses et de débits de doses définies.
À cet effet, l'apoptose induite sera mesurée par la détection in situ de la fragmentation de l'ADN (In Situ Cell Death Detection Kit, Roche) mais aussi par la quantification par western blot de marqueurs spécifiques (caspases).
L'analyse de la sénescence sera réalisée par détermination de l'activité SA-β-galactosidase. L'induction de la sénescence pourra également être mise en évidence par western blot pour détecter les niveaux d'expression de p21 et de p16 ainsi que l'expression et la phosphorylation de p53 et l'expression de la lamine B1. L'apoptose et la sénescence seront mesurées dans les conditions de doses et de débits de dose définies.

3.6.4 - Stress oxydatif cellulaire

L'excès de stress oxydant dans la cellule à la suite d'une irradiation est un facteur d'inflammation et de mutagenèse. La production de ERO (Espèce Réactive de l'Oxygène) dans la cellule peut être contrebalancée par des systèmes de défenses enzymatiques ou non-enzymatiques. La production de peroxyde d'hydrogène sera mesurée par l'introduction intracytoplasmique d'une sonde fluorescente CM-H2DCFDA (Invitrogen™). Les cellules ainsi traitées peuvent être analysées par cytométrie en flux afin de quantifier leur fluorescence qui sera proportionnelle à la quantité d'H2O2 produite. Les activités des principales enzymes antioxydantes (SOD, catalase, GPx), ainsi que le ratio de glutathion réduit/oxydé, seront également évalués. En complément, les oxydations des lipides (LPO) et des protéines (groupements carbonyls) pourront être mesurées. Ces phénomènes oxydatifs seront mesurés juste après l'irradiation et, à plus long terme, dans les conditions de doses et de débits de dose définies.

3.6.5 - Inflammation et sécrétion de facteurs solubles

L'inflammation et la transmission intercellulaire d'un signal inflammatoire et/ou bystander sont des phénomènes complexes et centraux dans la survenue des effets toxiques immédiats lors d'une irradiation. Le potentiel pro-inflammatoire des rayonnements ionisants devra être évalué dans le modèle 3D. Le chondrocyte a pour rôle de maintenir un parfait équilibre entre la synthèse et la dégradation des composants matriciels du cartilage grâce aux cytokines IL-1, IL-6, et TNF-alpha, et des facteurs de croissance locaux IGF-I, BMPs, et TGF-ß1. La composante inflammatoire de l'irradiation pourrait modifier la production de cytokines, mais aussi l'équilibre entre l'anabolisme et le catabolisme, la prolifération et la différenciation cellulaire nécessaires à l'homéostasie du cartilage.
Afin de mesurer les facteurs sécrétés, il est essentiel d'utiliser des méthodes sensibles, quantitatives et compatibles avec le dosage dans des milieux de culture cellulaire. Pour cela, nous allons développer trois approches complémentaires :

1. Le système de protéines sur biopuces (RayBio® Biotin Label-based Human Antibody Array. ref AAH-BLG-1-4) permettant de détecter simultanément les niveaux d'expression de plusieurs protéines. Ces protéines sont capturées par des anticorps fixés sur une lame de verre puis révélées par un système chimioluminescent. A l'aide de ce système, nous pourrons quantifier simultanément en quadriplicate 507 protéines humaines, majoritairement des chémokines, cytokines et des facteurs de croissance.
2. Le système de dosage Elisa multiplexe MSD (Mesoscale Discovery™, http://www.mesoscale.com) qui repose sur une combinaison exclusive de détection par électrochémiluminescence et de plaques 96 puits brevetées. En fait, la détection par électrochémiluminescence offre une combinaison unique de sensibilité, de gamme dynamique et de facilité d'utilisation. Pour cela, le lecteur MSD utilise des photodétecteurs ultra-sensibles et performants afin de collecter et de mesurer quantitativement la lumière émise par les microplaques. Ce sytème MSD permet la quantification de panels de cytokines/chimiokines (jusqu' à 30 analytes) compatibles avec des surnageants de culture en terme de sensibilité.
3. L'analyse différentielle du sécrétome par spectrométrie de masse directe ou par électrophorèse bidimensionnelle de milieux conditionnés [50] permettra une identification sans *a priori* des facteurs sécrétés modulés.

3.6.6 - Expression différentielle et modifications post-traductionnelles des protéines

Un stress génotoxique, tel qu'une irradiation, provoque une réponse cellulaire complexe où de multiples signaux conduisent à modifier l'expression mais aussi les activités de très nombreuses protéines soit par une modification de la quantité, soit par la modification de la structure (PTM). L'expression de protéines impliquées dans les voies métaboliques de réponses aux rayonnements ionisants sera évaluée par des techniques classiques de protéomique quantitative. L'analyse des

modifications post-traductionnelles des protéines de chondrocytes sains et tumoraux en culture 3D sera réalisée par une électrophorèse bidimensionnelle permettant de séparer, de visualiser puis d'identifier par spectrométrie de masse les protéines d'intérêt. De manière comparable, l'analyse phospho-protéomique permettra d'identifier les phosphorylations des protéines dans les conditions de doses et de débits de dose définies.

3.6.7 - Dégradation des protéines de la matrice extracellulaire du cartilage

Le traitement d'un chondrosarcome par hadronthérapie peut induire une dégradation partielle du cartilage sous la forme d'un relargage de fragments peptidiques. De tels fragments peuvent présenter une activité biologique de type bystander tissu spécifique. Ces fragments moléculaires de protéines de la matrice extracellulaire du cartilage produits après irradiations par des ions seront analysés en temps réel par un spectromètre de masse dédié.

3.7 - Résultats escomptés

Les caractéristiques de ce modèle *in vitro* [3D – physioxie] en font un outil idéal de la radiobiologie moderne en transposant un organe sain avasculaire humain en un outil *in vitro,* tout en s'affranchissant de l'expérimentation animale. Les expériences envisagées au plus proche du microenvironnement de la physiologie humaine nous permettront de déterminer l'existence avérée ou non d'un « RIBE » aussi bien sous irradiation par rayons X qu'à des TEL plus élevés.
En première intention, les séries d'expériences seront développées en irradiations par doses uniques. En deuxième intention, selon les résultats observés et les accessibilités aux temps de faisceaux dépendant de la programmation des ions délivrés au GANIL ou ultérieurement du Centre ARCHADE, des séries d'expériences avec des doses répétitives quotidiennes devront être envisagées, afin de mimer au mieux les conditions d'un protocole de radiothérapie conventionnelle ou non.
Si les données expérimentales obtenues prouvaient l'existence d'un tel effet dans les chondrocytes ou dans les fibroblastes normaux utilisés comme receveurs, aussi bien après irradiations par rayons X que par ions de hauts TEL, elles devront être impérativement prises en compte dans la mise au point et le déroulement d'un protocole de radiothérapie conventionnelle ou non, en raison du risque encouru sur les tissus sains chez des patients jeunes et notamment pédiatriques. Dans le cas contraire, ces expériences seraient en cohérence avec le principe de précaution devenu règle d'or en matière de protection sanitaire des patients.

3.8 - Conclusions - Perspectives

Ce projet de recherche a pour objectif de mieux définir les fondements de référence sous irradiation par rayons X pour l'hadronbiologie afin de mieux maîtriser les paramètres d'un TPS par ions carbone et d'envisager sereinement l'utilisation de ce type de faisceau balayé en routine clinique.
L'accumulation de connaissances nouvelles grâce à la réalisation de ce projet, par ailleurs transposable à d'autres types de tumeurs éligibles pour l'hadronthérapie, devra contribuer à valider ou non la supériorité curative des ions carbone versus protons pour le traitement de tumeurs dont l'origine de la radiorésistance avérée est, comme pour le chondrosarcome, totalement inconnue. Par ailleurs, il est légitime de s'intéresser aux effets des rayons X sur les CSMs, en raison de l'exposition de celles-ci lors de protocoles de radiothérapie de dernière génération comme l'arcthérapie. L'exploration simultanée de l'équilibre survie/sénescence et de l'instabilité génétique, associées à une démarche pertinente en terme de conditions de physioxie et de microenvironnement, permettra de fournir des données de référence concernant les effets des rayons X sur le caractère multipotent et la stabilité des CSMs. Ces données permettront également de déterminer si l'irradiation induit des altérations des capacités des chondrocytes et des CSM à se différencier. La prise en compte de la physioxie cellulaire, jusqu'ici négligée aussi bien après irradiations en rayons X qu'en protons et ions carbone, sera particulièrement importante pour des paramètres simples, tels que la clonogénicité, comme pour des phénomènes complexes telle que la modulation radio-induite de l'expression de gènes d'intérêt ou encore un effet « bystander ». Les complications de la radiothérapie conventionnelle sur l'os et le cartilage, chez l'enfant notamment, justifient l'intérêt porté à la radiosensibilité de ces tissus et de leurs progéniteurs que sont les CSMs de la moelle osseuse. Ces connaissances nouvelles pourront être à l'origine d'une nouvelle vision de la recherche d'EBRs en conditions de physioxie cellulaire et de leurs intégrations dans un TPS.

Mutation Research xxx (2014) xxx–xxx

Contents lists available at ScienceDirect

Mutation Research/Reviews in Mutation Research

journal homepage: www.elsevier.com/locate/reviewsmr
Community address: www.elsevier.com/locate/mutres

Review

Proteomic overview and perspectives of the radiation-induced bystander effects

François Chevalier *, Dounia Houria Hamdi, Yannick Saintigny, Jean-Louis Lefaix

LARIA - iRCM - DSV - CEA, GANIL, Campus Jules Horowitz, Bd Henri Becquerel, BP 55027, Caen 14076, France

ARTICLE INFO

Article history:
Received 7 April 2014
Received in revised form 22 September 2014
Accepted 18 November 2014
Available online xxx

Keywords:
Ionizing radiation
Bystander effect
Proteomics
Signal transduction
Secretome

ABSTRACT

Radiation proteomics is a recent, promising and powerful tool to identify protein markers of direct and indirect consequences of ionizing radiation. The main challenges of modern radiobiology is to predict radio-sensitivity of patients and radio-resistance of tumor to be treated, but considerable evidences are now available regarding the significance of a bystander effect at low and high doses. This "radiation-induced bystander effect" (RIBE) is defined as the biological responses of non-irradiated cells that received signals from neighboring irradiated cells. Such intercellular signal is no more considered as a minor side-effect of radiotherapy in surrounding healthy tissue and its occurrence should be considered in adapting radiotherapy protocols, to limit the risk for radiation-induced secondary cancer. There is no consensus on a precise designation of RIBE, which involves a number of distinct signal-mediated effects within or outside the irradiated volume. Indeed, several cellular mechanisms were proposed, including the secretion of soluble factors by irradiated cells in the extracellular matrix, or the direct communication between irradiated and neighboring non-irradiated cells *via* gap junctions. This phenomenon is observed in a context of major local inflammation, linked with a global imbalance of oxidative metabolism which makes its analysis challenging using *in vitro* model systems.

In this review article, the authors first define the radiation-induced bystander effect as a function of radiation type, *in vitro* analysis protocols, and cell type. In a second time, the authors present the current status of protein biomarkers and proteomic-based findings and discuss the capacities, limits and perspectives of such global approaches to explore these complex intercellular mechanisms.

Contents

Abbreviations: 2DE, two-dimensional electrophoresis; 2D-DIGE, two dimensional-differential gel electrophoresis; 3DCRT, three dimensional conformal radiotherapy; BE, bystander effect(s); BF, bystander factor(s); BR, bystander response(s); CyPA, cyclophilin A; DSB, double strand break(s); HMEC, human mammary epithelial cells; IEF, isoelectric focalization; IMRT, intensity-modulated radiation therapy; IR, ionizing radiation(s); LET, linear energy transfer; Mr, relative molecular mass; MS, mass spectrometry; NO, nitric oxide; NOS, nitric oxide synthase; NSCLC, non-small cell lung carcinoma; OS, oxidative stress; p*I*, isoelectric point; PTM, post-translational modifications; RIBE, radiation induced bystander effect; ROS, reactive oxygen species; SDS-PAGE, sodium dodecyl sulfate poly acrylamide gel electrophoresis; SELDI–TOF, surface enhanced laser desorption ionization–time of flight; UNSCEAR, United Nation Scientific Committee on the Effects of Atomic Radiation.

* Corresponding author. Tel.: +33 (0)2 31 45 45 64.
E-mail addresses: chevalier@ganil.fr, francois.chevalier@cea.fr (F. Chevalier).

http://dx.doi.org/10.1016/j.mrrev.2014.11.008
1383-5742/

1. Introduction of RIBE definition

Over the past 25 years, considerable evidence has accumulated regarding "radiation-induced bystander effects", RIBE, defined as a biological response of non-targeted and non-irradiated cells, neighboring to cells directly traversed by ionizing radiations. Bystander effect (BE) leads to non-irradiated cells injury with a biological response close to the direct response of irradiated cells [1–3].

When cells are exposed to ionizing radiation, a large amount of energy is deposed, and many molecules become non-functional. In the case of DNA molecules, major damages such as double-strand breaks are created, and un-repaired or mis-repaired damages lead to multiple chromosomal mutations and cell death. This irradiation strategy is the basis of radiotherapy, targeting specifically a tumor mass with the irradiator system beam, in order to reduce cancer cell viability. Experimental evidence shows that, in addition to this direct and targeted effect of radiation, a side or secondary effect is observed within the un-irradiated area. Irradiated cells relay a stress signal in the close proximity. Neighboring un-irradiated cells react to this signal, *i.e.*, BE with a specific "bystander response" (BR), characteristic of a biological context, but with a close relationship to the biological response typically associated with direct radiation exposure. Bystander responses and bystander factors (BF) secreted by irradiated cells were observed and studied in many physical and biological conditions, *in vitro* and *in vivo*. For a complete overview of BE, most experiments in this area were broadly reviewed from the years 1992 to 2006 in the UNSCEAR report [4], in a special issue of Oncogene in 2003 [5–12], and in several recent publications [1,3,13–20].

1.1. Effect classes: Bystander/abscopal/cohort

As explained by Blyth and Sykes [3], distinctions should be made between effect classes to define and delimit cell responses to radiations. Within the irradiated volume, irradiated cells communicate a stress signal to non-irradiated cells, *i.e.*, a BE; and irradiated cells also communicate this stress signal to irradiated cells, *i.e.*, a cohort effect, which can be the same, but mostly masked by the direct effect of radiation. These bystander and cohort effects, which appear at the same time, need to be considered carefully when designing analysis protocols and interpreting bystander results, especially with *in-vitro* models. During exposure of the body to radiation, an abscopal response can be observed outside of an irradiated volume, sent by the different irradiated tissues in the direction of the non-irradiated ones. Of course, such effects, involving a total body response *via* the blood vessel and immune system, is impossible to repeat *in vitro*.

1.2. Radiation source and dose

According to the quantitative model of Brenner et al. [16], at least in the case of α-particles, BE are important and dominate the overall response at doses below 50 cGy. This model transforms the approach about low-dose responses, which was extrapolated from intermediate doses and may lead to an underestimation of the risk. The dose-response relationship does not increase with increasing radiation dose [1]. In contrast to direct effects, BR reaches a plateau and become quickly saturated at relatively low doses (50–100 cGy). Such a remarkable dose-dependence response is still poorly understood and leads to contradictory results as a function of irradiation type and doses [3]. Since the complete cellular mechanism of the BE is not elucidated, it is difficult to explain such a saturated response. A hypothesis can only be proposed with, for example, a simple on/off response or a secretion limit of BF by irradiated cells.

In addition, BE are dependent on the radiation source and quality, and on the characteristics of the beam used for irradiation (LET, energy, dose rate, dose, etc.). A complete review of the recent *in vitro* studies of the BE as a function of cell type, radiation type (alpha particle, gamma radiation, X-rays, protons, neutrons, heavy ions), end point (chromosomal instability, plating efficiency) and origin of BE (micro-beam irradiation, medium transfer, etc.) was published in 2006 [4] by the United Nation Scientific Committee on the Effects of Atomic Radiation (UNSCEAR).

1.3. Biological effects

BE are translated at the cell level with numerous endpoints [13] associated with damaging, protective or undetermined consequences. Most biological effects are largely considered to be directly or indirectly linked with a prominent oxidative stress, inducing genetic instability, related to DNA damages [10,19,21–23,15,24]. An increased frequency of micronuclei formation and sister chromatid exchanges was reported, indicating unrepaired or

Please cite this article in press as: F. Chevalier, et al., Proteomic overview and perspectives of the radiation-induced bystander effects, Mutat. Res.: Rev. Mutat. Res. (2014), http://dx.doi.org/10.1016/j.mrrev.2014.11.008

miss-repaired single and double-strand breaks of DNA. An enhanced cell growth and radioresistance, an altered gene expression of regulatory and DNA repair pathways, the induction of apoptosis and neoplastic transformation were also observed in bystander cells [25], showing a large variety of biological responses of the BE, and its consequences in normal cells, surrounding the targeted irradiation area.

1.4. Cellular mechanisms

BE are observed in a large variety of biological systems, and are now well documented in radiobiology studies. However, there is still no consensus on a precise definition of the cellular mechanisms involved during these phenomena. Several mechanisms were alternatively proposed, including the production of reactive oxygen species and/or the secretion of BF by irradiated cells, or the direct cell to cell communication, *via* gap-junctions (Fig. 1). Most of the cellular mechanisms involved in radiation responses and BR are intimately linked to the balance of reactive oxygen species and inflammatory-related cytokines [26]. BE is at least in part driven to restore cellular and tissue homeostasis in response to IR inflammatory stress.

1.4.1. Cell type (signaler vs responder)

Following cell or tissue irradiation, signaler cells can transmit a stress response to neighboring cells in different ways (Fig. 1, cell 1). However not all cell types are signalers of a BE (Fig. 1, cell 2), independently of any direct effect of ionizing radiation, and without any rational or explained reason. With the exception of fibroblast cells, there is no general consensus for a conserved state as signaler and/or responder cells. Indeed, it is well established that fibroblasts usually answer to stimuli of BF as a positive control, a kind of universal responder [3]. A wide variety of bystander "competent" or "non-competent" cell types as signalers or responders have been described, but it is not possible to determine a global rule for such cell capacity, as all these studies were performed independently with specific irradiation protocol and different analysis methods. Nevertheless, it appears that the concept of signaler/responder cells is the key in the understanding and the control of the BE *in vivo*.

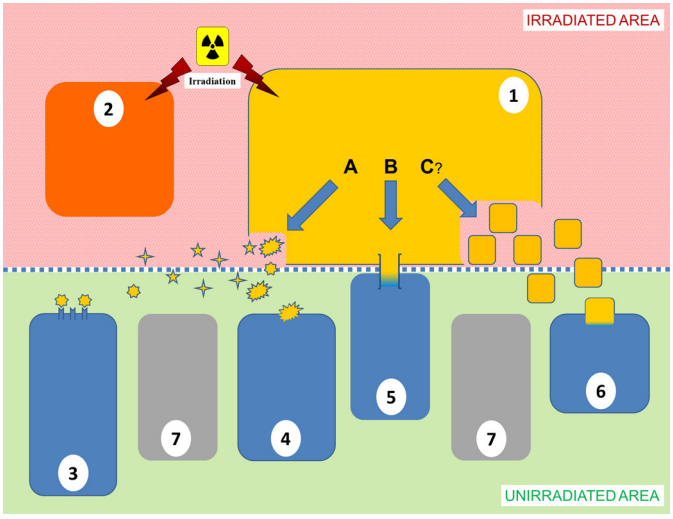

Fig. 1. Schematic representation of cellular mechanisms potentially involved in a bystander response to ionizing radiation. In the irradiated area (top red area), some cells, the signaler cells, can respond to direct radiation by producing bystander responses though several ways (orange cell 1); other irradiated cells (red cell 2) are not able to produce a bystander response. The bystander signal, by definition, is transmitted in the un-irradiated area and some cells, the responder cells (blue cells 3, 4, 5 and 6), competent to receive bystander signals, will display a characteristic bystander response. In the un-irradiated area, some cells (gray cells) can't receive or interpret the signal and do not develop a bystander response. Three cellular mechanisms of intercellular communication are proposed to be involved in the RIBE response: (i) direct secretion in the extracellular matrix of bystander factors (A) recognized by specific receptors of responder cells (cell 3) or directly incorporated inside the cellular membrane of responder cells (cell 4); (ii) direct connection between cytoplasms of signaler cells and responder cells (cell 5) via gap-junction (B); and (iii) secretion by signaler cell in the extracellular matrix close to responder cells (cell 6) of small vesicules such as exosomes (C). In the case of gap-junction communication and exosome secretion, a part of the cytoplasm content from irradiated signaler cells is transferred to the responder cells, including a large range of bioactive and/or oxidized molecules, with the potential capacity to induce a biological bystander response. (For interpretation of the references to color in this figure legend, the reader is referred to the web version of this article.)

1.4.2. Secretion of factors by irradiated cells

The secretion or release of diverse factors by irradiated cells is one of the two main mechanisms of the BE dissemination. Concerning the direct secretion of soluble factors in the intercellular matrix (Fig. 1, cell 1, mechanism A), several studies have shown clear evidences for a major implication of lipid peroxide products, reactive oxygen or nitrogen species, and cytokines. Such factors are also generally observed in inflammation diffusion within a tissue, following a stress stimulus. However, in the case of RIBE, it is likely that other factors are implicated, as BR could be closely related to direct effects of ionizing radiation. BF can interact with responder cells and being directly incorporated inside the cell by diffusion through the cell membrane (Fig. 1, cell 4) or they can be recognized by responder cell receptors, inducing a specific cell response (Fig. 1, cell 3). A final mechanism is coupled with the physiological relevance of shedding from native and irradiated cells [27]. This cellular mechanism corresponds to the secretion of small vesicles or exosomes by the responder cell, allowing the transport of various soluble or insoluble factors between cells (Fig. 1, cell 6 *via* mechanism C). An increased production of exosomes was observed in gamma-irradiated cells, in a p53-dependent manner [28].

1.4.3. Gap junction communication between cells

A second mechanism of inter-cell communication involves gap-junction channels [1,19,10], creating a direct communication between the cytoplasm of irradiated cell and the very close/touching surrounding nonirradiated cell (Fig. 1, cell 5 *via* mechanism B). The involvement of gap-junctions in the transmission of stress signals from irradiated to non-irradiated cells was demonstrated using low fluency radiation and chemical inhibitors of gap junction [29]. The absence of gap junction in a confluent fibroblast cell population reduced micronucleus formation after high LET radiation. In this study, inter-cell communication of BE *via* direct physical channels was observed in parallel to the secretion of unknown factors [29].

2. Analysis protocol

The transduction and propagation of a BE certainly involves several mechanisms of inter-cell communication, activated alternatively or at the same time, as a function of the biological context (signaler *vs* responder cell type and proximity between cells) and as a function of the radiation quality. To explore these mechanisms more deeply, *in vitro* model systems were analyzed to simplify and limit the communication possibilities between cells following irradiation.

2.1. In vitro *transfer of conditioned medium*

To show the secretion of active factors by irradiated cells, the medium of irradiated cells cultured *in vitro* was transferred to non-irradiated cells [30] (Fig. 2). This protocol allowed: (i) the analysis of direct effects of irradiation using irradiated cells; (ii) the analysis of indirect effects of irradiation using bystander cells; (iii) the

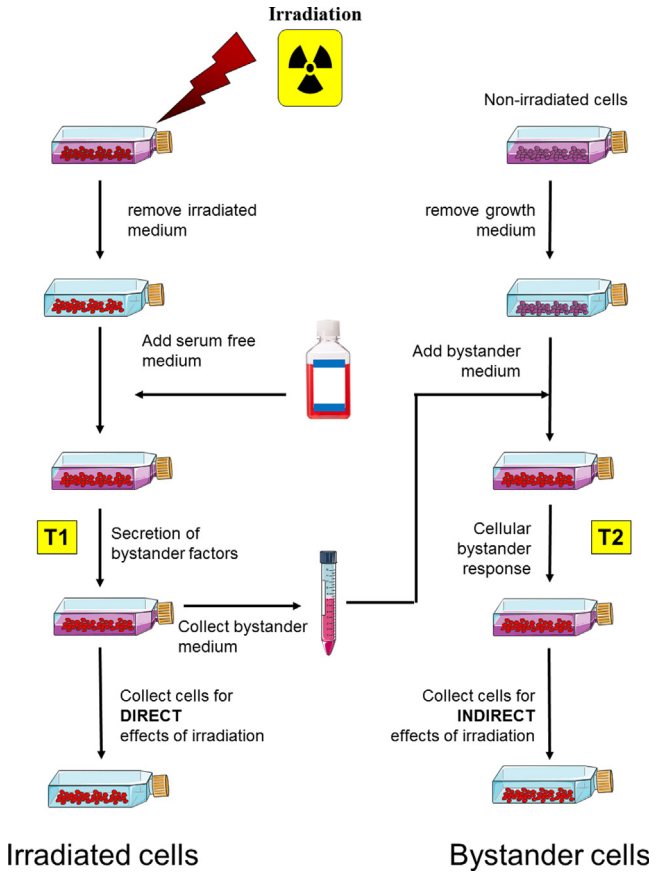

Fig. 2. Detailed "medium transfer" protocol proposed for the analysis of irradiated cells, bystander medium and bystander cells. Cells were first irradiated at the required dose, incubated with fresh serum-free medium during the determined period (T1), after which cell layer (irradiated cell sample) as well as bystander medium (conditioned medium sample) were collected. The bystander medium, which can be used for the direct identification of BF or non-irradiated cells, was incubated with bystander medium during the determined period (T2) after which cells were collected (bystander cell sample).

analysis of the bystander medium using biochemical and proteomics techniques, when a BE was effectively observed. The use of serum-free medium for the preparation of conditioned medium is required to reduce the molecular complexity and allows a proteomic identification of BF. Of course, again in case of this protocol, the choice of radiation source, its quality and dose and the choice of signaler and responder cells are critical to obtain a BR or not. The other critical points that need to be set up for each experiment, are the incubations times T1 and T2 (Fig. 2). Indeed, without identification of the BF, it is difficult to estimate the timing of the events in the bystander signaling process. In case of a secretion in the conditioned medium, the duration of the secretion, the functional stability and the bystander activity of a factor will determine a plateau or a maximum at a precise timing following cell irradiation. Depending on the experimental conditions, BE were observed in a range of time, from 10 min to 24 h following irradiation [31]. With the same idea, the contact time between bystander medium and un-irradiated cell, to produce a BE is linked to the concentration of the factor, its capacity to penetrate bystander cells and to induce a cellular response.

2.2. In vitro *co-culture*

A significant reduction in system complexity can be obtained when irradiated cells and non-irradiated cells are co-cultured. With this strategy, stages T1 and T2 of the conditioned medium transfer protocol (Fig. 2) are simultaneous, allowing a synchronized secretion of BF by signaler cells and reception of these factors by responder cells. *In vitro* co-culture of two different sets of cells usually requires a compartment system, with a physical separation of cells, and a medium exchange between compartments through a microporous membrane (Fig. 3A). The two populations of cells are placed within distance in both compartments to study secreted BF (Fig. 3B1), or placed on both sides of the upper compartment to study secreted and gap-junction-related BF (Fig. 3B2).

Others strategies of co-culture have been also tested *in vitro*. With specific protocols, it is possible to generate two populations of cells mixed together in the same flask. For example, using a mask screen during irradiation, a part of the cells in the culture flask was covered and didn't receive ionizing radiation; it was then possible to compare cell survival in field and out of field within the same flask in order to observe potential BE [32–34]. Second, using low fluences of α-particles, only a small portion of cells were traversed (<1%) and responses occurring in the whole cell population displayed a bystander-like effect, with an increased frequency (~30%) of sister chromatid exchange [35].

2.3. In vivo *protocols*

When analyzing such complex cell mechanisms, it is indeed easier to use a simplified cell system such as *in vitro* single cell to find partial or cell specific process with particular factors. However, the lack of realistic multicellular morphology prevents the observation of the whole phenomenon in a three-dimensional system, with cell-to-cell interactions between different tissue organizations in a close environment.

Considering the presumed proximity between directly irradiated cells and bystander non-irradiated cells, RIBE effects should

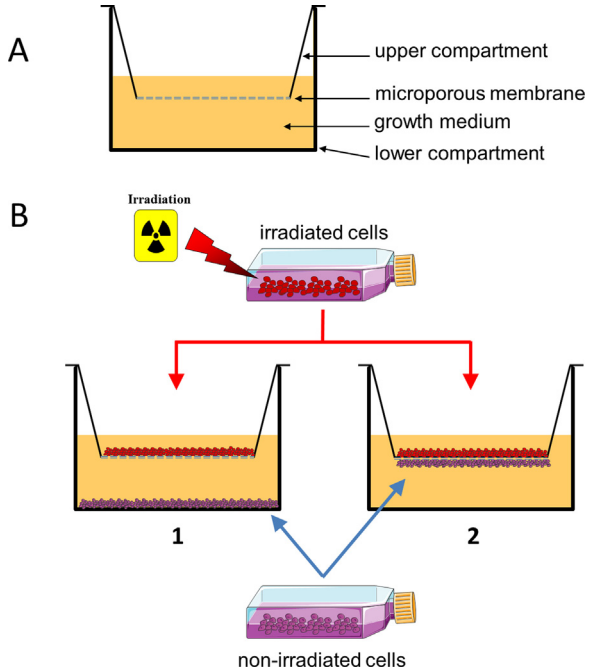

Fig. 3. Schematic of the device used to perform "co-culture" experiments. A cup with the bottom composed of a microporous membrane is positioned in a multi-well microplate (usually 6 or 24 wells per microplate). The membrane is designed to allow cell adherence and medium exchange between the upper and lower compartments (A). Irradiated cells are, for example, placed in the upper face of the cup. Secreted BF are released by irradiated cells and received by non-irradiated cells in the bottom of the well (B-1) or in the lower face of the cup (B-2). When irradiated and non-irradiated cells are placed on both sides of the microporous membrane (B-2), the close proximity allows an additional intercellular communication, *via* gap-junctions.

Please cite this article in press as: F. Chevalier, et al., Proteomic overview and perspectives of the radiation-induced bystander effects, Mutat. Res.: Rev. Mutat. Res. (2014), http://dx.doi.org/10.1016/j.mrrev.2014.11.008

be limited to the irradiated organ, or to the touching surrounding organs. Also, it appears that *in vivo* studies of RIBE included a whole body response, where blood vessels were involved in BF dissemination [36], or even an inter-individual communication of BF, when, for example, irradiated fishes communicated with non-irradiated fishes through the water environment [37]. These studies must be considered carefully, because the frontier between bystander and abscopal effects is hard to delimit *in vivo*, and the observed effects could be indirect without any relation to the irradiation treatment, considering the immune system response, or a potential global stress.

2.4. Prediction models

Recently, several models were sequentially developed to predict adverse effects of signaling cells following IR of a radiotherapy protocol [38,39,34,40]. These models were proposed to evaluate the impact of intercellular communication of irradiated cells on the real exposure of surrounding healthy tissues. A mathematical model based on *in vitro* observations of cell survival following modulated radiation exposures shows significant differences between adjusted signals and physical doses, with the largest increase in doses (from 23 to 33 Gy) in the low-dose regions, close to the target volume.

3. Proteomic studies of RIBE

Although RIBE has been demonstrated in numerous studies, it is still difficult to define a general process as it depends on a lot of physical, temporal and biological parameters, as described already in this review (Fig. 1). It is noted that the first cellular response to IR is, at least in part, related to an imbalanced red/ox status. In association with a denaturation and/or a partial destruction of bio-molecules, direct effects of IR leads to a massive deposit of energy inside living cells (normal and tumor cells). Of course, DNA damage and DSB are the most handicapping cellular lesions, inducing in turn repair processes to enable genetic stability. In addition to this well-studied cellular response, IR also induces the formation of free radicals with most bio-molecules. Lipids, proteins, water, DNA are ionized and release highly reactive free radicals. This very fast phenomenon (nanoseconds scale) produces an oxidative stress (OS): hydroxyl and superoxide radicals react with other molecules, amplifying the radical oxidation proportionally to the initial IR intensity. Molecular actors implicated in this IR-based OS are partly known and follow from studies related to more general OS homeostasis mechanisms. If OS can be transmitted from irradiated cells to bystander cells, it could be associated with such protein actors in a direct or indirect way, or maybe through other unknown factors. Such imbalance of OS observed in bystander cells is not necessarily induced by the OS-associated factors from irradiated cells. The whole cellular machinery is implicated in the maintenance of the ROS level, for example, to regulate cell proliferation [10]. A focus on specific proteins or enzymes is certainly not the best strategy to elucidate RIBE, as it involves lots of different cellular metabolism pathways. Without any *a priori* results, a non-targeted proteomic study is recommended to analyze variations of the protein content following strategically chosen irradiation protocols.

3.1. Experimental strategy

With the development of many different proteomic tools and the large availability of proteomic platforms in research centers, the ability of researchers to use such technologies is increasing fast. However, the access to such tools doesn't prevent the necessity to build a solid experimental strategy (Fig. 4). Proteomic is not a magic black box, allowing the easy discovery of biomarkers, whatever the biological questions, samples quality or protocols. Reference samples, positive and negative controls, robustness on sample producing, repeatability of staining protocol and compatibility with mass spectrometry are mandatory [41,42]. Even with the best proteomic tools available, when initial samples display a poor quality, final results will be of a poor quality too. A fractionation or enrichment in the studied compartments could be needed to prevent the hiding of proteins of interest by abundant proteins (*e.g.*, albumin in a serum sample). The choice of the proteomic strategy (for example 2-D electrophoresis or shotgun proteomics) must be linked with the biological endpoint to be compatible and feasible and will guide sample preparation, such as biological and technical replicates, protein amount or solubilization buffer.

3.2. Proteomic tools

Proteomic studies have increased exponentially during the last twenty years. Proteomic technologies involve most protein-dataset global analysis methods, including gel-based, gel-free and protein chips techniques. These post-genomic technologies were closely linked to the development of mass spectrometry, dedicated to the study of bio-molecules and peptides. Following the genome sequencing, it appears that the final biological product of DNA, *i.e.*, proteins, is one of the most essential biomolecules in the cell and in cell regulation and stability. One gene can potentially produce hundreds of unique proteins, thanks to special regulations, maturation and gene splicing during protein synthesis and, according to a number of post-translational modifications such as phosphorylation, acetylation, sumoylation, as a function of protein signalizations and cell stresses. Since the late 1990s, mass spectrometers are continuously improving in terms of accuracy and sensitivity to analyse deeper and deeper inside various proteomes. These machines are now intimately dedicated to the analysis of proteins and peptides, alone or in mixtures, with specificities for PTM (post-translational modifications) identification and/or quantification. To analyze a specific proteome, it is mandatory to reduce the complexity of protein or peptide mixtures with several and sequential steps of separation. Two major types of approaches are traditionally balanced for protein biomarker discovery: the analysis of intact separated proteins (top-down proteomics) and the analysis of peptide mixtures from digested proteins (bottom-up proteomics). A third technology, based on antibody assays, emerged as complementary to the classical proteomic approaches; proteins are observed and quantified using a miniaturized system, a microarray chip, dedicated to a specific scientific question, and allow a direct, targeted and sensitive analysis of proteomes (Fig. 4).

3.2.1. Top-down proteomic approaches

Top-down proteomics consists of separating intact proteins from complex biological samples using traditional separation techniques such as 2-D gel electrophoresis (2DE), followed by differential expression analysis using gel imaging platforms (Fig. 4 from "proteins separation technics" to "proteome observation"). Spots predicted to contain biomarkers are identified using MS. Gel-based proteomics largely centered on 2-D electrophoresis is a technique of choice for simultaneously visualizing and quantifying up to 2000 protein spots within the same gel [43,44]. Protein samples have first to be dissolved in a 2DE-compatible buffer, usually composed of urea and non-ionic or zwitterionic detergents. Proteins are then separated in a first dimension by isoelectric-focalization (IEF) as a function of isoelectric points in a native-like state. Following the first dimension, strips with separated proteins are equilibrated in SDS buffer to bind this anionic detergent to the

Please cite this article in press as: F. Chevalier, et al., Proteomic overview and perspectives of the radiation-induced bystander effects, Mutat. Res.: Rev. Mutat. Res. (2014), http://dx.doi.org/10.1016/j.mrrev.2014.11.008

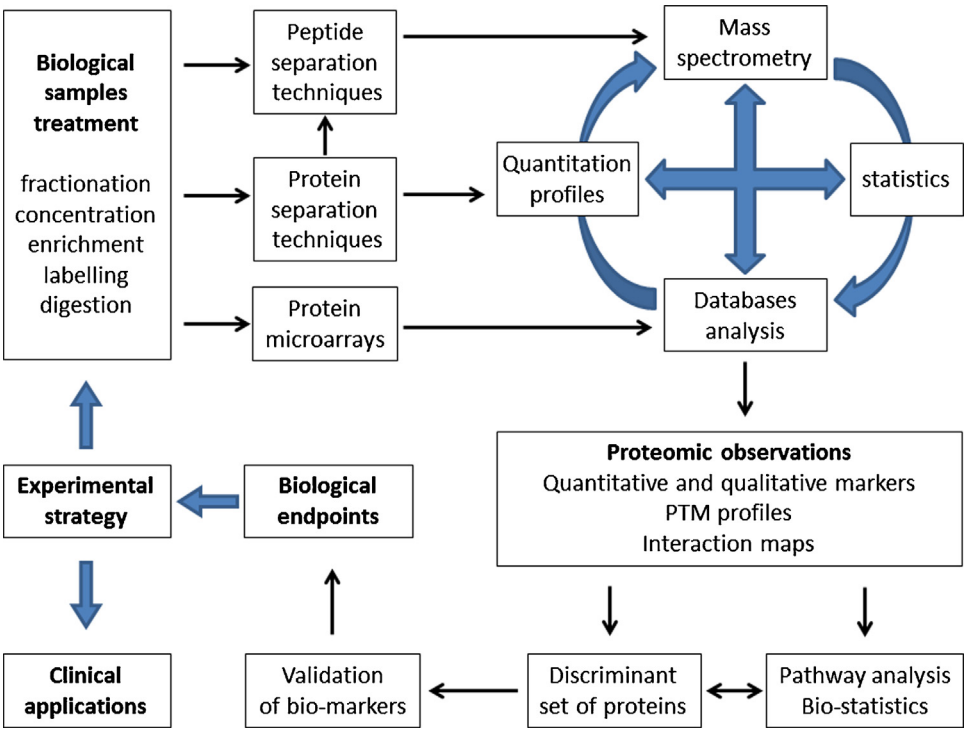

Fig. 4. Typical sequential process within large scale proteomic studies. The flowchart illustrates the three major proteomic strategies developed for a global analysis, from biological sample treatments to biological endpoints and clinical applications: gel-based proteomics, MS-based proteomics, and antibody-based proteomics. Prior to proteomic analysis, protein samples are specifically treated, solubilized or digested to be compatible with the subsequent proteomic strategies, and to reduce their complexity, thus increasing the chance of the identification and quantification of less abundant proteins. In typical gel-based (top-down proteomics) and shotgun proteomic approaches (bottom-up proteomics), proteins or peptides are separated by 2DE or by HPLC, respectively. The resulting spot proteins or peptide spectra are in turn sequentially submitted to MS identification, bio-informatic quantification, dedicated statistical analysis, and database analysis. In the case of protein microarrays, the antibody-based strategy allows targeting of specific proteins, with no need for MS identification. Following these steps, proteomic observations are interpreted and protein groups are analyzed as a function of the biological context using bio-informatics tools (e.g., interaction map, cellular pathways, known biological activity, previously published experiments in the same area). From the discriminant set of proteins, biomarkers are validated using unrelated experimental strategies to reach the biological endpoint. This final finding can then open new possibilities of (proteomic) experiments and clinical applications.

protein and to allow the second dimension of separation. During this equilibration step, proteins are reduced and alkylated, to reduce artefacts of separation and MS identification. The last step consists of SDS-PAGE of proteins, with a separation according to the protein molecular mass. An unreduced state of protein can be preserved during equilibration to study disulfide-linked polymers [45,46]. The separation power of 2DE is correlated with intrinsic characteristic of proteins involved in both orthogonal separations. Indeed, the 2DE is based on two independent biochemical characteristics of proteins. It typically combines isoelectric focusing (IEF), which separates proteins according to their global isoelectric point (related to amino acid nature, *i.e.*, acid/basic/neutral), and SDS-PAGE, which separates them further according to their molecular mass (related to amino acid number), as illustrated by the 2DE image of our recent study of the secretome of irradiated cells (Fig. 5). Currently, 2DE allows simultaneous detection and quantification of up to thousands of protein spots in the same gel [47]. Combined with subsequent mass spectrometry analysis, 2DE offers the possibility of identifying intact native proteins [48,49], comparing isoform abundance [50,51] and posttranslational modifications [52,53].

3.2.2. Bottom-up proteomic approaches

The bottom-up approach to protein profiling (proteolytic digestion of proteins prior to MS analysis) has been widely adopted in modern MS-based proteomics research (Fig. 4 from "peptides separation technics" to "proteome observation"). Known as "shotgun proteomics," the bottom-up proteomic approach consists of a direct digestion of a biological sample using a proteolytic enzyme to create a complex peptide mixture. The digested samples are then analyzed on specific high-resolution/high-performance mass spectrometers involving liquid chromatography and tandem mass spectrometry. These analytical systems are low-throughput by requirement, and basic biological questions are usually addressed using a small number of samples from simple model systems. The main advantage of the bottom-up approach is the ability to achieve high-resolution separations, producing protein identifications and relative expression for hundreds of proteins within a small number of samples.

3.2.3. Protein microarrays approaches

The conception of protein microarrays was a great challenge compared with DNA microarrays due to the absence of any amplification process adaptable to proteins, in order to generate large amounts of protein. To resolve this technological obstacle, sensitive and specific detection systems were set-up, using antibody-based technology coupled with dedicated labelling systems. Protein microarrays provide a valuable platform for both classical and functional proteome analysis and offer many advantages, the most important of which is the high-throughput analysis of thousands of proteins simultaneously. Protein microarrays are classified as analytical, reversed-phase and functional microarrays as a function of the substrate's nature immobilized onto the solid array surface [54]. In analytical arrays, antibodies are immobilized onto the array surface and incubated with the test sample. Targeted biomolecules are then captured on the array surface from the test lysate and can be detected by means of specific labeled secondary antibodies. Reversed-phase arrays are

Please cite this article in press as: F. Chevalier, et al., Proteomic overview and perspectives of the radiation-induced bystander effects, Mutat. Res.: Rev. Mutat. Res. (2014), http://dx.doi.org/10.1016/j.mrrev.2014.11.008

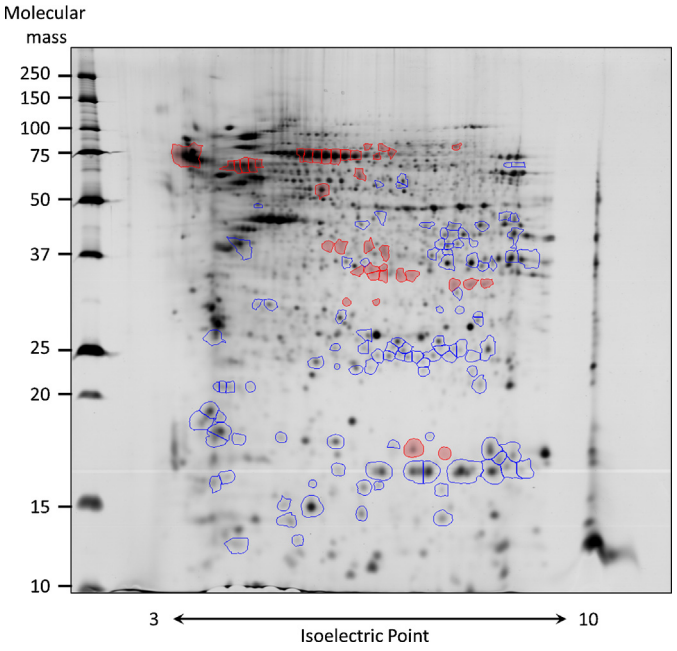

Fig. 5. An example of 2DE separation of proteins secreted by irradiated breast cancer cells [61]. Proteins are extracted by precipitation as presented in Fig. 8 (right part), from the bystander medium of irradiated cells obtained as presented in Fig. 2. Following protein quantification, 100 μg proteins were separated using 2DE, with a 3–10 p*I* range for the first dimension and a 12% acrylamide gel for the second dimension. Protein spots are silver stained and gel pictures of irradiated and non-irradiated secretome samples are compared with the Samespots software. Spots with an increased amount in irradiated samples are highlighted in blue, while spots with decreased amount in irradiated samples are highlighted in red.

generated by immobilizing the test sample on the array surface, which is then probed using a detection antibody against the target protein of interest. These antibodies are in turn detected by means of secondary tagging. Functional microarrays study the biochemical properties and functions of thousands of native proteins, peptides or domains printed onto a chip surface in their active state, after extensive purification using cell-based methods or by cell-free expression on the array.

3.2.4. Bioinformatics, from proteome to biological endpoints

All of these proteomic approaches involve specific bioinformatics and biostatistics tools to extract the valuable information. Several steps of each approach produce large datasets of protein or peptide characteristics and parameters. For example, using the gel-based proteomic approach, following 2DE separation of proteins, gel pictures are analyzed using specific software and several parameters are associated with each detected spot, such as gel location with observed p*I* and M*r*; spot intensity based on gray levels; spot variability between technological and/or biological replicates (fold change, ANOVA), spot area, background, etc. Spots of interest are then selected and submitted to biostatistics methods using dedicated tools to find those spots that show differences in expression between groups, using several statistical parameters to prevent false positive selection (*e.g.*, *p*-value, *q*-values, power of analysis). Spots with significant differences in intensity are then selected for the next step, the protein identification by MS. The MS analysis also involves numerous bioinformatics analysis of data, with specific MS-based statistics to study observed mass spectra and compare then with databases. Following this multi-axial and circular analysis, involving biophysics, biochemistry and bioinformatics tools (Fig. 4), a set of characteristics of the analyzed proteome can emerge with quantitative and qualitative markers for specific PTM modifications.

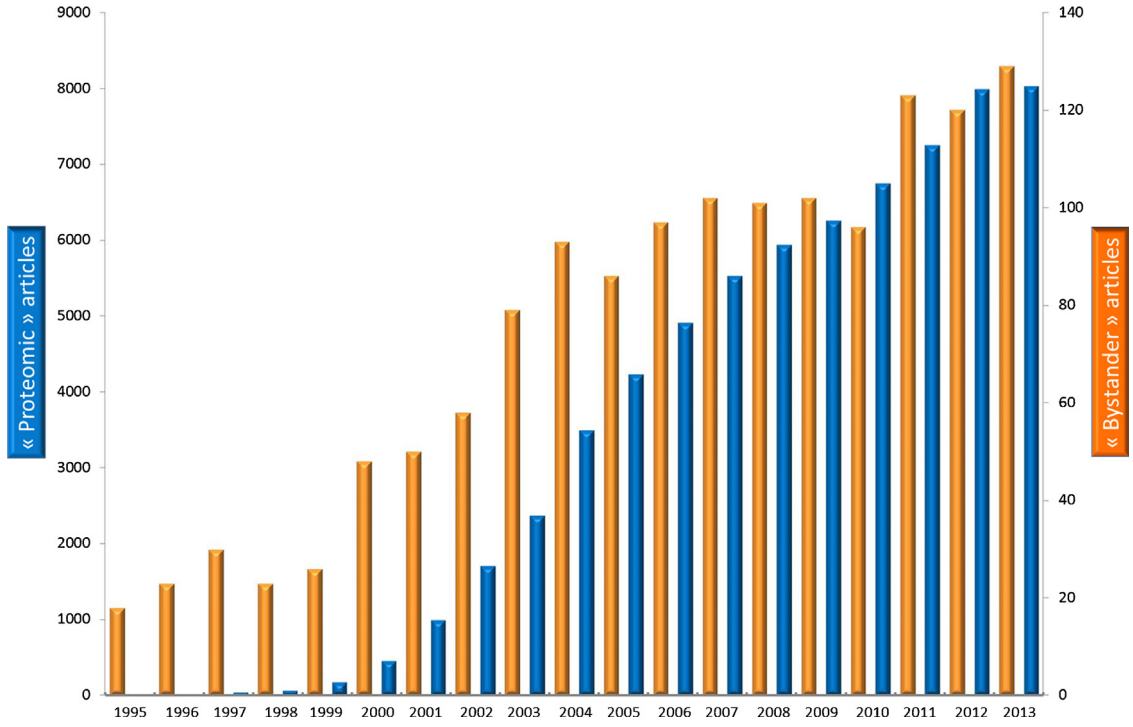

Fig. 6. Number of publications in the fields of bystander and proteomics between 1995 and 2013. For each year period, the number of publication in the field of "Bystander" (red histogram) and "Proteomic" (blue histogram) was estimated using the Pubmed tool "Results by year" at the address: http://www.ncbi.nlm.nih.gov/pubmed/; with the following criteria: bystander articles = pubmed – (irradiation OR irradiated OR radiation) AND ("conditioned medium" OR "diffusible factor" OR "secreted protein" OR bystander OR "bioactive molecule"); proteomic articles = pubmed – proteome OR proteomic OR secretome OR secretomic. (For interpretation of the references to color in this figure legend, the reader is referred to the web version of this article.)

Please cite this article in press as: F. Chevalier, et al., Proteomic overview and perspectives of the radiation-induced bystander effects, Mutat. Res.: Rev. Mutat. Res. (2014), http://dx.doi.org/10.1016/j.mrrev.2014.11.008

Biomarkers of a proteomic comparison arise from the analysis of the discriminant set of proteins, their relationships, the relevance of protein family members, cellular pathway implications, and their association and interaction in known protein complexes. Then, after all these bioinformatics steps, biological endpoints are obtained when biomarkers are validated using independent and distinct techniques, for example, quantitative Western blot analyses of new samples, biologically relevant activity tests, or knockout mutants.

3.3. Publication volume of proteomic and RIBE studies

According to such powerful capacity of investigation, proteomic approaches were applied to a large range of biosciences to find biomarkers, or to understand fundamental organization of living cells. The number of scientific articles including the term "proteomic" increased exponentially from 1999 to 2013 (Fig. 6 blue bars). In 2013, about 8000 articles were published in the proteomic field, in all areas of scientific research, referenced in PubMed. From 1995 to 2013, the number of scientific articles including the term "Bystander" (applied to radiation research) increased largely too (Fig. 6 orange bars). However, it appears clearly that, when both subjects were combined, very few articles were found. Indeed, only 15 studies were observed that associate RIBE and proteomic tools (Table 1) from 1999 to 2013. The low use of proteomic tools in RIBE studies could demonstrate the limited knowledge of radiobiologists in these technologies and their capacities of investigation. Historically, radiobiologists studied direct effect of radiations, using cellular and molecular tools, applied to DNA stability and DNA damages. The discovery of a RIBE implied a cellular response and inter-cell communication *via*, at least partially, protein factors. Proteomic analysis, which was massively used in fundamental cancer research and biomarkers finding, is now a new possibility offered to radiobiologists to understand direct and indirect cellular responses to IR.

3.4. Proteomic studies overview

Since a decade, several labs started to use proteomic strategies to study RIBE at various cellular levels with contrasting successes. The 15 studies related to the RIBE research are summarized in Table 1 and are discussed in the next sections, as a function of the experimental strategies employed.

3.4.1. MS-based proteomic studies of RIBE

RIBE has been analyzed *in vitro* with low dose irradiation of CHO cells [55] and HMEC (human mammary epithelial cells) [56]. In these studies, global changes in shed proteins in media taken from cells exposed to low-doses of radiation were analyzed using MS-based proteomics. Shed proteins are anchored at the cell surface, and released by regulated proteolysis, according to a general cellular process in response to various injuries. In these studies, the authors analyzed conditioned media of cells using a mass spectrometry-based global proteomic method. Media samples taken from irradiated CHO cells were analyzed using a combination of tandem- and Fourier transform-ion cyclotron resonance mass spectrometry [55]. About 500 proteins were identified and 20% were predicted as integral membrane proteins or membrane-associated proteins, suggesting as being derived from the cell surface, and released by a shedding process. The evaluation of quantitative changes didn't show any differences between control and irradiated samples. With a comparable experimental strategy, the same group analyzed shed proteins in medium from irradiated HMEC. From the 177 identified proteins, 23 sequences were attributed to membranes associated proteins, but with no changes in abundance reliable to radiation exposure. According to these two studies, following a 10 cGy irradiation with gamma-rays, no bystander factors were highlighted in medium after a secretion time of 5 h using CHO and HMEC cells.

An analysis of the secretome of zebrafish embryonic cells showed no specific bystander proteins following low-doses irradiation with chronic X-rays [57]. The factors secreted by a human skin model were analysed following irradiation using a multidimensional LC–MS strategy [58]. A set of 135 proteins were identified as specifically modulated and potentially involved in a BR.

Adaptive response to low-dose radiation of human lymphocytes was investigated *in vitro* using MS-based proteomics [59]. The authors characterized global expression profiles of proteins released in the medium from human lymphocytes first irradiated with 3 cGy, 4 hours prior to a 1-Gy gamma-ray irradiation. A list of 55 proteins was identified without quantitative difference between adaptive and non-adaptive groups, and a list of 48 proteins were identified with quantitative or qualitative specificities to adaptive groups. These proteins, related to an adaptive process, were secreted by irradiated cells and were potentially linked to a protective action of RIBE.

The secretory profile of NSCLC-associated fibroblasts was investigated *in vitro* after ablative radiotherapy using a combination of shotgun proteomics and ELISA multiplex assays [60]. Cancer associative fibroblasts (CAF), isolated from freshly resected human lung tumors, were exposed to ablative doses of IR (18 Gy) and analyzed for the secretion of paracrine bystander factors. In agreement with the data generated by multiplex protein assays, proteomic analysis showed a reduction of angiogenic regulators (TSP1 and TSP2) and IL-6 and an increase of macrophage migratory inhibitory factor in the supernatant of irradiated cells.

3.4.2. Gel-based proteomic studies of RIBE

Using a 2DE gel-based proteomic strategy, the secretion of bystander factors from several human breast cell lines following irradiation at 10 Gy was analyzed *in vitro* [61]. To limit the identification of false-positive secreted proteins, total and cytosolic cell extracts were performed in parallel to secretory protein extracts with un-irradiated controls and irradiated samples. Taken together, 2DE pictures from all samples and replicates were associated within the same software analysis, and only 37 protein spots were specifically modulated between irradiated and control conditioned media. From these spots, 17 distinct accessions were identified by MS, with a majority of secreted proteins. An increased secretion of Cyclophilin A (CyPA) was observed in 5 modulated spots, and confirmed by a 1D and 2D Western blotting analysis. As observed subsequently by a deeper MS analysis, these CyPA isoforms were modified by several post-translational modifications such as methylations and/or acetylations [61]. Moreover, the secreted form of CyPA was increased in radio-sensitive cell lines and potentially linked to a RIBE of that type of cells.

With a similar proteomic experimental strategy, the proliferative response of bystander rat liver cells was investigated *in vitro* using separated or co-cultures of un-irradiated and 5 Gy irradiated cells [62]. A confluent monolayer of rat liver cells were irradiated and mixed with a majority of un-irradiated cells (5/95) and co-cultured for 24 h. Total extract of un-irradiated cells was compared with extracts from irradiated or co-cultured cells using 2DE. Modulated protein spots were identified by MS and indicated that the presence of irradiated cells in a population of un-irradiated cells can affect nucleophosmin (NPM)-1 and alpha-enolase synthesis by a direct or indirect RIBE mechanism.

Bystander factors secreted by irradiation-induced senescent cancer cells were analyzed *in vitro* using a 2DE proteomic strategy [63]. Conditioned media from IR-induced senescent MCF-7 cells

Please cite this article in press as: F. Chevalier, et al., Proteomic overview and perspectives of the radiation-induced bystander effects, Mutat. Res.: Rev. Mutat. Res. (2014), http://dx.doi.org/10.1016/j.mrrev.2014.11.008

Table 1
List of studies on RIBE analysis, using a proteomic strategy.

Ref.	Year	Experiment	Biological sample	Radiation type and dose	Bystander methods	Time post-irradiation	Protein sampling	Proteomic method	Results
[55]	2005	*In vitro*	CHO cells	γ-Rays ^{60}Co 0.1 Gy	Conditioned medium	5 h	Medium concentration and glycosylated proteins enrichment	Gel-free; LC–MS/MS; FT-ICR MS; database analysis and blast against membrane sequences	20% of the 500 identified proteins were attributed to membrane proteins but without abundance changes linked to a bystander effect
[56]	2005	*In vitro*	Human mammary epithelial cells (HMEC)	γ-Rays ^{60}Co 0.1 Gy	Conditioned medium	5 h	Medium concentration	Gel-free; LC–MS/MS; database analysis	23 membrane associated proteins with no changes in abundance linked to radiation exposure
[62]	2007	*In vitro*	Rat liver epithelial cell (WB-F344)	γ-Rays ^{137}Cs 5 Gy	Co-culture (mixture of 95% unirradiated and 5% irradiated)	24 h	Total protein extraction from cell in 2DE compatible lysis buffer	2DE (p*I* 3–10; SDS-PAGE 9-18%; sypro ruby); MALDI–TOF–TOF MS/MS; western blotting	Expression changes of NPM-1 and alpha-enolase isoforms of bystander cells
[64]	2007	*In vivo*	Rainbow trout fish	X-rays 0.5 Gy	Co-culture and medium transfert (mixture of irradiated and unirradiated fish; unirradiated fish placed in water of irradiated fish)	2 + 2 h	Protein extraction from the gill tissue in 2DE compatible lysis buffer	2DE (p*I* 3–10; tricine SDS-PAGE 10% duracryl; sypro ruby); ESI Q–TOF MS/MS	Expression of hemopexin-like protein, RhoGDI, PDH and SCAF was modified in bystander fishs
[65]	2011	*In vivo*	Wild type and radiosensitive medaka fish	X-rays 0.5 Gy	Co-culture (irradiated and unirradiated fishs were placed in the same container partitioned by a mesh screen)	2 + 2 h	Protein extraction from the gill tissue in 2DE compatible lysis buffer	2DE (p*I* 3–10; tricine SDS-PAGE 10% duracryl; sypro ruby); ESI Q–TOF MS/MS	Annexin max3, annexin A4, creatine kinase, LDH, Wap65 and SCAF proteins were modulated in bystander medaka gills
[61]	2012	*In vitro*	Radioresistant and radiosensible human mammary cells (T-47D, MCF7, BT-20, ZR-75, MDA-MB-157, MDA-MB-231)	γ-Rays ^{137}Cs 10 Gy	Conditioned medium	18 h	Protein fractionation and precipitation	2DE (p*I* 3–10; SDS-PAGE 12%; silver nitrate); MALDI–TOF–TOF MS/MS; Nano-LC MS/MS; 1D and 2D western blotting; Q-RT-PCR	17 modulated proteins in conditioned medium including 5 isoforms of CyPA with a complex pattern of maturation and post-translational modifications
[63]	2012	*In vitro*	MCF7, MDA-MB-231, H460, HCT116, HUVEC	γ-Rays ^{137}Cs 6 Gy	Conditioned medium	36 h	Protein concentration with centricon	2DE (p*I* 3–10; SDS-PAGE 11%; silver nitrate); MALDI–TOF–TOF MS/MS; western blotting	RKIP, alpha-enolase, AKAP9 and MARK4 were increased in conditioned medium of irradiated cells
[59]	2012	*In vitro*	Primary blood lymphocyte	γ-Rays ^{137}Cs 0–1 Gy; 0.03–1 Gy	Conditioned medium	72 h	Protein concentration and lyophilisation	Gel-free; LC–MS/MS; database analysis	A list of 48 protein were differentially secreted following an adaptive response to radiation
[69]	2012	*In vitro*	Reconstructed human skin	X-rays 0.03, 0.1 and 2 Gy	Conditioned medium	24 or 48 h	No treatment	Protein microarray, ELISA	20 inflammatory proteins were evaluated, IFN-gamma and MIP-1alpha were modulated at 3 cGy; IL-2 at 10 cGy and IL-2, IL-10, IL-13, IFN-gamma, MIP-1alpha, TNF-alpha and VEGF at 200 cGy
[68]	2013	*In vivo*	Mouse	γ-Rays ^{60}Co 20, 40 and 80 Gy (20% total skin surface)	Blood serum	3 or 7 days	Depletion of major serum proteins	2D-DIGE (p*I* 4–7; SDS-PAGE 10%); MALDI–TOF–TOF MS/MS LC–MS/MS; SELDI-TOF)	15 proteins were selected as candidate proteins specifically modulated in blood following skin irradiation
[36]	2013	*In vivo*	Mouse, human	γ-Rays ^{60}Co 20, 40 and 80 Gy (20% total skin surface)	Blood serum	3 or 7 days	Depletion of major serum proteins with or without deglycosylation	2D-DIGE (p*I* 4–7; SDS-PAGE 10%); MALDI–TOF–TOF MS/MS LC–MS/MS; SELDI–TOF)	Several glycoproteins were modulated following high doses of radiation and serum cytokines (IL-1beta, IL-6 and TNF-alpha) were increased
[60]	2013	*In vitro*	Human CAF	X-rays single 2, 6, 12, 18 Gy or 6 × 3 Gy	Conditioned medium	4 or 6 days	Protein concentration	24 bands SDS-PAGE; nanoLC–Q–TOF	PEDF, TSP-1, TSP-2, IGF-2, GAS-6, MIF, CTGF and IL-6 were identified as modulated in CAF supernatant

Please cite this article in press as: F. Chevalier, et al., Proteomic overview and perspectives of the radiation-induced bystander effects, Mutat. Res.: Rev. Mutat. Res. (2014), http://dx.doi.org/10.1016/j.mrrev.2014.11.008

Table 1 (*Continued*)

Ref.	Year	Experiment	Biological sample	Radiation type and dose	Bystander methods	Time post-irradiation	Protein sampling	Proteomic method	Results
[66]	2013	*In vivo*	Rat brain	X-rays High energy microbeam or homogenous irradiation 35 and 350 Gy	Co-culture (right cerebral hemisphere irradiated and left cerebral hemisphere "bystander" non-irradiated)	4, 8 or 12 h	Protein extraction from the rat brain tissue in 2DE compatible lysis buffer	2DE (p*I* 3–10; SDS-PAGE 12%; sypro ruby); MALDI Q-TOF MS/MS	TPI, serum albumin, prohibitin, HSP71, Aconitase, DLD, Tubulin and GFAP were differentially modulated in the bystander left hemisphere following an irradiation of the right hemisphere
[58]	2014	*In vitro*	Reconstructed human skin	X-rays 0.03, 0.1 and 2 Gy	Conditioned medium	48 h	Depletion of major proteins	Gel-free; LC–MS/MS; database analysis	135 proteins showed a modulation following irradiation
[57]	2014	*In vitro*	Embryonic zebrafish fibroblasts ZF4	γ-Rays ^{137}Cs 0.007, 0.07, 0.7, 5.5 Gy	Conditioned medium	1–24 h	TCA precipitation	LC–MS/MS; database analysis	From the 127 identified proteins, no difference was observed

were collected 2.5 days following a 6 Gy irradiation. Senescent cells are supposed to secrete multiple growth regulatory proteins (*i.e.*, BF), which could alter the behavior of neighboring cells. In this study, the authors identified 24 senescent-associated proteins and the RAF kinase inhibitor protein was proposed to play a central role in neighboring cell migration following irradiation.

In three articles published between 2007 and 2012, the group of Carmel E. Mothersill observed a RIBE-like *in vivo* with adult rat, rainbow trout and medaka fishes using comparative 2DE proteomics. In the first study [64], a group of trouts was X-rays treated with 50 cGy, transferred in a partitioned container holding a non-irradiated trout on the other side of the partition, corresponding to the bystander effect communication by partner fish. Another non-irradiated trout was placed in the first container previously holding the irradiated fish, corresponding to bystander effect communication by waterborne exposure. Proteins were extracted from gills of controls, irradiated and bystander fishes and used to perform 2DE. Expression of hemopexin-like protein, Rho GDP dissociation inhibitor and pyruvate dehydrogenase were increased in bystander trouts, with a potential protective action against bystander ROS. In a second study of the same group [65], a group of medaka fish was X-rays irradiated with 50 cGy, transferred into a partitioned container holding non-irradiated fishes on the other side of the partition, corresponding to bystander fishes. Irradiated and bystander gill proteomes were compared by 2DE with wild-type and radiosensitive transgenic medaka. Several proteins were modulated as a function of irradiated or bystander samples and radiosensitivity of fishes, with an increase expression of annexin max3 or A4, creatine kinase and lactate dehydrogenase. The identified proteins could indicate both immediate protection and longer term adaptation to IR. In a third study [66], the authors investigated the use of microbeam and homogenous irradiations on rat brain. The right brain hemisphere of rats was irradiated with 35 or 350 Gy and several hours following irradiation, the right brain hemisphere (directly irradiated) and the left brain hemisphere (bystander) were collected and proteins were extracted and separated by 2DE. Modulated spots were identified by MS; levels of triosphosphate isomerase, prohibitin and tubulin were decreased and those of glial fibrillary acidic protein were increased in bystander brain samples, suggesting a potential function in ROS-mediated apoptosis.

Radiation-induced damages *in vivo* are complex and lead to specific and characteristic reactions, including inflammation, BR and immunological responses, depending on the tissues irradiated. Organisms respond to irradiation with an altered expression of proteins and/or PTM, and secretion of BF in the close environment of irradiation, which could be released in organic fluids such as blood or urine [67]. Biomarkers of irradiation have been explored in serum and plasma and can be associated with BF by an abscopal response to IR (see Section 1.1). The two following studies demonstrated the capacity of modern gel-based proteomic approaches to highlight serum protein modifications of irradiated animals. Using two complementary large-scale quantitative proteomic approaches, 2DE and SELDI-TOF-MS, proteins specifically secreted or modified in serum of irradiated mice were analyzed [68]. Blood of mice exposed to high doses of gamma-rays was collected 3 and 7 days after irradiation and the corresponding sera were compared using 2-D DIGE and SELDI-TOF. A list of 15 protein spots was observed as being differentially expressed post-irradiation and proposed as a set of protein candidates for triage and prognosis of this kind of irradiation. In a second study, PTM of serum proteins from irradiated mice was analyzed using gel-based and MS-based proteomic strategies [36]. The 2D-DIGE analysis showed a p*I*-shift of several spots as a function of irradiation, and a MS-based glycomic strategy revealed a modulated glycosylation of proteins in sera of locally irradiated mice.

3.4.3. Protein microarrays approach

Protein arrays and protein multiplex assays have been tested several times to simultaneously detect, quantify and analyze targeted molecules in complex samples. These functional proteomic approaches were used in a recent study of the effects of low-dose irradiation on a 3D reconstituted human skin [69]. The inflammatory response of a human skin model was tested using a set of 23 cytokines after 24 and 48 h of irradiation at 3, 10 or 200 cGy. Microarray and ELISA multiplex assays showed a modulation of three cytokines at low doses (10 cGy) and seven cytokines at high dose (200 cGy). An increase in pro-inflammatory cytokines (IL-1beta, IL-6 and TNF-alpha) was reported in the serum of irradiated mice using ELISA multiplex assays [36]. A decrease of angiogenic regulators (SDF-1alpha, ANG-1 and TSP-2) was observed following exposure of CAF to ablative doses of ionizing radiation, using multianalyte profiling assays [60].

4. RIBE proteomic capacities

As explained before, numerous parameters can activate and modulate BE. The proteomic study of RIBE can be summarized and simplified as presented in Fig. 7. The first step, before this proteomic analysis, is the choice of the cellular model, culture condition and irradiation plan. It is crucial and needs to be set up with adequate controls and a careful knowledge of the RIBE bibliography. The second step is the choice of the studied BE, which is related to the compatibility with the experimental strategy, the scientific question, and the potential application in clinical research.

4.1. RIBE proteomic subdivisions

The recent development and large availability of proteomic tools are challenging for the field of radiobiology [70,71]. Lots of exciting questions concerning the molecular and cellular mechanism of the RIBE are emerging thanks to these new technologies. Both MS-based and gel-based strategies display robustness and sensitivity expected for identifying a BF in an established system with known BE. This opens the doors to the study of many biological systems and IR conditions. For example, BF can be studied in systems comparing IR conditions: low *vs* high doses, low *vs* high dose rates, low *vs* high TEL. Studies comparing such IR conditions have already been done, with a successful observation of a BE [4], but the cellular mechanisms involved in such BE are unknown and the specificity of mechanism between BE and IR conditions has yet to be established. The analysis of RIBE can be performed at different levels. Direct and indirect effects can be compared using cellular extracts and associated with the secretion of BF (Fig. 7). Gel-based analysis of such samples allows a global analysis of IR consequences on the selected biological system and presents the advantages of limiting the selection of false-positive BF markers and the identification of direct effects and BE within the same examination [61]. The proteomic comparison of irradiated cells and bystander cells, using un-irradiated cells as control, will display protein biomarkers of direct and indirect effects of IR, with common or distinct cellular mechanisms. For this propose, the analysis protocol used should allow the collection of irradiated and bystander cells separately. The "medium transfer" and the "co-culture" protocols are compatible with such strategy, with some

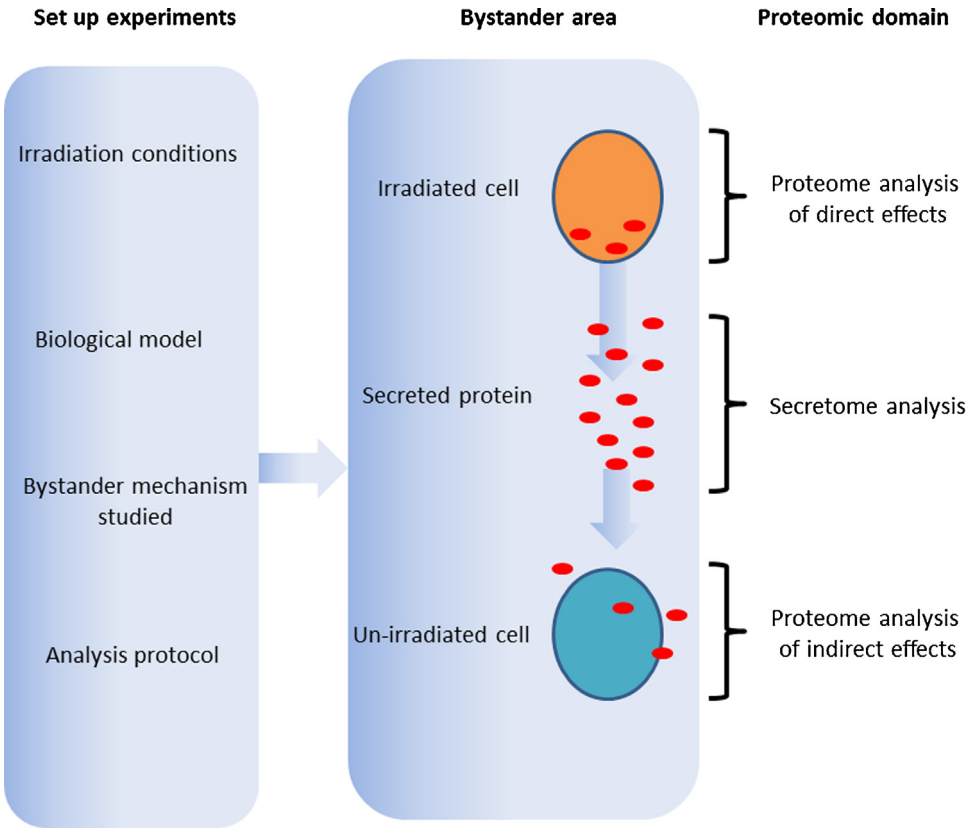

Fig. 7. Sequential scheme for the analysis of bystander samples using proteomic tools. Following the setup of the experimental conditions (irradiation conditions, biological model, analysis protocol and the studied RIBE mechanism), three areas can be analyzed separately using proteomic tools. The proteome analysis of direct effects can be realized using irradiated cells; the secretome analysis can be explored with the conditioned medium containing secreted proteins and BF; and the proteome analysis of indirect effects can be analyzed using un-irradiated/bystander cells, incubated with secreted factors.

Please cite this article in press as: F. Chevalier, et al., Proteomic overview and perspectives of the radiation-induced bystander effects, Mutat. Res.: Rev. Mutat. Res. (2014), http://dx.doi.org/10.1016/j.mrrev.2014.11.008

limits for the "co-culture" protocol, concerning the restricted amount of available cells.

4.2. Secretome analysis of RIBE

A comparison between proteome and secretome could be performed (Fig. 7), but using two distinct experiments to produce samples, as BF could be consumed by bystander cells (to generate a BE), reducing their relative amount available for MS identification. In addition, the extraction process of BF from conditioned medium should be compatible with the subsequent proteomic technology. Several protocols were developed by proteomic and biochemistry researchers to improve the extraction capacity and allow a correct separation of proteins by 2DE [61,72]. The main objective of such protein extraction is to concentrate proteins in a small amount of buffer, or to precipitate them as a pellet using centrifugation (Fig. 8). According to a method applied to secreted salivary proteins [50], a chemical precipitation protocol was developed, with some modifications [72], to improve protein recovery and 2D-gel quality (Fig. 8, right side). Such a protocol was successfully applied to the analysis of secreted proteins from irradiated mammary cells [61] or in saliva [48,50]. Another possibility consists of using a 5 kDa cut-off membrane that will concentrate proteins in the retentate solution. Concentrated solution of proteins can be lyophilized to eliminate buffer and the remaining powder may be solubilized in 2DE compatible buffer (Fig. 8, left side). The use of cut-off membrane is an easy way to concentrate a protein solution and is widely used in biochemical studies of conditioned media [55,56,59,60,63].

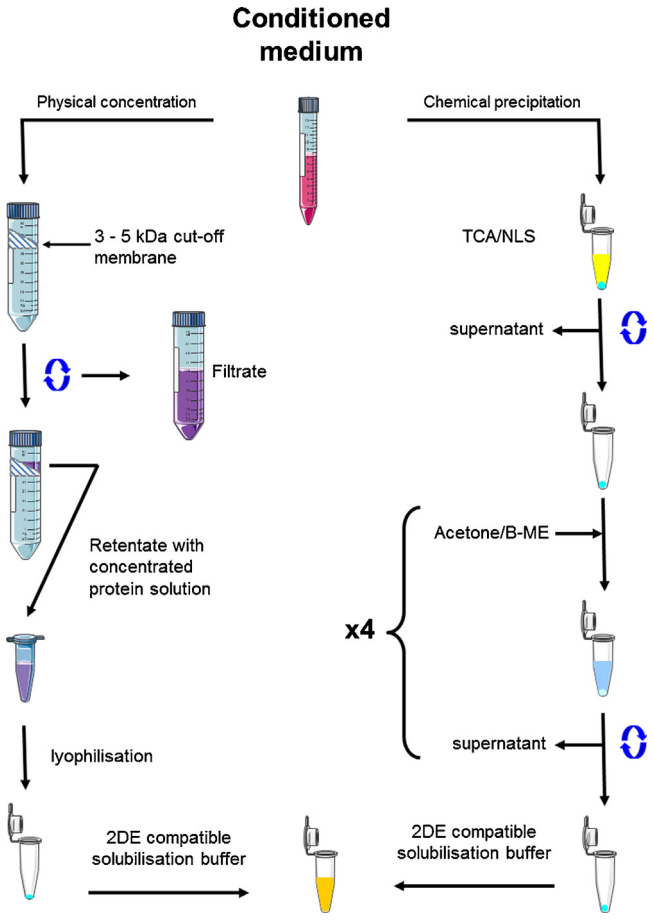

Fig. 8. Extraction and concentration of secreted proteins from conditioned medium and preparation of protein samples in 2DE compatible buffer. In case of chemical precipitation (right side), secreted proteins are precipitated using 7.5% TCA and 0.1% NLS (sodium lauryl sarcosinate), precipitated proteins are washed 4 times using cold acetone supplemented with 0.07% B-Me to remove 2DE un-compatible compounds such as TCA and NLS, and washed proteins are air-dried and dispersed with 2DE solubilization buffer. In the case of physical concentration (left side), conditioned medium with secreted protein is concentrated by centrifugation using a 3–5-kDa cut-off membrane. The retentate with concentrated solution is diluted several time to eliminate culture medium and finally lyophilized. Protein powder is re-suspended and solubilized in 2DE solubilization buffer.

4.3. Cellular models to confirm RIBE mechanisms

In addition to the irradiation conditions and analysis protocols (Fig. 7, left), the choice of the cellular model will allow the study of specific or general RIBE mechanisms (*e.g.*, gap junctions, proteins, ligands, exosomes, etc.). Several cell and tissue types were previously investigated for BE [3,4] but very few under the same irradiation conditions. As initially presented in Fig. 1, following IR, signaler cells (Fig. 1, cell 1) secrete BF *via* specific channels to receptor cells. Some cells are not able to secrete factors (red cells) and all cells are not able to receive these factors (gray cells). One way to analyze intercellular signaling pathways is to focus on a specific RIBE mechanism with a dedicated model. The functions of specific intercellular communications has been accurately studied in cellular models expressing gap-junctions channels composed of connexin43 [73] or either connexin26 or connexin32 [74], showing a modulation of clonogenic survival and metabolic activity as a function of connexin expression. Proteomic studies can reveal new protein targets involved in RIBE mechanisms and will open new possibilities of research using cellular models with characteristic expression of these protein targets (mutants or over-expression). Indeed, independently of the proteomic strategy selected (gel-based or MS-based), the comparison between treated and control samples will display a list of candidate biomarkers. These proteins need to be validated using a biological test, independent of the proteomic experiment (Fig. 4, validation of biomarkers). Such an approach is mandatory within a global proteomic strategy to reject false-positive biomarkers and allow the establishment of biological endpoints.

4.4. Applications in medicine and radiotherapy

One major consequence of the validation of biomarkers is the development of new scientific projects, new experimental strategies and its applications in medicine. Until now, most studies about RIBE were developed with cellular and molecular tools to focus on a specific BE determined by the irradiation system and the cellular model. Radiobiologists have analyzed over several decades various irradiation conditions, including comparisons between low and high doses or low and high TEL, with diverse successes. Most of these studies were performed with 2D culture models maintained in humidified incubators at 37 °C in an atmosphere of 5% CO_2 and 20% O_2. New developments for *in vitro* studies aim to get closer to *in vivo* conditions, but with functional and practical models related to irradiation constraints. The use of 3D culture models, with normoxic growth conditions (2–5% O2) is a great possibility for *in vitro* analysis of RIBE, without the need for animal experimentations [75]. It combines the flexibility and capacity of *in vitro* growth conditions with the conserved 3D cellular response close to animal tissues and *in vivo* oxygen concentrations. Indeed, such models could explain the differential radiosensitivity observed between cells in 2D cultures and cells included in a tissue. The normoxic growth conditions, close to *in vivo* experiments, will certainly modulate the RIBE effect linked to oxidative metabolism. ROS are considered as major BF and key pathways affecting bystander signal too. It is then mandatory to analyze BE in a controlled and coherent oxygen concentration during RIBE experiments. In radiotherapeutic treatment of tumors, the objective is, of course, to

Please cite this article in press as: F. Chevalier, et al., Proteomic overview and perspectives of the radiation-induced bystander effects, Mutat. Res.: Rev. Mutat. Res. (2014), http://dx.doi.org/10.1016/j.mrrev.2014.11.008

maximize BR inside the tumor mass and to limit or prevent BE in normal tissues surrounding tumor cells or in the way of the beam [1]. For this reason, the development of new irradiation protocols will require a better understanding of RIBE associated with the discovery of new biomarker targets.

5. Conclusion

Proteomics is a well-established set of technical tools for the study and comparison of complex protein mixture. Moreover, RIBE is a largely observed biological mechanism and this non-targeted effect of exposure to IR is now widely accepted by radiobiologists. In contrast to research performed in cancer-proteomics, it appears clearly that the proteomic study of RIBE is only at the first phase of investigation and from a more general point of view, proteomic tools are still under-used in radiation research [54,67,70,71,76,77]. From a fundamental point of view, proteomic tools could reveal general intercellular communication mechanisms, involving BF secreted by irradiated cells, protein receptors of bystander cells, the involvement of direct cell-to-cell communication *via* gap-junctions, or the secretion of small vesicles by irradiated cells before cell death. The observation of such intercellular communication will allow a better control of IR delivered during RT, to limit the BE on normal cells and to prevent inflammation processes around the tumor area. With the recent advances in delivery of external beam radiotherapy (3DCRT and IMRT) which enable a precise delivery of high doses of radiation to the tumor, a better treatment of the cancer could be associated with a higher risk of BE in the adjacent tissues. This hypothesis could be reasonably associated with the use of high LET radiations (hadrontherapy), in which the energy deposition is maximum in the targeted area. These last generations of radiotherapy treatments lead to numerous questions concerning the role of RIBE and its consequences, showing the huge efforts still needed to control this intercellular phenomenon.

Conflict of interest statement

The authors declare that there are no conflicts of interest.

References

[1] K.M. Prise, J.M. O'Sullivan, Radiation-induced bystander signalling in cancer therapy, Nat. Rev. Cancer 9 (2009) 351–360, http://dx.doi.org/10.1038/nrc2603.
[2] M. Mancuso, E. Pasquali, P. Giardullo, S. Leonardi, M. Tanori, V. Di Majo, et al., The radiation bystander effect and its potential implications for human health, Curr. Mol. Med. 12 (2012) 613–624.
[3] B.J. Blyth, P.J. Sykes, Radiation-induced bystander effects: what are they, and how relevant are they to human radiation exposures? Radiat. Res. 176 (2011) 139–157.
[4] UNSCEAR, Annex C. Non-targeted and Delayed Effects of Exposure to Ionizing Radiations, UNSCEAR, 2006.
[5] J.B. Little, W.F. Morgan, Oncogene 22 (2003) 6977, http://dx.doi.org/10.1038/sj.onc.1207045 (Guest Editors).
[6] J.B. Little, Genomic instability and bystander effects: a historical perspective, Oncogene 22 (2003) 6978–6987, http://dx.doi.org/10.1038/sj.onc.1206988.
[7] C. Mothersill, C. Seymour, Radiation-induced bystander effects, carcinogenesis and models, Oncogene 22 (2003) 7028–7033, http://dx.doi.org/10.1038/sj.onc.1206882.
[8] E.J. Hall, T.K. Hei, Genomic instability and bystander effects induced by high-LET radiation, Oncogene 22 (2003) 7034–7042, http://dx.doi.org/10.1038/sj.onc.1206900.
[9] K.M. Prise, M. Folkard, B.D. Michael, Bystander responses induced by low LET radiation, Oncogene 22 (2003) 7043–7049, http://dx.doi.org/10.1038/sj.onc.1206991.
[10] E.I. Azzam, S.M. de Toledo, J.B. Little, Oxidative metabolism, gap junctions and the ionizing radiation-induced bystander effect, Oncogene 22 (2003) 7050–7057, http://dx.doi.org/10.1038/sj.onc.1206961.
[11] S.A. Lorimore, P.J. Coates, E.G. Wright, Radiation-induced genomic instability and bystander effects: inter-related nontargeted effects of exposure to ionizing radiation, Oncogene 22 (2003) 7058–7069, http://dx.doi.org/10.1038/sj.onc.1207044.
[12] W.F. Morgan, Is there a common mechanism underlying genomic instability, bystander effects and other nontargeted effects of exposure to ionizing radiation? Oncogene 22 (2003) 7094–7099, http://dx.doi.org/10.1038/sj.onc.1206992.
[13] M.A. Chaudhry, Bystander effect: biological endpoints and microarray analysis, Mutat. Res. 597 (2006) 98–112, http://dx.doi.org/10.1016/j.mrfmmm.2005.04.023.
[14] C. Mothersill, C. Seymour, Radiation-induced bystander effects: past history and future directions, Radiat. Res. 155 (2001) 759–767.
[15] E.I. Azzam, J.-P. Jay-Gerin, D. Pain, Ionizing radiation-induced metabolic oxidative stress and prolonged cell injury, Cancer Lett. 327 (2012) 48–60, http://dx.doi.org/10.1016/j.canlet.2011.12.012.
[16] D.J. Brenner, J.B. Little, R.K. Sachs, The bystander effect in radiation oncogenesis: II. A quantitative model, Radiat. Res. 155 (2001) 402–408.
[17] W.F. Morgan, Non-targeted and delayed effects of exposure to ionizing radiation: I. Radiation-induced genomic instability and bystander effects in vitro, Radiat. Res. 159 (2003) 567–580.
[18] W.F. Morgan, Non-targeted and delayed effects of exposure to ionizing radiation: II. Radiation-induced genomic instability and bystander effects in vivo, clastogenic factors and transgenerational effects, Radiat. Res. 159 (2003) 581–596.
[19] N. Hamada, H. Matsumoto, T. Hara, Y. Kobayashi, Intercellular and intracellular signaling pathways mediating ionizing radiation-induced bystander effects, J. Radiat. Res. (Tokyo) 48 (2007) 87–95.
[20] C.A. Waldren, Classical radiation biology dogma, bystander effects and paradigm shifts, Hum. Exp. Toxicol. 23 (2004) 95–100.
[21] S.M. de Toledo, N. Asaad, P. Venkatachalam, L. Li, R.W. Howell, D.R. Spitz, et al., Adaptive responses to low-dose/low-dose-rate gamma rays in normal human fibroblasts: the role of growth architecture and oxidative metabolism, Radiat. Res. 166 (2006) 849–857, http://dx.doi.org/10.1667/RR0640.1.
[22] G. Kashino, K.M. Prise, K. Suzuki, N. Matsuda, S. Kodama, M. Suzuki, et al., Effective suppression of bystander effects by DMSO treatment of irradiated CHO cells, J. Radiat. Res. (Tokyo) 48 (2007) 327–333.
[23] M. Buonanno, S.M. de Toledo, D. Pain, E.I. Azzam, Long-term consequences of radiation-induced bystander effects depend on radiation quality and dose and correlate with oxidative stress, Radiat. Res. 175 (2011) 405–415, http://dx.doi.org/10.1667/RR2461.1.
[24] C. Laurent, A. Leduc, I. Pottier, V. Prévost, F. Sichel, J.-L. Lefaix, Dramatic increase in oxidative stress in carbon-irradiated normal human skin fibroblasts, PLoS One 8 (2013) e85158, http://dx.doi.org/10.1371/journal.pone.0085158.
[25] Z. Goldberg, B.E. Lehnert, Radiation-induced effects in unirradiated cells: a review and implications in cancer, Int. J. Oncol. 21 (2002) 337–349.
[26] D. Schaue, E.L. Kachikwu, W.H. McBride, Cytokines in radiobiological responses: a review, Radiat. Res. 178 (2012) 505–523, http://dx.doi.org/10.1667/RR3031.1.
[27] J. Albanese, N. Dainiak, Modulation of intercellular communication mediated at the cell surface and on extracellular, plasma membrane-derived vesicles by ionizing radiation, Exp. Hematol. 31 (2003) 455–464.
[28] X. Yu, S.L. Harris, A.J. Levine, The regulation of exosome secretion: a novel function of the p53 protein, Cancer Res. 66 (2006) 4795–4801, http://dx.doi.org/10.1158/0008-5472.CAN-05-4579.
[29] N. Autsavapromporn, M. Suzuki, T. Funayama, N. Usami, I. Plante, Y. Yokota, et al., Gap junction communication and the propagation of bystander effects induced by microbeam irradiation in human fibroblast cultures: the impact of radiation quality, Radiat. Res. (2013), http://dx.doi.org/10.1667/RR3111.1.
[30] L.A. Ryan, R.W. Smith, C.B. Seymour, C.E. Mothersill, Dilution of irradiated cell conditioned medium and the bystander effect, Radiat. Res. 169 (2008) 188–196, http://dx.doi.org/10.1667/RR1141.1.
[31] C. Mothersill, C.B. Seymour, Cell–cell contact during gamma irradiation is not required to induce a bystander effect in normal human keratinocytes: evidence for release during irradiation of a signal controlling survival into the medium, Radiat. Res. 149 (1998) 256, http://dx.doi.org/10.2307/3579958.
[32] K.T. Butterworth, C.K. McGarry, C. Trainor, S.J. McMahon, J.M. O'Sullivan, G. Schettino, et al., Dose, dose-rate and field size effects on cell survival following exposure to non-uniform radiation fields, Phys. Med. Biol. 57 (2012) 3197–3206, http://dx.doi.org/10.1088/0031-9155/57/10/3197.
[33] K.T. Butterworth, C.K. McGarry, C. Trainor, J.M. O'Sullivan, A.R. Hounsell, K.M. Prise, Out-of-field cell survival following exposure to intensity-modulated radiation fields, Int. J. Radiat. Oncol. Biol. Phys. 79 (2011) 1516–1522, http://dx.doi.org/10.1016/j.ijrobp.2010.11.034.
[34] S.J. McMahon, K.T. Butterworth, C. Trainor, C.K. McGarry, J.M. O'Sullivan, G. Schettino, et al., A kinetic-based model of radiation-induced intercellular signalling, PLoS One 8 (2013) e54526, http://dx.doi.org/10.1371/journal.pone.0054526.
[35] H. Nagasawa, J.B. Little, Induction of sister chromatid exchanges by extremely low doses of alpha-particles, Cancer Res. 52 (1992) 6394–6396.
[36] T. Chaze, M.-C. Slomianny, F. Milliat, G. Tarlet, T. Lefebvre-Darroman, P. Gourmelon, et al., Alteration of the serum *N*-glycome of mice locally exposed to high doses of ionizing radiation, Mol. Cell. Proteomics 12 (2013) 283–301, http://dx.doi.org/10.1074/mcp.M111.014639.
[37] C. Mothersill, R.W. Smith, N. Agnihotri, C.B. Seymour, Characterization of a radiation-induced stress response communicated in vivo between zebrafish, Environ. Sci. Technol. 41 (2007) 3382–3387.
[38] M. Partridge, A radiation damage repair model for normal tissues, Phys. Med. Biol. 53 (2008) 3595, http://dx.doi.org/10.1088/0031-9155/53/13/014.
[39] S.J. McMahon, K.T. Butterworth, C.K. McGarry, C. Trainor, J.M. O'Sullivan, A.R. Hounsell, et al., A computational model of cellular response to modulated radiation fields, Int. J. Radiat. Oncol. 84 (2012) 250–256, http://dx.doi.org/10.1016/j.ijrobp.2011.10.058.
[40] S.J. McMahon, C.K. McGarry, K.T. Butterworth, J.M. O'Sullivan, A.R. Hounsell, K.M. Prise, Implications of intercellular signaling for radiation therapy: a theoretical dose-planning study, Int. J. Radiat. Oncol. Biol. Phys. 87 (2013) 1148–1154, http://dx.doi.org/10.1016/j.ijrobp.2013.08.021.
[41] F. Chevalier, V. Rofidal, P. Vanova, A. Bergoin, M. Rossignol, Proteomic capacity of recent fluorescent dyes for protein staining, Phytochemistry 65 (2004) 1499–1506.

Please cite this article in press as: F. Chevalier, et al., Proteomic overview and perspectives of the radiation-induced bystander effects, Mutat. Res.: Rev. Mutat. Res. (2014), http://dx.doi.org/10.1016/j.mrrev.2014.11.008

[42] F. Chevalier, D. Centeno, V. Rofidal, M. Tauzin, O. Martin, N. Sommerer, et al., Different impact of staining procedures using visible stains and fluorescent dyes for large-scale investigation of proteomes by MALDI–TOF mass spectrometry, J. Proteome Res. 5 (2006) 512–520.
[43] F. Chevalier, Highlights on the capacities of Gel-based proteomics, Proteome Sci. 8 (2010) 23.
[44] J. Dépagne, F. Chevalier, Technical updates to basic proteins focalization using IPG strips, Proteome Sci. 10 (2012) 54, http://dx.doi.org/10.1186/1477-5956-10-54.
[45] F. Chevalier, C. Hirtz, N. Sommerer, A.L. Kelly, Use of reducing/nonreducing two-dimensional electrophoresis for the study of disulfide-mediated interactions between proteins in raw and heated bovine milk, J. Agric. Food Chem. 57 (2009) 5948–5955.
[46] F. Chevalier, A.L. Kelly, Proteomic quantification of disulfide-linked polymers in raw and heated bovine milk, J. Agric. Food Chem. 58 (2010) 7437–7444.
[47] F. Chevalier, O. Martin, V. Rofidal, A.D. Devauchelle, S. Barteau, N. Sommerer, et al., Proteomic investigation of natural variation between *Arabidopsis* ecotypes, Proteomics 4 (2004) 1372–1381.
[48] C. Hirtz, F. Chevalier, D. Centeno, J.C. Egea, M. Rossignol, N. Sommerer, et al., Complexity of the human whole saliva proteome, J. Physiol. Biochem. 61 (2005) 469–480.
[49] D. Peric, J. Labarre, F. Chevalier, G. Rousselet, Impairing the microRNA biogenesis pathway induces proteome modifications characterized by size bias and enrichment in antioxidant proteins, Proteomics 12 (2012) 2295–2302, http://dx.doi.org/10.1002/pmic.201100461.
[50] C. Hirtz, F. Chevalier, D. Centeno, V. Rofidal, J.C. Egea, M. Rossignol, et al., MS characterization of multiple forms of alpha-amylase in human saliva, Proteomics 5 (2005) 4597–4607.
[51] F. Chevalier, M. Rossignol, Proteomic analysis of *Arabidopsis thaliana* ecotypes with contrasted root architecture in response to phosphate deficiency, J. Plant Physiol. (2011), http://dx.doi.org/10.1016/j.jplph.2011.05.024.
[52] E. Armaforte, E. Curran, T. Huppertz, C. Ryan, M. Caboni, P. O'Connor, et al., Proteins and proteolysis in pre-term and term human milk and possible implications for infant formulae, Int. Dairy J. 20 (2010) 715–723, http://dx.doi.org/10.1016/j.idairyj.2010.03.008.
[53] T. Uniacke-Lowe, F. Chevalier, S. Hem, P.F. Fox, D.M. Mulvihill, Proteomic comparison of equine and bovine milks on renneting, J. Agric. Food Chem. 61 (2013) 2839–2850, http://dx.doi.org/10.1021/jf3045846.
[54] H. Chandra, P.J. Reddy, S. Srivastava, Protein microarrays and novel detection platforms, Expert Rev. Proteomics 8 (2011) 61–79, http://dx.doi.org/10.1586/epr.10.99.
[55] M. Ahram, E.F. Strittmatter, M.E. Monroe, J.N. Adkins, J.C. Hunter, J.H. Miller, et al., Identification of shed proteins from Chinese hamster ovary cells: application of statistical confidence using human and mouse protein databases, Proteomics 5 (2005) 1815–1826, http://dx.doi.org/10.1002/pmic.200401072.
[56] D.L. Springer, M. Ahram, J.N. Adkins, L.E. Kathmann, J.H. Miller, Characterization of medium conditioned by irradiated cells using proteome-wide, high-throughput mass spectrometry, Radiat. Res. 164 (2005) 651–654.
[57] S. Pereira, V. Malard, J.-L. Ravanat, A.-H. Davin, J. Armengaud, N. Foray, et al., Low doses of gamma-irradiation induce an early bystander effect in zebrafish cells which is sufficient to radioprotect cells, PLoS One 9 (2014) e92974, http://dx.doi.org/10.1371/journal.pone.0092974.
[58] Q. Zhang, M. Matzke, A.A. Schepmoes, R.J. Moore, B.-J. Webb-Robertson, Z. Hu, et al., High and low doses of ionizing radiation induce different secretome profiles in a human skin model, PLoS One 9 (2014) e92332, http://dx.doi.org/10.1371/journal.pone.0092332.
[59] K.N. Rithidech, X. Lai, L. Honikel, P. Reungpatthanaphong, F.A. Witzmann, Identification of proteins secreted into the medium by human lymphocytes irradiated in vitro with or without adaptive environments, Health Phys. 102 (2012) 39–53, http://dx.doi.org/10.1097/HP.0b013e31822833af.
[60] T. Hellevik, I. Pettersen, V. Berg, J. Bruun, K. Bartnes, L.-T. Busund, et al., Changes in the secretory profile of NSCLC-associated fibroblasts after ablative radiotherapy: potential impact on angiogenesis and tumor growth, Transl. Oncol. 6 (2013) 66–74.
[61] F. Chevalier, J. Depagne, S. Hem, S. Chevillard, J. Bensimon, P. Bertrand, et al., Accumulation of cyclophilin A isoforms in conditioned medium of irradiated breast cancer cells, Proteomics 12 (2012) 1756–1766, http://dx.doi.org/10.1002/pmic.201100319.
[62] B.I. Gerashchenko, A. Yamagata, K. Oofusa, K. Yoshizato, S.M. de Toledo, R.W. Howell, Proteome analysis of proliferative response of bystander cells adjacent to cells exposed to ionizing radiation, Proteomics 7 (2007) 2000–2008, http://dx.doi.org/10.1002/pmic.200600948.
[63] N.-K. Han, B.C. Kim, H.C. Lee, Y.-J. Lee, M.-J. Park, S.-G. Chi, et al., Secretome analysis of ionizing radiation-induced senescent cancer cells reveals that secreted RKIP plays a critical role in neighboring cell migration, Proteomics 12 (2012) 2822–2832, http://dx.doi.org/10.1002/pmic.201100419.
[64] R.W. Smith, J. Wang, C.P. Bucking, C.E. Mothersill, C.B. Seymour, Evidence for a protective response by the gill proteome of rainbow trout exposed to X-ray induced bystander signals, Proteomics 7 (2007) 4171–4180, http://dx.doi.org/10.1002/pmic.200700573.
[65] R.W. Smith, J. Wang, C.E. Mothersill, T.G. Hinton, K. Aizawa, C.B. Seymour, Proteomic changes in the gills of wild-type and transgenic radiosensitive medaka following exposure to direct irradiation and to X-ray induced bystander signals, Biochim. Biophys. Acta 1814 (2011) 290–298, http://dx.doi.org/10.1016/j.bbapap.2010.11.002.
[66] R.W. Smith, J. Wang, E. Schültke, C.B. Seymour, E. Bräuer-Krisch, J.A. Laissue, et al., Proteomic changes in the rat brain induced by homogenous irradiation and by the bystander effect resulting from high energy synchrotron X-ray microbeams, Int. J. Radiat. Biol. 89 (2013) 118–127, http://dx.doi.org/10.3109/09553002.2013.732252.
[67] O. Guipaud, Serum and plasma proteomics and its possible use as detector and predictor of radiation diseases, in: D. Leszczynski (Ed.), Radiat. Proteomics, Springer, Netherlands, 2013, pp. 61–86, ⟨http://link.springer.com/chapter/10.1007/978-94-007-5896-4_4⟩ (accessed November 29, 2013).
[68] T. Chaze, L. Hornez, C. Chambon, I. Haddad, J. Vinh, J.-P. Peyrat, et al., Serum proteome analysis for profiling predictive protein markers associated with the severity of skin lesions induced by ionizing radiation, Proteomes 1 (2013) 40–69, http://dx.doi.org/10.3390/proteomes1020040.
[69] S.M. Varnum, D.L. Springer, M.E. Chaffee, K.A. Lien, B.-J.M. Webb-Robertson, K.M. Waters, et al., The effects of low-dose irradiation on inflammatory response proteins in a 3D reconstituted human skin tissue model, Radiat. Res. 178 (2012) 591–599, http://dx.doi.org/10.1667/RR2976.1.
[70] S. Tapio, S. Hornhardt, M. Gomolka, D. Leszczynski, A. Posch, S. Thalhammer, et al., Use of proteomics in radiobiological research: current state of the art, Radiat. Environ. Biophys. 49 (2010) 1–4, http://dx.doi.org/10.1007/s00411-009-0263-7.
[71] O. Azimzadeh, M.J. Atkinson, S. Tapio, Proteomics in radiation research: present status and future perspectives, Radiat. Environ. Biophys. (2013), http://dx.doi.org/10.1007/s00411-013-0495-4.
[72] M. Chevallet, H. Diemer, A. Van Dorssealer, C. Villiers, T. Rabilloud, Toward a better analysis of secreted proteins: the example of the myeloid cells secretome, Proteomics 7 (2007) 1757–1770, http://dx.doi.org/10.1002/pmic.200601024.
[73] E.I. Azzam, S.M. de Toledo, J.B. Little, Expression of CONNEXIN43 is highly sensitive to ionizing radiation and other environmental stresses, Cancer Res. 63 (2003) 7128–7135.
[74] N. Autsavapromporn, S.M. De Toledo, J.-P. Jay-Gerin, A.L. Harris, E.I. Azzam, Human cell responses to ionizing radiation are differentially affected by the expressed connexins, J. Radiat. Res. (Tokyo) 54 (2013) 251–259, http://dx.doi.org/10.1093/jrr/rrs099.
[75] A. Carreau, B. El Hafny-Rahbi, A. Matejuk, C. Grillon, C. Kieda, Why is the partial oxygen pressure of human tissues a crucial parameter? Small molecules and hypoxia, J. Cell. Mol. Med. 15 (2011) 1239–1253, http://dx.doi.org/10.1111/j.1582-4934.2011.01258.x.
[76] O. Guipaud, M. Benderitter, Protein biomarkers for radiation exposure: towards a proteomic approach as a new investigation tool, Ann. Ist. Super. Sanita 45 (2009) 278–286.
[77] M.J. Atkinson, Radiation treatment effects on the proteome of the tumour microenvironment, Adv. Exp. Med. Biol. 990 (2013) 49–60, http://dx.doi.org/10.1007/978-94-007-5896-4_3.

Please cite this article in press as: F. Chevalier, et al., Proteomic overview and perspectives of the radiation-induced bystander effects, Mutat. Res.: Rev. Mutat. Res. (2014), http://dx.doi.org/10.1016/j.mrrev.2014.11.008

3.9 - Références

[1] H.A. Wolff, D.M. Wagner, L.-C. Conradi, S. Hennies, M. Ghadimi, C.F. Hess, et al., Irradiation with protons for the individualized treatment of patients with locally advanced rectal cancer: a planning study with clinical implications, Radiother. Oncol. J. Eur. Soc. Ther. Radiol. Oncol. 102 (2012) 30–37. doi:10.1016/j.radonc.2011.10.018.

[2] D.J. Brenner, J.B. Little, R.K. Sachs, The bystander effect in radiation oncogenesis: II. A quantitative model, Radiat. Res. 155 (2001) 402–408.

[3] S.J. McMahon, C.K. McGarry, K.T. Butterworth, J.M. O'Sullivan, A.R. Hounsell, K.M. Prise, Implications of Intercellular Signaling for Radiation Therapy: A Theoretical Dose-Planning Study, Int. J. Radiat. Oncol. Biol. Phys. 87 (2013) 1148–1154. doi:10.1016/j.ijrobp.2013.08.021.

[4] Dossier - Cancer : ARCHADE place la Basse-Normandie à la pointe de la recherche, (n.d.). http://www.connexions-normandie.fr/2013/06/20/dossier-cancer-archade-place-la-basse-normandie-a-la-pointe-de-la-recherche/ (accessed December 3, 2014).

[5] Médecine nucléaire à Caen : le projet Archade définitivement lancé - Tendance Ouest, (n.d.). http://www.tendanceouest.com/caen/actualite-80377-medecine-nucleaire-a-caen-le-projet-archade-definitivement-lance.html (accessed December 3, 2014).

[6] D. Schulz-Ertner, C.P. Karger, A. Feuerhake, A. Nikoghosyan, S.E. Combs, O. Jäkel, et al., Effectiveness of carbon ion radiotherapy in the treatment of skull-base chordomas, Int. J. Radiat. Oncol. Biol. Phys. 68 (2007) 449–457. doi:10.1016/j.ijrobp.2006.12.059.

[7] T.A. van de Water, A.J. Lomax, H.P. Bijl, M.E. de Jong, C. Schilstra, E.B. Hug, et al., Potential benefits of scanned intensity-modulated proton therapy versus advanced photon therapy with regard to sparing of the salivary glands in oropharyngeal cancer, Int. J. Radiat. Oncol. Biol. Phys. 79 (2011) 1216–1224. doi:10.1016/j.ijrobp.2010.05.012.

[8] S.G. Sawant, G. Randers-Pehrson, C.R. Geard, D.J. Brenner, E.J. Hall, The bystander effect in radiation oncogenesis: I. Transformation in C3H 10T1/2 cells in vitro can be initiated in the unirradiated neighbors of irradiated cells, Radiat. Res. 155 (2001) 397–401.

[9] K.M. Prise, J.M. O'Sullivan, Radiation-induced bystander signalling in cancer therapy, Nat. Rev. Cancer. 9 (2009) 351–360. doi:10.1038/nrc2603.

[10] F. Chevalier, D.H. Hamdi, Y. Saintigny, J.-L. Lefaix, Proteomic overview and perspectives of the radiation-induced bystander effects, Mutat. Res. Mutat. Res. (n.d.). doi:10.1016/j.mrrev.2014.11.008.

[11] UNSCEAR, Annex C : Non-targeted and delayed effects of exposure to ionizing radiations, 2006.

[12] N. Suchowerska, M.A. Ebert, M. Zhang, M. Jackson, In vitro response of tumour cells to non-uniform irradiation, Phys. Med. Biol. 50 (2005) 3041–3051. doi:10.1088/0031-9155/50/13/005.

[13] K.M. Prise, M. Folkard, B.D. Michael, Bystander responses induced by low LET radiation, Oncogene. 22 (2003) 7043–7049. doi:10.1038/sj.onc.1206991.

[14] G. Kashino, K.M. Prise, K. Suzuki, N. Matsuda, S. Kodama, M. Suzuki, et al., Effective suppression of bystander effects by DMSO treatment of irradiated CHO cells, J. Radiat. Res. (Tokyo). 48 (2007) 327–333.

[15] C. Shao, M. Folkard, K.M. Prise, Role of TGF-beta1 and nitric oxide in the bystander response of irradiated glioma cells, Oncogene. 27 (2008) 434–440. doi:10.1038/sj.onc.1210653.

[16] K.T. Butterworth, C.K. McGarry, C. Trainor, J.M. O'Sullivan, A.R. Hounsell, K.M. Prise, Out-of-field cell survival following exposure to intensity-modulated radiation fields, Int. J. Radiat. Oncol. Biol. Phys. 79 (2011) 1516–1522. doi:10.1016/j.ijrobp.2010.11.034.

[17] K.T. Butterworth, C.K. McGarry, C. Trainor, S.J. McMahon, J.M. O'Sullivan, G. Schettino, et al., Dose, dose-rate and field size effects on cell survival following exposure to non-uniform radiation fields, Phys. Med. Biol. 57 (2012) 3197–3206. doi:10.1088/0031-9155/57/10/3197.

[18] S.J. McMahon, K.T. Butterworth, C.K. McGarry, C. Trainor, J.M. O'Sullivan, A.R. Hounsell, et al., A Computational Model of Cellular Response to Modulated Radiation Fields, Int. J. Radiat. Oncol. 84 (2012) 250–256. doi:10.1016/j.ijrobp.2011.10.058.

[19] S.J. McMahon, K.T. Butterworth, C. Trainor, C.K. McGarry, J.M. O'Sullivan, G. Schettino, et al., A kinetic-based model of radiation-induced intercellular signalling, PloS One. 8 (2013) e54526. doi:10.1371/journal.pone.0054526.

[20] K.T. Butterworth, C.K. McGarry, B. Clasie, A. Carabe-Fernandez, J. Schuemann, N. Depauw, et al., Relative biological effectiveness (RBE) and out-of-field cell survival responses to passive

scattering and pencil beam scanning proton beam deliveries, Phys. Med. Biol. 57 (2012) 6671–6680. doi:10.1088/0031-9155/57/20/6671.
[21] C. Trainor, K.T. Butterworth, C.K. McGarry, F. Liberante, J.M. O'Sullivan, A.R. Hounsell, et al., Cell survival responses after exposure to modulated radiation fields, Radiat. Res. 177 (2012) 44–51.
[22] C. Trainor, K.T. Butterworth, C.K. McGarry, S.J. McMahon, J.M. O'Sullivan, A.R. Hounsell, et al., DNA damage responses following exposure to modulated radiation fields, PloS One. 7 (2012) e43326. doi:10.1371/journal.pone.0043326.
[23] C.K. McGarry, K.T. Butterworth, C. Trainor, S.J. McMahon, J.M. O'Sullivan, K.M. Prise, et al., In-vitro investigation of out-of-field cell survival following the delivery of conformal, intensity-modulated radiation therapy (IMRT) and volumetric modulated arc therapy (VMAT) plans, Phys. Med. Biol. 57 (2012) 6635–6645. doi:10.1088/0031-9155/57/20/6635.
[24] S.J. McMahon, K.T. Butterworth, C. Trainor, C.K. McGarry, J.M. O'Sullivan, G. Schettino, et al., A Kinetic-Based Model of Radiation-Induced Intercellular Signalling, PLoS ONE. 8 (2013) e54526. doi:10.1371/journal.pone.0054526.
[25] E.I. Azzam, S.M. de Toledo, J.B. Little, Oxidative metabolism, gap junctions and the ionizing radiation-induced bystander effect, Oncogene. 22 (2003) 7050–7057. doi:10.1038/sj.onc.1206961.
[26] E.I. Azzam, S.M. de Toledo, J.B. Little, Expression of CONNEXIN43 is highly sensitive to ionizing radiation and other environmental stresses, Cancer Res. 63 (2003) 7128–7135.
[27] S.M. de Toledo, N. Asaad, P. Venkatachalam, L. Li, R.W. Howell, D.R. Spitz, et al., Adaptive responses to low-dose/low-dose-rate gamma rays in normal human fibroblasts: the role of growth architecture and oxidative metabolism, Radiat. Res. 166 (2006) 849–857. doi:10.1667/RR0640.1.
[28] M. Pinto, E.I. Azzam, R.W. Howell, Investigation of adaptive responses in bystander cells in 3D cultures containing tritium-labeled and unlabeled normal human fibroblasts, Radiat. Res. 174 (2010) 216–227. doi:10.1667/RR1866.1.
[29] S.M. de Toledo, M. Buonanno, M. Li, N. Asaad, Y. Qin, G. Gonon, et al., The impact of adaptive and non-targeted effects in the biological responses to low dose/low fluence ionizing radiation: the modulating effect of linear energy transfer, Health Phys. 100 (2011) 290–292. doi:10.1097/HP.0b013e31820832d8.
[30] M. Buonanno, S.M. de Toledo, D. Pain, E.I. Azzam, Long-term consequences of radiation-induced bystander effects depend on radiation quality and dose and correlate with oxidative stress, Radiat. Res. 175 (2011) 405–415. doi:10.1667/RR2461.1.
[31] J.M. Akudugu, E.I. Azzam, R.W. Howell, Induction of lethal bystander effects in human breast cancer cell cultures by DNA-incorporated Iodine-125 depends on phenotype, Int. J. Radiat. Biol. 88 (2012) 1028–1038. doi:10.3109/09553002.2012.683511.
[32] E.I. Azzam, J.-P. Jay-Gerin, D. Pain, Ionizing radiation-induced metabolic oxidative stress and prolonged cell injury, Cancer Lett. 327 (2012) 48–60. doi:10.1016/j.canlet.2011.12.012.
[33] N. Autsavapromporn, S.M. De Toledo, J.-P. Jay-Gerin, A.L. Harris, E.I. Azzam, Human cell responses to ionizing radiation are differentially affected by the expressed connexins, J. Radiat. Res. (Tokyo). 54 (2013) 251–259. doi:10.1093/jrr/rrs099.
[34] G. Gonon, J.-E. Groetz, S.M. de Toledo, R.W. Howell, M. Fromm, E.I. Azzam, Nontargeted stressful effects in normal human fibroblast cultures exposed to low fluences of high charge, high energy (HZE) particles: kinetics of biologic responses and significance of secondary radiations, Radiat. Res. 179 (2013) 444–457. doi:10.1667/RR3017.1.
[35] N. Autsavapromporn, M. Suzuki, I. Plante, C. Liu, Y. Uchihori, T.K. Hei, et al., Participation of gap junction communication in potentially lethal damage repair and DNA damage in human fibroblasts exposed to low- or high-LET radiation, Mutat. Res. (2013). doi:10.1016/j.mrgentox.2013.07.001.
[36] N. Autsavapromporn, M. Suzuki, T. Funayama, N. Usami, I. Plante, Y. Yokota, et al., Gap Junction Communication and the Propagation of Bystander Effects Induced by Microbeam Irradiation in Human Fibroblast Cultures: The Impact of Radiation Quality, Radiat. Res. (2013). doi:10.1667/RR3111.1.
[37] O.V. Belyakov, S.A. Mitchell, D. Parikh, G. Randers-Pehrson, S.A. Marino, S.A. Amundson, et al., Biological effects in unirradiated human tissue induced by radiation damage up to 1 mm away, Proc. Natl. Acad. Sci. U. S. A. 102 (2005) 14203–14208. doi:10.1073/pnas.0505020102.
[38] H.J. Park, R.J. Griffin, S. Hui, S.H. Levitt, C.W. Song, Radiation-induced vascular damage in tumors: implications of vascular damage in ablative hypofractionated radiotherapy (SBRT and SRS), Radiat. Res. 177 (2012) 311–327.

[39] A. Carreau, B. El Hafny-Rahbi, A. Matejuk, C. Grillon, C. Kieda, Why is the partial oxygen pressure of human tissues a crucial parameter? Small molecules and hypoxia, J. Cell. Mol. Med. 15 (2011) 1239–1253. doi:10.1111/j.1582-4934.2011.01258.x.

[40] O.A. Sedelnikova, A. Nakamura, O. Kovalchuk, I. Koturbash, S.A. Mitchell, S.A. Marino, et al., DNA double-strand breaks form in bystander cells after microbeam irradiation of three-dimensional human tissue models, Cancer Res. 67 (2007) 4295–4302. doi:10.1158/0008-5472.CAN-06-4442.

[41] K. Suzuki, M. Nakashima, S. Yamashita, Dynamics of ionizing radiation-induced DNA damage response in reconstituted three-dimensional human skin tissue, Radiat. Res. 174 (2010) 415–423. doi:10.1667/RR2007.1.

[42] T.E. Schmid, G. Dollinger, V. Hable, C. Greubel, O. Zlobinskaya, D. Michalski, et al., Relative biological effectiveness of pulsed and continuous 20 MeV protons for micronucleus induction in 3D human reconstructed skin tissue, Radiother. Oncol. J. Eur. Soc. Ther. Radiol. Oncol. 95 (2010) 66–72. doi:10.1016/j.radonc.2010.03.010.

[43] A. Mezentsev, S.A. Amundson, Global gene expression responses to low- or high-dose radiation in a human three-dimensional tissue model, Radiat. Res. 175 (2011) 677–688. doi:10.1667/RR2483.1.

[44] P. Grabham, B. Hu, P. Sharma, C. Geard, Effects of ionizing radiation on three-dimensional human vessel models: differential effects according to radiation quality and cellular development, Radiat. Res. 175 (2011) 21–28. doi:10.1667/RR2289.1.

[45] S. Claus, N. Mayer, E. Aubert-Foucher, H. Chajra, E. Perrier-Groult, J. Lafont, et al., Cartilage-characteristic matrix reconstruction by sequential addition of soluble factors during expansion of human articular chondrocytes and their cultivation in collagen sponges, Tissue Eng. Part C Methods. 18 (2012) 104–112. doi:10.1089/ten.TEC.2011.0259.

[46] L. Basciano, C. Nemos, B. Foliguet, N. de Isla, M. de Carvalho, N. Tran, et al., Long term culture of mesenchymal stem cells in hypoxia promotes a genetic program maintaining their undifferentiated and multipotent status, BMC Cell Biol. 12 (2011) 12. doi:10.1186/1471-2121-12-12.

[47] C. Némos, L. Basciano, A. Dalloul, [Biological effects and potential applications of mesenchymal stem cell culture under low oxygen pressure], Pathol. Biol. (Paris). 60 (2012) 193–198. doi:10.1016/j.patbio.2011.07.004.

[48] Haute autorité de santé, Hadronthérapie par ions carbone : rapport préliminaire, (2010). http://www.has-sante.fr/portail/jcms/c_934208/fr/hadrontherapie-par-ions-carbone-rapport-preliminaire?xtmc=&xtcr=1.

[49] M. Wakatsuki, N. Magpayo, H. Kawamura, K.D. Held, Differential bystander signaling between radioresistant chondrosarcoma cells and fibroblasts after x-ray, proton, iron ion and carbon ion exposures, Int. J. Radiat. Oncol. Biol. Phys. 84 (2012) e103–108. doi:10.1016/j.ijrobp.2012.02.052.

[50] F. Chevalier, J. Depagne, S. Hem, S. Chevillard, J. Bensimon, P. Bertrand, et al., Accumulation of cyclophilin A isoforms in conditioned medium of irradiated breast cancer cells, Proteomics. 12 (2012) 1756–1766. doi:10.1002/pmic.201100319.